CONTRIBUTIONS ON SPECTRAL CONTROL FOR THE ASYMMETRICAL FULL BRIDGE MULTILEVEL INVERTER

Oscar Mauricio Muñoz Ramírez

ISBN: 978-84-693-7665-2
Dipòsit Legal: T.1747-2010

UNIVERSITAT ROVIRA I VIRGILI
CONTRIBUTIONS ON SPECTRAL CONTROL FOR THE ASYMMETRICAL FULL BRIDGE MULTILEVEL INVERTER
Oscar Mauricio Muñoz Ramírez
ISBN:978-84-693-7665-2/DL:T.1747-2010

DOCTORAL THESIS

Oscar Mauricio Muñoz Ramírez

CONTRIBUTIONS ON SPECTRAL CONTROL FOR THE ASYMMETRICAL FULL BRIDGE MULTILEVEL INVERTER

UNIVERSITAT ROVIRA I VIRGILI

Department
of Electronics, Electrical and Automatic Control Engineering

UNIVERSITAT ROVIRA I VIRGILI

Tarragona
2010

UNIVERSITAT ROVIRA I VIRGILI
CONTRIBUTIONS ON SPECTRAL CONTROL FOR THE ASYMMETRICAL FULL BRIDGE MULTILEVEL INVERTER
Oscar Mauricio Muñoz Ramírez
ISBN:978-84-693-7665-2/DL:T.1747-2010

UNIVERSITAT ROVIRA I VIRGILI
CONTRIBUTIONS ON SPECTRAL CONTROL FOR THE ASYMMETRICAL FULL BRIDGE MULTILEVEL INVERTER
Oscar Mauricio Muñoz Ramírez
ISBN:978-84-693-7665-2/DL:T.1747-2010

UNIVERSITAT ROVIRA I VIRGILI
CONTRIBUTIONS ON SPECTRAL CONTROL FOR THE ASYMMETRICAL FULL BRIDGE MULTILEVEL INVERTER
Oscar Mauricio Muñoz Ramírez
ISBN:978-84-693-7665-2/DL:T.1747-2010

UNIVERSITAT ROVIRA I VIRGILI
CONTRIBUTIONS ON SPECTRAL CONTROL FOR THE ASYMMETRICAL FULL BRIDGE MULTILEVEL INVERTER
Oscar Mauricio Muñoz Ramírez
ISBN:978-84-693-7665-2/DL:T.1747-2010

Oscar Mauricio Muñoz Ramírez

CONTRIBUTIONS ON SPECTRAL CONTROL FOR THE ASYMMETRICAL FULL BRIDGE MULTILEVEL INVERTER

DOCTORAL THESIS

Supervised by Dr. Hugo Valderrama-Blavi

Department
of Electronics, Electrical and Automatic Control Engineering

UNIVERSITAT ROVIRA I VIRGILI

Tarragona
2010

UNIVERSITAT ROVIRA I VIRGILI
CONTRIBUTIONS ON SPECTRAL CONTROL FOR THE ASYMMETRICAL FULL BRIDGE MULTILEVEL INVERTER
Oscar Mauricio Muñoz Ramírez
ISBN:978-84-693-7665-2/DL:T.1747-2010

UNIVERSITAT ROVIRA I VIRGILI
CONTRIBUTIONS ON SPECTRAL CONTROL FOR THE ASYMMETRICAL FULL BRIDGE MULTILEVEL INVERTER
Oscar Mauricio Muñoz Ramírez
ISBN:978-84-693-7665-2/DL:T.1747-2010

UNIVERSITAT
ROVIRA I VIRGILI
ESCOLA TÈCNICA SUPERIOR D'ENGINYERIA
DEPARTAMENT D'ENGINYERIA ELECTRONICA, ELÈCTRICA I AUTOMÀTICA

Avinguda dels Països Catalans, 26
Campus sescelades
43007 Tarragona
Tel. (977) 55 96 10
Fax (977) 55 96 05
e-mail: secelec@etse.urv.es
http://www.etse.urv.es/DEEEA/

I, Hugo Valderrama Blavi, Associate Professor of the Department of Electronics, Electrical and Automatic Control Engineering of the Rovira i Virgili University,

CERTIFY:

That the present research work, entitled "Contributions on Spectral Control for the Asymmetrical Full Bridge Multilevel Inverter", presented by Oscar Mauricio Muñoz Ramírez for the award of the degree of Doctor, has been carried out under my supervision at the Department of Electronics, Electrical and Automatic Control Engineering of this university.

Tarragona, May 6th 2010

UNIVERSITAT ROVIRA I VIRGILI
CONTRIBUTIONS ON SPECTRAL CONTROL FOR THE ASYMMETRICAL FULL BRIDGE MULTILEVEL INVERTER
Oscar Mauricio Muñoz Ramírez
ISBN:978-84-693-7665-2/DL:T.1747-2010

UNIVERSITAT ROVIRA I VIRGILI
CONTRIBUTIONS ON SPECTRAL CONTROL FOR THE ASYMMETRICAL FULL BRIDGE MULTILEVEL INVERTER
Oscar Mauricio Muñoz Ramírez
ISBN:978-84-693-7665-2/DL:T.1747-2010

Acknowledgements

I would like to express my gratitude to my academic advisor and mentor, Dr. Hugo Valderrama-Blavi for the completion of this work, who provided me guidance, patience, and support throughout my thesis stages. My sincere thanks go to Dr. Luis Martínez Salamero, Dr. Javier Maixé Altés, Dr. Roberto Giral and Dr. Abdelali El-Aroudi for their comments and general advice during the preparation of this thesis.

També vull agrair al Grup de Recerca en Automàtica i Electrònica Industrial, del Departament d'enginyeria electrònica, Elèctrica i Automàtica de la Universitat Rovira i Virgili, el seu suport acadèmic i financer que m'ha permès dur a terme aquest projecte.

I would like to thank all the laboratory staff at the GAEI, especially Josep M. Bosque and Antoni León, who assisted me with PCB design and supported me with all equipment and instrumentation during my stancy at the laboratory. I would also like to thank all of my friends and colleagues, who gave me ideas and suggestions to complete my thesis, mostly I thank Carlos Restrepo who guided me with genetics algorithms.

The persons not mentioned here, friends from the university, comrades in this journey, all of them are just in my mind and if you've been my guest at home, believe me, you're a truly friend: I apologize for not writing down your name here; lucky of me for such a long list of pals. So, my gratitude to these friends for the coffees, beers, dinners, movies and especially all the moments of reflections we shared in Tarragona.

Finally, I would like to thank my beloved family members. A mi abuela, quien me enseñó a leer y escribir y quien diariamente con su ejemplo me ha motivado a buscar la paz; a mis padres, quienes ofrendaron lo mejor de ellos para sus hijos; a mis hermanos, que son motivo de mi alegría y la razón de jamás claudicar ("Prométete a ti mismo", esta vá para vos David); a Yunuen, mi compañera en las vicisitudes; y a Dios, quién me dió la vida y me ha rodeado de personas tan bellas, pues Él es fuente de todos los tesoros que nos dá la existencia.

UNIVERSITAT ROVIRA I VIRGILI
CONTRIBUTIONS ON SPECTRAL CONTROL FOR THE ASYMMETRICAL FULL BRIDGE MULTILEVEL INVERTER
Oscar Mauricio Muñoz Ramírez
ISBN:978-84-693-7665-2/DL:T.1747-2010

UNIVERSITAT ROVIRA I VIRGILI
CONTRIBUTIONS ON SPECTRAL CONTROL FOR THE ASYMMETRICAL FULL BRIDGE MULTILEVEL INVERTER
Oscar Mauricio Muñoz Ramírez
ISBN:978-84-693-7665-2/DL:T.1747-2010

Abstract

Multilevel inverter (MI) topologies can work at higher voltage and higher power than conventional two-level converters. In addition, multilevel conversion reduces the output variables harmonic distortion and, sometimes, in spite of the devices-count increment, the conversion losses can also decrease by increasing the number of levels. The harmonic distortion reduction achieved by increasing the number of levels, can be used to further reducing the switching losses by decreasing the inverter carrier frequencies. To reduce even more the switching frequency without degrading output spectrum, we control the triangular carrier waveforms slopes.

First, to achieve this target, two analytical models have been created in order to predict the inverter output voltage spectrum, depending on diverse parameters: the amplitude modulation index M_A, the voltage distribution *K* of the inverter input sources, and the four carrier slopes $\{r_1, r_2, r_3, r_4\}$. The first model considers Natural Sampling and is based on Double Fourier Series (DFS) whereas the second model based on Simple Fourier Series (SFS), introduces the concept of Pseudo-Natural Sampling, as a digital approximation of the natural modulation. Both models are programmed in Matlab, verified with Pspice simulations and validated with a first experimental prototype with a DSP digital modulator.

The good agreement between natural and pseudo-natural modulations, as well as their respective DFS and SFS models, is exploited by a Genetic Algorithm (GA) application where THD is the cost function to minimize. After testing and properly tuning the GA, a framework matrix containing the optimized carriers set for a specific range of variables $\{M_A,K\}$ is generated and then, tested with a second, closed-loop prototype. A slow digital loop modifies the carrier slopes created by dsPIC microcontroller as PWM modulations, whose amplitude, once demodulated, are affected by a feed-forward loop. These carriers, compared with a sinusoidal reference, state-feedback modified, generate finally the closed-loop multilevel modulation. The final results demonstrates the feasibility of harmonic reduction by means of carrier slopes programming.

Keywords: multilevel inverter, PWM, harmonic distortion, spectral modeling, carrier slope, carriers set, level distribution, Double Fourier Series, Simple Fourier Series, natural sampling, regular sampling, pseudo-natural sampling, Genetic Algorithms.

UNIVERSITAT ROVIRA I VIRGILI
CONTRIBUTIONS ON SPECTRAL CONTROL FOR THE ASYMMETRICAL FULL BRIDGE MULTILEVEL INVERTER
Oscar Mauricio Muñoz Ramírez
ISBN:978-84-693-7665-2/DL:T.1747-2010

UNIVERSITAT ROVIRA I VIRGILI
CONTRIBUTIONS ON SPECTRAL CONTROL FOR THE ASYMMETRICAL FULL BRIDGE MULTILEVEL INVERTER
Oscar Mauricio Muñoz Ramírez
ISBN:978-84-693-7665-2/DL:T.1747-2010

Summary

As the electrical energy of renewable origin is still expensive, the improvement of the global conversion chain efficiency, going from the diverse transducers (PV panels, wind turbines, fuel cell stacks) to the diverse payloads, stockage forms, and distribution networks have become a key question.

Thus, most European governments have installation subsidies and granted research programs. In this frame, the current work explores new modulation methods to minimize switching losses in multilevel inverters, especially for the asymmetrical full bridge multilevel inverter.

A multilevel inverter (MI) is a switching converter where the appropriate control of an arrangement of switching devices allows combining diverse input voltages to synthesize a sinusoidal output voltage waveform. Multilevel conversion reduces the output variables harmonic distortion and, sometimes, in spite of the devices-count increment, the conversion losses can also decrease [Val08].

Precisely, the relationship between losses and harmonic content is a key question in this research work. The voltages blocked by the devices during the OFF-state in a multilevel converter are quite lower that the respective OFF-voltages in a two-level case. Therefore, all performance figures depending on those voltages can be improved substantially at equal switching frequency, load, and input-output voltage conditions. This is the case of the output voltage distortion and converter switching losses.

The distortion reduction achieved by increasing the number of levels, can be used to reduce further the switching losses decreasing slightly the inverter carrier frequencies without degrading excessively the output distortion. Besides, to reduce even more those switching losses, we have studied the possibility of modulating the slopes of the triangular carrier waveforms in order to achieve a set of optimum carrier signals. Feedback and Feedforward loops will reduce distortion, but as cleaner be the open-loop output voltage spectrum, the better will be the final result, once the control-loop is applied.

After presenting the contents and objectives of this work in the introduction, a review on the different multilevel topologies (diode-clamped, flying-capacitor, and cascaded full-bridge) emphasizes that the asymmetrical full bridge multilevel converter (AFBMI) is the five-level

ISBN:978-84-693-7665-2/DL:T.1747-2010

converter that uses less controllable switches, and therefore is the most suitable to reduce conduction and switching losses.

Different modulation and spectral analysis techniques are also revised here. On the one hand, we review the different harmonic performance parameters (WTHD, THD), as well as the concerns about the number of harmonics to be considered when applying such performance parameters. On the other hand, we classify the different modulations techniques according its spectral performance and operating mode.

Concerning the spectral performance the main differences come from the fact of using a fixed (PWM) and discrete spectrum, or variable, and even random switching frequency, where the output spectrum is smoothed. Concerning the modulation operating mode, we distinguish among on-line and off-line modulations. Our focus is oriented to on-line modulations, where we survey the different ways to organize the carriers of a multilevel modulation, and also, the different sampling techniques to decide the switching instants, natural and regular sampling among them.

According to diverse literature works, the natural PD-PWM modulation has better spectrum performance and is easier to implement [Cal98]. Consequently, we decided to restrict our study only to that modulation using the concepts found in the literature [Hol03]. On the other hand, we take the concept of contour plot to depict graphically the features of a sinusoidal modulation. Then, any contour plot identifies uniquely a certain modulation and its parameters. That graphical representation can be adapted mathematically by means of a double fourier series (DFS) because the integrals involved to calculate the DFS coefficients C_{mn} could be easily deduced from the contour plots.

Several simulations are done in order to prove that the spectrum of a PD modulation can be modified by means of selecting the slope of the vertically shifted carriers. The spectral results were analyzed using the FFT function of the PSPICE simulator. In particular, we corroborated that the contour plots were a good tool to distinguish the influence of different parameters in a modulation, as explained previously.

A model for the natural-sampled five-level PD-PWM modulation presented in (3.20) considers that all voltage levels are equal, that is, an inverter with balanced power supplies. We have extended such model to a situation were the levels be different, {−E, (K−1)·E, 0, KE, E} where 0<K<1, creating also the corresponding contour plots. Notice that, although the

ISBN:978-84-693-7665-2/DL:T.1747-2010

system have five levels available, the output voltage, can be synthesized using only 2, 3, or 4 of those levels. The number of used levels depend only on the amplitude modulation index M_a, and the level distribution parameter K. Such extended model is based on DFS and considers Natural Sampling, an inherent feature of analog modulation.

Natural sampling modulation requires a set of analog comparators working with their corresponding analog synchronized carriers and modulator signals. In addition, the slope and the amplitude of the carriers might be fully controllable. Amplitude control is required by the feed-forward loop, where the carriers should be proportional to the inverter power supplies. The feed-forward loop assures a good line regulation and linearizes the converter dynamics. The carriers slope control is required for spectrum optimization. Both, amplitude and slope controllability imply a serious implementation problem derived from the complexity of an analog modulator.

To overcome the implementation problem, we have explored two alternatives. First, we introduce the pseudo-natural modulation, a digital-made modulation, emulating reasonably well the natural sampling modulation. This digital modulation is a better approximation to the natural sampling because interpolates the sinusoidal waveform with two segments determined with the sampling points used by the preceding digital modulations ($T_C/4$, $T_C/2$, $3T_C/4$). A digital prototype confirmed the validity of pseudo-natural sampling.

In the second alternative, we implemented a closed-loop inverter prototype controlled by a mixed digital-analog modulator. A dsPIC microcontroller creates a set of carriers with a fully controllable slope. Those carriers are generated as PWM waveforms. Then, a series of low-pass filters and complementary circuits demodulate those signals to get the set of analog carriers vertically-shifted and their amplitudes proportionally adjusted to the inverter supply. Once these “analog” carriers have been created, they are compared analogically with a sinusoidal modulator created with the same method as the carriers. Thus, we have done a second approach to the natural modulation, created partially by digital means.

Visual comparison between the spectra of the natural sampling modulation and the pseudo-natural modulation are done in order to investigate if both spectra are sufficiently similar to consider the pseudo-natural modulation a promising candidate for a digital implementation of the natural modulation. Finally, thinking about future spectral comparisons and experimental validations, we begin to investigate the advantages and drawbacks of using the DFS

ISBN:978-84-693-7665-2/DL:T.1747-2010

coefficients C_{mn} for natural sampling or the SFS coefficients C_h for pseudo-natural sampling, where SFS appears as a faster and more precise option.

The first prototype consists of three main systems. The AFBMI converter board, the mosfet drivers, and the remaining system is a TMS320F2812 development kit where the pseudo-natural modulation is programmed. The amplitude modulation index and the level distribution K are written in the program code as set points. This means that when the modulation parameters must be changed the program execution must be stopped, modified and compiled again. When the program is executed, it calculates the switching instants and stores them in the DSP memory. Once the memory table is completed, the DSP board generates directly the AFBMI mosfet switching pulses from the data stored using two different internal counters.

Different test have been made to explore if the Pseudo-Natural PWM can be a good digital approximation of the analog natural sampling PWM. The first experiments pretended to verify if the DSP was implementing correctly the algorithms to calculate the switching instants for the Pseudo-Natural PWM. First, for two-level modulation different tests changing the carrier slope were made to verify the different spectra obtained. Once verified the system, we repeated the same experiments for a five-level modulation.

We have developed tools to predict the spectrum or finger print associated to a certain group of modulation parameters: the amplitude modulation index M_a, the level distribution K, and the carrier slopes $\{r_1, r_2, r_3, r_4\}$.We have also seen, that although the DFS and SFS can be used to predict analytically the value of each harmonic or spectral component in a multilevel modulation characterized by the preceding parameters, the mathematical operations are extremely complex. Actually, it is impossible to make the opposite calculation.

Given a certain output spectrum specification, for instance, the amplitudes of certain number of harmonics, or a certain THD or WTHD constraint, was impossible to solve the system of equations to know the appropriate carrier set $\{r_1, r_2, r_3, r_4\}$ assuring the fulfillment of the desired specifications. Therefore, an alternative carrier optimization method was required.

Genetic algorithms are used frequently as powerful tools to generate a family of training pairs for a neural network. Genetic algorithms are useful tools, reliable and accurate to solve search problems, because they are based on the evolution concept derived form Darwin's theory, where the best individual survives.

ISBN:978-84-693-7665-2/DL:T.1747-2010

The genetic algorithm iterative process is based on the natural selection, the crossover process, where two parents create two children, and finally the mutation phenomena that randomly affect the genetic representation of some individuals. In our case the genetic code of each individual is the set of carriers $\{r_1, r_2, r_3, r_4\}$. After a certain number of iterations or generations, according to certain natural selection criteria, for instance a THD threshold, the generations evolve, into a convergent solution, where a genetically optimum genetically finally appears. We have tested different parameters to tune the genetic algorithm, under different evolving constraint and initial population.

Optimizing the carrier slopes for any working point $\{M_a, K\}$ implies the execution of infinite genetic algorithms, one per point. Thus, in a practical implementation, the number of optimized working points must be reduced to decrease computing time-consumption. To reduce appropriately the number of points, we have considerated that in multilevel inverters, he amplitude modulation index is high to profit the input voltage supply, and therefore, such index can be restricted between $0.7 \leq M_a \leq 1$. In the same way, it is reasonable to consider level distribution between $0.3 \leq K \leq 0.7$. In the end, 221 working points were optimized using genetics algorithm.

The closed-loop prototype performs a vertically-shifted carrier modulator, with full carrier amplitude and slope control. A dsPIC microcontroller creates a set of carriers with a fully controllable slope. Those carriers are generated as PWM waveforms. Then, a series of fourth-order low-pass filters and complementary circuits demodulate those signals and combine them with some DC offsets, to get the set of analog carriers vertically shifted, with their amplitude proportional to the inverter supply. Once these “analog” carriers have been created, they are compared analogically with a sinusoidal modulator created with the same method as the carriers. Thus, we have created a slope-controllable natural modulation by mixed digital-analog means.

The prototype has three different closed loops. A digital control-loop actualizes five times per second the carrier slopes to optimize the output spectrum. The two analog loops are a classical feedforward, and state feedback loop. The feedforward loop linearizes the converter dynamics, assures ideal line regulation, and rejects the harmonics coming form the inverter DC power supplies. The state feedback loops improves the load regulation, increases the converter bandwidth, stabilizes the converter assuring a minimum damping factor at no-load conditions, and corrects the output voltage harmonic distortion coming from highly non-linear loads by means of reducing the inverter closed-loop output impedance.

ISBN:978-84-693-7665-2/DL:T.1747-2010

To assign an optimum carrier set to any operating point $\{M_a, K\}$ the digital control loop programs such set by finding the nearest of four optimized points that were pre-calculated with the GA and copying their respective carrier slopes. The spectrum optimization capability of this technique yields clear improvements on the output voltage spectrum, as can be seen in the given experimental results.

To conclude, we have proved that the base-band spectrum of a multilevel inverter output-voltage can be modified and improved by means of an appropriate selection of the carrier slopes, and we have developed two prototypes to verify that.

Future lines of work are also proposed in this thesis. Among them, the use of neural networks to interpolate the optimum slopes at any arbitrary working point. Other proposal for instance, would imply to investigate an slope control executing in real-time the genetic algorithms from data obtained directly from the measured output voltage spectrum.

UNIVERSITAT ROVIRA I VIRGILI
CONTRIBUTIONS ON SPECTRAL CONTROL FOR THE ASYMMETRICAL FULL BRIDGE MULTILEVEL INVERTER
Oscar Mauricio Muñoz Ramírez
ISBN:978-84-693-7665-2/DL:T.1747-2010

Glossary and Common Terms

AFBMI	*Asymmetric Full Bridge Multilevel Inverter*
APOD	*Alternative Phase Opposition Disposition*
C_{mn}	*Double Fourier Series Coefficient*
C_n	*Single Fourier Series Coefficient*
CSI, VSI	*Current, Voltage Source Inverter*
DC-AC	*Direct Current to Alternative Current*
DFS	*Double Fourier Series*
DFT	*Discrete Fourier Transform*
FFT	*Fast Fourier Transform*
GA	*Genetic(s) Algorithm(s)*
K	*Level Distribution Coefficient,* $V_D = K \cdot V_{dc}$, $V_U = (1-K) \cdot V_{dc}$
L_A, L_U	*Available Levels,* $L_A = \{-1, K-1, 0, K, 1\} \cdot V_{dc}$, *and Used Levels*
M_a , M_f	*Amplitude and Frequency Modulation Index,* $M_a = Vo/V_{dc}$, $M_f = F_C/F_O$
F_O , F_C	*Fundamental* $F_O = 50$ *Hz, and Switching Frequencies,* $F_C = 2.5$ *kHz*
MI	*Multilevel Inverter*
PCB	*Printed Circuit Board*
PD	*Phase Disposition*
POD	*Phase Opposition Disposition*
r_i	*Shape Factor of a Triangular Carrier,* $r_i = t_{rise}/T_C$
$\{r_1, r_2, r_3, r_4\}$	*Set of Shape factors in a 5-level MI*
SFS	*Single Fourier Series*
SPWM	*Sinusoidal Pulse Width Modulation*
T_C	*Triangular Carrier period (inverse of* F_C*)*
t_{rise}	*Rise time in a carrier signal,* $r_i = t_{rise}/T_C$
TDD	*Total Demand Distortion, referred to rated load current*
THD_I, THD_V	*Total Harmonic Distortion, referred to current or voltage harmonics*
THDn	*Total Harmonic Distortion for nth harmonic*
$V_O(t)$, V_O	*Inverter Output Voltage Waveform and Amplitude,* $V_O(t) = V_O \cdot \sin(2\pi F_O t)$
V_D, V_U, V_{dc}	*Voltage sources of an AFBMI, and total DC supply,* $V_D + V_U = V_{dc}$
$WTHD_0n$	*Weighted Total Harmonic Distortion for nth harmonic*

UNIVERSITAT ROVIRA I VIRGILI
CONTRIBUTIONS ON SPECTRAL CONTROL FOR THE ASYMMETRICAL FULL BRIDGE MULTILEVEL INVERTER
Oscar Mauricio Muñoz Ramírez
ISBN:978-84-693-7665-2/DL:T.1747-2010

UNIVERSITAT ROVIRA I VIRGILI
CONTRIBUTIONS ON SPECTRAL CONTROL FOR THE ASYMMETRICAL FULL BRIDGE MULTILEVEL INVERTER
Oscar Mauricio Muñoz Ramírez
ISBN:978-84-693-7665-2/DL:T.1747-2010

List of Figures

Figure 1.1 Comparison of Digital and Natural Modulations. 37
Figure 1.2 Optimization Matrix. 41

Figure 2.1 Single phase leg inverters. 47
Figure 2.2 Circuits based on three-level inverter leg. 48
Figure 2.3 Diode-Clamped multilevel inverter-leg. 49
Figure 2.4 Capacitor-Clamped multilevel inverter. 49
Figure 2.5 Cascaded inverters. 50
Figure 2.6 Mixed-Level multilevel inverter. 50
Figure 2.7 Asymmetric Full-Bridge Multilevel Inverter (AFBMI). 52
Figure 2.8 Ti-buck modeling of an Asymmetric Full-Bridge Multilevel Inverter. 53

Figure 3.1 Generalized stepped waveform synthesized by SHE. 64
Figure 3.2 Generalized three-level waveform synthesized by SHE. 64
Figure 3.3 Horizontally displaced carriers. 67
Figure 3.4 PD-SPWM. 68
Figure 3.5 POD-SPWM. 68
Figure 3.6 APOD-SPWM. 68
Figure 3.7 PS-SPWM. 68
Figure 3.8 Sampling methods of modulator signal in PWM. 70
Figure 3.9 Spectral amplitudes in a Pulse Width Modulated waveform. 71
Figure 3.10 Contour plot of 5-Level PD-SPWM Inverter. 73
Figure 3.11 Modulator signals in overmodulation conditions. 75
Figure 3.12 DC-DC conversion before DC-AC inversion. 76
Figure 3.13 Direct DC-AC inversion. 76

Figure 4.1 Spectra by FFT in Pspice simulation. 79
Figure 4.2 Synthesized waveforms by DFS model. 81
Figure 4.3 Refined waveforms by DFS. 83
Figure 4.4 Level distribution ratio K of input voltages. 86
Figure 4.5 Shape-factor representation of a carrier signal. 86
Figure 4.6 V_{PWM} Spectra by carriers programming. 90
Figure 4.7 Five-level PD-SPWM with modified carriers. 91
Figure 4.8 Switching angles (α_{ib},α_{is}) and carrier shape factors (r_i) . 92

ISBN:978-84-693-7665-2/DL:T.1747-2010

Figure 4.9 Switching Zones in 5-level modulation. 93
Figure 4.10 Five-level modulation (K=0.5, M_a=0.9). 97
Figure 4.11 Contour plot to calculate C_{mn} (K=0.5, M_a=0.9). 97
Figure 4.12 Five-level modulation (K=0.3, M_a=0.9). 98
Figure 4.13 Contour plot to calculate C_{mn} (K=0.3, M_a=0.9). 98
Figure 4.14 Five-level modulation (K=0.7, M_a=0.5). 99
Figure 4.15 Contour plot to calculate C_{mn} (K=0.7, M_a=0.5). 99
Figure 4.16 Five-level modulation (K=0.3, M_a=0.5). 101
Figure 4.17 Contour plot to calculate C_{mn} (K=0.3, M_a=0.5). 101
Figure 4.18 Five-level modulation (K=0.7, M_a=0.2). 103
Figure 4.19 Contour plot to calculate C_{mn} (K=0.7, M_a=0.2). 103
Figure 4.20 Continuos time signals using C_{mn}-Algorithm. 107
Figure 4.21 Comparisons between FFT and DFS performance. 108

Figure 5.1 Sampling Methods in SPWM. 113
Figure 5.2 Comparisons between C_{mn}-Algorithm and C_n-Algorithm. 117
Figure 5.3 Comparisons of Pseudo-Natural, Symmmetrical Regular and Asymmetrical Regular sampling. 118
Figure 5.4 Five, four and three levels modulation by C_n-Algorithm. 119

Figure 6.1.a Block Diagrams of the Open Loop System Prototype. 123
Figure 6.1.b Photo of the Open Loop System Prototype. 123
Figure 6.2 Asymmetric Full Bridge Inverter. 124
Figure 6.3 L-C Filter. 124
Figure 6.4 Load Connection by a two-position switch. 125
Figure 6.5 Current Amplifier Section of one Gate Driver. 125
Figure 6.6 Voltage Buffering Section and Optical Isolation. 126
Figure 6.7 Pseudo-Natural Sampling Method for SPWM. 126
Figure 6.8 Generation of switching edges X_d and X_u. 128
Figure 6.9 Timer1 Compare Units: PWM generation. 128
Figure 6.10 Ripple voltage at the input converter plug. 130
Figure 6.11 V_{pwm} voltage at the output plug converter. 130
Figure 6.12 Spectrum patterns for Ma=0.9 132
Figure 6.13 Case 1:{r1=0.5, r2=0.5, r3=0.5, r4=0.5}. 133
Figure 6.14 Case 2 :{r1=1.0, r2=1.0, r3=1.0, r4=1.0}. 133
Figure 6.15 Case 4:{ r1=1.0, r2=1.0, r3=0.0, r4=0.0}. 133
Figure 6.16 Wrong switching instants calculation, case4. 134
Figure 6.17 Oscilloscope-FFT, Case 4. 135

ISBN:978-84-693-7665-2/DL:T.1747-2010

Figure 6.18 Spectrum by C_n-Algorithm , Case 4. 135
Figure 6.19 Spectrum by Cmn-Algorithm, Case 4. 135
Figure 6.20 Pspice-FFT, Case 4. 135
Figure 6.21 Error Magnitude and Pearson-Correlation. 137
Figure 6.22 Spectra of theoretical and real case1. 140
Figure 6.23 Spectra of theoretical and real case12. 140
Figure 6.24 Spectra of theoretical and real case13. 140
Figure 6.25 Global $THD_{h=400}$, K=0.5. 141
Figure 6.26 Global $WTHDo_{h=400}$, K=0.5. 141
Figure 6.27 Best cases for $THD_{h=100}$, K=0.5. 142
Figure 6.28 Best cases for $WTHD_{oh=100}$, K=0.5. 142
Figure 6.29 Best cases for $THD_{h=10}$, K=0.5. 142
Figure 6.30 Evolving of THD to h=30. 142
Figure 6.31 Best cases for $WTHDo_{h=10}$, K=0.5. 142
Figure 6.32 PD, POD, APOD and Symmetrical and Asymmetrical Regular Sampling, Ma=0.9, K=0.5. 144
Figure 6.33 PD, POD, APOD and Symmetrical and Asymmetrical Regular Sampling, Ma=0.8, K=0.5. 144
Figure 6.34 PD, POD, APOD and Symmetrical and Asymmetrical Regular Sampling, Ma=0.7, K=0.5. 144
Figure 6.35 PD, POD, APOD and Symmetrical and Asymmetrical Regular Sampling, Ma=0.6, K=0.5. 144
Figure 7.1 Target Point $V_{target}(M_a,K)$ sorrounded by 4 pre-calculated points. 146
Figure 7.2 Distortion for 31 cases of carrier programming. 146
Figure 7.3 Basic Configuration of a Genetic (Evolutive) Algorithm. 149
Figure 7.4 Crossover simplified scheme. 149
Figure 7.5 Mutation simplified scheme. 149
Figure 7.6 Convergence Characteristics for different criteria of mutation. 153
Figure 7.7 Spectrum Optimization (Ma=0.9, K=0.3). 154
Figure 7.8 Optimized cases compared to typical carriers sets. 156
Figure 8.1 AFBMI circuit showing the two input voltage sources. 161
Figure 8.2 Tibuck Modeling applied to an AFBMI converter. 162
Figure 8.3.a Blocks Diagram of the Closed Loop System Prototype. 167
Figure 8.3.b Photo of the Closed Loop System Prototype. 167
Figure 8.4 Implemented SPWM scheme. 169
Figure 8.6 Drivers Circuitry (PCB N° 4). 170

ISBN:978-84-693-7665-2/DL:T.1747-2010

Figure 8.7 Power Stage of the AFBMI (PCB N° 5). 171
Figure 8.8 V_{PWM} and filtered output V_O signals. 172
Figure 8.9 Harmonic profiles with different local minimum THD. 173
Figure 8.10 Local minimization obtained by different objective functions. 173
Figure 8.13 Measured M_a peak (Channel3). 177
Figure 8.14 Adapted framework matrix. 177
Figure 8.15 Experimental Set-Up of the Prototype. 179
Figure 8.16 Optimized and Standard Carriers, $V_{target}(M_a=0.764,K=0.4)$. 181
Figure 8.17 Optimized and Standard Carriers, $V_{target}(M_a=0.764,K=0.5)$ 182
Figure 8.18 Optimized and Standard Carriers, $V_{target}(M_a=0.764,K=0.6)$. 183
Figure 8.19 Optimized and Standard Carriers, $V_{target}(M_a=0.84,K=0.4)$ 184
Figure 8.20 Optimized and Standard Carriers, $V_{target}(M_a=0.84,K=0.5)$. 185
Figure 8.21 Optimized and Standard Carriers, $V_{target}(M_a=0.84,K=0.6)$. 186
Figure 8.22 Optimized and Standard Carriers, $V_{target}(M_a=0.88,K=0.4)$. 187
Figure 8.23 Optimized and Standard Carriers, $V_{target}(M_a=0.88,K=0.5)$. 188
Figure 8.24 Optimized and Standard Carriers, $V_{target}(M_a=0.88,K=0.6)$ 189
Figure 8.25 Optimized Carriers Vs. Standard Carriers, ($M_a=0.764$). 190
Figure 8.26 Optimized Carriers Vs. Standard Carriers, ($M_a=0.84$). 191
Figure 8.27 Optimized Carriers Vs. Standard Carriers, ($M_a=0.88$). 192

Figure B.1 Comparison of Experimental and Modeled Spectra. 221
Figure B.2 Error Magnitude and Pearson-Correlation. 223
Figure B.3 Distortion Criterions for the cases of Table B.1. 224

Figure C.1 Schematic of AFBMI Power Stage. 227
Figure C.2 Schematic of switching pulses drivers. 228
Figure C.3 Schematic of Analogic 5-level PD-PWM modulator 229
and State Variables control loop. 229
Figure C.4 Schematic of demodulation and filtering of carriers and modulator signal 230
and Feedforward control loop. 230
Figure C.5 PCB-Layout at 10:8 scale of AFBMI Power Stage, top face. 231
Figure C.7 PCB-Layout at 10:8 scale of Drivers Circuits, top face. 233
Figure C.8 PCB-Layout at 10:8 scale of Drivers Circuits, bottom face. 234
Figure C.9 PCB-Layout at 10:8 scale of Analogic 5-level PD-PWM modulator 235
and State Variables control loop , top face. 235
Figure C.10 PCB-Layout at 10:8 scale of of Analogic 5-level PD-PWM modulator 236
and State Variables control loop , bottom face. 236

UNIVERSITAT ROVIRA I VIRGILI
CONTRIBUTIONS ON SPECTRAL CONTROL FOR THE ASYMMETRICAL FULL BRIDGE MULTILEVEL INVERTER
Oscar Mauricio Muñoz Ramírez
ISBN:978-84-693-7665-2/DL:T.1747-2010

Figure C.11 PCB-Layout at 10:8 scale of demodulation and filtering of carriers and modulator signal and Feedforward control loop, top face. 237

Figure C.12 PCB-Layout at 10:8 scale of demodulation and filtering of carriers and modulator signal and Feedforward control loop, bottom face. 238

UNIVERSITAT ROVIRA I VIRGILI
CONTRIBUTIONS ON SPECTRAL CONTROL FOR THE ASYMMETRICAL FULL BRIDGE MULTILEVEL INVERTER
Oscar Mauricio Muñoz Ramírez
ISBN:978-84-693-7665-2/DL:T.1747-2010

ISBN:978-84-693-7665-2/DL:T.1747-2010

List of Tables

Table 2.1 features of different five-level converters. 51

Table 3.1 Harmonics Limits of Standard EN 50160/1995. 61
Table 3.2 Harmonics Limits of Standard IEC 61000-3-2. 62
Table 3.3 Harmonics Limits of ANSI/IEEE 519-1992. 62

Table 4.1 Sideband Coefficients for Composing h_3. M_f=11, M_a=0.9. 82
Table 4.2 Overlap for Composing h_3 and h_{13}. M_f=11, M_a=0.9. 83
Table 4.3 Overlap for Composing h_3 and h_{13}. M_f=49, M_a=0.9. 84
Table 4.4 Distortion Indices Referred to the h^{th} Harmonic. 84
Table 4.5 Carriers of 5-level SPWM. 87
Table 4.6 Levels Collapsing. 87
Table 4.7 Comparisons Groups of Some Cases. 87
Table 4.8 Simulated Cases. M_a=0.9, M_f=50[Muñ05]. 88
Table 4.9 Best and Worst Results of Harmonic Distortion 89
Evaluation for 10 Harmonics. Ma=0.9, Mf=50[Muñ05]. 89
Table 4.10 Best and Worst Results in Harmonic Distortion 89
Evaluation for 100 Harmonics. Ma=0.9, Mf=50[Muñ05]. 89
Table 4.11 PD-SPWM Rules and Switching Angles Characteristics. 93
Table 4.13 Null integrals for C_{mn} when M_a > max(K,1-K). 96
Table 4.14 Limits of integration for the differential dx. 96
Table 4.15 Solution for C_{mn} when (1-K)< M_a <K. 100
Table 4.16 Null integrals for C_{mn} when (1-K)< M_a <K. 100
Table 4.17 Solution for C_{mn} when K < M_a < (1-K). 102
Table 4.18 Null integrals for C_{mn} when K < M_a < (1-K). 102
Table 4.19 Solution for C_{mn} when M_a <min(K,1-K). 104
Table 4.20 Null integrals for C_{mn} when M_a <min(K,1-K). 104
Table 4.21 Reorganization of limits of integration, dx. 105
Table 4.22 Examples of C_{mn} coefficients for composing one harmonic *h*. 106

Table 5.1 Comparison of Sampling Methods. 114

Table 6.1 Switching States and Voltage Levels. 127
Table 6.2 Compare Units of Timer T1 to generate the Driving Signals. 129
Table 6.3 Classification of working conditions to study spectral modeling. 129

ISBN:978-84-693-7665-2/DL:T.1747-2010

Table 6.4 Pearson-Correlation for h={2…100} M_a=0.9, K0.5. 138

Table 6.5 Pearson-Correlation h={2…100} M_a=0.9, K0.3. 138

Table 6.6 Pearson-Correlation h={2…20} M_a=0.9, K0.5. 138

Table 6.7 Pearson-Correlation h={2…20} M_a=0.9, K0.3. 138

Table 7.1 Evolution of the Carriers Set with fixed Mutation (0.05), Variance (0.1), P_{max}=5000, and forced initial population. 152

Table 7.2 Softly increased Mutation and Variance after the 300th generation. P_{max}=1500. No forced initial population. 152

Table 7.3 Optimized Carriers Set compared to Typical Sets. 155

Table 8.1 Tibuck Voltages. 163

Table 8.2 Switching States and Voltage Levels. 163

Table 8.3 Framework Matrix To Program The Carriers Set. 176

Table 8.4 Distortion results evaluated on ten harmonics. 179

Table 8.5 Qualification Results for closed-loop system. 193

Table B.1 Evaluated Carriers Sets for Pseudo-Natural PD-SPWM. 220

UNIVERSITAT ROVIRA I VIRGILI
CONTRIBUTIONS ON SPECTRAL CONTROL FOR THE ASYMMETRICAL FULL BRIDGE MULTILEVEL INVERTER
Oscar Mauricio Muñoz Ramírez
ISBN:978-84-693-7665-2/DL:T.1747-2010

Table of Contents

1. Introduction and Objectives **31**
1.1 Work Objectives 32
1.2 Document Contents and Organization 33
1.3 Derived Publications 43

2. Multilevel Inverter Survey **45**
2.1 Introduction to Multilevel Conversion 46
2.2 Half-Bridge Derived Structures 47
2.3 Clamping Voltage Techniques 48
2.4 Tibuck Modeling of the AFBMI 52
2.5 Concluding Remarks 53

3. Review of Modulation Techniques **57**
3.1 Spectral Performance Parameters and Standards 59
3.1.1 Distortion parameters 59
3.1.2 Spectral Performance and Power Quality 60
3.2 Programmed Modulations and Selective Harmonic Elimination 62
3.3 SPWM Carrier-based Modulation Types 66
3.5 Advantages of Spectrum Control 77

4. Spectral Modeling of Natural PD-PWM in Multilevel Inverters **79**
4.1 DFS Model for five-level standard PD-SPWM (K=0.5, $\forall r_i$'s=0.5) 80
4.2 Extension to Asymmetrical Carrier PD-SPWM cases 85
4.3 Extension of DFS Model to Asymmetrical Carriers 91
4.4 Contour Plots for the Five-Level Asymmetrical carrier PD-SPWM 94
4.4.1 Case M_a >max(K,1−K) 95
4.4.2 Case (1−K)< M_a <K 98
4.4.3 Case K< M_a <1−K 100
4.4.4 Case M_a <min(K,1−K) 102
4.4.5 DFS calculation example, case M_a>max(K,1−K) 104

5. Pseudo-Natural Modulation **111**
5.1 Natural and Regular Sampling Methods for SPWM 111
5.2 Definition of Pseudo-Natural Sampling SPWM 113
5.3 SFS Spectrum from Pseudo-Natural SPWM 115

6. Pseudo-Natural Modulation Performance **121**
6.1 Experimental Prototype Description 123
6.1.1 Power Stage Circuit 124
6.1.2 Driver Board Circuit 125
6.1.3 Pseudo-Natural PWM Realized with a TMS320F2812 (DSP) 126

UNIVERSITAT ROVIRA I VIRGILI
CONTRIBUTIONS ON SPECTRAL CONTROL FOR THE ASYMMETRICAL FULL BRIDGE MULTILEVEL INVERTER
Oscar Mauricio Muñoz Ramírez
ISBN:978-84-693-7665-2/DL:T.1747-2010

6.2 Natural Sampling and Pseudo-Natural Comparison 129
6.2.1 Checking the Carrier-Shape Modifications 131
6.2.2 Reliability of Pseudo-Natural Five-Level Modulation 132
6.2.3 Qualifying Pseudo-Natural Spectra using Pearson-Correlation 136
6.2.4 Checking the Switching Edges (X_d, X_u) 139
6.3 Evaluating the Pseudo-Natural Spectra with THD and $WTHD_0$ 140
6.4 Performance of PD, POD, APOD with Diverse Sampling Methods 143

7. Carriers Optimization with Genetic Algorithms 145
7.1 Carrier Set Optimization at a given working point (Ma, K) 145
7.2 Brief Description and Definition for GA's 148
7.3 Tunning GA's Parameters to Optimize the Carriers Sets 151
7.4 Experimental Results of a GA Optimized Spectra 155

8. Closed-Loop Harmonic Performance 159
8.1 Closed-Loop Prototype Introduction 159
8.2 Inverter Modeling and Closed-Loop Design 161
8.3 Closed-Loop Prototype Description 166
8.4 GA Optimization in a Matrix of Working Points (M_a,K) 172
8.5 Prototype Experimental Results 178

9. Conclusions 195

10. Perspectives and Future Works 201

Bibliography 203

APPENDIX A. Equations to Calculate C_{mn} 209

APPENDIX C. Schematics and PCB Layouts 227

APPENDIX D. MATLAB Source Code 239
D.1 C_{mn}-Algorithm 239
D.2 C_n-Algorithm 254
D.3 Genetic Algorithm For Matrix (M_a,K) 257

APPENDIX E. TMS32F2812 Source Code (DSP) 267

APPENDIX F. dsPIC30F6010A Source Code 273

UNIVERSITAT ROVIRA I VIRGILI
CONTRIBUTIONS ON SPECTRAL CONTROL FOR THE ASYMMETRICAL FULL BRIDGE MULTILEVEL INVERTER
Oscar Mauricio Muñoz Ramírez
ISBN:978-84-693-7665-2/DL:T.1747-2010

1. Introduction and Objectives

Although some issues like the environment are usually not considered when the cost of clean energies is compared to fossil, nuclear, and other conventional sources, the social acceptance of sustainable development policies have been driving and promoting the renewable energies expansion abroad.

As the electrical energy of renewable origin is still expensive, the improvement of the global conversion chain efficiency, going from the diverse transducers (PV panels, wind turbines, fuel cell stacks) to the diverse payloads, stockage forms, and distribution networks have become a key question.

Thus, most European governments have installation subsidies and granted research programs. In this frame, the current work, partially sponsored by the Spanish ministry of research under the grants DPI2006-15627 and DPI2009-14713, explores new modulation methods to minimize switching losses in multilevel inverters, especially for the asymmetrical full bridge multilevel inverter.

A multilevel inverter (MI) is a switching converter where the appropriate control of an arrangement of switching devices allows combining diverse input voltages to synthesize a sinusoidal output voltage waveform.

Multilevel systems were introduced to make high voltage and high-power converters feasible because it was difficult to realize them with two-level structures and conventional switching devices. As additional benefits, multilevel conversion reduces the output variables harmonic distortion and, sometimes, in spite of the devices-count increment, the conversion losses can also decrease [Val08].

Precisely, the relationship between losses and harmonic content is a key question in this research work. The voltages blocked by the devices during the OFF-state in a multilevel converter are quite lower that the respective OFF-voltages in a two-level case. Therefore, all performance figures depending on those voltages can be improved substantially at equal switching frequency, load, and input-output voltage conditions. This is the case of the output voltage distortion and converter switching losses.

UNIVERSITAT ROVIRA I VIRGILI
CONTRIBUTIONS ON SPECTRAL CONTROL FOR THE ASYMMETRICAL FULL BRIDGE MULTILEVEL INVERTER
Oscar Mauricio Muñoz Ramírez
ISBN:978-84-693-7665-2/DL:T.1747-2010

The distortion reduction achieved increasing the number of levels, can be used to reduce further the switching losses decreasing slightly the inverter carrier frequencies without degrading excessively the output distortion. Besides, to reduce even more those switching losses, we have studied the possibility of modulating the slopes of the triangular carrier waveforms in order to achieve a set of optimum carrier signals.

Output voltage harmonic distortion can have different causes: a) nonlinear or switching loads, b) harmonics generated by the PWM modulation itself, c) harmonics introduced by the inverter DC-voltage supplies, d) intermodulation products, and so on.

Feedback and Feedforward loops will reduce distortion, but as cleaner be the open-loop output voltage spectrum, the better will be the final result, once the control-loop is applied. A clean open-loop voltage spectrum is especially important, when modulating at low switching frequency (F_C=2.5 kHz), the tail of left-side part of the first alias, centered at the switching frequency, can contaminate the base-band, where the fundamental frequency F_O is placed.

1.1 Work Objectives

The research work realized in this PhD thesis, and explained in this document follows some key objectives:

First Objective.- To investigate if by means of adjusting the slope or shape factor of each carrier signal $\{r_1, r_2, r_3, r_4\}$, the spectrum of a natural SPWM can be modified, and eventually optimized.

Second Objective.- To develop mathematic models of the natural PD SPWM modulation to predict the spectrum content of any natural PD SPWM modulation whatever be its **parameters**: *levels number* 2, 3, 4 and 5, *level distribution* K, *amplitude modulation index* Ma, and the *set of carrier slope factors* $\{ r_1, r_2, r_3, r_4\}$.

Third Objective.- To implement a natural PD SPWM where all the previous modulation parameters be on-line or even off-line customizable by means of a pure analog circuit is unrealistic, as a result we want to create a digital modulation based on DSP, with the same spectral features as the natural modulation. Consequently, this modulation is named Pseudo-Natural Modulation. The system developed to modulate digitally can perform easily other types of SPWM such as POD and APOD, by changing a few parameters.

UNIVERSITAT ROVIRA I VIRGILI
CONTRIBUTIONS ON SPECTRAL CONTROL FOR THE ASYMMETRICAL FULL BRIDGE MULTILEVEL INVERTER
Oscar Mauricio Muñoz Ramírez
ISBN:978-84-693-7665-2/DL:T.1747-2010

Fourth Objective.- Assuming a 5-level distribution, to find a tool that calculates at least one optimum set of carrier shapes $\{r_1, r_2, r_3, r_4\}$ for any operating point allocated within a defined range in the plane (M_a, K) according to a certain optimizing criterion based for instance in an open-loop distortion level, spectral pattern or profile.

Fifth Objective.- To develop two experimental prototypes. The first one, in open-loop, will validate the results on spectral modeling and to verify the performance and accuracy of the Pseudo-Natural modulation. The second prototype will test the inverter performance in a system with two closed loops, the slow-one is a digital loop that optimizes the spectrum modifying periodically the carrier slopes. The faster loop is an analog circuit, and includes power supply feedforward and linear state-feedback.

Sixth Objective.- To measure the contribution of the inverter switching frequency in the converter losses, as well as to evaluate experimentally the influence of the set of slopes, in the inverter efficiency caused by output distortion changes.

1.2 Document Contents and Organization

The objectives above exposed will be discussed in this monograph prepared to fulfill the requirements of the Degree of Doctor of Philosophy by the Rovira i Virgili University. This document is organized as follows:

First Section: This chapter exposes the thesis objectives, describes the document contents and its organization, and introduces the motivation of this thesis: “Assuming that losses are reduced by switching at low frequency, let’s optimize the output voltage spectrum.”

Second Section: In this section, we review the different multilevel topologies (diode-clamped, flying-capacitor, and cascaded full-bridge) emphasizing that the asymmetrical full bridge multilevel converter (AFBMI) is the five-level converter that uses less controllable switches, and therefore is the most suitable to reduce conduction and switching losses. The results were presented at two conferences, and there is a journal paper at IET Power Electronics [Val08].

Third Section: This chapter reviews the state-of-the-art of the different modulation and spectral analysis techniques. By one side, this chapter deals with the different harmonic performance parameters (WTHD, THD), as well as the concerns about the number of harmonics to be considered when applying such performance parameters.

UNIVERSITAT ROVIRA I VIRGILI
CONTRIBUTIONS ON SPECTRAL CONTROL FOR THE ASYMMETRICAL FULL BRIDGE MULTILEVEL INVERTER
Oscar Mauricio Muñoz Ramírez
ISBN:978-84-693-7665-2/DL:T.1747-2010

In this chapter, we classify the different modulations techniques according its spectral performance and operating mode. Concerning the spectral performance the main differences come from the fact of using a fixed (PWM) and discrete spectrum, or variable, and even random switching frequency, where the output spectrum is smoothed.

Concerning the modulation operating mode, we distinguish among on-line and off-line modulations. Off-line modulations are those where the switching instants or angles are pre-calculated, and placed in a memory. An example of this situation is the well-known, selective harmonic elimination, Walsh modulations, etc. The on-line techniques are those where the switching instants come from comparing a modulating signal with a set of carriers, carriers that can be off-line optimized and programmed, as in our case.

Finally, this chapter reviews the different ways to organize the carriers of a multilevel modulation, and also, the different sampling techniques to decide the switching instants. Thus, the carriers can be horizontally shifted or vertically shifted, and among this last group, we can distinguish: phase-disposition (PD), alternative phase-disposition (APOD), phase opposition disposition (POD), and phase shift (PS) or hybrid modulation. Finally, concerning the sample techniques, we review the natural and the regular sampling. The first one is the most typical technique, and is implemented analogically; the second technique is specially adapted for digital inverters, and has two versions: the asymmetric and symmetric regular sampling.

According to diverse literature works, the natural PD-PWM modulation has better spectrum performance and is easier to implement [Cal98]. Consequently, we decided to restrict our study only to that modulation, constraining the thesis scope, to be more feasible work in a reasonable time.

Finally, in section III, we profit two concepts found in the literature[Hol03]. By one side, we take the concept of contour plot to depict graphically the features of a sinusoidal modulation. Then, any contour plot identifies uniquely a certain modulation and its parameters.

That graphical representation can be adapted mathematically by means of a double fourier series (DFS) because the integrals involved to calculate the DFS coefficients C_{mn} could be easily deduced from the countour plots. Nevertheless, the main drawback of modeling spectrally a modulation by means of a DFS, comes from the fact that the coefficients C_{mn} are not directly linked to the spectrum, because any spectral component is in fact, the sum of different infinite C_{mn} values.

UNIVERSITAT ROVIRA I VIRGILI
CONTRIBUTIONS ON SPECTRAL CONTROL FOR THE ASYMMETRICAL FULL BRIDGE MULTILEVEL INVERTER
Oscar Mauricio Muñoz Ramírez
ISBN:978-84-693-7665-2/DL:T.1747-2010

DFS (Double Fourier Series)	SFS (Single fourier Series)
$f(t)=\sum_{-\infty}^{\infty}\sum_{-\infty}^{\infty}C_{mn}e^{j(m\omega_c+n\omega_o)t}$	$f(t)=\sum_{-\infty}^{\infty}C_h e^{jh\omega_o t}$
$C_{mn}=\frac{1}{T_c T_o}\int_{-T_c/2}^{T_c/2}\int_{-T_o/2}^{T_o/2}f(t)\cdot e^{-j(m\omega_c+n\omega_o)t}dt^2$	$C_h=\frac{1}{T_o}\int_{-T_o/2}^{T_o/2}f(t)\,e^{-jh\omega_o t}dt$

$$C_h=\sum_{m=0}^{\infty}C_{m,h-mM_f}\approx\sum_{m=0}^{2}C_{m,h-mM_f}\ \text{where}\ \omega_c=M_F\cdot\omega_o$$

Nevertheless, if the frequency modulation index M_F is high, as in our case where M_F=50, the quickly decaying Bessel functions allows to calculate approximately any spectral component using only the two closer aliases, both, at the right and left side.

Fourth Section: In this chapter, we make several simulations to prove that the spectrum of a PD modulation can be modified by means of selecting the slope of the vertically shifted carriers. These results have been presented, also at two conferences, among them ISIE'05. The spectral results were analyzed using the FFT function of the PSPICE simulator. In particular, we corroborated that the contour plots were a good tool to distinguish different modulations, as explained previously.

Holmes, in his book "Pulse Width Modulation for Power Converters" (2003) had modeled the natural-sampled five-level PD-PWM modulation (3.20) considering that all voltage levels were equal, that is considering an inverter with balanced power supplies.

In this chapter, we extend the model proposed by him, to a situation were the voltage levels could be different, {–E, (K–1)·E, 0, KE, E} where 0<K<1, creating also the corresponding contour plots. Notice that, the Holmes model was addressed to an ideal situation, with five equal levels (K=0.5) and the modulation index M_a sufficiently high to avoid level collapsing.

In fact, although the system have five levels available, the output voltage, can be synthesized using only 2, 3, or 4 of those levels. Realize that, the number of levels used, depend only on the amplitude modulation index M_a, and the level distribution parameter K. Consequently, we generalize the Holmes model to all these situations were the output voltage is modulated with less than 5 levels, introducing the concept of "level collapsing" to describe those situations were less than 5 levels were required to modulate the output voltage waveform.

UNIVERSITAT ROVIRA I VIRGILI
CONTRIBUTIONS ON SPECTRAL CONTROL FOR THE ASYMMETRICAL FULL BRIDGE MULTILEVEL INVERTER
Oscar Mauricio Muñoz Ramírez
ISBN:978-84-693-7665-2/DL:T.1747-2010

Fifth Section: In past sections, we have seen that the output voltage spectrum can be improved by means of controlling the slopes of the carriers in a natural sampling PWM scheme. Realize that this modulation is analogical, and should be implemented analogically.

Realizing a natural sampling modulation requires a set of analog comparators working with their corresponding analog synchronized carriers and modulator signals. In addition, the slope and the amplitude of the carriers might be fully controllable. Amplitude control is required by the feed-forward loop, where the carriers should be proportional to the inverter power supplies. The feed-forward loop assures a good line regulation and linearizes the converter dynamics. The carriers slope control was required for spectrum optimization. Both, amplitude and slope controllability imply a serious implementation problem derived from the complexity of such system.

Analog carrier implementation, could be attempted combining several function generator integrated circuits, such as ICL8038 or XR2206 parts, but although those parts were very common some years ago, currently are fully unavailable.

To overcome the implementation problem, we have explored two alternatives. In this section, we introduce the pseudo-natural modulation, a digital-made modulation, emulating reasonably well, the natural sampling modulation.

In section 8, when the closed-loop inverter prototype is presented, we develop a mixed digital-analog modulator. A dsPIC microcontroller creates a set of carriers with a fully controllable slope. Those carriers are generated as PWM waveforms. Then, a series of low-pass filters and complementary circuits demodulate those signals to get the set of analog carriers vertically-shifted and with their amplitude proportional to the inverter supply. Once these “analog” carriers have been created, they are compared analogically with a sinusoidal modulator created with the same method as the carriers. Thus, we have done a second approach to the natural modulation, created partially by digital means.

Coming back to section V, a fully-digital implemented natural modulation is intended. To do that, we begin comparing the performances of the state-of-the-art digital modulations with the desired natural modulation. Besides, this will also help to evaluate and contextualize our implementation. Thus, we have compared, at various points, the duty ratios and the switching instants produced by the natural sampling modulation, with the angles and switching instants produced by the symmetrical and the asymmetrical regular samplings (digital modulations).

UNIVERSITAT ROVIRA I VIRGILI
CONTRIBUTIONS ON SPECTRAL CONTROL FOR THE ASYMMETRICAL FULL BRIDGE MULTILEVEL INVERTER
Oscar Mauricio Muñoz Ramírez
ISBN:978-84-693-7665-2/DL:T.1747-2010

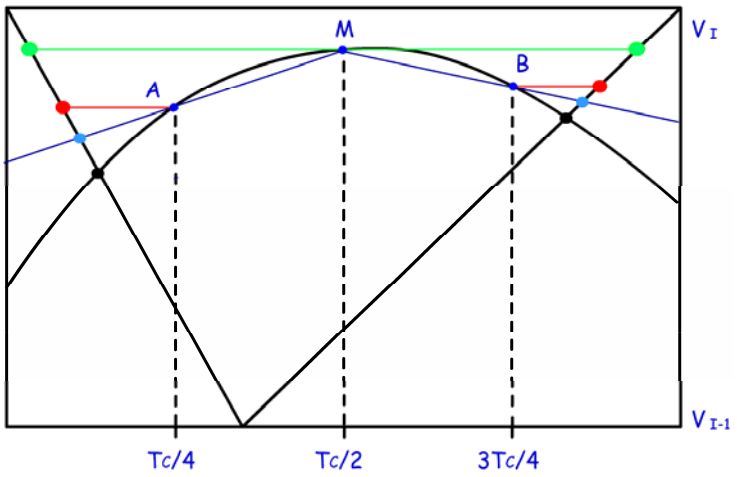

Figure 1.1 Comparison of Digital and Natural Modulations.

From that study, we observed that the symmetrical regular sampling used only one sample (Tc/2) per cycle to compute the switching instants and pulse width, whereas the asymmetrical regular sampling considers two samples per switching cycle ($T_C/4$, $3T_C/4$). Consequently, the spectrum and switching instants of the asymmetrical regular sampling were more similar to those from the natural sampling modulation.

Nevertheless, as the similitude degree between the natural and the asymmetrical regular sampling, was not sufficient, and we developed a new digital modulation called "Pseudo-Natural Modulation". This digital modulation is a better approximation to the natural sampling because interpolates the sinusoidal waveform with two segments determined with the sampling points used by the preceding digital modulations ($T_C/4$, $T_C/2$, $3T_C/4$).

In figure 1.1, we have exaggerated the sinusoidal modulator curvature to show the differences between the natural and the diverse digital modulations. The switching instants are given by the carriers intersection points. Black points belong to the natural sampling, green and red ones correspond to the symmetrical and asymmetrical regular samplings respectively, and finally, the blue points belong to the pseudo-natural modulation.

Chapter fifth concludes with a visual comparison between the spectrums of the natural sampling modulation and the pseudo-natural modulation to investigate if both spectra are sufficiently similar to consider the pseudo-natural modulation a promising candidate for a digital implementation of the natural modulation.

UNIVERSITAT ROVIRA I VIRGILI
CONTRIBUTIONS ON SPECTRAL CONTROL FOR THE ASYMMETRICAL FULL BRIDGE MULTILEVEL INVERTER
Oscar Mauricio Muñoz Ramírez
ISBN:978-84-693-7665-2/DL:T.1747-2010

Finally, thinking about future spectral comparisons and experimental validations, we begin to investigate the advantages and drawbacks of using the DFS coefficients C_{mn} or the SFS coefficients C_h, where SFS appears as a faster and more precise option.

Sixth Section: In this chapter, we develop an open-loop prototype. This prototype consists of three main systems. The AFBMI converter board, the mosfet drivers, and the remaining system is a TMS320F2812 development kit where the pseudo-natural modulation is programmed. The amplitude modulation index and the level distribution K are written in the program code as set points. This means that when the modulation parameters must be changed the program execution must be stopped, modified and compiled again. When the program is executed, it calculates the switching instants and stores them in the DSP memory. Once the memory table is completed, the DSP board generates directly the AFBMI mosfet switching pulses from the data stored using two different internal counters.

Different test have been made to explore if the Pseudo-Natural PWM can be a good digital approximation of the analog natural sampling PWM.

The first experiments pretended to verify if the DSP was implementing correctly the algorithms to calculate the switching instants for the Pseudo-Natural PWM. To do that we reduced initially the 5-level modulation to a conventional 2-level modulation, and different tests changing the carrier slope were made to verify the different spectra obtained. Once verified the system, we repeated the same experiments for a five-level modulation.

To compare both modulations, the natural and the pseudo-natural we have tested many different operating points or modulation cases. Each case is given by a certain amplitude modulation index M_A, level distribution K, and r_1, r_2, r_3, r_4 carrier slopes, and each case has its own different spectrum, is like finger print.

Those spectrums have been compared in several ways. First, we have compared the theoretical natural modulation spectrum coming form the DFS obtained form the contour plots, secondly, the simulated natural modulation spectrum from the PSPICE FFT, third, the pseudo-natural spectrum deduced from the SFS applied to the switching instants calculated by the DSP, and finally the real experimental pseudo-natural spectrum obtained from the oscilloscope FFT measuring the inverter output voltage at open loop, and before the output filter, that is in the output of the AFBMI bridge.

UNIVERSITAT ROVIRA I VIRGILI
CONTRIBUTIONS ON SPECTRAL CONTROL FOR THE ASYMMETRICAL FULL BRIDGE MULTILEVEL INVERTER
Oscar Mauricio Muñoz Ramírez
ISBN:978-84-693-7665-2/DL:T.1747-2010

Besides the PD pseudo-natural modulation, to show the versatility of the developed system, by means of few changes in the DSP program parameters, our system is able to implement practically any kind of multilevel modulations and sampling methods, for example: Pseudo-natural POD and APOD, and the asymmetrical and symmetrical regular sampling PD.

Seventh Section: In the preceding sections of this document we have demonstrated that different values of carrier slopes in a multilevel modulation lead to a different output voltage spectra. By other side, we have developed tools to predict the spectrum or finger print associated to a certain group of modulation parameters: the amplitude modulation index M_a, the level distribution K, and the carrier slopes $\{r_1, r_2, r_3, r_4\}$.

We have seen also, that although the DFS and SFS can be used to predict analytically the value of each harmonic or spectral component in a multilevel modulation characterized by the preceding parameters, the mathematical operations are extremely complex. In fact, it is impossible to make the opposite calculation. That is, given a certain output spectrum specification, that can be the amplitudes of certain number of harmonics, or a more relaxed specification like a certain THD or WTHD, value is impossible, to solve the system of equations to know the appropriate values of the carrier set $\{r_1, r_2, r_3, r_4\}$ that assure the fulfillment of the desired specifications.

Therefore, the only realistic goal is to reduce the output voltage distortion, by means of cleaning as much as possible the output voltage base-band spectrum. This noise reduction cannot focus or specify the amplitude of each specific harmonic, it can only focus to a certain distortion figure, appearing in the literature. Among them the WTHD in case of inductive loads, and more generally the THD evaluated up to a certain number of harmonics: 10, 20, and sometimes even 40.

Our final goal is to optimizing the output voltage spectrum, by means of reducing the base-band noise measured according one of the preceding figures. By means of hard simulation work, we have observed that certain set of slopes give a cleaner base-band spectrum, but as explained before, as analytically, becomes impossible to find such slopes, we needed an appropriate tool to help us in the selection the appropriate set of slopes, to that clean base-band spectrum at any modulation condition given by a certain amplitude modulation index M_a, and level distribution K.

UNIVERSITAT ROVIRA I VIRGILI
CONTRIBUTIONS ON SPECTRAL CONTROL FOR THE ASYMMETRICAL FULL BRIDGE MULTILEVEL INVERTER
Oscar Mauricio Muñoz Ramírez
ISBN:978-84-693-7665-2/DL:T.1747-2010

Among the possible selection or classification tools, that can be adapted to our purposes, we could consider the neural networks and the genetic algorithms. A neural network must be trained with an important number of training pairs given the operating points $\{M_a, K\}$ with their respective optimum slopes $\{r_1, r_2, r_3, r_4\}$. When trained, the neural network could help to find the optimum slopes for a new operating point given by $\{M_a, K\}$.

Realize, that the neural network is not solving our problem, because we need an important number of training pairs, and to have this family of training pairs, we need to find previously the optimum set of carriers for the training family members.

In fact, according to the literature, genetic algorithms are used frequently as power tools to generate a family of training pairs for a neural network. Genetic algorithms are useful tools, reliable and accurate to solve search problems, because are based on the evolution concept derived form Darwin's theory, where the best individual survives.

The genetic algorithm iterative process is based on the natural selection, the crossover process, where two parents create two children, and finally the mutation phenomena that randomly affect the genetic representation of some individuals. In our case the genetic code of each individual is the set of carriers $\{r_1, r_2, r_3, r_4\}$. After a certain number of iterations or generations, according to certain natural selection criteria, for instance a THD threshold, the generations evolve, into a convergent solution, where a genetically optimum genetically finally appears. We have tested different parameters to tune the genetic algorithm, under different evolving constraint and initial population.

Optimizing the carrier slopes for any working point $\{M_a, K\}$ implies the execution of infinite genetic algorithms, one per point. Thus, in a practical implementation, the number of optimized working points must be reduced to decrease computing time-consumption.

Figure 1.2 shows an optimization matrix with two different regions: A) The light grey region depicts low probability working points. At these points, the carrier slopes are not optimized and conventional or standard carriers are used. Those carriers have the typical isosceles triangular waveform $\{r_1=r_2=r_3=r_4=0.5\}$. Although in a buck-based inverter, the amplitude modulation index is high to profit the input voltage supply, such index can vary between $0.7<M_a<1$. B) The dark grey region depicts the optimized zone, where the black dots show the 63 operating points where a genetic algorithm has been applied.

UNIVERSITAT ROVIRA I VIRGILI
CONTRIBUTIONS ON SPECTRAL CONTROL FOR THE ASYMMETRICAL FULL BRIDGE MULTILEVEL INVERTER
Oscar Mauricio Muñoz Ramírez
ISBN:978-84-693-7665-2/DL:T.1747-2010

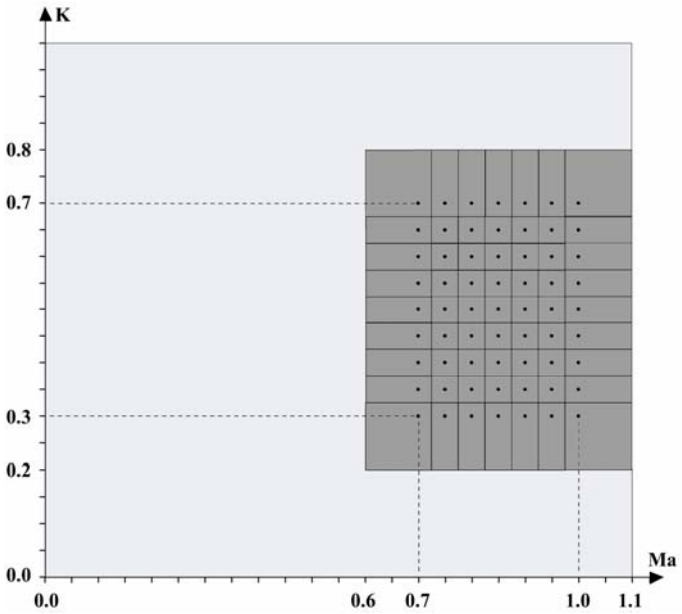

Figure 1.2 Optimization Matrix.

Eighth Section: This chapter begins with the description of the closed-loop prototype, from the most generic concepts to the diverse block diagrams, and precise development details. The development of vertically-shifted carrier modulator, with full carrier amplitude and slope control, is especially important for this prototype.

A dsPIC microcontroller creates a set of carriers with a fully controllable slope. Those carriers are generated as PWM waveforms. Then, a series of fourth-order low-pass filters and complementary circuits demodulate those signals and combine them with some DC offsets, to get the set of analog carriers vertically shifted, with their amplitude proportional to the inverter supply. Once these "analog" carriers have been created, they are compared analogically with a sinusoidal modulator created with the same method as the carriers. Thus, we have created a slope-controllable natural modulation by mixed digital-analog means.

The prototype has three different closed loops. Two of them are analogical and the last one is digital. The digital control-loop actualizes five times per second the carrier slopes to optimize the output spectrum. The two analog loops are a classical feedforward, and state feedback loop. The feedforward loop linearizes the converter dynamics, assures ideal line regulation, and rejects the harmonics coming form the inverter DC power supplies. The state feedback loops improves the load regulation, increases the converter bandwith, stabilizes the converter assuring a minimum damping factor at no-load conditions, and corrects the output voltage harmionic distortion coming from highly non-linear loads by means of reducing the inverter closed-loop output impedance.

UNIVERSITAT ROVIRA I VIRGILI
CONTRIBUTIONS ON SPECTRAL CONTROL FOR THE ASYMMETRICAL FULL BRIDGE MULTILEVEL INVERTER
Oscar Mauricio Muñoz Ramírez
ISBN:978-84-693-7665-2/DL:T.1747-2010

As exposed in the preceding section, in the closed-loop prototype, assigning an optimum carrier set to a certain operating point $\{M_a, K\}$ requires to evaluate which is the operating point, classifying or placing it inside the operation matrix of figure 1.2. As the switching devices generate noise, to reduce its influence in the optimized spectrum, we need to work with a matrix where there is a considerable distance among its points, so in the practice, as depicted in figure 1.2, only 63 different working points $\{M_a, K\}$, depicted in that figure as black dots, have been optimized.

Besides, the uncertainty in the measured value of $\{M_a, K\}$ caused by the switching noise have decided us to avoid any kind of interpolation process, for instance using a neural network, to estimate the optimum slopes for any working point $\{M_a, K\}$, from the four nearest GA optimized points (dark dots). Instead of that, we have assigned to all the operating points inside a dark-grey square contouring a black dot, the same set of slopes $\{r_1, r_2, r_3, r_4\}$ corresponding to that black dot.

Although, this simplification limites theoretically, the spectrum optimization capability of our technique, clear improvements of the output voltage spectrum are achieved, as can be seen in the given experimental results.

Ninth Section: This chapter begins with a quick exposition of the main general conclusion of this research work. Next, further detailed conclusions are given concerning more particular issues, concerning the prototypes or the spectral modeling.

Among them it is important to realize that we have proved that the base-band spectrum of a multilevel inverter output-voltage can be modified and improved by means of an appropriate selection of the carrier slopes, and the two developed prototypes to verify that.

The first prototype, is fully digital, and is able to implement any kind of digital PWM modulation: POD, PD, APOD, and sampling: asymmetrical and symmetrical regular sampling and Pseudo-Natural PD PWM modulation. When the digital protoype performs the Pseudo-Natural PD PWM modulation, the working point $\{M_a, K\}$, and the set of slopes $\{r_1, r_2, r_3, r_4\}$ can be easily changed. With the DPS output signals, the inverter performs an output voltage that can be used to evaluate the spectrum of a certain slope set, among other experiments.

The second prototype, mixed digital-analog, implements a thee-loop prototype, with two analog loops, feed-froward and state feedback, and with a slow digital loop performing the slope carrier actualization to optimize the output spectrum.

Among the modeling conclusions the SFS harmonic coefficients C_h give directly a signal spectrum, whereas the DFS is less precise, because to evaluate numerically a certain harmonic component a certain number of alias must be neglected.

Tenth Section: In this chapter, we explain different ways to continue the research work made in this pHD thesis. Among them, the use of neural networks to interpolate the optimum slopes at any arbitrary working point. Other proposal for instance, would imply to investigate an slope control executing in real-time the genetic algorithms from data obtained directly from the measured output voltage spectrum.

Appendix A: In this chapter, we give the solutions for the DFS integral applied to a natural sampling PD PWM five-level modulation, without considering level collapsing. Thus formulas are given to illustrate the complexity of the mathematics involved.

Appendix B: In this section, we give additional experimental results concerning the Pseudo-Natural Modualtion developed and implemented in section VI. The results are placed here to avoid increasing excessively the size of that section.

Appendix C: Here, we give the schematics and the printed board circuits lay-outs corresponding to both prototypes, the DSP open-loop prototype implementing the Pseudo-Natural Modulation, explained in section VI, and the closed-loop prototype of Section VIII.

Appendix D: This chapter offers the different MATLAB codes corresponding to: SFS and DFS algorithms, as well as the GA algorithms implementation.

Appendix E: This chapter offers the different DSP program codes. Basically, such programs implement the Pseudo-Natrual Modulation.

Appendix F: This chapter offers the different dsPIC program codes, corresponding to the carrier implementation and actualization in the closed-loop prototype.

1.3 Derived Publications

The present research work has motivated the following publications, one Spanish conference, two international conference contributions, and a paper published at the IET Power Electronics. Besides, two additional journal papers more are in course.

[Muñ5] MUÑOZ-RMIREZ, M., VALDERRAMA-BLAVI, H., MAIXE, J, LEYVA R,.VIDAL, E., "Programación Armónica de Portadoras en Inversores Multinivel PWM", http://www.teisa.unican.es/gim/saaei05/en/papers.htm
http://www.teisa.unican.es/gim/res/P14.htm

[Val05] VALDERRAMA-BLAVI, H.; MUNOZ-RAMIREZ, M.; MAIXE, J.; GIRAL, R.; CALVENTE, J.; "Low frequency multilevel inverters for renewable energy systems" Industrial Electronics, 2005. ISIE 2005. Proceedings of the IEEE International Symposium on, vol.3, no., pp. 1019- 1024 vol. 3, 20-23 June 2005, doi: 10.1109/ISIE.2005.1529063. http://ieeexplore.ieee.org/stamp/stamp.jsp?tp=&arnumber=1529063&isnumber=32654

[Val06] VALDERRAMA-BLAVI, H.; MAIXE, J.; BOSQUE-MONCUSI, J. M.; MARTINEZ -SALAMERO, L.; MUNOZ, M.; "Multilevel AC Current Source with Sliding-Mode Control for Renewable Energy Grid Systems", Power Electronics and Motion Control Conference, 2006. EPE-PEMC 2006. 12th International , vol., no., pp.1866-1872, Aug. 30 2006-Sept.1 2006, doi: 10.1109/EPEPEMC.2006.4778677
http://ieeexplore.ieee.org/stamp/stamp.jsp?tp=&arnumber=4778677&isnumber=4778360.

[Val08] VALDERRAMA-BLAVI, H.; BOSQUE, J.M.; BARRADO, J.A.; MUNOZ, M.; CALVENTE, J.; "Design of a sinusoidal current source using a sliding-mode-controlled asymmetrical full-bridge multilevel converter", Power Electronics, IET , vol.1, no.2, pp.203-213, June 2008, doi:10.1049/iet-pel:20070321.
http://ieeexplore.ieee.org/stamp/stamp.jsp?tp=&arnumber=4539507&isnumber=4539504.

UNIVERSITAT ROVIRA I VIRGILI
CONTRIBUTIONS ON SPECTRAL CONTROL FOR THE ASYMMETRICAL FULL BRIDGE MULTILEVEL INVERTER
Oscar Mauricio Muñoz Ramírez
ISBN:978-84-693-7665-2/DL:T.1747-2010

2. Multilevel Inverter Survey

A multilevel inverter (MI) is a switching converter where the appropriate control of an arrangement of switching devices allows combining diverse input voltages to synthesize a sinusoidal output voltage waveform.

The first multilevel inverter circuits appeared in the middle 70's in different application fields, representing a high potential for the realization not only of inverter topologies, but also power converters applications [Bow175]. Among these applications: rectifiers, active filters, power factor correctors, high power amplifiers, inverters can be referenced in the literature. In industrial applications such as electrical drives, furnaces, and locomotive systems [Nik98], the neutral-point-clamped (NPC) branch structure has been frequently used as a building block for three-phase inverters and rectifiers [Nab81].

Multilevel technologies represented a significant advance to overcome the traditional problem of developing high-voltage and high-power applications with off-the-shelf devices. Multilevel converters continue to receive more and more attention because of their increasing voltage and power operation rates, lower losses and better output voltage spectrum.

Multilevel conversion is also suitable for photovoltaic and wind power plants [Cal98]. For instance, photovoltaic power plants placed at big flat fields, with quite uniform photovoltaic (PV) fields, can use a high-power centralized inverter. Nevertheless, multilevel inverters are not only adequate for high power centralized systems. In domestic power plants, often integrated in roofs and façades, where very irregular shadowing can occur, the full-bridge cascade multilevel inverter [Alo03], seems to be a practical solution, because is an easily scalable topology, and each bridge can process the energy coming from a single panel with individualized maximum power point tracking.

With the advances in power mosfet's and igbt's technology during this last decade, the switching transients and the corresponding losses have been reduced. Moreover, multilevel topologies allow using devices with a reduced breakdown voltage, which means a lower conduction resistance if mosfet devices are used. Thus, a higher converter efficiency can be achieved by means of a simple hard-switching technique avoiding typical soft-switching complications, specially concerning modulation issues.

UNIVERSITAT ROVIRA I VIRGILI
CONTRIBUTIONS ON SPECTRAL CONTROL FOR THE ASYMMETRICAL FULL BRIDGE MULTILEVEL INVERTER
Oscar Mauricio Muñoz Ramírez
ISBN:978-84-693-7665-2/DL:T.1747-2010

Because of the simplicity of hard-switching, this technique is commonly used for multilevel conversion, especially for more than three levels applications. Considering this, only inverter topologies with hard-switching techniques will be treated.

2.1 Introduction to Multilevel Conversion

A multilevel inverter (MI) is a DC-AC electronic switching converter which utilizes an arrangement of semiconductor devices in order to generate a sinusoidal waveform from various DC sources. A multilevel inverter, as any switching converter, is an electronic circuit consisting of some energy storage elements and a matrix of switches connecting those storage elements with the converter input and output ports. Therefore, the multilevel inverter must comply with the operating electrical rules of switching converters:

A) An inductor or current source is incompatible with open circuits, and similarly a capacitor or a voltage source can never be short-circuited.
B) Parallel voltage sources and series-connected current sources are not allowed.

Considering now the input port, a multilevel converter can be seen as VSI (voltage source inverter) or as CSI (current source inverter) depending on the capacitive or inductive character of the DC supplies. From the load point of view, the multilevel inverter is considered as VSI if operates as a stand-alone inverter, or must behave like a CSI when is connected to the grid.

For instance, in some PV systems, many times the inverter must be able to operate grid-connected (as a CSI), but when the grid falls, after disconnecting itself from the grid, the inverter must supply the local loads behaving as VSI.

Hereinafter, in order to avoid confusion describing the inverter, we introduce the following nomenclature and classification: voltage-fed VSI, voltage-fed CSI, current-fed VSI, and current-fed CSI. The first three types are the most used and studied cases.

Multilevel Inverters have become an attractive choice as a partial solution to the improvement of the global conversion chain efficiency imposed by the renewable energies systems. In terms of power electronics, there has been a considerable research emphasis to operate MI's at increased voltages and power levels.

When comparing multilevel and two-level converters, some advantages and drawbacks can be observed. Among the multilevel inverters advantages, we find:

UNIVERSITAT ROVIRA I VIRGILI
CONTRIBUTIONS ON SPECTRAL CONTROL FOR THE ASYMMETRICAL FULL BRIDGE MULTILEVEL INVERTER
Oscar Mauricio Muñoz Ramírez
ISBN:978-84-693-7665-2/DL:T.1747-2010

A) Output voltage waveform with lower distortion at equal switching frequency.
B) Lower switching losses at equal output voltage distortion.
C) As the blocking voltage is divided by a greater number of devices, high voltage and high power inverters can be realized with off-the-shelf components.

Some inconvenient features can be derived from the increased number of switching devices and voltage sources which means a more complex control strategy. The continuous price reduction in power electronics components and also in digital signal processors can lead to the extension of multilevel technologies to low power applications. The extra number of devices might not necessarily mean an increment of conduction losses.

Finally, among the wide variety of proposed MI circuits, the following classification is the most broadly accepted: diode-clamped, capacitor-clamped (flying capacitors) and cascaded multiple-cells (with separate DC sources).

2.2 Half-Bridge Derived Structures

In converter topologies, there are two ways to switch the power devices: hard-switching and soft-switching techniques. Literature reports some significant improvement in converter efficiency when soft-switching techniques are used [Jan05]. However, some drawbacks are associated with design and implementation of soft-switching. One of them is the low modulation index range caused by the restrictions to implement the ZVS or ZCS instants. On the other hand, more power devices are required increasing control complexity.

Because of the simplicity of hard-switching, this technique is commonly used for multilevel conversion, especially for more than three levels applications. Considering this, only inverter topologies with hard-switching techniques will be treated.

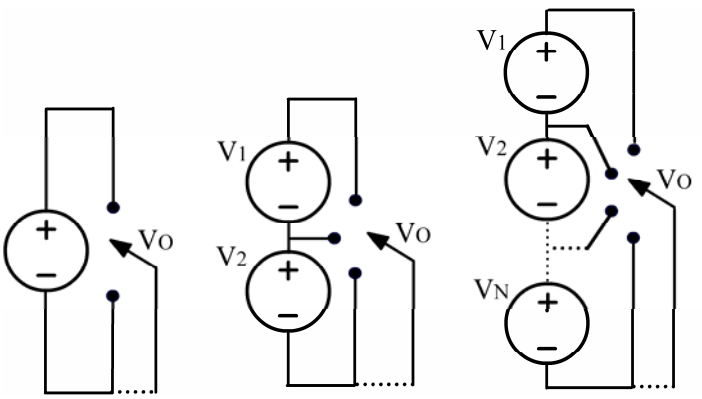

Figure 2.1 Single phase leg inverters.

UNIVERSITAT ROVIRA I VIRGILI
CONTRIBUTIONS ON SPECTRAL CONTROL FOR THE ASYMMETRICAL FULL BRIDGE MULTILEVEL INVERTER
Oscar Mauricio Muñoz Ramírez
ISBN:978-84-693-7665-2/DL:T.1747-2010

Figure 2.1, depicts a N+1 level single-phase leg structure using N voltage supplies. Traditionally, it has been assumed that all the DC sources have the same values. From this basic single-phase inverter leg, different structures can be developed. For example, three-phase structures, or full-bridge single phase topologies can be derived, as illustrated in figure 2.2a and 2.2b

A half-bridge multilevel inverter consists of one phase leg that needs N voltage sources to modulate a N+1 levels output waveform. Using the same number of DC sources, the full-bridge inverter would synthesize a 2N+1 level output waveform, if those sources are balanced. When the DC sources have different voltages (unbalanced), the full bridge output waveform can have even more levels. Anyway, the full bridge configuration is mostly preferred because the output voltage of this arrangement is twice the ouput of the half-bridge inverter.

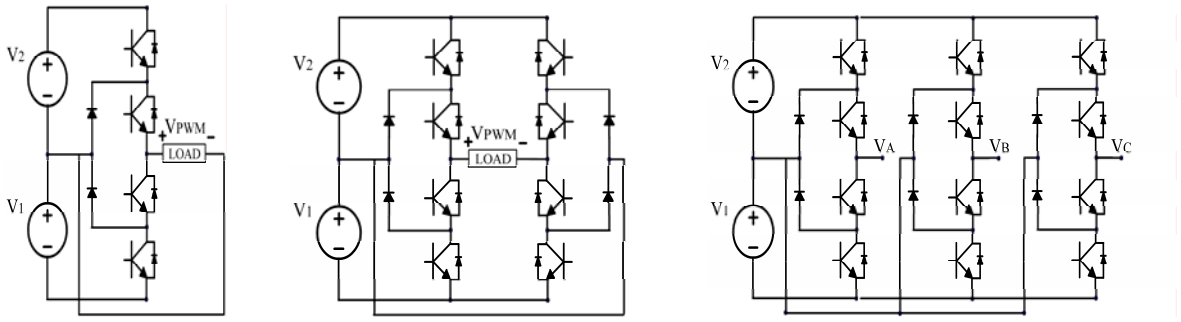

a) half bridge. b) full bridge. c) three phase.

Figure 2.2 Circuits based on three-level inverter leg.

Finally, although by increasing the number of levels in the inverter, the output voltage has less harmonic distortion, the control complexity, and the hardware cost increase.

2.3 Clamping Voltage Techniques

There are three basic families of multilevel inverters, according to the voltage clamping mechanism: diode, capacitor and cascade clamping.

The first topology is the Diode Clamped half-bridge, illustrated for three and five level configurations (figure2.3). The middle point of the diodes give the partial voltages in the inverter circuit. The key components that distinguish this circuit from a conventional two level inverter are the diodes; sometimes varios diodes are placed in series to share the off-state voltage, as in figure 2.3b. Generally, those diodes must have a fast recovering characteristic.

UNIVERSITAT ROVIRA I VIRGILI
CONTRIBUTIONS ON SPECTRAL CONTROL FOR THE ASYMMETRICAL FULL BRIDGE MULTILEVEL INVERTER
Oscar Mauricio Muñoz Ramírez
ISBN:978-84-693-7665-2/DL:T.1747-2010

The Capacitor-Clamped topology is also illustrated for three and five level configurations. This topology is also called the flying capacitor inverter. These converters have been deeply studied by many people, and among them, Meynard in his laboratory at Toulouse, France [Mey95, Dem02]. Although there are no diodes, the capacitors increase the volume and weight. Another important aspect is that the capacitors voltage must be controlled using redundant states to assure the required balance. Nevertheless, the capacitor-clamped converters are usually less difficult to control because they have more switching combinations that lead to the same powering or freewheeling states.

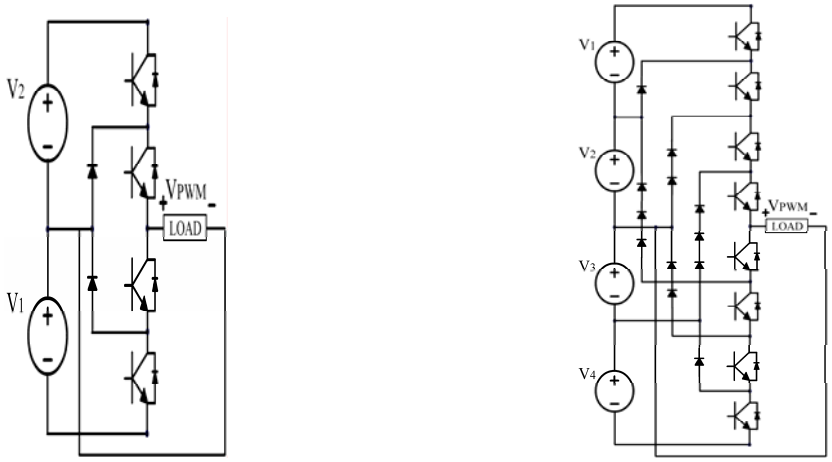

a) Three-level. b) Five-level.

Figure 2.3 Diode-Clamped multilevel inverter-leg.

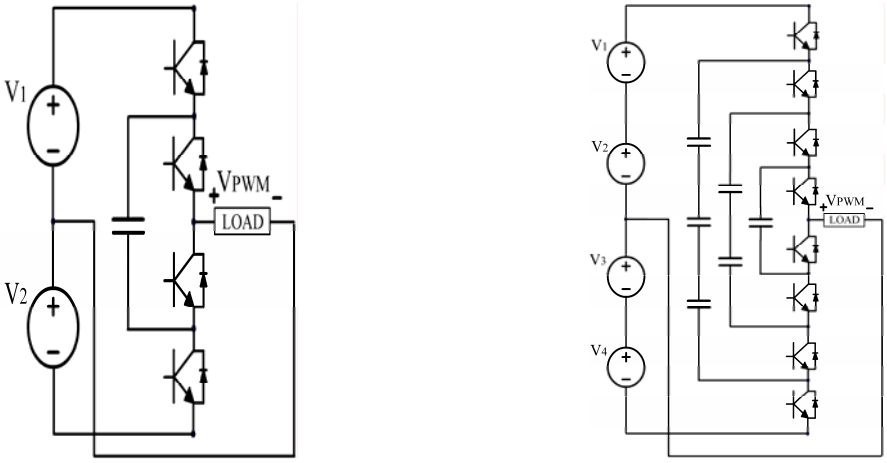

a) Three level. b) Five level.

Figure 2.4 Capacitor-Clamped multilevel inverter.

The cascaded inverters are illustrated in figure 2.5a and 2.5b, with two and three full-bridges respectively. As can be easily deduced, this structure is the most scalable. The resulting phase

UNIVERSITAT ROVIRA I VIRGILI
CONTRIBUTIONS ON SPECTRAL CONTROL FOR THE ASYMMETRICAL FULL BRIDGE MULTILEVEL INVERTER
Oscar Mauricio Muñoz Ramírez
ISBN:978-84-693-7665-2/DL:T.1747-2010

voltage is synthesized by the addition of the voltages generated by the different cells. Each cell delivers its power by the action of a full-bridge that adds or substracts an step or level voltage to the output wave. In the particular case of seven-level, each phase leg has three cells or DC sources as depicted in figure 2.5.b.

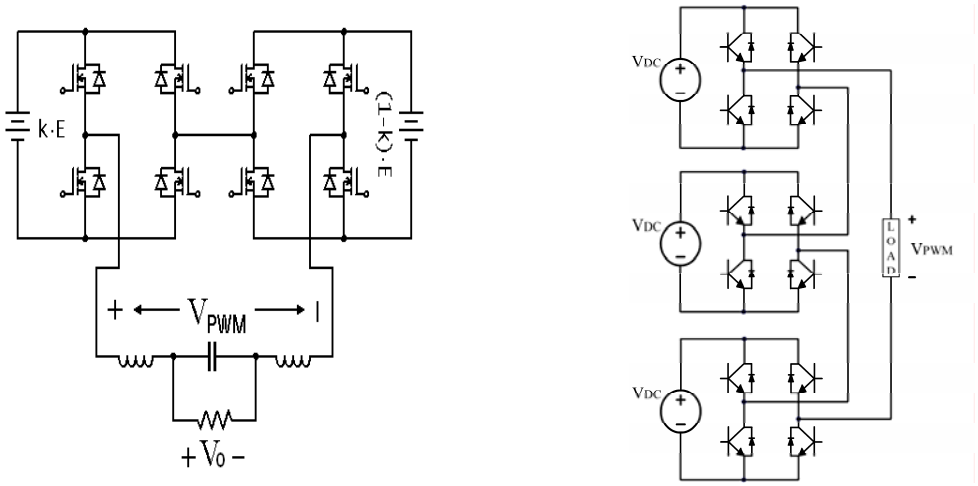

a) 5-level if k=0.5, 9-level k≠0.5 [Val03]. b) Seven-level, balanced input voltages.

Figure 2.5 Cascaded inverters.

To design and implement a inverter with a high number of levels, one solution could be the adoption of diode-clamped or capacitor clamped half-bridges to replace the conventional 2-level inverter legs in the full-bridges of cascaded inverters. This solution is often known as a Mixed-Level Hybrid Multilevel Inverter because it incorporates flying-capacitors inside a cascade configuration, an can be seen in figure 2.6.

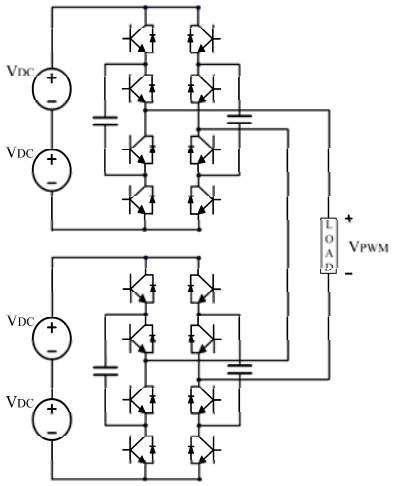

Figure 2.6 Mixed-Level multilevel inverter.

UNIVERSITAT ROVIRA I VIRGILI
CONTRIBUTIONS ON SPECTRAL CONTROL FOR THE ASYMMETRICAL FULL BRIDGE MULTILEVEL INVERTER
Oscar Mauricio Muñoz Ramírez
ISBN:978-84-693-7665-2/DL:T.1747-2010

After reviewing the different alternatives derived from the basic topologies, it can be stated that multilevel inverter systems are generally classified as diode-clamping inverters, cascaded inverters topologies, and flying capacitor or multicell inverters. The selection of a certain topology sometimes depends on the number of converter switching devices and available levels. Sometimes, a high number of switches causes switching redundancy, as certain output voltage levels can be generated by various switching states. Redundant states can be used to balance the switches power sharing, but are specially appreciated in flying capacitor converters because those additional freedom degrees are very useful to keep the capacitors voltages balanced [Kan05, Val08]. In general, the number of available levels and redundant states depends on the converter topology, and the balanced or unbalanced nature of the input voltages.

Under the dynamics point of view, the converter selection has also influence in the control-loop design. Thus, the flying-capacitor converter is always more complex than the equivalent diode-clamped circuits, where the only memory circuit is the LC output filter. The diode-clamped circuit is always a second-order system, whereas the flying capacitor is an Nth order system, with an inductor and $1+(N-2)\cdot(N-1)/2$ capacitors, where only $N-1$ are independent.

TABLE 2.1 FEATURES OF DIFFERENT FIVE-LEVEL CONVERTERS.

Converter Name	Available Levels	Redundant States	Mosfets	Clamping Diodes	Clamping Capacitors	Input Voltages	Order Dynamics
Diode Clamping Half Bridge	5	0	8	6	0	4	2
Flying Capacitor Half Bridge	5	11	8	0	6	1	5
Full Bridge using NPC (3-level) Legs	5 (B)	5 (B)	8	4	0	2	2
	7 (U)	3 (U)					
Asymmetrical Full Bridge (AFBMC)	5	1	6	2	0	2	2
Two "Normal" Full Bridges Cascaded	5 (B)	11 (B)	8	0	0	2	2
	9 (U)	7 (U)					

To compare diverse multilevel circuits, we show at table 2.1 some features of diverse 5-level circuits with balanced (B) or unbalanced (U) voltage supplies. The cascaded inverter and the asymmetrical full-bridge multilevel converter (AFBMC), both of them with second-order dynamics, require less number of devices than any other five-level circuit [Val03-05], and therefore a simpler control can be expected. Since such circuits have a reduced number of switching devices, we can expect lower conduction and switching losses, and become especially interesting for our study.

UNIVERSITAT ROVIRA I VIRGILI
CONTRIBUTIONS ON SPECTRAL CONTROL FOR THE ASYMMETRICAL FULL BRIDGE MULTILEVEL INVERTER
Oscar Mauricio Muñoz Ramírez
ISBN:978-84-693-7665-2/DL:T.1747-2010

Although the cascaded full bridge has attracted much research interest because it is easily scalable by adding more full bridges and can be driven with off-the-shelf commercial integrated full-bridge controllers, the AFBMI, a converter less found in the literature [Kai04], is also scalable, and has less controllable devices than the cascaded full bridge, that is, only six MOSFETs. This last reason has motivated the selection of this last converter as the platform to evaluate all our research on harmonic programming for multilevel inverters.

2.4 Tibuck Modeling of the AFBMI

To study the spectral phenomenon related with different modulation methods for multilevel inverters and, but simultaneously, to reduce the scope of the work, we have decided to choose the Asymmetric Full-Bridge Multilevel Inverter (AFBMI) as the representative converter to particularize the research task realized in this thesis about harmonic modeling and control.

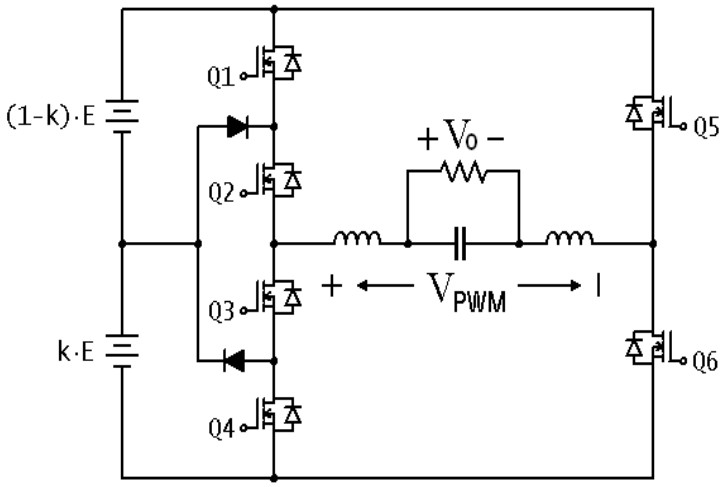

Figure 2.7 Asymmetric Full-Bridge Multilevel Inverter (AFBMI).

The AFBMI topology economizes devices compared to other topologies having the same levels number and the same dynamics, as the cascaded full-bridge. Comparing this circuit with the half-bridge in figure 2.3, only two DC sources are required instead of four. The AFBMI circuit is depicted in figure 2.7.

To understand the behavior of the AFBMI, we proposed to model this converter as a sequence of N–1 Tibuck cells operating sequentially in time, where each cell is supplied with a part of the input voltage determined by adjacent voltage levels (V_I–V_J), where the Tibuck sequence is directly driven by the output voltage.

UNIVERSITAT ROVIRA I VIRGILI
CONTRIBUTIONS ON SPECTRAL CONTROL FOR THE ASYMMETRICAL FULL BRIDGE MULTILEVEL INVERTER
Oscar Mauricio Muñoz Ramírez
ISBN:978-84-693-7665-2/DL:T.1747-2010

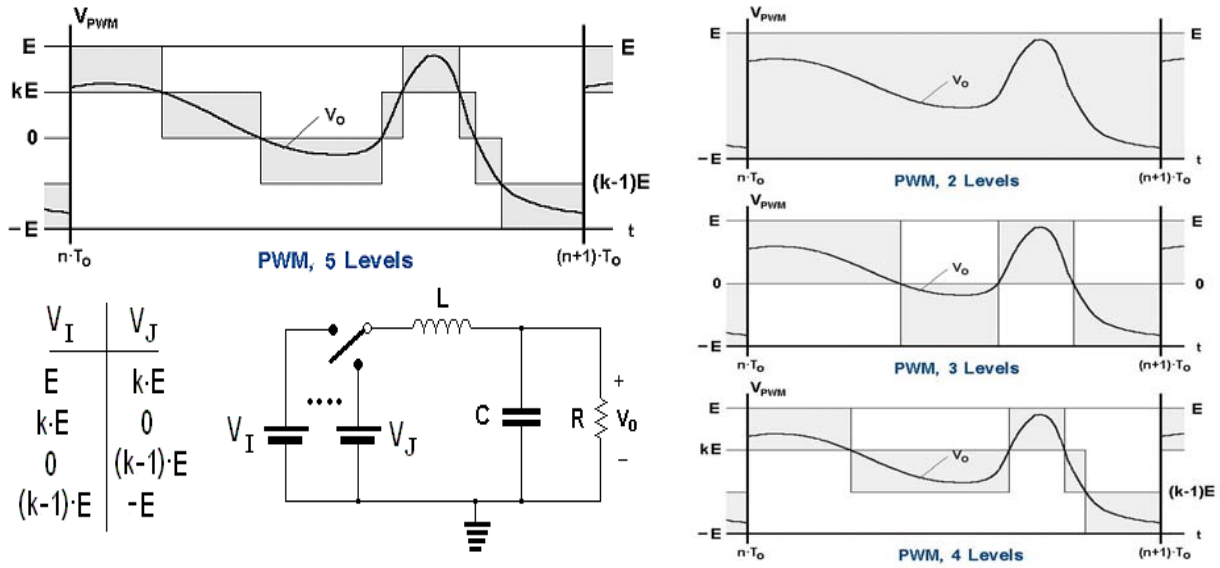

Figure 2.8 Ti-buck modeling of an Asymmetric Full-Bridge Multilevel Inverter.

Figures 2.8 shows the feasibility of modeling the AFBMI as a sequence of adjacent TIbuck's, and also how is reduced the voltage blocked by the devices as the number of levels increase, and therefore the switching losses. Since a multilevel converter can be seen as N–1 buck converters operating sequentially, its averaged switching losses could be estimated with (2.1), where expression (2.2) estimates linearly such losses in a single Tibuck converter.

$$P_{SW} = \sum_{i=1}^{N-1} \frac{\Delta T_i}{T_o} P_{SW}(i) \quad T_o = \sum_{i=1}^{N-1} \Delta T_i \tag{2.1}$$

$$P_{SW}(i) \approx \frac{1}{2} \cdot \Delta t \cdot f_S \cdot (V_I - V_J) \cdot |I_{On}| \tag{2.2}$$

Finally, an additional advantage of multilevel conversion is llustrated in figure 2.8, where by simple inspection, we observe that harmonic distortion decreases as the number of levels increase, assuming that the switching frequency, and the output filter remain unchanged.

2.5 Concluding Remarks

As previously explained, in a system with 5 balanced levels, only 25% of the buck converter switching losses can be ideally expected at the same switching frequency. Such losses reduction makes MI an atractive choice in power conversion systems, whereas the harmonic distortion reduction remains as an additional important advantage. Indeed, the relationship between losses and harmonic content is the cornerstone of this research work.

UNIVERSITAT ROVIRA I VIRGILI
CONTRIBUTIONS ON SPECTRAL CONTROL FOR THE ASYMMETRICAL FULL BRIDGE MULTILEVEL INVERTER
Oscar Mauricio Muñoz Ramírez
ISBN:978-84-693-7665-2/DL:T.1747-2010

Realize, that the distortion reduction achieved by increasing the number of levels, can be used to reduce further the switching losses decreasing the inverter carrier or switching frequency. Indeed, one step forward is possible, and in order to reduce even more those switching losses, we can try to minimize the output voltage harmonic distortion modulating the slopes of the triangular carrier waveforms in order to achieve a set of optimum carrier signals.

Generally, the output voltage distortion has three different causes: a) nonlinear or switching loads, b) harmonics generated by the PWM modulation itself, c) harmonics introduced by the DC-voltage ripple caused by the non-zero impedance of the sources supplying the inverter.

Although, the harmonics in the DC-supply are also caused by PWM modulation, the most important contribution is caused by the inverter load current. In case of pure resistive load, and balanced level distribution, the main DC component will be the typical 100 Hz ripple.

$$V_o(t) = mV_{dc}\sin(\omega_o t) \tag{2.3}$$

$$V_{IN}(t) = V_{dc} - Z_o I_{IN}(t) = V_{dc}\left[1 - \frac{m^2}{2\eta R}\left[1+\sin(2\omega_o t)\right]\right] \tag{2.4}$$

where formula (2.4) assumes a non-power dependent inverter efficiency η in (2.5), and a low ripple hypothesis. This hypothesis used in (2.6) to calculate the input current component, hides other minor magnitude harmonics due to different inter-modulation products.

$$P_o(t) = \eta P_{IN}(t) = \frac{m^2 V_{dc}^2}{R}\cdot\sin^2(\omega_o t) = \frac{m^2 V_{dc}^2}{2R}\left[1+\sin(2\omega_o t)\right] \tag{2.5}$$

$$P_{IN}(t) \approx V_{dc} I_{IN}(t) \Rightarrow I_{IN}(t) \approx \frac{m^2 V_{dc}}{2\eta R}\left[1+\sin(2\omega_o t)\right] \tag{2.6}$$

As explained previously, different originated harmonics can be compensated theoretically by different control loops, althoguh as the different loops apply to the same system, it could be a difficult task, in the final protoype to evaluate which is the sharing between the different loops in the final harmonic optimization. This task is proposed as a future work.

By one side, the harmonics coming from the DC sources voltage ripple should be greatly rejected or eliminated by means of the linearizing feed-forward loop. Harmonics coming from nonlinear loads, sudden transients, etc. should be attenuated by means of a wide-band linear state-feed-back loop, where the closed-loop transfer-functions have to be designed carefully, to avoid resonance peaks that could amplify some harmonics instead of rejecting them.

UNIVERSITAT ROVIRA I VIRGILI
CONTRIBUTIONS ON SPECTRAL CONTROL FOR THE ASYMMETRICAL FULL BRIDGE MULTILEVEL INVERTER
Oscar Mauricio Muñoz Ramírez
ISBN:978-84-693-7665-2/DL:T.1747-2010

And finally, the harmonics generated by the PWM modulaiton itself, should be reduced or eliminated by means of the slow-digital control-loop modifying the carriers of the multilevel PWM modulation.

Anyway, closed-loop harmonic compensation is never perfect, so as cleaner be the open-loop output voltage spectrum, better will be the final result, once the control-loop is applied. This is specially important, when modulating at low switching frequencies, and the left side of the fist alias, centered at the switching frequency F_C, can introduce harmonic content near the fundamental frequency F_O (50 Hz).

In this thesis, we focus our interest in the harmonic modeling of a multilevel inverter, to prove that by means of controlling the carriers slope, a better spectrum can be achieved.

UNIVERSITAT ROVIRA I VIRGILI
CONTRIBUTIONS ON SPECTRAL CONTROL FOR THE ASYMMETRICAL FULL BRIDGE MULTILEVEL INVERTER
Oscar Mauricio Muñoz Ramírez
ISBN:978-84-693-7665-2/DL:T.1747-2010

3. Review of Modulation Techniques

In the last decades, an extended variety of topics related to multilevel conversion have been investigated and discussed on scientific literature. Among these topics, in the last chapter we reviewed circuits and applications structures; in this section control and modulation techniques are considered. When revising literature it can be appreciated the diverse classification criteria and several approaches to categorize most of modulation techniques. There is not a unified criterion and neither a clear frontier to distinguish them, and thus modulation techniques classification is a subject of controversy and not a trivial task [Pin02, Mas03, Wal99, Fran08].

We proposed a scope for some of the most cited modulation schemes by considering the way of calculating the switching edges. Off-line and on-line methods are those ways that constitute traditional Pulse Width Modulation (PWM) schemes. Off-line or pre-calculated methods assemble a set of switching angles for a whole fundamental period. Such methods aim to eliminate, or reduce within an acceptable range, some chosen harmonics from the low frequency band and because of this reason such methods are named as Selective Harmonic Elimination (SHE) and Selective Harmonic Minimization (SHM). They require sophisticated mathematical resources in hardware and software and although they have been reported with attractive results they can not react to transients quickly. Moreover, by displacing incorrectly one angle the optimized spectrum might upset. On the contrary, on-line methods, mostly known as multicarrier-based, calculate switching instants either at the beginning or during the switching cycle and such property permits to these methods to respond to transients much better than off-line methods. The only limitatation is the bandwidth which in theory is $F_C/2$ and in practice it has been reported as $F_C/3$ [Des05].

Then, on-line methods offer better performance since efficiency and reliability are the first two motivations or objectives in constructing any power converter. After achieving those targets, spectral performance is a growing important factor, especially for MI and others DC-AC converters. Spectral performance can be determined by measurements after executing a modulation scheme, or it can be predicted by models that can be exploited to improve the design stages before implementing a MI circuit and a modulation technique. Often, attached to research on control and modulation techniques, there are spectral models that are based on modulation schemes. The spectrum is then calculated according to the switching instants of

UNIVERSITAT ROVIRA I VIRGILI
CONTRIBUTIONS ON SPECTRAL CONTROL FOR THE ASYMMETRICAL FULL BRIDGE MULTILEVEL INVERTER
Oscar Mauricio Muñoz Ramírez
ISBN:978-84-693-7665-2/DL:T.1747-2010

the modulation. Spectral models, in the light of harmonic distortion, permit to predict and to analyze the impact and viability of a MI. Choosing the proper number of harmonics is a criterion to be considered. For most applications, it is sufficient to consider the harmonic range from the 2^{nd} to the 25^{th}, but most standards specify up to the 50^{th} [Arr03]. However, in our particular case, most of the time we will focus calculating the distortion indeces to the tenth harmonic since we are concerned to optimize the baseband frequencies.

Another important issue is synchronization between the generated pulses and the fundamental frequency, a common requirement to all modulation techniques. Synchronization ensures that the switching frequency f_c is an integer multiple M_f of the synthesized fundamental frequency f_o. Then, the spectrum of the PWM waveform will consist of discrete frequencies at multiples of the fundamental frequency. Additionally, if M_f is an integer multiple of f_o, no sub-harmonics or frequency components below fundamental frequency f_o will exist. Undesired sub-harmonics, near zero frequency, even small in amplitude, can cause large currents to flow in inductive loads. Apart of of sub-harmonics, DC offset must be avoided in modulating MI, especially in connections with transformers.

Although perfect synchronization is practically impossible due to electrical component drifts, we can consider that both methods, off-line on-line, produce a spectrum of discrete and grouped frequencies. A third common method to generate PWM pulses is characterized by operating a variable switching frequency as hysteresis control, spread spectrum clock generation. Such methods do not accomplish synchronization and generate a continuous spectrum, with the known advantages and disadvantages. A hysteresis band modulator calculates the error between the reference waveform and the measured output. When the error leaves the hysteresis band (exceeds a defined bound) then the state of the switching devices changes. Hysteresis control is closed loop by nature and very simple to implement and makes it a very attractive choice. Nevertheless, its spectrum is continuous and spread, rather than discrete and grouped; besides, sub-harmonics may be present since the variable nature of switching cycle of hysteresis control.

To resume, among the three basic ways of PWM calculations and implementations, we chose a specific on-line method since harmonics will be discrete components, bandwidth will be good enough by properly selecting M_F, and switching instants can be easily calculated if compared to those obtained by SHE.

UNIVERSITAT ROVIRA I VIRGILI
CONTRIBUTIONS ON SPECTRAL CONTROL FOR THE ASYMMETRICAL FULL BRIDGE MULTILEVEL INVERTER
Oscar Mauricio Muñoz Ramírez
ISBN:978-84-693-7665-2/DL:T.1747-2010

3.1 Spectral Performance Parameters and Standards

3.1.1 Distortion parameters

Several distortion criterions and performance indexes can be found to evaluate the output waveform degradation due to undesirable harmonics. Concerning to voltage and current harmonics amplitudes, the most common criterions are:

$$THD_V = \sqrt{\sum_{n=2}^{\infty}\left(\frac{V_n}{V_1}\right)^2}\ ,\ where\ V_1=M_aV_{dc} \tag{3.1}$$

$$THD_I = \sqrt{\sum_{n=2}^{\infty}\left(\frac{I_n}{I_1}\right)^2}\ ,\ where\ I_1=\frac{V_1}{Z_{load}} \tag{3.2}$$

$$WTHD = \sqrt{\sum_{n=2}^{\infty}\frac{1}{n^2}\left(\frac{V_n}{V_1}\right)^2} = \frac{1}{M_a}\cdot WTHD_0 = \frac{\omega L}{V_1}THD_I\ \ (inductive\ load) \tag{3.3}$$

$$WTHD_0 = \sqrt{\sum_{n=2}^{\infty}\frac{1}{n^2}\left(\frac{V_n}{V_{dc}}\right)^2}\ \ where\ V_{dc}\ is\ the\ sum\ of\ all\ d.c.\ sources \tag{3.4}$$

THD figure can be applied to voltage and current harmonics interchangeable, giving the figures THD_V, THD_I. In expressions (3.1) to (3.4), V_1 and I_1 are the fundamental voltage and current, whereas the harmonic order is defined by *n*. According to standards on harmonic distortion, the summation operator is evaluated from *n=2* to the harmonic order considered by a specific requirement. THD formula in (3.1) assumes that there is not DC content in the output voltage. This is a very frequent hypothesis when computing THD figures for inverters.

Linear loads like R, L, and C do not create new harmonic frequencies, whereas with nonlinear loads, inter-modulation products cause new harmonic and sub-harmonic components that are added in the spectrum by superposition. Consequently, the THD value of a voltage signal can be very different from that of current THD. This means that harmonic current and harmonic voltages must be measured individually in the case of nonlinear loads in order to compute and compare their respective THD_I and THD_V.

Sometimes, inverter loads are induction or synchronous machines. Those loads are highly inductive, and WTHD figure is usually preferred instead of THD. The WTHD (Weighted Total Harmonic Distortion) takes into account an additional normalization with respect to the quantity $V_1/\omega L$. This merit figure is equivalent to find the THD_I in a system where the load is practically a pure inductor with a relatively small resistance [Lipo00].

UNIVERSITAT ROVIRA I VIRGILI
CONTRIBUTIONS ON SPECTRAL CONTROL FOR THE ASYMMETRICAL FULL BRIDGE MULTILEVEL INVERTER
Oscar Mauricio Muñoz Ramírez
ISBN:978-84-693-7665-2/DL:T.1747-2010

Finally, the $WTHD_0$ is derived from normalized WTHD with respect to the amplitude modulation index M_a [Age198, Age298]. Note that for a multilevel inverter with a constant DC bus and M_a getting progressively close to zero, THD and WTHD approach rapidly to infinite, whereas the parameter $WTHD_0$ remains as an useful performance figure that is not masked by small values of M_a.

Current distortion levels can also be characterized by a THD_I value but it can give a wrong conclusion when the fundamental load current is low compared with the short circuit or rated load current at the point of common coupling in any AC bus, i.e. the electrical grid or a transformer. A high THD_I value for a low input current may not be of significant concern if the rated load I_R is higher, since the magnitude of the harmonic current is low. To avoid such ambiguity a Total Demand Distortion (TDD) factor is used instead, and is defined as:

$$TDD_I = \sqrt{\sum_{n=2}^{\infty}\left(\frac{I_n}{I_R}\right)^2} \tag{3.5}$$

Applied on ANSI/IEEE 519-1992 standard, this factor is similar to THD but the distortion is expressed as a percentage of the rated or maximum load current I_R, rather than as a percentage of the fundamental current; for instance, at 100% of load operation $I_1=I_R$. Since electrical power supply systems are designed to withstand the rated or maximum load current, the impact of current distortion on the system will be more realistic if the distortion is evaluated on the designed values, rather than on a reference that changes with the load levels [Arr03].

In scientific literature, all these distortion criterions written before are the most used in order to validate or discuss results concerning with harmonic performance; otherwise, in commercial and industrial literature, to certificate the compliance with a specific standard of harmonics, it is only given one distorion index and usually no further details are given such as the number of harmonics considered. There is not a fixed protocol to select one distortion criterion or the other in order to qualify a certain spectrum; it is more recommended to observe some of those indices, for example, THD_V vs. $WTHD_0$ or TDH_V vs. THD_I as well as to consider more than one scope such as evaluating a few frequency components or a bigger number of harmonics, that is $THD_{V,h=10}$ vs. $THD_{V,h=40}$.

3.1.2 Spectral Performance and Power Quality

Spectral performance is one of the studied subjects in the field of power quality. This field has been emerging during the last three or four decades in power generation and power

UNIVERSITAT ROVIRA I VIRGILI
CONTRIBUTIONS ON SPECTRAL CONTROL FOR THE ASYMMETRICAL FULL BRIDGE MULTILEVEL INVERTER
Oscar Mauricio Muñoz Ramírez
ISBN:978-84-693-7665-2/DL:T.1747-2010

conversion systems. Power quality gathers in different categories the problems associated with the utilization of power converters. Often, the same devices that cause power quality problems can also be used to solve these problems [Ras07]. A growing attention has been dedicated to not only in solving the problem that cause quality disturbance, for instance active harmonic filters, power factor correctors, and so on, but also emerging techniques aimed to improve the power quality when harmonics are not yield rather than compensated, as in the case of DC-AC power converters that mainly work as VSI or CSI but as additional feature such converters yield a minimized distortion.

As a brief survey, power quality can be classified by categories as follows:

1. Steady-state voltage magnitude and frequency
2. Voltage sags
3. Grounding
4. Harmonics
5. Voltage fluctuations and flicker
6. Transients
7. Monitoring and measurement

It is considered that most of power electronic equipment causes harmonics and any DC-AC converter is one of them. Any AC. current flowing through any circuit at any frequency will produce a voltage drop at that same frequency. Harmonic currents are caused by loads and yield voltage drops in the power supply impedance at each respective frequency. The final result is a distorted output voltage. Then, spectral performance indicates how harmonics composition will affect power quality and hence the harmonics shall be ruled by standards.

TABLE 3.1 HARMONICS LIMITS OF STANDARD EN 50160/1995.

Harmonic number (integer multiple of h_1) Harmonics are given in percentage of h_1. These values are referred to voltage values.													
Odd harmonics											**Even harmonics**		
h_3	**h_5**	**H_7**	**h_9**	**h_{11}**	**h_{13}**	**h_{15}**	**h_{17}**	**h_{19}**	**h_{21}**	**h_{23}**	**h_2**	**h_4**	**$h_6 \ldots h_{24}$**
5%	6%	5%	1.5%	3.5%	3%	0.5%	2%	1.5%	0.5%	1.5%	2%	1%	0.5%
Maximum THD_V=8%, computing this formula from the 2nd harmonic up to the 40th harmonic.													

Harmonics are regulated by different standards which are adopted or recommended according to the policies of every country. Tables T3.1, T3.2 and T3.3 show the maximum values

concerned with maximum limits of harmonics; these tables are taken from three standards, namely, EN 50160/1995, IEC 61000-3-2 (for A class equipments) and ANSI/IEEE 519-1992.

TABLE 3.2 HARMONICS LIMITS OF STANDARD IEC 61000-3-2.

Maximum harmonic currents (integer multiple of h_1) Harmonics are given in Amperes.										
Odd harmonics							**Even harmonics**			
h_3	**h_5**	**h_7**	**h_9**	**h_{11}**	**h_{13}**	**$h_{15}\leq h\leq h_{39}$**	**h_2**	**h_4**	**h_6**	**$h_8\leq h\leq h_{40}$**
2.3	1.14	0.77	0.4	0.33	0.21	2.25/h	1.08	0.43	0.3	1.84/h
This standard is applied to equipments with output current less than 16 Amperes. There is not specification for THD.										

In Spain, UNIPEDE (Unión de Productores y Distribuidores de Electricidad) has accepted THD_V=5% as maximum distortion, computing this index from the 2nd harmonicto40th harmonic.

TABLE 3.3 HARMONICS LIMITS OF ANSI/IEEE 519-1992.

Maximum harmonic currents (integer multiple of h_1) Harmonics are given in percentage of h_1. They concern to the range 120 V-69 kV.						
I_{SC}/I_1	**Odd harmonics**					**Maximum distortion**
	h<11	**11≤h<17**	**17≤h<23**	**23≤h<35**	**35≤h**	**TDD(%)**
<20*	4.0	2.0	1.5	0.6	0.3	5.0
20-50	7.0	3.5	2.5	1.0	0.5	8.0
50-100	10.0	4.5	4.0	1.5	0.7	12.0
100-1000	12.0	5.5	5.0	2.0	1.0	15.0
>1000	15.0	7.0	6.0	2.5	1.4	20.0
Even harmonics are limited to 25% of the odd harmonic limits above. No d.c. offset allowed. *All power generation equipment is limited to these values of current distortion, regardless of the ratio I_{SC}/I_1.						

I_{SC} is the short circuit current at the PCC (point of common coupling). PCC is the point at which harmonics shall be evaluated. I_1 is the maximum fundamental current at the same point.

The practice of these standards should be utilized as an evaluation and diagnostic tool in developing power converters and validating research experiments as well as certifying compliance requirements in commercial and industrial products of power converter and power systems. For instance, ANSI/IEEE 519-1922 standard is a recommended practice, since the harmonics limits are merely suggested values; it is necessary to consider the size of the user and its maximum or rated load, and also, to consider the strength of the system (its impedance and short circuit current).

3.2 Programmed Modulations and Selective Harmonic Elimination

Both Selective Harmonic Elimination (SHE) and Selective Harmonic Minimization (SHM) are off-line modulation methods that aim at low frequency components to be eliminated or

UNIVERSITAT ROVIRA I VIRGILI
CONTRIBUTIONS ON SPECTRAL CONTROL FOR THE ASYMMETRICAL FULL BRIDGE MULTILEVEL INVERTER
Oscar Mauricio Muñoz Ramírez
ISBN:978-84-693-7665-2/DL:T.1747-2010

reduced by optimizing a cost function (a distortion figure). Low frequency harmonics are undesired, and when they are present, very difficult to eliminate by means of a passive filter. Pre-calculated angles for some targets or working points (M_{a1}, M_{a2},… M_{aMAX}) are located in a look-up table. The on-line controller uses this set of values to adjust the switching edges for a specific compensated or regulated M_a signal.

Usually, triplen harmonics are not eliminated since they do not cause any current flow in a balanced three phase system because the line-to-line voltages at triplen harmonics can be cancelled [Ras07]. Therefore, odd non triplen components are selected, such as the 5^{th}, 7^{th}, 11^{th} and 13^{th} harmonics; higher components can be filtered or just accepted if their influence on a distortion criterion is below standard requirements. This criterion is supported on the assumption of synthesizing a quarter-wave and half-wave symmetric signal that ensures that no even harmonics are not present in the spectrum.

When performing SHE or SHM, the chopped waveform can be modulated with different amplitude settings depending on the DC sources and the MI circuit architecture. A bipolar waveform can be synthesized from a half-bridge inverter by means of one carrier signal and commuting the output between two values $+V_{dc}$ and $-V_{dc}$ in both fundamental semi-cycles. Using a full-bridge inverter, an unipolar waveform is modulated between $+V_{dc}$ and 0 during positive semi-cycle and between $-V_{dc}$ and 0 during negative semi-cycle [Chi04]. Bipolar modulation can be defined as a 2-level scheme whereas unipolar modulation is a 3-level scheme. Finally, a the stepped waveform can be synthesized by adding several DC sources when more than three levels compose the output voltage; usually, seven, nine or eleven levels are used for this kind of waveforms. A stepped or staircase waveform is preferred since the block-voltage is reduced for each switching device. Notice that in both bipolar and unipolar signals and in stepped wave, the number of switching angles are directly related to the number of controlled harmonics.

The general rule for SHE is that modulating the fundamental component f_o, with N switching angles in a quarter-cycle, there are $N–1$ harmonic components that can be eliminated. In the case of a stepped waveform, with N sources of direct current, it is possible to obtain a $2*N+1$ level scheme and $N–1$ harmonics are be eliminated [Chi03,Chi04].

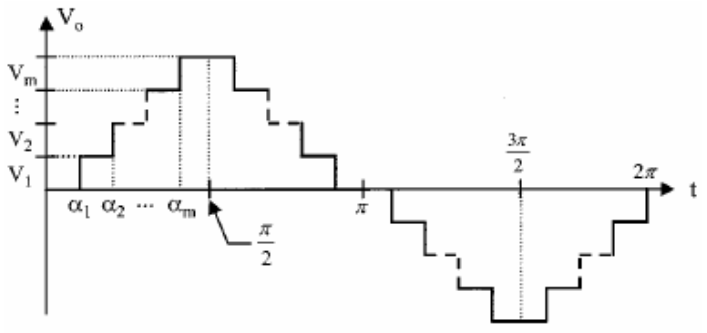

Figure 3.1 Generalized stepped waveform synthesized by SHE [Sir02].

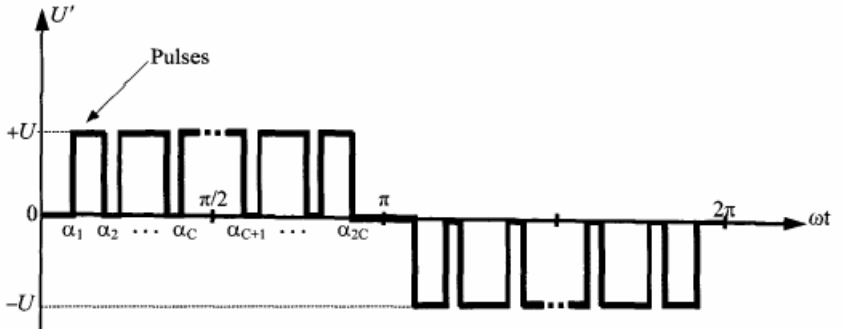

Figure 3.2 Generalized three-level waveform synthesized by SHE[Sir99].

To illustrate briefly how the switching angles are found, generally after assuming quarter-wave symmetry for a stteped signal, the equations to be solved start from writing the single Fourier Series coefficients as:

$$a_n = \frac{4}{\pi}\int_0^{\pi/2} F(\omega t)\sin(n\omega t)d(\omega t) \tag{3.6}$$

$a_n = 0$, for even n (3.7)

$$b_n = 0 \tag{3.8}$$

Where $F(\omega t) = V_L(\omega t)$, and L is the switched level between two angles, L={1,2,3,...2*N+1} for a stepped waveform based on N input voltages. From the switching angles, replacing (3.6) the harmonic coefficient is $c_n=a_n+jb_n$:

$$c_n = \frac{4}{\pi}\left[\int_{\alpha 1}^{\alpha 2} E_1\sin(n\omega t)d(\omega t) + \int_{\alpha 2}^{\alpha 3} E_1\sin(n\omega t)d(\omega t) + \ldots + \int_{\alpha N-1}^{\alpha N} E_N\sin(n\omega t)d(\omega t)\right] \tag{3.9}$$

$$c_n = \frac{4}{\pi}\left[E_1\cos(n\alpha_1) + \left((E_2 - E_1)\cos(n\alpha_2)\right) + \ldots + \left((E_N - E_{N-1})\cos(n\alpha_N)\right)\right] \tag{3.10}$$

This last equation leads to the general output waveform expression:

$$V_{PWM}(\omega t)=\sum_{n=1}^{\infty}\left[\frac{4E}{n\pi}\sum_{k=1}^{N}\cos(n\alpha_k)\right]\sin(\omega t) \tag{3.11}$$

And the amplitude of the harmonic C_n is:

$$c_n=\frac{4E}{n\pi}\sum_{k=1}^{N}\cos(n\alpha_k) \tag{3.12}$$

For example, assuming equal DC sources ($E=E_1=E_2=\dots E_N$), with N=5 and eliminating the fifth and the seventh harmonics, (3.9) is re-written as follows:

$$c_n=\frac{4E}{\pi}\left[\cos(n\alpha_1)+\cos(n\alpha_2)+\cos(n\alpha_3)\right] \tag{3.13}$$

The fundamental harmonic amplitude is then:

$$c_1=\frac{4E}{\pi}\left[\cos(1\alpha_1)+\cos(1\alpha_2)+\cos(1\alpha_3)\right]=M_a 4E \tag{3.14}$$

The two eliminated and controlled harmonics are depicted by:

$$c_5=\frac{4E}{\pi}\left[\cos(5\alpha_1)+\cos(5\alpha_2)+\cos(5\alpha_3)\right]=0 \tag{3.15}$$

$$c_7=\frac{4E}{\pi}\left[\cos(7\alpha_1)+\cos(7\alpha_2)+\cos(7\alpha_3)\right]=0 \tag{3.16}$$

When finding the solutions, the angles will fulfill the condition $\alpha_1<\alpha_2<\alpha_3...<\alpha_N$. The nature of these equations is non transcendental and there are some methods that find their solutions. Initial approximations are used as initial conditions for numerical methods based on Rampson-Newton algorithm or theory of resultants [Chi05]. New formulation are cited in more recent publications, where a new formulation places the switching initial angles inside a half-partitioned rectangle according to equal area criteria [Wan09,Ahm09]. This new formulation permits to find the solution faster than methods based on Rampson-Newton or theory of resultants.

It must be highlighted that most of literature reports have been focused on equal DC sources, accomplishing quarter-wave and half-wave symmetry [Tol98]. Lately, some contributions have been done with non-equal DC sources in modulating symmetric waveforms [Tol05]. Despite all the progress in SHE and its attractiveness, in the asymmetric waveform situation, the quarter-wave condition is not valid, and thus the complexity of equations (3.6), (3.7), (3.8) and (3.9) increases. The asymmetric situation is very common in practical applications and

the possibility of even harmonics produced at the output signal can not be ignored. Furthermore, ripple effects in DC sources are not considered until the present in literature reports.

Innovations and advances in solving methods continue and therefore, the calculation time for finding the solutions of these transcendental equations decreases. Faster solving times permit to handle higher order equations with more switching angles permitting to include more steps from DC supplies or more pulses in the case or unipolar and bipolar waves. However, the relation *N* d.c. sources eliminating *N–1* harmonics by means of a SHE stepped-waveform has an important drawback which is precisely the hardware complexity concerning to the number of d.c. sources or capacitors, switching devices and driving circuitry. Moreover, eliminating a group of harmonics means to translate the energy of such set to another place in the spectrum which can cause the first non eliminated harmonics to increase their amplitudes. Finally, if the available d.c. sources only permits to implement a small *N–1* group to be eliminated then the output filter will be designed for a excessive low cut-off frequency. For instance, with four d.c. sources a 5-level stepped waveform can be synthesized and if quarter-wave symmetry exists then 5^{th}, 7^{th}, 11^{th} and 13^{th} can be eliminated and the cut-off frequency will be higher than 650 Hz (a practical situation); if the waveform is asymmetric, then 2^{nd}, 4^{th}, 8^{th} harmonics will be present and therefore reducing the cut-off frequency and increasing the filter size.

3.3 SPWM Carrier-based Modulation Types

On-line methods for Pulse Width Modulation are schemes or algorithms where a modulating signal is compared with a carriers set. Normally, in inverters modulation, the modulating signal is a sinusoidal reference for open-loop systems or the same reference plus a compensating signal for closed-loop systems. Because of the sinusoidal shape of desired output, whether it be a voltage or a current output, the modulation scheme can be denoted as as Sinusoidal PWM, i.e. SPWM. The modulating signal has a fundamental frequency F_O and the carriers have a switching frequency F_C that satisfies the ratio $M_F=F_C/F_O$. Such ratio, the frequency modulation index, must be an integer value in order to obtain a discrete spectrum comprised of integer harmonic multiple.

The carriers can be displaced horizontally or vertically depending on the type of output phase configuration; either vertical or horizontal displacement are schemes easy to implement. In three-phase circuits, horizontal displacement is frequently used where each carrier is placed

UNIVERSITAT ROVIRA I VIRGILI
CONTRIBUTIONS ON SPECTRAL CONTROL FOR THE ASYMMETRICAL FULL BRIDGE MULTILEVEL INVERTER
Oscar Mauricio Muñoz Ramírez
ISBN:978-84-693-7665-2/DL:T.1747-2010

120 degrees respect to the others. In such case, every phase is modulated between two amplitude-limits and each carrier controlling one phase. For example, in figure 3.3 three modulating signals are compared with two horizontally displaced carriers. In this case, each carrier is used for positive and negative semi-cycles respectively.

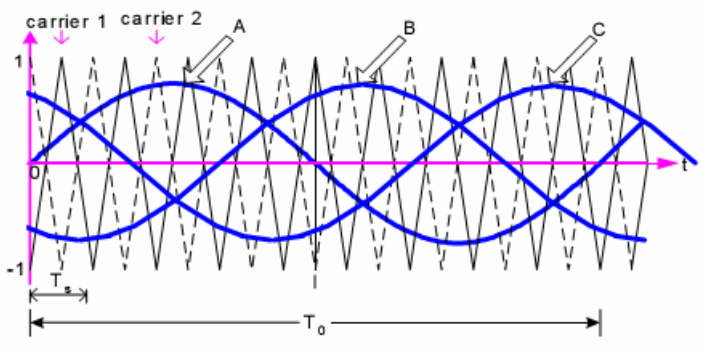

Figure 3.3 Horizontally displaced carriers [Fen04].

The phase-to-phase voltage is a three-level waveform as a result of adding the pulses between two phases. However, if the phase-to-phase voltage should be synthesized with more than three levels, a vertical multi-carrier set for each phase is preferred since vertical displacement is easier to implement than horizontal ly shifted carriers.

In general, to synthesize a N-level output per phase, *N–1* carriers are needed in vertical displacement and *N–1* amplitude-intervals are defined by the limits of the carrier amplitudes. One sinusoidal waveform is then compared with the carriers, where the modulated pulses switch between a couple of levels bounded by the amplitude-interval that the sinusoidal signal is crossing in a switching period. These pair of levels, corresponding to the amplitude limits of one carrier, depicts the amplitudes of the switching zone. Thus, there are *N–1* switching zones for *N–1* carriers. The obtained waveform is the line-to-neutral voltage V_{PWM} which can be added to an equivalent but displaced wave to form a line-to-line voltage. To obtain such line-to-line voltage, each output phase must be modulated by a different sinusoidal modulating wave with 120 degrees displacement. Then, three modulating signals are needed to synthesize a set of three-phase output waveforms.

The concept of vertical displacement is detailed in figure 3.4 and it can be extended to other arrangement of multiple carriers. The sinusoidal waveform modulates pulses along *N–1* amplitude-intervals, where each interval is an switching zone bounded by the carrier amplitudes. In one carrier period, the switching zone normally makes one pulse (consisting of two edges, one rising and the other falling) except in some transition instants between two

UNIVERSITAT ROVIRA I VIRGILI
CONTRIBUTIONS ON SPECTRAL CONTROL FOR THE ASYMMETRICAL FULL BRIDGE MULTILEVEL INVERTER
Oscar Mauricio Muñoz Ramírez
ISBN:978-84-693-7665-2/DL:T.1747-2010

adjacent zones where there is only one single edge since the modulating signal leaves the boundary of the switching zone. For spectral performance, during such transitions intervals, it is preferred to have only one edge in one switching period instead of having more than two edges.

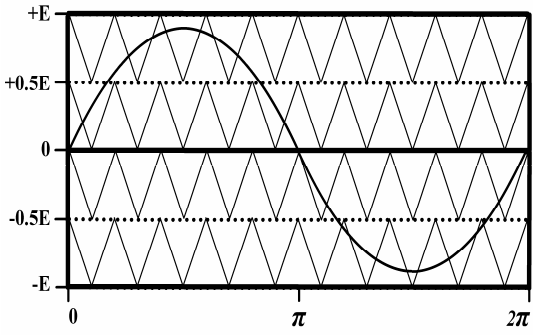

Figure 3.4 PD-SPWM.

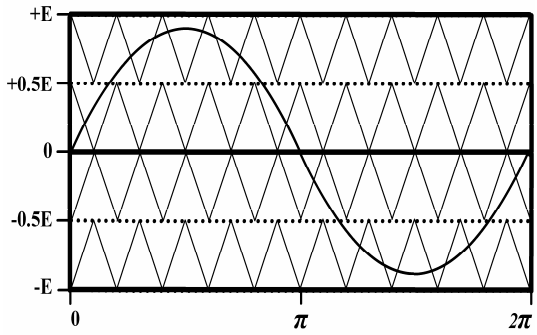

Figure 3.5 POD-SPWM.

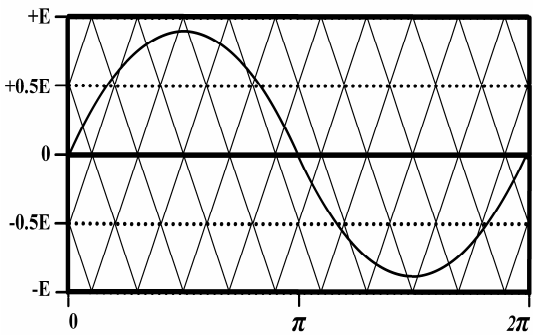

Figure 3.6 APOD-SPWM.

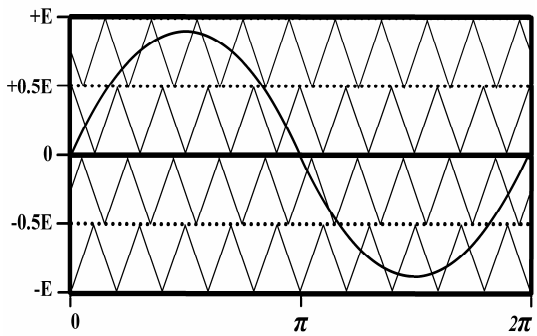

Figure 3.7 PS-SPWM.

TABLE 3.4 TYPES OF DISPOSITION FOR VERTICAL MULTICARRIER SPWM.

Type of SPWM	Meaning	Description
PD	Phase Disposition	All carriers have the same phase (figure 3.4)
POD	Phase Opposition Disposition	All carriers located above zero reference have the same phase, but they have 180º phase displacement respect to those located below zero reference (figure 3.5)
APOD	Alternative Phase Opposition Disposition	A 180º phase displacement is imposed between each carrier (figure 3.6)
PS	Phase Shifted	For each carrier, phase displacement equals $360/(N-1)$º and is successively added on the next carrier (figure 3.7)

Vertical displacement of a multi-carrier set in a single-phase modulating circuit can have different arrangements of SPWM. Figure 3.4 is the representation of a classic and particular arrangement of vertical displacement; in such case, symmetric triangular carriers are in Phase Disposition. Double-edged triangular carriers (i.e. scalene triangle) are the most used shapes

UNIVERSITAT ROVIRA I VIRGILI
CONTRIBUTIONS ON SPECTRAL CONTROL FOR THE ASYMMETRICAL FULL BRIDGE MULTILEVEL INVERTER
Oscar Mauricio Muñoz Ramírez
ISBN:978-84-693-7665-2/DL:T.1747-2010

in SPWM implementations and their classification, in the light of vertical displacement, can be stated as table 3.4 does:

The same types of SPWM can be extended to others carrier shapes, such as saw-tooth or exponential signals, also used in SPWM schemes.

The analysis on SPWM types plays an important role for establishing which method best suits an application. In particular, for multiple carriers SPWM several results concerning on types of SPWM have been published in previous works where those methods have been compared. Phase Disposition has been reported as the best method in most of cases when compared against other methods such as POD and APOD [McG02,Age198], especially in Diode-Clamped inverters. However, it is recommendable to complement analysis based on simulations and formulations with experimental data analysis. Some conditions such as sampling methods, the ratio F_C/F_O and the non-linear characteristics of switching devices have influence on the obtained experimental waveform and its spectrum.

Depending on the approaches and their conditions taken for simulations, model formulation and algorithm implementation, the expected results can be lightly or significantly different from real results. For instance, a PD-SPWM spectral analysis can be supported by means of circuit simulation obtaining the time domain signal and its respective spectrum is computed applying FFT to either simulated or experimentally obtained data. Also, a direct way is posible by modeling its output spectra with analytic formulation.

Simulation analysis made by means of common electrical simulation programs use a FFT algorithm to calculate the DFT of the sampled signals. Nevertheless, there are differences between the real and the simulated spectra due to small errors during simulations such as step size used in circuit simulation and the number of considered fundamental cycles. The FFT analysis can require a very large number of sampled points in order to obtain an acceptable accuracy; however FFT is a valuable analysis tool for simulated and experimental data. Alternatively, analytical approaches based on Double Fourier Series, firstly introduced by [Bla53], have been developed to determine the exact theoretical harmonic content of SPWM waveforms and lately studied by [Bow175,Bow275] and more recently by Holmes [Hol98,Hol03].

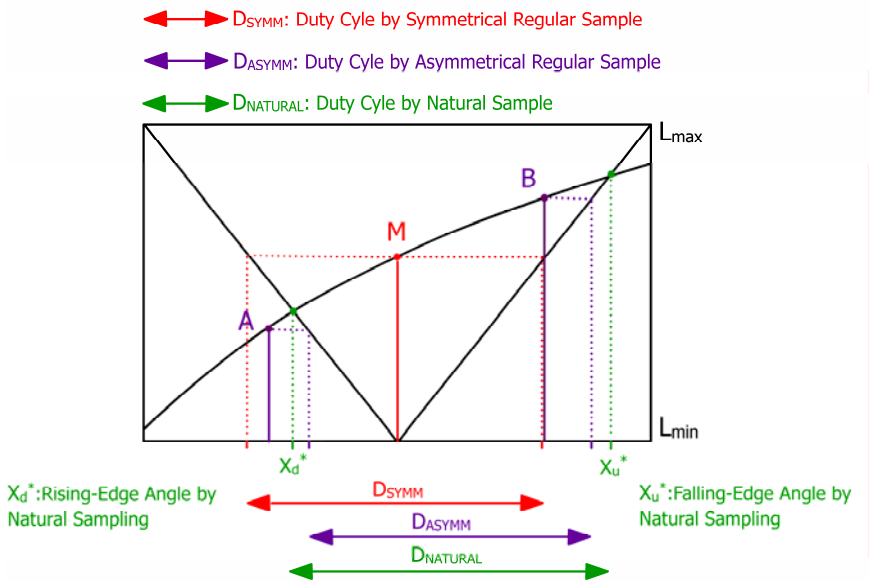

Figure 3.8 Sampling methods of modulator signal in PWM.

When determining the spectrum of any type of SPWM, the sampling method is an important condition to be considered in the comparison task between the modulating reference and the carriers. The way in which modulating and carriers signals are generated has important differences that are reflected in the spectrum. The DFS analytical approaches have been developed for natural and regular sampling methods. Analog circuits can realize natural sampling method while digital circuits are usually applied in regular sampling methods. Natural sample occurs when the modulator signal is continuously compared with the triangular carrier. Symmetrical regular sample occurs when the reference is sampled at the center of the carrier ($T_c/2$) and is held constant to be compared with the triangular carrier. Asymmetrical regular sample uses the two values intersected at the midpoints of falling time ($T_c/4$) and rise time ($3T_c/4$). These sampling methods are showed in figure 3.8 where X_D and X_U are rising and the falling edges respectively. These instantants can be obtained by differents sampling methods and in figure 3.8 such methods are natural sampling and the two variants of regular sampling: symmetrical and asymmetrical.

Certainly, the implementation of vertically displaced carrier PWM techniques led to their analysis and spectral formulations, rather than practical application of these techniques as a consequence of the initial theory. Natural PWM modulator can be implemented by analog hardware. The triangular carrier can be generated by integrating a square wave clock. A comparator generates the PWM output by comparing the input reference and triangular carrier signals. A multilevel modulator requires a number of synchronized triangular carriers with a type of phase arrangement. This implies more complexity in the analog hardware. In any of these analog implementations, performance is limited by noise and inaccuracy; both caused

UNIVERSITAT ROVIRA I VIRGILI
CONTRIBUTIONS ON SPECTRAL CONTROL FOR THE ASYMMETRICAL FULL BRIDGE MULTILEVEL INVERTER
Oscar Mauricio Muñoz Ramírez
ISBN:978-84-693-7665-2/DL:T.1747-2010

by temperature variations as well as white noise in the analog circuit components, mainly resistances and capacitors.

Although natural sampling implementation in analog hardware becomes more complex as the levels of the inverter increase, this method is the most suitable in order to synthesize a multilevel waveform with a high degree of fidelity. The fundamental component is the exact reproduction of the modulating signal and additionally, the content of non expected harmonics is reduced for practical circuits. Moreover, natural sampling method is the easiest comparing condition to formulate a SPWM analytical approach based on DFS and it constitutes a valuable starting point in order to study other alternatives of SPWM sampling such as Symmetrical Regular and Asymmetrical Regular sampling. These studies can be based on a simpler mathematical model (natural sampling) and the implementation can achieve highly approximate results when implementing regular sampling SPWM.

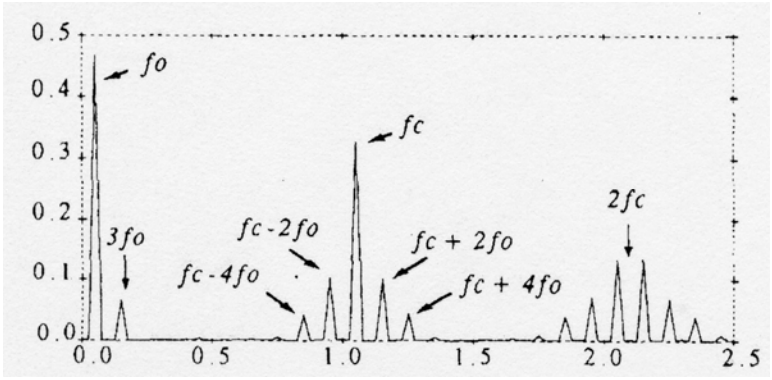

Figure 3.9 Spectral amplitudes in a Pulse Width Modulated waveform [Age96].

In order to know the spectrum of a particular type of SPWM, it is necessary to compute the coefficients of every harmonic, including the fundamental frequency. The harmonics amplitudes of a MI waveform are obtained from the coefficients C_{mn} of the Double Fourier Series for a doubled variable (x,y) controlled waveform [Hol03] and are calculated by the following expression:

$$C_{mn} = A_{mn} + jB_{mn} = \frac{1}{2\pi^2}\int_{-\pi}^{\pi}\int_{-\pi}^{\pi} f(x,y)e^{j(mx+ny)}dxdy \qquad (3.17)$$

The two variables of these coefficients are the carrier angle x and the fundamental angle y. Replacing x by $\omega_c t + \theta_c$ (carrier signal) and y by $\omega_o t + \theta_o$ (modulating signal), the evaluation of this coefficient is separated in four main divisions (showed at figure 3.9) and arranged by the m and n suffixes:

UNIVERSITAT ROVIRA I VIRGILI
CONTRIBUTIONS ON SPECTRAL CONTROL FOR THE ASYMMETRICAL FULL BRIDGE MULTILEVEL INVERTER
Oscar Mauricio Muñoz Ramírez
ISBN:978-84-693-7665-2/DL:T.1747-2010

DC Offset:	C_{00}
Fundamental Components and Baseband Harmonics:	C_{0n}
Carrier Harmonics:	C_{m0}
Sideband Harmonics:	C_{mn} (n ≠ 0)

For a multilevel inverter it is necessary that no zero-frequency component exist in the output voltage spectrum. As can be observed on left side in figure 3.9, it can be appreciated that there is not DC offset for a certain output signal and the first component of its spectrum is the fundamental frequency f_o, followed by the baseband harmonics ($2f_o$, $3f_o$, $4f_o$, $5f_o$, etc). In the middle part of the same figure, the first bell-shaped group of harmonics is formed by the first multiple of the switching frequency ($1f_c$) and its associate sideband harmonics ($f_c \pm f_o$, $f_c \pm 2f_o$, $f_c \pm 3f_o$, etc); such group of harmonics is known as the first alias and on right side of figure 3.9 the second alias group is also outlined. One alias is comprised by a carrier frequency multiple and it is sorrounded by sideband frequency components. When switching frequency is low, the alias components produce an effect known as overlap which consists of the superposition of frequency components that belong to different carrier multiple groups; for instance, the left part of the first alias are the major overlap components that affects the low frequency components alocated in the baseband and because of this reason M_F must be high enough to minimize the adition of harmonics components over the baseband and at the same time low as posible to reduce the switching losses.

When coefficients C_{mn} are calculated, the time-varying function of a PWM output voltage can be expressed as a summatory of sines and cosines functions which yields the formal expression of a DFS series as it is defined in (3.18) .

$$\underbrace{f(t)=\frac{A_{00}}{2}+\sum_{n=1}^{\infty}\left[A_{0n}\cos\left(n\left[\omega_0 t+\theta_0\right]\right)+B_{0n}\sin\left(n\left[\omega_0 t+\theta_0\right]\right)\right]}$$

DC Offset, Fundamental Component and Baseband Harmonics

$$\underbrace{+\sum_{m=1}^{\infty}\left[A_{m0}\cos\left(m\left[\omega_c t+\theta_c\right]\right)+B_{m0}sin\left(m\left[\omega_c t+\theta_c\right]\right)\right]}$$

Carrier Harmonics

$$\underbrace{+\sum_{m=1}^{\infty}\sum_{\substack{n=-\infty,\\ n\neq 1}}^{\infty}\left[A_{mn}\cos\left(m\left[\omega_c t+\theta_c\right]+n\left[\omega_0 t+\theta_0\right]\right)+B_{mn}sin\left(m\left[\omega_c t+\theta_c\right]+n\left[\omega_0 t+\theta_0\right]\right)\right]} \qquad (3.18)$$

Sideband Harmonics

UNIVERSITAT ROVIRA I VIRGILI
CONTRIBUTIONS ON SPECTRAL CONTROL FOR THE ASYMMETRICAL FULL BRIDGE MULTILEVEL INVERTER
Oscar Mauricio Muñoz Ramírez
ISBN:978-84-693-7665-2/DL:T.1747-2010

It is stated that a harmonic or multiple of the fundamental frequency, the harmonic h, satisfies the condition:

$$h = m \cdot M_f + n \tag{3.19}$$

Then, each harmonic is the composition of several C_{mn} coefficients; for example, when M_f=50, the third harmonic composition implies that $h_3=C_{0,3} + C_{1,-47} + C_{2,-97} + \ldots$etc. In theory, an infinite number of terms must be added; however, when executing programmed calculations, it is enough to consider no more than twenty C_{mn} coefficients that satisfies the condition (3.19).

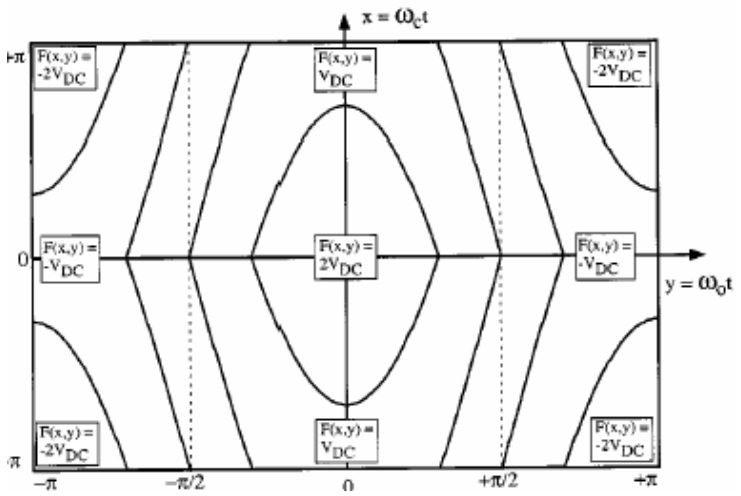

Figure 3.10 Contour plot of 5-Level PD-SPWM Inverter [Hol03]

When evaluating C_{mn}, the inner limits of the double integral that defines C_{mn} are dependent on the variable x (carrier signal: $x = \omega_c t + \theta_c$). The outer limits are defined by the variable y (modulator signal: $y = \omega_o t + \theta_o$) and indicates the switching zone. For PD-PWM it is assumed that $\theta_o=\theta_c=0$. Figure 3.10 shows a contour plot diagram for the C_{mn} coefficients of a five-level PD-SPWM modulation by natural sampling. In such contour, the limits of the outer integral are plotted in the y axe; these limits are within the intervals depicted by the angles where modulating signal amplitude passes from one level to the next, that is, when changes of TiBuck cell or switching zone. Since level distribution is symmetric, those angles are 0, $\pm\arccos(1/2M_a)$, $\pm\pi/2$ and $\pm\pi$. Similarly, the limits of the inner integral are also plotted in the x axe but their values are precisely dependent on the intersection points betwen modulator and carrier signals which yields sinusoidal functions for each limit of the inner integral.

The DFS analytical approach to calculate the output voltage spectrum in general case is difficult to obtain. Equation (3.16) is analyzed according to the contour plot of figure 3.10 where solving C_{mn} formula is quite extensive to be written here. When C_{mn} coefficients are

UNIVERSITAT ROVIRA I VIRGILI
CONTRIBUTIONS ON SPECTRAL CONTROL FOR THE ASYMMETRICAL FULL BRIDGE MULTILEVEL INVERTER
Oscar Mauricio Muñoz Ramírez
ISBN:978-84-693-7665-2/DL:T.1747-2010

calculated then they are substituted in Equation (3.17) which gives the DFS that defines the analytical expression of voltage. The analytical expression for a particular type of SPWM is founded in [Hol03]. This is the DFS model expresion (3.20) for the single-phase output voltage $V_{an}(t)$ obtained for PD-SPWM-natural sampling 5-Level Inverter with equal DC sources, plus the condition $0.5<M_a<1.0$ and where $\varphi=\arccos(1/2M_a)$.

$$V_{an}(t) = M_a Vdc\cos(\omega_o t) + \ldots$$

$$\ldots + \frac{4V_{dc}}{\pi^2}\sum_{m=0}^{\infty}\left\{\frac{1}{2m+1}\sum_{k=0}^{\infty}\left\{\frac{J_{2k+1}(2\pi(2m+1)M_a)}{2k+1}\left[1-2\cos(k\pi)\sin((2k+1)\varphi)\right]\right\}\cos((2m+1)\omega_c t)\right\} + \ldots$$

$$\ldots + \frac{V_{dc}}{\pi}\sum_{m=1}^{\infty}\sum_{\substack{n=-\infty \\ n\neq 0}}^{\infty}\frac{1}{2m}J_{2n-1}(4m\pi)\cos((n-1)\pi)\cos(2m\omega_c t + (2n-1)\omega_o t) + \ldots$$

$$\ldots + \frac{2V_{dc}}{\pi^2}\sum_{m=0}^{\infty}\frac{1}{2m+1}\sum_{\substack{n=-\infty \\ n\neq 0}}^{\infty}\left\{\begin{array}{l}\displaystyle\sum_{q=1}^{\infty}J_{2q-1}([2m+1]2\pi M_a)\cos(q\pi) \\ \times\left[\begin{array}{l}\dfrac{\cos([n-q]\pi)+2\sin([2q-1-2n]\varphi)}{2q-1-2n} \\ +\dfrac{\cos([n+q]\pi)+2\sin([2q-1+2n]\varphi)}{2q-1+2n}\end{array}\right]\end{array}\right\}\times\cos((2m+1)\omega_c t)+2n\omega_o t) \quad (3.20)$$

It is remarkable that most of hypothesis for spectral analytical approaches in SPWM consider that multilevel inverters operate with DC sources with equal values and that the carriers are the typical isosceles triangles or the less used saw-tooth carriers. There are not many references where variations on geometry of the carrier triangle is modified and therefore no further spectral analysis have been done.

The types of dispositon for vertical multicarriers schemes are the most used alternatives for multilevel converters and they can be applied on both single-phase and three-phase circuits. Up to this point we consider the modulation range defined as $M_a\leq 1.0$. However, in three-phase circuits the output fundamental voltage can be increased by overmodulating hence increasing the power rate. This condition led to develop techniques such as third harmonic injection, dead band and vectorial control. Since these methods are concerned to three-phase systems we only do a short description here. Dead band and third harmonic injection are methods where modulating signal is not a pure sinusoidal signal. These methods are used only in three phase inverters, where the cancellation of triplen-multiple harmonics is exploited. In dead band method each phase is inactive 120 over 360 degrees (figure 3.11.a) whereas in third harmonic injection method (figure 3.11.b) a third harmonic component is added to the

UNIVERSITAT ROVIRA I VIRGILI
CONTRIBUTIONS ON SPECTRAL CONTROL FOR THE ASYMMETRICAL FULL BRIDGE MULTILEVEL INVERTER
Oscar Mauricio Muñoz Ramírez
ISBN:978-84-693-7665-2/DL:T.1747-2010

reference or modulating signal as expressed in (3.21), and so the inverter voltage gain is increased. Vectorial control or Space Vector Modulation identifies the status of a three-phase inverter output as a vector, then a reference sample is a vector composition of the two nearest vectors.

$$V_{REF} = 1.15M_a \sin(\omega_o t) + 0.19M_a \sin(3\omega_o t) \tag{3.21}$$

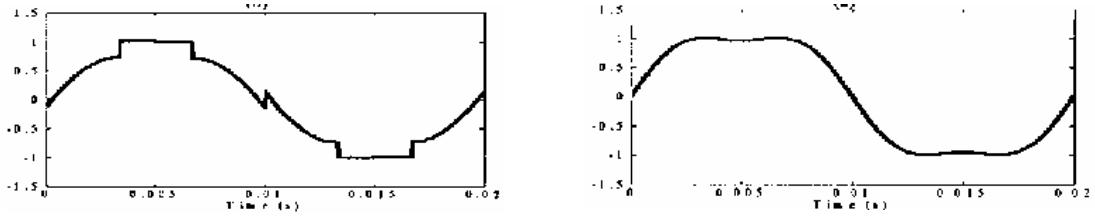

a) Dead Band PWM b) Third Harmonic Injection

Figure 3.11 Modulator signals in overmodulation conditions.

3.4 Spectrum Knowledge and Benefits

For an operator providing energy from any forms of renewable source, reliability and low cost are the most important aspects in such power systems. However, power quality is a matter with increasing importance and among power quality issues, the distortion of the power converter output is one such issues.

As an important example where spectral performance is a key factor, photovoltaic conversion systems include an inverter stage connected to the grid or local loads. The more PV generation systems connected to grid, the more the need to reduce the injected distortion caused by each generator element in the grid. Since the inverter is the link between DC-side and AC-side, it is the inverter that must adapt to AC-side supply conditions; the input supply of the inverter may be derived directly from a PV array or from a DC-DC converter.

In order to extract efficiently energy from PV sources, Maximum Power Tracking Point (MPPT) algorithms are extensively used strategies for PV applications where DC-DC converter structures extracts the maximum available power of PV arrays before the final DC-AC conversion; the output power is the maximum available one and to achieve that power, the regulated output voltage V_o changes in each DC-DC module (figure 3.12), then the available levels of the inverter are stable and stiffed during minutes intervals but are not equal during the whole daytime. In such applications it is expected that during daytime DC regulated output sources change and although the DC-DC modules are regulated, their

UNIVERSITAT ROVIRA I VIRGILI
CONTRIBUTIONS ON SPECTRAL CONTROL FOR THE ASYMMETRICAL FULL BRIDGE MULTILEVEL INVERTER
Oscar Mauricio Muñoz Ramírez
ISBN:978-84-693-7665-2/DL:T.1747-2010

temporal values change depending on extracted power-conditions. Long-term balanced DC voltages and consequently uniform level distribution are not garanteed.

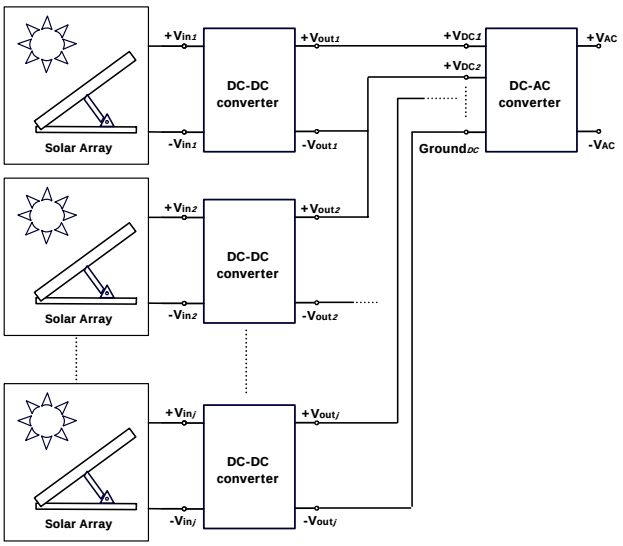

Figure 3.12 DC-DC conversion before DC-AC inversion.

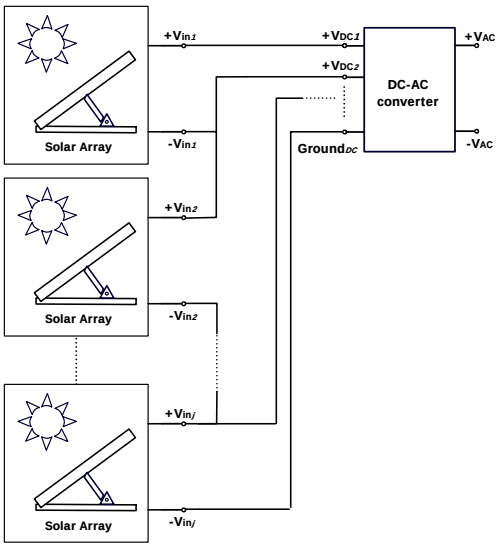

Figure 3.13 Direct DC-AC inversion.

Others PV installations do not work with MPPT applications and there is direct connection between PV array and DC-AC inverter producing faster changes in the available levels of the inverter (figure 3.13). Regardless of if these supplies are regulated or not, DC values are not fixed during daylight and therefore inverter structures would inject varying spectrum content as a consequence of input DC supplies conditions; as it is detailed on next chapter, the level distribution ratio has influence on the output voltage spectrum. Spectral programming can be added to modulation strategy when input DC supplies change, keeping distortion requirements below minimum permitted distortion or at least keeping an optimized spectrum.

UNIVERSITAT ROVIRA I VIRGILI
CONTRIBUTIONS ON SPECTRAL CONTROL FOR THE ASYMMETRICAL FULL BRIDGE MULTILEVEL INVERTER
Oscar Mauricio Muñoz Ramírez
ISBN:978-84-693-7665-2/DL:T.1747-2010

3.5 Advantages of Spectrum Control

The main requirements for a MI are quality and efficiency. Then, a trade-off is established between the reduction of losses and the minimum switching speed that reproduces an acceptable modulated waveform. By applying appropriate modulation schemes, these two goals can be achieved simultaneously. Modeling the spectrum for SPWM-scheme and moreover, predicting its content for given conditions (i.e. Ma, K, load type), is a useful information that can be exploited to guarantee a feasible performance.

In order to improve the output waveform of the inverter, its harmonic content must be reduced especially at the low-frequency base-band. This also permits to reduce the filter size used and the EMI levels generated by the switching operation.

Multilevel technology promises a number of advantages over the conventional technologies, especially for high level applications. However, such methods are easily applicable in medium and low power applications and a number of them suit in the PV applications and other renewable sources conversion systems. Several advantages of MI over conventional ones include an improved output waveform, since the multilevel signal approaches the sinusoidal signal closer than the three-level signal, smaller filter size, lower switching losses, lower EMI and lower acoustic noise.

Since MI inverter cannot deliver undesired harmonics, as minimum, harmonics must be below the accepted values. Depending on the load, the harmonics currents and voltages may present different profiles, since the load could be a resistance, an electric bulb, a motor, a rectifier circuit, etc. For every type of load it is possible to adopt a different pattern of SPWM strategy by means of programming different carrier-shape-factors. As a first step, we started by studying the harmonics effects on a resistive load, where the current harmonics (I_o) are directly proportional to the voltage harmonics (V_o). The tunning or adjustments done on a specific spectral programming are based on the modeled interaction of resistive load. It means that a specific carriers set is optimized and its harmonic performance can be applied on not resistive load connections.

UNIVERSITAT ROVIRA I VIRGILI
CONTRIBUTIONS ON SPECTRAL CONTROL FOR THE ASYMMETRICAL FULL BRIDGE MULTILEVEL INVERTER
Oscar Mauricio Muñoz Ramírez
ISBN:978-84-693-7665-2/DL:T.1747-2010

UNIVERSITAT ROVIRA I VIRGILI
CONTRIBUTIONS ON SPECTRAL CONTROL FOR THE ASYMMETRICAL FULL BRIDGE MULTILEVEL INVERTER
Oscar Mauricio Muñoz Ramírez
ISBN:978-84-693-7665-2/DL:T.1747-2010

4. Spectral Modeling of Natural PD-PWM in Multilevel Inverters

Modeling the theoretical spectrum is very useful when both reduced harmonic content and high output power are required, especially when a particular design of power conversion compels to use a low commutation frequency. In particular, analysis on different patterns of spectrum can lead to the best possible selection among the available alternatives of SPWM schemes. These analyses can be done on the basis of Fast Fourier Transforms algorithms or mathematical models. A FFT processes the information of a sampled signal that has already taken place in past time. On the contrary, a mathematical model can predict such information.

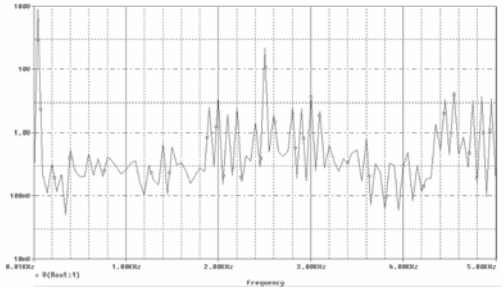

a) 1 cycle, Step Time=40µS

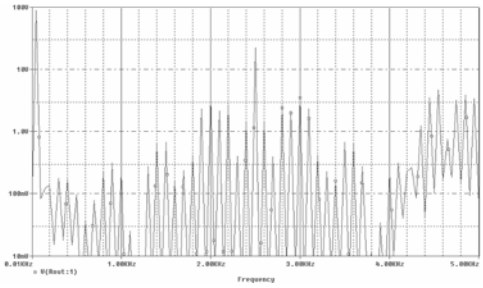

b) 2 cycles, Step Time=40 µS

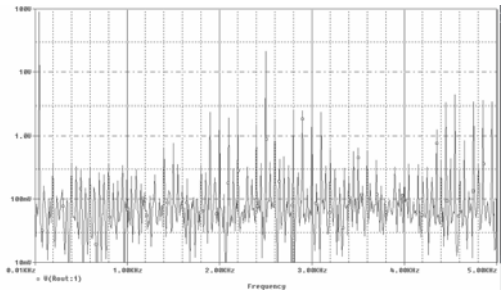

c) 5 cycles, Step Time=40µS

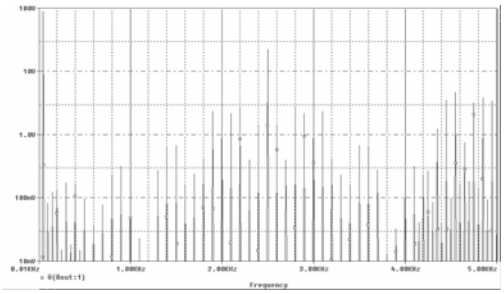

d) 5 cycles, Step Time=0.4 µS

Figure 4.1 Spectra by FFT in Pspice simulation.

Traditionally, FFT is used as a spectral analysis tool in circuit simulations and experimental data obtained from circuit implementations. FFT analysis uses a sampled representation of the switched waveform, and such task requires a large collecting-time of sampled data. Usually, from empiric knowledge, it is recommended that the sampled data must cover an interval of time greater or equal than five times the fundamental period and the sampling rate must be ten times lower than the switching period. FFT does not calculate the exact spectrum since it is very susceptible to sampling parameters. Actually, FFT is a simplification of a Discrete

UNIVERSITAT ROVIRA I VIRGILI
CONTRIBUTIONS ON SPECTRAL CONTROL FOR THE ASYMMETRICAL FULL BRIDGE MULTILEVEL INVERTER
Oscar Mauricio Muñoz Ramírez
ISBN:978-84-693-7665-2/DL:T.1747-2010

Fourier Series which would require a much longer computational time. Moreover, for a FFT, the obtained sample representation from circuit simulations can contain errors if the step time is incorrectly selected; in particular, the step time is a parameter of numerical analysis method used in Pspice.

Figure 4.1 shows four different results for a 5-level simulated waveform where length of time and step time vary; the test is realized for a PD-SPWM scheme with M_a=0.9 and M_f=50. On these figures is evident that small errors from FFT configuration can substantially degrade the calculated spectrum, especially on base-band harmonics. These harmonics are the most important to calculate because they are the target to minimize. It is clearly justified that the exact calculation of the spectrum is an important matter.To calculate the exact spectrum, analytical approaches are based on mathematical models that can predict the harmonic content of a SPWM waveform. Since phase disposition method has been referenced as a suitable method for SPWM, we developed for this type of vertical displacement a model that includes the carrier shapes and the asymmetry of unbalanced DC sources.

4.1 DFS Model for five-level standard PD-SPWM (K=0.5, $\forall r_i$'s=0.5)

Equation 3.19 written in chapter 3 calculates the exact output voltage in the time domain. For quickly consulting is re-written here as (4.1):

$$V_{an}(t) = M_a Vdc\cos(\omega_o t) + \ldots$$

$$\ldots + \frac{4V_{dc}}{\pi^2}\sum_{m=0}^{\infty}\left\{\frac{1}{2m+1}\sum_{q=0}^{\infty}\left\{\frac{J_{2q+1}(2\pi(2m+1)M_a)}{2q+1}\left[1-2\cos(q\pi)\sin((2q+1)\varphi)\right]\right\}\cos((2m+1)\omega_c t)\right\} + \ldots$$

$$\ldots + \frac{V_{dc}}{\pi}\sum_{m=1}^{\infty}\sum_{\substack{n=-\infty \\ n\neq 0}}^{\infty}\frac{1}{2m}J_{2n-1}(4m\pi)\cos((n-1)\pi)\cos(2m\omega_c t + (2n-1)\omega_o t) + \ldots$$

$$\ldots + \frac{2V_{dc}}{\pi^2}\sum_{m=0}^{\infty}\frac{1}{2m+1}\sum_{\substack{n=-\infty \\ n\neq 0}}^{\infty}\left\{\begin{array}{l}\displaystyle\sum_{q=1}^{\infty}J_{2q-1}([2m+1]2\pi M_a)\cos(q\pi) \\ \times\left[\begin{array}{l}\dfrac{\cos([n-q]\pi)+2\sin([2q-1-2n]\varphi)}{2q-1-2n} \\ +\dfrac{\cos([n+q]\pi)+2\sin([2q-1+2n]\varphi)}{2q-1+2n}\end{array}\right]\end{array}\right\}\times\cos((2m+1)\omega_c t)+2n\omega_o t) \quad (4.1)$$

UNIVERSITAT ROVIRA I VIRGILI
CONTRIBUTIONS ON SPECTRAL CONTROL FOR THE ASYMMETRICAL FULL BRIDGE MULTILEVEL INVERTER
Oscar Mauricio Muñoz Ramírez
ISBN:978-84-693-7665-2/DL:T.1747-2010

The first term contains the fundamental harmonic and it proves that there is not dependency on PD-SPWM properties such as carrier shapes or level distributions. The second term computes the amplitude for carrier multiples. On the one hand, the third term calculates the odd sideband components around even carrier multiples, and on the other hand the fourth term gives the even sideband components that surrounds odd carrier multiples.

In practice, to synthesize the signal, it is enough to consider the first ten carrier multiples and for the carrier sidebands it is necessary to include $10*M_f$ fundamental multiples, then the harmonics can be determined with high accuracy. These considerations are obtained by observing equation (4.1), and the minimum scale values for indexes m and n of coefficients C_{mn} are explained and determined later. It is interesting how frequency index M_f and Bessel function have an important influence on the sum operators of Equation 3.19.

When checking equation (4.1) it is possible to see the role of Bessel function in the second term (second row that corresponds to carrier multiples) and for the third and fourth terms (rows related to carrier multiples combined with fundamental multiples).Bessel functions explain the minimum scale given for indexes m and n of sum operators. Bessels functions are expressed in the form $J_q(x)$, where q is the order of the function and x is its argument. For a Bessel function its value is neglected when q>20. Special to mention is the attenuation due to the order of Bessel function in third term which is faster than the attenuation produced in fourth term. In third term, the order of Bessel function varies with n, whereas in fourth term q determines the attenuation of such function.

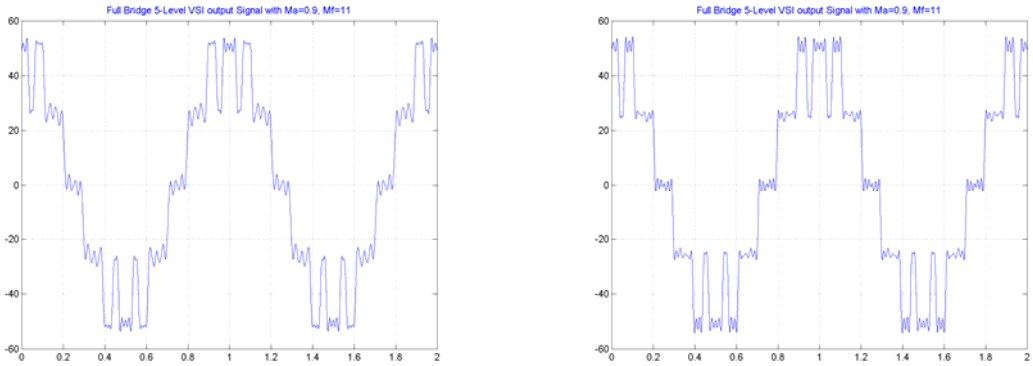

a) q_{max}=5 for Bessel function, fourth term of (3.19)

b) q_{max}=20 for Bessel function, fourth term of (3.19)

Figure 4.2 Synthesized waveforms by DFS model.

UNIVERSITAT ROVIRA I VIRGILI
CONTRIBUTIONS ON SPECTRAL CONTROL FOR THE ASYMMETRICAL FULL BRIDGE MULTILEVEL INVERTER
Oscar Mauricio Muñoz Ramírez
ISBN:978-84-693-7665-2/DL:T.1747-2010

Figure 4.2 shows the comparison between two output voltages when two different values for maximum *q* are used when computing (3.19); others input parameters of the used algorithm to calculate (4.1) are m_{max}=5, n_{max}=1*M_f. M_a=0.9, M_f=11. Here, a low value of M_f is selected to simplify visual illustration.

It can be observed the effects of using a specific frequency index M_f over the harmonic amplitudes. Equation (3.19), re-written here as $h = m*M_f + n$, gives the condition for composing the harmonic by adding its related C_{mn} coefficients. For example, if M_f=11, then the third harmonic h_3 will be the superposition of C_{mn} coefficients as follows:

$$h_3 = C_{0,3} + C_{1,-8} + C_{2,-19} + C_{3,-30} + C_{4,-41} + C_{5,-52} + \ldots \quad (4.2)$$

The coefficient $C_{0,3}$ is the third fundamental multiple (n=3) when the carrier multiple is zero and thus $C_{0,3}$ is null because there is no term in Equation 3.20 containing $\cos(0\omega_c t + n\,\omega_o t)$. Meanwhile, the others terms are sideband components who belong to the m^{th} carrier multiple and are displaced to the left by the n^{th} fundamental multiple. More examples of how to compose an harmonic *h* by adding C_{mn} coefficients can be checked later in table 4.22.

If M_f is a low switching frequency index, say $M_f < 32$, the contribution of mainly the first ten sideband components affects the total amplitude of baseband harmonics, namely h_2, h_3, h_4 and so up to the harmonic with the index equal to $M_f/2$. The sideband components have a decreasing contribution since their values are mitigated when *m* and *n* increase. The mitigation effect is related to the function depicted by each of the terms that constitute the sideband components in Equation (3.19). In table 4.1 the first twelve sidebands C_{mn} coefficients to compose h_3 illustrate the decreasing contribution mentioned above. All values are referenced to 50 Vdc.

TABLE 4.1 SIDEBAND COEFFICIENTS FOR COMPOSING H_3. M_F=11, M_A=0.9.

$C_{1,-8}$	$C_{2,-19}$	$C_{3,-30}$	$C_{4,-41}$	$C_{5,-52}$	$C_{6,-63}$
-1.0739	-0.0024	0.1388	0.0	-0.0604	0.0
$C_{7,-74}$	$C_{8,-85}$	$C_{9,-96}$	$C_{10,-107}$	$C_{11,-118}$	$C_{12,-129}$
0.0368	0.0	-0.0044	0.0	0.0010677	0.0

Including more side band coefficients leads to a more accurate value when composing an harmonic *h*. The inclusion of more C_{mn} coefficients is the effect we call here as overlap where the sideband component satisfies the condition in equation (3.18). To compute an m^{th} overlap

UNIVERSITAT ROVIRA I VIRGILI
CONTRIBUTIONS ON SPECTRAL CONTROL FOR THE ASYMMETRICAL FULL BRIDGE MULTILEVEL INVERTER
Oscar Mauricio Muñoz Ramírez
ISBN:978-84-693-7665-2/DL:T.1747-2010

group by using equation (4.1) then n must be m times M_f; in other words, the maximum overlap is reached when $n=m_{max}*M_f$. For example, the coeeficient $C_{10,-107}$ belongs to the tenth overlap group, and if it is included to compose h_3 then n_{max} must be at least equal to ten. Figure 4.3 shows two signals obtained with different overlap groups where the input parameters of (4.1) are the same, having m_{max}=10, q_{max}=20, M_a=0.9, M_f=11; the only difference is in the parameter n_{max}. The contribution of a sideband component on a harmonic composition is significant when its index m is greater or equal than 10. See how in figure 4.3.b the Gibb's effect is reduced and the obtained signal is flatter. Additional contributions from higher values of index m cause insignificant variations on the composition for any harmonic h, as it is verified in table 4.2 where the maximum limit for m is specified by the number of overlap groups. An overlap group is a multiple of carrier frequency ($m*M_f$) and its sideband harmonics ($\pm n$); having the shape of a cathedral in spectrum graphics, in this document we refer to these groups as alias or aliases.

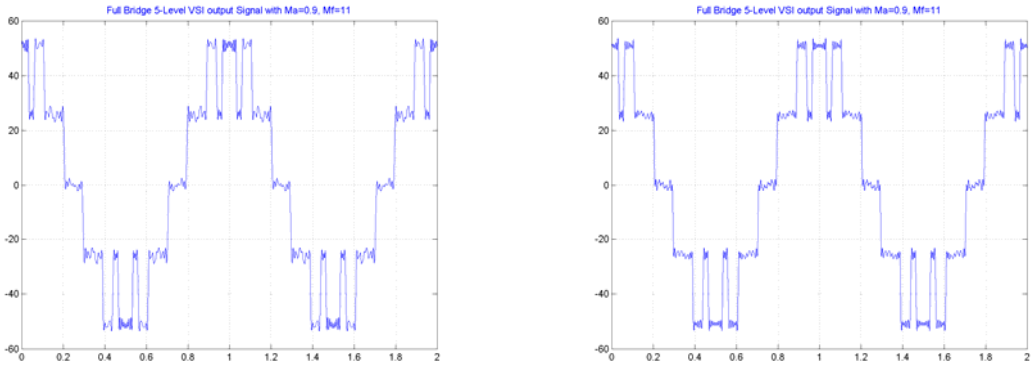

a) Overlap is $n_{max}=2*M_f$ b) Overlap is $n_{max}=10*M_f$

Figure 4.3 Refined waveforms by DFS.

TABLE 4.2 OVERLAP FOR COMPOSING H_3 AND H_{13}. M_F=11, M_A=0.9.

Overlap: n_{max}	$2*M_f$	$5*M_f$	$10*M_f$	$20*M_f$	$50*M_f$	$100*M_f$
h_3	-1.0763	-0.9979	-0.9656	-0.9630	-0.9631	-0.9631*
h_3 error to *	11.7%	3.6%	0.26%	0.001%	0%	0%
h_{13}	2.3451	2.4729	2.4224	2.4202	2.4202	2.4202**
h_{13} error to **	3.1%	2.2%	0.09%	0%	0%	0%

If M_f is a middle switching frequency number, say $M_f > 31$, then overlap is reduced since all sidebands components are now more far from any harmonic to be composed. If assuming M_f=49, it can be verified that the composition for h_3 is mainly determined by the first five

overlapping groups of baseband components. The next groups have a neglected overlap effect.

When M_f is a large number, say $M_f > 100$, it can be concluded that overlap effect is practically eliminated since the values of *n* in the third and fourth terms of Equation 3.19 have a strong mitigating effect. When implementing an algorithm for Equation 3.19, these considerations on the size of M_f are important in order to optimize computing time and accuracy by adjusting the scale for *m* and *n*.

TABLE 4.3 OVERLAP FOR COMPOSING H_3 AND H_{13}. M_F=49, M_A=0.9.

Overlap	2	5	10	20	50	100
h_3	0.0108	0.0130	0.0118	0.0111	0.0111	0.0111*
h_3 error to *	2.7%	17%	6.3%	0%	0%	0%
h_{13}	0.0065	0.0037	0.0046	0.0050	0.0050	0.0050*
h_3 error to **	30%	26%	8%	0%	0%	0%

Concerning to multilevel inverters and its output waveform synthesis, it is a good practice to include ten overlap groups if the frequency index is low, five groups if this index is medium or just two groups when the switching frequency is high. However, two points of view arise when using a formulation such as Equation (4.1). If the purpose is to reproduce a time domain signal, it is necessary to include more multiples *m* of carrier frequency and more overlap groups in order to obtain a more accurate signal. Nevertheless, if low frequency harmonics are the target of main interest, it is enough to consider as many multiples *m* of carrier as the range of this target is covered. For example, if M_f=11 and the distortion index includes fifty harmonics, it is sufficient to calculate the harmonics with m_{max}=5. The overlap effect can be sized to the second group if low frequency harmonics are the aim, as demonstrated in table 4.4 where the used input parameters are M_f=11, M_a=0.9. Therefore, distortion indices are practically not affected by the low refinement degree when including only one or two overlapping alias.

TABLE 4.4 DISTORTION INDICES REFERRED TO THE H^{TH} HARMONIC.

Overlap	2	10
$THD_{h=10}$	4.685%	4.685%
$THD_{h=50}$	26.409%	26.409%
$WTHDo_{h=10}$	0.94991%	0.94991%
$WTHDo_{h=50}$	2.1566%	2.1566%

UNIVERSITAT ROVIRA I VIRGILI
CONTRIBUTIONS ON SPECTRAL CONTROL FOR THE ASYMMETRICAL FULL BRIDGE MULTILEVEL INVERTER
Oscar Mauricio Muñoz Ramírez
ISBN:978-84-693-7665-2/DL:T.1747-2010

Distortion indices are strongly influenced by the selected frequency index M_f. Obviously, these distortion indices are reduced with higher switching frequency. In our work, we have chosen M_f=50 which permits us to study and optimize the harmonics on the low frequency band, where the presence of unexpected components are more linked to the non linear mechanisms of SPWM. In theory, with M_f=50, the first twenty frequencies amplitudes are practically not affected by overlap. Besides, such frequency index has an integer carrier period, 400μS, which is easy to implement in hardware and eliminates the condition of imprecise switching rate that might result into sub-harmonics. In the context of this work, M_f is stiff; however, in other research contexts, such index can be modulated in order to spread the output spectrum or adapted to some specific integer values in accordance to the modulating signal slope. Such contexts could be partially studied with the same therical background we propose here for stiff M_f index.

To summarize, when using an equation that performs DFS of a multilevel PWM voltage waveform, if the distortion index is calculated with the first ten harmonics then the analysis of harmonic distortion is strongly influenced by the low order harmonics and their amplitudes changes are important when there are several spectra to be compared. When considering a small group of frequencies, that is the baseband or half of frequency modulation index $M_f/2$, the differences in their calculated amplitudes can be noticeable when a low or medium switching frequency index is chosen; the amplitudes of baseband frequencies must be calculated with sufficient overlap groups in the DSF composition, in accordance with the size of index M_f.

4.2 Extension to Asymmetrical Carrier PD-SPWM cases

Traditional phase displacements strategies in multicarrier SPWM have been analyzed by means of circuit simulation or analysis approach [Hol98, Hol03]. However, it is remarkable that only triangular carriers with equal rise-and-falling edges have been used in most of the referenced works. These carriers have also equal peak-to-peak amplitude. Thus, the carriers are symmetric in amplitude as well as in rise-and-falling times.

Figure 4.4 presents an asymmetric inverter where the peak-to-peak amplitudes in SPWM scheme are not symmetric between them since the input voltages are unbalanced when $K \neq 0.5$; E is the total sum of the input voltages and in many cases is also referred as V_{dc}. In the context of asymmetrical level distribution, the DFS model given by (3.19) is not valid and the analysis on spectrum needs another tool or method to calculate the harmonics.

UNIVERSITAT ROVIRA I VIRGILI
CONTRIBUTIONS ON SPECTRAL CONTROL FOR THE ASYMMETRICAL FULL BRIDGE MULTILEVEL INVERTER
Oscar Mauricio Muñoz Ramírez
ISBN:978-84-693-7665-2/DL:T.1747-2010

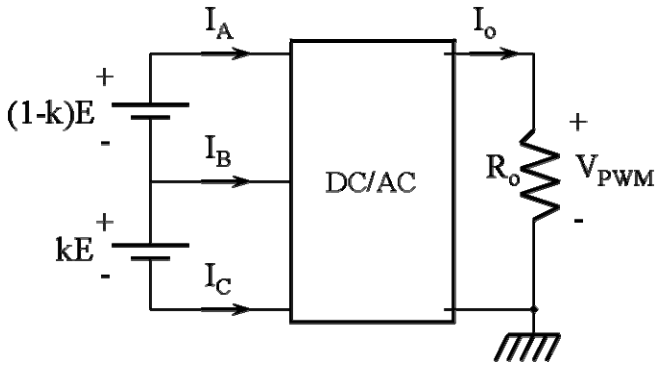

Figure 4.4 Level distribution ratio K of input voltages.

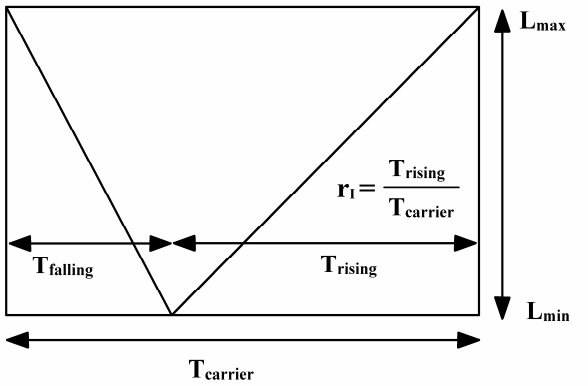

Figure 4.5 Shape-factor representation of a carrier signal.

Additionally, since the DC supply has asymmetric distribution, it is expected that the harmonic distortion is increased. However, the harmonic distortion can be reduced by controlling the relation between the rise-time and the falling-time of the carriers as depicted in figure 4.5. The shape-factor or the carrier shape which is one of the studied parameters in the context of this thesis and it is written as follows:

$$r_I = \frac{T_{\text{rising}}}{T_{\text{carrier}}} \tag{4.3}$$

For example, for trailing edge carrier the factor shape is 1.0 and for double edge carrier the factor shape is 0.5. The shape-factor can vary between 0 and 1 which gives an infinite number of possibilities to program the carriers. The subscript *i* indicates the carrier linked to the switching zone limited between two levels, L_{max} and L_{min}, as shown in table 4.5. L_{max} is equivalent to V_I and L_{min} is equivalent to V_J as it is indicated in Tibuck modeling; because of programming implementation and to avoid errors when writing the algorithm code the nomenclature of these variables, L_{max} and L_{min}, is preferred. In general, for a N-level inverter the I^{th} carrier is between the superior level L_{max} and the inferior level L_{min}; for i it is stated that i={1, 2, …N-1}.

UNIVERSITAT ROVIRA I VIRGILI
CONTRIBUTIONS ON SPECTRAL CONTROL FOR THE ASYMMETRICAL FULL BRIDGE MULTILEVEL INVERTER
Oscar Mauricio Muñoz Ramírez
ISBN:978-84-693-7665-2/DL:T.1747-2010

TABLE 4.5 CARRIERS OF 5-LEVEL SPWM.

I^{th} Carrier	**L_{max}**	**L_{min}**
$Carrier_1$	+E	+K·E
$Carrier_2$	+K·E	0
$Carrier_3$	0	-(1-K)·E
$Carrier_4$	-(1-K)·E	-E

Considering five-level and four-level modulation cases, and depending on amplitude index M_a, there are three modes of operation of the inverter. In Table 4.6, it can be observed that in some cases, all the available levels are not used in the conversion process. We call this phenomenon "level collapsing" where K and M_a present different combinations that yields several situations of level modulation with five or less number of levels.

TABLE 4.6 LEVELS COLLAPSING.

Collapse	**Available Levels**	**5**	**4**
No	$M_a>max(K,1-K)$	5	4
Yes	$min(K,1-K)<M_a<max(K,1-K)$	4	3
Yes	$M_a<min(K,1-K)$	3	2

If modulation index is sufficiently high to perform 5-level modulation, then we have the maximum number of carriers to be programmed. If the collapse phenomenon is presented, then the number of active carriers decreases. Under our point of view, by varying the shape-factor, there are unlimited combinations that can be concentrated into a limited and affordable quantity of cases to be studied.

TABLE 4.7 COMPARISONS GROUPS OF SOME CASES.

Group	**N-Levels**	**Collapse**	**Level Distribution (K)**
1	5	No	0.5
2	5	No	0.3
3	4	No	0.5
4	4	No	0.3
5	3	No	---
6	2	No	---

Amplitude Modulation Index $M_a=0.9$

In order to observe the effects of carriers programming, two values for level distribution have been selected, *K=0.5* and *K=0.3*. From this basis, six groups are defined for N-level modulation as detailed in table 4.7. The first four groups, those having four and five levels

modulation, interact with level distributions. Oppositely, level distribution has no sense for those cases with two and three levels.

Various simulation sets have been studied by considering particular cases with different arrangements of carrier shapes. Some of these simulation cases are detailed in Table 4.8 where the shape-factors are given for some cases. Case 1 utilizes typical isosceles triangular shape for all carriers in SPWM. Case 2 uses saw-tooth shape for all carriers. The remainder of the cases have different combinations of carrier shapes.

TABLE 4.8 SIMULATED CASES. M_A=0.9, M_F=50[MUÑ05].

Groups 1 & 2					**Groups 3 & 4**				**Group 5**			**Group 6**	
Set	$\mathbf{r_1}$	$\mathbf{r_2}$	$\mathbf{r_3}$	$\mathbf{r_4}$	**Set**	$\mathbf{r_1}$	$\mathbf{r_2}$	$\mathbf{r_3}$	**Set**	$\mathbf{r_1}$	$\mathbf{r_2}$	**Set**	$\mathbf{r_1}$
1	0.5	0.5	0.5	0.5	**1**	0.5	0.5	0.5	**1**	0.5	0.5	**1**	0.5
2	1.0	1.0	1.0	1.0	**2**	1.0	1.0	1.0	**2**	1.0	1.0	**2**	1.0
3	0.0	0.0	1.0	1.0	**3**	0.0	1.0	0.0	**3**	0.2	0.6	**3**	0.0
4	0.2	0.65	0.35	0.8	**4**	0.2	0.6	0.8	---	---	---	---	---
5	1.0	0.0	0.0	1.0	**5**	1.0	0.0	1.0	---	---	---	---	---
6	0.0	0.0	0.0	0.0	**6**	0.0	0.0	0.0	---	---	---	---	---

These cases were simulated with Pspice which calculated their respective spectra using its embedded FFT tool, and followed by such task in Pspice, the related data were analyzed with a Matlab algorithm that calculated and compared the harmonic distortion index, $WTHD_0$; the output voltage V_{PWM} is a non-filtered signal. These comparisons are done over two targets that include firstly ten harmonics and secondly one hundred harmonics in order to observe two frequencies ranges.

Revising distortion index in table 4.9 it is confirmed our hypothesis: low frequency harmonics can be reduced by optimization or by elimination when carrier shapes in a SPWM process are properly programmed. Superior spectral performance can be achieved using different combinations of carriers, and the best founded set of cases are normally non standard carriers slopes, i.e., all carriers are not uniformly equal to 0.5 nor 1.0. The rows “Best Case”, “Typical Case” and “Worst Case” demonstrate how the typical carriers of case 1 rarely benefit the spectral performance. The last row presents the percentage of improvement where the

UNIVERSITAT ROVIRA I VIRGILI
CONTRIBUTIONS ON SPECTRAL CONTROL FOR THE ASYMMETRICAL FULL BRIDGE MULTILEVEL INVERTER
Oscar Mauricio Muñoz Ramírez
ISBN:978-84-693-7665-2/DL:T.1747-2010

distortion is reduced by more than 50% in all the groups. Despite of these good results, at this point it is undetermined the mechanism or the decision criterion to select a specific combination of carrier shapes and thus to have the best case. Nevertheless, it is verified by means of circuit simulations that spectrum can be indeed improved by programming the carriers.

TABLE 4.9 BEST AND WORST RESULTS OF HARMONIC DISTORTION EVALUATION FOR 10 HARMONICS. MA=0.9, MF=50[MUÑ05].

h=1…10		**Comparison Group**					
		1	**2**	**3**	**4**	**5**	**6**
Best Case	$WTHD_0$[%]	0.04146	0.04569	0.03947	0.03385	0.00956	0.01783
	Case	6	2	6	1	2	2
Typical Case	*$WTHD_0$[%]*	*0.07978*	*0.08039*	*0.05341*	*0.03385*	*0.07492*	*0.02789*
Worst Case	$WTHD_0$[%]	0.08115	0.08039	0.05341	0.06218	0.07492	0.02813
	Case	4	1	1	3	1	3
$\frac{Best}{Worst}$[%]		51.09	56.83	73.9	54.43	12.76	63.38

TABLE 4.10 BEST AND WORST RESULTS IN HARMONIC DISTORTION EVALUATION FOR 100 HARMONICS. MA=0.9, MF=50[MUÑ05].

h=1…100		**Comparison Group**					
		1	**2**	**3**	**4**	**5**	**6**
Best Case	$WTHD_0$[%]	0.49276	0.56827	0.67854	0.71063	0.89832	1.6402
	Case	1	1	1	1	3	1
Typical Case	*$WTHD_0$[%]*	*0.49276*	*0.56827*	*0.67854*	*0.71063*	*0.89867*	*1.6402*
Worst Case	$WTHD_0$[%]	0.49701	0.57321	0.68595	0.72029	0.90612	1.6465
	Case	2	2	6	2	2	3
$\frac{Best}{Worst}$[%]		99.14	99.14	98.92	98.66	99.14	99.62

Revising a different distortion criteria, when is considered a high number of harmonics, it is observed that increasing the number of levels makes the output waveform to be closer in resemblance to the fundamental reference, as shown in table 4.10. Superior spectral performance is only dependent on the used N-levels and on the level distribution. Carrier shapes programming has neglected influence on distortion evaluated in wider bands of

UNIVERSITAT ROVIRA I VIRGILI
CONTRIBUTIONS ON SPECTRAL CONTROL FOR THE ASYMMETRICAL FULL BRIDGE MULTILEVEL INVERTER
Oscar Mauricio Muñoz Ramírez
ISBN:978-84-693-7665-2/DL:T.1747-2010

frequency components. In this context, the high number of included harmonics concerns with electromagnetic compatibility rather than with distortion reduction in low frequency. It is important to remind that the current harmonics are related with the voltage harmonics and the type of load. If voltage distortion is reduced, the current distortion is also decreased; it is expected to have lower switching losses by reading results of $WTHD_0$ as done in table 4.10.

Figure 4.6 shows four spectra obtained by FFT in circuit simulation with Pspice. The spectra correspond to five-level PD-PWM output waveforms, V_{PWM}, from the set of simulations of tables 4.7 and 4.8 for a [Muñ05]. On the left-upper corner, typical carriers (case 1) exhibit inferior spectral performance compared to the cleaner low frequency band that is obtained with the case of right-upper corner. Case 3 in group 1 (Figure 4.6 c) is interesting since even harmonics are eliminated despite M_f is an even number. Case 4 for group 2, on the right-lower corner, shows that inappropriate carrier shapes can worsen the spectrum. Therefore, carrier programming is not a random method but proper selection is necessary to optimize the low frequency band.

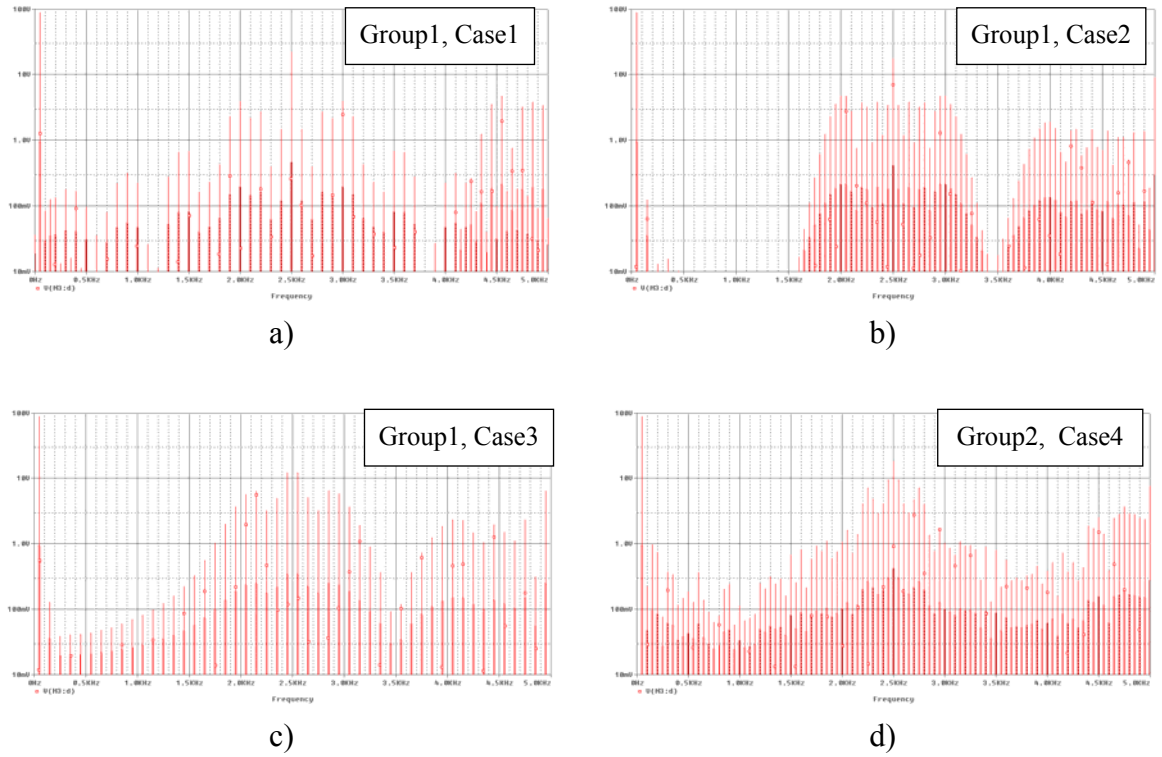

Figure 4.6 V_{PWM} Spectra by carriers programming [Muñ05].

The possibility of having many combinations and its respective advantages when such combinations of carriers sets pass a speficic distorion criterion states a new quest with two main questions: What tools or models will permit to calculate the spectrum for a given

carriers set modifying its rising-and-falling ratios?, How to find the optimum case for a given working point (M_a, K)?. The working point bears a challenge since the possibilities of diverse values M_a and K is infinite. Exactitude in spectrum amplitudes is not only a feature to be considered in the methods that solves the first previous question, but convergence, speed, proper sizing of a finite set of working points (M_a, K) and facilities to compute a spectrum from any combination are important issues when developing optimizing methods.

4.3 Extension of DFS Model to Asymmetrical Carriers

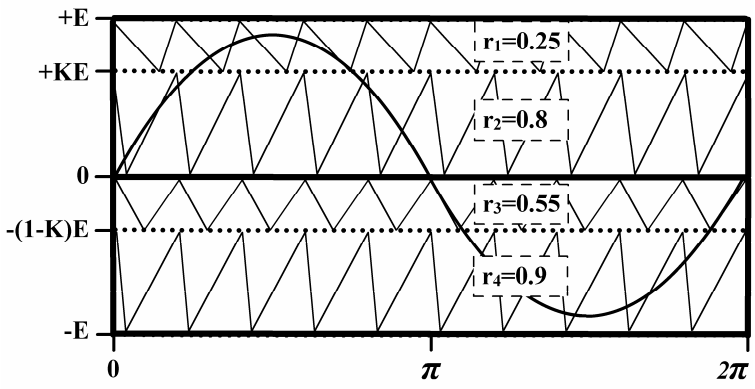

Figure 4.7 Five-level PD-SPWM with modified carriers.

Decisions on suitable carriers programming can be supported on an analytical approach for 5-level modulation that considers both carriers modification and level distribution, as shown in figure 4.7. These new variables are included in our new formulation which is an extension of Equation 3.20 and to deal with such formulation C_{mn} coefficients are recalculated according to the new conditions; thus the composition for every harmonic h can be realized as equation (3.19) indicates. Such compositions for each harmonic h is part of the whole calculation of two arrays: the first contains the sinus terms related to the real part of h, and the second contains the cosine terms related to the imaginary part of h. The time domain signal can be synthesized by using the sinus and cosine array. The harmonics amplitudes are calculated from the magnitude of h. Since the starting point to calculate h is the computation of its related C_{mn} coefficients, let us recall the next expression:

$$\overline{C_{mn}} = A_{mn} + jB_{mn} = \frac{1}{2\pi^2}\int_{-\pi}^{\pi}\int_{-\pi}^{\pi} f(x,y)e^{j(mx+ny)}dxdy \qquad (4.4)$$

In (4.4) carrier signal domain is represented by $x = \omega_c t + \theta_c$*, and modulator signal is represented by* $y = \omega_o t + \theta_o$*. For PD-SPWM it is assumed that* $\theta_o = \theta_c = 0$*.*

UNIVERSITAT ROVIRA I VIRGILI
CONTRIBUTIONS ON SPECTRAL CONTROL FOR THE ASYMMETRICAL FULL BRIDGE MULTILEVEL INVERTER
Oscar Mauricio Muñoz Ramírez
ISBN:978-84-693-7665-2/DL:T.1747-2010

Writing again equation (3.17) as (4.4) which defines C_{mn}, and in this expression it can be observed that there are two differentials *dx* and *dy* which make reference to carrier and modulator angles respectively; both differentials establish the integration intervals between –π and +π and hence it is justified the bi-dimensional nature of DFS.

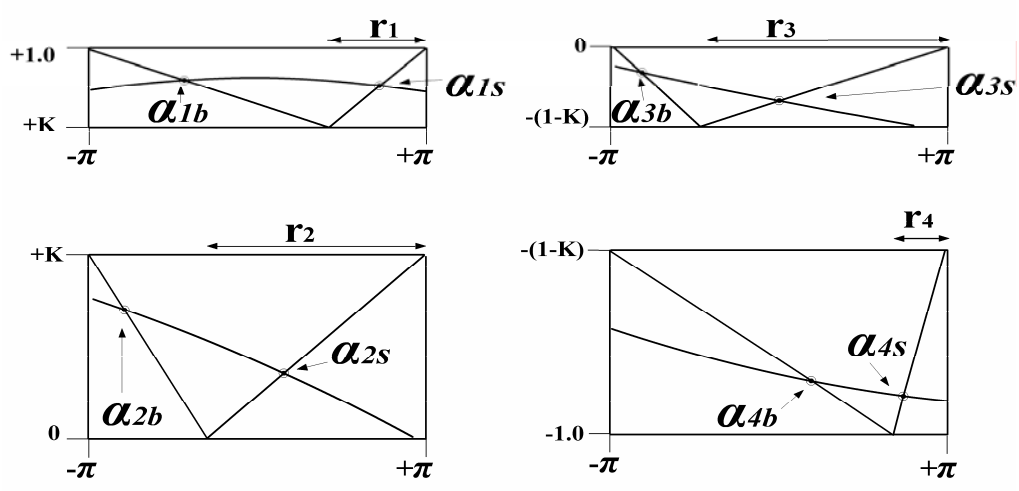

Figure 4.8 Switching angles (α_{ib},α_{is}) and carrier shape factors (r_i) .

Looking at the inner limits of the double integral, it can be observed that they are dependent on the variable *x*. The intersection points of the modulating signal and its related switching carrier are located within these inner limits and such intersections are repeatedly calculated for each carrier period T_c. These intersection points are indeed the switching angles during one carrier period, say α_{ib} and α_{is}; numerical suffix indicates the related carrier: suffix b indicates the begining of the rising-edge angle, otherwise, suffix s indicates the stop of the falling-edge angle.

Of course, there is only one activated carrier or in other words an activated Tibuck cell, where the ith-*carrier* is permanetly compared to the modulator as long as the modulator is between the carrier amplitudes limits producing a pulse for each carrier period. This solely interval of time comprises an active zone or Tibuck cell, wherein two adjacent voltages are assigned as the commuting levels. The function *f(x,y)*, the commuted level, is evaluated along the differential *dx* which is in the carrier domain. Figure 4.8 depicts this mechanism wherein basically there are three steps to complete one interval of integration in one active carrier period. First, from –π to α_{ib} modulator signal is below the carrier amplitude and *f(x,y)* commutes to the low voltage L_{min}. Then, from α_{ib} to α_{is} modulator signal is higher than the carrier making *f(x,y)* to commute to the high voltage L_{max}. Finally, from α_{is} to π modulator signal returns to be below the carrier and *f(x,y)* is back again to the low voltage L_{min}; at this

UNIVERSITAT ROVIRA I VIRGILI
CONTRIBUTIONS ON SPECTRAL CONTROL FOR THE ASYMMETRICAL FULL BRIDGE MULTILEVEL INVERTER
Oscar Mauricio Muñoz Ramírez
ISBN:978-84-693-7665-2/DL:T.1747-2010

point the interval over one carrier period is covered and this is how the inner integration is conducted through differential *dx*.

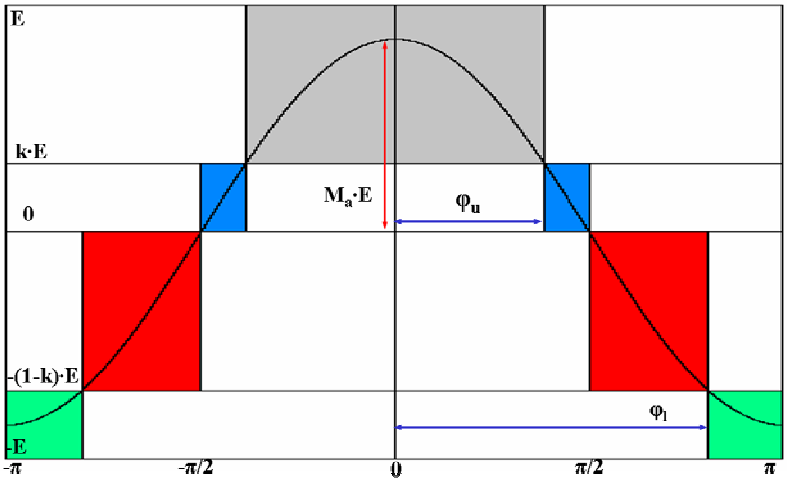

Figure 4.9 Switching Zones in 5-level modulation.

TABLE 4.11 PD-SPWM RULES AND SWITCHING ANGLES CHARACTERISTICS.

Switching Zone: Active Tibuck	**condition**	***f(x,y)***	**Interval of integration, *dx***	**Interval of integration, *dy***
1: $M_a(t) \geq +K\cdot E$	$M_a(t) > carrier_1(t)$	$+1\cdot E$	$[\alpha_{1b},\alpha_{1s}]$	$[\varphi_u,-\varphi_u]$
	$carrier_1(t) > M_a(t) > carrier_2(t)$	$+K\cdot E$	$[-\pi,\alpha_{1b}]$, $[\alpha_{1s},\pi]$	$[-\pi/2,-\varphi_u]$, $[\varphi_u,\pi/2]$
2: $K\cdot E > M_a(t) \geq 0$	$carrier_1(t) > M_a(t) > carrier_2(t)$	$+K\cdot E$	$[\alpha_{2b},\alpha_{2s}]$	
	$carrier_2(t) > M_a(t) > carrier_3(t)$	0	$[-\pi,\alpha_{2b}]$, $[\alpha_{2s},\pi]$	$[-\pi/2,-\varphi_u]$, $[\varphi_u,\pi/2]$, $[-\varphi_l,-\pi/2]$, $[-\pi/2,\varphi_l]$
3: $0> M_a(t) \geq -(1-K)\cdot E$	$carrier_2(t) > M_a(t) > carrier_3(t)$	0	$[\alpha_{3b},\alpha_{3s}]$	
	$carrier_3(t) > M_a(t) > carrier_4(t)$	$-(1-K)\cdot E$	$[-\pi,\alpha_{3b}]$, $[\alpha_{3s},\pi]$	$[-\varphi_l,-\pi/2]$, $[-\pi/2,\varphi_l]$
4: $M_a(t) \geq -E$	$carrier_3(t) > M_a(t) > carrier_4(t)$	$-(1-K)\cdot E$	$[\alpha_{4b},\alpha_{4s}]$	
	$M_a(t) < carrier_4(t)$	$-1\cdot E$	$[-\pi,\alpha_{4b}]$, $[\alpha_{4s},\pi]$	$[-\pi,-\varphi_l]$, $[\varphi_l,\pi]$

For every carrier period, the previous process is repeated M_f times then one modulator period is covered and the second integral is conducted through the differential *dy* which is in the modulator domain. The outer limits defined by the variable *y* indicate the angles of transition at which the modulator signal is going from one switching zone to another. In other words, they indicate where the modulator amplitude is placed between the maximum and minimum levels within each switching zone. Figure 4.9 shows the working zones in five-level modulation for a cosine modulator over one fundamental period $[-\pi,+\pi]$ and their related

UNIVERSITAT ROVIRA I VIRGILI
CONTRIBUTIONS ON SPECTRAL CONTROL FOR THE ASYMMETRICAL FULL BRIDGE MULTILEVEL INVERTER
Oscar Mauricio Muñoz Ramírez
ISBN:978-84-693-7665-2/DL:T.1747-2010

angles of transition, namely φ_u and φ_l. Table 4.11 summarizes the rules for 5-level PD-SPWM and resumes the limits of integration that are needed to compose the coefficients C_{mn}.

4.4 Contour Plots for the Five-Level Asymmetrical carrier PD-SPWM

A contour plot is a useful guide in order to write the double-integrals that define the C_{mn} coefficients. The original five-level countour plot from figure 3.10, is now modified by the influence of carriers modifications. Those modifications are manifested in the limits of integration written before in table 4.11. Moreover, depending on M_a amplitude, the contour plot can have additional modifications. Actually, if M_a is not sufficiently high, the contour plot is somewhat simplified and the five-level inverter can only produce a level-collapsed output with four, three or two levels, as previously indicated in table 4.6.

On the other hand, f(x,y) takes a value that depends on the switching level state. Taking into account the five level states [+E, +K·E, 0, -(1-K)·E, - E] for full-scaled $V_{PWM}(t)$ or [+1, +K, 0, -(1-K), -1] for normalized values, two types of integrals are defined. One type consist of a set of non-zero double integrals whereas the other type has a set of null double integrals where f(x,y)=0 V. The null integrals are only written here as an anecdotal illustration for further comprehension when defining the double-integrals for C_{mn} and their respective limits of integration.

Depending on the level distribution K and the amplitude modulation index M_a, the angles of transition are limits of integration along the differential dy, where $y=\omega_o t$; in fact, these limits are in the external integral of C_{mn} formula. First, φ_u in the positive half-cycle, delimits the transition between +E and +K· E. Second, φ_l in the negative half-cycle, delimits the transition of the switching zones that share the boundary between -(1-K)·E and -E. Equation (4.5) defines those angles as follows:

$$\begin{aligned} \phi_l &= \cos^{-1}\left[(K-1)/M_a\right] \\ \phi_u &= \cos^{-1}\left(K/M_a\right) \end{aligned} \tag{4.5}$$

Up to four collapsing-situations can be presented when modulating a five-level inverter and these cases will depend on the amplitude modulation, M_a, and the level distribution, K. First, let us consider a symmetric level distribution ($K = 0.5$) and later, an asymmetric level distribution ($K \neq 0.5$). In the first situation, the modulation process can synthesize, a three level waveform if $M_a < K$, and a five-level waveform if $M_a > K$, and under this assumption (K

UNIVERSITAT ROVIRA I VIRGILI
CONTRIBUTIONS ON SPECTRAL CONTROL FOR THE ASYMMETRICAL FULL BRIDGE MULTILEVEL INVERTER
Oscar Mauricio Muñoz Ramírez
ISBN:978-84-693-7665-2/DL:T.1747-2010

= 0.5) only two cases can be present. In contrast, the other situation can have two more cases, both with four levels when *min(K,1-K)* < M_a <*max(K,1-K)*, since K ≠ 0.5. To depict a contour plot, there can be up to four different situations:

- M_a >max(*K*,1-*K*), five levels are synthesized, see figures 4.10 to 4.13.
- 1-*K* < M_a <*K* where *K* > 0.5, four levels are synthesized, see figures 4.14 and 4.15.
- *K*< M_a < 1-*K* where *K* < 0.5, four levels are synthesized see figures 4.16 and 4.17.
- M_a <min(*K*,1-*K*) , three levels are synthesized, see figures 4.18 and 4.19.

For each of these situations there is a different contour plot that depicts the limit functions to evaluate the the double integral of C_{mn}, then there is a different solution for these coefficients that depends on the situation established by *K* and M_a. The solution for C_{mn} is the addition of the integrations from each portion encircled inside the contour plot.

4.4.1 Case M_a >max(K,1−K)

For this first situation where all five levels are available, as shown in figures 4.10 and 4.12 with *K* equal to 0.5 and 0.3 respectively, a set of fifteen non-zero integrals are obtained in order to calculate C_{mn}. The definition of these integrals is supported on contour plot from figures 4.11 (with K=0.5) and 4.13 (with K=0.3) that satisfy the condition M_a>max(K,1−K). The solution for C_{mn} is defined as equation (4.6) and because of its complexity is organized in table 4.12 as a set of fifteen non-zero defined integrals; its computation is done by an algorithm, DFS based-on C_{mn}-Algorithm , developed in Matlab software which means that the numerical solution of each defined integral is computed and added from the first integral to the last one. On the other hand, six null integrals are detailed in table 4.13.

As for composing one double-ntegral, let us take as example integral I_{15} where the active Tibuck cell is linked to the highest carrier, $carrier_1$, and f(x,y) is switched to +E. The external factor of the integral is always $1/2\pi^2$. Then, the outer integral evualuates the switched pulse along the horizontal axis $y=\omega_o t$, where the interval is comprised between $-\varphi_u$ and φ_u. Next, the inner integral is evaluated between the limits marked by the switching edges α_{1b} and α_{1s}.These limits are in vertical axis $x=\omega_c t$ and they indicate the beginning and end of the switched level. For every switched level, there are a group of double integrals and finally the total sum of all these integrals yields a C_{mn} coefficient.

UNIVERSITAT ROVIRA I VIRGILI
CONTRIBUTIONS ON SPECTRAL CONTROL FOR THE ASYMMETRICAL FULL BRIDGE MULTILEVEL INVERTER
Oscar Mauricio Muñoz Ramírez
ISBN:978-84-693-7665-2/DL:T.1747-2010

Equation (4.6):

TABLE 4.12 SOLUTION FOR C_{MN} WHEN M_A >MAX(K,1-K).

$I_1 = \frac{1}{2\pi^2}\int_{-\pi}^{-\varphi_l}\int_{-\pi}^{\alpha_{4b}} -Ee^{j(mx+ny)}dxdy$	$I_2 = \frac{1}{2\pi^2}\int_{-\pi}^{-\varphi_l}\int_{\alpha_{4b}}^{\alpha_{4s}} -(1-K)Ee^{j(mx+ny)}dxdy$
$I_3 = \frac{1}{2\pi^2}\int_{-\pi}^{-\varphi_l}\int_{\alpha_{4s}}^{\pi} -Ee^{j(mx+ny)}dxdy$	$I_4 = \frac{1}{2\pi^2}\int_{-\varphi_l}^{-\pi/2}\int_{-\pi}^{\alpha_{3b}} -(1-K)Ee^{j(mx+ny)}dxdy$
$I_5 = \frac{1}{2\pi^2}\int_{-\varphi_l}^{-\pi/2}\int_{\alpha_{3s}}^{\pi} -(1-K)Ee^{j(mx+ny)}dxdy$	$I_6 = \frac{1}{2\pi^2}\int_{-\pi/2}^{-\varphi_u}\int_{\alpha_{2b}}^{\alpha_{2s}} KEe^{j(mx+ny)}dxdy$
$I_7 = \frac{1}{2\pi^2}\int_{-\varphi_u}^{\varphi_u}\int_{-\pi}^{\alpha_{1b}} KEe^{j(mx+ny)}dxdy$	$I_8 = \frac{1}{2\pi^2}\int_{-\varphi_u}^{\varphi_u}\int_{\alpha_{1s}}^{\pi} KEe^{j(mx+ny)}dxdy$
$I_9 = \frac{1}{2\pi^2}\int_{-\varphi_u}^{\varphi_u}\int_{\alpha_{1b}}^{\alpha_{1s}} Ee^{j(mx+ny)}dxdy$	$I_{10} = \frac{1}{2\pi^2}\int_{\varphi_u}^{\pi/2}\int_{\alpha_{2b}}^{\alpha_{2s}} KEe^{j(mx+ny)}dxdy$
$I_{11} = \frac{1}{2\pi^2}\int_{\pi/2}^{\varphi_l}\int_{-\pi}^{\alpha_{3b}} -(1-K)Ee^{j(mx+ny)}dxdy$	$I_{12} = \frac{1}{2\pi^2}\int_{\pi/2}^{\varphi_l}\int_{\alpha_{3s}}^{\pi} -(1-K)Ee^{j(mx+ny)}dxdy$
$I_{13} = \frac{1}{2\pi^2}\int_{\varphi_l}^{\pi}\int_{\alpha_{4b}}^{\alpha_{4s}} -(1-K)Ee^{j(mx+ny)}dxdy$	$I_{14} = \frac{1}{2\pi^2}\int_{\varphi_l}^{\pi}\int_{-\pi}^{\alpha_{4b}} -Ee^{j(mx+ny)}dxdy$
$I_{15} = \frac{1}{2\pi^2}\int_{\varphi_l}^{\pi}\int_{\alpha_{4s}}^{\pi} -Ee^{j(mx+ny)}dxdy$	

TABLE 4.13 NULL INTEGRALS FOR C_{MN} WHEN M_A > MAX(K,1-K).

$I_{Z1} = \frac{1}{2\pi^2}\int_{-\varphi_l}^{-\pi/2}\int_{\alpha_{3b}}^{\alpha_{3s}} 0e^{j(mx+ny)}dxdy$	$I_{Z2} = \frac{1}{2\pi^2}\int_{-\pi/2}^{-\varphi_u}\int_{\alpha_{2s}}^{\pi} 0e^{j(mx+ny)}dxdy$
$I_{Z3} = \frac{1}{2\pi^2}\int_{-\pi/2}^{-\varphi_u}\int_{-\pi}^{\alpha_{2b}} 0e^{j(mx+ny)}dxdy$	$I_{Z4} = \frac{1}{2\pi^2}\int_{\varphi_u}^{\pi/2}\int_{\alpha_{2s}}^{\pi} 0e^{j(mx+ny)}dxdy$
$I_{Z5} = \frac{1}{2\pi^2}\int_{\varphi_u}^{\pi/2}\int_{-\pi}^{\alpha_{2b}} 0e^{j(mx+ny)}dxdy$	$I_{Z6} = \frac{1}{2\pi^2}\int_{\pi/2}^{\varphi_l}\int_{\alpha_{3b}}^{\alpha_{3s}} 0e^{j(mx+ny)}dxdy$

TABLE 4.14 LIMITS OF INTEGRATION FOR THE DIFFERENTIAL DX.

$\alpha_{1s} = \pi - 2\pi\frac{r_1}{1-K} + 2\pi\frac{r_1}{1-K}M\cos y$	$\alpha_{1b} = -\pi + 2\pi\frac{r_1-1}{K-1} + 2\pi\frac{1-r_1}{K-1}M\cos y$
$\alpha_{2s} = \pi - 2\pi r_2 + 2\pi\frac{r_2}{K}M\cos y$	$\alpha_{2b} = -\pi + 2\pi(1-r_2) + 2\pi\frac{r_2-1}{K}M\cos y$
$\alpha_{3s} = \pi + 2\pi\frac{r_3}{1-K}M\cos y$	$\alpha_{3b} = -\pi + 2\pi\frac{1-r_3}{K-1}M\cos y$
$\alpha_{4s} = \pi + 2\pi r_4\frac{1-K}{K} + 2\pi\frac{r_4}{K}M\cos y$	$\alpha_{4b} = -\pi + 2\pi(r_4-1)\frac{1-K}{K} + 2\pi\frac{r_4-1}{K}M\cos y$

UNIVERSITAT ROVIRA I VIRGILI
CONTRIBUTIONS ON SPECTRAL CONTROL FOR THE ASYMMETRICAL FULL BRIDGE MULTILEVEL INVERTER
Oscar Mauricio Muñoz Ramírez
ISBN:978-84-693-7665-2/DL:T.1747-2010

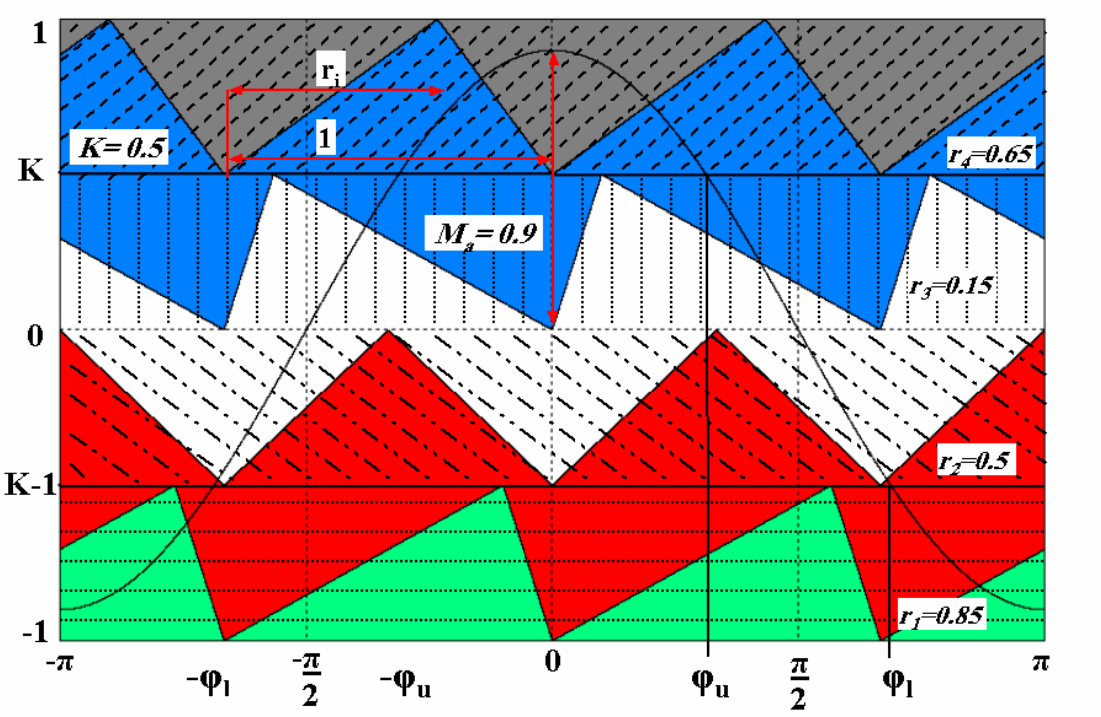

Figure 4.10 Five-level modulation (K=0.5, M_a=0.9).

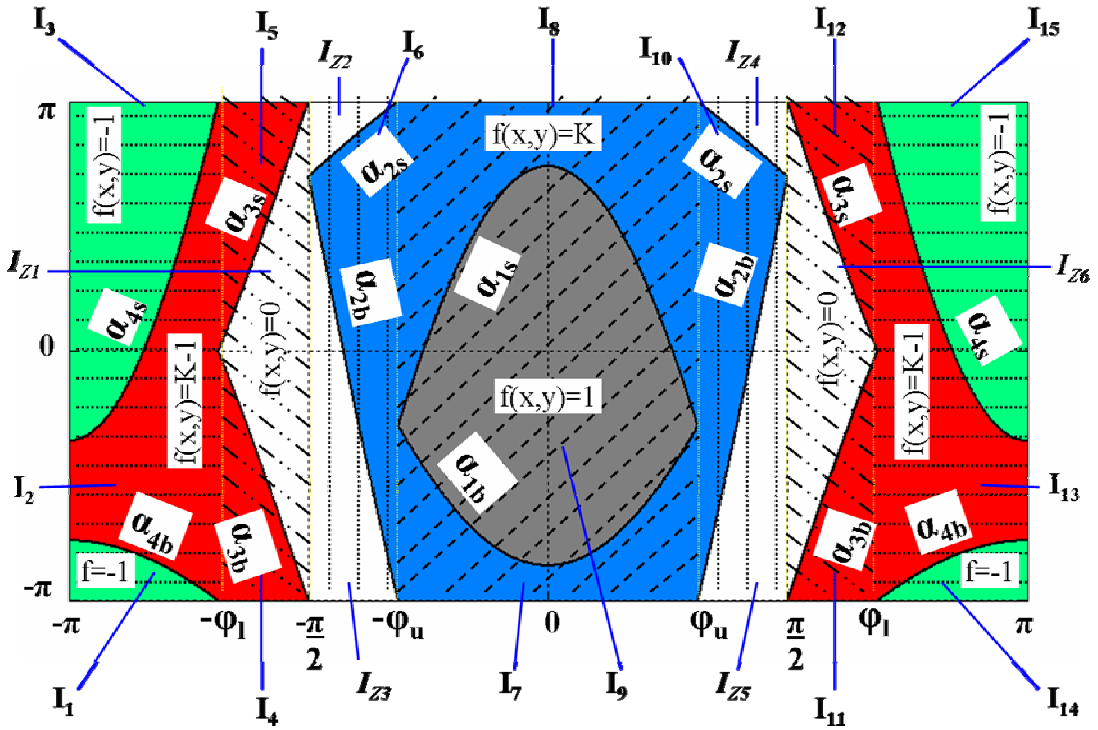

Figure 4.11 Contour plot to calculate C_{mn} (K=0.5, M_a=0.9).

UNIVERSITAT ROVIRA I VIRGILI
CONTRIBUTIONS ON SPECTRAL CONTROL FOR THE ASYMMETRICAL FULL BRIDGE MULTILEVEL INVERTER
Oscar Mauricio Muñoz Ramírez
ISBN:978-84-693-7665-2/DL:T.1747-2010

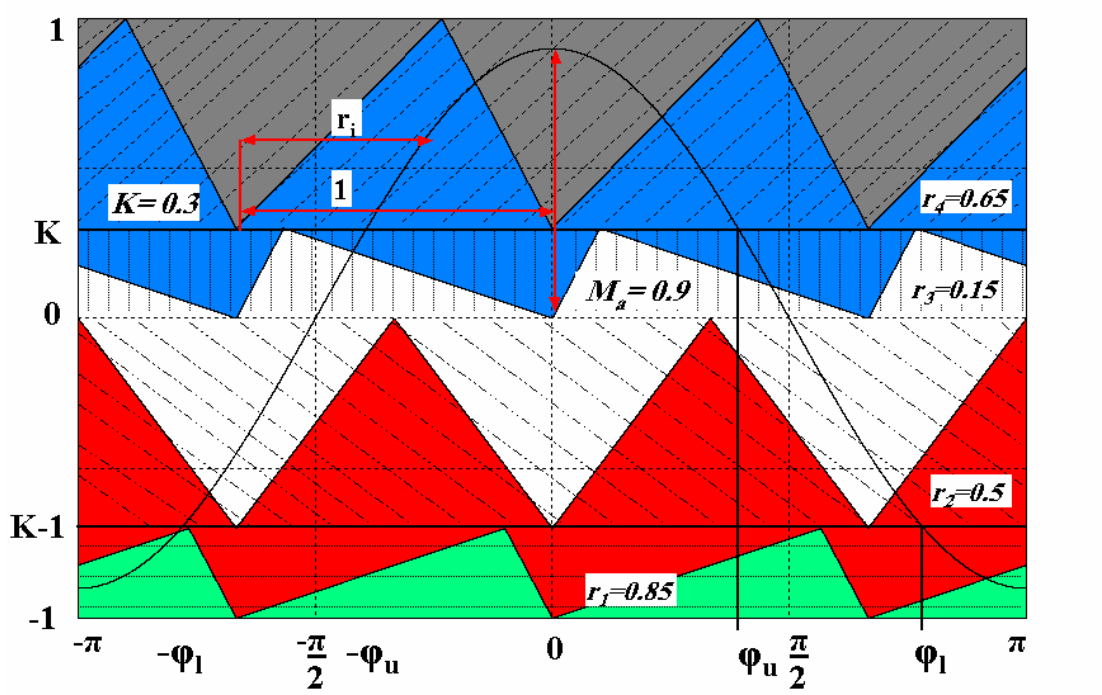

Figure 4.12 Five-level modulation (K=0.3, M_a=0.9).

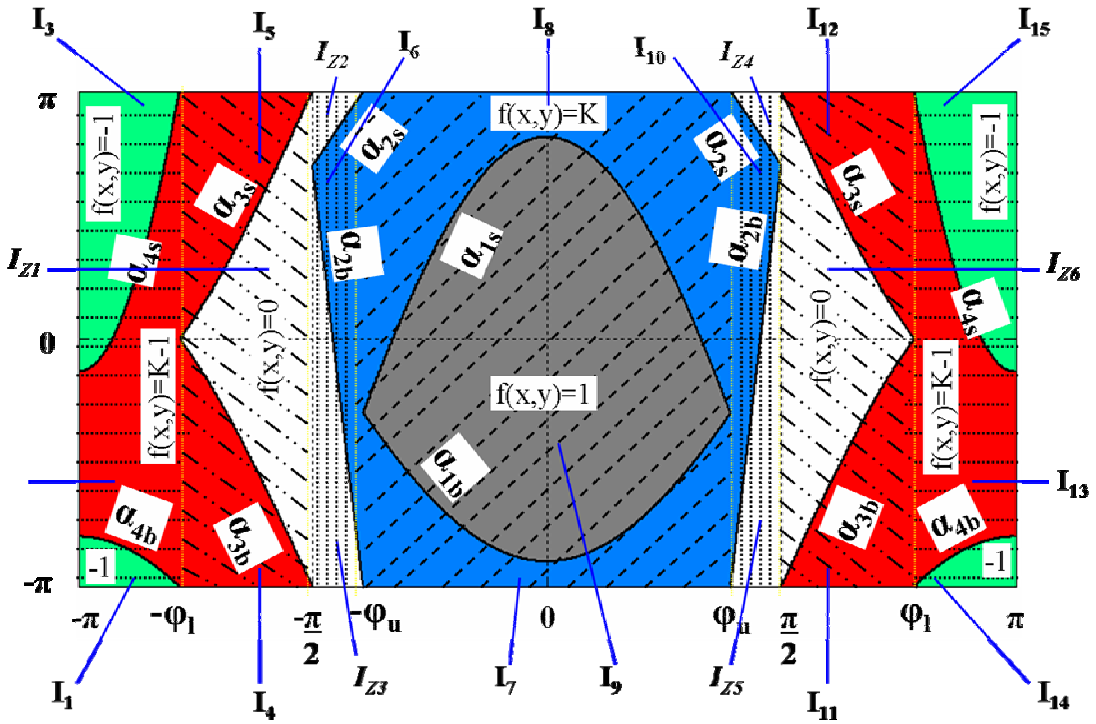

Figure 4.13 Contour plot to calculate C_{mn} (K=0.3, M_a=0.9).

4.4.2 Case (1–K)< M_a <K

For the second situation, as shown in figure 4.14, a set of 11 non-zero integrals are obtained in order to calculate C_{mn}; φ_u does not show in the external integral limits since the modulating

UNIVERSITAT ROVIRA I VIRGILI
CONTRIBUTIONS ON SPECTRAL CONTROL FOR THE ASYMMETRICAL FULL BRIDGE MULTILEVEL INVERTER
Oscar Mauricio Muñoz Ramírez
ISBN:978-84-693-7665-2/DL:T.1747-2010

signal does not switch to +E state. The definition of these integrals is supported on contour plot from figure 4.15. The solution for C_{mn} is summarized in table 4.15. The zero-null integrals are written in table 4.16.

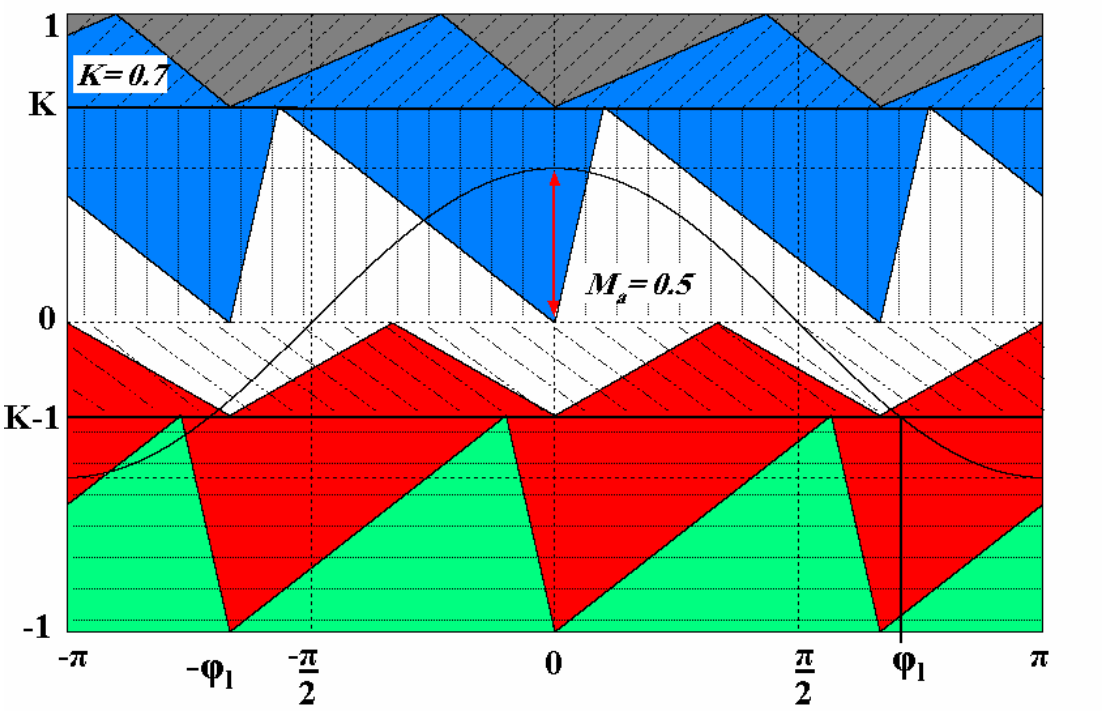

Figure 4.14 Five-level modulation (K=0.7, M_a=0.5).

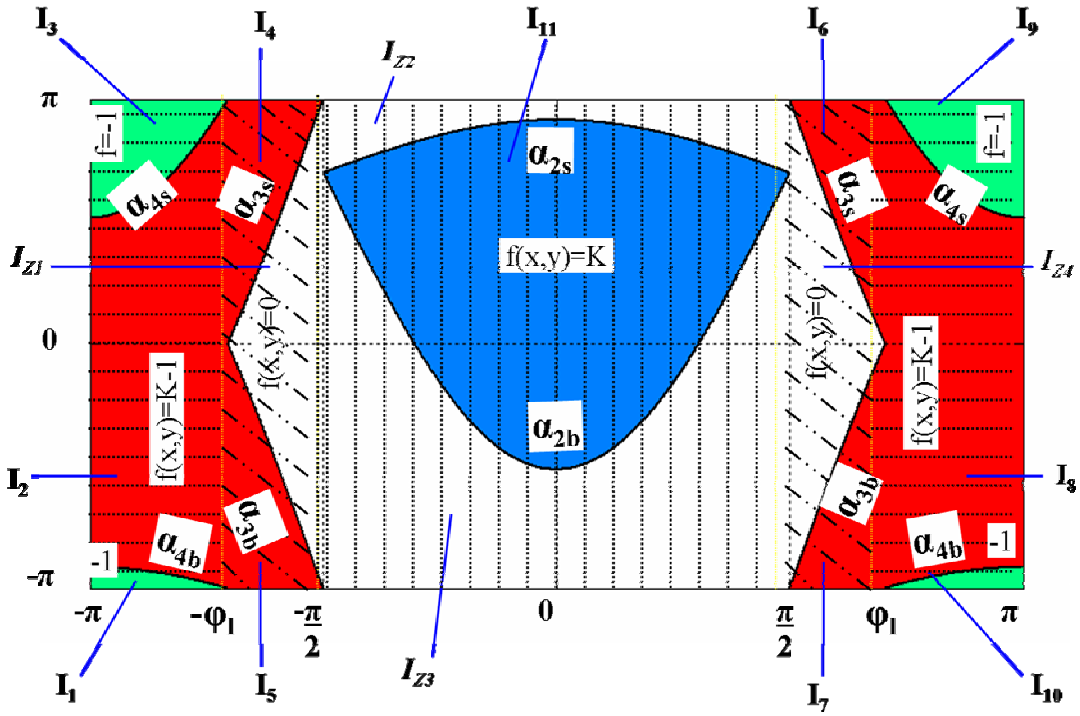

Figure 4.15 Contour plot to calculate C_{mn} (K=0.7, M_a=0.5).

UNIVERSITAT ROVIRA I VIRGILI
CONTRIBUTIONS ON SPECTRAL CONTROL FOR THE ASYMMETRICAL FULL BRIDGE MULTILEVEL INVERTER
Oscar Mauricio Muñoz Ramírez
ISBN:978-84-693-7665-2/DL:T.1747-2010

TABLE 4.15 SOLUTION FOR C_{MN} WHEN (1-K)< M_A <K.

$I_1 = \frac{1}{2\pi^2}\int_{-\pi}^{-\varphi_l}\int_{-\pi}^{\alpha_{4b}} -Ee^{j(mx+ny)}dxdy$	$I_2 = \frac{1}{2\pi^2}\int_{-\pi}^{-\varphi_l}\int_{\alpha_{4b}}^{\alpha_{4s}} -(1-K)Ee^{j(mx+ny)}dxdy$
$I_3 = \frac{1}{2\pi^2}\int_{-\pi}^{-\varphi_l}\int_{\alpha_{4s}}^{\pi} -Ee^{j(mx+ny)}dxdy$	$I_4 = \frac{1}{2\pi^2}\int_{-\varphi_l}^{-\pi/2}\int_{\alpha_{3s}}^{\pi} -(1-K)Ee^{j(mx+ny)}dxdy$
$I_5 = \frac{1}{2\pi^2}\int_{-\varphi_l}^{-\pi/2}\int_{-\pi}^{\alpha_{3b}} -(1-K)Ee^{j(mx+ny)}dxdy$	$I_6 = \frac{1}{2\pi^2}\int_{\pi/2}^{\varphi_l}\int_{\alpha_{3s}}^{\pi} -(1-K)Ee^{j(mx+ny)}dxdy$
$I_7 = \frac{1}{2\pi^2}\int_{\pi/2}^{\varphi_l}\int_{-\pi}^{\alpha_{3b}} -(1-K)Ee^{j(mx+ny)}dxdy$	$I_8 = \frac{1}{2\pi^2}\int_{\varphi_l}^{\pi}\int_{\alpha_{4b}}^{\alpha_{4s}} -(1-K)Ee^{j(mx+ny)}dxdy$
$I_9 = \frac{1}{2\pi^2}\int_{\varphi_l}^{\pi}\int_{\alpha_{4s}}^{\pi} -Ee^{j(mx+ny)}dxdy$	$I_{10} = \frac{1}{2\pi^2}\int_{\varphi_l}^{\pi}\int_{-\pi}^{\alpha_{4b}} -Ee^{j(mx+ny)}dxdy$
$I_{11} = \frac{1}{2\pi^2}\int_{-\pi/2}^{\pi/2}\int_{\alpha_{2b}}^{\alpha_{2s}} KEe^{j(mx+ny)}dxdy$	

TABLE 4.16 NULL INTEGRALS FOR C_{MN} WHEN (1-K)< M_A <K.

$I_{Z1} = \frac{1}{2\pi^2}\int_{-\varphi_l}^{-\pi/2}\int_{\alpha_{3b}}^{\alpha_{3s}} 0e^{j(mx+ny)}dxdy$	$I_{Z2} = \frac{1}{2\pi^2}\int_{-\pi/2}^{\pi/2}\int_{\alpha_{2s}}^{\pi} 0e^{j(mx+ny)}dxdy$
$I_{Z3} = \frac{1}{2\pi^2}\int_{-\pi/2}^{\pi/2}\int_{-\pi}^{\alpha_{2b}} 0e^{j(mx+ny)}dxdy$	$I_{Z4} = \frac{1}{2\pi^2}\int_{\pi/2}^{\varphi_l}\int_{\alpha_{3b}}^{\alpha_{3s}} 0e^{j(mx+ny)}dxdy$

4.4.3 Case K< M_a <1−K

For the third situation, as shown in figure 4.16, a set of 9 non-zero integrals are obtained in order to calculate C_{mn}; φ_l does not show in the external integral limits since the modulating signal does not switch to -E state. The definition of these integrals is supported on contour plot from figure 4.17. On the other hand, four null integrals are obtained. The solution for C_{mn} is summarized in table 4.17 whereas in table 4.18 six null integrals are given.

UNIVERSITAT ROVIRA I VIRGILI
CONTRIBUTIONS ON SPECTRAL CONTROL FOR THE ASYMMETRICAL FULL BRIDGE MULTILEVEL INVERTER
Oscar Mauricio Muñoz Ramírez
ISBN:978-84-693-7665-2/DL:T.1747-2010

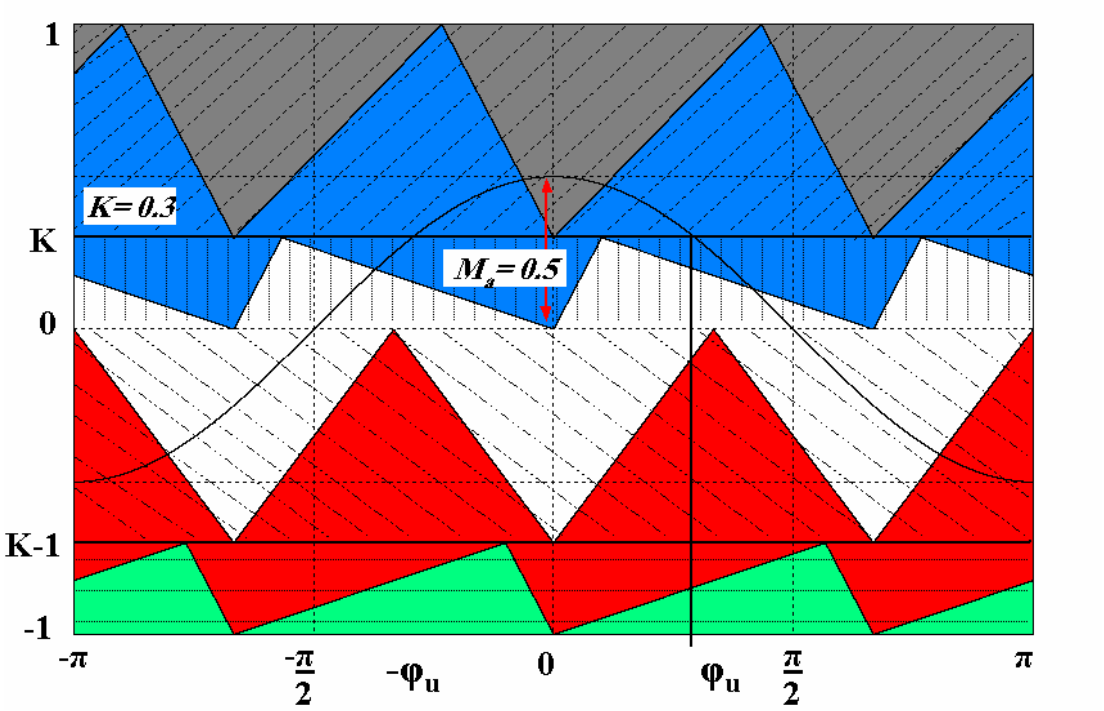

Figure 4.16 Five-level modulation (K=0.3, M_a=0.5).

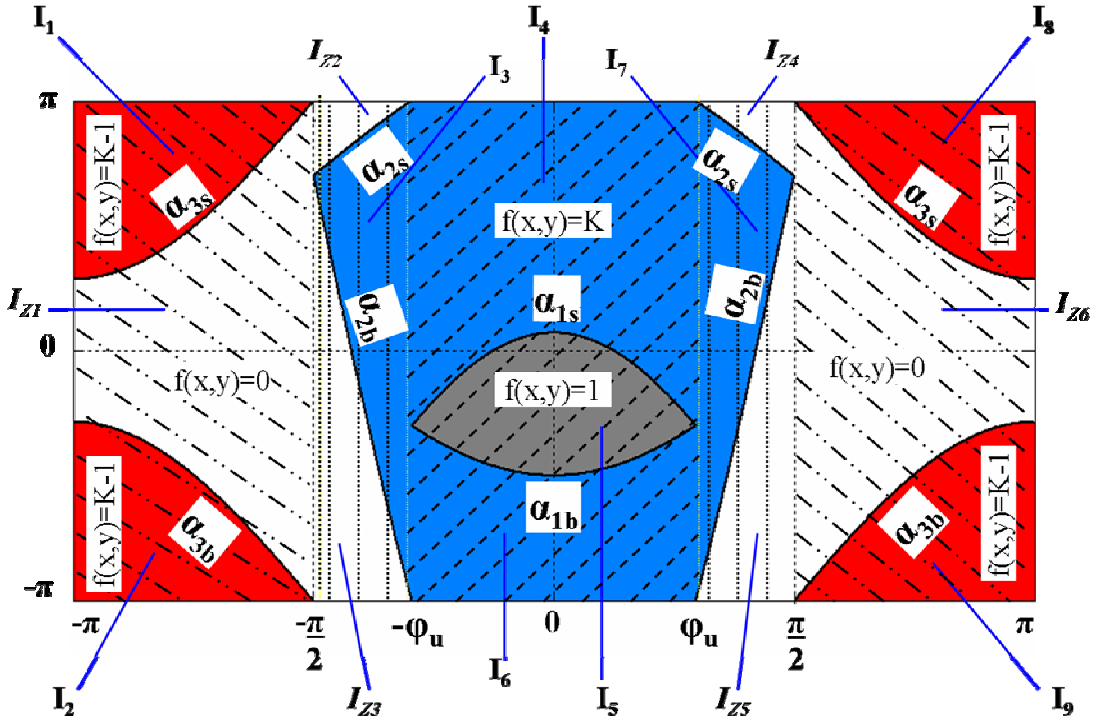

Figure 4.17 Contour plot to calculate C_{mn} (K=0.3, M_a=0.5).

UNIVERSITAT ROVIRA I VIRGILI
CONTRIBUTIONS ON SPECTRAL CONTROL FOR THE ASYMMETRICAL FULL BRIDGE MULTILEVEL INVERTER
Oscar Mauricio Muñoz Ramírez
ISBN:978-84-693-7665-2/DL:T.1747-2010

TABLE 4.17 SOLUTION FOR C_{MN} WHEN $K < M_A < (1-K)$.

$I_1 = \frac{1}{2\pi^2}\int_{-\pi}^{-\pi/2}\int_{\alpha_{3s}}^{\pi} -(1-K)Ee^{j(mx+ny)}dxdy$	$I_2 = \frac{1}{2\pi^2}\int_{-\pi}^{-\pi/2}\int_{-\pi}^{\alpha_{3b}} -(1-K)Ee^{j(mx+ny)}dxdy$
$I_3 = \frac{1}{2\pi^2}\int_{-\pi/2}^{-\varphi_u}\int_{\alpha_{2b}}^{\alpha_{2s}} KEe^{j(mx+ny)}dxdy$	$I_4 = \frac{1}{2\pi^2}\int_{-\varphi_u}^{\varphi_u}\int_{\alpha_{1s}}^{\pi} KEe^{j(mx+ny)}dxdy$
$I_5 = \frac{1}{2\pi^2}\int_{-\varphi_u}^{\varphi_u}\int_{\alpha_{1b}}^{\alpha_{1s}} Ee^{j(mx+ny)}dxdy$	$I_6 = \frac{1}{2\pi^2}\int_{-\varphi_u}^{\varphi_u}\int_{-\pi}^{\alpha_{1b}} KEe^{j(mx+ny)}dxdy$
$I_7 = \frac{1}{2\pi^2}\int_{\varphi_u}^{\pi/2}\int_{\alpha_{2b}}^{\alpha_{2s}} KEe^{j(mx+ny)}dxdy$	$I_8 = \frac{1}{2\pi^2}\int_{\pi/2}^{\pi}\int_{\alpha_{3s}}^{\pi} -(1-K)Ee^{j(mx+ny)}dxdy$
$I_9 = \frac{1}{2\pi^2}\int_{\pi/2}^{\pi}\int_{-\pi}^{\alpha_{3b}} -(1+K)Ee^{j(mx+ny)}dxdy$	

TABLE 4.18 NULL INTEGRALS FOR C_{MN} WHEN $K < M_A < (1-K)$.

$I_{Z1} = \frac{1}{2\pi^2}\int_{-\pi}^{-\pi/2}\int_{\alpha_{3b}}^{\alpha_{3s}} 0e^{j(mx+ny)}dxdy$	$I_{Z2} = \frac{1}{2\pi^2}\int_{-\pi/2}^{-\varphi_u}\int_{\alpha_{2s}}^{\pi} 0e^{j(mx+ny)}dxdy$
$I_{Z3} = \frac{1}{2\pi^2}\int_{-\pi/2}^{-\varphi_u}\int_{-\pi}^{\alpha_{2b}} 0e^{j(mx+ny)}dxdy$	$I_{Z4} = \frac{1}{2\pi^2}\int_{\varphi_u}^{\pi/2}\int_{\alpha_{2s}}^{\pi} 0e^{j(mx+ny)}dxdy$
$I_{Z5} = \frac{1}{2\pi^2}\int_{\varphi_u}^{\pi/2}\int_{-\pi}^{\alpha_{2b}} 0e^{j(mx+ny)}dxdy$	$I_{Z6} = \frac{1}{2\pi^2}\int_{\pi/2}^{\pi}\int_{\alpha_{3b}}^{\alpha_{3s}} 0e^{j(mx+ny)}dxdy$

4.4.4 Case M_a <min(K,1−K)

Finally, in the fourth situation, as shown in figure 4.18, a set of five non-zero integrals are obtained in order to calculate C_{mn}; φ_u does not show in the external integral limits, neither does φ_l, since the modulating signal does not switch to $+E$ nor $-E$ level states. The definition of these integrals is supported on contour plot from figure 4.19. The four null integrals are detailed in table 4.20 and the solution for C_{mn} is summarized in table 4.19.

UNIVERSITAT ROVIRA I VIRGILI
CONTRIBUTIONS ON SPECTRAL CONTROL FOR THE ASYMMETRICAL FULL BRIDGE MULTILEVEL INVERTER
Oscar Mauricio Muñoz Ramírez
ISBN:978-84-693-7665-2/DL:T.1747-2010

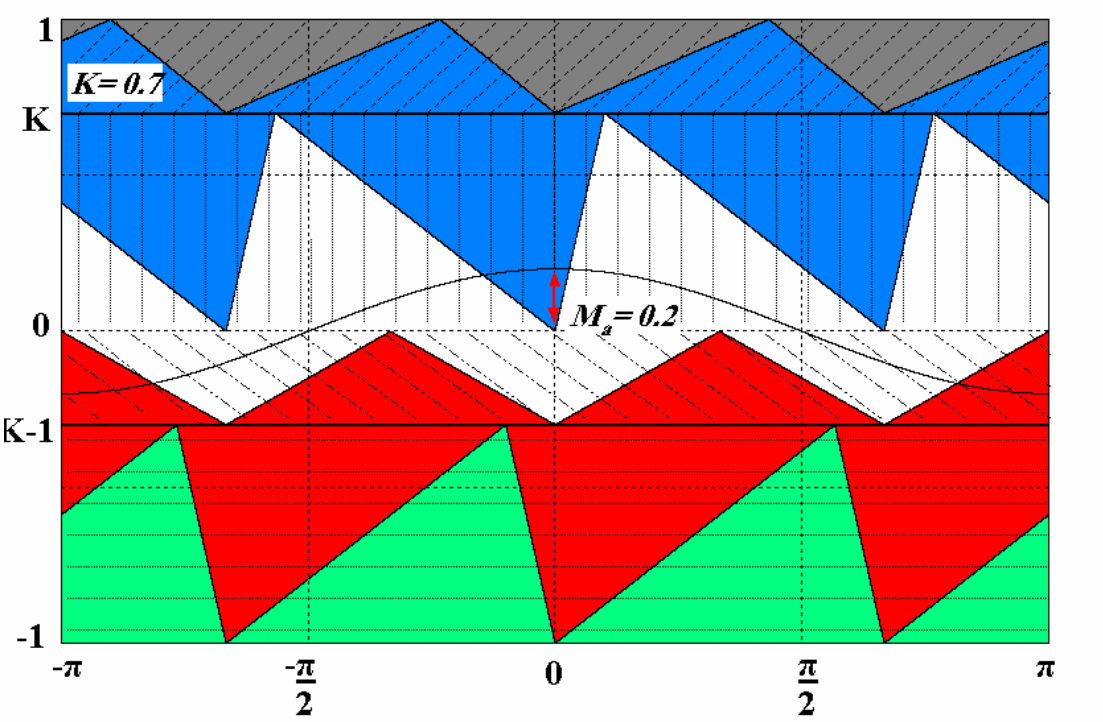

Figure 4.18 Five-level modulation (K=0.7, M_a=0.2).

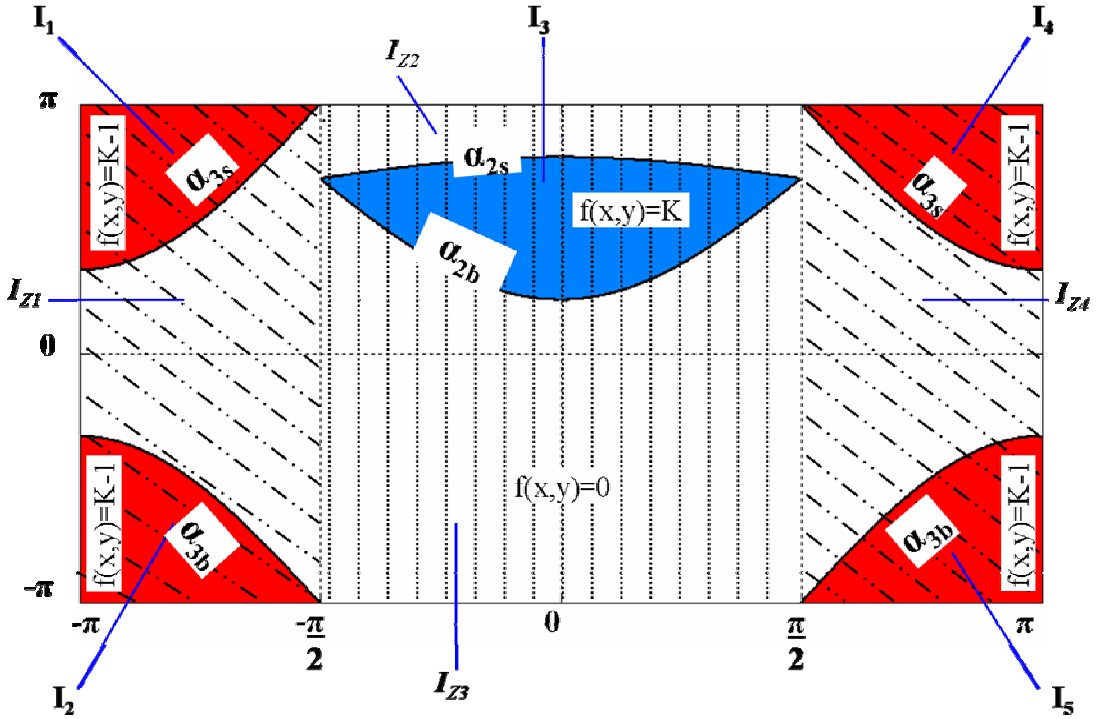

Figure 4.19 Contour plot to calculate C_{mn} (K=0.7, M_a=0.2).

UNIVERSITAT ROVIRA I VIRGILI
CONTRIBUTIONS ON SPECTRAL CONTROL FOR THE ASYMMETRICAL FULL BRIDGE MULTILEVEL INVERTER
Oscar Mauricio Muñoz Ramírez
ISBN:978-84-693-7665-2/DL:T.1747-2010

TABLE 4.19 SOLUTION FOR C_{MN} WHEN M_A <MIN(K,1-K).

$I_1 = \frac{1}{2\pi^2}\int_{-\pi}^{-\pi/2}\int_{\alpha_{3s}}^{\pi} -(1-K)Ee^{j(mx+ny)}dxdy$	$I_2 = \frac{1}{2\pi^2}\int_{-\pi}^{-\pi/2}\int_{-\pi}^{\alpha_{3b}} -(1-K)Ee^{j(mx+ny)}dxdy$
$I_3 = \frac{1}{2\pi^2}\int_{-\pi/2}^{\pi/2}\int_{\alpha_{2b}}^{\alpha_{2s}} KEe^{j(mx+ny)}dxdy$	$I_4 = \frac{1}{2\pi^2}\int_{\pi/2}^{\pi}\int_{\alpha_{3s}}^{\pi} KEe^{j(mx+ny)}dxdy$
$I_5 = \frac{1}{2\pi^2}\int_{\pi/2}^{\pi}\int_{-\pi}^{\alpha_{3b}} KEe^{j(mx+ny)}dxdy$	

TABLE 4.20 NULL INTEGRALS FOR C_{MN} WHEN M_A <MIN(K,1-K).

$I_{Z1} = \frac{1}{2\pi^2}\int_{-\pi}^{-\pi/2}\int_{\alpha_{3b}}^{\alpha_{3s}} 0e^{j(mx+ny)}dxdy$	$I_{Z2} = \frac{1}{2\pi^2}\int_{-\pi/2}^{\pi/2}\int_{\alpha_{2s}}^{\pi} 0e^{j(mx+ny)}dxdy$
$I_{Z3} = \frac{1}{2\pi^2}\int_{-\pi/2}^{\pi/2}\int_{-\pi}^{\alpha_{2b}} 0e^{j(mx+ny)}dxdy$	$I_{Z4} = \frac{1}{2\pi^2}\int_{\pi/2}^{\pi}\int_{\alpha_{3b}}^{\alpha_{3s}} 0e^{j(mx+ny)}dxdy$

4.4.5 DFS calculation example, case M_a>max(K,1–K)

$$\text{Carrier}_1:\quad I_8 \equiv \int_{-\varphi_u}^{\varphi_u}\int_{\alpha_{1s}}^{\pi} K \;+ I_7 \equiv \int_{-\varphi_u}^{\varphi_u}\int_{-\pi}^{\alpha_{1b}} K \;+ I_9 \equiv \int_{-\varphi_u}^{\varphi_u}\int_{\alpha_{1b}}^{\alpha_{1s}} +1 \;+\ldots$$

$$\text{Carrier}_2:\quad I_6 \equiv \int_{-\pi/2}^{-\varphi_u}\int_{\alpha_{2b}}^{\alpha_{2s}} K \;+ I_{10} \equiv \int_{\varphi_u}^{\pi/2}\int_{\alpha_{2b}}^{\alpha_{2s}} K +\ldots$$

$$\text{Carrier}_3:\quad I_5 \equiv \int_{-\varphi_l}^{-\pi/2}\int_{\alpha_{3b}}^{\pi} -(1-K) \;+ I_4 \equiv \int_{-\varphi_l}^{-\pi/2}\int_{-\pi}^{\alpha_{3b}} -(1-K) \;+\ldots$$

$$I_{12} \equiv \int_{\pi/2}^{\varphi_l}\int_{\alpha_{3s}}^{\pi} -(1-K) \;+ I_{11} \equiv \int_{\pi/2}^{\varphi_l}\int_{-\pi}^{\alpha_{3b}} -(1-K) \;+\ldots$$

$$\text{Carrier}_4:\quad I_{15} \equiv \int_{\varphi_l}^{\pi}\int_{\alpha_{4s}}^{\pi} -1 \;+ I_{13} \equiv \int_{\varphi_l}^{\pi}\int_{\alpha_{4b}}^{\alpha_{4s}} -(1-K) \;+ I_{14} \equiv \int_{\varphi_l}^{\pi}\int_{-\pi}^{\alpha_{4b}} -1 +\ldots$$

$$I_1 \equiv \int_{-\pi}^{-\varphi_l}\int_{\alpha_{4b}}^{\pi} -1 \;+ I_2 \equiv \int_{-\pi}^{-\varphi_l}\int_{\alpha_{4b}}^{\alpha_{4s}} -(1-K) \;+ I_3 \equiv \int_{-\pi}^{-\varphi_l}\int_{-\pi}^{\alpha_{4b}} -1 \qquad (4.7)$$

Observing the inner integral definition (the differential *dx*), the limits of integration can be organized using the order of carriers, starting from the highest carrier to the lowest carrier. Besides, two well discernible groups define the contributions in the positive semi-cycle and the negative semi-cycle of the fundamental frequency. The non-zero integrals are organized

UNIVERSITAT ROVIRA I VIRGILI
CONTRIBUTIONS ON SPECTRAL CONTROL FOR THE ASYMMETRICAL FULL BRIDGE MULTILEVEL INVERTER
Oscar Mauricio Muñoz Ramírez
ISBN:978-84-693-7665-2/DL:T.1747-2010

according to these criterions, and for some facility, we gathered the integrals in separated groups by following the order of the carriers, starting with the highest carrier, carrier$_1$, and ending with the lowest carrier, carrier$_4$. The sketch of expression (4.7) was useful when implementing the algorithm that computed all the definite integrals.

The sum of these fifteen integrals is what finally computes one C_{mn} coefficient. Later, the DFS is performed by composing every harmonic h using the condition $h = m*M_f + n$. In order to make more flexible the formulation with all the integrals, some manipulation on the angle expressions is done, as shown in table 4.21. Reorganizing the inner limits of integration was helpful when the code was finally written and executed by the algorithm done in Matlab, namely C_{mn}-Algorithm.

TABLE 4.21 REORGANIZATION OF LIMITS OF INTEGRATION, DX.

$\alpha_{4s} = \alpha_4 + \Delta_4 \cos y$ $\alpha_4 = \pi + 2\pi r_4 \frac{1-K}{K};\ \Delta_4 = 2\pi \frac{r_4}{K} M$	$\alpha_{4b} = \beta_4 - \lambda_4 \cos y$ $\beta_4 = -\pi - 2\pi(1-r_4)\frac{1-K}{K};\ \lambda_4 = 2\pi \frac{1-r_4}{K} M$
$\alpha_{3s} = \alpha_3 + \Delta_3 \cos y$ $\alpha_3 = \pi;\ \Delta_3 = 2\pi \frac{r_3}{1-K} M$	$\alpha_{3b} = \beta_3 - \lambda_3 \cos y$ $\beta_3 = -\pi;\ \lambda_3 = 2\pi \frac{(1-r_3)}{1-K} M$
$\alpha_{2s} = \alpha_2 + \Delta_2 \cos y$ $\alpha_2 = \pi - 2\pi r_2;\ \Delta_2 = 2\pi \frac{r_2}{K} M$	$\alpha_{2b} = \beta_2 - \lambda_2 \cos y$ $\beta_2 = -\pi + 2\pi(1-r_2);\ \lambda_2 = 2\pi \frac{1-r_2}{K} M$
$\alpha_{1s} = \alpha_1 + \Delta_1 \cos y$ $\alpha_1 = \pi - 2\pi \frac{r_1}{1-K};\ \Delta_1 = 2\pi \frac{r_1}{1-K} M$	$\alpha_{1b} = \beta_1 - \lambda_1 \cos y$ $\beta_1 = -\pi + 2\pi \frac{1-r_1}{1-K};\ \lambda_1 = 2\pi \frac{1-r_1}{1-K} M$

In particular, detailed description of solving the solution of C_{mn} coefficients for 5-level PD-PWM modulation can be seen at Appendix A whereas the numerical computation code is referenced to Appendix D. In both appendices A and D, this particular solution is partitioned and presented in the four portions that a modulated signal comprises its spectrum:

the fundamental harmonic, $C_{01}=A_{01}+jB_{01}$

the fundamental multiple harmonics, $C_{0n}=A_{0n}+jB_{0n}$, where $n=2\ldots\infty$

the carrier multiple harmonics and, $C_{m\,0}=A_{m\,0}+jB_{m\,0}$, where $m=1\ldots\infty$

the sideband harmonics, $C_{mn}=A_{mn}+jB_{mn}$, where $m=1\ldots\infty$ and, $n=-\infty\ldots\infty$ and $n\neq 0$

UNIVERSITAT ROVIRA I VIRGILI
CONTRIBUTIONS ON SPECTRAL CONTROL FOR THE ASYMMETRICAL FULL BRIDGE MULTILEVEL INVERTER
Oscar Mauricio Muñoz Ramírez
ISBN:978-84-693-7665-2/DL:T.1747-2010

The following table helps to trace the composition of some harmonics, in order to check the correct computation of the spectrum components.

TABLE 4.22 EXAMPLES OF C_{MN} COEFFICIENTS FOR COMPOSING ONE HARMONIC *H*.

Harmonic *h*	**M_f=50**	**M_f=11**
1	$C_{0,1}$ $C_{1,-49}$ $C_{2,-99}\cdots$	$C_{0,1}$ $C_{1,-10}$ $C_{2,-21}$ $C_{3,-32}\cdots$
2	$C_{0,2}$ $C_{1,-48}$ $C_{2,-98}\cdots$	$C_{0,2}$ $C_{1,-9}$ $C_{2,-20}$ $C_{3,-31}\cdots$
3	$C_{0,3}$ $C_{1,-47}$ $C_{2,-97}\cdots$	$C_{0,3}$ $C_{1,-8}$ $C_{2,-19}$ $C_{3,-30}\cdots$
4	$C_{0,4}$ $C_{1,-46}$ $C_{2,-96}\cdots$	$C_{0,4}$ $C_{1,-7}$ $C_{2,-18}$ $C_{3,-29}\cdots$
5	$C_{0,5}$ $C_{1,-45}$ $C_{2,-95}\cdots$	$C_{0,5}$ $C_{1,-6}$ $C_{2,-17}$ $C_{3,-28}\cdots$
6	$C_{0,5}$ $C_{1,-44}$ $C_{2,-94}\cdots$	$C_{0,6}$ $C_{1,-5}$ $C_{2,-16}$ $C_{3,-27}\cdots$
7	$C_{0,5}$ $C_{1,-43}$ $C_{2,-93}\cdots$	$C_{0,7}$ $C_{1,-4}$ $C_{2,-15}$ $C_{3,-26}\cdots$
8	$C_{0,5}$ $C_{1,-42}$ $C_{2,-92}\cdots$	$C_{0,8}$ $C_{1,-3}$ $C_{2,-14}$ $C_{3,-25}\cdots$
9	$C_{0,5}$ $C_{1,-41}$ $C_{2,-91}\cdots$	$C_{0,9}$ $C_{1,-2}$ $C_{2,-13}$ $C_{3,-24}\cdots$
10	$C_{0,5}$ $C_{1,-40}$ $C_{2,-90}\cdots$	$C_{0,10}$ $C_{1,-1}$ $C_{2,-12}$ $C_{3,-23}\cdots$
11	$C_{0,5}$ $C_{1,-39}$ $C_{2,-89}\cdots$	$C_{0,11}$ $C_{1,0}$ $C_{2,-11}$ $C_{3,-22}\cdots$
12	$C_{0,5}$ $C_{1,-38}$ $C_{2,-88}\cdots$	$C_{0,12}$ $C_{1,1}$ $C_{2,-10}$ $C_{3,-21}\cdots$
13	$C_{0,5}$ $C_{1,-37}$ $C_{2,-87}\cdots$	$C_{0,13}$ $C_{1,2}$ $C_{2,-9}$ $C_{3,-20}\cdots$
14	$C_{0,5}$ $C_{1,-36}$ $C_{2,-86}\cdots$	$C_{0,14}$ $C_{1,3}$ $C_{2,-8}$ $C_{3,-19}$ $C_{4,-30}\cdots$
15	$C_{0,5}$ $C_{1,-35}$ $C_{2,-85}\cdots$	$C_{0,15}$ $C_{1,4}$ $C_{2,-7}$ $C_{3,-18}$ $C_{4,-29}\cdots$
16	$C_{0,5}$ $C_{1,-34}$ $C_{2,-84}\cdots$	$C_{0,16}$ $C_{1,5}$ $C_{2,-6}$ $C_{3,-17}$ $C_{4,-28}\cdots$
17	$C_{0,5}$ $C_{1,-33}$ $C_{2,-83}\cdots$	$C_{0,17}$ $C_{1,6}$ $C_{2,-5}$ $C_{3,-16}$ $C_{4,-27}\cdots$
18	$C_{0,5}$ $C_{1,-32}$ $C_{2,-82}\cdots$	$C_{0,18}$ $C_{1,7}$ $C_{2,-4}$ $C_{3,-15}$ $C_{4,-26}\cdots$
19	$C_{0,5}$ $C_{1,-31}$ $C_{2,-81}\cdots$	$C_{0,19}$ $C_{1,8}$ $C_{2,-3}$ $C_{3,-14}$ $C_{4,-25}\cdots$
20	$C_{0,5}$ $C_{1,-30}$ $C_{2,-80}\cdots$	$C_{0,20}$ $C_{1,9}$ $C_{2,-2}$ $C_{3,-13}$ $C_{4,-24}\cdots$
21	$C_{0,5}$ $C_{1,-29}$ $C_{2,-79}\cdots$	$C_{0,21}$ $C_{1,10}$ $C_{2,-1}$ $C_{3,-12}$ $C_{4,-23}\cdots$
22	$C_{0,5}$ $C_{1,-28}$ $C_{2,-78}\cdots$	$C_{0,22}$ $C_{1,11}$ $C_{2,0}$ $C_{3,-11}$ $C_{4,-22}\cdots$
23	$C_{0,5}$ $C_{1,-27}$ $C_{2,-77}\cdots$	$C_{0,23}$ $C_{1,12}$ $C_{2,1}$ $C_{3,-10}$ $C_{4,-21}\cdots$
24	$C_{0,5}$ $C_{1,-26}$ $C_{2,-76}\cdots$	$C_{0,24}$ $C_{1,13}$ $C_{2,2}$ $C_{3,-9}$ $C_{4,-20}\cdots$
25	$C_{0,5}$ $C_{1,-25}$ $C_{2,-75}\cdots$	$C_{0,25}$ $C_{1,14}$ $C_{2,3}$ $C_{3,-8}$ $C_{4,-19}\cdots$

Figure 4.20 comprises six waveforms for the situation $M_a > max(K,1-K)$ where two cases of carrier programming are calculated for three values of level distribution; such waveforms are obtained using equation (4.6) with the input parameters E=50 V, M_a=0.9. The systematic calculation of the harmonics uses the condition $h = m*M_f + n$, yielding the DFS that represents the continuos time signal. This method is simply called C_{mn}-Algorithm, an application implemented in Matlab software. Figure 4.20 shows two different carrier sets and

UNIVERSITAT ROVIRA I VIRGILI
CONTRIBUTIONS ON SPECTRAL CONTROL FOR THE ASYMMETRICAL FULL BRIDGE MULTILEVEL INVERTER
Oscar Mauricio Muñoz Ramírez
ISBN:978-84-693-7665-2/DL:T.1747-2010

three values of K. For an easy and quick visual demonstration, frequency index M_f is selected as eleven.

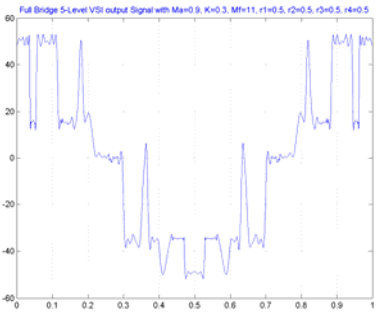

a) K=0.3, r_1=0.5, r_2=0.5, r_3=0.5, r_4=0.5

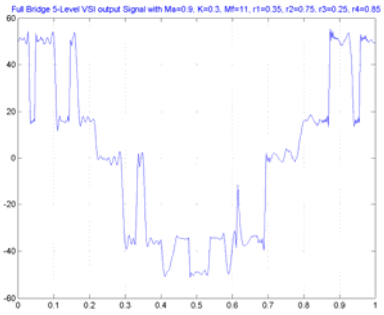

d) r_1=0.35, r_2=0.75, r_3=0.25, r_4=0.85

b) K=0.5, r_1=0.5, r_2=0.5, r_3=0.5, r_4=0.5

e) K=0.5, r_1=0.35, r_2=0.75, r_3=0.25, r_4=0.85

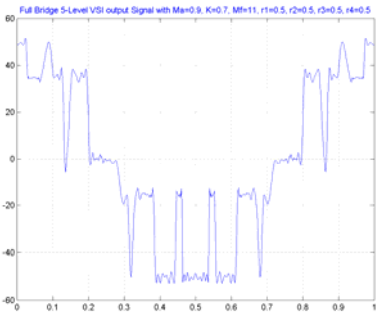

c) K=0.7, r_1=0.5, r_2=0.5, r_3=0.5, r_4=0.5

f) K=0.7, r_1=0.35, r_2=0.75, r_3=0.25, r_4=0.85

Figure 4.20 Continuos time signals using C_{mn}-Algorithm.

Although differences can be noticed between cases of carrier sets, the task of selecting a optimum case can become ambiguos when more cases are analyzed if time domain waveforms are used. Spectra comparisons are more suitable for such task, especially if M_f=50. However, the waveforms in figure 4.20 illustrates the good performance of the algorithm implemented in Matlab software which computes the solution of C_{mn} coefficients based on equation (4.6), E=50 V, M_a=0.9, M_f=11.

UNIVERSITAT ROVIRA I VIRGILI
CONTRIBUTIONS ON SPECTRAL CONTROL FOR THE ASYMMETRICAL FULL BRIDGE MULTILEVEL INVERTER
Oscar Mauricio Muñoz Ramírez
ISBN:978-84-693-7665-2/DL:T.1747-2010

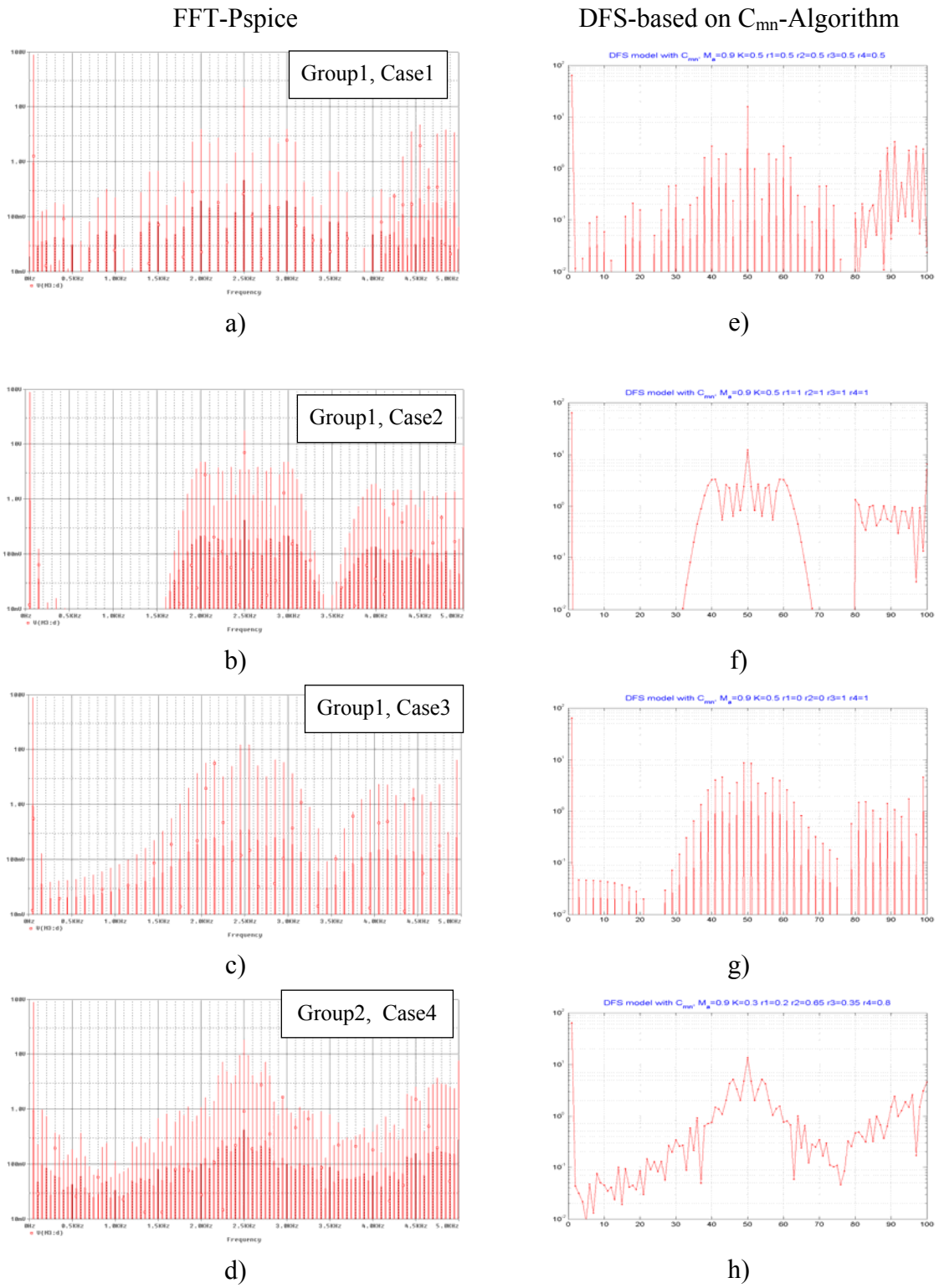

Figure 4.21 Comparisons between FFT and DFS performance.

Figure 4.20 has continuos time waveforms and if compared to their homologus waveform obtaind with a circuit simulator, the conclusions about resemblance would be imprecise. In contrast to continuos time signals, spectral comparison between two harmonic predictive tools is easier; for instance, such comparison is dealt in figure 4.21 where M_f=50 and the

resemblance can be detected easier than if continuos time signals were compared. On left column there are spectra based on circuit simulator FFT and on the right column there are the spectra modeled with C_{mn}-Algorithm.

Spectra obtained using Pspice simulations were done with ten fundamental cycles and 100ns of step size. The input parameters of C_{mn}-Algortihm to calculate the harmonics amplitudes are: m_{max}=5, q_{max}=20, and five overlap groups which means $n_{max}=M_f*m_{max}$. The couples of figures a-e, as well as b-f, have great resemblance; on the other hand, pairs c-g and d-h though being identycal do not give an immediate conclusion about their resemblance. Larger values for input parameters, m_{max} and q_{max}, refine the calculation of C_{mn}-Algorithm and the decision of increasing computing time depends on whether a continuos time waveform is required or a wide band of harmonics is pictured. For narrower band, such as the baseband of the AFBMI, the metioned input parameters are sufficient.

Various theoretical spectra can be observed at Appendix B where it is demonstrated the validity of equation (4.6), written in table 4.12. In this appendix, for various cases of carrier programming, the theoretical spectra are compared with experimental spectra and with a more simplified spectra model based on SFS and detailed on the following chapter. Comparing the spectra is much easier than comparing their respective time domain signals; then the effects of carrier programming using equation (4.6) can be studied when observing the spectra. Equation (4.6) calculates the exact spectrum by means of coefficients C_{mn} and on the basis of Natural Sampling. Such coefficients compose every calculated harmonic in accordance to the condition given in (3.19), re-written as $h = m*M_f + n$, and finally performing the DFS that synthesizes the output voltage waveform. Experimental spectrum and simplified spectrum model match the spectrum of modulation based on Pseudo-Natural Sampling, a terminology that we introduced and explain in Chapter 5.

UNIVERSITAT ROVIRA I VIRGILI
CONTRIBUTIONS ON SPECTRAL CONTROL FOR THE ASYMMETRICAL FULL BRIDGE MULTILEVEL INVERTER
Oscar Mauricio Muñoz Ramírez
ISBN:978-84-693-7665-2/DL:T.1747-2010

ISBN:978-84-693-7665-2/DL:T.1747-2010

5. Pseudo-Natural Modulation

5.1 Natural and Regular Sampling Methods for SPWM

There are two options to calculate and transmit the switching pulses that are generated by a N-level-SPWM modulator, wherein a modulating waveform is compared with N-1 carrier signals and as a result, the appropriate gating sequence of the switching devices is generated. Natural Sampling and Regular Sampling are the most common ways of obtaining the commutation instants by means of an analog or a digital circuit. Natural Sampling is the mechanism where the modulator signal is continuously sampled, otherwise, when the modulator signal is sampled at discrete instants the process is named Regular Sample.

The DFS formulation is a useful tool that can be validated for harmonics calculation with a SPWM circuit based on Natural Sample method. It means that SPWM decisions must be realized by an analog control circuit wherein the reference and the carriers are generated as continuous signals. An analog circuit computes immediately the exact solution at which the sinusoidal reference and the carrier intersect. Thus, the output waveform contains a spectrum that can be represented by using a DFS formulation. However, when accomplishing the exact solution for switching instants, such analog modulator can have some difficulties when it must adapt the shape-factor for its carrier signals. Such task, although not impossible to implement, is somewhat tedious for successive reconfigurations which means extra time costs. Even having in advance simulations based-on designs, working with an analog modulator is a slow and exhaustive quest when it is necessary to find the suitable harmonic profiles that are obtained by modifying shape-factor cases. Aditionally, an analog implementation has some drawbacks such as tolerance in passive elements, susceptibility to noise and temperature dependence. Additionally, a analog modulator does not have flexibility if extra configurations for other types of SPWM such as POD and APOD are needed.

Because of its nature, a digital circuit is intended to implement a Regular Sampling function whereas an analog circuit can have the exactitude to calculate the instants of Natural Sample. The solution of a sinusoidal reference intersecting a carrier can be found by solving a transcendental equation; this is done intrinsically in the analog modulator. On the other hand, the digital circuit might require a long time to compute such solution within a certain interval of accuracy but it will never be the exact solution. To avoid such a long computing time, the most extended choice is to take one sample (*Symmetrical Regular Samplingl*) or two samples

(*Asymmetrical Regular Sampling*) of the reference signal and by plotting a projection to the falling and rising slopes of the carrier, then the commutation instants are easily calculated with an acceptable accuracy.

Digital implementation of SPWM is broadly realized since this option offers some advantages such as small noise for carriers and modulator comparisons which is limited to the quantization error equal to one half of least significant bit, no temperature dependence and fast configurations, which in our particular case enables carriers slope programming. Furthermore, the same digital modulator can be easily re-configured to permorm different types of phase disposition such as POD and APOD and even more, combining switching frequency indexes to speed up the response at the regions of high dv/dt in the modulating signal. This last issue could be attempted if for example M_f=100 when $M_a(t)$ is ±30 ° in the boundary of zero-crossing and M_f is lowered, say to 50, for other instants of the modulating signal.

As a precedent, the work of Geoffrey Walker [Wal99,Wal03] was a implementation of digitally calculated switching instants, defined by the author as Digitally-Generated Natural Sampling PWM. Basically, the method consisted of re-sampling the modulator signal according to the Re-Sampling Ratio rsr=$F_S/2F_C$, that is, when rsr=4 four modulator samples were taken along each slope in one-carrier period T_C. Therefore, for symmetrical sampling the re-sampling ratio is rsr=1 whereas for asymmetrical sampling rsr=2. Such method was implemented by TMS320C31 DSP and supported with Altera FLEX 8820 FPGA where carriers were generated using a controller board based on those circuits and twelve bit resolution; such carriers were standard shaped. Another precedent was the approach developed by Mariethoz [Mar04, Mar05] where the curve of sinusoidal modulating signal is assumed as one single secant line along the carrier period; for every carrier interval there is a elementary cell that represents the states of the inverter and their respective switching instants. Using the basis of such elementary cell, a harmonic predictive model was developed to study in advance different PWM strategies implemented later with standard carriers by digital means. In this chapter, we propose an alternative method to model and realize SPWM as close and accurate as possible to Natural Sampling methods. Such method, namely Pseudo-Natural Sampling, permits to perform harmonic modeling and later experimental implementation of SPWM using whether a simulation tool or a digital control board and considering the opportunity to modify the carriers slopes.

UNIVERSITAT ROVIRA I VIRGILI
CONTRIBUTIONS ON SPECTRAL CONTROL FOR THE ASYMMETRICAL FULL BRIDGE MULTILEVEL INVERTER
Oscar Mauricio Muñoz Ramírez
ISBN:978-84-693-7665-2/DL:T.1747-2010

5.2 Definition of Pseudo-Natural Sampling SPWM

Although a digital modulator would not produce the exact switching pulses, its accuracy is sufficiently high in order to synthesize the fundamental reference. However, its harmonic content differs from that obtained by a Natural Sampling analog modulator. Thus, the DFS model based on Natural Sampling can not be validated in 100% of precision since the harmonics produced in a Regular Sampling digital modulator are the result of switching instants calculated by interpolation of discrete samples and the carriers. In this context, we developed the concept of Pseudo-Natural Sampling that can be observed in figure 5.1 wherein its switching instants decisions are compared with the previously mentioned sampling methods.

Pseudo-Natural Sampling method is achieved by calculating the intersection point between two pair of segments; thus, the intersection abscise is assigned to the respective switching instant. In one pair of segment there are the carrier slope and a secant-segment; such secant-segment approximates the modulating signal along one half of the carrier period. This secant can be accepted as a good approximation of the tangent line that would appear in the exact intersection derived from a pure Natural Sampling function. In other words, the secant-segments AM and MB replace the modulating signal. The pair of segments AM and the falling slope are intersected to find X_d. In the same way, the pair of segments MB and the rising slope are intersected to solve X_u.

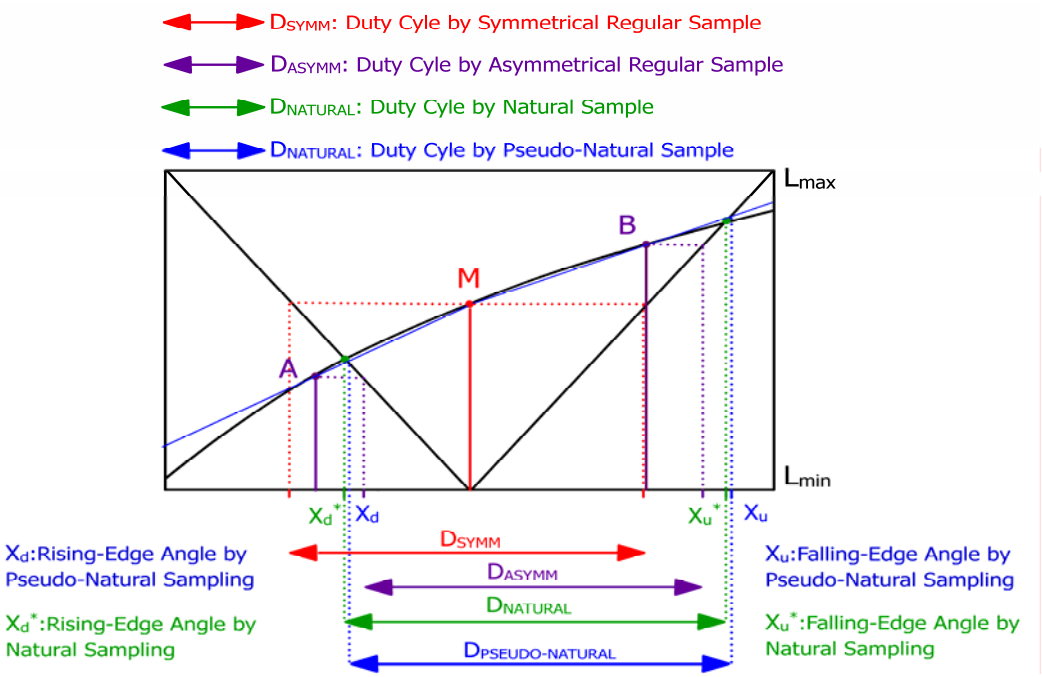

Figure 5.1 Sampling Methods in SPWM.

UNIVERSITAT ROVIRA I VIRGILI
CONTRIBUTIONS ON SPECTRAL CONTROL FOR THE ASYMMETRICAL FULL BRIDGE MULTILEVEL INVERTER
Oscar Mauricio Muñoz Ramírez
ISBN:978-84-693-7665-2/DL:T.1747-2010

To depict the secant lines in both rising and falling edge intervals, three samples are taken as follows: one sample at the carrier period T_c mid-point, namely Sample M; on left side, at the falling edge interval mid-point, namely Sample A; and finally, on right side, at the rising edge interval mid-point, namely Sample B. By taking Sample M, the switching zone is defined with its respective output levels. X_d is calculated using the segment determined by Sample A and Sample M. Similarly, X_u is calculated using the segment determined by Sample M and Sample B. Then, the pulse width and its position in an interval of time are determined.

TABLE 5.1 COMPARISON OF SAMPLING METHODS.

Switching time	**Natural Sampling**	**Pseudo-Natural Sampling**		**Symmetrical Regular Sampling**		**Asymmetrical Regular Sampling**	
X_d	179.74µS	179.7µS	-0.024%	177.43µS	-1.28%	188.73µS	5%
X_u	225.54µS	225.48µS	-0.028%	222.66µS	-1.28%	233.93µS	3.72%
$D=X_d-X_u$	45.8µS	45.78µS	-0.044%	45.23µS	-1.2445%	45.2µS	-1.31%

*A=0.9*sin(1.8°), M=0.9*sin(3.6°), B=0.9*sin(5.4°).*
Switching parameters obtained by Matlab and Pspice simulations.

Table 5.1 shows the comparison among switching instants and duty cycles with four sampling methods, including the introduced Pseudo-Natural method. The switching values are delimited in the first carrier period, that is $0 \leq t \leq T_c < T_o$, for a switching ratio M_f=50. Taking this example is very illustrative, since the first carrier period is in the boundary of zero-crossing and the sinusoidal reference presents a high derivative. In table 5.1 it is also demonstrated how the duty cycle D in a carrier period can have different widths and be modulated at different instants if the four sampling methods are compared among them. The differences rely on the fact that the input signal is not constant during a carrier period, especially on the the boundary of zero-crossing where the high derivative property implies that any digital sampling method should synthesize the incoming modulating signal as natural sampling does. Pseudo-Natural sampling method is the option that best fits in replacing natural sampling by means of a digital modulator.

Then, it is confirmed that both secant-segments defined by Pseudo-Natural Sampling are a high fidelity synthesization of the original reference signal. The use of such segments can be compared to curve fitting techniques where basically low order functions are used in distributed intervals along the variable domain (in this case time domain) replacing a high order function. Our statement is that Pseudo-Natural sampling produces a duty cycle that is sufficiently close to that obtained with Natural sampling. This enables us to implement a

UNIVERSITAT ROVIRA I VIRGILI
CONTRIBUTIONS ON SPECTRAL CONTROL FOR THE ASYMMETRICAL FULL BRIDGE MULTILEVEL INVERTER
Oscar Mauricio Muñoz Ramírez
ISBN:978-84-693-7665-2/DL:T.1747-2010

SPWM modulation by means of digital hardware where an experimental output waveform must present a low degrading effect over the expected spectrum. This means that a spectrum obtained by Pseudo-Natural sampling can have neglected differences from that spectrum produced by using Natural sampling. Moreover, the experimental spectra by Pseudo-Natural sampling can validate the data calculated by our analytical formulation introduced in Chapter 4, Equation (4.4).

5.3 SFS Spectrum from Pseudo-Natural SPWM

Since a digital control circuit can accomplish successive reconfigurations for different shape-factor cases, we needed to develop a software-tool that calculated the spectrum of a Pseudo-Natural PD-SPWM waveform. This algorithm, namely C_n-Algorithm, calculates the switching instants saving them in two arrays of length M_f; one array for X_d and the other for X_u. Also, the switched output level is assigned according to the modulation rule and is saved in another array of length $2*M_f$ since it is expected to have two output level states for each carrier period; in some intervals of time, there is only one commutation due to the transition pass of the modulating signal between two adjacent Tibuck cells.

Having the switching instants and the output voltages assigned to the intervals of time, a Simple Fourier Series (SFS) is implemented where the C_n coefficients are defined according to the expression $c_n = a_n + b_n$, where:

$$a_n = \frac{2}{T_o}\int_0^{To} F(t)\cos(n\omega_o t)dt \tag{5.1}$$

$$b_n = \frac{2}{T_o}\int_0^{To} F(t)\sin(n\omega_o t)dt \tag{5.2}$$

A for-loop finds the solutions of equations (5.1) and (5.2) by solving the integrals delimited by the switching instants where the commuted level $V_{pwm}(t)$ is fixed for every interval. These solutions are written as:

$$a_n = \frac{2}{T_o}\sum_{p=1}^{M_F}\left(\int_{(p-1)T_C}^{X_D[pT_C]} V_{I-1}\cos(n\omega_o t)dt + \int_{X_D[pT_C]}^{X_U[pT_C]} V_I\cos(n\omega_o t)dt + \int_{X_U[pT_C]}^{pT_C} V_{I-1}\cos(n\omega_o t)dt\right) \tag{5.3}$$

$$b_n=\frac{2}{T_o}\sum_{p=1}^{M_F}\left(\int_{(p-1)T_C}^{X_D[pT_C]}V_{I-1}\sin(n\omega_o t)dt+\int_{X_D[pT_C]}^{X_U[pT_C]}V_I\sin(n\omega_o t)dt+\int_{X_U[pT_C]}^{pT_C}V_{I-1}\sin(n\omega_o t)dt\right) \quad (5.4)$$

Replacing (5.3) and (5.4) the output voltage can be synthesized by superposition of the sine and cosine functions as equation (5.5) states.

$$V_{PWM}(t)=\sum_{n=1}^{\infty}[a_n\cos(n\omega_o t)+b_n\sin(n\omega_o t)] \quad (5.5)$$

In figure 5.2 both DFS formulation (4.4) and SFS formulation (5.3 and 5.4) are compared by executing their respective algorithms, namely C_{mn}-Algorithm and C_n-Algorithm. These algorithms are implemented in Matlab to predict the spectra of several cases of SPWM with E=50 V, M_a=0.9, the y-scale range: [0,4] V_{rms}, and the x-range: 225 harmonics. The experimental output signal spectrum from oscilloscope generates data and photos with a scale measured in V_{rms}, thus, the final comparisons will consider such scale for visual inspection of the resemblance among the different ways to calculate or measure spectra for identical cases of carriers set.

The y-scale is adjusted to focus on the non fundamental harmonics rather than the fundamental 50 Hz component and then comparisons can be done. The similarity between both types of spectra modeling confirms that Pseudo-Natural sampling is a suitable approximation to implement the PD-SPWM by means of a digital modulator.

More spectra obtained, by Pseudo-Natural sampling method and using the tool C_n-Algorithm, can be observed at Appendix B-Figure B.1 where it is confirmed the validity of equations (5.3) and (5.4) that calculates the harmonics and thus reproduces the continuos output voltage V_{pwm} represented with (5.5). The spectra obtained by C_n-Algorithm requires a much shorter time of computation, giving an extra advantage when using this tool. Moreover, this algorithm can be easily modified so that the switching instants from (5.3) and (5.4) can be calculated for both Symmetrical and Asymmetrical sampling methods considering PD-PWM for multicarrier disposition.

These modifications permitted us to obtain the spectra for the three sampling methods that can be implemented by a digital modulator. Some results of these spectra are observed in figure 5.3 where it is clearly confirmed the superiority of Pseudo-Natural sampling over both Symmetrical and Regular sampling methods.

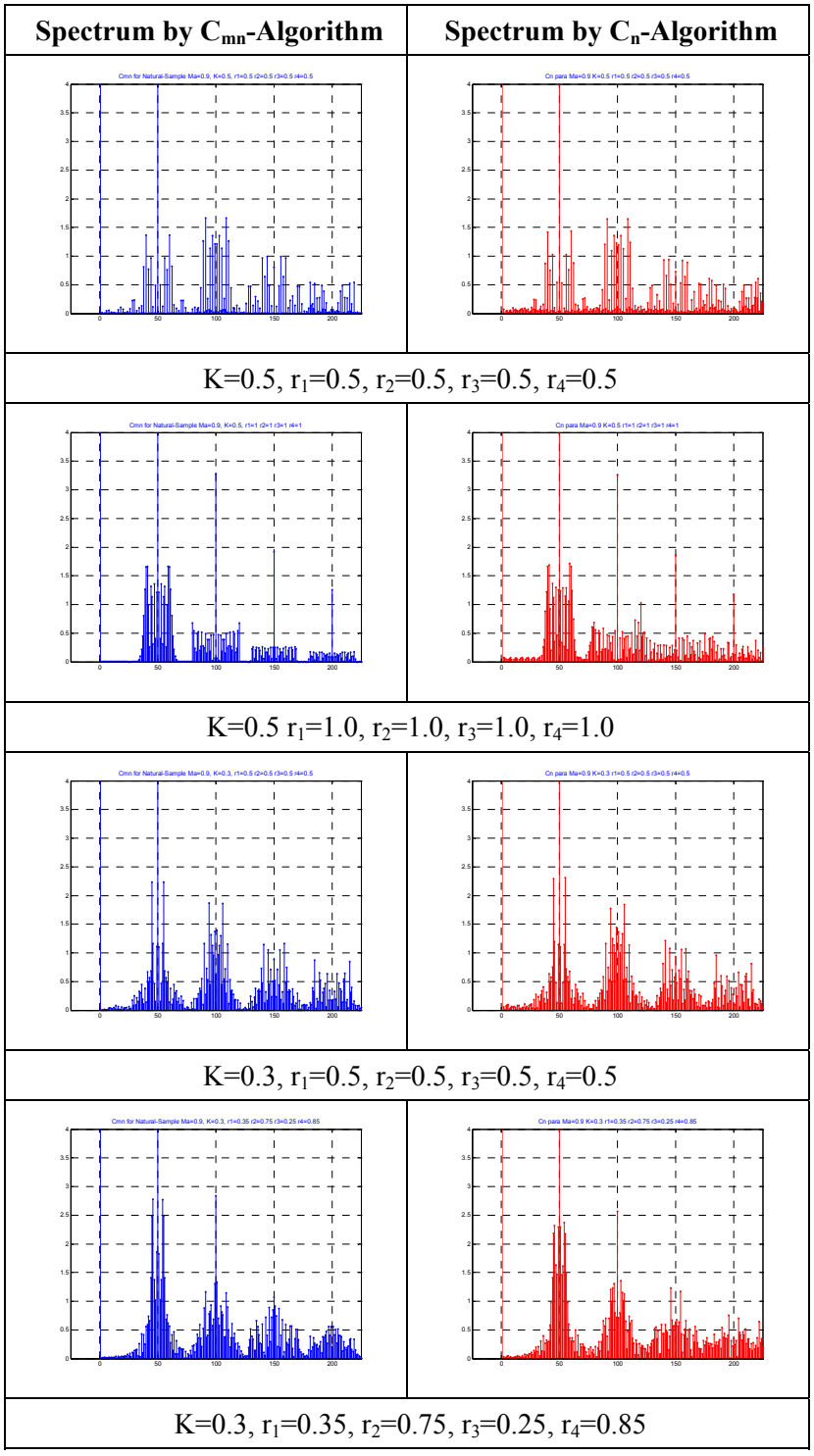

Figure 5.2 Comparisons between C_{mn}-Algorithm and C_n-Algorithm.

Figure 5.3 illustrates the spectral differences of Pseudo-Natural, Symmmetrical and Asymmetrical Regular sampling methods. The harmonics ara calculated by the tool C_n-Algorithm implemented in Matlab for a PD-SPWM scheme with E=50 Vdc, M_a=0.9, the y-scale: [0,4]V_{rms}, and the x-range:225 harmonics.

UNIVERSITAT ROVIRA I VIRGILI
CONTRIBUTIONS ON SPECTRAL CONTROL FOR THE ASYMMETRICAL FULL BRIDGE MULTILEVEL INVERTER
Oscar Mauricio Muñoz Ramírez
ISBN:978-84-693-7665-2/DL:T.1747-2010

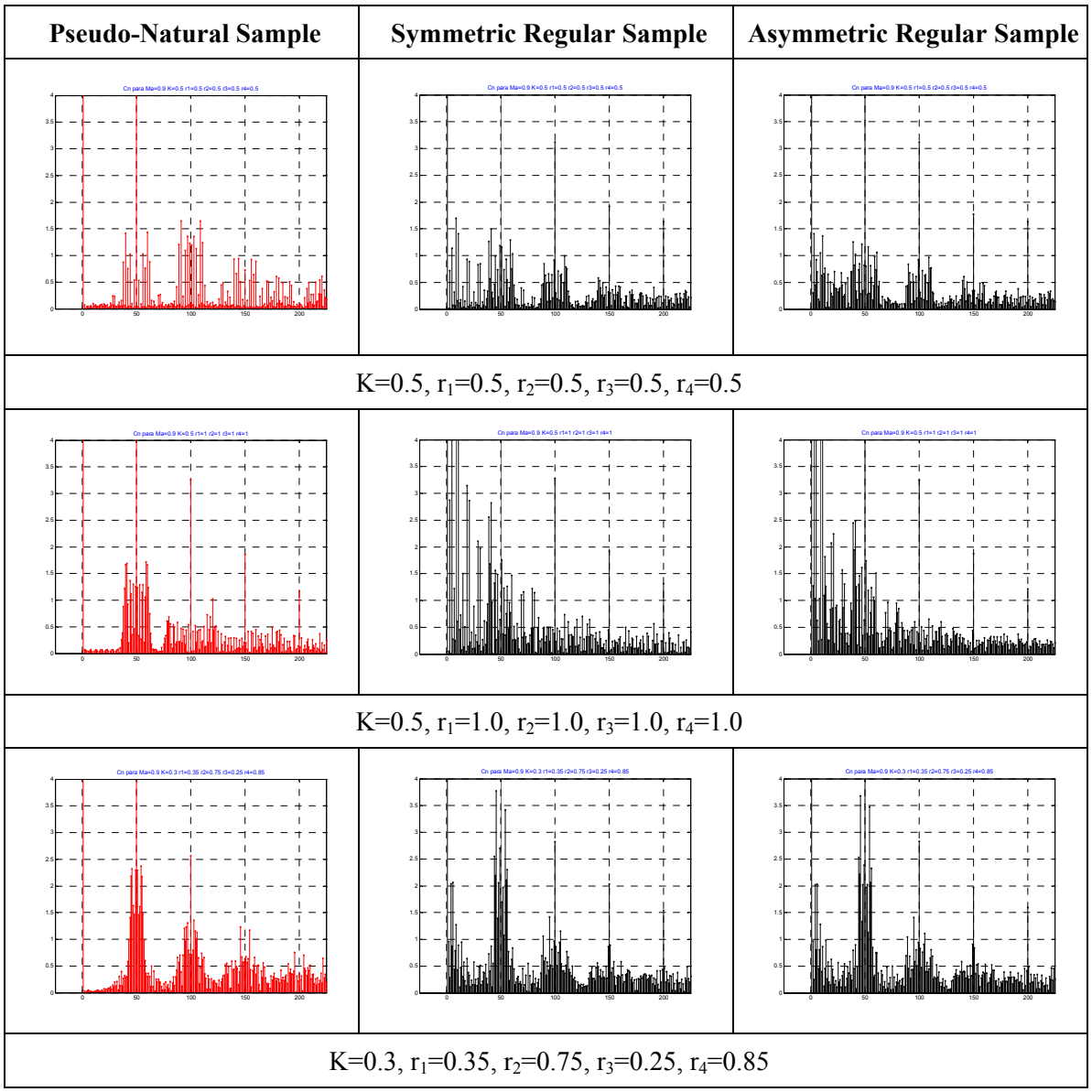

Figure 5.3 Comparisons of Pseudo-Natural, Symmmetrical Regular and Asymmetrical Regular sampling.

Other benefit of C_n-Algorithm is its ability to explore modulation schemes with four, three or two levels where the carriers set is adapted according to the criterion N levels, N-1 carriers. Formulation for SFS is much easier than DFS formulation, since in the same program of C_n-Algorithm the carriers assignment and the angles computing is an easy task whereas in the case C_{mn}-Algorithm the formulas related to the diagram of contours are entirely modified by collapsing situations of amplitude index and by the number of levels. The algorithm developed for DFS formulation is restricted by the collapsing condition M_a>max(K,1-K) referred in table 4.6, chapter 4. So far, the tool C_{mn}-Algorithm only performs five-level simulation of voltage spectrum. On the contrary, the algorithm for SFS formulation computes the harmonics for any level number equal or less than five and for any level distribution K.

UNIVERSITAT ROVIRA I VIRGILI
CONTRIBUTIONS ON SPECTRAL CONTROL FOR THE ASYMMETRICAL FULL BRIDGE MULTILEVEL INVERTER
Oscar Mauricio Muñoz Ramírez
ISBN:978-84-693-7665-2/DL:T.1747-2010

5-Level Modulation	4-Level Modulation	3-Level Modulation
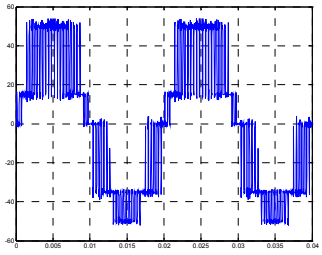	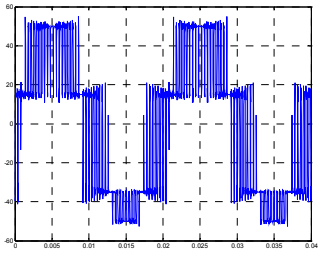	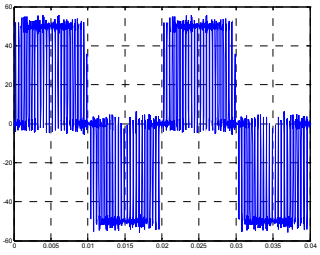
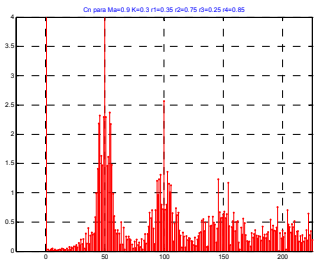	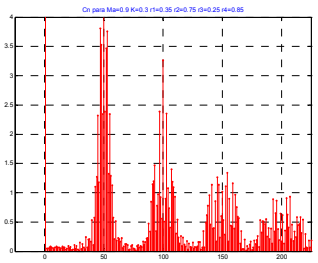	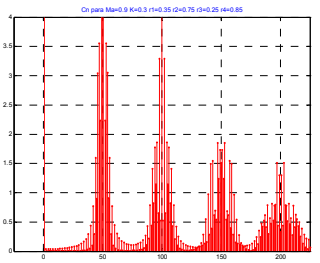
K=0.3, r_1=0.35, r_2=0.75, r_3=0.25, r_4=0.85	K=0.3, r_1=0.35, r_2=0.75, r_3=0.25	r_1=0.35, r_2=0.75

Figure 5.4 Five, four and three levels modulation by C_n-Algorithm.

Figure 5.4 shows the waveforms and spectra for a particular carriers set with five, four and three levels modulation in a PD-SPWM scheme, with E=50 V, and M_a=0.9. Those frequency amplitudes and their respective time domain output waveforms are calculated by C_n-Algorithm. C_{mn}-Algorithm calculates the exact theoretical spectrum wherein Natural Sampled PWM implementation is needed. The execution time is quite significant and the calculated spectrum is lightly different from Pseudo-Natural PWM. Accepting those little differences and considering the fact of having a fast calculated spectrum, C_n-Algorithm is a suitable option when many cases are to be tested. C_n-Algorithm works on the basis of calculating the spectrum with single Fourier series for a Pseudo-Natural Sampled signal. In both algorithms, the calculated spectrum can contains more than one hundred harmonics. The time-domain output signal is quite the same from that obtained by Pspice. It is concluded that C_n-Algorithm offers a realistic and best approximated output spectrum simulation tool if compared to DFS model based on C_{mn} coefficients or spectrum simulation based on FFT.

In a digital control circuit, the switching instants can obtained by means of Pseudo-Natural Sampling method. This means that the PD-SPWM process can be carried out with satisfactory results. This is the motivation for seeking the alternatives to work out a digital implementation able to emulate natural-sample PWM. Modifications of the digital modulator are easy to implement; this is a benefit for future experiments where other types of SPWM

and sampling methods can be studied. Although our research work was focused on PD-SPWM, other phase disposition strategies for multicarrier schemes are easy to be implemented by a digital modulator. Among those strategies POD and APOD are the most representative. The carrier slope factor in those strategies can also be modified which means a broad set of paths to be explored. Since the our aim of exploring multicarrier schemes is to reduce harmonic distortion by means of carriers slope programming, we decided to explore and only to optimize PD-SPWM.

UNIVERSITAT ROVIRA I VIRGILI
CONTRIBUTIONS ON SPECTRAL CONTROL FOR THE ASYMMETRICAL FULL BRIDGE MULTILEVEL INVERTER
Oscar Mauricio Muñoz Ramírez
ISBN:978-84-693-7665-2/DL:T.1747-2010

6. Pseudo-Natural Modulation Performance

Chapters four and five have concentrated on the theoretical spectral analysis of pulse width modulation, exploring and modeling the technique of modifying the carrier-shapes in a multilevel scheme. The main benefit of this technique is to obtain a cleaner base-band content than standard carrier-shapes can produce for a PWM scheme of vertically displaced carriers. As amplitude index or level distribution change so the harmonic distortion varies; it is possible to search a more suitable set of carrier shapes that keep the harmonic content as low as possible.

The theory and harmonic modeling algorithms (DFS based on C_{mn}-Algorithm, SFS based on C_n-Algorithm) of previous chapters are important since when building a power inverter the output spectra can be controlled by proper modulation adjustments. This means that switching sequence must follow a law of control commanded by the selected type of PWM; in particular, the set of carrier shapes. There is limited value in knowing the theoretical spectrum for a given modulation scheme if the hardware/software platform switches incorrectly, or even worse, causes switching errors because noise or wrong calculations are injected through the control electronics. The physical implementation needs that the experimental prototype works as close as possible to the modeled output spectrum and vice versa. Actually, the design of a practical application requires several prototype developments assigned in different stages wherein new working conditions are added according to its complexity. Similarly, models are proposed and developed by progressively including the variables that describe the phenomena and mechanisms of an application.

Similarity between a theoretical and its respective experimental spectrum is measured and discussed along this chapter. Resistive loads produce spectra with high degree of similarity to their respective modeled spectra. Additionally, their voltage and current voltage are linear since current is directly proportional to voltage. The core of this thesis is the modeling of ideal spectra for output voltages performed by different carriers set. Then, a resistive load in an open loop control is suitable to such matter since the output voltage only has a constant and small drop with respect the DC input voltages leaving the switched levels with constant values. However, if the load is R-L-C type, the output current will distort the switched levels with no constant drop values due to the sinusoidal pattern of the current. In which case, the consistency of those optimum carriers set for spectra based on resistive load is evaluated

UNIVERSITAT ROVIRA I VIRGILI
CONTRIBUTIONS ON SPECTRAL CONTROL FOR THE ASYMMETRICAL FULL BRIDGE MULTILEVEL INVERTER
Oscar Mauricio Muñoz Ramírez
ISBN:978-84-693-7665-2/DL:T.1747-2010

when the second order filter is added and thus the correspondence between their respective spectra is examined. If the resistance changes, the filter can present an overdamped response and some harmonics can be increased instead. In this context, the need of closed loop control and carrier amplitude compensation is justified. We recall that in a first stage, the spectrum optimization starts from modeling a resistive load system in open loop condition where the modulator signal has one single frequency component, thus the best possible conditions of modulation are placed in the system. In a final stage, the modulator signal coming from a closed loop control is yield to the PWM controller; the modulator signal contains indeed more than one frequency components. Although the modeling of output spectra for close loop is not developed in this thesis, we expect that those best possible conditions given by open loop optimization additionally contribute to diminish the measured error in a close loop scheme. In other words, the compensator block in the feedback system will handle a less perturbed output since its harmonic distortion is smaller.

This chapter provides a description of the main characteristics of the experimental system comprising the power switching devices, the driving circuitry of the generated pulses and the PWM controller which is implemented with programmable hardware. Several examples were generated with this experimental prototype and the results presented here are intended to evaluate the experimental spectra for some cases based on Pseudo-Natural modulation and comparing them with their respective theoretical spectra.

Within the constraints of available power switching devices and hardware/software limitations, we implemented the Pseudo-Natural Sampling method for a Phase Disposition PWM controller around the TMS320F2812 Development Kit. Such kit is a embedded system that comprises a hardware/software platform where a DSP (in this case the TMS320F2812 Digital Signal microProcessor) can be reprogrammed, monitored and reconfigured by using a communication protocol, namely JTAG (Joint Test Action Group) which is often used for debugging and for probing the pins of the DSP. This protocol is used by a C/C++ software manager interface (CCS, Code Composer Studio) where a PWM algorithm can be written, compiled and executed as a program. From a personal computer, the CCS loads the executable code into the DSP. In the TMS320F2812 Development Kit, the configuration of output and input ports as well as internal hardware are flexible and the switching pulses of the asymmetric full bridge multilevel inverter can be transferred through an optically isolated driving circuitry.

UNIVERSITAT ROVIRA I VIRGILI
CONTRIBUTIONS ON SPECTRAL CONTROL FOR THE ASYMMETRICAL FULL BRIDGE MULTILEVEL INVERTER
Oscar Mauricio Muñoz Ramírez
ISBN:978-84-693-7665-2/DL:T.1747-2010

6.1 Experimental Prototype Description

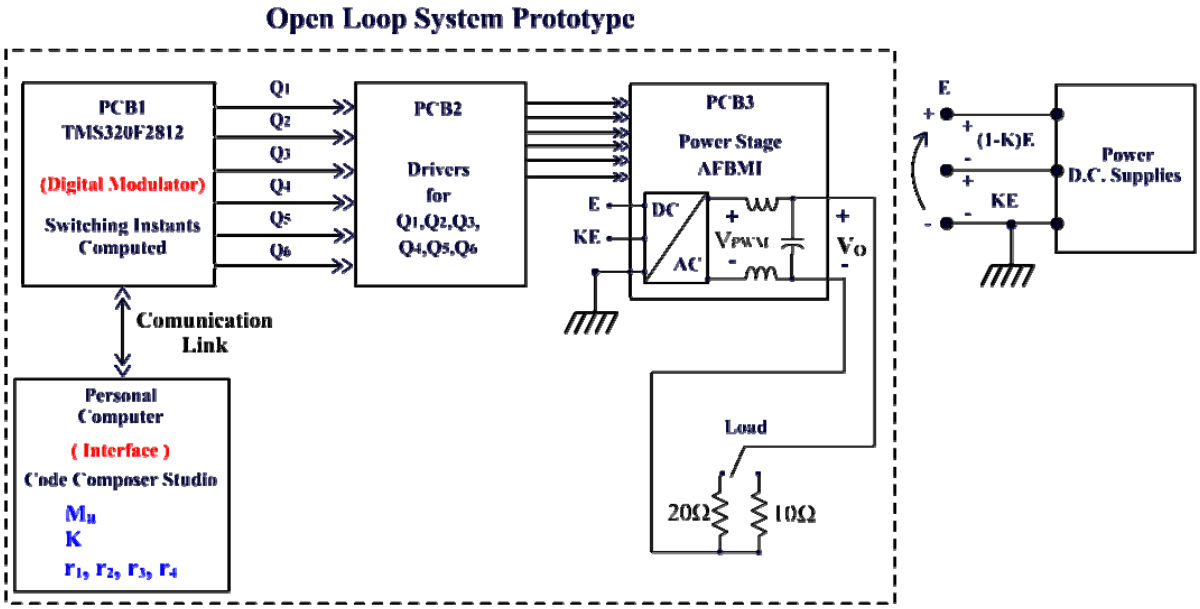

Figure 6.1.a Block Diagrams of the Open Loop System Prototype.

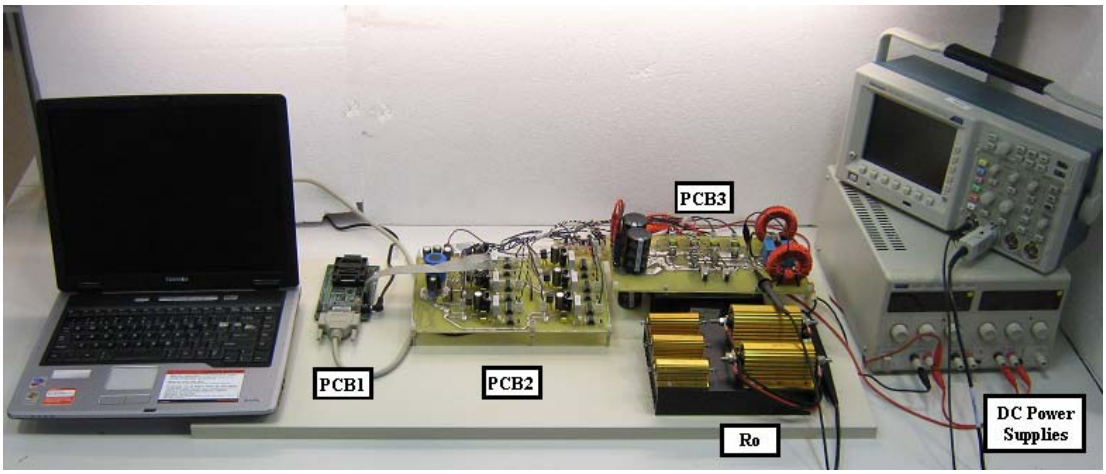

Figure 6.1.b Photo of the Open Loop System Prototype.

The experimental prototype consists of three main sections namely the Power Stage Circuit, the Driving Circuitry and the Modulation Controller System, as illustrated in figure 6.1.a. The Power Stage section contains the power switching components, the connection plugs for input and output voltages and, the group of reservoir capacitors to stiff the input voltages. In the second section, the pulses calculated and generated by the DSP are optically isolated and conditioned for each MOSFET. These signals originally operate in a 3.3 V range and the gate-to-source activation voltage must be within a 10 V range. A multiple output transformer is used in order to obtain the input AC supplies for seven auxiliary DC sources: one for the optical isolators and six more for each dedicated buffering circuit that transmits the pulses to their respective MOSFETS. Finally, the Modulation Controller Systems, as previously

UNIVERSITAT ROVIRA I VIRGILI
CONTRIBUTIONS ON SPECTRAL CONTROL FOR THE ASYMMETRICAL FULL BRIDGE MULTILEVEL INVERTER
Oscar Mauricio Muñoz Ramírez
ISBN:978-84-693-7665-2/DL:T.1747-2010

introduced, comprises the PWM algorithm with the ability of modifying the carriers set. Figure 6.1.b is a picture of the experimental prototype implemented and utilized at the GAEI laboratory.

6.1.1 Power Stage Circuit

The power stage, PCB3 in photo, was built on a single PCB where six power N-channel MOSFETs are placed in H-bridge configuration in order to achieve five-level modulation. Two clamping diodes establish the paths for the intermediate levels, i.e. $+K{\cdot}E$ and $-(1-K){\cdot}E$. Figure 6.2 shows the capacitors that fix the input voltage supply and next to them there are the arrangement of the main power switching devices. For each power MOSFET there is an inverse current by-pass diode connected between the drain and the source pins. The output connections of the H-bridge, namely V_{pwm1} and V_{pwm2}, are the terminals of the output PWM waveform. The resistive load can be connected directly to these terminals or via the L-C filter as detailed in figures 6.3 and 6.4. Then, for R-load connection tests the output voltage is $V_o = V_{pwm}$ and for R-L-C connection, the output voltage is the filtered signal obtained from V_{pwm}.

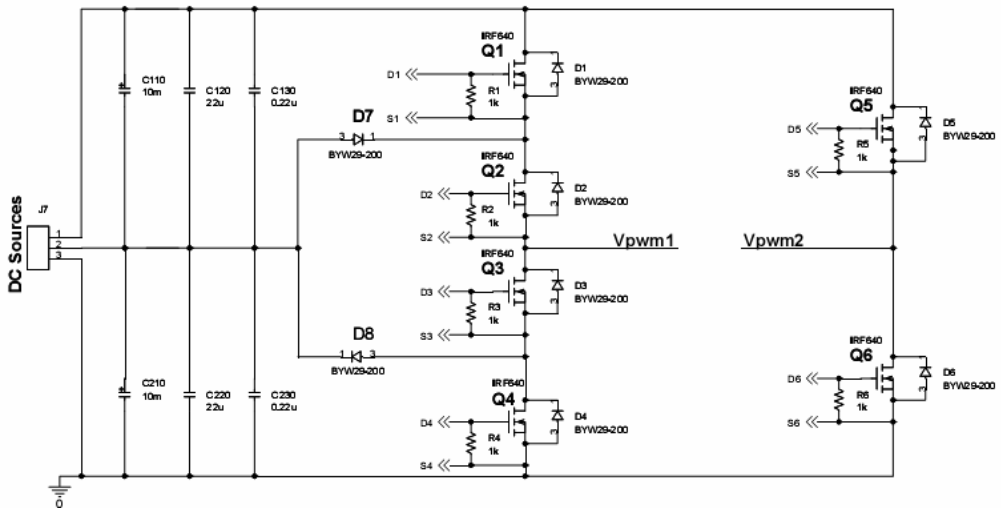

Figure 6.2 Asymmetric Full Bridge Inverter.

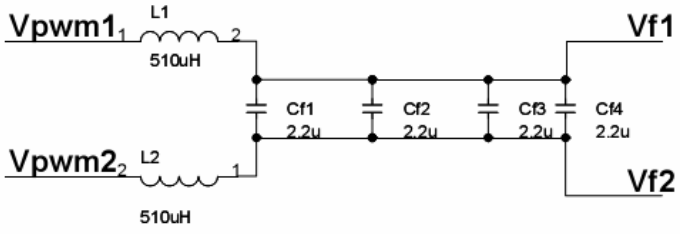

Figure 6.3 L-C Filter.

UNIVERSITAT ROVIRA I VIRGILI
CONTRIBUTIONS ON SPECTRAL CONTROL FOR THE ASYMMETRICAL FULL BRIDGE MULTILEVEL INVERTER
Oscar Mauricio Muñoz Ramírez
ISBN:978-84-693-7665-2/DL:T.1747-2010

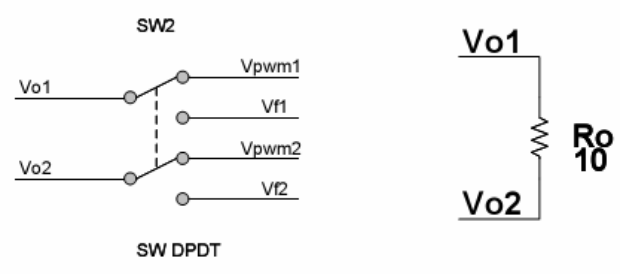

Figure 6.4 Load Connection by a two-position switch.

6.1.2 Driver Board Circuit

The Driving Circuitryhas three functions: to isolate optically the incoming DSP signals, to convert their working voltage range from 3.3 V to 10 V and to give galvanic isolation to each pulse that arrives at the gate-to-source port in the MOSFET. In the same PCB from Power Stage Circuit, the current amplifier section, figure 6.5, from the gate driving circuitry is placed here. This current amplifier is basically built with two transistors working on a complementary pair or push-pull configuration and its output is connected to the MOSFET gate pin as close as possible. We decided to put this section in order to reduce EMI effects along the pulse transmitting wire by placing the components that ensures the current injection every time the pulse triggers the gate.

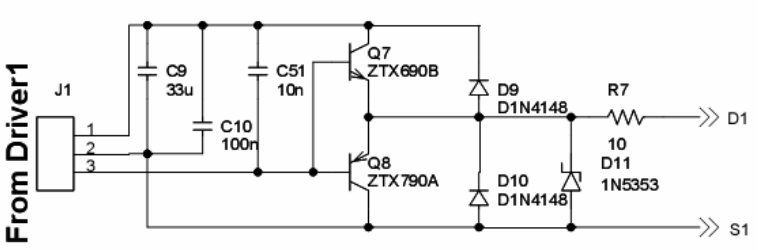

Figure 6.5 Current Amplifier Section of one Gate Driver.

Figure 6.6 shows how in right side the outgoing signals contain the voltage-amplified pulse and the supply voltage which is regulated in this PCB2 as showed in photo. In other words, for the six incoming driving pulses, the power stage PCB3 contains the current amplifier section for each driver circuit leaving the voltage-amplifier section in PCB2 which receives the pulses from the DSP (PCB1); this PCB contains the auxiliary DC supplies.

UNIVERSITAT ROVIRA I VIRGILI
CONTRIBUTIONS ON SPECTRAL CONTROL FOR THE ASYMMETRICAL FULL BRIDGE MULTILEVEL INVERTER
Oscar Mauricio Muñoz Ramírez
ISBN:978-84-693-7665-2/DL:T.1747-2010

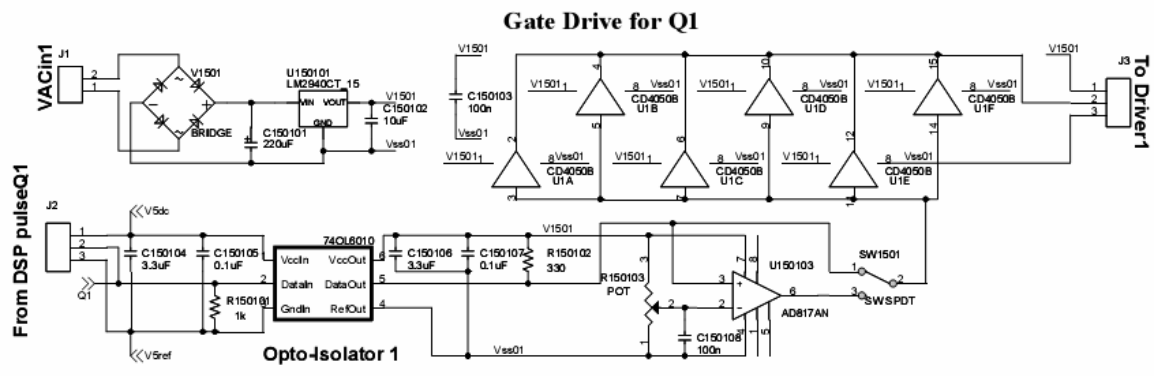

Figure 6.6 Voltage Buffering Section and Optical Isolation.

6.1.3 Pseudo-Natural PWM Realized with a TMS320F2812 (DSP)

The control program for five level modulation is implemented on a DSP which can be accessed through a development kit as was mentioned before; this kit is showed in the photo of figure 6.1.b. To control the AFBMI, six driving signals are delivered from this DSP. This PWM implementation has the limitations of a digital circuit and normally it would modulate by Regular Sampling. Nevertheless, Pseudo-Natural Sampling PD-SPWM is attempted by calculating the intersection point of two lines with the carrier slopes that approaches the natural sampling of the sinus in one carrier period. Figure 6.7 shows both rising and falling edges and their respective instants, i.e. X_{DP} and X_{UP} for.Pseudo-Natural sampling and X_D and X_U for Natural sampling Recalling table 4.5 this figure illustrates the sampling process for one switching zone where its respective carrier r_i is active with two output level states, i.e. V_I and V_J. Then four switching zones are delimited by five level modulation.

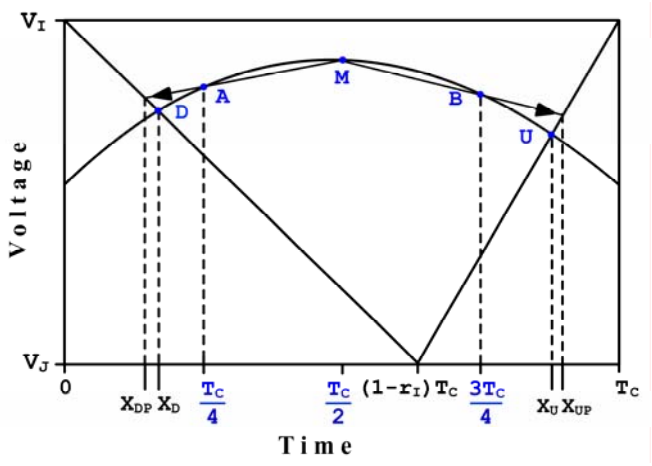

Figure 6.7 Pseudo-Natural Sampling Method for SPWM.

Once the switching instants are calculated in a modulation zone, the driving pulses are assigned for each level at the inverter output. These signals are distributed to activate six

UNIVERSITAT ROVIRA I VIRGILI
CONTRIBUTIONS ON SPECTRAL CONTROL FOR THE ASYMMETRICAL FULL BRIDGE MULTILEVEL INVERTER
Oscar Mauricio Muñoz Ramírez
ISBN:978-84-693-7665-2/DL:T.1747-2010

topologies or status-devices in order to accomplish the five level outputs. Every switching zone (1, 2, 3 and 4) works with a pair of complementary signals. That is only two switching devices commute between the two levels.

It can be said that in each of these zones the AFBMI assumes the role of Buck converter where two output levels are synthesized by comparing the actual modulating-segment with its respective carrier. Two redundant states are available to obtain the mid-point level or zero-voltage at the inverter output. table 6.1 summarizes the binary values for each MOSFET in every switched level or status at the output of the inverter.

TABLE 6.1 SWITCHING STATES AND VOLTAGE LEVELS.

State	Level	Q_1	Q_2	Q_3	Q_4	D_1	D_2	Q_5	Q_6
S_1	E	1	1	X	0	0	0	0	1
S_2	k·E	0	1	1	0	1	1	0	1
S_3	0	0	0	1	1	0	0	0	1
S_4	0	1	1	0	0	0	0	1	0
S_5	(k−1)·E	0	1	1	0	1	1	1	0
S_6	−E	0	X	1	1	0	0	1	0

Observing table 6.1 it is remarkable that only one of the three complementarily pairs commutes at every switching zone, except for the transition status for 0^+ and 0^-. Those pairs are $\{Q_1,Q_3\}$, $\{Q_2, Q_4\}$ and $\{Q_5, Q_6\}$. These three pairs of driving signals needs an arrangement of three comparators with complementary outputs and the switching edges must be refreshed or re-loaded every T_c seconds.

In the light of generating three complementary pair of driving signals, we take advantage of the available hardware in the DSP, where a master timer **T0** is used as the carrier period generator and a slave timer **T1** is reconfigured every T_c seconds by the master timer interruption **INT_T0**. Timer **T0** generates this interruption every 400 μs and timer **T1** is refreshed by reloading its registers, namely Period Register (X_u) and Compare Register (X_d); this mechanism is depicted in figure 6.8. Due to the internal clock configuration in the DSP, the maximum value for Period Register is 30000 counts which is equivalent to the maximum X_u value, 400μS. The resolution of Period Register is high enough as to generate the switching times in every carrier period. The Counter Registers starts its count from zero and increase it until it is reached the actual Period Register value, and at the same time, comparing its value with that of Compare Register. When the Counter Register is bigger than

UNIVERSITAT ROVIRA I VIRGILI
CONTRIBUTIONS ON SPECTRAL CONTROL FOR THE ASYMMETRICAL FULL BRIDGE MULTILEVEL INVERTER
Oscar Mauricio Muñoz Ramírez
ISBN:978-84-693-7665-2/DL:T.1747-2010

Compare Register, then the timer T1 output state is high or active; on the contrary, if Compare Register is lower than Counter Register, T1 state is low or inactive.

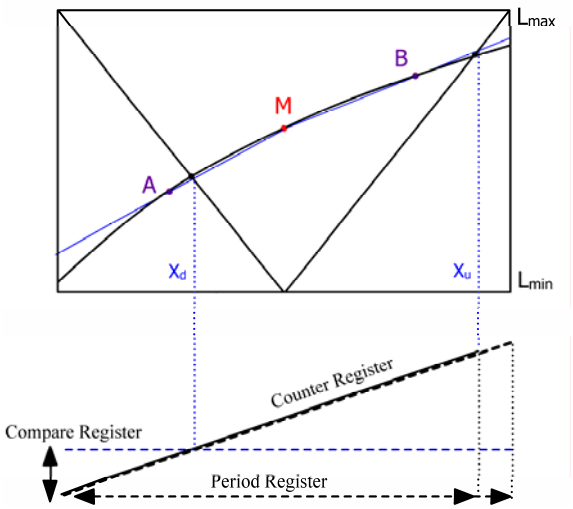

Figure 6.8 Generation of switching edges X_d and X_u.

When Counter Register has reached the Period Register value, it is latched to zero until it is re-loaded with a new value in the next carrier period. In the same manner, the Period Register is re-loaded. For every carrier period t_{fi} there is a modulator sample $M_{[i]}$ where $i=\{1,2\ldots M_f\}$.

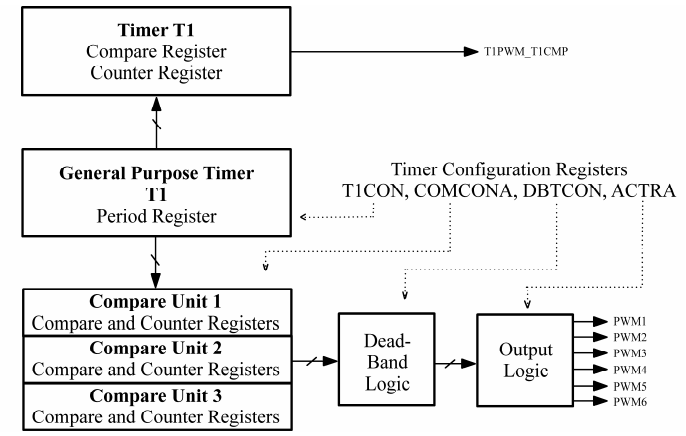

Figure 6.9 Timer1 Compare Units: PWM generation.

In figure 6.9 it is illustrated how Timer **T1** and its registers are connected to 3 comparators, namely Compare Unit 1, 2 and 3. Each of these compare units has two outputs pins that can be reconfigured as complementary pins or latched to a fix state. Additionally, the dead-band time can be configured in the compare output pins. Here is where the benefits of the DSP are exploited to generate the driving signals.

Since three pairs are needed to modulate the AFBMI, the three compare units of timer **T1** are enough to realize this task by controlling output pins $PWM_{1,2,3,4,5,6}$. X_d and X_u edges are executed by the assigned pin configuration on Compare Units. At each carrier period, an

UNIVERSITAT ROVIRA I VIRGILI
CONTRIBUTIONS ON SPECTRAL CONTROL FOR THE ASYMMETRICAL FULL BRIDGE MULTILEVEL INVERTER
Oscar Mauricio Muñoz Ramírez
ISBN:978-84-693-7665-2/DL:T.1747-2010

switching zone is defined with every sample $M_{[i]}$ and therefore a switching configuration is selected. ACTRA register allows the new changes on PWM_x pins (Active-Hi, Active-Low, Forced-Set, Forced-Reset). The pins distribution is shown on table 6.2.

TABLE 6.2 COMPARE UNITS OF TIMER T1 TO GENERATE THE DRIVING SIGNALS.

$CMPR_1$		**$CMPR_2$**		**$CMPR_3$**	
PWM_1	PWM_2	PWM_3	PWM_4	PWM_5	PWM_6
Q_1	Q_3	Q_2	Q_4	Q_5	Q_6

The TMS320F2812 DSP has three more timers, namely **T2**, **T3** and **T4**. As timer **T1**, timer **T3** has three PWM compare units, but they are no further needed for this prototype.

6.2 Natural Sampling and Pseudo-Natural Comparison

SPWM implementation is done under conditions that are not the same as those considered when modeling such process. Therefore, it is necessary to establish the bounds of study for SPWM that permit us to realize the assessment of our results about harmonics. The resemblance between theoretical and experimental spectra is closer as long as the working conditions are adapted or compensated. Some of these conditions are presented in table 6.3 in order to distinguish the criterions for testing and also, to do correct interpretations about observations on spectra.

TABLE 6.3 CLASSIFICATION OF WORKING CONDITIONS TO STUDY SPECTRAL MODELING.

Cause of disturbances	**Characteristic**	**Commentary**
DC sources	ripple voltage	Ripple mainly comprises 2^{nd}, 3^{rd} or 5^{th} multiples of $\mathbf{f_o}$(50 Hz)
Load type	R, L-R, R-L-C, grid connection, non-linear load	For preliminary indicators, R load is suitable for spectral model validation
Filtering action	none, first order , second order	Filtering action masks the harmonic profile. Resonance must be avoided
Non-linear characteristics and other effects	delay-time, switching losses, cupper losses, parasitic effects, L and C dependancy on frequency.	Output spectrum is degraded. Resemblance between real and theoretical spectra is challenging

DC sources are not ideal and their output impedance can distort the input voltages (E, K·E) of the inverter when input demanded current increases. A step voltage drop can be present if the load is R type and a waving drop is present with R-L-C type. Big capacitors combined with small capacitors (see figure 6.2) help to diminish the DC input distortion if they are placed closely to the input inverter plug. Figure 6.10 shows the AC component of these distortions

UNIVERSITAT ROVIRA I VIRGILI
CONTRIBUTIONS ON SPECTRAL CONTROL FOR THE ASYMMETRICAL FULL BRIDGE MULTILEVEL INVERTER
Oscar Mauricio Muñoz Ramírez
ISBN:978-84-693-7665-2/DL:T.1747-2010

on the darkest blue graphs, where voltage drop at the input converter plug due to R-L-C load is present due to the impedance of the DC supply with E=40 V_{dc}, M_a=0.9, K=0.5, R=10 Ω, L=1900 μH, C=6.6 μF.

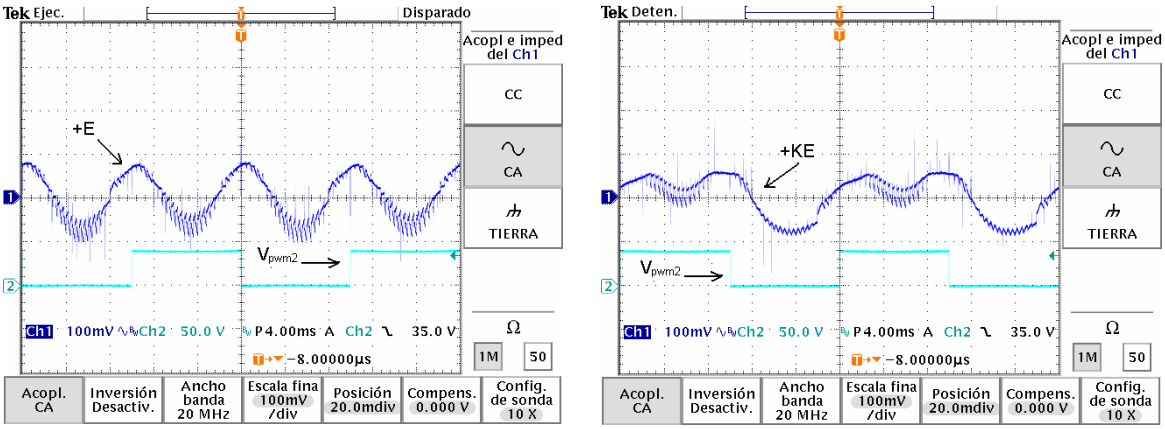

a) Waving drop < 0.5% at node +E b) Waving drop < 0.5% at node +K·E

Figure 6.10 Ripple voltage at the input converter plug.

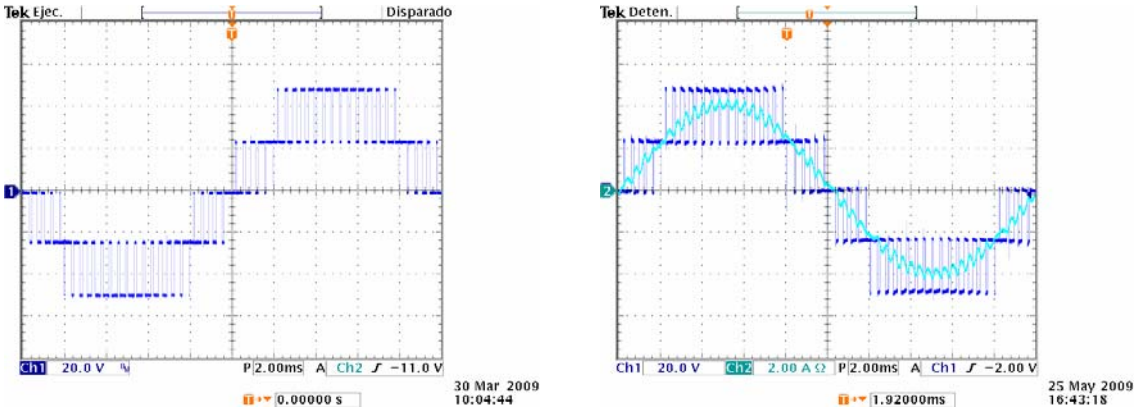

a) R-load: I_o has the same shape as V_{pwm}; drop in V_{pwm} is constant. b) R-L-C load: I_o is sinusoidal and V_{pwm} has a waving drop proportional to $I_O R_{DS\text{-}ON}$.

Figure 6.11 V_{pwm} voltage at the output plug converter.

In figure 6.10, the first cause of disturbance mentioned in working conditions from table 6.3 is somewhat easy to compensate. Brighter blue graphs correspond to Drain-to-Source Voltage of Q_6. According to MOSFET manufacturer and after our experimental measurements, the $R_{DS\text{-}ON}$ resistance is determined as 0.178 Ω. Assuming this value for all switching elements, a load resistance of 10 Ω has a gain about 95% in the voltage divisor established along the active interrupters and the resistance, thus R load is suitable for spectral model validation and the second cause of disturbance is assumed as negligible.

Other types of load such as a DC motor, a rectifier or a grid connection present different properties that can change with time, temperature or frequency as well as to present non-linear

UNIVERSITAT ROVIRA I VIRGILI
CONTRIBUTIONS ON SPECTRAL CONTROL FOR THE ASYMMETRICAL FULL BRIDGE MULTILEVEL INVERTER
Oscar Mauricio Muñoz Ramírez
ISBN:978-84-693-7665-2/DL:T.1747-2010

or unpredictable characteristics. In such cases, the modeling approaches can become a problem hard to tackle requiring major time-and-effort investments. The inferior complexity of a spectrum model based on R-load and non-ripple DC sources is a good trade off between time-and-effort investments and the resemblance obtain in experimental results.

Filtering action is necessary since standards of harmonic distortion must be accomplished or any other design requirement implies a determined cut-off frequency. The chosen values for L and C in a second order filter must assure no resonance at the cut-off frequency boundaries. If not, the base-band harmonics will be amplified. Although well designed, the L-C filter will contain an unavoidable and small distortion on V_{pwm} which is reflected mainly in the second and the third harmonics and consequently in the output voltage V_o. Although the input DC sources (E, K·E) are compensated and their ripple is negligible, the activated levels (E, K·E, K·E-1, -E) at V_{pwm} are mainly distorted by voltage drop $I_O R_{DS\text{-}ON}$. Nevertheless, by filtering action the experimental spectrum V_o is improved yet.

Finally, the switching devices are not ideal elements and the inductance has mainly copper losses. The welder junctions add more losses as well as the PCB design has parasitic effects that are out of hand. Up to this point, we have reviewed the main causes that can introduce differences in the measurements of the spectra. Spectra tested for R-load are basically used to verify the coherence between theoretical and experimental carriers set. Spectra tested for R-L-C load with no resonance are used to verify the optimization methods for some points of operation (M_a,K).

6.2.1 Checking the Carrier-Shape Modifications

The first experimental test was realized by using a single output pin from DSP. A simple program executes modulation algorithm where a sinusoidal wave modulates a low-power two-level signal that comes from the output pin T1PWM_T1CMP. The modulating signal is software-compared with a single carrier signal. This means that both the modulating and the carrier signals are sample-generated. These samples are chosen in such way that pseudo-natural modulation can be executed by the DSP. In this experiment, no power stage is needed on a PCB application; using a single output pin only permits to verify PWM execution by an algorithm. The output pin has a 0-3.3 V range. Thus the output signal shows a spectrum with a DC component. The generated modulating signal is calculated for M_a=0.9 and is compared and tested with different shape-carrier coefficients. The PWM switching frequency is 2.5 kHz.

UNIVERSITAT ROVIRA I VIRGILI
CONTRIBUTIONS ON SPECTRAL CONTROL FOR THE ASYMMETRICAL FULL BRIDGE MULTILEVEL INVERTER
Oscar Mauricio Muñoz Ramírez
ISBN:978-84-693-7665-2/DL:T.1747-2010

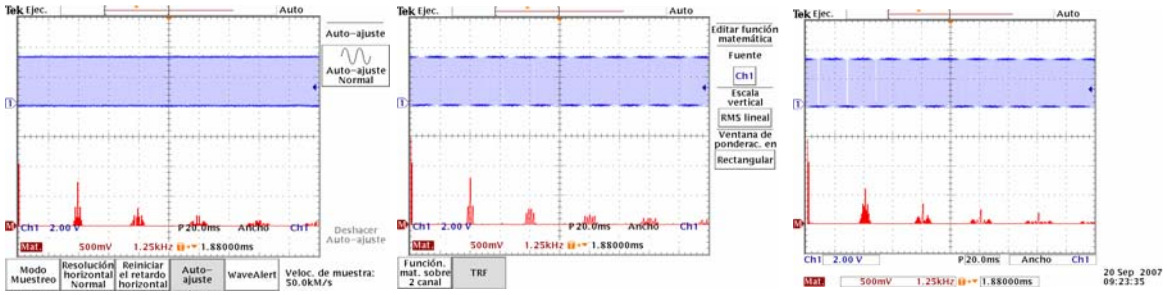

a) r=0.75 b) r=0.5 c) r=1.0

Figure 6.12 Spectrum patterns for Ma=0.9

In figure 6.12 it is observed and confirmed the carrier-shape influence on the spectrum. The spectral patterns are clearly differenced on the first carrier-multiple then on the adjacent carrier-multiples they are lesser and lesser differenced. Every carrier-multiple is surrounded by side-band harmonics (fundamental harmonic multiples that add or subtract from the carrier multiple) that are also affected by the carrier-shape. This simple experiment demonstrates the viability of implementing a pseudo-natural sampling modulation by means of digital hardware. The easy configuration of *r*-factor justifies the substitution of analog circuitry for PWM pulse-train generation.

6.2.2 Reliability of Pseudo-Natural Five-Level Modulation

There must be coherence between an obtained signal and a desired signal. To accomplish such evaluation some tests and methods were carried out and observed. First at all, correct driver signals from DSP must be obtained and with proper selection of tools for spectrum analysis the reliability on the tested spectra can be measured. The tools we used for spectra analysis are the FFT functions done by the oscilloscope and by Pspice and the C_{mn} and C_n algorithms done on Matlab.

Once the six driver signals are obtained and synchronized correctly, the power stage was connected with the driving circuitry. A preliminary test is done in order to prove the reliability of the Pseudo-Natural Five-Level PD-SPWM algorithm. The algorithm is executed by DSP, where the four r shape factors are modified in 31-cases. All these cases are detailed in Appendix B, table B.1, but here in this chapter only a few on them will be showed.

UNIVERSITAT ROVIRA I VIRGILI
CONTRIBUTIONS ON SPECTRAL CONTROL FOR THE ASYMMETRICAL FULL BRIDGE MULTILEVEL INVERTER
Oscar Mauricio Muñoz Ramírez
ISBN:978-84-693-7665-2/DL:T.1747-2010

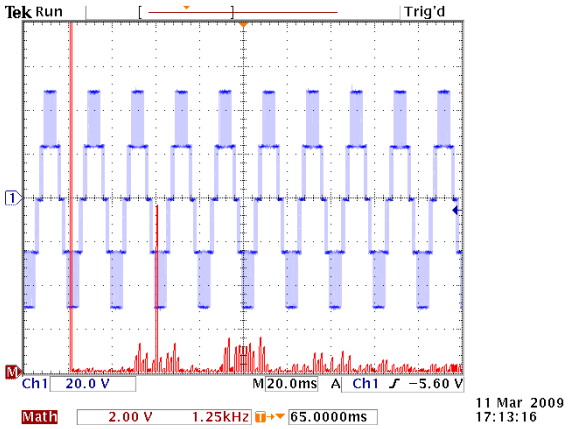

Figure 6.13 Case 1:{r1=0.5, r2=0.5, r3=0.5, r4=0.5}.

From figure 6.13 to figure 6.21 the spectral tests were realized with V_{dc}=50 V and M_a=0.9 and were obtained with the oscilloscope. Among these cases, we observed that Case 1 and case 2 (figures 6.13, 6.14) presented acceptable results when the output signal is analyzed by the oscilloscope FFT tool. In a first attempt, case-2 spectrum had some small harmonics on the base-band zone. We consider the base-band from the 2nd to 30th harmonic, then first side-band of the first carrier multiple appears as Bessel functions suggest. Those harmonics and their amplitudes might be considered negligible and then one might think the signal modulation as correct for case-1 and case-2.

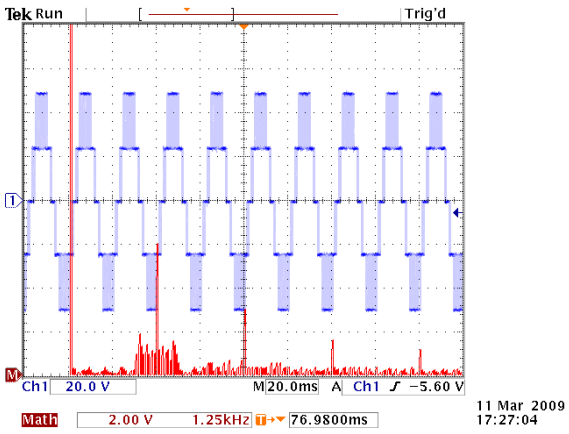

Figure 6.14

Case 2 :{r1=1.0, r2=1.0, r3=1.0, r4=1.0}.

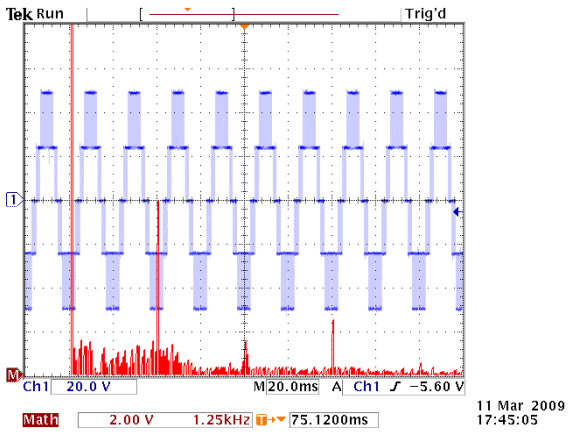

Figure 6.15

Case 4:{ r1=1.0, r2=1.0, r3=0.0, r4=0.0}.

However, after proving case 4 (figure 6.15) which presented several and significant wrong components on the base-band zone, some adjustments were done for the DSP algorithm code. The presence of those wrong harmonics means an incorrect reproduction of the modulation signal. The switching instants X_d and X_u, illustrated in figures 6.7 and 6.8, were first calculated by the expressions:

UNIVERSITAT ROVIRA I VIRGILI
CONTRIBUTIONS ON SPECTRAL CONTROL FOR THE ASYMMETRICAL FULL BRIDGE MULTILEVEL INVERTER
Oscar Mauricio Muñoz Ramírez
ISBN:978-84-693-7665-2/DL:T.1747-2010

$$X_d = \frac{M - L_{\max} + \dfrac{A-M}{r_i}}{\dfrac{L_{\min} - L_{\max}}{1-r_i} + 2\dfrac{A-M}{r_i}} \times 30000 counts \tag{6.1}$$

$$X_u = \frac{M - L_{\max} + \dfrac{M-B}{1-r_i} + \dfrac{L_{\max} - L_{\min}}{r_i}}{\dfrac{L_{\max} - L_{\min}}{r_i} + 2\dfrac{M-B}{1-r_i}} \times 30000 counts \tag{6.2}$$

After revising the algorithm code, it was detected overflow conditions, and then expressions for X_d and X_u were synthesized by rewriting the equations that determines the intersections of figure 6.8. The dependence of r as a denominator that produces overflow conditions is eliminated as equations 6.3 and 6.4 prove it.

$$X_d = \frac{(1-r_i)(2A - M - L_{\max})}{L_{\min} - L_{\max} + 4(1-r_i)(M-A)} \times 30000 counts \tag{6.3}$$

$$X_u = \frac{r_i(3M - 2B - L_{\max}) + L_{\max} - L_{\min}}{L_{\max} - L_{\min} + 4r_i(B-M)} \times 30000 counts \tag{6.4}$$

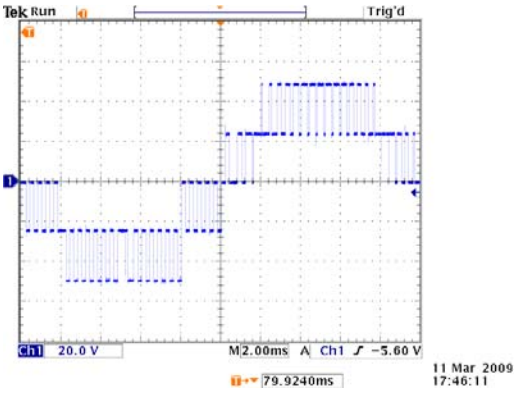

a) Experimental output signal

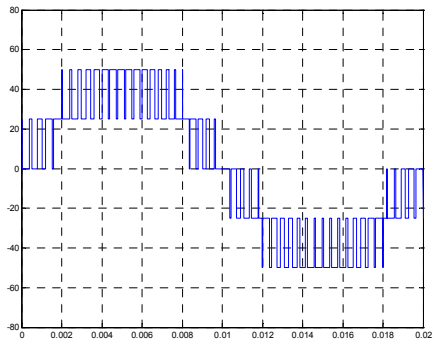

b) Simulated output signal

Figure 6.16 Wrong switching instants calculation, case4.

In the same case-4 (figure. 6.15) we could observe one fundamental cycle in time domain, where figure 6.16.a shows two missing pulses in the experimental signal obtained with the previous equations 6.1 and 6.1; meanwhile figure 6.16.b shows the simulated signal obtained with C_n-Algorithm in Matlab. Unfortunately, checking every switching pulse along one fundamental cycle is a tedious task. Finding a missing or extra pulse may take a short time, but checking exact instants of commutation is further difficult. Even after revising and correcting the expressions that computes X_d and X_u, it is necessary a systematic protocol that evaluate any spectrum quickly. To prove the exactitude of a modulated signal, the comparison

UNIVERSITAT ROVIRA I VIRGILI
CONTRIBUTIONS ON SPECTRAL CONTROL FOR THE ASYMMETRICAL FULL BRIDGE MULTILEVEL INVERTER
Oscar Mauricio Muñoz Ramírez
ISBN:978-84-693-7665-2/DL:T.1747-2010

between a simulated spectrum and an experimental spectrum is then justified. Hence, we use spectrum comparison as the basic evidence or primary data source. Case-4 is revised again and the obtained experimental spectrum (figure 6.17) is by far more accurate if compared with theoretical spectrum (figures 6.18, 6.19, 6.20).

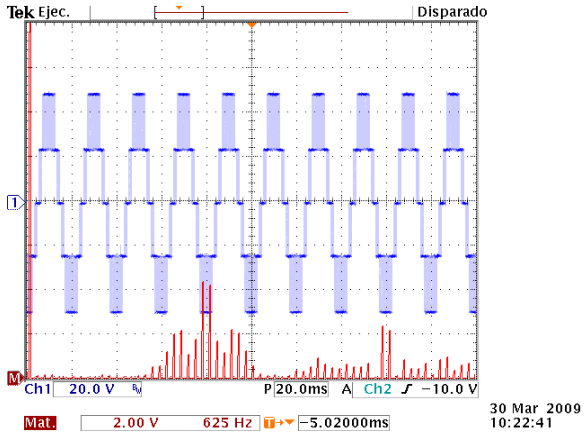

Figure 6.17 Oscilloscope-FFT, Case 4.

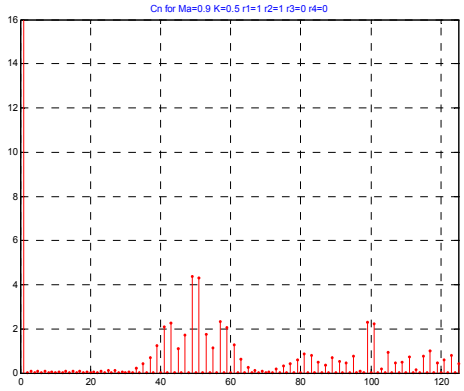

Figure 6.18 Spectrum by C_n-Algorithm , Case 4.

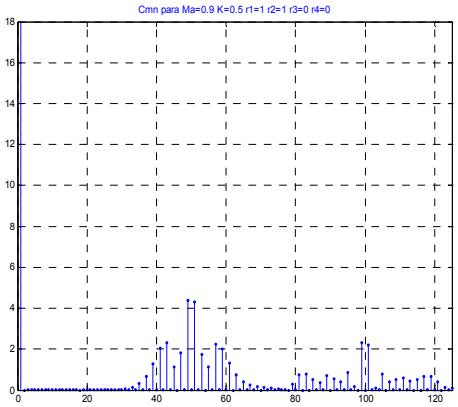

Figure 6.19 Spectrum by Cmn-Algorithm, Case 4.

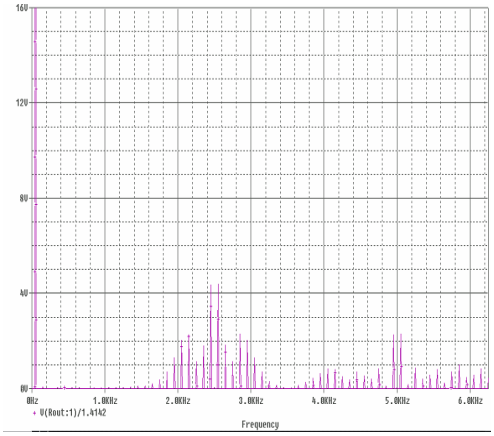

Figure 6.20 Pspice-FFT, Case 4.

Since the modulation frequency index is an exact integer (M_f=50) and the load is resistive (MOSFETS-losses are negligible,) thus signal reproduction is highly linear and only the fundamental component f_o=50 Hz should highlight over the base-band zone. Looking at figures 6.17, 6.18, 6.19 and B.1-Appendix B, it is observed that the base-band harmonics are below 1% of the main component. Then, the base-band zone is considered as neat. It can be concluded that presenting clean base-band for an open loop PWM with resistive load is a good indication of correct modulation process. This conclusion is based on visual inspection over the four types of previous calculated spectra. Visual inspection of the spectra is a valid and widely accepted method. Distortion parameters such as THD and $WTHD_0$ are quality indicators of signals, but they do not indicate the resemblance between theoretical and

UNIVERSITAT ROVIRA I VIRGILI
CONTRIBUTIONS ON SPECTRAL CONTROL FOR THE ASYMMETRICAL FULL BRIDGE MULTILEVEL INVERTER
Oscar Mauricio Muñoz Ramírez
ISBN:978-84-693-7665-2/DL:T.1747-2010

experimental sets of signals. Next sections introduce more strict methods that reinforce the evaluation of spectra and the resemblance between theoretical and experimental signals.

6.2.3 Qualifying Pseudo-Natural Spectra using Pearson-Correlation

Visual inspection of figures 6.17, 6.18, 6.19 and B.1-Appendix B demonstrates that experimental results are good enough to pass. However, visual inspection only qualifies but does not quantify how good or bad are these very results or other results. From figure B.1, in appendix B, the experimental spectra calculated by FFT-function embedded in oscilloscope are compared with their respective theoretical spectra calculated by Pspice FFT-function, C_n-Algorithm and C_{mn}-Algorithm. The sets of spectrum-tools were organized as pairs, and by subtracting them the error-magnitude is calculated on six pairs of arrays: $|C_{mn}-C_n|$, $|C_{mn}$-Dsp|, $|C_{mn}$-Pspice|, $|C_n$-Dsp|, $|C_n$-Pspice| and |Dsp-Pspice|. These arrays are obtained by the different harmonic calculation methods used in this thesis and their respective indexes are explained as follows:

C_{mn}: this index corresponds to the harmonics calculated by C_{mn}-Algorithm in Matlab.
C_n: this index corresponds to the harmonics calculated by C_n-Algorithm in Matlab.
Pspice: this index corresponds to the harmonics calculated by FFT-function of Pspice in circuit simulation.
Dsp: this index corresponds to the harmonics calculated by FFT-function of oscilloscope applied to the circuit controlled by DSP-modulator.

Drawing the error-magnitude of these arrays does not clearly conclude about the resemblance between the pairs of spectrum-methods as can be observed in figure 6.21. To attempt resemblance quantification, the Pearson correlation coefficient is used for our comparisons. It is widely used in the sciences as a measure of the strength of linear dependence between two variables. In statistics, the Pearson correlation coefficient (sometimes referred to as the PMCC, and typically denoted in statics as r) is a measure of the correlation between two variables X and Y, giving a value between +1 and −1 inclusive [Wik10, Rod88]; such coeffient is dimensionless. The two variables to be compared are the pair of spectrum-tools, e.g, C_{mn} *vs.* $C_{n.}$ To avoid misunderstanding, we denote this coefficient as Pearson-Correlation whose formula is written in (6.5); this formula is one of therteen ways of calculating correlation and it was the first one to be used by its author [Rod88]. The Pearson-Correlation can be described as is the quotient between the covariance of two variables X and Y and the product of their respective standard deviations. A value of 1 implies that a linear equation

UNIVERSITAT ROVIRA I VIRGILI
CONTRIBUTIONS ON SPECTRAL CONTROL FOR THE ASYMMETRICAL FULL BRIDGE MULTILEVEL INVERTER
Oscar Mauricio Muñoz Ramírez
ISBN:978-84-693-7665-2/DL:T.1747-2010

describes the relationship between X and Y perfectly, with all data points lying on a line for which Y increases as X increases. A value of −1 implies that all data points lie on a line for which Y decreases as X increases. A value of 0 implies that there is no linear correlation between the variables.

$$PearsonCorrelation = \frac{\sum_{i=1}^{n}\left(x_i - \bar{x}\right)\sum_{i=1}^{n}\left(y_i - \bar{y}\right)}{\sqrt{\sum_{i=1}^{n}\left(x_i - \bar{x}\right)}\sqrt{\sum_{i=1}^{n}\left(y_i - \bar{y}\right)}} \tag{6.5}$$

This coefficient is useful to compare different combinations of pairs that we want to compare. for instance, in figure 6.21 the error magnitude per harmonic amplitude is calculated for six pairs of arrays resulting of different combinations of of harmonic calculation methods. Pearson-Correlation is much easier to use in order to quantify if a pair of arrays match or do not match as a pair of correlated data which in particular means a match-quantification between two harmonic calculation methods.

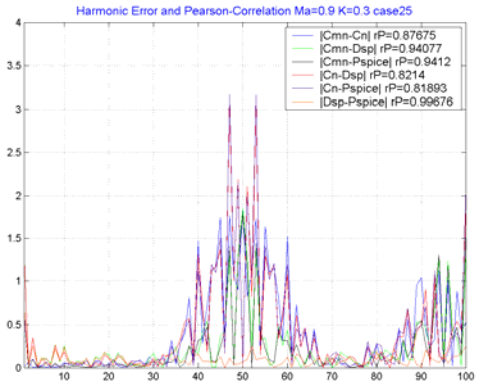

Figure 6.21 Error Magnitude and Pearson-Correlation.

More results based on Pearson-Correlation are calculated to the sets of spectrum-methods for each case from figure B.1, appendix B. The results are resumed in Tables 6.4, 6.5, 6.6 and 6.7 where the fourth rows contain the pair C_n *vs. Dsp* which is pair of most interest since it evaluates the resemblance between the theoretical spectrum calculated by C_n-Algorithm and the experimental spectrum.. The results of these tables are also placed in figure B.2 which shows error-magnitude curves for the pairs of spectrum-tools evaluated in each case previously visualized in figure B.1. Those graphs can have different interpretation but the Pearson-Correlation offers an alternative and complementary aid.

TABLE 6.4 PEARSON-CORRELATION FOR H={2…100} M_A=0.9, K0.5.

Pair of Harmonics Arrays	Case1	Case2	Case12	Case25
C_{mn} vs. C_n	0.7993	0.8939	0.8794	0.8767
C_{mn} vs. Dsp	0.7762	0.8973	0.878	0.8756
C_{mn} vs. Pspice	0.8024	0.9003	0.8842	0.8855
C_n vs. Dsp	0.9959	0.9985	0.9972	0.9968
C_n vs. Pspice	0.9991	0.9983	0.9994	0.9991
Dsp vs. Pspice	0.9959	0.9964	0.9972	0.997

TABLE 6.5 PEARSON-CORRELATION H={2…100} M_A=0.9, K0.3.

Pair of Harmonics Arrays	Case1	Case2	Case12	Case25
C_{mn} vs. C_n	0.7993	0.8939	0.8794	0.8767
C_{mn} vs. Dsp	0.9967	0.9953	0.9641	0.9408
C_{mn} vs. Pspice	0.9998	0.9993	0.9716	0.9412
C_n vs. Dsp	0.8035	0.9005	0.8971	0.8214
C_n vs. Pspice	0.7989	0.8939	0.8991	0.8189
Dsp vs. Pspice	0.9972	0.9959	0.9966	0.9967

TABLE 6.6 PEARSON-CORRELATION H={2…20} M_A=0.9, K0.5.

Pair of Harmonics Arrays	Case1	Case2	Case12	Case25
C_{mn} vs. C_n	0.046	-0.1158	0.4402	0.1159
C_{mn} vs. Dsp	-0.1819	-0.0705	-0.1467	-0.2591
C_{mn} vs. Pspice	-0.0962	-0.1827	0.3065	0.0371
C_n vs. Dsp	0.1186	0.336	0.1163	-0.1916
C_n vs. Pspice	0.0776	0.2139	-0.0191	-0.0526
Dsp vs. Pspice	0.3305	0.616	0.2906	0.4828

TABLE 6.7 PEARSON-CORRELATION H={2…20} M_A=0.9, K0.3.

Pair of Harmonics Arrays	Case1	Case2	Case12	Case25
C_{mn} vs. C_n	0.046	-0.1158	0.4402	0.1159
C_{mn} vs. Dsp	-0.2516	0.0644	-0.1098	0.1019
C_{mn} vs. Pspice	0.615	0.0133	0.4097	0.5676
C_n vs. Dsp	0.0972	0.3661	-0.3461	-0.1019
C_n vs. Pspice	-0.255	0.2302	-0.1118	-0.1765
Dsp vs. Pspice	0.1041	0.4468	0.718	0.5218

UNIVERSITAT ROVIRA I VIRGILI
CONTRIBUTIONS ON SPECTRAL CONTROL FOR THE ASYMMETRICAL FULL BRIDGE MULTILEVEL INVERTER
Oscar Mauricio Muñoz Ramírez
ISBN:978-84-693-7665-2/DL:T.1747-2010

First, in Tables 6.4 and 6.5 the evaluated interval comprises the harmonics *h={2…100}*. The weight of this interval is centered around the first carrier multiple and its side-band harmonics, *h={30…1*M_f…70}* and the evaluation by Pearson-Correlation mainly falls over them. Second, in Tables 6.6 and 6.7 the evaluated interval comprises the harmonics *h={2…20}*. This narrower interval focuses the evaluation by Pearson-Correlation on the base-band harmonics since their amplitudes are barely distinguishable when compared with the interval *h={2…100}*.

To conclude this section, from tables 6.4 and 6.5 the resemblance of the first carrier-multiple and its side-bands in all the pairs is large since all the Pearson-Correlation coefficients are bigger than 0.75. The rows of pair C_{mn} *vs.* C_n confirms that Natural Sampling and Pseudo-Natural are closely the same modulation and therefore Pseudo-Natural is a suitable technique to be implemented. The pairs C_{mn} *vs. Dsp*, C_n *vs. Dsp* and *Dsp vs. Pspice* confirm that experimental spectra are accurate when interval *h={2…100}* is evaluated. However, from Tables 6.5 and 6.6, the conclusion is that resemblance for base-band harmonics is poor. This means that when synthesizing a PWM waveform, the base-band zone is affected by other non modeled characteristics of the modulation in the AFBMI, e.g. the non linear effects (last row from table 6.3).

6.2.4 Checking the Switching Edges (X_d, X_u)

Since Pearson-Coefficient for base-band harmonics shows a poor coherence between the theoretical and experimental signals (pair C_n *vs. Dsp* from Tables 6.5 and 6.6), it is necessary to revise the computation of switching edges. For this purpose, the spectrum calculated by C_n-Algorithm is compared with its respective spectrum computed by the DSP by means of the registers X_d and X_u. These registers are read from DSP, and using Matlab the harmonics are calculated. We highlight that these registers are used to compute their expected spectrum, not the experimental spectrum which is measured at the prototype PWM voltage output. Despite corrections done on equations (6.1) and (6.2) which resulted in (6.3) and (6.4), it is necessary to confirm the correctness of registers X_d and X_u. Checking the switching edges proves whether the base-band zone is altered by incorrect functioning of DSP or by non linear effects or other characteristics not evident to be modeled. The next graphs, figures 6.22, 6.23 and 6.24, correspond to the spectra obtained by C_n-Algorithm and DSP-Algorithm and all of them have match exactly; the working conditions are V_{dc}=E=40 V, M_a=0.9, K=0.7. Pearson-Correlation is calculated between the theoretical spectrum obtained by C_n-Algorithm and the

UNIVERSITAT ROVIRA I VIRGILI
CONTRIBUTIONS ON SPECTRAL CONTROL FOR THE ASYMMETRICAL FULL BRIDGE MULTILEVEL INVERTER
Oscar Mauricio Muñoz Ramírez
ISBN:978-84-693-7665-2/DL:T.1747-2010

spectrum based on the switching instants associate to Timer1 registers and calculated by DSP; the range comprises harmonics h={2…20}. It is verified that the computation of switching edges by DSP is correct and the hypothesis that the base-band zone is affected by non modeled characteristics of the AFBMI modulation is proved. This ensures us that Pseudo-Natural sampling method is correctly applied by the experimental prototype we use. The protocol we established by using Pearson-Correlation which is used to evaluate a particular range of harmonics demonstrates to be a reliable tool for complementary spectra analysis.

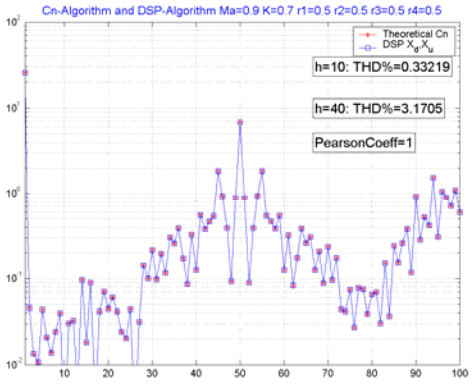

Figure 6.22 Spectra of theoretical and real case1.

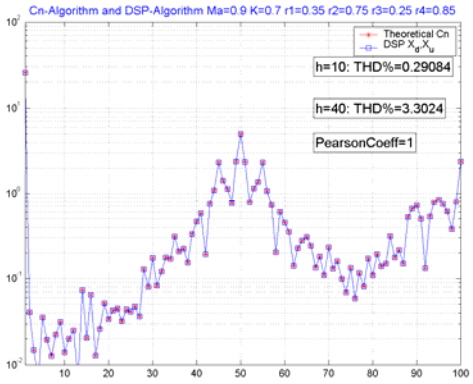

Figure 6.23 Spectra of theoretical and real case12.

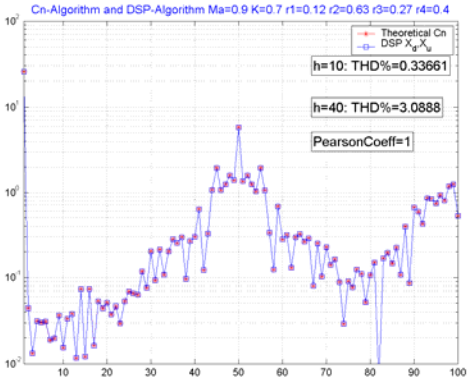

Figure 6.24 Spectra of theoretical and real case13.

6.3 Evaluating the Pseudo-Natural Spectra with THD and $WTHD_0$

In this section we present the results for some operating points $M_a=0.9$, $K=\{0.5,0.4,0.3\}$.THD and $WTHD_0$ offer different scopes or interpretations in spectral analysis that depend on the number of harmonics to be considered. Thirty-one cases were evaluated for the AFBMI with R-load connection. Figures 6.25 to 6.31 corresponds to the operating point $M_a=0.9$, $K=0.5$. In appendix B, the respective graphs of operating points $M_a=0.9$, $K=\{0.4,0.3\}$ are in figure B.3.

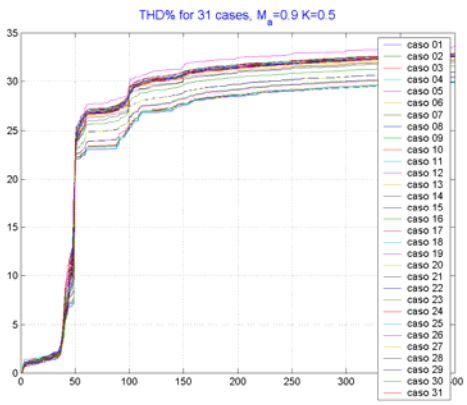

Figure 6.25 Global $THD_{h=400}$, K=0.5.

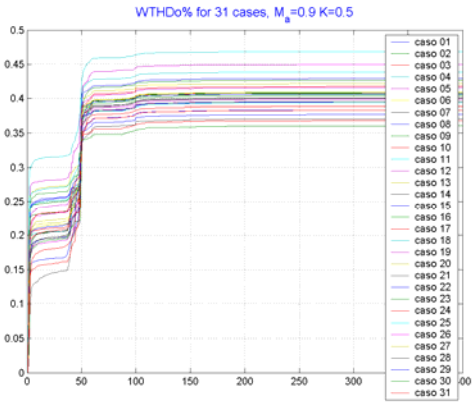

Figure 6.26 Global $WTHDo_{h=400}$, K=0.5.

When considering a broad spectrum, *h={2…100 or more}*, the global value of THD can be used as an indication of the amount of EMI as shown in figure 6.25.

For inverters with transformerless connections, global THD is an interesting data and the shape-carrier modification is an alternative to reduce global THD, but transformerless-connections are mainly oriented to higher switching frequency applications (M_f>50).

A global $WTHD_0$ mainly reflects the impact of the second and third harmonics because of the low attenuation of *1/n*, and of the first carrier multiple with its side-band harmonics because their major amplitudes, see figure 6.26. Global $WTHD_0$ gives information about the main harmonics related to ripple-voltage in DC-supplies, *h={2,3}*, but masks the others base-band harmonics, *h={2…30}*. Moreover, the second rise in these curves is an indication of the main ripple currents and voltages (*h={30…70}*) in storage elements such as the capacitor and inductance in a second order filter.

The curve with smallest change in its rise will be the most suitable if low ripple is specified. This is shown in some cases (see figures 6.13, 6.14 and 6.17) where the first carrier multiple amplitude can be reduced which hypothetically reduces the main ripple currents and voltages frequencies. Figures 6.27 and 6.28 are the respective selections of the best five cases for global THD and $WTHD_0$ including one hundred harmonics.

However, global distortion parameters are not used for our purposes. Due to the compensation over the base-band zone, ten harmonics are to be included in computing partial THD and $WTHD_0$. Figure 6.29 results in *case5* as the most suitable for *h=10*. However, in this graph it can be observed that *case14* has a minor impact originated from the second-and-third harmonics and because of this reason this case might be selected. After revising figure 6.30,

UNIVERSITAT ROVIRA I VIRGILI
CONTRIBUTIONS ON SPECTRAL CONTROL FOR THE ASYMMETRICAL FULL BRIDGE MULTILEVEL INVERTER
Oscar Mauricio Muñoz Ramírez
ISBN:978-84-693-7665-2/DL:T.1747-2010

the extension to the 30th harmonic of the five curves previously selected by the criterion $THD_{h=10}$, indicates that although *case14* has the smallest second-and-third harmonics this case can inject more distortion since a conventional filter has cut-off frequency nearby the 20th or 30th harmonic.

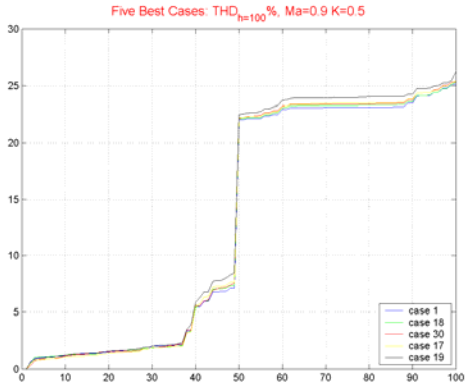

Figure 6.27 Best cases for $THD_{h=100}$, K=0.5.

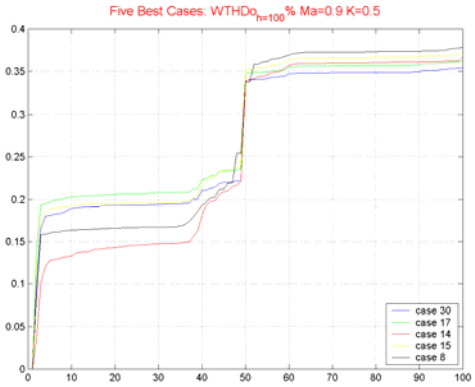

Figure 6.28 Best cases for $WTHD_{oh=100}$, K=0.5.

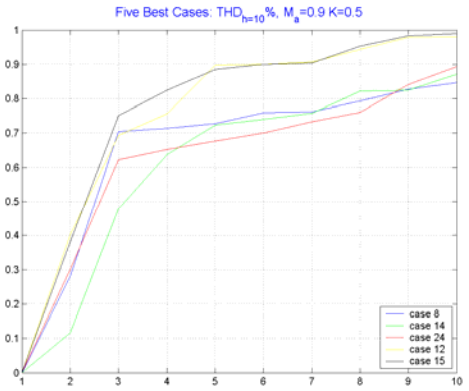

Figure 6.29 Best cases for $THD_{h=10}$, K=0.5.

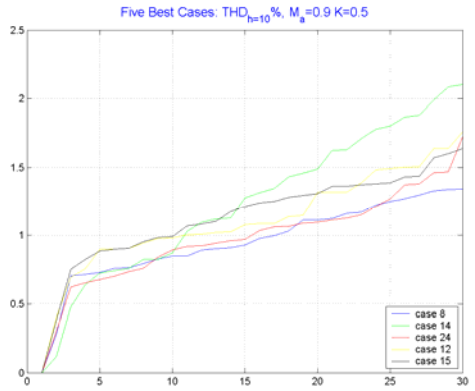

Figure 6.30 Evolving of THD to h=30.

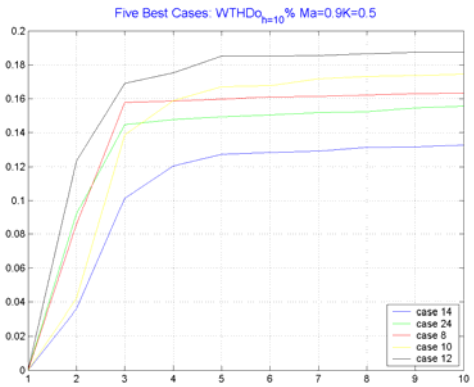

Figure 6.31 Best cases for $WTHDo_{h=10}$, K=0.5.

Figure 6.31 only gives information about *h={2,3}*, whereas the others base-band harmonics (*h={4…30}*) are masked. Partial $WTHD_0$ is only useful for highly inductive loads. The results

of this section demonstrate the importance of modifying the carrier-shapes but also show that distortion parameters must be properly chosen and interpreted.

Although a considerable amount of cases were evaluated (thirty-one cases of table B.1), there is not certainty of finding the best carrier-shape combination. However, it shows a path to be explored and leads to find good solutions that can improve the spectra. When attempting this results, it was how we stated the need of an optimization tool such as GA.

6.4 Performance of PD, POD, APOD with Diverse Sampling Methods

Our main interest in this thesis is Phase Disposition SPWM done by Pseudo-Natural sampling method. Nevertheless, in this section we briefly present some results on other types of modulation to demonstrate the flexibility of our modulator based on DSP. Two sampling methods, Regular Asymmetrical and Regular Symmetrical, were proved on the Phase Disposition scheme. Additionally, we proved Phase Opposition Disposition and Alternative Phase Opposition. These two last schemes are executed by using Pseudo-Natural sampling method; notice that for these phase disposition methods the symmetrical or asymmetrical sampling can be used giving a large number of combinations.

In all these experiments we only used the standard carrier (r_i=0.5); however in these methods we remark that as future works it is possible to explore the effect of modifying the carriers set. Such works can be focused in similar aspects as well as the items we have studied here with PD-SPWM. The sampling methods (natural, pseudo-natural, symmetrical and asymmetrical) can be used for any type of SPWM such as PD, POD, APOD or PS. Thus, the combinations may lead to an unaffordable research. By using optimization tools, the PD-SPWM algorithm can be used to compensate the carriers set in order to achieve a low distortion profile even better that any other type of SPWM. Notice that in figures 6.33 to 6.35 all the types of PWM schemes have diverse harmonic profile with different local minima, where their plotting curves show different locations where a specific scheme is better that the rest, but such properties are not consistent along a particular plotting.

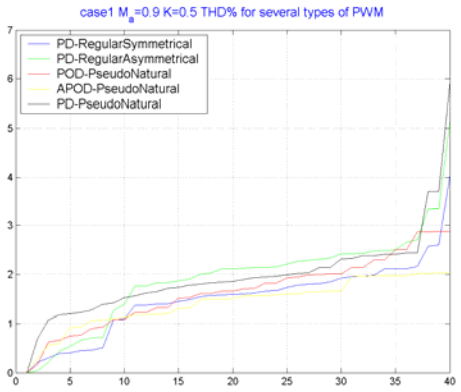

Figure 6.32 PD, POD, APOD and Symmetrical and Asymmetrical Regular Sampling, Ma=0.9, K=0.5.

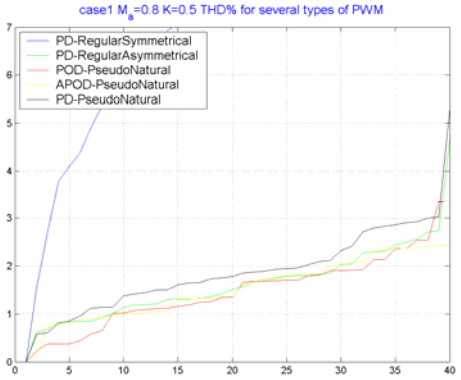

Figure 6.33 PD, POD, APOD and Symmetrical and Asymmetrical Regular Sampling, Ma=0.8, K=0.5.

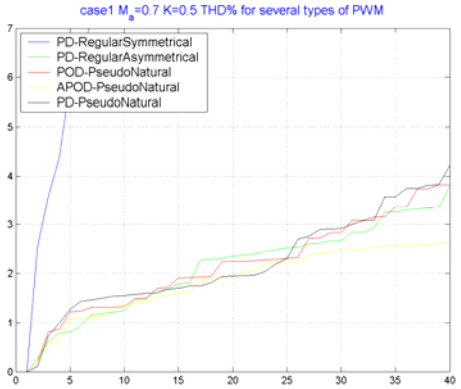

Figure 6.34 PD, POD, APOD and Symmetrical and Asymmetrical Regular Sampling, Ma=0.7, K=0.5.

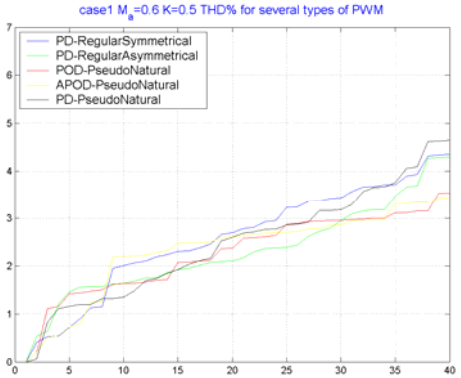

Figure 6.35 PD, POD, APOD and Symmetrical and Asymmetrical Regular Sampling, Ma=0.6, K=0.5.

UNIVERSITAT ROVIRA I VIRGILI
CONTRIBUTIONS ON SPECTRAL CONTROL FOR THE ASYMMETRICAL FULL BRIDGE MULTILEVEL INVERTER
Oscar Mauricio Muñoz Ramírez
ISBN:978-84-693-7665-2/DL:T.1747-2010

7. Carriers Optimization with Genetic Algorithms

7.1 Carrier Set Optimization at a given working point (Ma, K)

Having predictive models that determine the spectrum for a defined set of carrier-shapes are useful tools; C_{mn}-Algorithm and C_n-Algorithm have proved it. Such tools or methods offer a reliable path to select a suitable carriers set when a low harmonic profile is desired in SPWM modulation. For a particular operating point $V_{pwm}(M_a,K)$, such suitable carriers set can be found after some trail and error iterations; an acceptable although not optimum carriers set can be found. Despite of their usefulness, our developed tools both C_{mn}-Algorithm and C_n-Algorithm, can not predict on-line a new and optimum set of carrier-shapes for a different operating point $V_{pwm}(M_a,K)$. This means the spectrum model can not provide instant information concerning to carrier-shapes, when in the light of stationary regime, a closed loop system compensates its control signal or the reference signal is modified which is the case of M_a, e.g. load variations. A similar situation is presented when the DC supplies have varying voltage which results in changing K. Since in a practical application the load and the DC sources are changing, as far as the range of operating point $V_{pwm}(M_a,K)$ expands so should do the carriers set in order to cover such points.

For calculating on-line/off-line an optimum set of carrier-shapes, arises the need of developing a tool able to explore a wide number of sets for one single operating point. After exploring this wide but not unaffordable number of sets, such tool evaluates the harmonic distortion that will cause every set. Then, by comparing the sets, an optimum solution-set can be founded yielding an optimized operating point in the plane M_a,K. For any arbitrary and non-optimized operating point, its optimum carriers set can be obtained by using four surrounding optimized points, namely V_{pwmA}, V_{pwmB}, V_{pwmC}, and V_{pwmD}. With their four solution-sets, we intend to develop a formula or technique that permits to interpolate the solution for any intermediate operating point located among the four points; this idea is depicted in figure 7.1. The purpose of this approach is developing a tool that calculates an optimum set of carrier-shapes for any operating point allocated within a defined range in the plane M_a,K.

UNIVERSITAT ROVIRA I VIRGILI
CONTRIBUTIONS ON SPECTRAL CONTROL FOR THE ASYMMETRICAL FULL BRIDGE MULTILEVEL INVERTER
Oscar Mauricio Muñoz Ramírez
ISBN:978-84-693-7665-2/DL:T.1747-2010

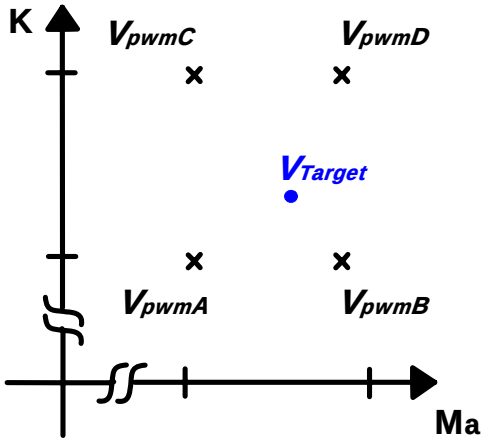

Figure 7.1 Target Point $V_{target}(M_a,K)$ sorrounded by 4 pre-calculated points.

As mentioned before in Chapter 3, the shape factor has a range between zero and one. Practical modifications in this factor are equal or greater than 0.01 so that the spectrum can be modified. For simplicity, let us consider three typical values for one single carrier-shape, r_i:{0.0, 0.5, 1.0}. For a 5-level SPWM scheme, four carriers are needed which leads us to deal with 3^4=81 sets. If Δr_i=0.01, that is a resolution of 1%, the number of sets is about one hundred million.

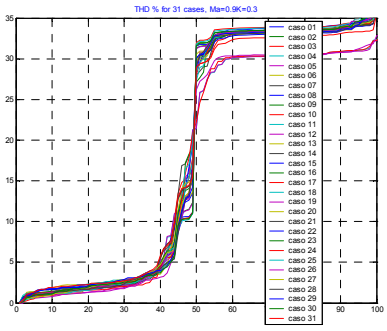

a) THD%, h=100

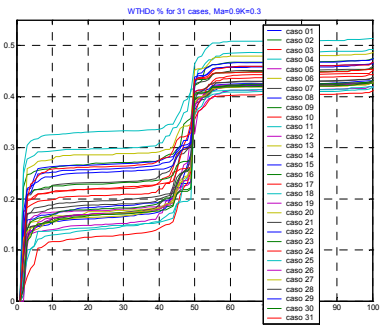

c) $WTHD_0$%, h=100

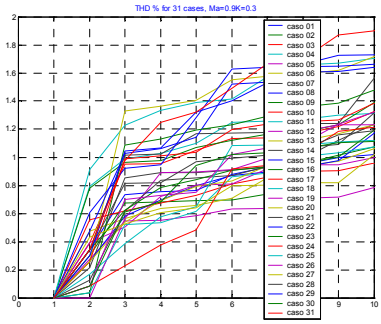

b) THD%, h=10

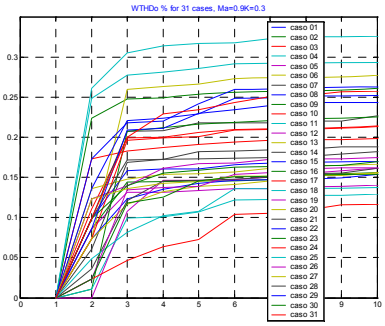

d) $WTHD_0$%, h=10

Figure 7.2 Distortion for 31 cases of carrier programming.

UNIVERSITAT ROVIRA I VIRGILI
CONTRIBUTIONS ON SPECTRAL CONTROL FOR THE ASYMMETRICAL FULL BRIDGE MULTILEVEL INVERTER
Oscar Mauricio Muñoz Ramírez
ISBN:978-84-693-7665-2/DL:T.1747-2010

In advance, consider one single operating point, where a finite number of cases were analyzed in experimental prototype. Thirty-one cases were tested and compared to find the best case among them as depicted on figure 7.2 where the working point is (Ma=0.9, K=0.3). Nevertheless, the best case or at least the most possible optimal case is hardly detected as a global solution. How many cases should then be enough?, Three hundred?, Two thousand?. Testing a high number of sets is dramatically costly in time and effort and finding a proper trade-off quantity of tests is not a trivial matter. Either C_{mn}-Algorithm or C_n-Algorithm can be used as a sub-routine which is executed by a master program that explores the global solution for an operating point. Such master program must perform a greater number of iterations than those realized in an experimental prototype where human errors are uncontrollable.

Because of the reasons above, we took into consideration Genetics Algorithms as an alternative research tool. Genetics Algorithms (GA) are a useful resource that is efficient, reliable and accurate. GA are efficient, since they find a solution with minimum effort; they are reliable, because the found solution is acceptable regardless the process description complexity; and they are accurate since the solution is the best possible. And this last remark is the answer to the question attached to any operating point (M_a, K) for the AFBMI. –Which solution or case is the best possible for any operating point?

Before describing how a GA works, an introduction to lexis referenced in GA literature must be done. The term *individual* or *solution* refers, in our case, to a singular set of carrier-shape. Each individual has a genetic profile or code, its own identity defined as chromosomal representation. The general chromosomal representation of a solution is: $solution_p=\{gen_1, gen_2, gen_3, gen_4...\}$. In particular, for 5-level SPWM one solution contains information of the four carrier-shape ($case_p=\{r_1=c_1, r_2=c_2, r_3=c_3, r_4=c_4\}$). The *population* is the number of solutions existing for a generation (one iteration in the algorithm). A fitted solution refers to the individual that satisfies a performance criterion, i.e. *Objective Function*, and hence the solution is classified as a good candidate or parent. The fittest solutions are the best individuals from a generation, and they constitute the *elite population*. Depending on the purpose, the Objective Function may be used to find a minimum or maximum value. In our case, THD for first ten harmonics is the function to be minimized.

The solution given by GA is classified after some iterations, wherein a wide number of solutions evolve during the generations performed by the algorithm. A wide number of solutions must be interpreted as high enough as to pick from well distributed samples from a big population and, as low enough as to converge rapidly to the optimal solution. Until now,

UNIVERSITAT ROVIRA I VIRGILI
CONTRIBUTIONS ON SPECTRAL CONTROL FOR THE ASYMMETRICAL FULL BRIDGE MULTILEVEL INVERTER
Oscar Mauricio Muñoz Ramírez
ISBN:978-84-693-7665-2/DL:T.1747-2010

we can state that using a GA is an exceptional tool to explore the best possible solutions for a given set of operating points. At each of these points some randomly chosen cases are tested, selecting the best solutions according to lowest harmonic distortion criterion (objective function for a GA).

GA plays the same role, as environment play in nature systems. They are based on Charles Darwin's simplest version of evolution. The best individuals have the major chances to survive and to transmit knowledge and heritage to their descendants. In this process random variation and natural selection participate. This solving-problem technique has been used for unlimited number of applications.

7.2 Brief Description and Definition for GA's

In the 1950s and 1960s several researchers worked independently with the idea that evolution theory could be used as an optimization tool for engineering problems [Mel96]. Optimization tools have been implemented on systems that create, evaluate and select a population of solutions to a given problem. To perform creation and selection of candidate solutions, genetic operators are used. These operators are inspired in natural genetic variation and natural selection. The following figure depicts the flowchart with the basic steps for a Genetic Algorithm.

Before working with a GA, solution representation must be encoded into the chromosomal representation. Three basics approaches are cited on literature [Ade07,Mel96]:

- Encoding solutions as binary strings sequences of 1s and 0s where the digit position represents some aspect of the solution.
- Encoding solutions as integer or decimal number sequences, allowing a more complex or continuous representation of the solution.
- Encoding solutions as character strings, where each letter represents a specific aspect of the solution.

UNIVERSITAT ROVIRA I VIRGILI
CONTRIBUTIONS ON SPECTRAL CONTROL FOR THE ASYMMETRICAL FULL BRIDGE MULTILEVEL INVERTER
Oscar Mauricio Muñoz Ramírez
ISBN:978-84-693-7665-2/DL:T.1747-2010

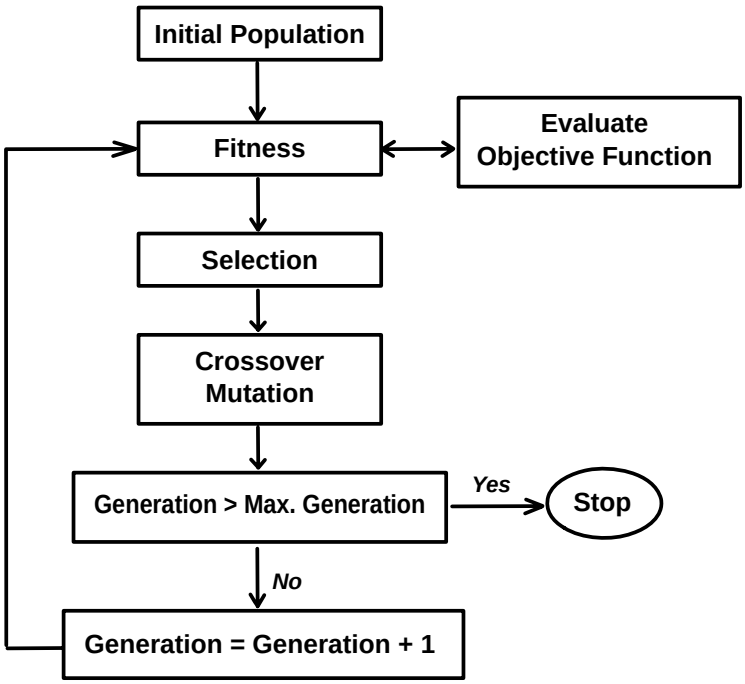

Figure 7.3 Basic Configuration of a Genetic (Evolutive) Algorithm.

Once it is defined the encoding representation, the first step starts by constructing the Initial Population P_i from a random selection of solution. Then all the solutions are evaluated by checking their fitness. Fitness means how close an individual is to solve the assigned problem. This evaluation is accomplished by Objective Function that determines which are the fitter solutions and with them, Selection randomly chooses the couples of parents (P_1,P_2) from the fitter solutions (elite population).

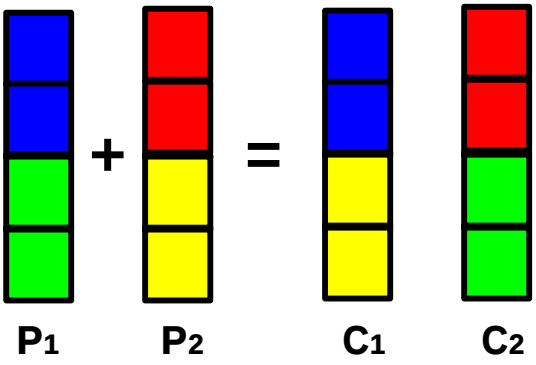

Figure 7.4 Crossover simplified scheme.

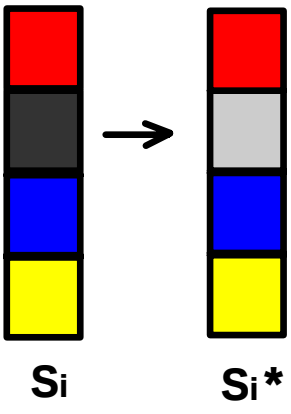

Figure 7.5 Mutation simplified scheme.

Coming from each selected couple, two children or descendants (C_1,C_2) are the new solutions that inherit the best characteristics from both their parents; they are created by crossover (recombination of parent's genes), see figure 7.4. With new solutions, the initial population is

expanded by crossover from an initial population to a Maximum Population P_{max}. After that, mutation randomly modifies some solutions from the population altering one gene in each mutant solution as illustrated in figure 7.5.

At this point, the algorithm re-starts at Fitness step, initiating a new generation which begins from a New Initial Population. The steps Fitting, Selection, reproduction and population expansion (up to P_{max}) by Crossover, and Mutation are repeated for G generations. After all the generations (iterations), the expected result is an optimal population with the most possible adapted, evolved and improved solutions. To resume, GA consist of Chromosomal Representation, Initial Population, Fitness evaluation, Selection, Crossover and Mutation. These steps are done over a population that evolves for a number of generations. There is no rigor to implement GA since both the variety of problems and the strategies for tuning differ from one application to another. Actually, many reports can be found on literature; a survey in GA subjects is a task concerning to evolutionary and genetic computation area and because of these reasons we only give the details concerning to our application in this thesis.

Further details are worth for commenting about selection, crossover and mutation. *Selection* has to be balanced with variation from crossover and mutation (exploitation/exploration balance). That means that too strong selection fits suboptimal individuals in new generations, reducing the needed diversity for further changes and progresses. On the contrary, weak selection results in slow evolution increasing convergence time for a GA [Mel96]. It is remarkable that selection has different strategies such as elitist selection, linear rank selection, roulette wheel selection, tournament selection and others strategies mentioned on the literature. In particular, when using our spectral modeling to search optimum cases, elitist selection is the strategy applied to GA that finds solutions for AFBMI. Elitist selection only takes the most fitted solutions for the next generation. The simplest version of *Crossover* takes the half-subsequences from two parents and by interchanging them, two offspring or descendants are the new built solutions. *Mutation* occurs in randomly assigned solutions, where the probability of alteration in one gene is small, i.e. the variance.

Additionally, two questions can be stated. When should we apply GA for a given problem since we are not clearly sure of the solution space size? How do we tune population size, crossover and mutation? In the evolutionary computation literature, many authors have reported a variety of approaches to parameter tuning. [Mel96] mentions others authors who reported an interesting conclusion about GA tuning criterion: they were independent of the problem in their tests. Reported settings were: population size 20-30, crossover rate 0.75-0.95

UNIVERSITAT ROVIRA I VIRGILI
CONTRIBUTIONS ON SPECTRAL CONTROL FOR THE ASYMMETRICAL FULL BRIDGE MULTILEVEL INVERTER
Oscar Mauricio Muñoz Ramírez
ISBN:978-84-693-7665-2/DL:T.1747-2010

and mutation rate 0.005-0.01. For crossover and mutation rates more details will be explained in describing our particular GA application.

7.3 Tunning GA's Parameters to Optimize the Carriers Sets

In order to create a framework which covers all the points within a defined bi-dimensional range [minM_a: maxM_a, minK:maxK], we executed the GA for some chosen points, separated by short intervals namely 0.025. We consider the limits of this range as practical in most of experimental applications. Then the amplitude index is covered within the range [0.7 : 0.025 : 1.0] and the level distribution comprises the range [0.3 : 0.025 : 0.7]; the bi-dimensional range yields in 221 operating points. For every point, $V_{PWM}(M_a,K)$, the parameters used for implementing our version of GA were:

- N=20 (initial population)
- N_{max}=50 (maximum population)
- G=5000 generations or iterations
- Mutation rate= 0.05 (5% probability that one solution mutates one of its genes)
- Population Variance =0.1 (maximum variation for a designed mutating gene r_i)
- Crossover operator: $$C_i = 0.5[(1+\beta)P_1 + (1-\beta)P_2]$$ $$C_{i+1} = 0.5[(1-\beta)P_1 + (1+\beta)P_2]$$
- where P_1 and P_2 represent the Parents and C_i and C_{i+1} represent the Children or solutions.
- For crossover operator, the coverage factor is: $$\beta = \begin{cases} (2\mu)^{1/\eta} & ,\mu \geq 0.5 \\ \dfrac{1}{2(1-\mu)}^{1/\eta} & ,\mu < 0.5 \end{cases}$$
- Coverage factor is a probabilistic distributed function, and it permits to crossover-operator to assigns two complementary factors for generating new genes. This guarantees an equal range of values for each gene, conserving the chromosomal representation [Res07]. The coverage factor makes crossover implementation more sophisticated than simply interchanging a sequence of genes as proposed in figure 7.5. Then, recombination of two parents genes falls in two "complementary-twin" genes gaining more resemblance between them and their parents genes.
- In the coverage factor, μ is a random number [0…1], $2 \leq \eta \leq 5$ and for our case η=4.
- Objective Function: $THD_{h=10}$. Despite of $WTHD_0$ advantages for analysis interpretation, we chose $THD_{h=10}$ parameter since it computes all the components with the same

UNIVERSITAT ROVIRA I VIRGILI
CONTRIBUTIONS ON SPECTRAL CONTROL FOR THE ASYMMETRICAL FULL BRIDGE MULTILEVEL INVERTER
Oscar Mauricio Muñoz Ramírez
ISBN:978-84-693-7665-2/DL:T.1747-2010

weight. Besides, the accumulated value changes substantially when increasing the term-frequency addition which permits detecting the presence of subsequent harmonics.

In all tested executions, it was observed that convergence is reached after two thousand iterations. The convergence is confirmed for all the execution-experiments of this algorithm. Convergence means finding an acceptable and optimized solution but not finding the global best one. The inclusion of ten components for calculating $THD_{h=10}$ must be interpreted as the combination of different frequencies whom can vary their amplitudes distribution for an equal reached $THD_{h=10}$. This means that for the same reached objective function value there is more that one solution. However, the main reason of using a GA is obtaining an optimized but feasible solution. Several executions were done for the same operating point, and the same procedure were repeated for more points, thus precision is confirmed for having the same solutions in the same evaluated points.

TABLE 7.1 EVOLUTION OF THE CARRIERS SET WITH FIXED MUTATION (0.05), VARIANCE (0.1), P_{MAX}=5000, AND FORCED INITIAL POPULATION.

Objective Function ($THD_{h=10}$%)	**r1**	**r2**	**r3**	**r4**	**Generation**
0.33413	0.5	0.0	0.0	0.5	1
0.13643	0.54111	0.96104	0.9988	0.92583	10
0.094291	0.48545	0.94896	0.89227	1	10
0.094111	0.48296	0.94518	0.88883	1	1000
0.080314	0.47597	0.94689	0.89168	0	5000

TABLE 7.2 SOFTLY INCREASED MUTATION AND VARIANCE AFTER THE 300TH GENERATION. P_{MAX}=1500. NO FORCED INITIAL POPULATION.

Objective Function ($THD_{h=10}$%)	**r1**	**r2**	**r3**	**r4**	**Generation**
0.23626	0.26514	0.8161	0.92466	0.91131	1
0.14538	0.40163	1	0.87274	1	10
0.094113	0.48253	0.94552	0.88874	1	100
0.080315	0.47609	0.94692	0.89182	0	1000

Tables 7.1 and 7.2 summarize the evolution of the individuals comprised by the chromosomal expression given as a set of carrier-shapes. After testing the algorithm with different criteria of mutation, we observed two important features in convergence and evolution: the first

UNIVERSITAT ROVIRA I VIRGILI
CONTRIBUTIONS ON SPECTRAL CONTROL FOR THE ASYMMETRICAL FULL BRIDGE MULTILEVEL INVERTER
Oscar Mauricio Muñoz Ramírez
ISBN:978-84-693-7665-2/DL:T.1747-2010

feature is that the initial population at iteration one can be declared with random individuals or they can be pre-assigned with some specific values, .e. a declared initial condition. It is confirmed that GA are no dependant of initial conditions to find an optimum solution. The second feature is the effect of mutation and its effect over convergence. When using a static and low mutation coefficient, the algorithm gains stability while is evolving. However it needs a high number of generations so an incoming mutant solution has major probabilities to be evaluated by the objective function; this comprises a long computing cost. In order to reduce the convergence time, and furthermore, to explore more possible local minima, the mutation and variance can be softly increased.

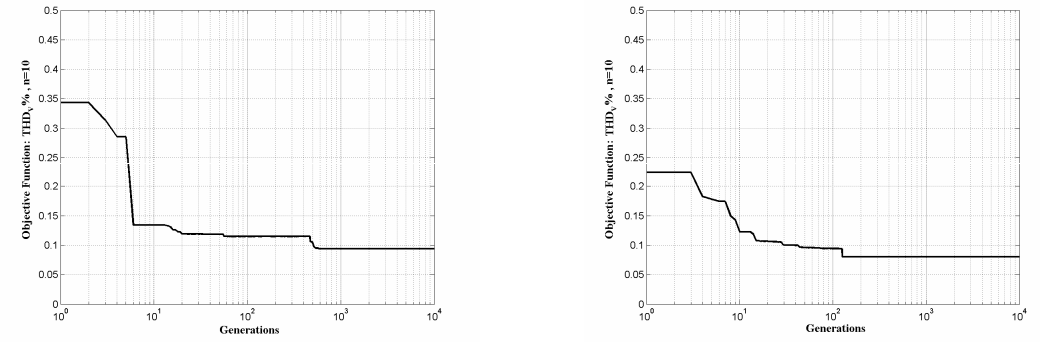

a) Evolution with forced initial population and fixed mutation and variance.

b) Evolution with random initial population and varying mutation and variance.

Figure 7.6 Convergence Characteristics for different criteria of mutation.

This procedure can be done after evolving along stable iterations, say 300 iterations, where the individuals of the population present a stable genetic code. In our application, after 300 iterations evaluating the spectra modeled by subroutine "C_n-Algorithm", we state that it is worth to try increased mutation and variance to reduce the convergence time. Figure 7.6 is an example of convergence (optimized point: $V_{target}=\{M_a=0.8,K=0.3\}$) and how a GA evolves faster by manipulating its mutation operators. After the 300^{th} generation, mutation and convergence were increased in 5% every one hundred generations up to a certain limit which in this case was 50%; after passing such limit, mutation and variance are set to their original values.

Optimization over the base-band is hardly distinguished if visual inspection on linear plots is done. A semi-logarithmical scale is more recommendable, although it is not commonly used in many publications. However, measuring or modeling the spectrum to calculate $THD_{h=10}$ permits to analyze the base-band harmonics for any particular case of carrier programming . Figure 7.7 shows two good spectra, where a) is the best fitted solution obtained in the first

UNIVERSITAT ROVIRA I VIRGILI
CONTRIBUTIONS ON SPECTRAL CONTROL FOR THE ASYMMETRICAL FULL BRIDGE MULTILEVEL INVERTER
Oscar Mauricio Muñoz Ramírez
ISBN:978-84-693-7665-2/DL:T.1747-2010

generation, and b) is the optimum spectrum obtained by the best solution after GA has stopped.

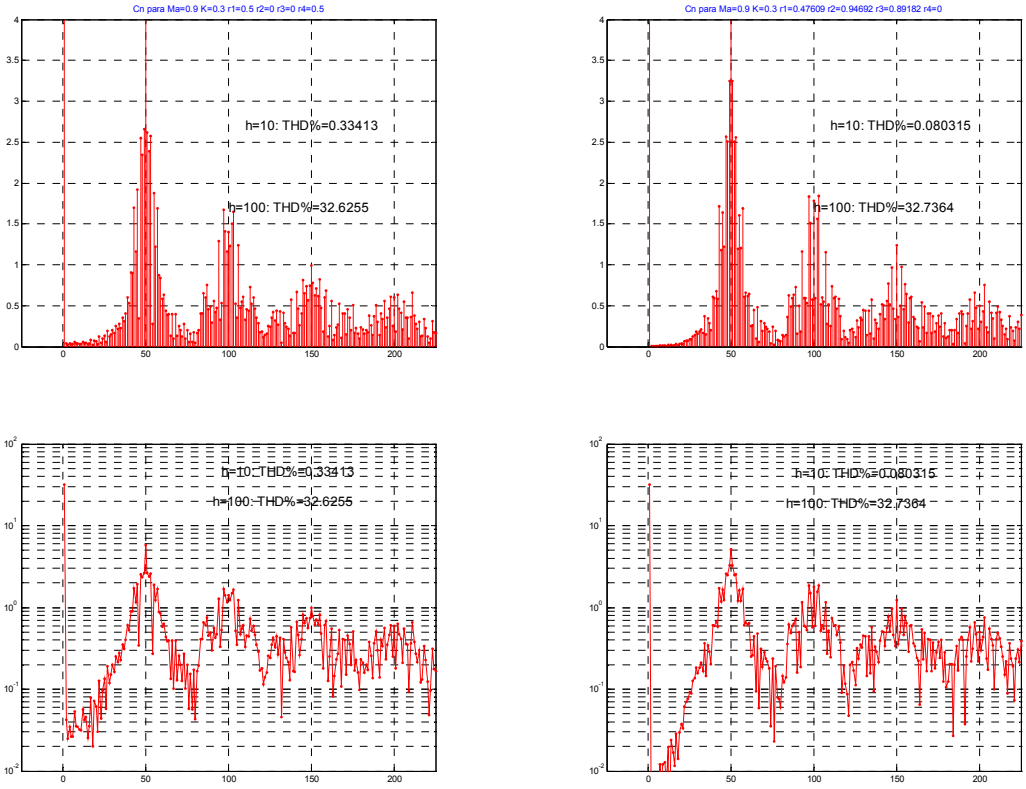

a) Best Fitted Solution from first iteration: {r1=0.5, r2=0, r3=0.0, r4=0.5}

b) Optimal Solution from last iteration: {r1=0.4451, r2=0.9357, r3=0.1195, r4=0.9845}

Figure 7.7 Spectrum Optimization (Ma=0.9, K=0.3).

The usefulness of GA as optimizing tool is demonstrated in this application and its extension to others applications is viable. In particular, for an analog SPWM modulator, the C_{mn}-Algorithm is the suitable sub-routine GA can utilize since such DFS-based on model considers the pure and exact modulation method with exact switching instants. For pseudo-natural sampling modulation or regular sampling modulation GA needs an adapted spectrum formulation as is the case of SFS-based on C_n-Algorithm which is used to optimize pseudo-natural modulation. For a digital modulator, depending on hardware resources and critical time requirements, a GA can be further exploited as an off-line or on-line optimizing resource; an on-line GA application would require a high performance embedded system, probably based on techniques suchs distributed or pararell procesors real-time features. These advantages still open interesting paths in research since systematic analysis can be performed for broader explorations by calculating any selected distortion criterion.

UNIVERSITAT ROVIRA I VIRGILI
CONTRIBUTIONS ON SPECTRAL CONTROL FOR THE ASYMMETRICAL FULL BRIDGE MULTILEVEL INVERTER
Oscar Mauricio Muñoz Ramírez
ISBN:978-84-693-7665-2/DL:T.1747-2010

7.4 Experimental Results of a GA Optimized Spectra

Next results are obtained by using GA where the harmonic distortion profile is kept as low as possible. THD curves can present different plots where the accumulated value for a determined interval of harmonics can be low but after passing a number of harmonic the curve tends to a higher distortion value.

The final version for our GA takes into account the local accumulated values at the harmonics ten, twenty and forty, i.e. $THD_{h=10}$, $THD_{h=20}$ and $THD_{h=40}$. This ensures that the found solution presents a low distortion along the whole base-band zone. In case this is not accomplished, as minimum, the first ten harmonics should be minimized. The second order filter consist of L=1900μH and C=6.6μF and since the load is R=10 Ω, the frequency transfer function has not overdamped response at the cut-off frequency.

TABLE 7.3 OPTIMIZED CARRIERS SET COMPARED TO TYPICAL SETS.

Working Point (M_a,K)	Case	r_1	r_2	r_3	r_4	Below case1	Below case2
(0.8,0.3)	Optimum1	0.0	0.54	0.47	0.934	Yes	No
	Optimum2	0.0	0.5	0.5	1.0	Yes	Yes
(0.8,0.5)	Optimum1	0.0	0.91	0.296	0.795	No	No
	Optimum2	0.0	1.0	0.5	0.5	No	No
(0.9, 0.4)	Optimum1	0.37	0.9811	0.393	0.57	Yes	No
	Optimum2	0.5	1.0	0.5	0.5	Yes	No
(0.9,0.5)	Optimum1	0.0	0.954	0.273	0.674	Yes	No
	Optimum2	0.0	1.0	0.5	0.5	Yes	No
(0.825,0.425)	Optimum1	1.0	0.512	0.529	0.65	Yes	Yes
	Optimum2	1.0	0.5	0.5	0.5	Yes	Yes
(0.8,0.4)	Optimum1	0.0	0.485	0.469	0.402	No	No
	Optimum2	0.0	0.5	0.5	0.5	No	No
(0.875,0.475)	Optimum1	0.0	0.99	0.362	0.705	Yes	Yes
	Optimum2	0.0	1.0	0.5	0.5	Yes	Yes
(0.85,0.45)	Optimum1	0.0	0.923	0.278	0.621	No	No
	Optimum2	1.0	0.0	0.5	0.5	Yes	No

Table 7.3 contains the carrier slope factors of different sets that correspond to the two optimum solutions evaluated in each working point. Those cases are compared with two typical or standard carriers sets: case1 where all r's are equal to 1; and case2 where all r's are

UNIVERSITAT ROVIRA I VIRGILI
CONTRIBUTIONS ON SPECTRAL CONTROL FOR THE ASYMMETRICAL FULL BRIDGE MULTILEVEL INVERTER
Oscar Mauricio Muñoz Ramírez
ISBN:978-84-693-7665-2/DL:T.1747-2010

equal to 1.0. The two last columns on the left side of table 7.3 give the global qualification of distortion profile comparing each optimized case with a standard case, namely case1 or case2.

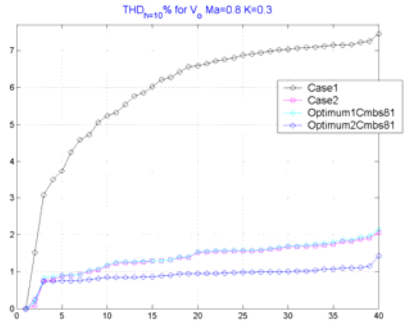

a) Ma=0.8 K=0.3

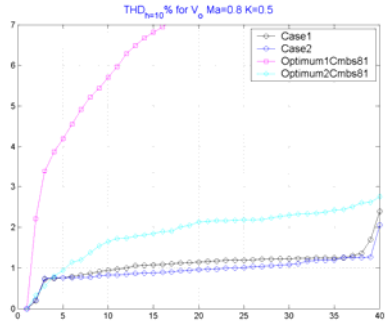

b) Ma=0.8 K=0.5

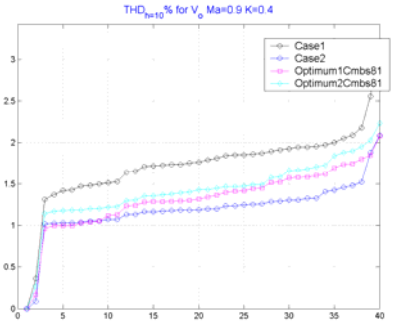

c) Ma=0.9 K=0.4

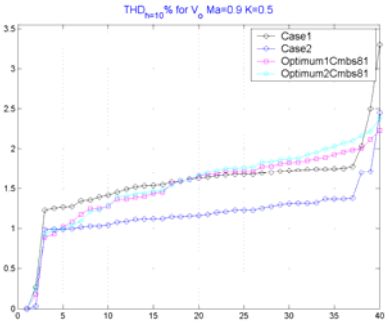

d) Ma=0.9 K=0.5

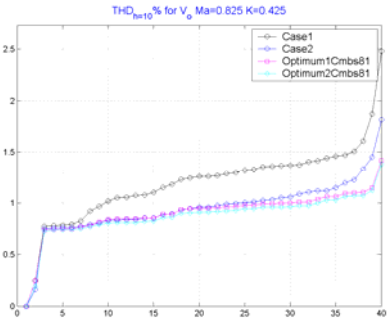

e) Ma=0.825 K=0.425

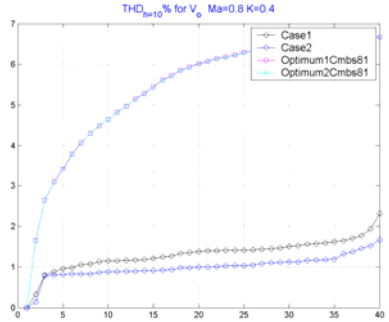

f) Ma=0.8 K=0.4

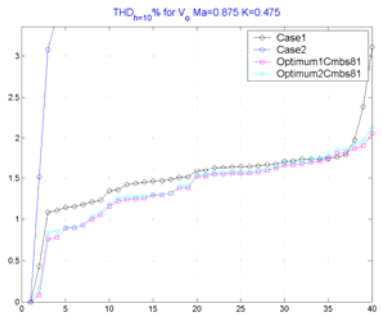

g) Ma=0.875 K=0.475

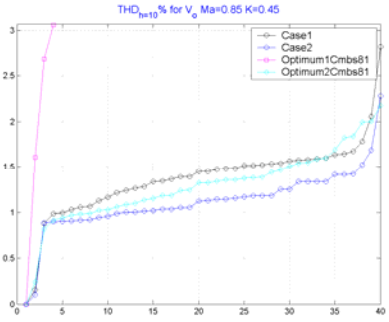

h) Ma=0.85 K=0.45

Figure 7.8 Optimized cases compared to typical carriers sets.

UNIVERSITAT ROVIRA I VIRGILI
CONTRIBUTIONS ON SPECTRAL CONTROL FOR THE ASYMMETRICAL FULL BRIDGE MULTILEVEL INVERTER
Oscar Mauricio Muñoz Ramírez
ISBN:978-84-693-7665-2/DL:T.1747-2010

Figure 7.8 contains the results of optimized carriers sets found by the GA when its fitting criterion is $THD_{h=10}$. Two optimum cases were obtained after evolving iterations for each working point (M_a,K): first optimum case is the last and best optimized solution after the end of GA algorithm execution, that is after the maximun number of generations are created; second optimum case is the best solution of the first generation. The two optimum cases are precalculated on the basis of predicting the harmonincs by means of SFS-based C_n-Algorithm, used as an auxiliar function of the implemented GA.

The results of figure 7.8 are the distortion evaluation of output voltages obtained in open loop conditions and are resumed in table 7.3 where only half of the comparisons passed. In some of these cases the local improvement on the second or third harmonic is achieved. Nevertheless, a global improvement over the harmonic profile or plot is prefered since most standards consider forty harmonics. In those figures, the harmonic profiles are proof of non considered elements when the spectrum of PD-PWM is modeled by DFS or SFS. The expected results are not satisfactory at all because of two main reasons: the first one, the MOSFET's R_{DS-ON} resistance plays an important role and if not dimensioned correctly, its degrading effect on the resulting signal is significative. Then, a modification in the power stage PCB will be introduced, reducing the mosfet R_{DS-ON} resistance as detailed chapter eight. The second reason of these poor qualified results of figure 7.7 is that open loop system has inferior performance features if compared to closed loop system that is reinforced by feedforward action. In closed loop system, the inductance can be reduced, which means an reduction in cupper losses of the pasive element. In advance, those pasive filter elements for closed loop prototuype are: $C=44\mu F$, $2Lo=1mH$, and $5<R<\infty$, where the damping factor lays between $0<\zeta<0.47$ due to adopted control strategie as a state variables feedback loop.

The benefits of optimized carriers sets by means of GA comprises a harmonic control loop that can not work by itself; it is necessary the interaction with feedback and feedforward loops and the following chapter will explain how this interaction is achieved.

UNIVERSITAT ROVIRA I VIRGILI
CONTRIBUTIONS ON SPECTRAL CONTROL FOR THE ASYMMETRICAL FULL BRIDGE MULTILEVEL INVERTER
Oscar Mauricio Muñoz Ramírez
ISBN:978-84-693-7665-2/DL:T.1747-2010

UNIVERSITAT ROVIRA I VIRGILI
CONTRIBUTIONS ON SPECTRAL CONTROL FOR THE ASYMMETRICAL FULL BRIDGE MULTILEVEL INVERTER
Oscar Mauricio Muñoz Ramírez
ISBN:978-84-693-7665-2/DL:T.1747-2010

8. Closed-Loop Harmonic Performance

In the first section of this chapter, we describe the functional blocks of the experimental prototype. A second section is dedicated to the state-variable space converter modeling and control loop design. After, we describe how the carriers optimization technique has been adapted and implemented in the prototype, and finally the definitive experimental set-up as well as the harmonic performance results are explained. Two main contributions are derived from our experimental results: how to apply the carriers optimization technique in a real inverter working with a certain range of operating points $V_{target}(M_a,K)$, and the performance improvement in the closed loop system caused by the carriers optimization.

8.1 Closed-Loop Prototype Introduction

The carriers optimization technique has been tested in a AFBMI prototype designed to perform like a VSI at closed loop. The control-loop has two parts: a feedforward-loop to linearize the converter dynamics, a good line regulation, and power-supply harmonics rejection, and secondly, an state feedback control-loop to assure a good load regulation, high quality sinusoidal waveform, and fast dynamic response, even at non-linear load conditions.

The control objective is to generate a sinusoidal output voltage V_o. Different inductive and non-linear loads have been tested, although for analysis purposes only resistive loads will be considered. Among the loads, many experiments have been done using two 10 Ω resistors connected either in series or in parallel, to get 5, 10, and 20 Ω.

The manipulated variables are the six PWM driving signals belonging to the respective inverter switches Q_1 to Q_6. This is accomplished by means of comparing a modulating signal U(t) with a set of four vertically-shifted carriers, and after applying some extra combinational logic circuits. In fact, the control signal U(t) is a sinusoidal signal, which amplitude modulation index M_a depends on a fixed reference, the output voltage and current errors.

The main difference of the proposed system is that in our case, the slopes of the four carrier signals are not constant, and are periodically changed in order to optimize the output spectrum. In our system, the changes on the carrier slopes take place each 200 ms, and only depend on the amplitude modulation index *Ma,* and the level distribution parameter *K*.

UNIVERSITAT ROVIRA I VIRGILI
CONTRIBUTIONS ON SPECTRAL CONTROL FOR THE ASYMMETRICAL FULL BRIDGE MULTILEVEL INVERTER
Oscar Mauricio Muñoz Ramírez
ISBN:978-84-693-7665-2/DL:T.1747-2010

An important objectives of our system was to reduce switching losses via reducing drastically the switching frequency (2.5 kHz). At this frequency, the output voltage alias spectrum alias are closer, and the left tail of the first alias (at 2.5 kHz) can easily contaminate the base-band alias, and distorting the output voltage waveform.

The inverter output voltage low frequency harmonics caused by the conjoint action of non-linear loads and bad output impedances are cancelled by the feed-forward and feedback control loops, theoretically under 1.25 kHz. When the bad output impedance belongs to the inverter power supplies, the feed-forward loop will be the main responsible to reduce the harmonic noise. Then, the feedback loop will compensate the harmonics generated by the conjoint action of nonlinear loads and the resistive losses of the switching devices, by means of reducing the inverter output impedance.

Anyway, as exposed previously, our system is operating at very low switching frequency. That means that even assuming zero-output impedance for the power supplies and the inverter, some harmonics could be generated by the interference of the first alias tail over the base band spectrum. Theoretically, the closed-loop system will try to reduce the value of this harmonic contamination, but a total elimination is impossible. Additionally, the inverter is a nonlinear system, and harmonics intermodulate creating new harmonics and subharmonics.

As a result, as more clean be the output voltage base-band spectrum, without considering the effect of any correcting control-loop, more clean will be real output voltage spectrum once the effect of the feed-forward and feedback control loops are applied.

We have demonstrated in this research work, that the harmonic content of the base-band spectrum of the inverter output sinusoidal waveform, switching at low frequency, depends strongly on the carriers slope, the amplitude modulation index Ma, and the level distribution K. That is the reason to adapt periodically the carriers slope.

Although changes in the inverter load, and the power supply voltages can be sudden and fast, normally in a real system, under the scope of long term operation those changes are produced occasionally. In a domestic stand-alone inverter (1-5 kW) supplied with a battery system, load changes causing deep variations on battery voltages will happen maybe twice per minute or twice per hour. Additionally, the power-supply voltage evolution will be normally quite slow. At these conditions to actualize the slope values more than 5 times per second, to clean the open-loop base-band spectrum is clearly not required.

UNIVERSITAT ROVIRA I VIRGILI
CONTRIBUTIONS ON SPECTRAL CONTROL FOR THE ASYMMETRICAL FULL BRIDGE MULTILEVEL INVERTER
Oscar Mauricio Muñoz Ramírez
ISBN:978-84-693-7665-2/DL:T.1747-2010

As a result, we have a three-loop system to compensate harmonics from diverse origin, but to design the converter closed-loop dynamics the effect, the digital close-loop, that actualizes 5 times or less per second the carriers slopes can be neglected, and the system can be presented as a traditional two-loop system with a feed-forward-loop, and a state-feedback loops.

8.2 Inverter Modeling and Closed-Loop Design

The AFBMI circuit is shown in figure 8.1. This AFBMI converter combines a conventional two-level inverter leg with a Neutral Point Clamped Half-Bridge. Therefore, the converter requires two input voltage supplies to operate. This structure, presented in [Val08] has the smallest number of controllable switching devices to generate a five-level output voltage.

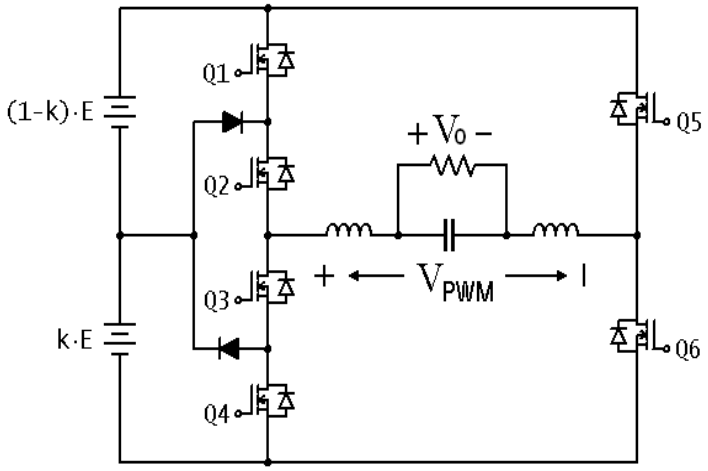

Figure 8.1 AFBMI circuit showing the two input voltage sources.

In fact, such topology, shown in figure 8.1 can operate with two, three, four or five levels by simply changing two small micro-switches (two bits) in the control board. Nevertheless, for this application, we have chosen to operate only with five-levels.

Assuming low input ripples $\Delta v_d(t)$, $\Delta v_u(t)$, the inverter input voltages $V_d(t)$ and $V_u(t)$ are given in expression (8.1).

$$\left.\begin{aligned} V_u(t) &= [1-K]E + \Delta v_u(t) \\ V_d(t) &= K\cdot E + \Delta v_d(t) \end{aligned}\right\} \text{ with } \quad 0 \le K \le 1 \tag{8.1}$$

UNIVERSITAT ROVIRA I VIRGILI
CONTRIBUTIONS ON SPECTRAL CONTROL FOR THE ASYMMETRICAL FULL BRIDGE MULTILEVEL INVERTER
Oscar Mauricio Muñoz Ramírez
ISBN:978-84-693-7665-2/DL:T.1747-2010

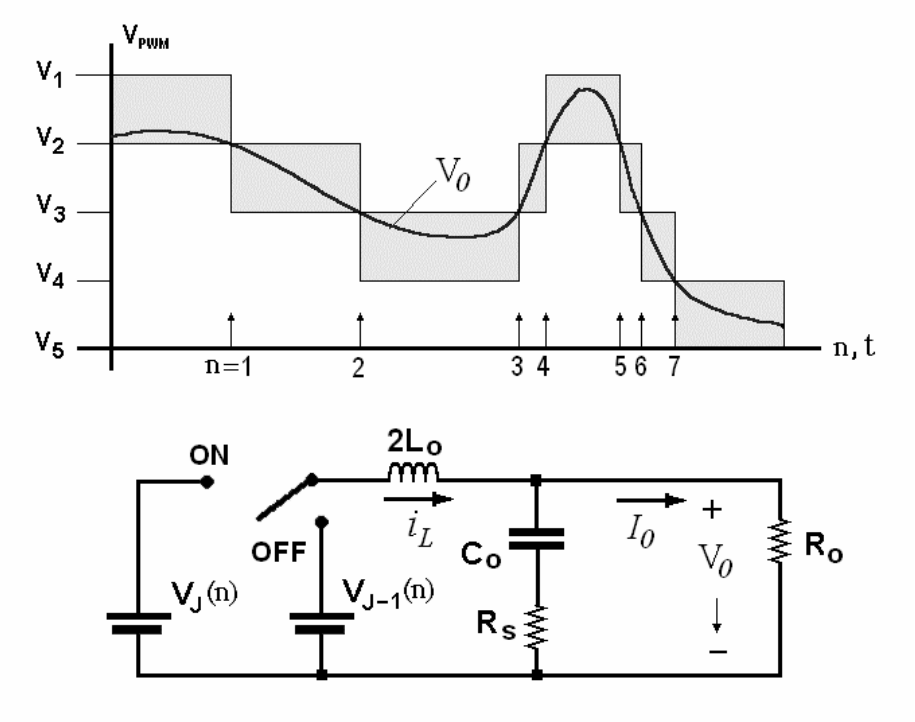

Figure 8.2 Tibuck Modeling applied to an AFBMI converter.

As can be seen in figure 8.2, the converter is always switching between adjacent levels $\{V_J, V_{J-1}\}$ except during deep-load transients. The converter output voltage $V_o(t)$ can be calculated using a local duty cycle D(n,t). The letter "n" indicates which Tibuck converter is operating at certain instant. This behaviour is represented in figure 8.2 using thick dark-grey arrows indicating the instant where the Tibuck changing events occur.

$$V_o(t) = V_J(n) \cdot D(n,t) + V_{J-1}(n) \cdot [1 - D(n,t)] \tag{8.2}$$

$V_o(t)$ is evolving following a sinusoidal waveform until D(n,t) becomes saturated. Then, the output voltage $V_o(t)$ cross the level borders $\{V_J, V_{J-1}\}$ to satisfy (8.2) and is then modulated by the next level pair or Tibuck converter (8.3). Each time that D(n,t) saturates, the actual Tibuck converter evolves to the next. This process generates a sequence of voltage controlled events given by expression (8.3).

$$\begin{cases} D(n,t) = 0 \quad \Rightarrow V_J(n+1) = V_{J-1}(n) \\ \\ D(n,t) = 1 \quad \Rightarrow V_{J-1}(n+1) = V_J(n) \end{cases} \tag{8.3}$$

As explained previously, the AFBMI structure allows the realization of PWM modulations with different number of levels. Table 8.1 gives the input voltage levels $V_J(t)$ and $V_{J-1}(t)$ of each Tibuck, depending on the number of levels used in the modulation.

UNIVERSITAT ROVIRA I VIRGILI
CONTRIBUTIONS ON SPECTRAL CONTROL FOR THE ASYMMETRICAL FULL BRIDGE MULTILEVEL INVERTER
Oscar Mauricio Muñoz Ramírez
ISBN:978-84-693-7665-2/DL:T.1747-2010

TABLE 8.1 TIBUCK VOLTAGES.

	5-Level Modulation				2-Level
$V_J(t)$	$E+\Delta v_u+\Delta v_d$	$k\cdot E+\Delta v_d$	0	$(k-1)\cdot E-\Delta v_u$	$E+\Delta v_u+\Delta v_d$
$V_{J-1}(t)$	$k\cdot E+\Delta v_d$	0	$(k-1)\cdot E-\Delta v_u$	$-E-\Delta v_u-\Delta v_d$	$-E-\Delta v_u-\Delta v_d$
	4-Level Modulation			**3-Level Modulation**	
$V_J(t)$	$E+\Delta v_u+\Delta v_d$	$k\cdot E+\Delta v_d$	$(k-1)\cdot E-\Delta v_u$	$E+\Delta v_u+\Delta v_d$	0
$V_{J-1}(t)$	$k\cdot E+\Delta v_d$	$(k-1)\cdot E-\Delta v_u$	$-E-\Delta v_u-\Delta v_d$	0	$-E-\Delta v_u-\Delta v_d$

Finally, Table 8.2, previously presented in Section 7, gives the logic states of the switching devices for each voltage level.

TABLE 8.2 SWITCHING STATES AND VOLTAGE LEVELS.

State	Level	Q_1	Q_2	Q_3	Q_4	D_1	D_2	Q_5	Q_6
S_1	E	1	1	X	0	0	0	0	1
S_2	k·E	0	1	1	0	1	1	0	1
S_3	0	0	0	1	1	0	0	0	1
S_4	0	1	1	0	0	0	0	1	0
S_5	(k–1)·E	0	1	1	0	1	1	1	0
S_6	–E	0	X	1	1	0	0	1	0

The AFBMI structure is a voltage event controlled sequence of different operating Tibucks, and obviously is a variable structure system (VSS). In fact, any system where there be switching devices can be considered a variable structure system, and therefore, the Tibuck converter itself, is also a variable structure system.

Nevertheless, comparing the Tibuck and Boost converters, although both have two different states or circuits (ON, OF), each of them linear and invariant circuits, the whole converters are quite different. Thus, the Tibuck converter can be approximated as a linear invariant circuit because ON-OFF topologies are identical, whereas boost converter is considered highly non-linear and time-variant, because both states, ON and OFF have different circuits.

As exposed previously, the AFBMI converter is a voltage event controlled sequence of operating Tibuck converters, and consequently, analyzing the dynamic behaviorof the AFBMI converter implies to study the Tibuck dynamic model.

UNIVERSITAT ROVIRA I VIRGILI
CONTRIBUTIONS ON SPECTRAL CONTROL FOR THE ASYMMETRICAL FULL BRIDGE MULTILEVEL INVERTER
Oscar Mauricio Muñoz Ramírez
ISBN:978-84-693-7665-2/DL:T.1747-2010

The Tibuck converter has two identical topologies with different excitations. The input voltage is V_J in the ON state, and V_{J-1} during the OFF state. Equation (8.4) gives the system dynamics during the ON state, whereas (8.5) gives the dynamics at the OFF state. At both equations, the inductor and capacitor series resistances are neglected for simplicity, and therefore, the capacitor voltage v_C and the output voltage $V_o(t)$ are equal.

$$\begin{bmatrix} \frac{di_L(t)}{dt} \\ \frac{dv_C(t)}{dt} \end{bmatrix} = \underbrace{\begin{bmatrix} 0 & \frac{-1}{2L_o} \\ \frac{-1}{C_o} & \frac{-1}{R_oC_o} \end{bmatrix}}_{A_{ON}} \cdot \begin{bmatrix} i_L(t) \\ v_C(t) \end{bmatrix} + \underbrace{\begin{bmatrix} \frac{V_J}{2L_o} \\ 0 \end{bmatrix}}_{B_{ON}} \tag{8.4}$$

$$\begin{bmatrix} \frac{di_L(t)}{dt} \\ \frac{dv_C(t)}{dt} \end{bmatrix} = \underbrace{\begin{bmatrix} 0 & \frac{-1}{2L_o} \\ \frac{-1}{C_o} & \frac{-1}{R_oC_o} \end{bmatrix}}_{A_{OFF}} \cdot \begin{bmatrix} i_L(t) \\ v_C(t) \end{bmatrix} + \underbrace{\begin{bmatrix} \frac{V_{J-1}}{2L_o} \\ 0 \end{bmatrix}}_{B_{OFF}} \tag{8.5}$$

By means of a binary control signal $u(t)=\{1\rightarrow ON,\ 0\rightarrow OFF\}$ both partial dynamics can be combined into a single expression (8.6) valid during the whole switching period, where the control signal u(t) is given by four vertically-shifted PWM modulators by comparing a modulating signal M(t) with the corresponding carrier

$$\overset{o}{X}(t) = [A_{ON}X(t) + B_{ON}]u(t) + [A_{OFF}X(t) + B_{OFF}][1-u(t)] \tag{8.6}$$

As the ON and OFF states have the same dynamics, expression (8.6) yields (8.7), and we can calculate the output voltage $V_o(t)$ by replacing u(t) in expression by average value D(n,t).

$$\overset{o}{X}(t) = A_{ON}X(t) + B_{OFF} + [B_{ON} - B_{OFF}]u(t) \tag{8.7}$$

$$D(n,t) = \frac{V_{ref}(t) - V_{J-1}}{V_J - V_{J-1}} \quad \rightarrow \quad V_O(t) = V_{ref}(t) = E{\cdot}M_a(t) = E{\cdot}M_a\sin(\omega_o t) \tag{8.8}$$

To reject line variations and harmonics, the carriers are chosen to be proportional to the inverter input voltages, implementing a classical feed-forward loop. Nevertheless, as can be

deduced by simple inspection of system matrix A_{ON}, the open-loop poles are strongly dependent on the converter load (8.9), where the damping factor is given by (8.10).

$$p(s)=\det[A_{ON}-sI]=\begin{bmatrix}-s & -\frac{-1}{2L_o}\\ \frac{-1}{C_o} & \frac{-1}{R_oC_o}-s\end{bmatrix}=s^2+\frac{1}{R_oC_o}s+\frac{1}{2L_oC_o} \tag{8.9}$$

$$\zeta=\frac{1}{R_o}\sqrt{\frac{L_o}{2C_o}} \quad where \quad p(s)=s^2+2\zeta\omega_n s+\omega_n^2 \tag{8.10}$$

Considering the component values: C=44μF, 2Lo=1mH, and 5<R<∞, the damping factor lays between 0<ζ<0.47, and the natural frequency $\omega_n=4.67\cdot10^3$ rad/s (760 Hz). As can be seen, at no load conditions, the poles would be directly over the jω axis in the complex plane. Obviously the converter losses will stabilize the system, but the damping factor will remain excessively low. To improve the relative stability of the system, and to compensate tracking errors in the output voltage, a state feedback loop is considered.

$$D(n,t)=\frac{1}{V_J-V_{J-1}}\left\{V_{ref}(t)+K_V\left[V_{ref}(t)-V_O(t)\right]+K_I\left[i_L(t)-I_O(t)\right]-V_{J-1}\right\} \tag{8.11}$$

$$Ic(t)=i_L(t)-I_O(t)=i_L(t)-\frac{V_o(t)}{R_o}=C_o\frac{dV_o(t)}{dt} \tag{8.12}$$

As can be easily deduced, i_L-I_O is the simply the inverter capacitor current Ic(t), that introduces a derivative term in the control loop $V_o(t)$ that stabilizes the system, making the damping factor, practically independent form the converter load. Applying the state-feedback law (8.11) to expression (8.7), the closed-loop system dynamics are given by (8.13), where A_{RE} is the new state matrix, once applied the state-feedback loop.

$$p(s)=\det[A_{RE}-sI]=\begin{bmatrix}-s+\frac{K_I}{2L_o} & -\frac{(K_V+1)+K_I/R_o}{2L_o}\\ \frac{-1}{C_o} & \frac{-1}{R_oC_o}-s\end{bmatrix}=s^2+\left[\frac{1}{R_oC_o}-\frac{K_I}{2L_o}\right]s+\frac{K_V+1}{2L_oC_o} \tag{8.13}$$

As the inverter switching frequency is f_S=2.5 kHz, the maximum available bandwidth according to Nyquist criterium is 1.25 kHz. Therefore, we have selected this last frequency as the 3dB bandwith (BW_{3dB}). Considering that a second order system has a frequency decay of

UNIVERSITAT ROVIRA I VIRGILI
CONTRIBUTIONS ON SPECTRAL CONTROL FOR THE ASYMMETRICAL FULL BRIDGE MULTILEVEL INVERTER
Oscar Mauricio Muñoz Ramírez
ISBN:978-84-693-7665-2/DL:T.1747-2010

-40db/dec, and assuming a good damping factor $\zeta>0.7$, avoiding any kind of resonance in the output filter, a 3 dB bandwidth of 1.25 kHz, implies a natural frequency $\omega_n=6.28\cdot10^3$ rad/s, or equivalently, at 1 kHz.

In fact, besides correcting output voltage errors and stabilizing the system, the state-feedback loop allows, using an adequate damping factor, avoiding resonance peaks of the inverter output filter. Those resonance peaks could amplify some base-band harmonics, loosing all the harmonic optimization achieved by means carriers programming.

According to the last criteria, closed loop $\omega_{nC}=6.28\cdot10^3$ rad/s, and damping factor over $\zeta>0.7$ at any load condition, the feedback constants are deduced in expression (8.14).

$$\begin{cases} \omega_{nC}^2 = \dfrac{K_V+1}{2L_oC_o} & \rightarrow K_V \approx 0.74 \\ 2\zeta\omega_{nC} = \dfrac{1}{R_oC_o} - \dfrac{K_I}{2L_o} & \rightarrow K_I \approx -8.79 \end{cases} \tag{8.14}$$

At maximum load Ro=5 Ω, the damping ratio is $\zeta=1.06$, and the phase-shift introduced by the output-reference transfer function (8.15) at 50 Hz lays between $-6º<\Delta\varphi<-4º$, where the maximum lag between the output and the reference occurs at full load conditions. This little phase-shift, can be corrected by introducing a lead-phase network, with parameters $\alpha=0.95$ and $\tau=3.184\cdot10^{-4}$ s, in the reference signal, if required.

$$H(s)=\frac{V_o(s)}{V_{ref}(s)}=\frac{\dfrac{K_V+1}{2L_oC_o}\cdot\alpha\left[1+s\tau\right]}{s^2+\left[\dfrac{1}{R_oC_o}-\dfrac{K_I}{2L_o}\right]\cdot s+\dfrac{K_V+1}{2L_oC_o}} \tag{8.15}$$

8.3 Closed-Loop Prototype Description

Figure 8.3.a depicts the main blocks and variables of the closed loop system as well as the D.C. voltage supplies to power the different circuit blocks. Figure 8.3.b is a photograph of the experiemental prototype implemented and utilized at the GAEI laboratory.

UNIVERSITAT ROVIRA I VIRGILI
CONTRIBUTIONS ON SPECTRAL CONTROL FOR THE ASYMMETRICAL FULL BRIDGE MULTILEVEL INVERTER
Oscar Mauricio Muñoz Ramírez
ISBN:978-84-693-7665-2/DL:T.1747-2010

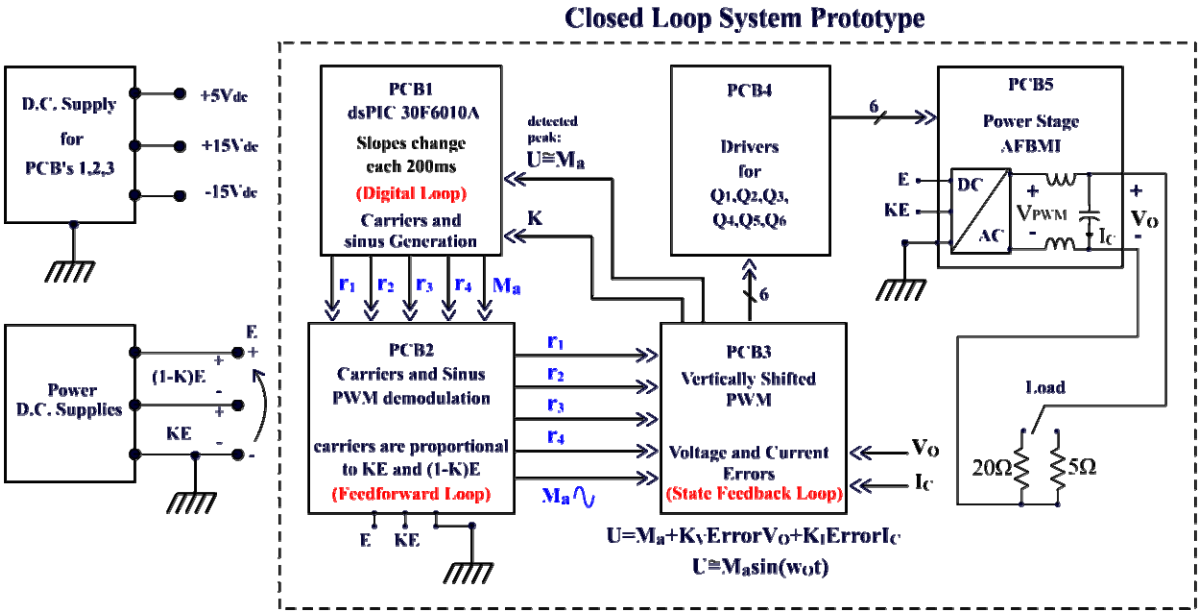

Figure 8.3.a Blocks Diagram of the Closed Loop System Prototype.

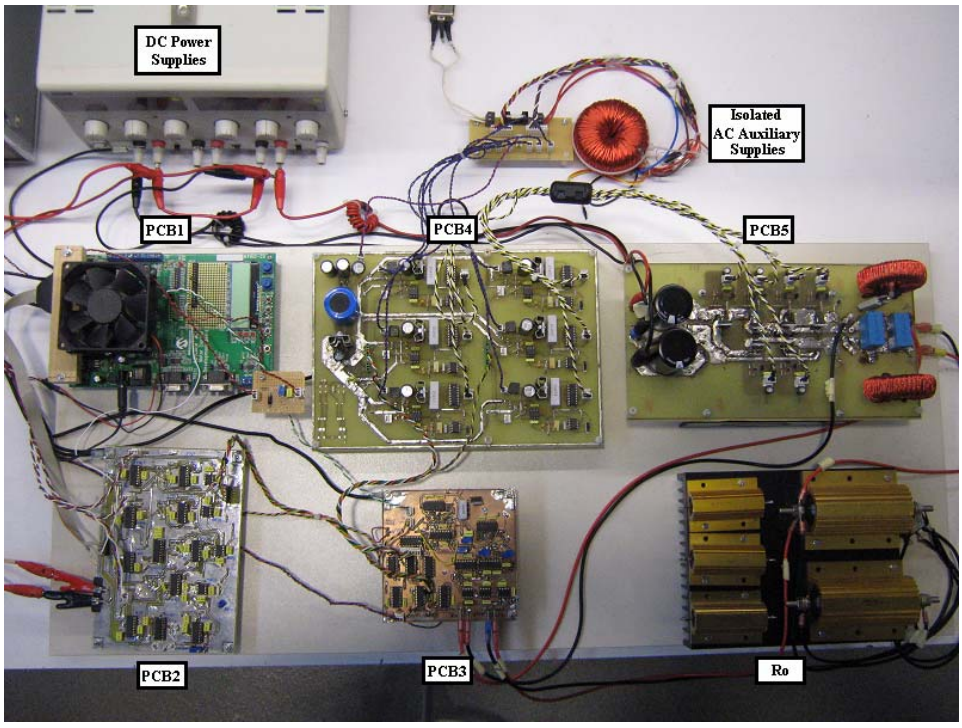

Figure 8.3.b Photo of the Closed Loop System Prototype.

Auxiliary supplies are used by digital and analog circuit blocks, namely PCB_1, PCB_2, PCB_3 and PCB_4. For digital purposes, a 5 Vdc supply is utilized by PCB_1. In the same way, a dual +15/-15 Vdc supply powers PCB_2 and PCB_3 in order to perform analog functions. The main power supply is connected to PCB_5 where two input D.C. voltages namely K·E and (1-K)·E comprise the chopped staircase-amplitudes of the synthesized output waveform V_{PWM}.

UNIVERSITAT ROVIRA I VIRGILI
CONTRIBUTIONS ON SPECTRAL CONTROL FOR THE ASYMMETRICAL FULL BRIDGE MULTILEVEL INVERTER
Oscar Mauricio Muñoz Ramírez
ISBN:978-84-693-7665-2/DL:T.1747-2010

Within the boundary of dashed lines in figure 8.3.a, it can be seen the flux of the signals and their description; starting by the first block, the functional blocks are:

PCB_1 .- The main function of this block is to generate uninterruptedly the carriers and the modulator which are generated in PWM form by means of the internal hardware timers working at 277 kHz in a amplitude-range of 0 to 5 V. These signals are buffered by comparators in a amplitude-range of 0 to 15 V and then connected to the second block PCB_2 where they are filtered and adjusted. Two analogic input signals M_a and K make the dsPIC algorithm to choose a carriers set every ten periods of fundamental frequency, i.e. 200 ms. Further descriptions of the implemented algorithms in this block are written in next section.

PCB_2 .- The input carriers signals are filtered by four low-pass 4^{th}-order Butterworth filters obtaining four clean 2500 Hz triangular carriers. Similarly, the modulator passes through a single low pass RC-filter to get a 50 Hz-unitary sinusoidal waveform (M_a=1.0). The cut-off frequency of the carrier filters is 100 kHz and 500 Hz for the modulator. Since the amplitude range for all these signals is 0 to 15 V, they are compensated in offset and amplitude. The carriers are adjusted from 0 to 1 V and the modulator from –1 to 1 V which are unitary scales. Since the maximum total input voltage E for the inverter is 120 V, the upper carrier and the lower carrier limits as well as the modulator peaks are scaled to one tenth of the input D.C. supply. The final SPWM scheme is represented within a range of ±12 V in one tenth of E and is defined as follows: Carrier1, the upper carrier has a gain of (1–K)·E/10 and K·E/10 as offset. Below Carrier1 is placed Carrier2 which has a gain of KE/10 and zero offset. Then Carrier3 is amplified by the gain factor (1–K)·E/10 and is displaced by the offset level –(1–K)·E/10. The lowest carrier, Carrier4, has a gain of K·E/10 and –E/10 as offset. These signals are connected to the third block PCB_3 where the SPWM scheme is finally executed. The modulator signal remains in unitary scale with only one frequency component $M_a(F_O)$ and is subsequently adjusted in PBC_3.

Figure 8.4 shows the implementation of SPWM with variable r_i-shape factor for the carriers signals and the modulator signal. The first three columns on the left correspond to the circuitry of PBC_1 where the carriers and the modulator are generated. Filtering and amplitude compensation are represented by the next two columns which are the functions of PCB_2.

UNIVERSITAT ROVIRA I VIRGILI
CONTRIBUTIONS ON SPECTRAL CONTROL FOR THE ASYMMETRICAL FULL BRIDGE MULTILEVEL INVERTER
Oscar Mauricio Muñoz Ramírez
ISBN:978-84-693-7665-2/DL:T.1747-2010

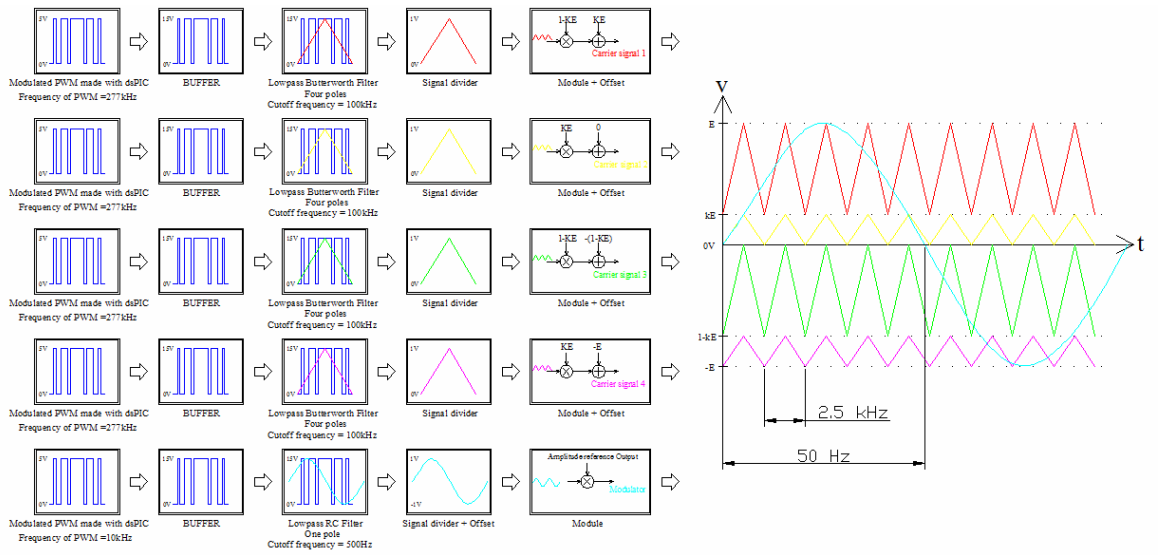

Figure 8.4 Implemented SPWM scheme.

PCB$_3$.- This part of the prototype is the core of control loop and modulation. Among the incoming signals, there are the four carriers and the modulator signal from PCB$_2$. Additionally, two signals from PCB$_2$ namely K·E/10 and E/10 obtained by two voltage divisor R-networks are used to calculate K. The modulator signal is scaled to E/10 when a potentiometer is at 100% span. By displacing the potentiometer, the reference control signal $M_a(F_O)$ is indicated to the control circuit that compares the reference signal with the errors measured in I_c and V_o. Thus, the control circuit compensates the modulating signal according to the expressions (8.1) and (8.2):

$$U(t) \cong Ma(t) = Ma(F_O, 2F_O, 3F_O \ldots) = Ma(F_O) + K_V e_{Vo} + K_I e_{IC} \quad (8.13)$$

$$Ma(t) = Ma_1 \sin(\varpi_O t + \varphi_1) + Ma_2 \sin(2\varpi_O t + \varphi_2) + \ldots + Ma_N \sin(N\varpi_O t + \varphi_N) \quad (8.14)$$

Modulator signal is finally compensated by means of closed loop control, and four comparators outputs are activated or deactivated which are the input of a combinatory logic circuit as is illustrated in figure 8.5. This circuit produces six necessary pulses to drive the inverter and they share the same ground or reference with a 5 V operating range. The function of isolating these pulses is subsequently done by PCB$_4$.

PCB$_4$.- This block has the only function to convert the mosfet's pulses from common-ground 5 V to isolated-ground voltage supply for every mosfet's gates Q_1, Q_2, Q_3, Q_4, Q_5, Q_6. Seven isolated AC supplies power the circuits of rectifiers and DC voltage regulators that provides one 5 V bus and six 10 V independent sources V_{EE1} to V_{SS1}, V_{EE2} to V_{SS2}, V_{EE3} to V_{SS3}, V_{EE4} to V_{SS4}, V_{EE5} to V_{SS5}, V_{EE6} to V_{SS6}. Each driver has a optical-isolator where its input pins are connected to the 5 V bus whereas its output is connected through a pull-up resistor to its

UNIVERSITAT ROVIRA I VIRGILI
CONTRIBUTIONS ON SPECTRAL CONTROL FOR THE ASYMMETRICAL FULL BRIDGE MULTILEVEL INVERTER
Oscar Mauricio Muñoz Ramírez
ISBN:978-84-693-7665-2/DL:T.1747-2010

respective V_{EE} to V_{SS} supply. This output activates a voltage-buffering stage as is indicated in figure 8.6 . The rest of the driver circuit is placed in PCB_5 since we initially intended to put as close as possible the driving signal connections to the gate-to-source in every mosfet. For this reason, voltage-buffering is realized in PCB_4 but current-buffering is done in PCB_5.

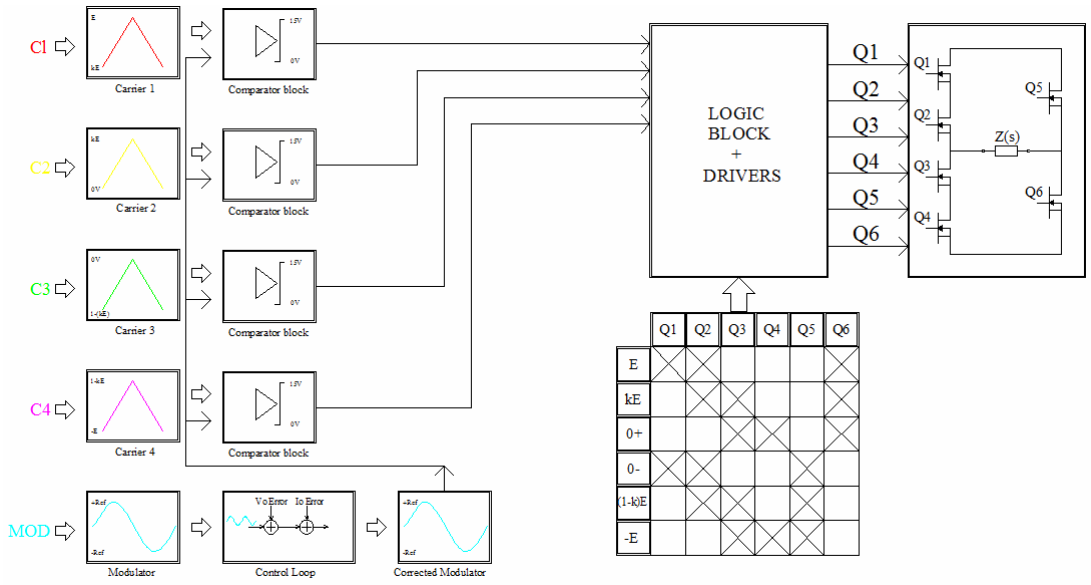

Figure 8.5 Generation of pulses for the AFBMI.

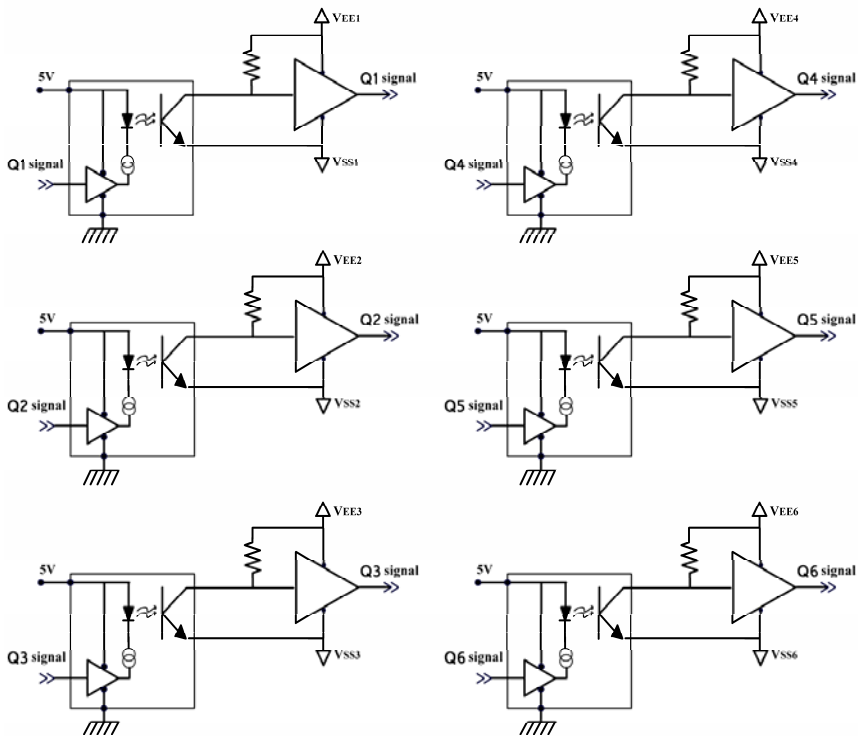

Figure 8.6 Drivers Circuitry (PCB N° 4).

PCB$_5$.- The power stage circuit consist of eight switching devices comprise the basic AFBMI architecture: six switching mosfets (Q_1, Q_2, Q_3, Q_4, Q_5, Q_6) and two clamping diodes (D_7, D_8). Each mosfet has a free-wheeling diode and contains the current-buffer stage of its respective

UNIVERSITAT ROVIRA I VIRGILI
CONTRIBUTIONS ON SPECTRAL CONTROL FOR THE ASYMMETRICAL FULL BRIDGE MULTILEVEL INVERTER
Oscar Mauricio Muñoz Ramírez
ISBN:978-84-693-7665-2/DL:T.1747-2010

driver. Thus, each current-buffer stage is connected to the respective driving signal and supply pins ($Q_i$signal,V_{EEi},V_{SSi}), see figure 8.7 where every independent isolated driving signal is current mode amplified; its respective incoming signal is voltage mode amplified and isolated from PCB4.

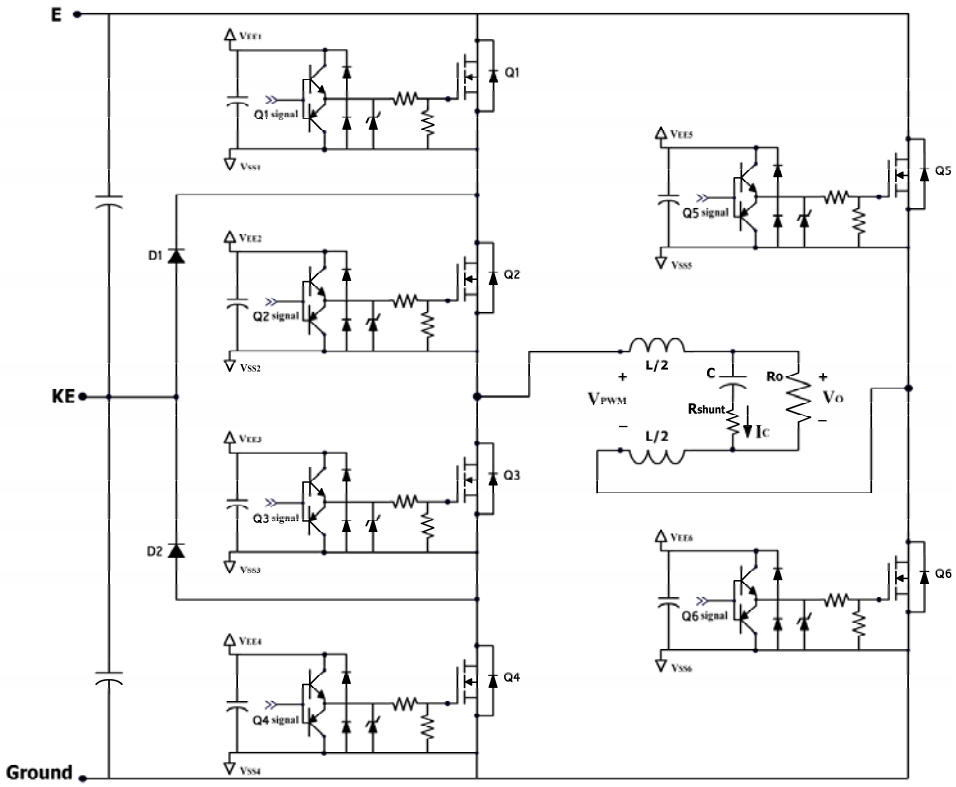

Figure 8.7 Power Stage of the AFBMI (PCB N° 5).

Additionally, at the inverter input there are two pairs of 10000 uF capacitors that stiff the input voltages K·E and (1−K)·E. The output of the bridge is the voltage V_{PWM}, this is the five-level output signal that is filtered through a second order R-L-C network obtaining the output voltage V_O. The second order filter consist of L=1000 μH and C=44 μF and since the load is R= 5 Ω, the frequency transfer function has over-damped response and the cut-off frequency is at 900 Hz. The second to fifth harmonics are not amplified, whereas the amplification from the sixth to fifteenth harmonics can be neglected since the resulting amplitudes are too small. After the 20^{th} and 30^{th} harmonics, the attenuation increases and this permits to maintain any typical compensation of harmonics. Considerations of trade-off must be taken when designing the filter; first, the second and third harmonics are more bigger than expected from simulations and any amplification is not permitted on these harmonics. Second, the inductor can be reduced to minimize copper losses and the capacitor increased always maintaining an acceptable over-damped characteristic positioned around the smaller frequency amplitudes. Figure 8.8 shows that although over-damped characteristic in filter transfer function, the base-

UNIVERSITAT ROVIRA I VIRGILI
CONTRIBUTIONS ON SPECTRAL CONTROL FOR THE ASYMMETRICAL FULL BRIDGE MULTILEVEL INVERTER
Oscar Mauricio Muñoz Ramírez
ISBN:978-84-693-7665-2/DL:T.1747-2010

band-harmonics are not modified by means of filtering action. Overdamped response peak and cut-off frequency are between the 10th and 20th harmonics and the output components though slightly amplified their impact is minimal.

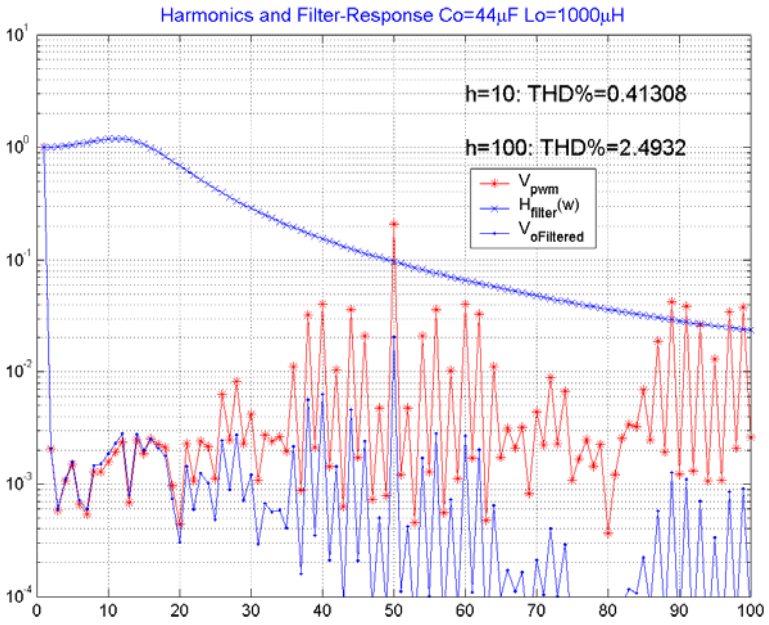

Figure 8.8 V_{PWM} and filtered output V_O signals.

8.4 GA Optimization in a Matrix of Working Points (M_a,K)

Before discussing the features of the adopted strategy for our implemented genetic algorithm, we remark that most distortion standards encompasses the first forty harmonics, e.g. IEEE 519-1992. Thus, the current bandwidth is ruled by such standards embracing h={2…40} Despite the frequency modulation index of our converter (M_f=50), we focused the optimization along the current bandwidth where the harmonic profiles of PWM output waveforms, represented by THD curves, are evaluated for the first forty frequency amplitudes.

The optimization of harmonic distortion for a particular and pre-calculated operating point $V_{PWM}(M_a,K)$, as previously explained in Chapter 6, was achieved using a GA. For each operating point it exists one optimal solution; this optimal solution contains information about the four carrier-factors, i.e. $case_{optimal}=\{r_1, r_2, r_3, r_4\}$. Then, by means of GA, a optimized carriers set can be found in order to minimize the harmonic distortion profile plotted in a THD curve. An objective function was used to find the minimum distortion when the spectrum of

UNIVERSITAT ROVIRA I VIRGILI
CONTRIBUTIONS ON SPECTRAL CONTROL FOR THE ASYMMETRICAL FULL BRIDGE MULTILEVEL INVERTER
Oscar Mauricio Muñoz Ramírez
ISBN:978-84-693-7665-2/DL:T.1747-2010

$V_{PWM}(M_a,K)$ is modeled by Cn-Algorithm. Initially, THD for first ten harmonics was thought as the function to be minimized.

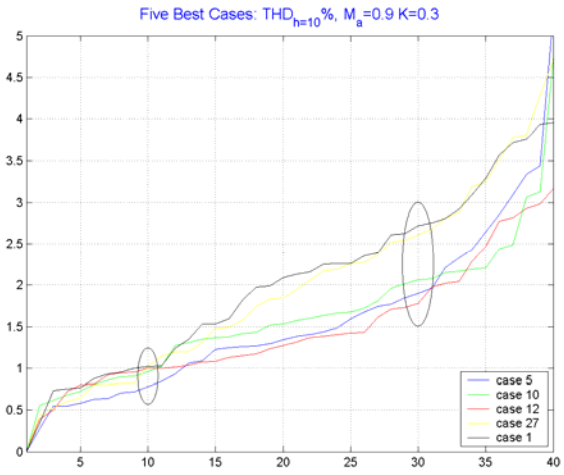

Figure 8.9 Harmonic profiles with different local minimum THD.

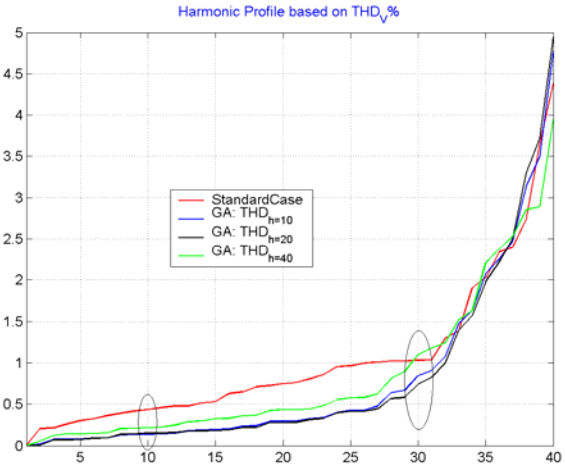

Figure 8.10 Local minimization obtained by different objective functions.

However, when proving some sets of carriers in open loop as detailed in Chapter 7, the harmonic profiles traced by THD curves suggested inconsistency on these profiles since a particular curve with a low THD in the harmonic h_1 can be classified as a optimum or at least as a good harmonic profile at from a particular set of carriers. The same particular curve can have a higher THD if compared with other different harmonic profile that presents a local minimum at the harmonic h_2. For example, assuming four arbitrary curves A, B, C and D, and that curve A can have a local minimum at the 10th harmonic, curve B presents a local minimum at the 20th harmonic, then curve C was selected for presenting a local minimum at the 30th harmonic and lastly, curve D was selected for presenting a local minimum at the 40th harmonic. Figures 6.2.b and 6.29 are examples of this dilemma where a particular carriers set

UNIVERSITAT ROVIRA I VIRGILI
CONTRIBUTIONS ON SPECTRAL CONTROL FOR THE ASYMMETRICAL FULL BRIDGE MULTILEVEL INVERTER
Oscar Mauricio Muñoz Ramírez
ISBN:978-84-693-7665-2/DL:T.1747-2010

can minimize its respective objective function THD_h defined at a local harmonic *h* whereas at different harmonics such minimization is represented by other carriers set. The objective function THD_h is only a measure at a punctual harmonic but does not give a global evaluation on the current bandwidth, h={2…40}.

Figure 8.9 shows again this situation for a few harmonic profiles derived from five particular carriers set. The cases of these figure are the best of thirty one cases tested in an experiment for one operating point (M_a=0.9,K=0.3). Blue line presents a local minimum at the harmonic h=10 but is exceeded at harmonic h=20 by red line which maintains a low profile up to the harmonic h=40. Since a GA explores a great number of different solutions, it can be adapted to keep the lowest harmonic profile along the current harmonic bandwidth.

Although we stated that base-band harmonics (h<11) are our main target to minimize, we did not ignore the possibility that a particular carriers set optimizes the THD plot at the first ten harmonics and at the same time such carriers set can degrades the THD plot at the location of higher harmonics. Therefore, to guarantee uniform and global minimization of distortion profile at several harmonic positions (h={2…40}), we added a new condition to our GA. Since the C_n-Algorithm calculates the harmonics for any carriers set, the modeled distortion can be predicted for the standard set, i.e. $case_{STANDARD}$={r_1=0.5, r_2=0.5, r_3=0.5, r_4=0.5}. Thus, the explored carriers set can be compared with such standard case comparing their respective distortion profiles.

$$\begin{cases} THD_{\substack{h=10 \\ Explored\,Set}} < THD_{\substack{h=10 \\ Standard\,Set}} \\ THD_{\substack{h=20 \\ Explored\,Set}} < THD_{\substack{h=20 \\ Standard\,Set}} \\ THD_{\substack{h=30 \\ Explored\,Set}} < THD_{\substack{h=30 \\ Standard\,Set}} \\ THD_{\substack{h=40 \\ Explored\,Set}} < THD_{\substack{h=40 \\ Standard\,Set}} \end{cases} \tag{8.14}$$

The four conditions from expression (8.14) must be satisfied and so, the explored carriers set is marked as a valid solution that finally is part of the expanding population of solutions throughout the generations or iterations of the GA. These conditions makes the GA to find an optimal solution (a carriers set) with a distortion profile that is always below of its homologous distortion profile based on standard carriers. In other words, the frontier of minimization layer is lowered in all the harmonics locations.

UNIVERSITAT ROVIRA I VIRGILI
CONTRIBUTIONS ON SPECTRAL CONTROL FOR THE ASYMMETRICAL FULL BRIDGE MULTILEVEL INVERTER
Oscar Mauricio Muñoz Ramírez
ISBN:978-84-693-7665-2/DL:T.1747-2010

In figure 8.10 the harmonic profile of the standard carriers set, in red color, is compared with the harmonic profiles of the solutions obtained by three types of objective functions: in blue color, the objective function was used by the GA to minimize the THD of ten harmonics; the black line corresponds to $THD_{h=20}$. These two last profiles present optimum solutions at their respective local minima, i.e. h=10 and h=20; nevertheless, their plots pass over the standard profile in the boundary of the fortieth harmonic. Green line shows an acceptable harmonic profile and although its THD values at h=10 and h=20 are not completely optimized they do maintain a spread distortion minimization over the forty harmonics encompassed by standard IEEE519-1992.

Once the GA's objective function was refined to optimize the harmonic distortion through the current bandwidth, the GA can be applied to find the solutions for several operating points, namely $V_{PWM}(M_a^*,K^*)$.

Such solutions are the basis of the information used in our experimental prototype and to assist closed loop control that regulates the AFBMI as a VSI, it is necessary to build a matrix that contains the information of carriers sets for several operating points, i.e. $case_{optimal}=\{r_1, r_2, r_3, r_4\}$. Pre-calculated operating points $V_{PWM}(M_a^*,K^*)$, comprise a framework where the arbitrary set-point, denoted as $V_{target}= (M_a,K)$, is assisted with a carriers set and by modulation process it yields V_O.

Thus any required reference signal M_a is a working point $V_{target}(M_a,K)$ that can be modulated with the proper carriers set by simply taking the closest location from the previously pre-calculated points $V_{PWM}(M_a^*,K^*)$.

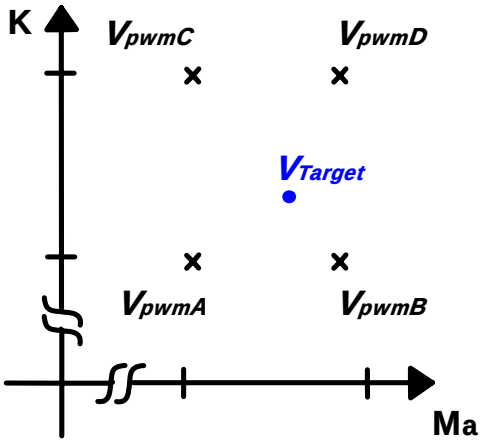

Figure 8.11 Working Point $V_{target}(M_a,K)$ in a cell of 4-points.

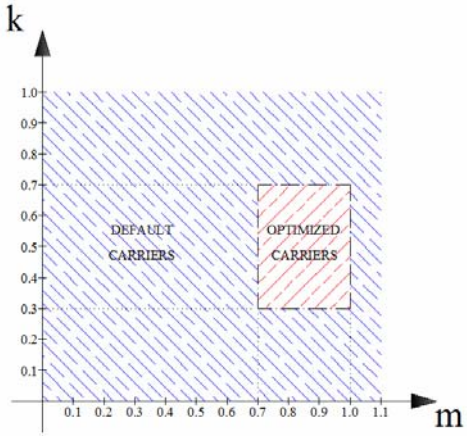

Figure 8.12 Framework matrix to program the optimized carriers set.

Figure 8.11 shows the cell where V_{target} is sorrounded by a cell; such cell is comprised by four pre-calculated points, namely $V_{PWM}A$, $V_{PWM}B$, $V_{PWM}C$ and $V_{PWM}D$. Each pre-calculated point is a two-dimensional element, M_a^* and K^*, that contains the information of its respective optimized carriers set when GA has been applied for such element, e.g. $V_{PWM}D(M_a^*{}_A, K^*{}_D)$. When PCB1 reads the analog inputs M_a and K, the algorithm that works in its dsPIC puts the corresponding operating point $V_{target}(M_a,K)$ in the cell comprised by $V_{PWM}A$, $V_{PWM}B$, $V_{PWM}C$ and $V_{PWM}D$.

In turn, a cell is a part of a framework which is a matrix limited by the maximum and minimum values of M_a and K. We restricted the ranges of carriers programming for the experimental prototype as it is detailed in table 8.3 and figure 8.12. When a target point does not falls inside the framework, the default output carriers is a standard set, i.e. $case_{STANDARD}=\{r_1=0.5, r_2=0.5, r_3=0.5, r_4=0.5\}$.

To implement the framework, firstly we built a 221-points matrix when resolution is ruled by step-size equals to 0.025. Similarly, a second matrix has 63-points matrix when its resolution is defined by step-size equals to 0.05. These matrix are used as look-up tables, since after reading the input signals M_a and K, the algorithm associates and activates the closest point $V_{PWM}(M_a^*,K^*)$ by comparing it with the actual target point $V_{target}(M_a,K)$. However, the associated carriers for such activated point are not modified; they are only adopted for the actual target point.

TABLE 8.3 FRAMEWORK MATRIX TO PROGRAM THE CARRIERS SET.

Input Signal	minimum	step-size	maximum	Resolution
Ma	0.7	0.025	1.0	221 points
K	0.3		0.7	
Ma	0.7	0.05	1.0	63 points
K	0.3		0.7	

In a first attempt, the 221-points matrix was tested and no computing delay was observed in the dsPIC performance. Nevertheless, such matrix, although offering high resolution, was very susceptible to input noise that was present in signals M_a and K. These signals are sampled by dsPIC in order to associate and activate the suitable point that programs the carriers set.

UNIVERSITAT ROVIRA I VIRGILI
CONTRIBUTIONS ON SPECTRAL CONTROL FOR THE ASYMMETRICAL FULL BRIDGE MULTILEVEL INVERTER
Oscar Mauricio Muñoz Ramírez
ISBN:978-84-693-7665-2/DL:T.1747-2010

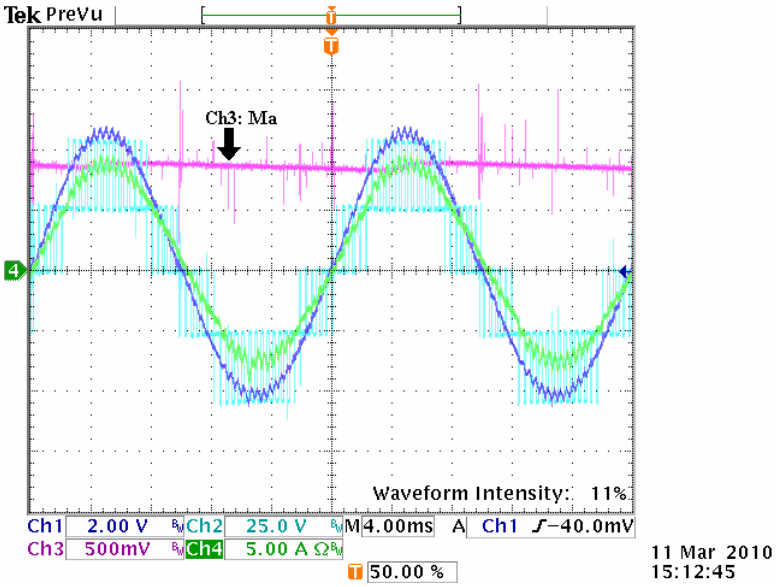

Figure 8.13 Measured M_a peak (Channel3).

Figure 8.13 shows the noise perturbations that affects the samples done by dsPIC; M_a is represented in violet color and scaled in 0 to 1V, V_{PWM} is traced with blue color, the output current with green color and the compensated modulator signal U(t) is pictured in dark blue color. For example, if V_{target} has M_a =0.95 or K=0.32, noise levels amplitudes at the measurement pin of signals M_a and K in PCB1 make that their respective samples fall outside the framework due to the proximity of any or both signals to the framework limits; an undesired condition to perform the framework matrix.

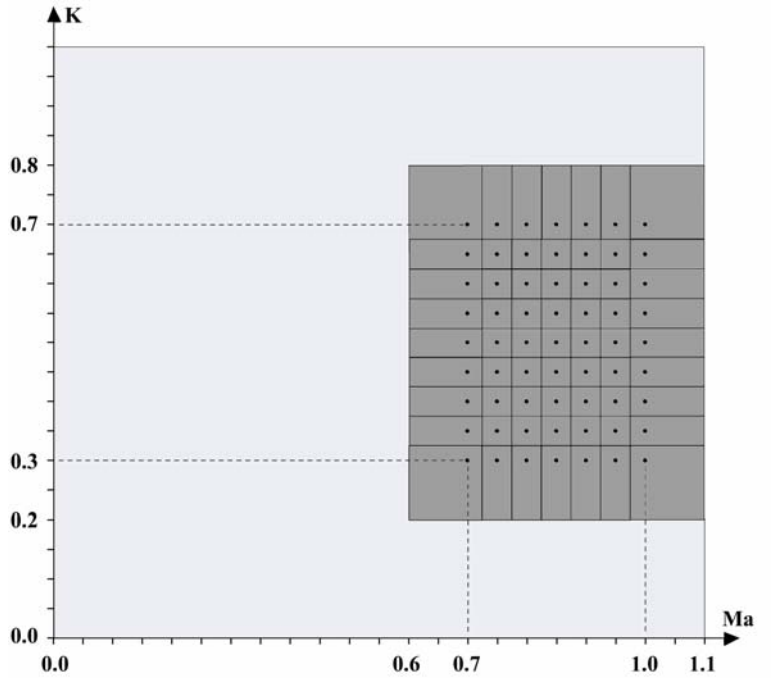

Figure 8.14 Adapted framework matrix.

UNIVERSITAT ROVIRA I VIRGILI
CONTRIBUTIONS ON SPECTRAL CONTROL FOR THE ASYMMETRICAL FULL BRIDGE MULTILEVEL INVERTER
Oscar Mauricio Muñoz Ramírez
ISBN:978-84-693-7665-2/DL:T.1747-2010

Although the experimental prototype was working in steady state conditions, as a result, the generated carriers were ruled by two intermittent sets, that is, the carriers set fluctuated between standard values and optimized values since the samples M_a and K were disturbed by noise. As another example, if V_{target} has M_a =0.83 and K=0.52, the activated point certainly falls in the framework center but the generated carriers were still ruled by intermittent sets. In a second attempt we tested the 63-points matrix and a tolerance gap equals to 0.1 was added to the external contours of the framework traced by the its own limits and as a result we solved the fault condition of intermittent sets. In other words, the theoretical framework matrix proposed, as figure 8.12 depicts it, was not practical due to the coinstraints of the boundary on such matrix. A tolerance gap was added to this framework and the intermittent sets condition was eliminated by assuming the same carriers values to those working points that were allocated in the vecinity of the original framework. This adaptation of added gaps is illustrated in figure 8.14 where the 63-points matrix performs optimized carriers for the dual range: 0.7<Ma<1.0. The initial 221-points was calculated with a step-resolution equal to 0.025; by simply changing such resolution to 0.05, the resultat bi-dimensional matrix contains 63 points and it is not necessay to calculate them due to this last samll matrix is a sub-set of the first large matrix.

8.5 Prototype Experimental Results

The performance of carriers programming was tested with the following material:

- System prototype based on the AFBMI, controlled as a VSI by state-feedback loop, offset and amplitude carriers controlled by feed-forward loop and harmonic distortion controlled by carriers programming.
- Two oscilloscopes.
- Two multimeters.
- One dual power DC supply, maximum KE=35 V, maximum (1-K)E=35 V.
- Auxiliaries supplies for analog and digital circuits, +15 V, -15 V and 5 V.

This material comprises the experimental set-up which is shown in figure 8.15 where auxiliary power supplies are not detailed, only the main input sources KE and (1-K)E.

UNIVERSITAT ROVIRA I VIRGILI
CONTRIBUTIONS ON SPECTRAL CONTROL FOR THE ASYMMETRICAL FULL BRIDGE MULTILEVEL INVERTER
Oscar Mauricio Muñoz Ramírez
ISBN:978-84-693-7665-2/DL:T.1747-2010

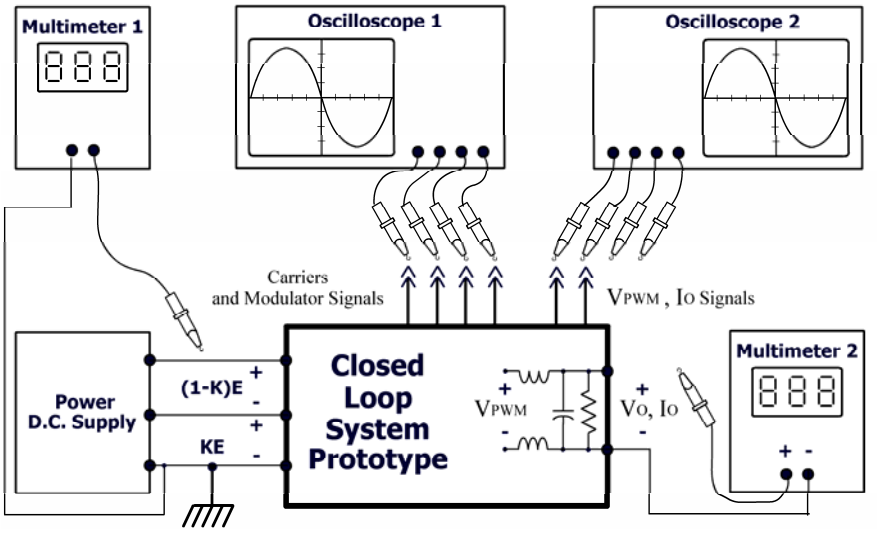

Figure 8.15 Experimental Set-Up of the Prototype.

The total harmonic distortion were evaluated for the first ten harmonics since we focus our attention on the low frequency base-band harmonics. Optimized cases which performed programmed carriers set are compared with standard cases which use standard carriers. The five-level modulated signal V_{pwm} is evaluated with the parameter $THD_{V,n=10}$. In the same way, the output filtered signal V_o is evaluated with the parameter $THD_{I,n=10}$.

Table 8.4 summarizes the harmonic analysis evaluated for some input conditions, namely M_a and K. They are the input conditions to the system comprising the operating point V_{target} which is allocated in the matrix of optimized solutions. Three values of M_a (0.764,0.84,0.88) are progressively measured with three combinations of K (0.4,0.5,0.6).

TABLE 8.4 DISTORTION RESULTS EVALUATED ON TEN HARMONICS.

Operating Point			Optimized Case		Standard Case	
V_{target}	M_a	K	$THD_{V,n=10}$%	$THD_{I,n=10}$%	$THD_{V,n=10}$%	$THD_{I,n=10}$%
1	0.764	0.4	4.5	0.94	3.72	0.80
2		0.5	3.04	0.64	3.74	0.76
3		0.6	3.46	0.77	4.79	1.09
4	0.84	0.4	3.70	0.73	3.69	0.75
5		0.5	3.78	0.83	4.06	0.86
6		0.6	3.41	0.65	4.25	0.88
7	0.88	0.4	3.49	0.66	3.49	0.68
8		0.5	2.44	0.54	2.96	0.68
9		0.6	3.04	0.67	3.50	0.74

In total, nine operating points were measured and recorded in order to evaluate their harmonic performance according to their correspondent programmed carriers set. Additionally, detailed pictures (figures 8.16 to 8.24) show how in most of the nine cases the harmonic distortion is

UNIVERSITAT ROVIRA I VIRGILI
CONTRIBUTIONS ON SPECTRAL CONTROL FOR THE ASYMMETRICAL FULL BRIDGE MULTILEVEL INVERTER
Oscar Mauricio Muñoz Ramírez
ISBN:978-84-693-7665-2/DL:T.1747-2010

improved especially on the second and third harmonics. The carriers shape and the modulator are depicted as well. Finally, THD curves were plotted in order to gather the plots of THD for ten harmonics and the main changes to be observed in the second and third harmonics.

In eight of nine cases, optimization was achieved as is confirmed by $THD_{V,\ n=10}$ and $THD_{I,\ n=10}$. Revising distortion parameters to the tenth harmonic is the first step to obtain quick diagnosis. With only these last criterions, it would be state that poor improvement was realized on the operating points V_{target} 4, 5 and 7. Although V_{target} 4, 5 and 7 were barely improved, it is worth to look further in the spectra pictures and their respective THD curves, where it can be observed that second harmonic was optimized but the next harmonics were not.

UNIVERSITAT ROVIRA I VIRGILI
CONTRIBUTIONS ON SPECTRAL CONTROL FOR THE ASYMMETRICAL FULL BRIDGE MULTILEVEL INVERTER
Oscar Mauricio Muñoz Ramírez
ISBN:978-84-693-7665-2/DL:T.1747-2010

$V_{target}1$: M_a=0.764, K=0.4, E=55 V, Ro=5 Ω, V_o=42 V_p=29.7 V_{rms}

Results with Optimized Carriers

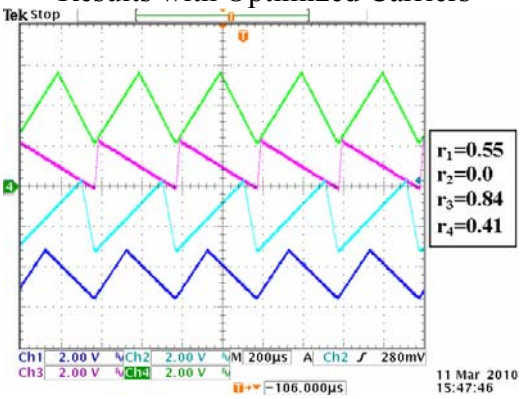

a) Optimized Carriers, 2V/200µs

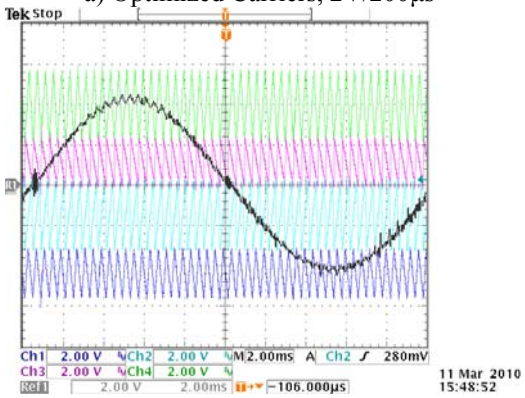

b) Optimized SPWM scheme, 2V/2ms

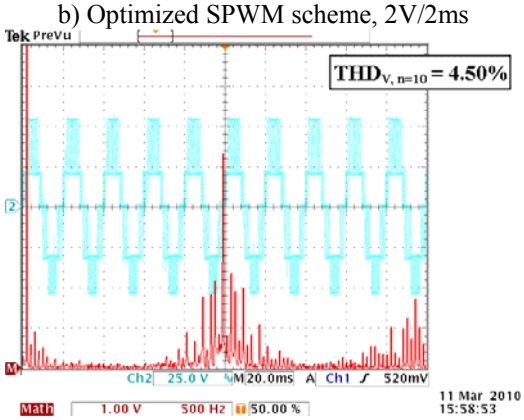

c) Spectrum for V_{pwm}, $1V_{rms}$/500Hz

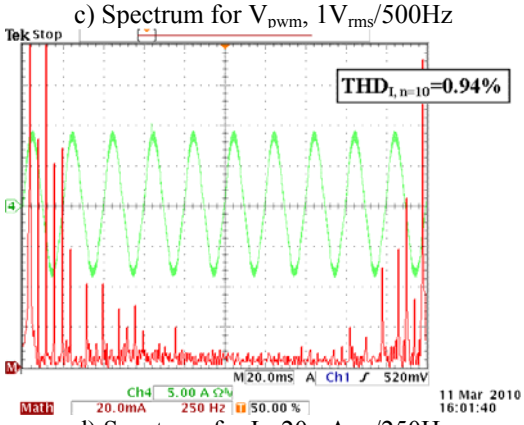

d) Spectrum for I_o, $20mA_{rms}$/250Hz

Results with Standard Carriers

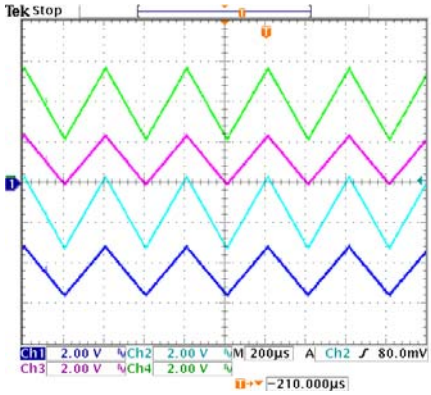

e) Standard Carriers, 2V/200µs

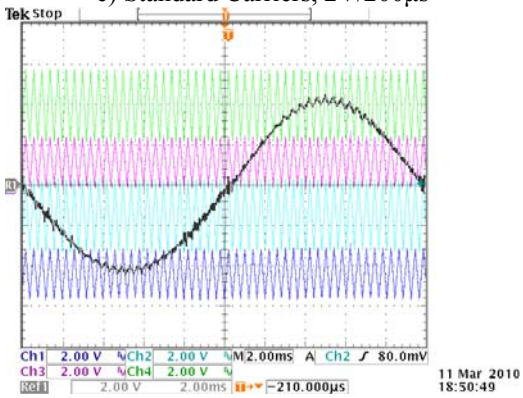

f) Standard SPWM scheme, 2V/2ms

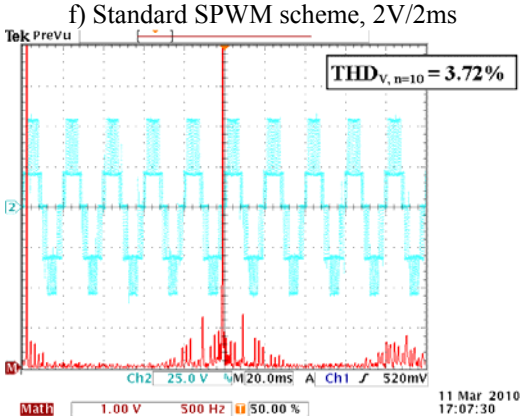

g) Spectrum for V_{pwm}, $1V_{rms}$/500Hz

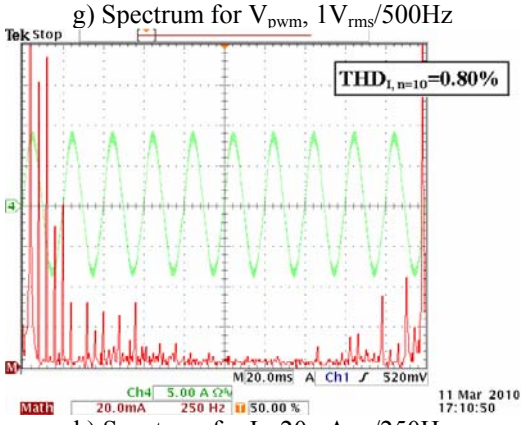

h) Spectrum for I_o, $20mA_{rms}$/250Hz

Figure 8.16 Optimized and Standard Carriers, V_{target}(M_a=0.764,K=0.4).

ISBN:978-84-693-7665-2/DL:T.1747-2010

$V_{target}2$:M_a=0.764, K=0.5, E=55 V, Ro=5 Ω, V_o=42 V_p=29.7 V_{rms}

Results with Optimized Carriers

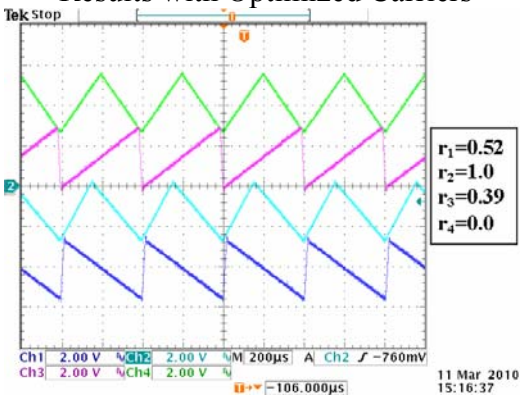

a) Optimized Carriers, 2V/200µs

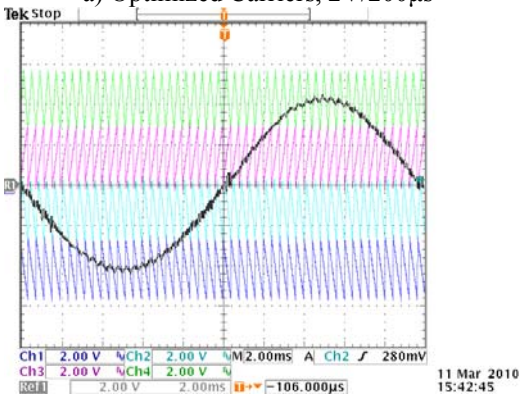

b) Optimized SPWM scheme, 2V/2ms

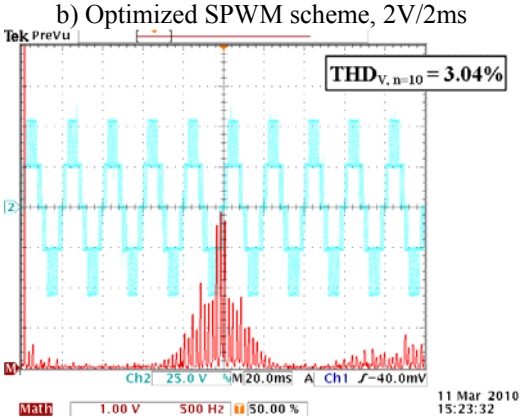

c) Spectrum for V_{pwm}, $1V_{rms}$/500Hz

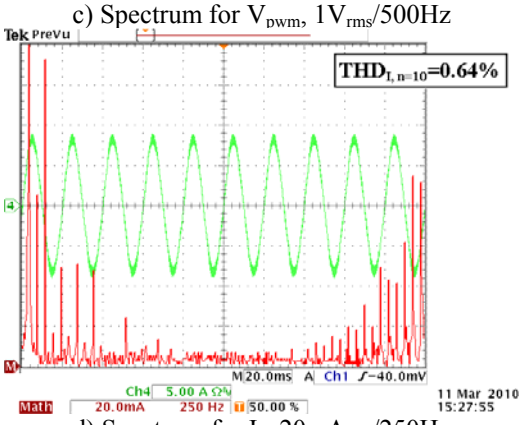

d) Spectrum for I_o, $20mA_{rms}$/250Hz

Results with Standard Carriers

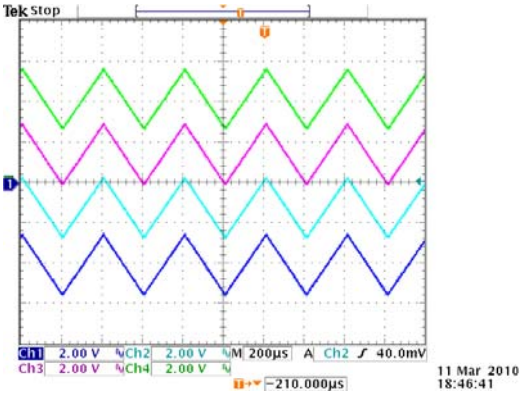

e) Standard Carriers, 2V/200µs

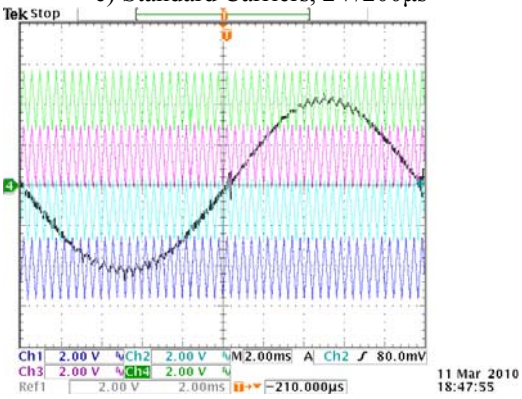

f) Standard SPWM scheme, 2V/2ms

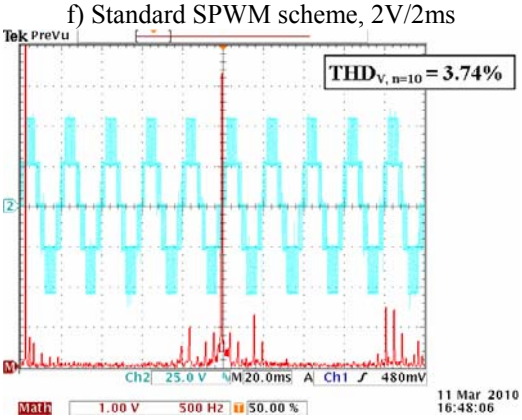

g) Spectrum for V_{pwm}, $1V_{rms}$/500Hz

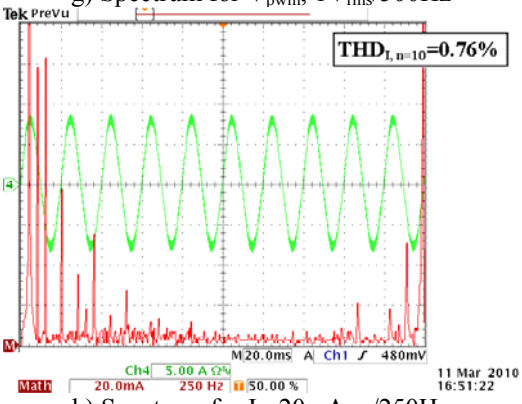

h) Spectrum for I_o, $20mA_{rms}$/250Hz

Figure 8.17 Optimized and Standard Carriers, V_{target}(M_a=0.764,K=0.5)

ISBN:978-84-693-7665-2/DL:T.1747-2010

$V_{target}3$: M_a=0.764, K=0.6, E=55 V, Ro=5 Ω, V_o=42 V_p=29.7 V_{rms}

Results with Optimized Carriers

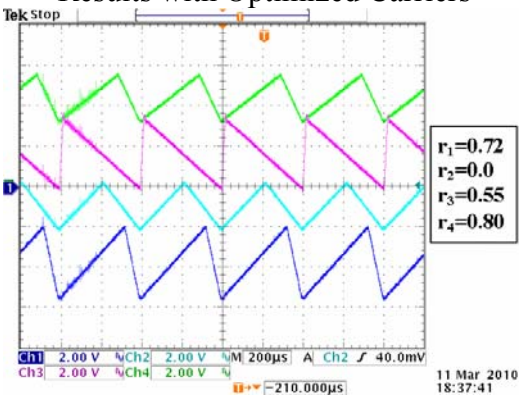

a) Optimized Carriers, 2V/200µs

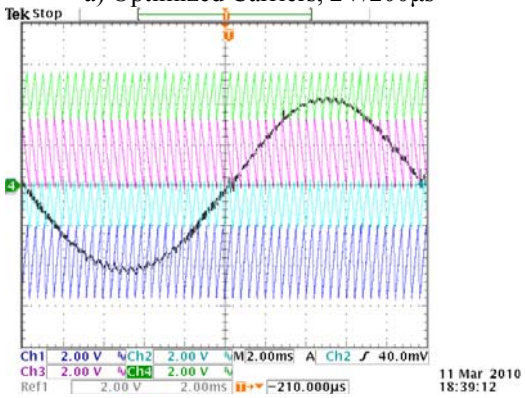

b) Optimized SPWM scheme, 2V/2ms

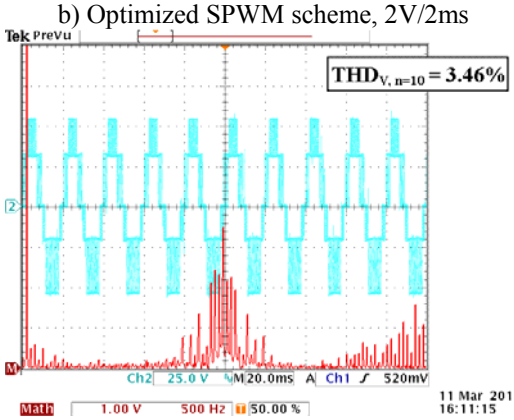

c) Spectrum for V_{pwm}, $1V_{rms}$/500Hz

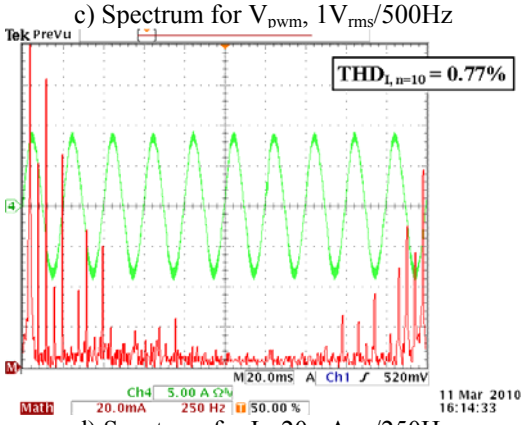

d) Spectrum for I_o, $20mA_{rms}$/250Hz

Results with Standard Carriers

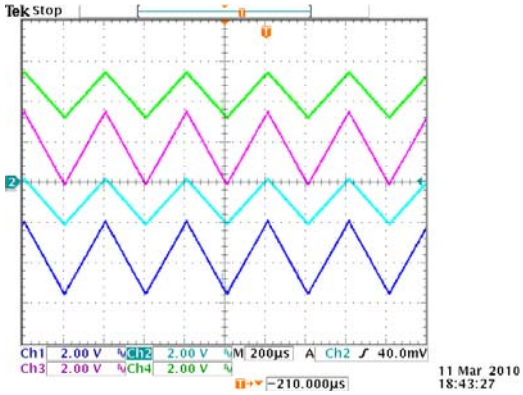

e) Standard Carriers, 2V/200µs

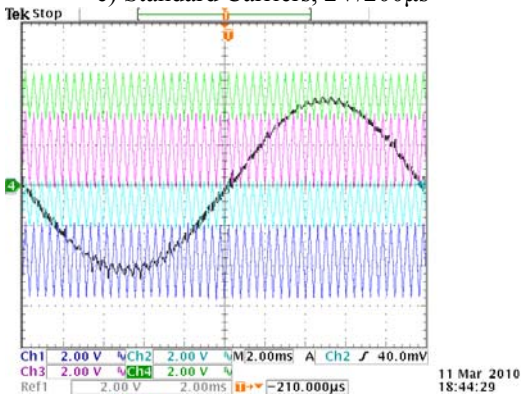

f) Standard SPWM scheme, 2V/2ms

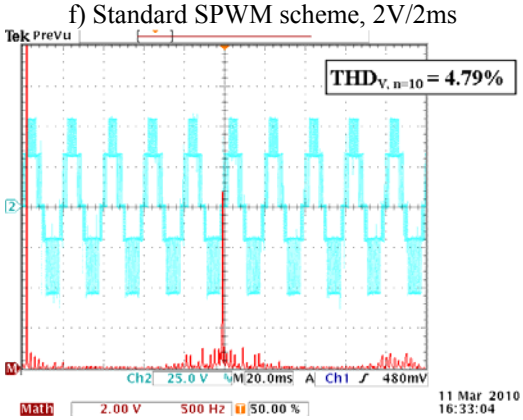

g) Spectrum for V_{pwm}, $2V_{rms}$/500Hz

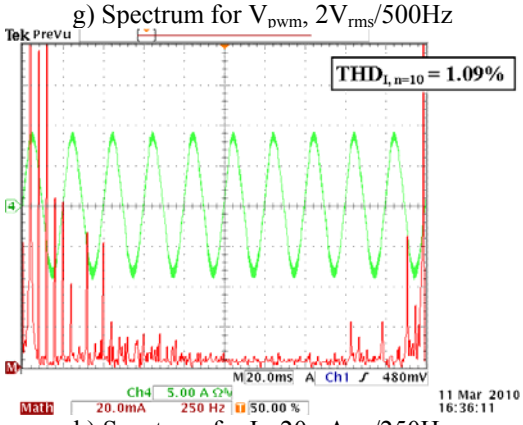

h) Spectrum for I_o, $20mA_{rms}$/250Hz

Figure 8.18 Optimized and Standard Carriers, V_{target}(M_a=0.764,K=0.6).

ISBN:978-84-693-7665-2/DL:T.1747-2010

$V_{target}4$: M_a=0.84, K=0.4, E=50 V, Ro=5 Ω, V_o=42 V_p=29.7 V_{rms}

Results with Optimized Carriers

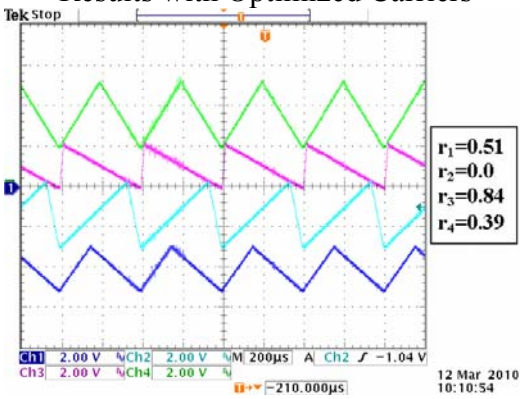

a) Optimized Carriers, 2V/200µs

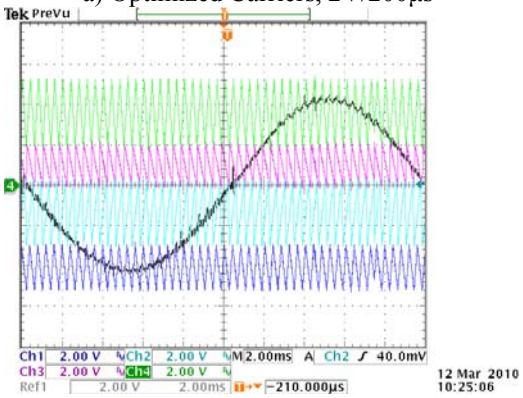

b) Optimized SPWM scheme, 2V/2ms

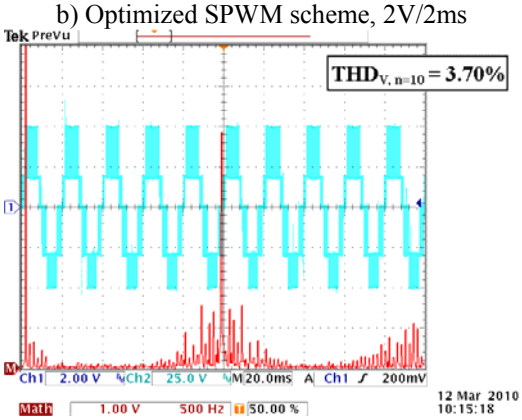

c) Spectrum for V_{pwm}, $1V_{rms}$/500Hz

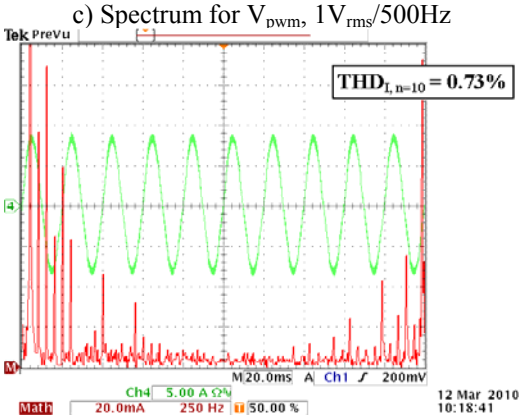

d) Spectrum for I_o, $20mA_{rms}$/250Hz

Results with Standard Carriers

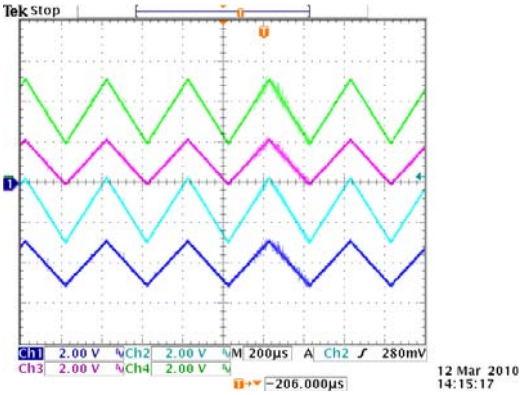

e) Standard Carriers, 2V/200µs

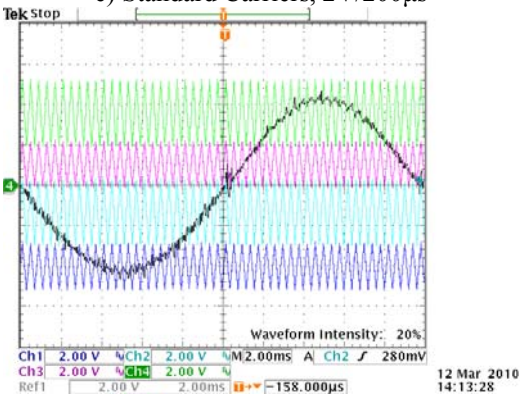

f) Standard SPWM scheme, 2V/2ms

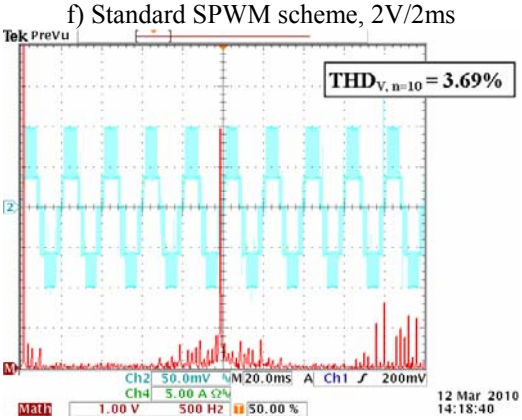

g) Spectrum for V_{pwm}, $1V_{rms}$/500Hz

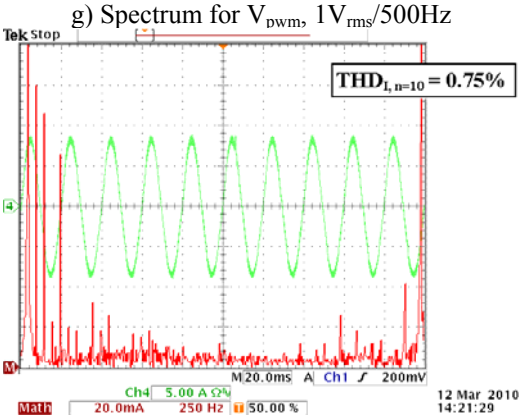

h) Spectrum for I_o, $20mA_{rms}$/250Hz

Figure 8.19 Optimized and Standard Carriers, V_{target}(M_a=0.84,K=0.4)

ISBN:978-84-693-7665-2/DL:T.1747-2010

$V_{target}5$: M_a=0.84, K=0.5, E=50 V, Ro=5 Ω, V_o=42 V_p=29.7 V_{rms}

Results with Optimized Carriers

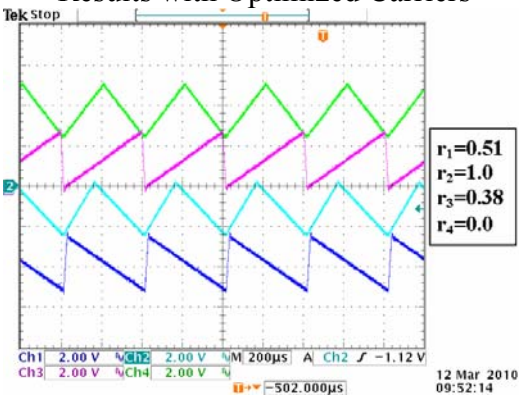

a) Optimized Carriers, 2V/200µs

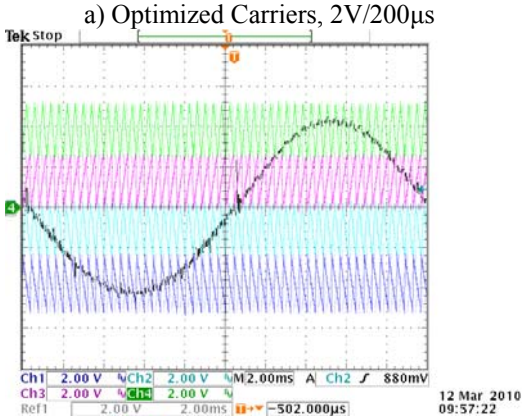

b) Optimized SPWM scheme, 2V/2ms

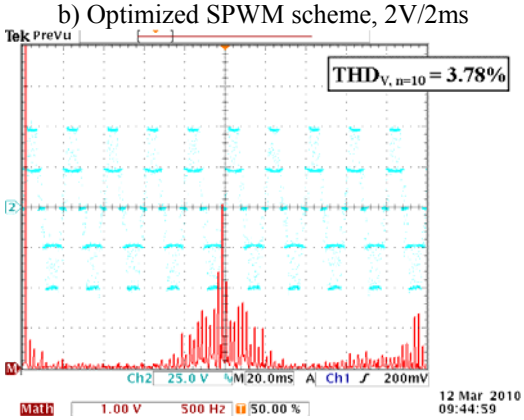

c) Spectrum for V_{pwm}, $1V_{rms}$/500Hz

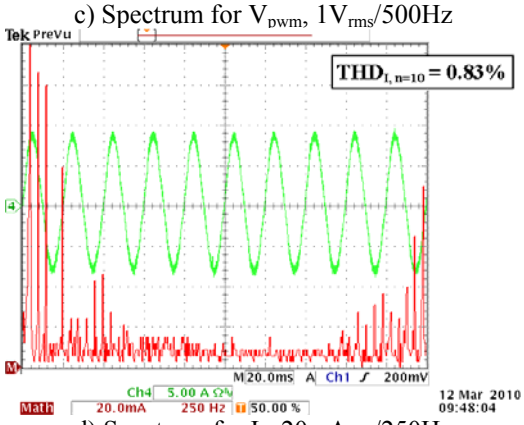

d) Spectrum for I_o, $20mA_{rms}$/250Hz

Results with Standard Carriers

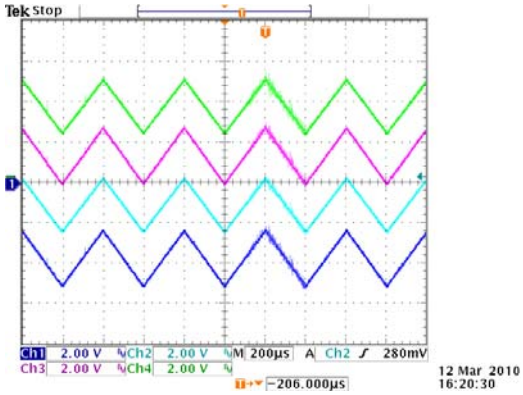

e) Standard Carriers, 2V/200µs

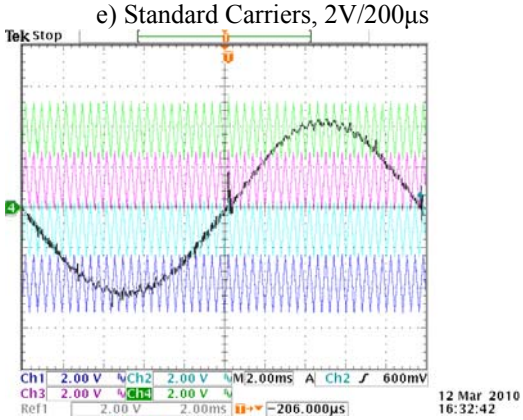

f) Standard SPWM scheme, 2V/2ms

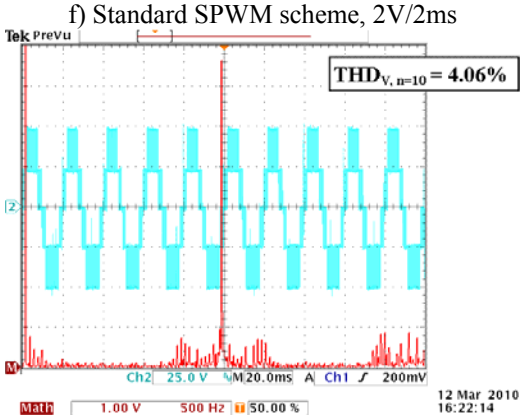

g) Spectrum for V_{pwm}, $1V_{rms}$/500Hz

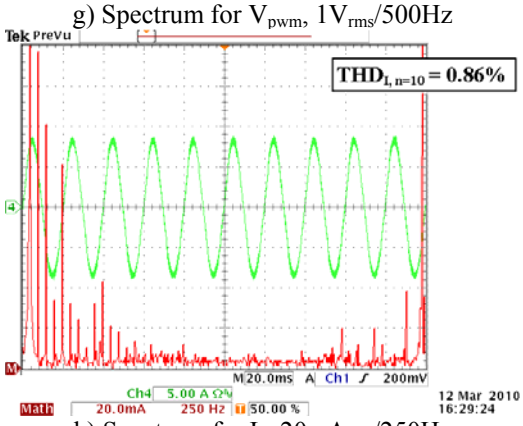

h) Spectrum for I_o, $20mA_{rms}$/250Hz

Figure 8.20 Optimized and Standard Carriers, V_{target}(M_a=0.84,K=0.5).

$V_{target}6$: M_a=0.84, K=0.6, E=50 V, Ro=5 Ω, V_o=42 V_p=29.7 V_{rms}

Results with Optimized Carriers

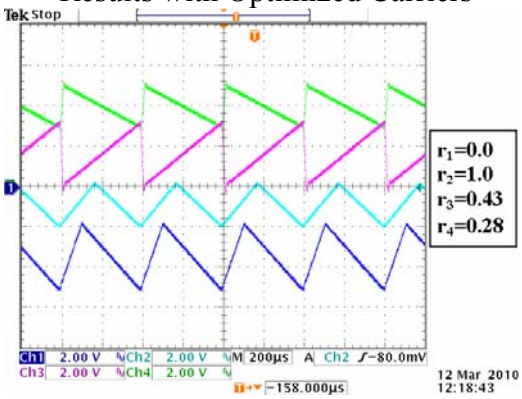

a) Optimized Carriers, 2V/200µs

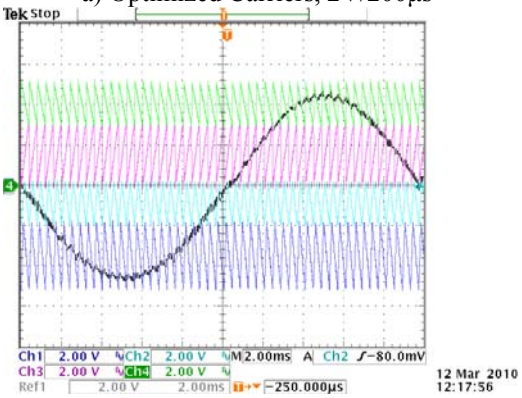

b) Optimized SPWM scheme, 2V/2ms

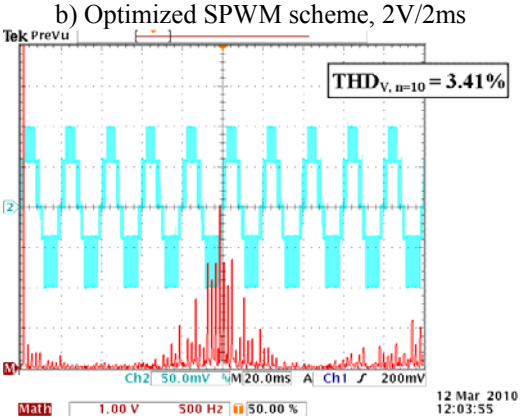

c) Spectrum for V_{pwm}, $1V_{rms}$/500Hz

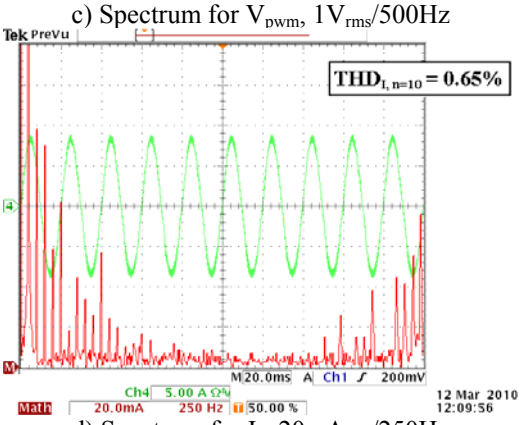

d) Spectrum for I_o, $20mA_{rms}$/250Hz

Results with Standard Carriers

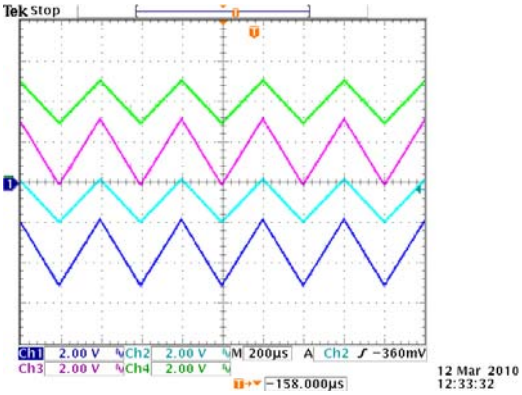

e) Standard Carriers, 2V/200µs

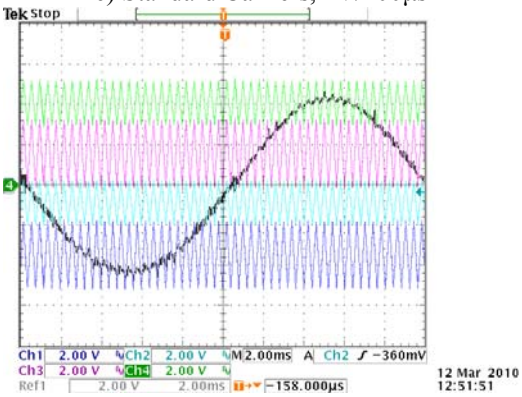

f) Standard SPWM scheme, 2V/2ms

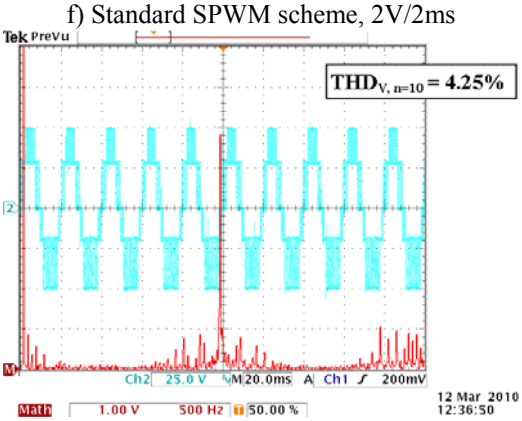

g) Spectrum for V_{pwm}, $1V_{rms}$/500Hz

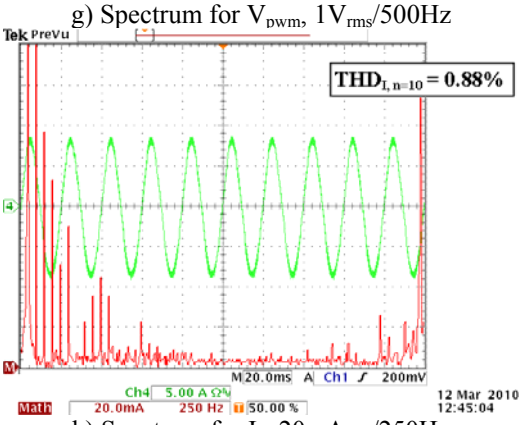

h) Spectrum for I_o, $20mA_{rms}$/250Hz

Figure 8.21 Optimized and Standard Carriers, V_{target}(M_a=0.84,K=0.6).

ISBN:978-84-693-7665-2/DL:T.1747-2010

V_{target}7: M_a=0.88, K=0.4, E=45 V, Ro=5 Ω, V_o=39.6 V_p=28 V_{rms}

Results with Optimized Carriers

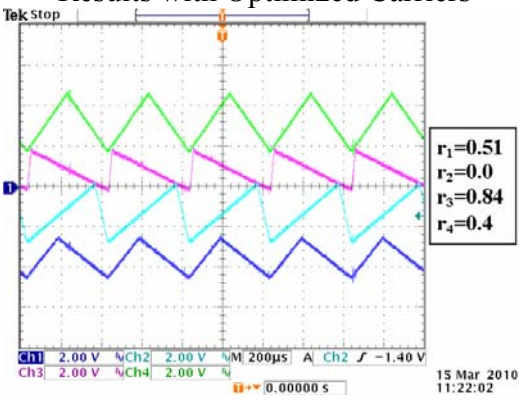

a) Optimized Carriers, 2V/200µs

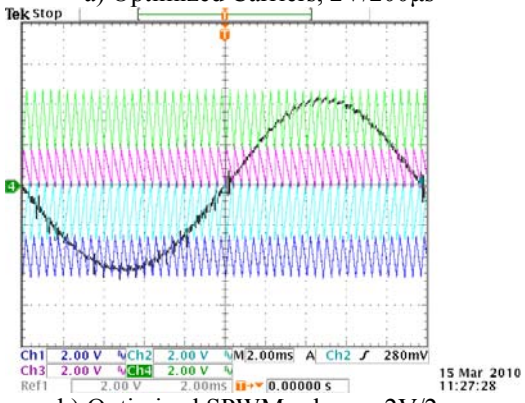

b) Optimized SPWM scheme, 2V/2ms

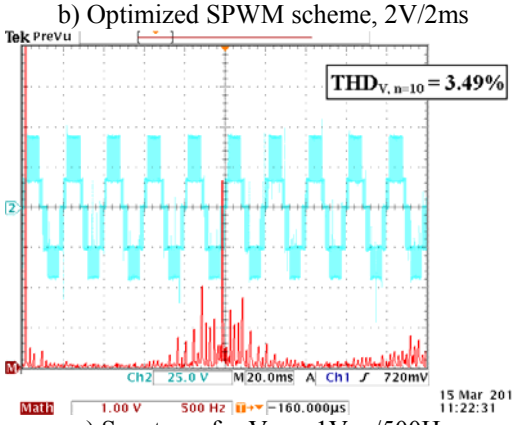

c) Spectrum for V_{pwm}, $1V_{rms}$/500Hz

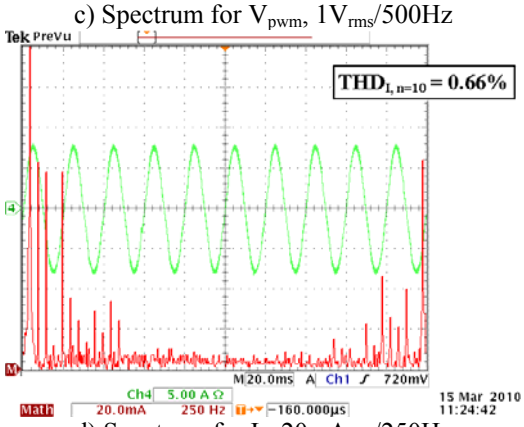

d) Spectrum for I_o, $20mA_{rms}$/250Hz

Results with Standard Carriers

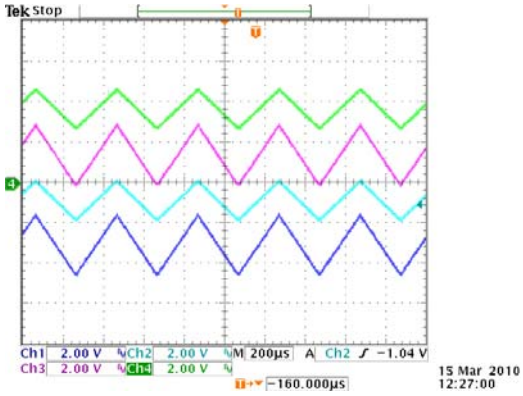

e) Standard Carriers, 2V/200µs

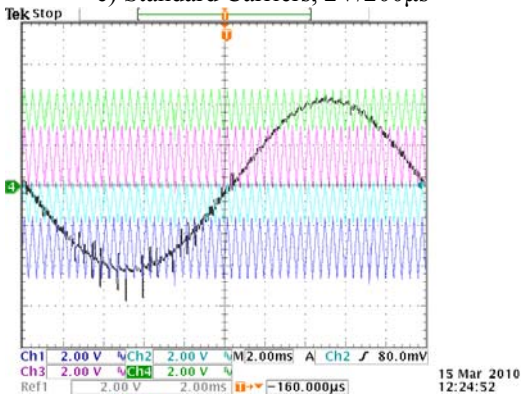

f) Standard SPWM scheme, 2V/2ms

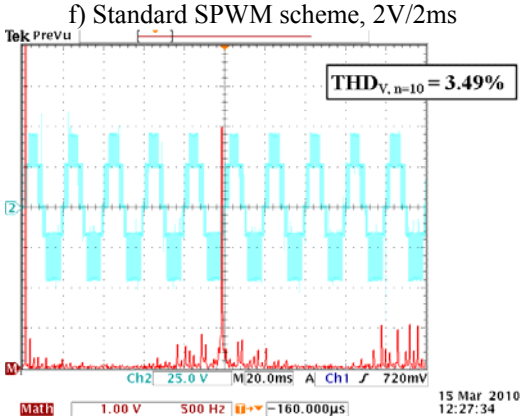

g) Spectrum for V_{pwm}, $1V_{rms}$/500Hz

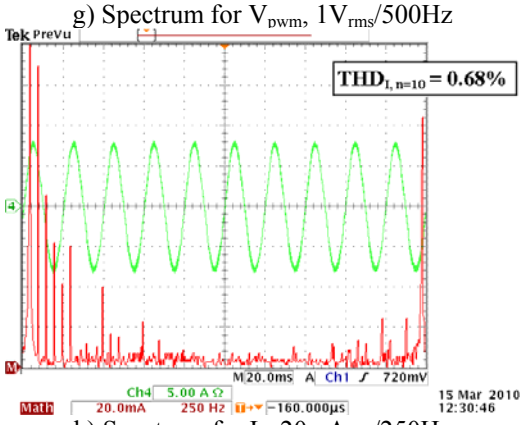

h) Spectrum for I_o, $20mA_{rms}$/250Hz

Figure 8.22 Optimized and Standard Carriers, V_{target}(M_a=0.88,K=0.4).

V_{target}8: M_a=0.88, K=0.5, E=45 V, Ro=5 Ω, V_o=39.6 V_p=28 V_{rms}

Results with Optimized Carriers

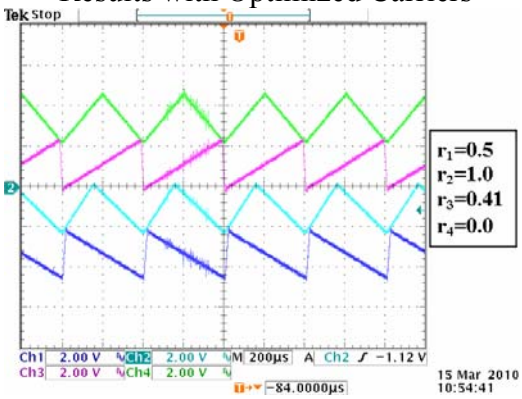

a) Optimized Carriers, 2V/200µs

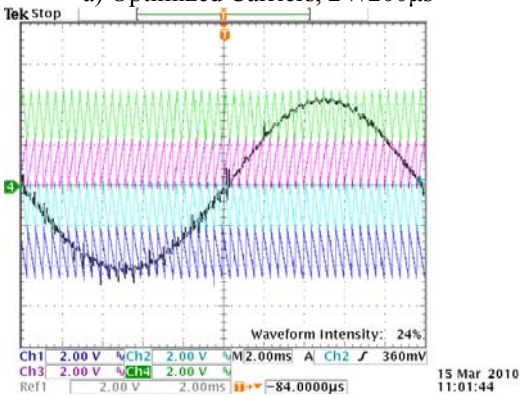

b) Optimized SPWM scheme, 2V/2ms

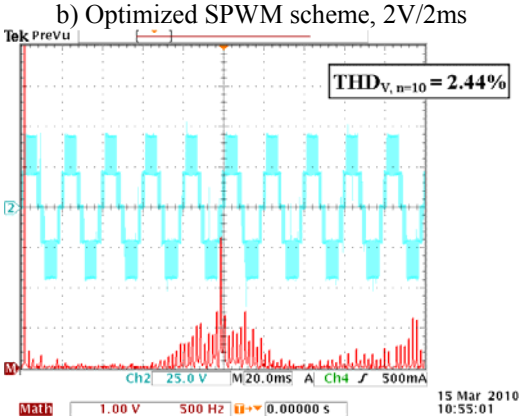

c) Spectrum for V_{pwm}, $1V_{rms}$/500Hz

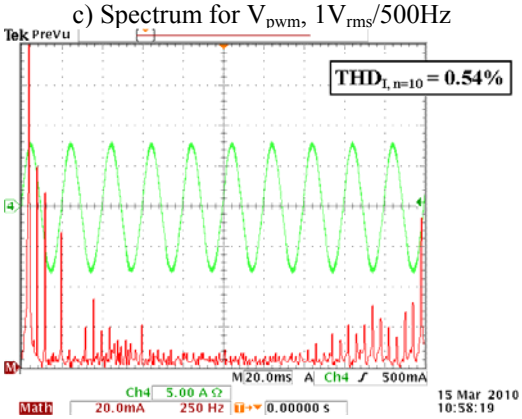

d) Spectrum for I_o, $20mA_{rms}$/250Hz

Results with Standard Carriers

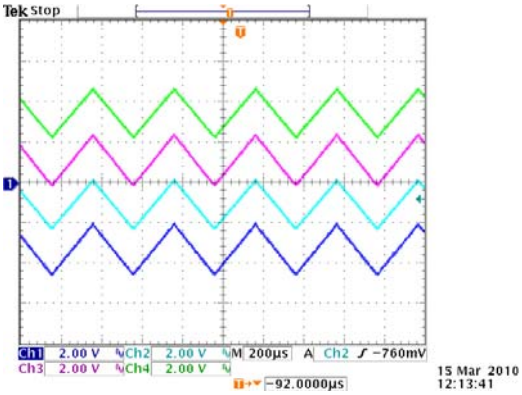

e) Standard Carriers, 2V/200µs

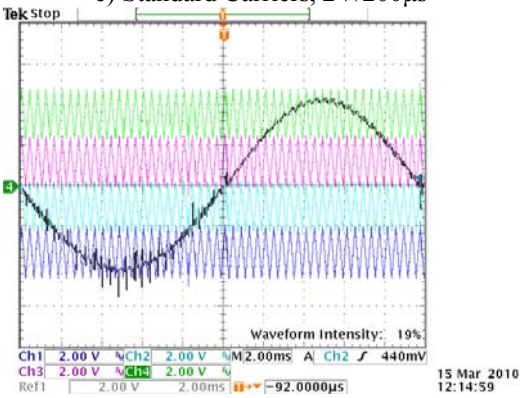

f) Standard SPWM scheme, 2V/2ms

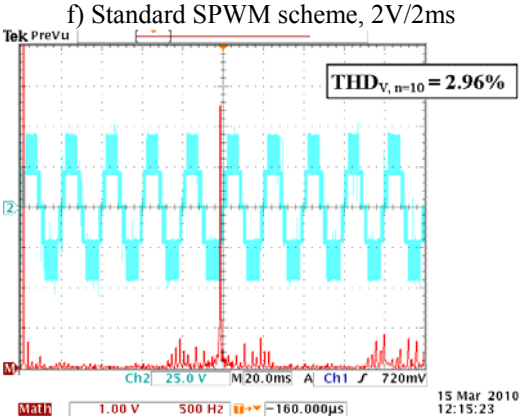

g) Spectrum for V_{pwm}, $1V_{rms}$/500Hz

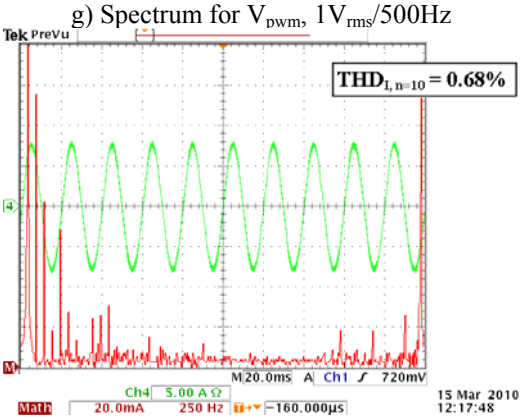

h) Spectrum for I_o, $20mA_{rms}$/250Hz

Figure 8.23 Optimized and Standard Carriers, V_{target}(M_a=0.88,K=0.5).

ISBN:978-84-693-7665-2/DL:T.1747-2010

$V_{target}9$: M_a=0.88, K=0.6, E=45 V, Ro=5 Ω, V_o=39.6 V_p=28 V_{rms}

Results with Optimized Carriers

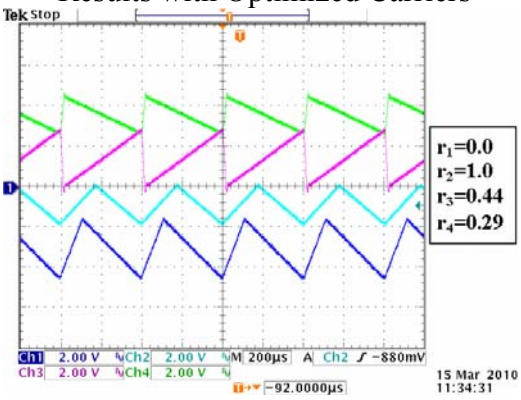

a) Optimized Carriers, 2V/200µs

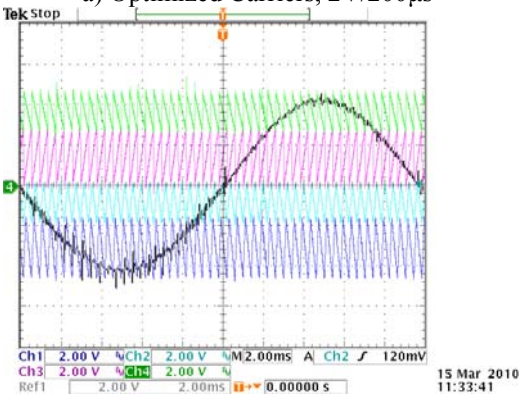

b) Optimized SPWM scheme, 2V/2ms

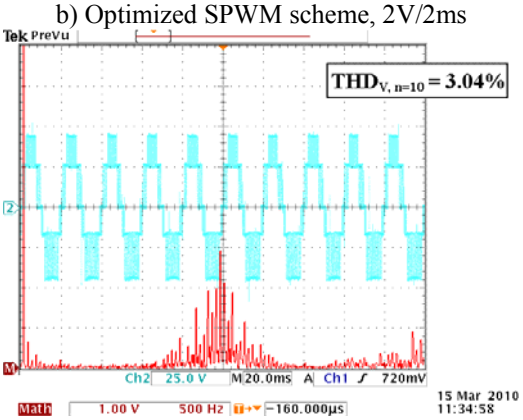

c) Spectrum for V_{pwm}, $1V_{rms}$/500Hz

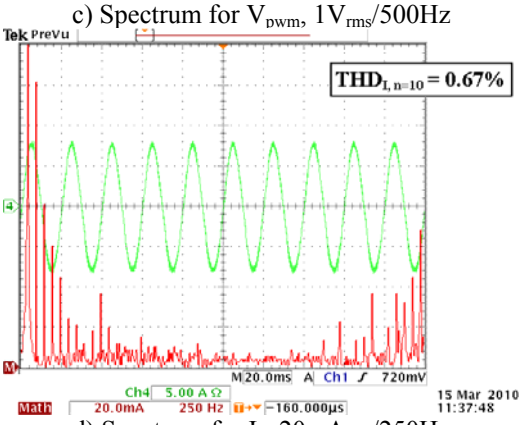

d) Spectrum for I_o, $20mA_{rms}$/250Hz

Results with Standard Carriers

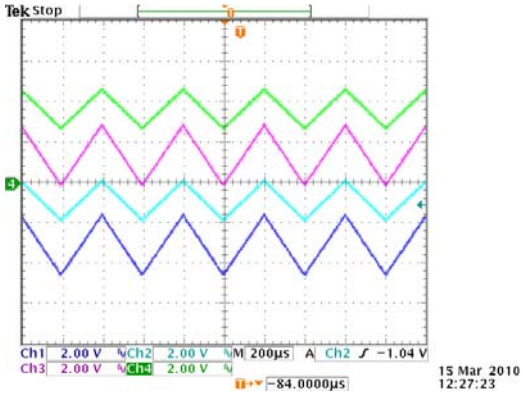

e) Standard Carriers, 2V/200µs

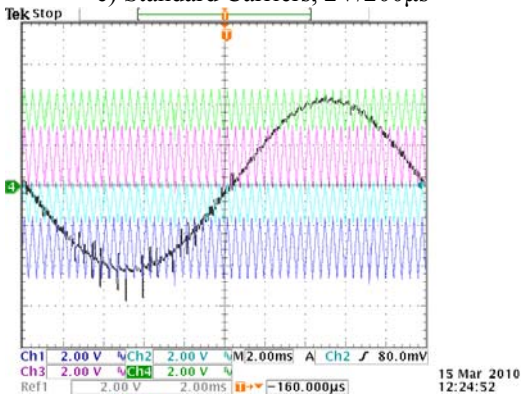

f) Standard SPWM scheme, 2V/2ms

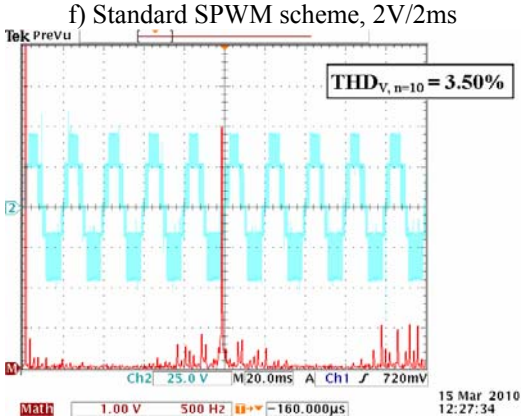

g) Spectrum for V_{pwm}, $1V_{rms}$/500Hz

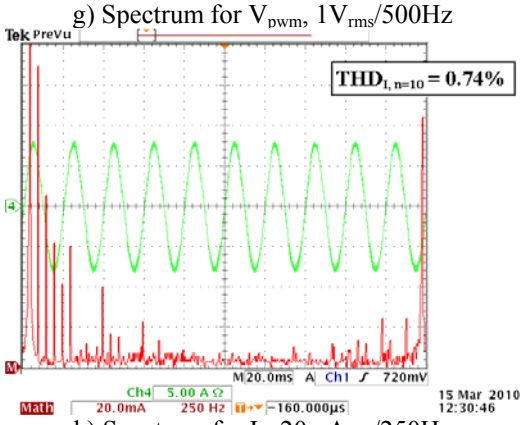

h) Spectrum for I_o, $20mA_{rms}$/250Hz

Figure 8.24 Optimized and Standard Carriers, V_{target}(M_a=0.88,K=0.6)

UNIVERSITAT ROVIRA I VIRGILI
CONTRIBUTIONS ON SPECTRAL CONTROL FOR THE ASYMMETRICAL FULL BRIDGE MULTILEVEL INVERTER
Oscar Mauricio Muñoz Ramírez
ISBN:978-84-693-7665-2/DL:T.1747-2010

$V_{target}1$: M_a=0.764, K=0.4, E=55 V, Ro=5 Ω, V_o=42 V_p=29.7 V_{rms}

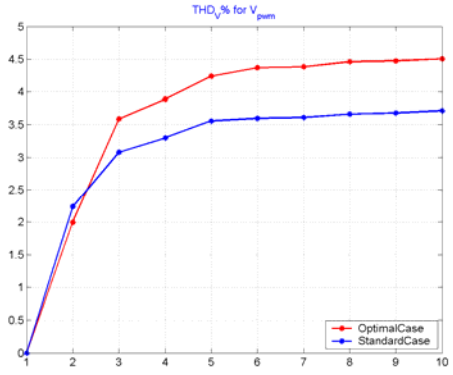

a) THD_V for V_{pwm}, Optimized Vs. Standard

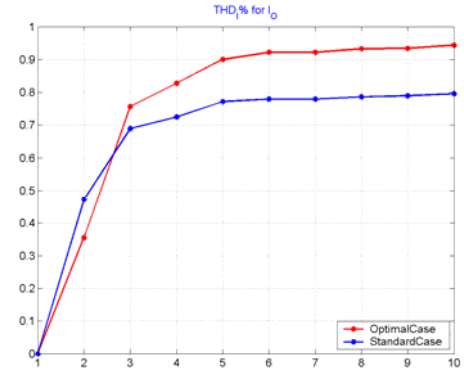

d) THD_I for I_o, Optimized Vs. Standard

$V_{target}2$: M_a=0.764, K=0.5, E=55 V, Ro=5 Ω, V_o=42 V_p=29.7 V_{rms}

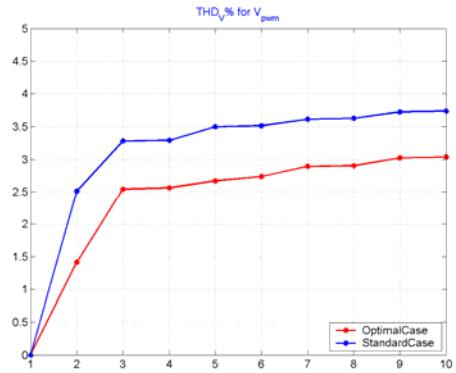

b) THD_V for V_{pwm}, Optimized Vs. Standard

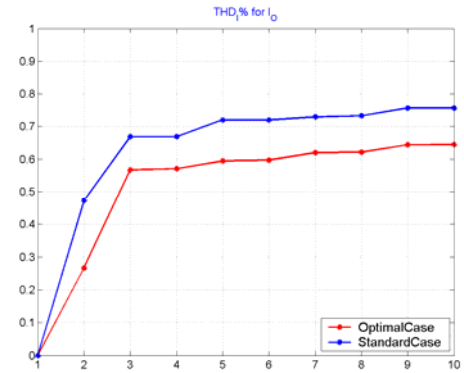

e) THD_I for I_o, Optimized Vs. Standard

$V_{target}3$: M_a=0.764, K=0.6, E=55 V, Ro=5 Ω, V_o=42 V_p=29.7 V_{rms}

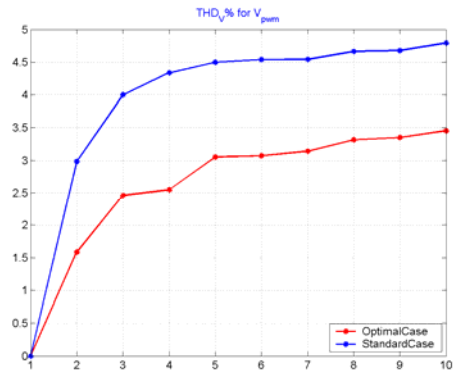

c) THD_V for V_{pwm}, Optimized Vs. Standard

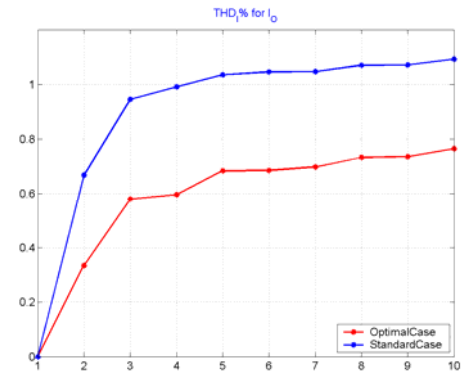

f) THD_I for I_o, Optimized Vs. Standard

Figure 8.25 Optimized Carriers Vs. Standard Carriers, (M_a=0.764).

Figure 8.25 gathers the three cases when M_a=0.764 and K= {0.4,0.5,0.6} and it can be observed that the derivative slope of their lines indicate the contribution of each harmonic every time the subsequent harmonic *h* is introduced in the summon factor used to calculate THD. Red lines correspond to harmonic profiles obtained by means of optimized carriers. Blue lines depicte harmonic profiles based on standard carriers. In figure 8.25, sub-figures a and d show that third harmonic has worsened and its slope is higher than in standard case; In the other cases, sub-figures shows good performance of carriers optimization.

$V_{target}4$: M_a=0.84, K=0.4, E=50 V, Ro=5 Ω, V_o=42 V_p=29.7 V_{rms}

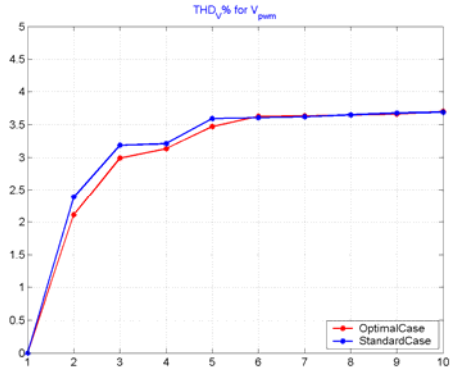

a) THD_V for V_{pwm}, Optimized Vs. Standard

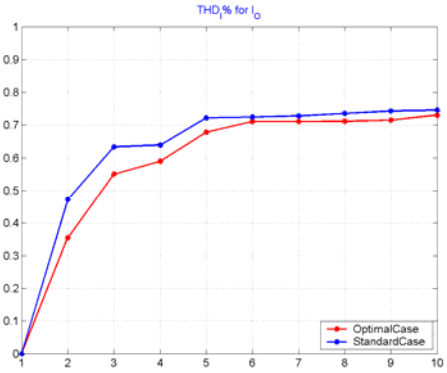

d) THD_I for I_o, Optimized Vs. Standard

$V_{target}5$: M_a=0.84, K=0.5, E=50 V, Ro=5 Ω, V_o=42 V_p=29.7 V_{rms}

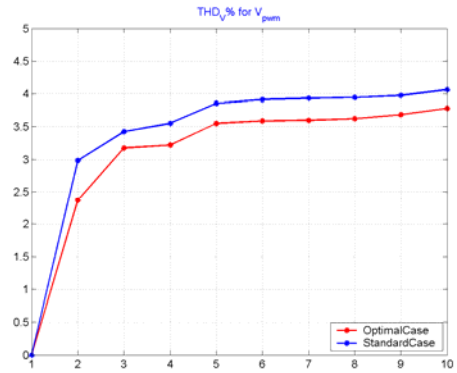

b) THD_V for V_{pwm}, Optimized Vs. Standard

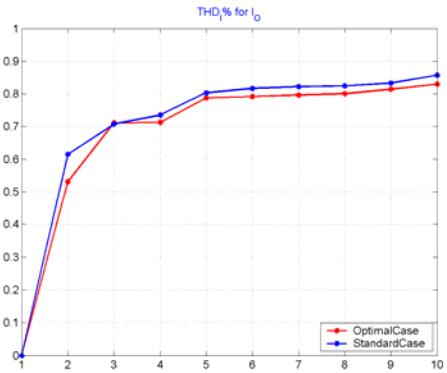

e) THD_I for I_o, Optimized Vs. Standard

$V_{target}6$: M_a=0.84, K=0.6, E=50 V, Ro=5 Ω, V_o=42 V_p=29.7 V_{rms}

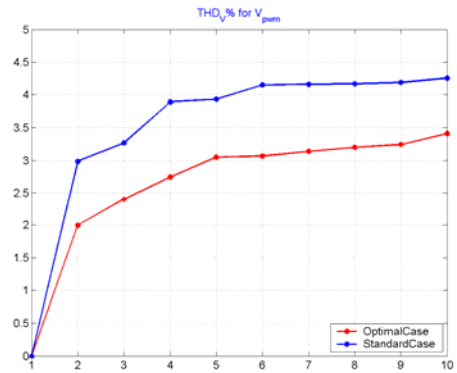

c) THD_V for V_{pwm}, Optimized Vs. Standard

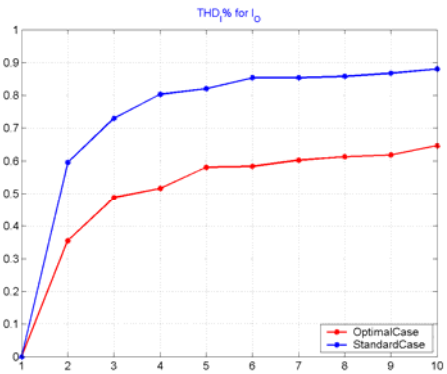

f) THD_I for I_o, Optimized Vs. Standard

Figure 8.26 Optimized Carriers Vs. Standard Carriers, (M_a=0.84).

When Ma=0.84 and K={0.4,0.5,0.6}, it can be observed that in all three cases optimization was achieved especially as shown in sub-figures 8.26 c), 8.26 f). Sub-figures a,d and b,e suggest that second and third harmonic have contributions that are not modeled yet by any of our developed algorithms to such predict frequency amplitudes. Despite of this disadvantage, the overall performance of the experimental prototype has been improved when mosfet's were selected with the lowest switched-on resistance $R_{DS\text{-}ON}$ available in the market.

UNIVERSITAT ROVIRA I VIRGILI
CONTRIBUTIONS ON SPECTRAL CONTROL FOR THE ASYMMETRICAL FULL BRIDGE MULTILEVEL INVERTER
Oscar Mauricio Muñoz Ramírez
ISBN:978-84-693-7665-2/DL:T.1747-2010

$V_{target}7$: M_a=0.88, K=0.4, E=45 V, Ro=5 Ω, V_o=39.6 V_p=28 V_{rms}

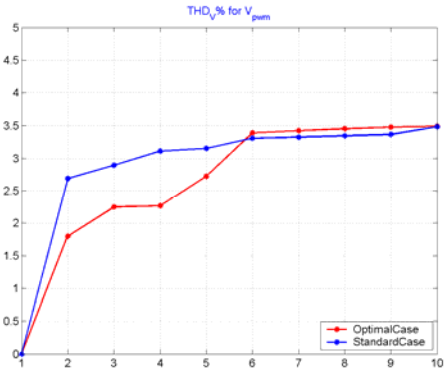

a) THD_V for V_{pwm}, Optimized Vs. Standard

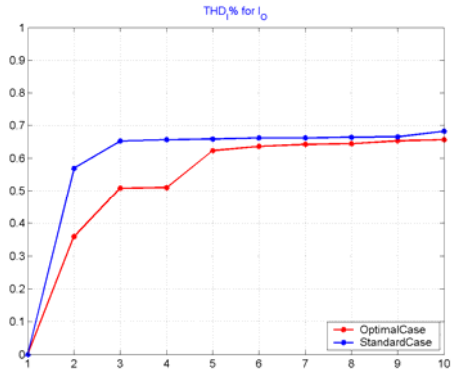

d) THD_I for I_o, Optimized Vs. Standard

$V_{target}8$: M_a=0.88, K=0.5, E=45 V, Ro=5 Ω, V_o=39.6 V_p=28 V_{rms}

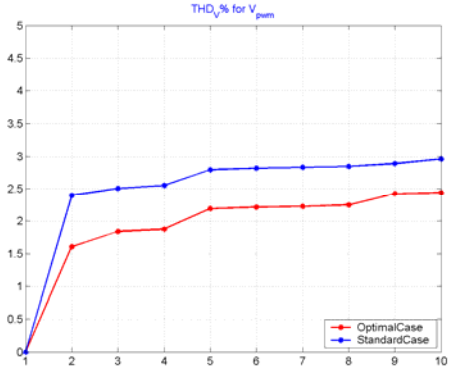

b) THD_V for V_{pwm}, Optimized Vs. Standard

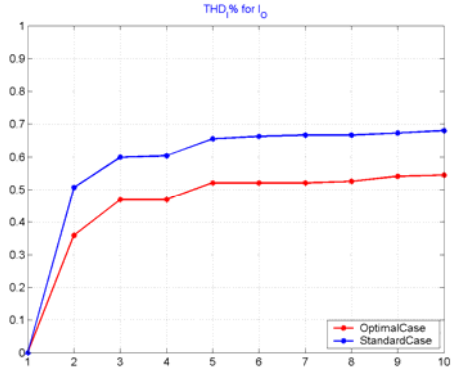

e) THD_I for I_o, Optimized Vs. Standard

$V_{target}9$: M_a=0.88, K=0.6, E=45 V, Ro=5 Ω, V_o=39.6 V_p=28 V_{rms}

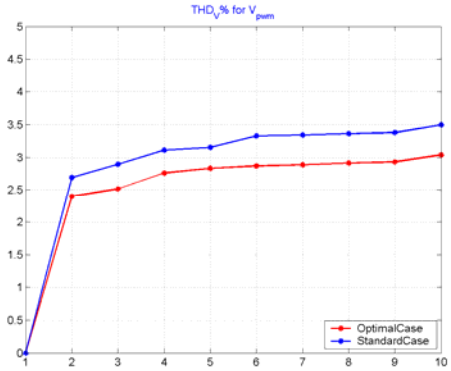

c) THD_V for V_{pwm}, Optimized Vs. Standard

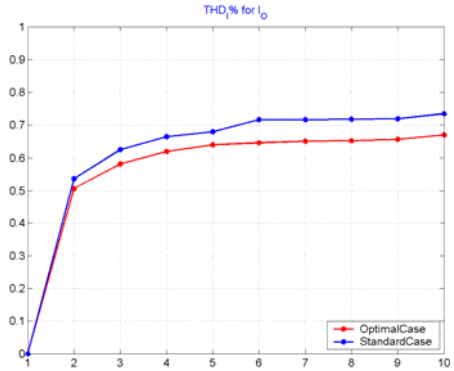

f) THD_I for I_o, Optimized Vs. Standard

Figure 8.27 Optimized Carriers Vs. Standard Carriers, (M_a=0.88).

Finally, in the last group that corresponds to M_a=0.88, optimization in all three cases is successful, especially with K=0.4 and 0.5.

When comparing V_{pwm} spectra, it is observed that carrier-frequency amplitude is reduced by optimizing the carriers set. The only exception is the fourth tested point, V_{target}(0.84,0.4). In general, it is observed that the concentrated energy in the first carrier-multiple by standard modulation is then spread over its lateral flaps when the set of carries is modified; this

UNIVERSITAT ROVIRA I VIRGILI
CONTRIBUTIONS ON SPECTRAL CONTROL FOR THE ASYMMETRICAL FULL BRIDGE MULTILEVEL INVERTER
Oscar Mauricio Muñoz Ramírez
ISBN:978-84-693-7665-2/DL:T.1747-2010

phenomenon is what improves or worsens the harmonic profile and for this reason the optimum carriers set is searched by the GA. The low frequency harmonics are measured by using semi-logarithmical graphs which are not placed in this text. Their amplitudes permitted to calculate accurately the distortion parameters presented here, $THD_{V,n=10}$ and $THD_{I,n=10}$, as well as their respective plotting curves that depicts their harmonic profiles in figures 8.25 to 8.27. These THD-calculations are a complement to the visual inspection realized on the V_{pwm} and I_o spectra from figures 8.16 to 8.24.

TABLE 8.5 QUALIFICATION RESULTS FOR CLOSED-LOOP SYSTEM.

Operating Point			**Optimization Chekcking**
V_{target}	**M_a**	**K**	**Pass**
1	0.764	0.4	No
2		0.5	Yes
3		0.6	Yes
4	0.84	0.4	Yes
5		0.5	Yes
6		0.6	Yes
7	0.88	0.4	Yes
8		0.5	Yes
9		0.6	Yes

The objective function evaluates the harmonics that has been predicted by means of C_n-Algorithm. Since our models (C_{mn}-Algorithm and C_n-Algorithm) do not consider the effects of input supply impedance ($Z_{O\text{-}supply)}$ and converter losses ($Z_{O\text{-}converter}$), the objective function used by the GA can not evaluate accurately the total contributions, mainly on the second and third harmonics where discrepancies are notorious. Despite of this disadvantage, the distortion introduced by $Z_{O\text{-}supply}$ and $Z_{O\text{-}converter}$ can be modified and improved by programming optimized carriers. The developed techniques for carriers optimization are a useful tool when harmonic distortion is to improve.

As long as is $R_{DS\text{-}ON}$ reduced, the resemblance between experimental harmonics amplitudes and modeled amplitudes is stronger. Additionally, core losses can be reduced if inductor is modified, however the filter cut-off frequency must be redesigned and the new filtered harmonics should not exceed the limits of distortion standard.

It is remarkable that in open loop system we used mosfet's with $R_{DS\text{-}ON}$=0.18 Ω and these preliminary experiments showed unsatisfactory modifications on the second and third harmonics. By reducing $R_{DS\text{-}ON}$=0.04 Ω when we changed mosfet's, the experiments in close loop systems yields results with distortion reduction that agree with the expected goal when GA were adopted as an optimization tool for carriers programming. The second and third

UNIVERSITAT ROVIRA I VIRGILI
CONTRIBUTIONS ON SPECTRAL CONTROL FOR THE ASYMMETRICAL FULL BRIDGE MULTILEVEL INVERTER
Oscar Mauricio Muñoz Ramírez
ISBN:978-84-693-7665-2/DL:T.1747-2010

harmonics are still a challenge and a objective for modeling. Since the inductor current of the output filter and the supply input currents add important contributions mainly on the second and third harmonics, and the dependency on this variables is attached to the carriers shapes and therefore to the switching instants, C_n-Algorithm and C_{mn}-Algorithm can be further improved. In this thesis, we restricted these algorithms by assuming ideal DC supplies and zero converter losses and the obtained voltage harmonics for a resistive load could be multiplied by the transfer function of an ideal filter. These assumptions were done in order to converge the research efforts and to avoid extra delays.

One advantage of the analog programmed carriers generator is that this system (comprised by PCB 1 and 2) does not need an exhaustive carriers validation as was the case of carriers generated by DSP in open loop condition, as commented on chapter 7. No pearson-coefficient must be applied to verify via-harmonics comparisons between real and simulated harmonics for the obtained signal, since PCB1,2 and 3 realize SPWM that can be checked instantly by visual inspection and using a oscilloscope.

UNIVERSITAT ROVIRA I VIRGILI
CONTRIBUTIONS ON SPECTRAL CONTROL FOR THE ASYMMETRICAL FULL BRIDGE MULTILEVEL INVERTER
Oscar Mauricio Muñoz Ramírez
ISBN:978-84-693-7665-2/DL:T.1747-2010

9. Conclusions

The cornerstone of this work was to find appropriate tools to optimize the output voltage spectrum of a multilevel inverter. The main constraint was that such converter might switch at very low frequency to reduce as much as possible the losses. That objective led to investigate the possibility of controlling the carrier slopes of a natural sampling PD-PWM modulation.

In parallel to the final goal, diverse spectrum modeling taskes have been realized. We have evaluated diverse modeling tools like DFS, SFS, FFT, and performance parameters as: WTHD, THD. This evaluation has been done by means of diverse simulator programs, and experimental measurements. We have also extended the concept of contour plot to a five-level PD PWM modulation, modeling also the level collapsing phenomena.

The main problem of implementing a multilevel natural modulation with full control of the carrier amplitudes and slopes, was precisely, how to create the carrier signals, or at least how to find the inverter MOSFET gating pulses. Two attempts have been made, and explained respectively, in section VI, and section VIII.

The prorotype presented and section VI, creates directly the pulses for the inverter switching devices. This protype implements a digital modulation, specially developed in this research work that reproduces accurately the features of the analog natural modulation. We call consequently this modulation “Pseudo-Natural Modulation”. This digital implementation was realized with a Texas Instruments DSP Development Kit for the TMS320F2812.

By simply changing a few DSP program parameters, the DSP can implement any kind of PWM POD, PD, and APOD digital modulations. Digital modulations are characterized because there are no analog carriers that can be used to compare with a sinusoidal modulation signal and create the modulation. Instead of that, digital modulations work directly with switching instants, that are stored in a memory table or calculated analytically. To avoid compelx trigonometric equations, many approximations of the sinusoidal signal inside a switching cycle can be considered. Among them, we have: the Pseudo-natural sampling, the asymmetrical regular sampling, and the symmetrical regular sampling. As explained in the text, the Pseudo-Natural sampling, realizing a two-section segment interpolation per carrier period, approximates much better a sinusoidal waveform, and therefore the natural sampling.

The digital prototype, by adjusting some few numerical constants, to modify off-line the working point $\{M_a, K\}$, and the set of slopes$\{r_1, r_2, r_3, r_4\}$ of a Pseudo-Natural PD PWM. After, the program is compiled again, the inverter creates the corresponding output voltage, which spectrum can be easily visualized by the oscilloscope FFT.

By other side, to correct the inverter output-voltage spectrum a closed-loop prototype is much more appropriated. If such closed-loop prototype were based on "Pseudo-Natural Modualtion" it would demand excesive computing effort to the DSP. Consequently, a second prototype, presented in section VIII was planified and realized.

In this second prototype, a dsPIC 30F6010A development kit is used. The micro-processor creates the carriers and the sinuosidal signal as PWM modulations. Those signals, conveniently demodulated and processed, become a set of vertically-shifted analog carries whith their amplitude and slope easily controllables. Those carriers, compared with the sinusoidal modulation signal, create the expected natural sampled multilevel modulation.

This second prototype has three control-loops, two of them are analog: feed-forward and state-feedback, and the third is a slow digital loop. The state-feedback loop involves the sinusoidal modulating signal, and the remaining two affect the carriers. The feed-forward one modifies the carriers amplitude, whereas the digital loop changes the carrier slopes.

Other important issue during this research work was to find an appropriate tool to optimize the carrier slopes. Although, from the beginning, we proved that the carrier slopes were able to modify the spectrum, an easy tool was required to optimize them to achieve a certain output voltatge harmonic goal, at any given working point. The solution came, at the end of this thesis through the genetic algorithms, as explained in section VII.

Genetic algorithms wer introduced as a feasible tool to optimize the carrier slope sets, because this tool was based in the natural evolution theory, and avoided the impossible task of solving the enormous trigonometric equation system to calculate analytically the slope sets. The unique concern when we adopted genetic algorithms was if they were or not convergent into an optimum unique solution, or at least to a set of improved solutions. Surely, that convergence would depend on the strictness degree of the constraint used as final goal of the genetic evolution. Probably is more easily covergent an evolution with a final distortion goal around 5%, than a distortion level below 1%. The real problem in fact, is to know which is the minimum distorsion achievable, because below that, the evolution convergence is impossible

UNIVERSITAT ROVIRA I VIRGILI
CONTRIBUTIONS ON SPECTRAL CONTROL FOR THE ASYMMETRICAL FULL BRIDGE MULTILEVEL INVERTER
Oscar Mauricio Muñoz Ramírez
ISBN:978-84-693-7665-2/DL:T.1747-2010

To control the output harmonics, our research work required an useful tool to understand, predict, or model the inverter output voltage spectrum. At the beginning we searched an analytical expression to predict the spectrum associated to a certain working point {Ma, K} and slope set {r1, r2, r3, r4}. Once predicted the spectrum, some mathematical manipulations could be used to calculate the slope set to achieve a certain spectral goal.

The first spectral tool we used was the DFS. Indeed, by making some integrals, the DFS could give us an analytical expression of the output voltage spectrum where the influence of the slope parameters were explicitly shown. Besides, the contour plots used to understand the influence of the slopes in the spectrum led practically to the DFS adoption because the integration limits of DFS came directly from that countour plots. We used this tool to calculate analytically, through the C_{mn} coefficients the analytical expression of the output voltage in a five level PD PWM natural sampled modulation where $M_a>\max(K,1-K)$. This case regards a five-level modulation where no collapsing is produced. That is, if we have 5 available levels, all of them are used to synthesize the sinusoidal output.

For other situations, were level collapsing occurs, and the final modulation has lees levels than expected, such as $1-K<M_a<K$, $K<M_a<1-K$, and $M_a>\min(K,1-K)$, their respective DFS models were written, the respective integrals wer made, but the output voltage final expression coming form simplifying all those previous hard expressions were not finally calculated. Indeed, level collapsing is undesired, because implies a reduced amplitude modulaiton index M_a, which is equivalent to say that all the voltage avialable in the inverter power supplies is not fully used, and higher current levels would be required for an hypothetic output transformer to give the same output voltage. As we use MOSFETS, this implies a efficiency reduction.

Concerning spectral modeling, we have verified that the FFT is dependent on simulation parameters as: switching frequency, simulator step-size, number of considered fundamental frequency cycles, and function windows (Hamming, Hanning, Rectangular, etc). DFS-based spectrums instead, are independent from all these factors and are more accurate. In spite fo the FFT evident lacks, it is widely used because has very simple implementation algorithms, and is installed by default in many oscilloscopes and circuit simulators.

Spectrum modeling through a DFS, was introduced because its direct relationship with the contour plots structure, and yields an exact expression for the inverter output voltage in the time-domain. Nevertheless, its performance in the frequency domain has some lacks compared to SFS, because the frequency information in the DFS is dispersed among the infinite C_{mn}

coefficients, whereas in the SFS, its coefficients C_h give directly the harmonic amplitudes. Nevertheless, in many cases the Bessel functions decay allows a two-alias approximation, specially if the switching frequency is sufficiently high.

$$C_h = \sum_{m=0}^{\infty} C_{m,h-mM_f} \approx \sum_{m=0}^{2} C_{m,h-mM_f} \tag{9.1}$$

Consequently, SFS modeling is more flexible, accurate and faster than the preceding ones.. Additionally, the numerical solution used to calculate the SFS coefficients C_h is very easy, and can be programmed in a MATLAB algorithm. Aditionally, the algorithm is always the same, without complications like level collapsing, because such algorithms involve M_F simple trigonometric calculations as shown in (9.3) where M_F is the frequency modulation index, and [a, b] defines the duration of a voltage pulse.

$$V_o(t) = \sum_{h=0}^{\infty} C_h e^{jh\omega_o t} \rightarrow C_h = \frac{1}{T_o} \sum_{p=1}^{M_F} \left[\int_a^b V_J \cos(h\omega_o t)dt - j\int_a^b V_J \sin(h\omega_o t)dt \right] \tag{9.2}$$

As exposed before, we have used up to four different tools to analyze the spectrum of a sinusoidal modulation, namely: ocscilloscope FFT, PSPICE FFT, and the algorithms used to calculate the DFS C_{mn}, and the SFS C_h coefficients. If the mesasurement and simulation procedure are made carefully the four tools could give the same spectrum. Normally spectrum are compared visually, but when the spectrums are quite similar, an additional interpretation tool to compare them is required. We have used the Person-Coefficients ρ_{xy}. This correlation coefficient measures the degree of linear-similitude of different signals, in this case discrete spectrums. Thus, if two spectrums are equal or proportional ρ_{xy}=1, if they are independent or non-linearly dependent ρ_{xy}=0, and finally if are inversely poroportional ρ_{xy}=–1. Indeed, as the different spectrums represent the same signal, when ρ_{xy}=1 both spectrums must be equal.

Nevertheless, Pearosn coefficient shave ot be applied carefulness. Realize that any sinusoidal modulation, has a first harmonic at 50 Hz much bigger than the remaining harmonics. Two different spectrums compared by Peraosn including the 50 Hz component will appear always as very similar. As a result, when Pearson coefficient has been used to extract conclusions the fundamental harmonic, dependent only on the amplitude emodulation index Ma, has been always neglected.

UNIVERSITAT ROVIRA I VIRGILI
CONTRIBUTIONS ON SPECTRAL CONTROL FOR THE ASYMMETRICAL FULL BRIDGE MULTILEVEL INVERTER
Oscar Mauricio Muñoz Ramírez
ISBN:978-84-693-7665-2/DL:T.1747-2010

Pearson coefficient tool has been used to corroborate that the spectrum of the Pseudo-Natural digital modulation is very similar, to the spectrum of the natural modulation, and therefore, Pseudo-Natural Modulation can be a good implementation for the analog modulaiotn. In general the Pearson-Coefifcients can be used to quantify at which extent, any kind of new modulation is really a good aproximation of a preexisting one. This idea is also, an additional contribution of the present research work.

UNIVERSITAT ROVIRA I VIRGILI
CONTRIBUTIONS ON SPECTRAL CONTROL FOR THE ASYMMETRICAL FULL BRIDGE MULTILEVEL INVERTER
Oscar Mauricio Muñoz Ramírez
ISBN:978-84-693-7665-2/DL:T.1747-2010

UNIVERSITAT ROVIRA I VIRGILI
CONTRIBUTIONS ON SPECTRAL CONTROL FOR THE ASYMMETRICAL FULL BRIDGE MULTILEVEL INVERTER
Oscar Mauricio Muñoz Ramírez
ISBN:978-84-693-7665-2/DL:T.1747-2010

10. Perspectives and Future Works

Concerning the closed-loop prototype, different improvements can be investigated. By now, a genetic algortihm executed by MATLAB optimizes, based on THD constraints, the slopes for all the operating points $\{Ma, K\}_g$ in a grid or matrix. The mixed digital-analog modulator described in Section VIII, use those off-line calculated values to optimize the output spectrum at the deseired target point. Once, the dsPIC has acquired the actual $\{Ma, K\}_m$ value, this point receives as "optimized" carrier slope set, the same slope set that was assigned to the nearest matrix point $\{Ma, K\}_g$ by the genetic algorithm.

A first improvement would affect the algorithm used to assign an "optimum" slope set to a target point point $\{Ma, K\}_m$ that not coincides expressely with any of the available matrix points $\{Ma, K\}_g$. We propose some different strategies.

The first proposal interpolates the optimum slope set for a certain target point $\{Ma, K\}_m$ using the slope sets from the four-six nearest $\{Ma, K\}_g$ matrix points. This interpolation should consider the relative distances between the target point and each one of the nearest points. As lower be the distance between the target and matrix point, bigger will be the weight of this point in the interpolation.

The second approach will use a neural network to calculate the optimum slope set associated to the target point $\{Ma, K\}_m$. The neural network inputs will be the target components: M_a and K, whereas the neural network ouputs will be the slope set $\{r_1, r_2, r_3, r_4\}$. This neural network will be trained with 63 or 221 optimum points given by the genetic algorithm optimization.

A possible third improvement, would consist on executing on-line directly in the dsPIC the genetic algorithms to find directly the optimum set of slopes for the target points $\{Ma, K\}_m$. according to the real output voltage spectrum at any given load condition, linear and nonlinear. This option requires a more powerful micro-processor, and also improving the accuracy and reducing the noise of the sampling process to acquire the target or working point $\{Ma, K\}_m$.

Another interesting subject will be to investigate if the optimum slopes calculated by the genetic algorithm are the best and/or the unique solution for any target point $\{M_a, K\}$. We have tested many target points, repeating many times the evolution process for the same point, obtaining always the same slope set for a given point. Althoguh we have made several

UNIVERSITAT ROVIRA I VIRGILI
CONTRIBUTIONS ON SPECTRAL CONTROL FOR THE ASYMMETRICAL FULL BRIDGE MULTILEVEL INVERTER
Oscar Mauricio Muñoz Ramírez
ISBN:978-84-693-7665-2/DL:T.1747-2010

experiments, we have no analytical method to prove that such “optimum” points correspond the minimum distortion possible. Among the experiments, we tested different initial populations, random and forced, and to avoid the attraction of local THD dwells that could stuck the evolution around a local THD minimum, high mutation levels were used.

Concerning other types of PWM modulations as POD and APOD, another future work could investigate if carrier slopes control, could be used to optimize the output voltage spectrum with those modulations. Similarly, assuming that slope control requires analog or natural sampled modulations, which would be the control strategy that should be applied to digital sampling techniques, to achieve similar spectrum improvements wit the asymmetrical and symmetrical regular samplings.

Concerning to harmonic modeling, many second order effects have not been considered. Probably, the most important one, is the real influence of the feed-forward and state-feedback analog loops. Feed-forward loop compensated the effect of the DC power supply spectrum in the inverter output, specially the 100 Hz component. State feed-back loop would reduce the harmonicscaused by the losses and nonlinearities introduced by the inductor, the switching devices, and certain loads. Another future task should investigate, using for instance the superposition theorem, which part of output voltage harmonic reduction comes from each one of the three inverter control loops.

Bibliography

[Ade07] ADEDEJI, A.A.; "Genetic (Evolutionary) Algorithm: Introduction and Its Use as an Engineering and Design Tool", Department of Civil Engineering, University of Ilorin, Olad Publishers and Printing Enterprisers, Ilorin, Nigeria, ISBN: 978-8115-86-1, 2007.

[Age96] AGELIDIS, V.G.; ZIOGAS, P.D.; JOOS, G.; , "'"Dead-band" PWM switching patterns," Power Electronics, IEEE Transactions on , vol.11, no.4, pp.522-531, Jul 1996, doi: 10.1109/63.506117.

[Age198] AGELIDIS, V.G.; CALAIS, M.; , "Application specific harmonic performance evaluation of multicarrier PWM techniques," Power Electronics Specialists Conference, 1998. PESC 98 Record. 29th Annual IEEE , vol.1, no., pp.172-178 vol.1, 17-22 May 1998, doi: 10.1109/PESC.1998.701896.

[Age298] AGELIDIS, V.G.; GOH, H.C.;, "Low-distortion variable-level PWM technique," Electric Power Applications, IEE Proceedings - , vol.145, no.2, pp.73-78, Mar 1998, ISSN: 1350-2352.

[Ahm09] AHMADI, D., JIN WANG, "Full Study of a Precise and Practical Harmonic Elimination Method for Multilevel Inverters," Applied Power Electronics Conference and Exposition, 2009. APEC 2009. Twenty-Fourth Annual IEEE , vol., no., pp.871-876, 15-19 Feb. 2009: 10.1109/APEC.2009.4802764.

[Alo03] ALONSO O., SANCHIS P., GUBIA E., ET AL., "Cascaded H-bridge multilevel converter for grid connected photovoltaic generators with independent maximum power point tracking of each solar array". Proc. IEEE 34th Power Electronics Specialist Conf. (PESC'03), 15–19 June 2003, vol. 2, pp. 731–735.

[Arr03] ARRILLAGA, J., WATSON, N.R.; "Power System Harmonics", Second Edition, John Wiley & Sons, Ltd, 2003, Print ISBN: 0-470-85129-5 / 9780470851296, Online ISBN: 780470871225, doi: 10.1002/0470871229.

[Bla53] BLACK, H.S.; "Modulation Theory", D. Van Nostrand, 1953. Library of congress Catalogue Card No. 53-10091.

[Bow175] BOWES S.R., BIRD B.M., "Novel Approach to the analysis and synthesis of modulation processes in power convertors", Proc. IEE Vol. 122, No. 5, May 1975, pg:507-513, doi: 10.1049/piee.1975.0141.

[Bow275] BOWES S.R., "New Sinusoidal Pulsewidth modulated invertor", Proc. IEE Vol. 122, No. 11, November 1975, pg:1279-1285. ISSN: 0020-3270, doi: 10.1049/piee.1975.0312.

[Cal98] CALAIS M., AGELIDIS V.G., "Multilevel converters for single-phase grid connected photovoltaic systems-an overview". Proc. IEEE Int. Symp. Industrial Electronics (ISIE'98), 7–10, July 1998, vol. 1, pp. 224–229, doi: 10.1109/ISIE.1998.707781.

[Chi03] CHIASSON, J.N., TOLBERT, L.M., MCKENZIE K.J., DU, ZHONG, "Control of a Multilevel Converter Using Resultant Theory", IEEE Trans. on Control Systems Technology, Vol. 11, No 3, May 2003, doi: 10.1109/TCST.2003.810382.

[Chi04] CHIASSON, J.N., TOLBERT, L.M., MCKENZIE K.J., DU, ZHONG, "A complete Solution to the Harmonic Elimination Problem", IEEE Trans. on Power Electronics, Vol. 19, No 2, March 2004, doi: 10.1109/TPEL.2003.823207.

[Chi05] CHIASSON, J.N., TOLBERT, L.M., MCKENZIE, K.J., ZHONG DU, "Elimination of harmonics in a multilevel converter using the theory of symmetric polynomials and resultants," Control Systems Technology, IEEE Transactions on , vol.13, no.2, pp. 216- 223, March 2005, doi: 10.1109/TCST.2004.839556.

[Dem02] DEMAS, L.; MEYNARD, T.A.; FOCH, H.; GATEAU, G., "Comparative study of multilevel topologies: NPC, multicell inverter and SMC with IGBT", IECON 02, IEEE 2002 28th Annual Conference of the Industrial Electronics Society, Volume 1, 5-8 Nov. 2002 Page(s):828 - 833 vol.1.

[Des05] DESLAURIERS, I.; AVDIU, N.; BOON TECK OOI; , "Naturally sampled triangle carrier PWM bandwidth limit and output spectrum," Power Electronics, IEEE Transactions on , vol.20, no.1, pp. 100- 106, Jan. 2005, doi: 10.1109/TPEL.2004.839829(410) 20.

[Fra08] FRANQUELO, L.G.; RODRIGUEZ, J.; LEON, J.I.; KOURO, S.; PORTILLO, R.; PRATS, M.A.M., "The age of multilevel converters arrives", Industrial Electronics Magazine, IEEE , vol.2, no.2, pp.28-39, June 2008. doi: 10.1109/MIE.2008.923519.

[Fen04] FENG, C.; AGELIDIS, V.G.; , "A DSP-based controller design for multilevel flying capacitor converters," Applied Power Electronics Conference and Exposition, 2004. APEC '04. Nineteenth Annual IEEE , vol.3, no., pp. 1740- 1744 Vol.3, 2004, doi: 10.1109/APEC.2004.1296101.

[Hol98] HOLMES, D.G.; , "A general analytical method for determining the theoretical harmonic components of carrier based PWM strategies," Industry Applications Conference, 1998. Thirty-Third IAS Annual Meeting. The 1998 IEEE , vol.2, no., pp.1207-1214 vol.2, 12-15 Oct 1998, doi: 10.1109/IAS.1998.730300.

[Hol03] D.G. HOLMES, THOMAS A. LIPO, "Pulse Width Modulation for Power Converters, principles and practice", IEEE Series on Power Engineering, Mohammed E. El-Hawary, Series Editor, 2003, ISBN 0-471-20814-0.

[IEE93] IEEE Standard 519-1922, "IEEE Recommended Practices and Requirements for Harmonic Control in Electrical Power systems", © IEEE 1993.

[IEC] Standard IEC-61000-3-2, " Electromagnetic compatibility (EMC) - Part 3-2: Limits for harmonic current emissions (equipment input current ≤ 16 A per phase)".

[Jan05] JANG, Y.; JOVANOVIC, M.M., "A new three-level soft-switched converter", Power Electronics, IEEE Transactions on, Volume 20, Issue 1, Jan. 2005 Page(s):75 – 81, doi: 10.1109/TPEL.2004.839832(410) 20.

[Kai04] KAI D., YUN-PING Z., ZHENG-YING C., ET AL.,"A novel single-phase 5-level asymmetric inverter". Proc. 4th Int. Power Electronics and Motion Control Conf. (IPEMC'2004), 14–16 August 2004, vol. 2, pp. 7932798.

[Kan05] KANG D.-W., LEE B.-K., JEON J.-H., ET AL., "A symmetric carrier technique of CRPWM for voltage balance method of flying-capacitor multilevel inverter", IEEE Trans. Ind. Electron., 2005, 52, (3), pp. 879–888, doi: 10.1109/TIE.2005.847574.

[Lip00] LIPO, THOMAS A.; "An Improved Weighted Total Harmonic Distortion Index For Induction Motor Drives", OPTIM, Brasov, Romania. 2000. Vol. 2, pp 311-22. http://www.ece.wisc.edu/~lipo/2000pub/00-06.PDF.

[Mar04] MARIETHOZ, S. ; RUFER, A.; "A New Single-Phase Multilevel Modulator - A Fast and Accurate Method to Compute the Modulator Harmonic Spectra", EPE-PEMC 2004; 11th International Conference on Power Electronics and Motion Control, Riga, Latvia, 2-4 September 2004, Reference: LEI-CONF-2006-022.

[Mar05] MARIÉTHOZ, JEAN-SÉBASTIEN ; Rufer, Alfred (director), "Etude formelle pour la synthèse de convertisseurs multiniveaux asymétriques: topologies, modulation et commande", Ph.D. Thesis, École Polytechnique Fédérale de Lausanne, EPFL Lausanne, 2005.

[Mas03] MASSOUD, A.M.; FINNEY, S.J.; WILLIAMS, B.W., "Control techniques for multilevel voltage source inverters", Power Electronics Specialist Conference, 15th to 19th of June 2003, PESC '03, IEEE 34th Annual, Volume 1, Page(s):171 - 176 vol.1. 2003.

[McG102] MCGRATH, B.P.; HOLMES, D.G.; , "An analytical technique for the determination of spectral components of multilevel carrier-based PWM methods," Industrial Electronics, IEEE Transactions on , vol.49, no.4, pp. 847- 857, Aug 2002, doi: 10.1109/TIE.2002.801071.

[McG202] MCGRATH, B.P.; HOLMES, D.G.;, "Multicarrier Pwm Strategies For Multilevel Inverters," Industrial Electronics, Ieee Transactions On , Vol.49, No.4, pp. 858-867, Aug 2002, doi: 10.1109/tie.2002.801073.

[Mel96] MELANIE, MITCHELL;, "An Introduction to Genetic Algorithms", The MIT Press, Copyright © 1996 Massachusetts Institute of Technology, ISBN 0-262-13316-4 (HB), 0-262-63185-7 (PB).

[Mey95] MEYNARD, T.A.; FOCH, H., "Multilevel converters and derived topologies for high power conversion", Industrial Electronics, Control, and Instrumentation, 1995., Proceedings of the 1995 IEEE IECON 21st International Conference on, Volume 1, 6-10 Nov. 1995 Page(s):21 - 26 vol.1, doi: 10.1109/IECON.1995.483327.

[Muñ05] M. MUÑOZ-RAMÍREZ, H. VALDERRAMA-BLAVI, J. MAIXÉ, R. LEYVA, E. VIDAL;, " Programación Armónica de Portadoras en Inversores Multinivel PWM", Seminario Anual de Automática, Electrónica Industrial e Instrumentación 2005, SAAEI'05, Septiembre 2005.

[Nab81] NABAE, A.; TAKAHASHI, I.; AKAGI, H., "A New Neutral-Point-Clamped PWM Inverter," Industry Applications, IEEE Transactions on , vol.IA-17, no.5, pp.518-523, Sept. 1981, doi: 10.1109/TIA.1981.4503992.

[Nik98] NIKOLAUS P., NGUYEN T., RUFER A.C., "A three-phase multilevel converter for high-power induction motors", IEEE Transactions Power Electronics., 1998, 13, (5), pp. 978–985, doi: 10.1109/63.712325.

[Pin02] PINDADO RICO, R., POU FÉLIX, J., "Convertidores Multinivel CC/CA: Topologías básicas", Mundo Electrónico, ISSN 0300-3787, Nº 332, 2002, pags. 28-35.

[Ras07] RASHID, M.H., editor, "Power Electronics Handbook", Academic Press, Elsevier Inc., ISBN 13: 978-0-12-068479-7, ISBN 10: 0-12-068479-8, 2007.

[Res07] RESTREPO P., CARLOS et ali, "Diseño de los Parámetros de un Estabilizador de Sistemas de Potencia (PPS) basado en una Técnica Evolutiva", Scientia et Technica Año XIII, No 37, Diciembre de 2007, Universidad Tecnológica de Pereira. ISSN: 0122-1701,

http://www.utp.edu.co/ciencia/index.php?UnArt=32&id=1038&anoFecha=2007&mesFecha=12

[Rod88] RODGERS, JOSEPH LEE; NICEWANDER, W. ALAN;, "Thirteen Ways to Look at the Correlation Coefficient", The American Statistician, Vol. 42, No. 1 (Feb., 1988), pp. 59-66, http://www.jstor.org/stable/2685263?seq=1

[Rod02] RODRIGUEZ, J.; JIH-SHENG LAI; FANG ZHENG PENG; , "Multilevel inverters: a survey of topologies, controls, and applications," Industrial Electronics, IEEE Transactions on , vol.49, no.4, pp. 724- 738, Aug 2002, doi: 10.1109/TIE.2002.801052.

[Ruf95] RUFER, A.-C.; , "An aid in the teaching of multilevel inverters for high power applications," Power Electronics Specialists Conference, 1995. PESC '95 Record., 26th Annual IEEE , vol.1, no., pp.347-352 vol.1, 18-22 Jun 1995, doi: 10.1109/PESC.1995.474834.

[Sir02] SIRISUKPRASERT, S., JIH-SHENG LAI; TIAN-HUA LIU, , "Optimum harmonic reduction with a wide range of modulation indexes for multilevel converters," Industrial Electronics, IEEE Transactions on , vol.49, no.4, pp. 875-881, Aug 2002, doi: 10.1109/TIE.2002.801226.

[Sir99] SIRISUKPRASERT, SIRIROJ, "Optimized Harmonic Stepped-Waveform Multilevel Inverter", MS Thesis, Virginia Polytechnique Institute, Virginia State University, September 1999.

[Tol198] TOLBERT, L.M.; PENG, F.Z.; HABETLER, T.G.; , "Multilevel inverters for electric vehicle applications", Power Electronics in Transportation, 1998 , vol., no., pp.79-84, 22-23 Oct 1998, doi: 10.1109/PET.1998.731062.

[Tol05] TOLBERT, L.M., CHIASSON, J.N., DU, ZHONG, MCKENZIE K.J., "Elimination of Harmonics in a Multilevel Converter with Nonequal DC Sources", IEEE Trans. on Industry Applications, Vol. 41, No 1, January-February 2005, doi: 10.1109/TIA.2004.841162.

[Val01] H. VALDERRAMA-BLAVI, "Gestión Inteligente de un Ondulador Modular para Aplicaciones Fotovoltaicas", Universitat Politècnica de Catalunya, Departament d'Engenyeria Electrònica, Febrero 2001. Doctoral Thesis

[Val03] VALDERRAMA-BLAVI H., ALONSO C., ESTIBALS B., ET AL., "Grid connected asymmetric full-bridge multilevel inverter", Proc. 10th European Power Electronics Conf. (EPE'03), Toulouse, France, 2–4 September, ISBN: 90-75815-07-7.

[Val05] VALDERRAMA-BLAVI H., MUNOZ-RAMIREZ M., MAIXE J., ET AL., "Low frequency multilevel inverters for renewable energy systems", Proc. IEEE Int. Symp on Industrial Electronics (ISIE 2005), 20–23 June 2005, vol. 3, pp. 1019–1024, doi: 10.1109/ISIE.2005.1529063.

[Val06] VALDERRAMA-BLAVI, HUGO; MAIXE, JAVIER; BOSQUE-MONCUSI, JOSEP MARIA; MARTINEZ-SALAMERO, LUIS; MUNOZ, MAURICIO; , "Multilevel AC Current Source with Sliding-Mode Control for Renewable Energy Grid Systems," Power Electronics and Motion Control Conference, 2006. EPE-PEMC 2006. 12th International , vol., no., pp.1866-1872, Aug. 30 2006-Sept. 1 2006, doi: 10.1109/EPEPEMC.2006.4778677.

[Val08] VALDERRAMA-BLAVI H., BOSQUE J.M, BARRADO J.A, MUÑOZ M., CALVENTE J., "Design of a sinusoidal current source using a sliding-mode-

controlled asymmetrical full-bridge multilevel converter", IET Power Electron., 2008, Vol. 1, No. 2, pp. 203–213/211, doi: 10.1049/iet-pel:20070321.

[Wal99] WALKER, G.R., "Modulation and Control of Multilevel Converters", Ph.D Thesis, Deparment of Computer Science and Electrical Engineering, University of Queensland, November 1999.

[Wal03] WALKER, G.R.; , "Digitally-implemented naturally sampled PWM suitable for multilevel converter control," Power Electronics, IEEE Transactions on , vol.18, no.6, pp. 1322- 1329, Nov. 2003, doi: 10.1109/TPEL.2003.818831.

[Wan09] WANMIN FEI, XINBO RUAN, BIN WU, "A Generalized Formulation of Quarter-Wave Symmetry SHE-PWM Problems for Multilevel Inverters", IEEE Trans. on Power Electronics, Vol. 24, No. 7, July 2009, doi: 10.1109/TPEL.2009.2018094.

[Wik10] Wikipedia article, "Pearson product-moment correlation coefficient", URL: http://en.wikipedia.org/wiki/Pearson_product-moment_correlation_coefficient

[Wil06] WILKINSON R.H., MEYNARD T.H., DU TOIT MOUTON H., "Natural balance of multicell converters: the general case", IEEE Trans. Power Electron., 2006, 21, (6), pp. 1658–1666, doi: 10.1109/TPEL.2006.882951.

UNIVERSITAT ROVIRA I VIRGILI
CONTRIBUTIONS ON SPECTRAL CONTROL FOR THE ASYMMETRICAL FULL BRIDGE MULTILEVEL INVERTER
Oscar Mauricio Muñoz Ramírez
ISBN:978-84-693-7665-2/DL:T.1747-2010

UNIVERSITAT ROVIRA I VIRGILI
CONTRIBUTIONS ON SPECTRAL CONTROL FOR THE ASYMMETRICAL FULL BRIDGE MULTILEVEL INVERTER
Oscar Mauricio Muñoz Ramírez
ISBN:978-84-693-7665-2/DL:T.1747-2010

APPENDIX A. Equations to Calculate C_{mn}

Note: The Jacobi-Anger Expansions are identities used to evaluate the integrals defined by C_{mn}. Such expansions are used during the computational implementation in DFS C_{mn}-Algorithm in Matlab.

$$\cos(\zeta\cos\vartheta) = J_0(\zeta) + 2\sum_{q=1}^{\infty}\cos(k\pi)J_{2q}(\zeta)\cos(2q\vartheta)$$

$$sin(\zeta\cos\vartheta) = 2\sum_{q=1}^{\infty}\cos(k\pi)J_{2q+1}(\zeta)\cos([2q+1]\vartheta)$$

DFS coeeficients are gathered in four groups: firstly, C_{01} is calculated and it is equal to the fundamental output modulated waveform, M_aV_{dc}. Then, the others coefficient are calculated according to their related groups: C_{0n} (n=2...∞), C_{m0} (m=1...∞), C_{mn} (m=1...∞, and -∞<n<∞ and n≠1). That means that the groups of coefficients are separated as Modulated Signal, Baseband Harmonics, Carrier Multiple Harmonics and Sideband Harmonics. The solution of these coeffients are the arrange in order to calculate the harmonic frequencies according the condition $h = mM_f + n$; this solution is attempted in DFS C_{mn}-Algorithm.

Group $C_{01}=A_{01}+jB_{01}$

$Level \quad +E:$

$$I_9 = \frac{E}{2\pi^2}\left\{\left[(\alpha_1-\beta_1)\cdot -je^{jy}\Big|_{-\varphi_u}^{\varphi_u}\right] + \left[(\Delta_1+\lambda_1)\left(-j\frac{e^{j2y}}{4}+\frac{y}{2}\right)\Big|_{-\varphi_u}^{\varphi_u}\right]\right\}$$

$Level \quad +K\cdot E:$

$$I_8 + I_7 = \frac{K\cdot E}{2\pi^2}\left\{\left[(2\pi+\beta_1-\alpha_1)\cdot -je^{jy}\Big|_{-\varphi_u}^{\varphi_u}\right] - \left[(\Delta_1+\lambda_1)\left(-j\frac{e^{j2y}}{4}+\frac{y}{2}\right)\Big|_{-\varphi_u}^{\varphi_u}\right]\right\}$$

UNIVERSITAT ROVIRA I VIRGILI
CONTRIBUTIONS ON SPECTRAL CONTROL FOR THE ASYMMETRICAL FULL BRIDGE MULTILEVEL INVERTER
Oscar Mauricio Muñoz Ramírez
ISBN:978-84-693-7665-2/DL:T.1747-2010

$$I_6=\frac{K\cdot E}{2\pi^2}\left\{\left[(\alpha_2-\beta_2)\cdot -je^{jy}\Big|_{-\pi/2}^{-\varphi_u}\right]+\left[(\Delta_2+\lambda_2)\left(-j\frac{e^{j2y}}{4}+\frac{y}{2}\right)\Big|_{-\pi/2}^{-\varphi_u}\right]\right\}$$

$$I_{10}=\frac{K\cdot E}{2\pi^2}\left\{\left[(\alpha_2-\beta_2)\cdot -je^{jy}\Big|_{\varphi_u}^{\pi/2}\right]+\left[(\Delta_2+\lambda_2)\left(-j\frac{e^{j2y}}{4}+\frac{y}{2}\right)\Big|_{\varphi_u}^{\pi/2}\right]\right\}$$

Level $-(1-K)\cdot E$:

$$I_2=\frac{-(1-K)\cdot E}{2\pi^2}\left\{\left[(\alpha_4-\beta_4)\cdot -je^{jy}\Big|_{-\pi}^{-\varphi_l}\right]+\left[(\Delta_4+\lambda_4)\left(-j\frac{e^{j2y}}{4}+\frac{y}{2}\right)\Big|_{-\pi}^{-\varphi_l}\right]\right\}$$

$$I_{13}=\frac{-(1-K)\cdot E}{2\pi^2}\left\{\left[(\alpha_4-\beta_4)\cdot -je^{jy}\Big|_{\varphi_l}^{\pi}\right]+\left[(\Delta_4+\lambda_4)\left(-j\frac{e^{j2y}}{4}+\frac{y}{2}\right)\Big|_{\varphi_l}^{\pi}\right]\right\}$$

$$I_5+I_4=\frac{-(1-K)\cdot E}{2\pi^2}\left\{\left[(2\pi+\beta_3-\alpha_3)\cdot -je^{jy}\Big|_{-\varphi_l}^{-\pi/2}\right]-\left[(\Delta_3+\lambda_3)\left(-j\frac{e^{j2y}}{4}+\frac{y}{2}\right)\Big|_{-\varphi_l}^{-\pi/2}\right]\right\}$$

$$I_{12}+I_{11}=\frac{-(1-K)\cdot E}{2\pi^2}\left\{\left[(2\pi+\beta_3-\alpha_3)\cdot -je^{jy}\Big|_{\pi/2}^{\varphi_l}\right]-\left[(\Delta_3+\lambda_3)\left(-j\frac{e^{j2y}}{4}+\frac{y}{2}\right)\Big|_{\pi/2}^{\varphi_l}\right]\right\}$$

Level $-E$:

$$I_1+I_3=\frac{-E}{2\pi^2}\left\{\left[(2\pi+\beta_4-\alpha_4)\cdot -je^{jy}\Big|_{-\pi}^{-\varphi_l}\right]-\left[(\Delta_4+\lambda_4)\left(-j\frac{e^{j2y}}{4}+\frac{y}{2}\right)\Big|_{-\pi}^{-\varphi_l}\right]\right\}$$

$$I_5+I_4=\frac{-E}{2\pi^2}\left\{\left[(2\pi+\beta_4-\alpha_4)\cdot -je^{jy}\Big|_{\varphi_l}^{\pi}\right]-\left[(\Delta_4+\lambda_4)\left(-j\frac{e^{j2y}}{4}+\frac{y}{2}\right)\Big|_{\varphi_l}^{\pi}\right]\right\}$$

UNIVERSITAT ROVIRA I VIRGILI
CONTRIBUTIONS ON SPECTRAL CONTROL FOR THE ASYMMETRICAL FULL BRIDGE MULTILEVEL INVERTER
Oscar Mauricio Muñoz Ramírez
ISBN:978-84-693-7665-2/DL:T.1747-2010

Group $C_{0n}=A_{0n}+jB_{0n}$, n=2…∞

Level $+E$:

$$I_9=\frac{E}{2\pi^2}\left\{\left[(\alpha_1-\beta_1)\cdot-j\frac{e^{jny}}{n}\Big|_{-\varphi_u}^{\varphi_u}\right]+\left[(\Delta_1+\lambda_1)\left(-j\frac{e^{j(n+1)y}}{2(n+1)}-j\frac{e^{j(n-1)y}}{2(n-1)}\right)\Big|_{-\varphi_u}^{\varphi_u}\right]\right\}$$

Level $+K\cdot E$:

$$I_8+I_7=\frac{K\cdot E}{2\pi^2}\left\{\left[(2\pi+\beta_1-\alpha_1)\cdot-j\frac{e^{jny}}{n}\Big|_{-\varphi_u}^{\varphi_u}\right]-\left[(\Delta_1+\lambda_1)\left(-j\frac{e^{j(n+1)y}}{2(n+1)}-j\frac{e^{j(n-1)y}}{2(n-1)}\right)\Big|_{-\varphi_u}^{\varphi_u}\right]\right\}$$

$$I_6=\frac{K\cdot E}{2\pi^2}\left\{\left[(\alpha_2-\beta_2)\cdot-j\frac{e^{jny}}{n}\Big|_{-\pi/2}^{-\varphi_u}\right]+\left[(\Delta_2+\lambda_2)\left(-j\frac{e^{j(n+1)y}}{2(n+1)}-j\frac{e^{j(n-1)y}}{2(n-1)}\right)\Big|_{-\pi/2}^{-\varphi_u}\right]\right\}$$

$$I_{10}=\frac{K\cdot E}{2\pi^2}\left\{\left[(\alpha_2-\beta_2)\cdot-j\frac{e^{jny}}{n}\Big|_{\varphi_u}^{\pi/2}\right]+\left[(\Delta_2+\lambda_2)\left(-j\frac{e^{j(n+1)y}}{2(n+1)}-j\frac{e^{j(n-1)y}}{2(n-1)}\right)\Big|_{\varphi_u}^{\pi/2}\right]\right\}$$

Level $-(1-K)\cdot E$:

$$I_2=\frac{-(1-K)\cdot E}{2\pi^2}\left\{\left[(\alpha_4-\beta_4)\cdot-j\frac{e^{jny}}{n}\Big|_{-\pi}^{-\varphi_l}\right]-\left[(\Delta_4+\lambda_4)\left(-j\frac{e^{j(n+1)y}}{2(n+1)}-j\frac{e^{j(n-1)y}}{2(n-1)}\right)\Big|_{-\pi}^{-\varphi_l}\right]\right\}$$

$$I_{13}=\frac{-(1-K)\cdot E}{2\pi^2}\left\{\left[(\alpha_4-\beta_4)\cdot-j\frac{e^{jny}}{n}\Big|_{\varphi_l}^{\pi}\right]-\left[(\Delta_4+\lambda_4)\left(-j\frac{e^{j(n+1)y}}{2(n+1)}-j\frac{e^{j(n-1)y}}{2(n-1)}\right)\Big|_{\varphi_l}^{\pi}\right]\right\}$$

ISBN:978-84-693-7665-2/DL:T.1747-2010

$$I_5+I_4=\frac{-(1-K)\cdot E}{2\pi^2}\left\{\left[(2\pi+\beta_3-\alpha_3)\cdot -j\frac{e^{jny}}{n}\Big|_{-\varphi_l}^{-\pi/2}\right]+\left[(\Delta_3+\lambda_3)\left(-j\frac{e^{j(n+1)y}}{2(n+1)}-j\frac{e^{j(n-1)y}}{2(n-1)}\right)\Big|_{-\varphi_l}^{-\pi/2}\right]\right\}$$

$$I_{12}+I_{11}=\frac{-(1-K)\cdot E}{2\pi^2}\left\{\left[(2\pi+\beta_2-\alpha_2)\cdot -j\frac{e^{jny}}{n}\Big|_{\pi/2}^{\varphi_l}\right]+\left[(\Delta_2+\lambda_2)\left(-j\frac{e^{j(n+1)y}}{2(n+1)}-j\frac{e^{j(n-1)y}}{2(n-1)}\right)\Big|_{\pi/2}^{\varphi_l}\right]\right\}$$

Level $-E$:

$$I_1+I_3=\frac{-E}{2\pi^2}\left\{\left[(2\pi+\beta_4-\alpha_4)\cdot -je^{jy}\Big|_{-\pi}^{-\varphi_l}\right]+\left[(\Delta_4+\lambda_4)\left(-j\frac{e^{j2y}}{4}+\frac{y}{2}\right)\Big|_{-\pi}^{-\varphi_l}\right]\right\}$$

$$I_5+I_4=\frac{-E}{2\pi^2}\left\{\left[(2\pi+\beta_4-\alpha_4)\cdot -j\frac{e^{jny}}{n}\Big|_{\varphi_l}^{\pi}\right]+\left[(\Delta_4+\lambda_4)\left(-j\frac{e^{j(n+1)y}}{2(n+1)}-j\frac{e^{j(n-1)y}}{2(n-1)}\right)\Big|_{\varphi_l}^{\pi}\right]\right\}$$

Group $C_{m0}=A_{m0}+jB_{m0}$, m=1…∞

Level $+E$:

$$I_9=\frac{E}{2\pi^2 m}\cdot\left[\begin{array}{l}-je^{jm\alpha_4}J_0(m\Delta_1)y\Big|_{-\varphi_u}^{\varphi_u}\\ -e^{jm\alpha_4}2\sum_{q=1}^{\infty}j^{q+1}J_q(m\Delta_1)\cdot\frac{\sin(qy)}{q}\Big|_{-\varphi_u}^{\varphi_u}\\ +je^{jm\beta_4}J_0(m\cdot-\lambda_1)y\Big|_{-\varphi_u}^{\varphi_u}\\ +e^{jm\beta_4}2\sum_{q=1}^{\infty}j^{q+1}J_q(m\cdot-\lambda_1)\cdot\frac{\sin(qy)}{q}\Big|_{-\varphi_u}^{\varphi_u}\end{array}\right]$$

UNIVERSITAT ROVIRA I VIRGILI
CONTRIBUTIONS ON SPECTRAL CONTROL FOR THE ASYMMETRICAL FULL BRIDGE MULTILEVEL INVERTER
Oscar Mauricio Muñoz Ramírez
ISBN:978-84-693-7665-2/DL:T.1747-2010

Level $+K\cdot E$:

$$I_8+I_7=\frac{K\cdot E}{2\pi^2 m}\cdot\left[\begin{array}{l}-je^{jm\beta_4}J_0(m\cdot-\lambda_1)y\Big|_{-\varphi_u}^{\varphi_u}\\ -e^{jm\beta_4}2\sum_{q=1}^{\infty}j^{q+1}J_q(m\cdot-\lambda_1)\cdot\frac{\sin(qy)}{q}\Big|_{-\varphi_u}^{\varphi_u}\\ +je^{jm\alpha_4}J_0(m\Delta_1)y\Big|_{-\varphi_u}^{\varphi_u}\\ +e^{jm\alpha_4}2\sum_{q=1}^{\infty}j^{q+1}J_q(m\Delta_1)\cdot\frac{\sin(qy)}{q}\Big|_{-\varphi_u}^{\varphi_u}\end{array}\right]$$

$$I_6=\frac{K\cdot E}{2\pi^2 m}\cdot\left[\begin{array}{l}-je^{jm\alpha_3}J_0(m\Delta_2)y\Big|_{-\pi/2}^{-\varphi_u}\\ -e^{jm\alpha_3}2\sum_{q=1}^{\infty}j^{q+1}J_q(m\Delta_2)\cdot\frac{\sin(qy)}{q}\Big|_{-\pi/2}^{-\varphi_u}\\ +je^{jm\beta_3}J_0(m\cdot-\lambda_2)y\Big|_{-\pi/2}^{-\varphi_u}\\ +e^{jm\beta_3}2\sum_{q=1}^{\infty}j^{q+1}J_q(m\cdot-\lambda_2)\cdot\frac{\sin(qy)}{q}\Big|_{-\pi/2}^{-\varphi_u}\end{array}\right]$$

$$I_{10}=\frac{K\cdot E}{2\pi^2 m}\cdot\left[\begin{array}{l}-je^{jm\alpha_3}J_0(m\Delta_2)y\Big|_{\varphi_u}^{\pi/2}\\ -e^{jm\alpha_3}2\sum_{q=1}^{\infty}j^{q+1}J_q(m\Delta_2)\cdot\frac{\sin(qy)}{q}\Big|_{\varphi_u}^{\pi/2}\\ +je^{jm\beta_3}J_0(m\cdot-\lambda_2)y\Big|_{\varphi_u}^{\pi/2}\\ +e^{jm\beta_3}2\sum_{q=1}^{\infty}j^{q+1}J_q(m\cdot-\lambda_2)\cdot\frac{\sin(qy)}{q}\Big|_{\varphi_u}^{\pi/2}\end{array}\right]$$

UNIVERSITAT ROVIRA I VIRGILI
CONTRIBUTIONS ON SPECTRAL CONTROL FOR THE ASYMMETRICAL FULL BRIDGE MULTILEVEL INVERTER
Oscar Mauricio Muñoz Ramírez
ISBN:978-84-693-7665-2/DL:T.1747-2010

Level $-(1-K)\cdot E$:

$$I_2=\frac{(1-K)\cdot E}{2\pi^2 m}\cdot\left[\begin{array}{l} je^{jm\alpha_1}J_0(m\Delta_4)y\Big|_{-\pi}^{-\varphi_l} \\ +e^{jm\alpha_1}2\sum_{q=1}^{\infty}j^{q+1}J_q(m\Delta_4)\cdot\frac{\sin(qy)}{q}\Big|_{-\pi}^{-\varphi_l} \\ -je^{jm\beta_1}J_0(m\cdot-\lambda_4)y\Big|_{-\pi}^{-\varphi_l} \\ -e^{jm\beta_1}2\sum_{q=1}^{\infty}j^{q+1}J_q(m\cdot-\lambda_4)\cdot\frac{\sin(qy)}{q}\Big|_{-\pi}^{-\varphi_l} \end{array}\right]$$

$$I_{13}=\frac{(1-K)\cdot E}{2\pi^2 m}\cdot\left[\begin{array}{l} je^{jm\alpha_1}J_0(m\Delta_4)y\Big|_{\varphi_l}^{\pi} \\ +e^{jm\alpha_1}2\sum_{q=1}^{\infty}j^{q+1}J_q(m\Delta_4)\cdot\frac{\sin(qy)}{q}\Big|_{\varphi_l}^{\pi} \\ -je^{jm\beta_1}J_0(m\cdot-\lambda_4)y\Big|_{\varphi_l}^{\pi} \\ -e^{jm\beta_1}2\sum_{q=1}^{\infty}j^{q+1}J_q(m\cdot-\lambda_4)\cdot\frac{\sin(qy)}{q}\Big|_{\varphi_l}^{\pi} \end{array}\right]$$

$$I_5+I_4=\frac{(1-K)\cdot E}{2\pi^2 m}\cdot\left[\begin{array}{l} je^{jm\beta_2}J_0(m\cdot-\lambda_3)y\Big|_{-\varphi_l}^{-\pi/2} \\ +e^{jm\beta_2}2\sum_{q=1}^{\infty}j^{q+1}J_q(m\cdot-\lambda_3)\cdot\frac{\sin(qy)}{q}\Big|_{-\varphi_l}^{-\pi/2} \\ -je^{jm\alpha_2}J_0(m\Delta_3)y\Big|_{-\varphi_l}^{-\pi/2} \\ -e^{jm\alpha_2}2\sum_{q=1}^{\infty}j^{q+1}J_q(m\Delta_3)\cdot\frac{\sin(qy)}{q}\Big|_{-\varphi_l}^{-\pi/2} \end{array}\right]$$

$$I_{12}+I_{11}=\frac{(1-K)\cdot E}{2\pi^2 m}\cdot\left[\begin{array}{l} je^{jm\beta_2}J_0(m\cdot-\lambda_3)y\Big|_{\pi/2}^{\varphi_l} \\ +e^{jm\beta_2}2\sum_{q=1}^{\infty}j^{q+1}J_q(m\cdot-\lambda_3)\cdot\frac{\sin(qy)}{q}\Big|_{\pi/2}^{\varphi_l} \\ -je^{jm\alpha_2}J_0(m\Delta_3)y\Big|_{\pi/2}^{\varphi_l} \\ -e^{jm\alpha_2}2\sum_{q=1}^{\infty}j^{q+1}J_q(m\Delta_3)\cdot\frac{\sin(qy)}{q}\Big|_{\pi/2}^{\varphi_l} \end{array}\right]$$

UNIVERSITAT ROVIRA I VIRGILI
CONTRIBUTIONS ON SPECTRAL CONTROL FOR THE ASYMMETRICAL FULL BRIDGE MULTILEVEL INVERTER
Oscar Mauricio Muñoz Ramírez
ISBN:978-84-693-7665-2/DL:T.1747-2010

Level $-E$:

$$I_1+I_3=\frac{E}{2\pi^2 m}\cdot\left[\begin{array}{l} je^{jm\beta_1}J_0(m\cdot-\lambda_4)y\Big|_{-\pi}^{-\varphi_l} \\ +e^{jm\beta_1}2\sum_{q=1}^{\infty}j^{q+1}J_q(m\cdot-\lambda_4)\cdot\frac{\sin(qy)}{q}\Big|_{-\pi}^{-\varphi_l} \\ -je^{jm\alpha_1}J_0(m\Delta_4)y\Big|_{-\pi}^{-\varphi_l} \\ -e^{jm\alpha_1}2\sum_{q=1}^{\infty}j^{q+1}J_q(m\Delta_4)\cdot\frac{\sin(qy)}{q}\Big|_{-\pi}^{-\varphi_l} \end{array}\right]$$

$$I_{15}+I_{14}=\frac{E}{2\pi^2 m}\cdot\left[\begin{array}{l} je^{jm\beta_1}J_0(m\cdot-\lambda_4)y\Big|_{\varphi_l}^{\pi} \\ +e^{jm\beta_1}2\sum_{q=1}^{\infty}j^{q+1}J_q(m\cdot-\lambda_4)\cdot\frac{\sin(qy)}{q}\Big|_{\varphi_l}^{\pi} \\ -je^{jm\alpha_1}J_0(m\Delta_4)y\Big|_{\varphi_l}^{\pi} \\ -e^{jm\alpha_1}2\sum_{q=1}^{\infty}j^{q+1}J_q(m\Delta_4)\cdot\frac{\sin(qy)}{q}\Big|_{\varphi_l}^{\pi} \end{array}\right]$$

Group $C_{mn}=A_{mn}+jB_{mn}$, $m=1\ldots\infty$, $n=-\infty\ldots\infty$ and $n\neq 0$

Level $+E$:

$$I_9=\frac{E}{2\pi^2 m}\cdot\left[\begin{array}{l} -e^{jm\alpha_4}J_0(m\Delta_1)\frac{e^{jny}}{n}\Big|_{-\varphi_u}^{\varphi_u} \\ -e^{jm\alpha_4}\sum_{q=1}^{\infty}j^{q}J_q(m\Delta_1)\cdot\left\{\frac{e^{j(n+q)y}}{(n+q)}\Big|_{-\varphi_u}^{\varphi_u}+\frac{e^{j(n-q)y}}{(n-q)}\Big|_{-\varphi_u}^{\varphi_u}\right\} \\ +e^{jm\beta_4}J_0(m\cdot-\lambda_1)\frac{e^{jny}}{n}\Big|_{-\varphi_u}^{\varphi_u} \\ +e^{jm\beta_4}\sum_{q=1}^{\infty}j^{q}J_q(m\cdot-\lambda_1)\cdot\left\{\frac{e^{j(n+q)y}}{(n+q)}\Big|_{-\varphi_u}^{\varphi_u}+\frac{e^{j(n-q)y}}{(n-q)}\Big|_{-\varphi_u}^{\varphi_u}\right\} \end{array}\right]$$

UNIVERSITAT ROVIRA I VIRGILI
CONTRIBUTIONS ON SPECTRAL CONTROL FOR THE ASYMMETRICAL FULL BRIDGE MULTILEVEL INVERTER
Oscar Mauricio Muñoz Ramírez
ISBN:978-84-693-7665-2/DL:T.1747-2010

Level $+K\cdot E$:

$$I_8+I_7=\frac{K\cdot E}{2\pi^2 m}\cdot\left[\begin{array}{l}
-e^{jm\beta_4}J_0(m\cdot-\lambda_1)\dfrac{e^{jny}}{n}\Big|_{-\varphi_u}^{\varphi_u}\\
-e^{jm\beta_4}\displaystyle\sum_{q=1}^{\infty}j^q J_q(m\cdot-\lambda_1)\cdot\left\{\frac{e^{j(n+q)y}}{(n+q)}\Big|_{-\varphi_u}^{\varphi_u}+\frac{e^{j(n-q)y}}{(n-q)}\Big|_{-\varphi_u}^{\varphi_u}\right\}\\
+e^{jm\alpha_4}J_0(m\Delta_1)\dfrac{e^{jny}}{n}\Big|_{-\varphi_u}^{\varphi_u}\\
+e^{jm\alpha_4}\displaystyle\sum_{q=1}^{\infty}j^q J_q(m\Delta_1)\cdot\left\{\frac{e^{j(n+q)y}}{(n+q)}\Big|_{-\varphi_u}^{\varphi_u}+\frac{e^{j(n-q)y}}{(n-q)}\Big|_{-\varphi_u}^{\varphi_u}\right\}
\end{array}\right]$$

$$I_6=\frac{K\cdot E}{2\pi^2 m}\cdot\left[\begin{array}{l}
-e^{jm\alpha_3}J_0(m\Delta_2)\dfrac{e^{jny}}{n}\Big|_{-\pi/2}^{-\varphi_u}\\
-e^{jm\alpha_3}\displaystyle\sum_{q=1}^{\infty}j^q J_q(m\Delta_2)\cdot\left\{\frac{e^{j(n+q)y}}{(n+q)}\Big|_{-\pi/2}^{-\varphi_u}+\frac{e^{j(n-q)y}}{(n-q)}\Big|_{-\pi/2}^{-\varphi_u}\right\}\\
+e^{jm\beta_3}J_0(m\cdot-\lambda_2)\dfrac{e^{jny}}{n}\Big|_{-\pi/2}^{-\varphi_u}\\
+e^{jm\beta_3}\displaystyle\sum_{q=1}^{\infty}j^q J_q(m\cdot-\lambda_2)\cdot\left\{\frac{e^{j(n+q)y}}{(n+q)}\Big|_{-\pi/2}^{-\varphi_u}+\frac{e^{j(n-q)y}}{(n-q)}\Big|_{-\pi/2}^{-\varphi_u}\right\}
\end{array}\right]$$

ISBN:978-84-693-7665-2/DL:T.1747-2010

$$I_{10}=\frac{K\cdot E}{2\pi^2 m}\cdot\left[\begin{array}{l}
-e^{jm\alpha_3}J_0(m\Delta_2)\dfrac{e^{jny}}{n}\Big|_{\varphi_u}^{\pi/2}\\
-e^{jm\alpha_3}\displaystyle\sum_{q=1}^{\infty}j^q J_q(m\Delta_2)\cdot\left\{\frac{e^{j(n+q)y}}{(n+q)}\Big|_{\varphi_u}^{\pi/2}+\frac{e^{j(n-q)y}}{(n-q)}\Big|_{\varphi_u}^{\pi/2}\right\}\\
+e^{jm\beta_3}J_0(m\cdot-\lambda_2)\dfrac{e^{jny}}{n}\Big|_{\varphi_u}^{\pi/2}\\
+e^{jm\beta_3}\displaystyle\sum_{q=1}^{\infty}j^q J_q(m\cdot-\lambda_2)\cdot\left\{\frac{e^{j(n+q)y}}{(n+q)}\Big|_{\varphi_u}^{\pi/2}+\frac{e^{j(n-q)y}}{(n-q)}\Big|_{\varphi_u}^{\pi/2}\right\}
\end{array}\right]$$

Level $-(1-K)\cdot E$:

$$I_2=\frac{(1-K)\cdot E}{2\pi^2 m}\cdot\left[\begin{array}{l}
e^{jm\alpha_1}J_0(m\Delta_4)\dfrac{e^{jny}}{n}\Big|_{-\pi}^{-\varphi_l}\\
+e^{jm\alpha_1}\displaystyle\sum_{q=1}^{\infty}j^q J_q(m\Delta_4)\cdot\left\{\frac{e^{j(n+q)y}}{(n+q)}\Big|_{-\pi}^{-\varphi_l}+\frac{e^{j(n-q)y}}{(n-q)}\Big|_{-\pi}^{-\varphi_l}\right\}\\
-e^{jm\beta_1}J_0(m\cdot-\lambda_4)\dfrac{e^{jny}}{n}\Big|_{-\pi}^{-\varphi_l}\\
-e^{jm\beta_1}\displaystyle\sum_{q=1}^{\infty}j^q J_q(m\cdot-\lambda_4)\cdot\left\{\frac{e^{j(n+q)y}}{(n+q)}\Big|_{-\pi}^{-\varphi_l}+\frac{e^{j(n-q)y}}{(n-q)}\Big|_{-\pi}^{-\varphi_l}\right\}
\end{array}\right]$$

$$I_{13}=\frac{(1-K)\cdot E}{2\pi^2 m}\cdot\left[\begin{array}{l}
e^{jm\alpha_1}J_0(m\Delta_4)\dfrac{e^{jny}}{n}\Big|_{\varphi_l}^{\pi}\\
+e^{jm\alpha_1}\displaystyle\sum_{q=1}^{\infty}j^q J_q(m\Delta_4)\cdot\left\{\frac{e^{j(n+q)y}}{(n+q)}\Big|_{\varphi_l}^{\pi}+\frac{e^{j(n-q)y}}{(n-q)}\Big|_{\varphi_l}^{\pi}\right\}\\
-e^{jm\beta_1}J_0(m\cdot-\lambda_4)\dfrac{e^{jny}}{n}\Big|_{\varphi_l}^{\pi}\\
-e^{jm\beta_1}\displaystyle\sum_{q=1}^{\infty}j^q J_q(m\cdot-\lambda_4)\cdot\left\{\frac{e^{j(n+q)y}}{(n+q)}\Big|_{\varphi_l}^{\pi}+\frac{e^{j(n-q)y}}{(n-q)}\Big|_{\varphi_l}^{\pi}\right\}
\end{array}\right]$$

UNIVERSITAT ROVIRA I VIRGILI
CONTRIBUTIONS ON SPECTRAL CONTROL FOR THE ASYMMETRICAL FULL BRIDGE MULTILEVEL INVERTER
Oscar Mauricio Muñoz Ramírez
ISBN:978-84-693-7665-2/DL:T.1747-2010

$$I_5+I_4=\frac{(1-K)\cdot E}{2\pi^2 m}\cdot\left[\begin{array}{l} e^{jm\beta_2}J_0(m\cdot-\lambda_3)\dfrac{e^{jny}}{n}\Big|_{-\varphi_l}^{-\pi/2} \\ +e^{jm\beta_2}\displaystyle\sum_{q=1}^{\infty}j^q J_q(m\cdot-\lambda_3)\cdot\left\{\frac{e^{j(n+q)y}}{(n+q)}\Big|_{-\varphi_l}^{-\pi/2}+\frac{e^{j(n-q)y}}{(n-q)}\Big|_{-\varphi_l}^{-\pi/2}\right\} \\ -e^{jm\alpha_2}J_0(m\Delta_3)\dfrac{e^{jny}}{n}\Big|_{-\varphi_l}^{-\pi/2} \\ -e^{jm\alpha_2}\displaystyle\sum_{q=1}^{\infty}j^q J_q(m\Delta_3)\cdot\left\{\frac{e^{j(n+q)y}}{(n+q)}\Big|_{-\varphi_l}^{-\pi/2}+\frac{e^{j(n-q)y}}{(n-q)}\Big|_{-\varphi_l}^{-\pi/2}\right\} \end{array}\right]$$

$$I_{12}+I_{11}=\frac{(1-K)\cdot E}{2\pi^2 m}\cdot\left[\begin{array}{l} e^{jm\beta_2}J_0(m\cdot-\lambda_3)\dfrac{e^{jny}}{n}\Big|_{\pi/2}^{\varphi_l} \\ +e^{jm\beta_2}\displaystyle\sum_{q=1}^{\infty}j^q J_q(m\cdot-\lambda_3)\cdot\left\{\frac{e^{j(n+q)y}}{(n+q)}\Big|_{\pi/2}^{\varphi_l}+\frac{e^{j(n-q)y}}{(n-q)}\Big|_{\pi/2}^{\varphi_l}\right\} \\ -e^{jm\alpha_2}J_0(m\Delta_3)\dfrac{e^{jny}}{n}\Big|_{\pi/2}^{\varphi_l} \\ -e^{jm\alpha_2}\displaystyle\sum_{q=1}^{\infty}j^q J_q(m\Delta_3)\cdot\left\{\frac{e^{j(n+q)y}}{(n+q)}\Big|_{\pi/2}^{\varphi_l}+\frac{e^{j(n-q)y}}{(n-q)}\Big|_{\pi/2}^{\varphi_l}\right\} \end{array}\right]$$

UNIVERSITAT ROVIRA I VIRGILI
CONTRIBUTIONS ON SPECTRAL CONTROL FOR THE ASYMMETRICAL FULL BRIDGE MULTILEVEL INVERTER
Oscar Mauricio Muñoz Ramírez
ISBN:978-84-693-7665-2/DL:T.1747-2010

Level $-E$:

$$I_1+I_3=\frac{E}{2\pi^2 m}\cdot\left[\begin{array}{l} e^{jm\beta_1}J_0(m\cdot-\lambda_4)\dfrac{e^{jny}}{n}\Big|_{-\pi}^{-\varphi_l} \\ +e^{jm\beta_1}\displaystyle\sum_{q=1}^{\infty}j^q J_q(m\cdot-\lambda_4)\cdot\left\{\frac{e^{j(n+q)y}}{(n+q)}\Big|_{-\pi}^{-\varphi_l}+\frac{e^{j(n-q)y}}{(n-q)}\Big|_{-\pi}^{-\varphi_l}\right\} \\ -e^{jm\alpha_1}J_0(m\Delta_4)\dfrac{e^{jny}}{n}\Big|_{-\pi}^{-\varphi_l} \\ -e^{jm\alpha_1}\displaystyle\sum_{q=1}^{\infty}j^q J_q(m\Delta_4)\cdot\left\{\frac{e^{j(n+q)y}}{(n+q)}\Big|_{-\pi}^{-\varphi_l}+\frac{e^{j(n-q)y}}{(n-q)}\Big|_{-\pi}^{-\varphi_l}\right\} \end{array}\right]$$

$$I_{15}+I_{14}=\frac{E}{2\pi^2 m}\cdot\left[\begin{array}{l} e^{jm\beta_1}J_0(m\cdot-\lambda_4)\dfrac{e^{jny}}{n}\Big|_{\varphi_l}^{\pi} \\ +e^{jm\beta_1}\displaystyle\sum_{q=1}^{\infty}j^q J_q(m\cdot-\lambda_4)\cdot\left\{\frac{e^{j(n+q)y}}{(n+q)}\Big|_{\varphi_l}^{\pi}+\frac{e^{j(n-q)y}}{(n-q)}\Big|_{\varphi_l}^{\pi}\right\} \\ -e^{jm\alpha_1}J_0(m\Delta_4)\dfrac{e^{jny}}{n}\Big|_{\varphi_l}^{\pi} \\ -e^{jm\alpha_1}\displaystyle\sum_{q=1}^{\infty}j^q J_q(m\Delta_4)\cdot\left\{\frac{e^{j(n+q)y}}{(n+q)}\Big|_{\varphi_l}^{\pi}+\frac{e^{j(n-q)y}}{(n-q)}\Big|_{\varphi_l}^{\pi}\right\} \end{array}\right]$$

UNIVERSITAT ROVIRA I VIRGILI
CONTRIBUTIONS ON SPECTRAL CONTROL FOR THE ASYMMETRICAL FULL BRIDGE MULTILEVEL INVERTER
Oscar Mauricio Muñoz Ramírez
ISBN:978-84-693-7665-2/DL:T.1747-2010

APPENDIX B. Pseudo-Natural PWM, more Results

TABLE B.1 EVALUATED CARRIERS SETS FOR PSEUDO-NATURAL PD-SPWM.

Case Number	r_1	r_2	r_3	r_4
1	0.5	0.5	0.5	0.5
2	1.0	1.0	1.0	1.0
3	0.0	0.0	0.0	0.0
4	1.0	1.0	0.0	0.0
5	0.0	0.0	1.0	1.0
6	0.5	1.0	0.5	1.0
7	1.0	0.5	1.0	0.5
8	0.5	1.0	1.0	0.5
9	1.0	0.5	0.5	1.0
10	1.0	0.5	0.0	0.5
11	1.0	0.0	0.5	0.5
12	0.35	0.75	0.25	0.85
13	0.12	0.63	0.27	0.4
14	0.1	0.1	0.1	0.1
15	0.2	0.2	0.2	0.2
16	0.3	0.3	0.3	0.3
17	0.4	0.4	0.4	0.4
18	0.6	0.6	0.6	0.6
19	0.7	0.7	0.7	0.7
20	0.8	0.8	0.8	0.8
21	0.9	0.9	0.9	0.9
22	0.2	0.4	0.6	0.8
23	0.1	0.2	0.3	0.4
24	0.15	0.35	0.28	0.9
25	0.2	0.6	0.7	0.4
26	0.2	0.4	0.6	0.7
27	0.8	0.9	0.6	0.35
28	0.7	0.85	0.55	0.1
29	0.5	0.9	0.4	0.8
30	0.45	0.55	0.47	0.53
31	0.95	0.93	0.97	0.94

The cases above were implemented by meas of DSP and the different methods of calculating or measuring the spectrum for Pseudo-Natural Phase-Disposition SPWM are compared in fibure B.1, where V_{dc}=E=50 V, M_a=0.9.

ISBN:978-84-693-7665-2/DL:T.1747-2010

Figure B.1 Comparison of Experimental and Modeled Spectra.

Experimental Pseudo-Natural Sampled PD-PWM	**Spectrum by C_n-Algorithm**	**Spectrum by C_{mn}-Algorithm**
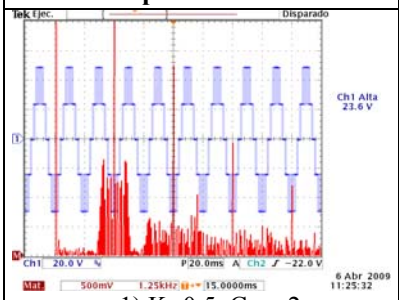 a.1) K=0.5, Case 2	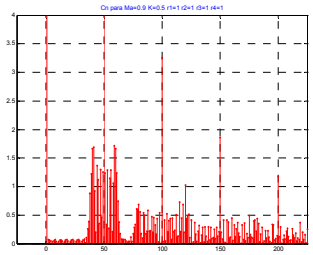 a.2) K=0.5, Case 2	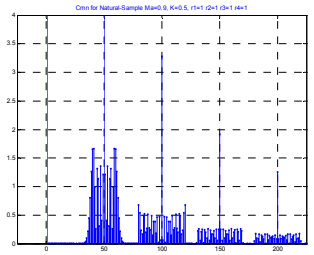 a.3) K=0.5, Case 2
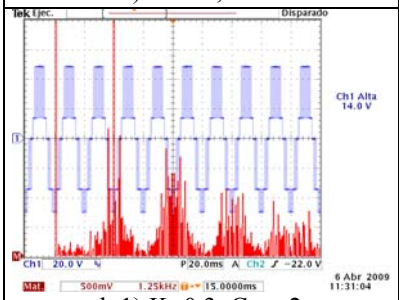 b.1) K=0.3, Case 2	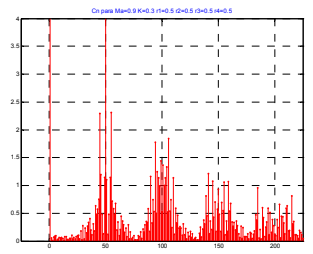 b.2) K=0.3, Case 2	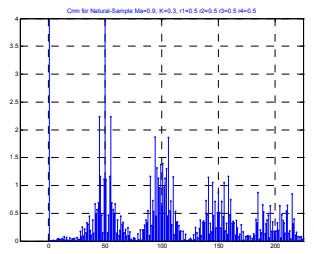 b.3) K=0.3, Case 2
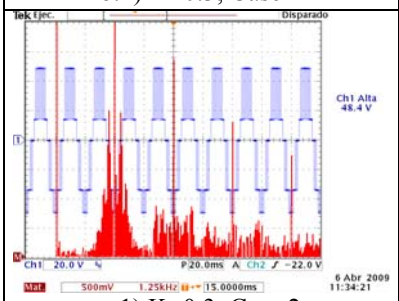 c.1) K=0.3, Case 2	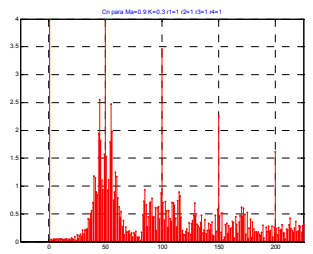 c.2) K=0.3, Case 2	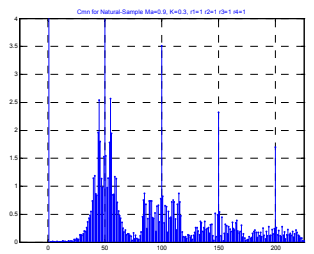 c.3) K=0.3, Case 2
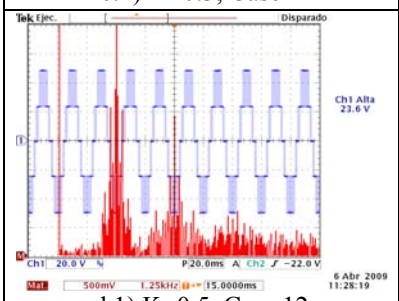 d.1) K=0.5, Case 12	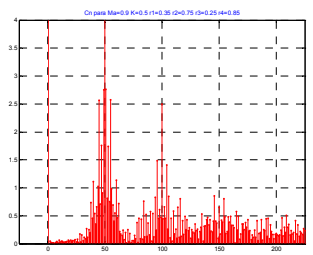 d.2) K=0.5, Case 12	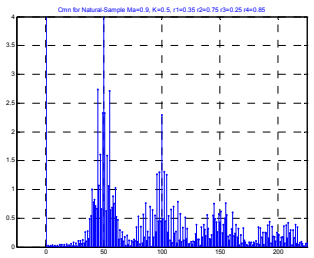 d.3) K=0.5, Case 12
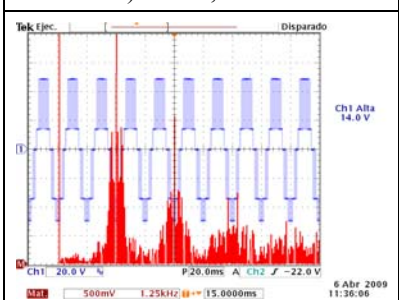 e.1) K=0.3, Case 12	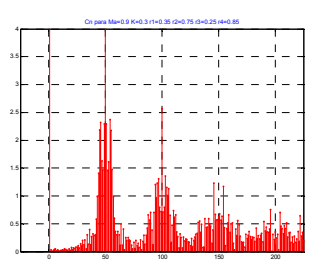 e.2) K=0.3, Case 12	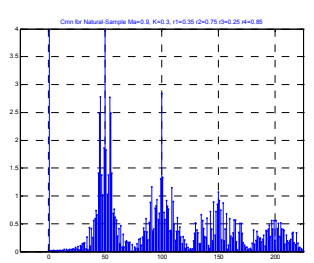 e.3) K=0.3, Case 12

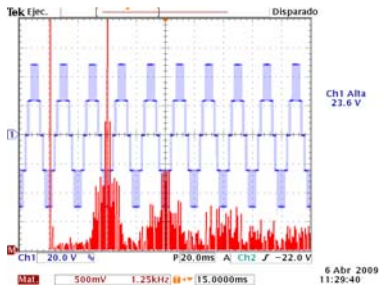

f.1) K=0.5, Case 25

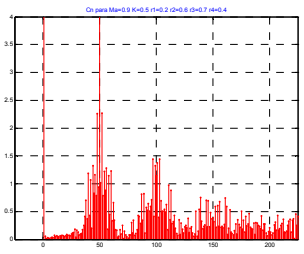

f.2) K=0.5, Case 25

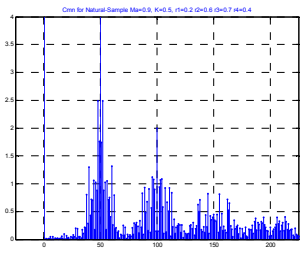

f.3) K=0.5, Case 25

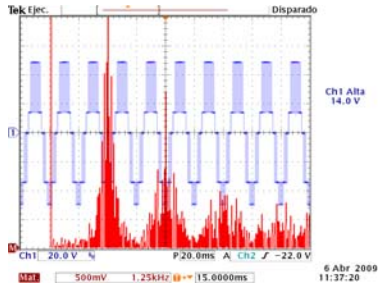

g.1) K=0.3, Case 25

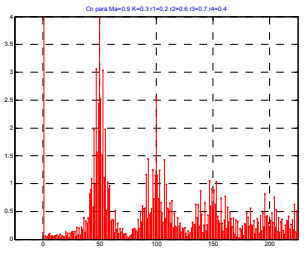

g.2) K=0.3, Case 25

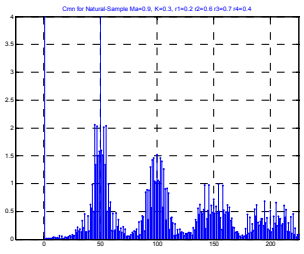

g.3) K=0.3, Case 25

Figure B.2 Error Magnitude and Pearson-Correlation.

<table>
<tr>
<td> 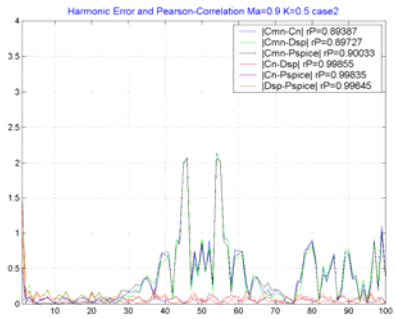

b.1) K=0.5, Case 2</td>
<td> 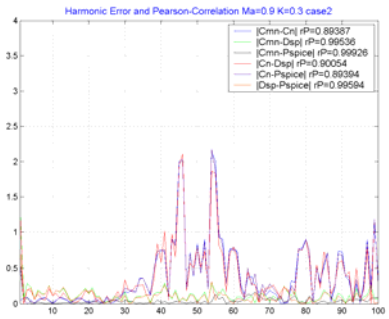

b.2) K=0.3, Case 2</td>
</tr>
<tr>
<td> 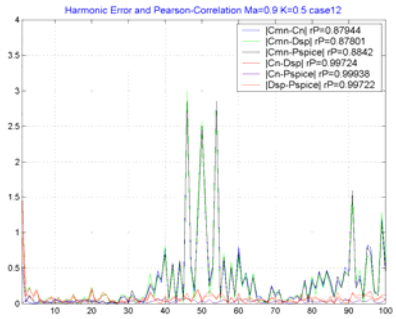

c.1) K=0.5, Case 12</td>
<td> 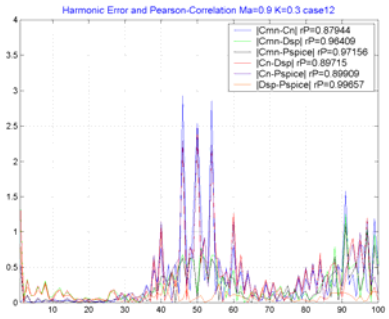

c.2) K=0.3, Case 12</td>
</tr>
<tr>
<td> 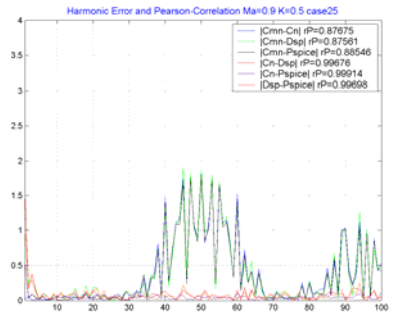

d.1) K=0.5, Case 25</td>
<td> 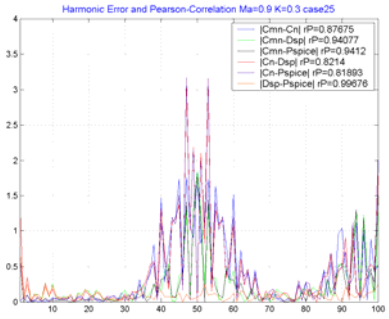

d.2) K=0.3, Case 25</td>
</tr>
<tr>
<td> 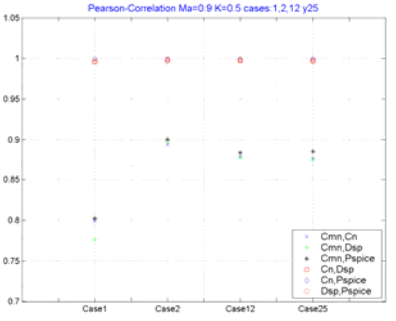

e.1) K=0.5, Pearson-Correlation Cases 1, 2, 12 and 25</td>
<td> 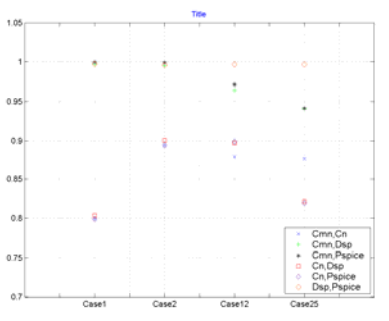

e.2) K=0.3, Pearson-Correlation Cases 1, 2, 12 and 25</td>
</tr>
</table>

UNIVERSITAT ROVIRA I VIRGILI
CONTRIBUTIONS ON SPECTRAL CONTROL FOR THE ASYMMETRICAL FULL BRIDGE MULTILEVEL INVERTER
Oscar Mauricio Muñoz Ramírez
ISBN:978-84-693-7665-2/DL:T.1747-2010

Figure B.3 Distortion Criterions for the cases of Table B.1.

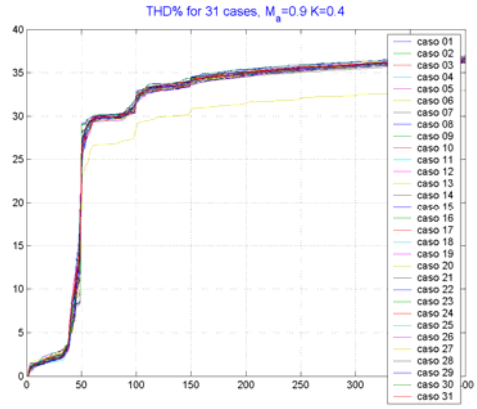

a.1) Global THD,$THD_{h=400}$, K=0.4

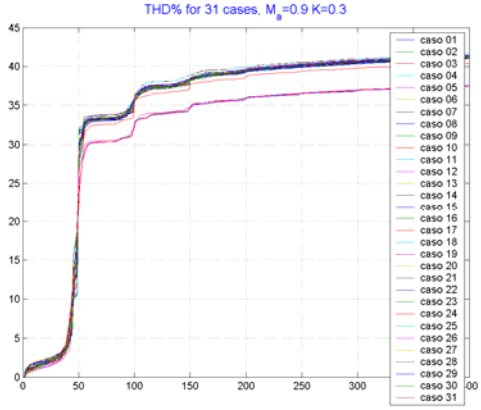

a.2) Global THD, $THD_{h=400}$, K=0.3

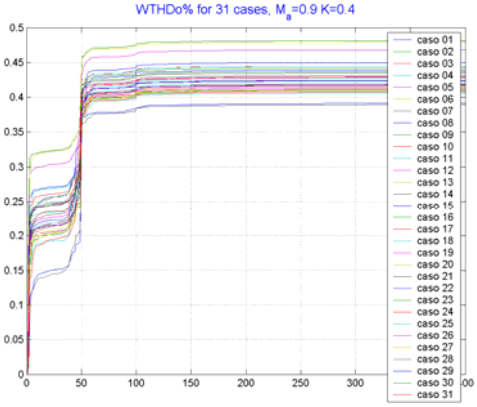

b.1) Global $WTHD_0$,$WTHDo_{h=400}$, K=0.4

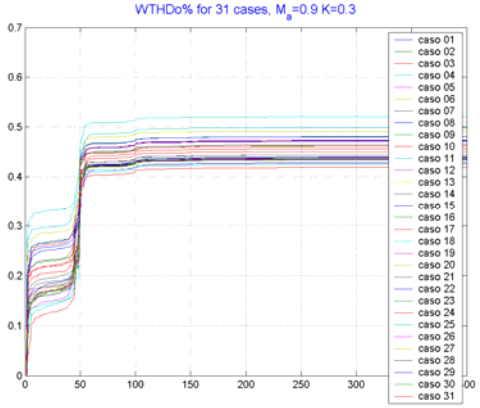

b.2) Global $WTHD_0$,$WTHDo_{h=400}$, K=0.3

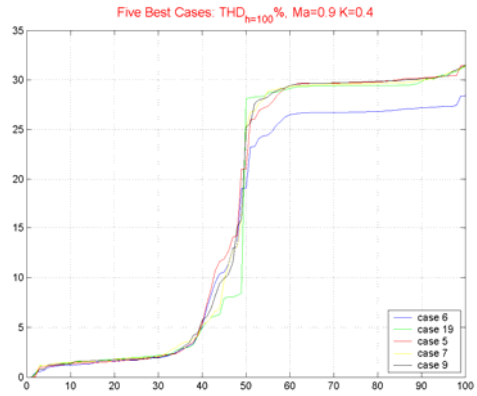

c.1) Best cases for $THD_{h=100}$, K=0.4

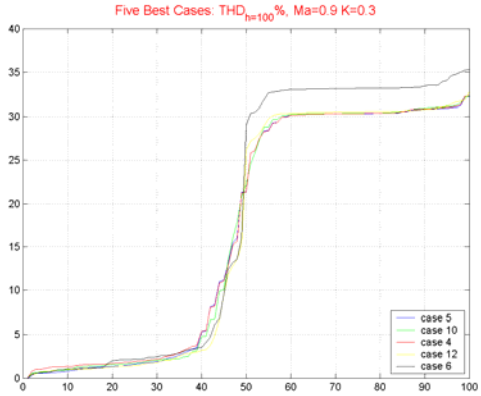

c.2) Best cases for $THD_{h=100}$, K=0.3

ISBN:978-84-693-7665-2/DL:T.1747-2010

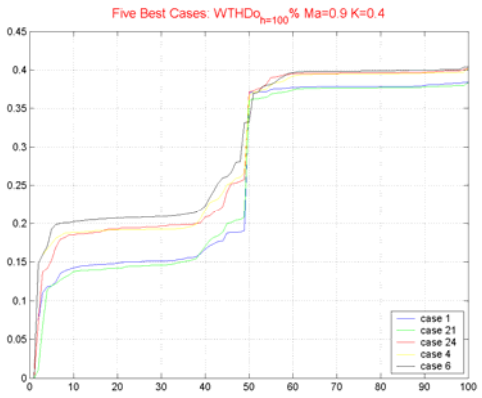

d.1) Best cases for $WTHDo_{h=100}$, K=0.4

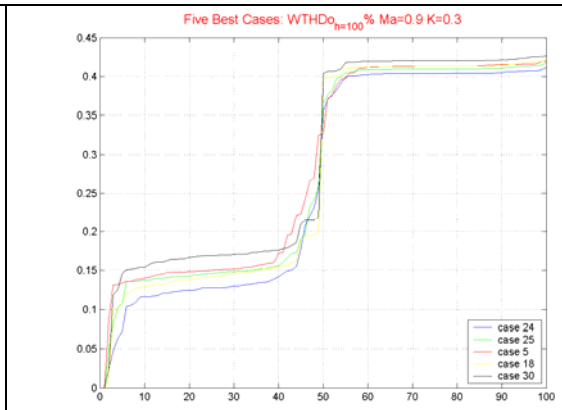

e.2) Best cases for $WTHDo_{h=100}$, K=0.3

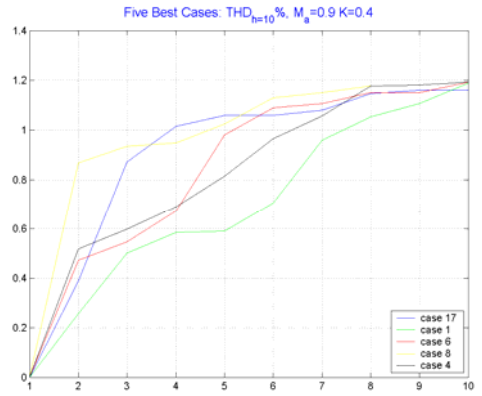

e.1) Best cases for $THD_{h=10}$, K=0.4

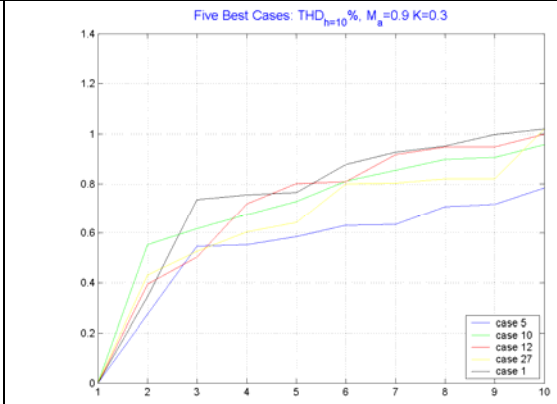

e.2) Best cases for $THD_{h=10}$, K=0.3

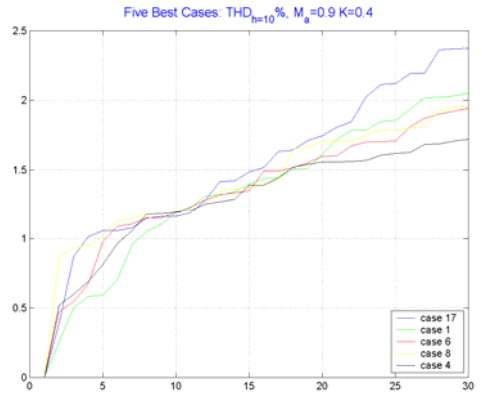

f.1) Best cases for $THD_{h=10}$, extended to h=30, K=0.4

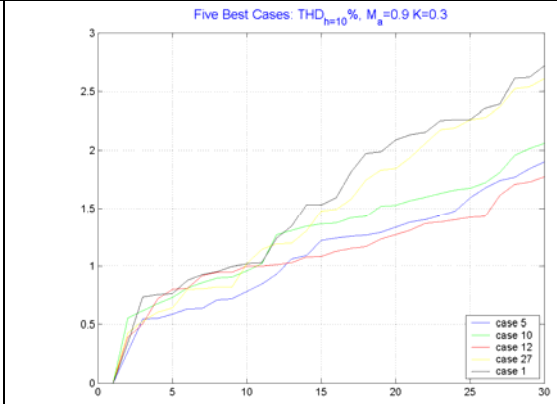

f.2) Best cases for $THD_{h=10}$, extended to h=30, K=0.3

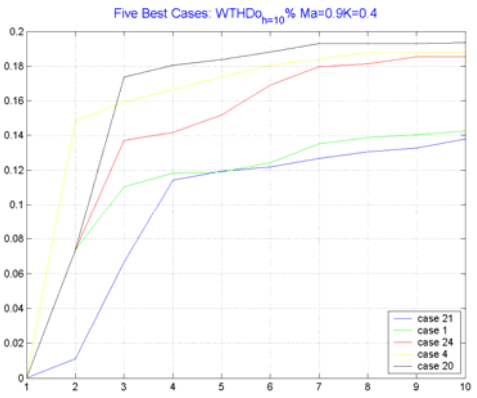

g.1) Best cases for WTHDo$_{h=10}$, K=0.4

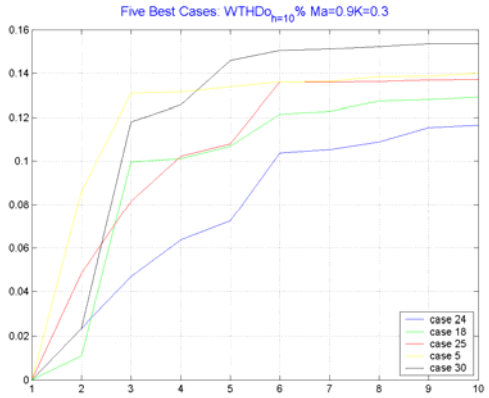

g.2) Best cases for WTHDo$_{h=10}$, K=0.3

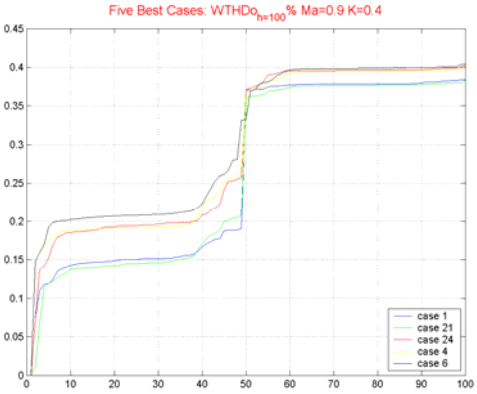

g.1) WTHDo$_{h=100}$, K=0.4

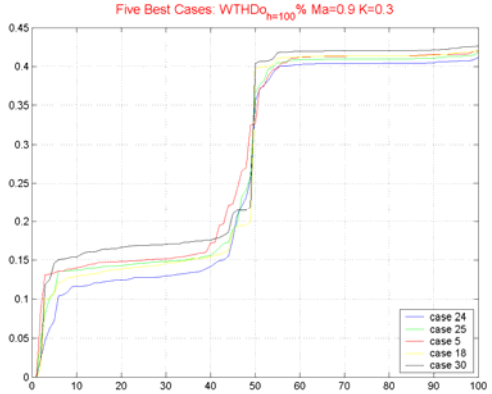

g.2) WTHDo$_{h=100}$, K=0.3

UNIVERSITAT ROVIRA I VIRGILI
CONTRIBUTIONS ON SPECTRAL CONTROL FOR THE ASYMMETRICAL FULL BRIDGE MULTILEVEL INVERTER
Oscar Mauricio Muñoz Ramírez
ISBN:978-84-693-7665-2/DL:T.1747-2010

APPENDIX C. Schematics and PCB Layouts

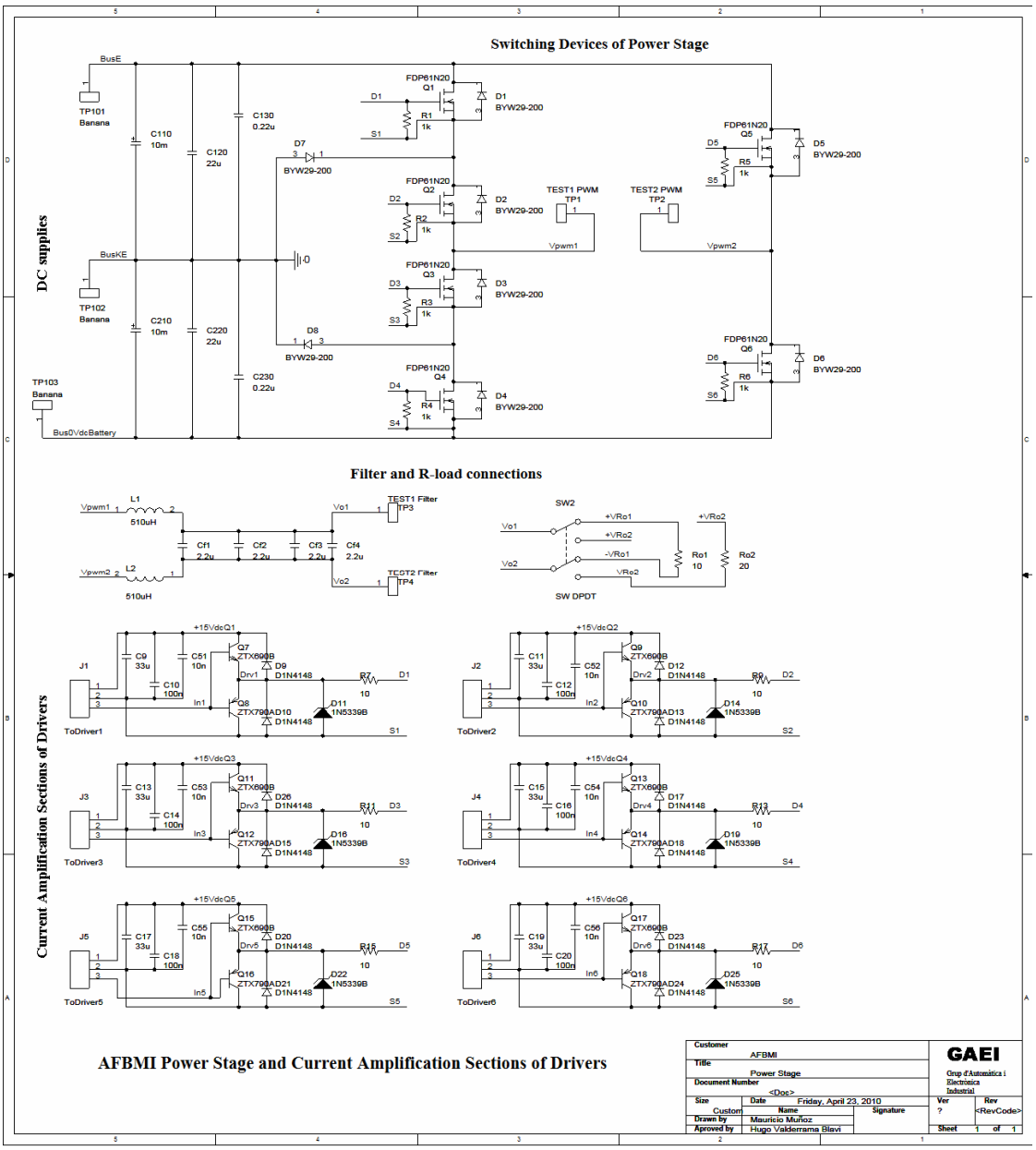

Figure C.1 Schematic of AFBMI Power Stage.

UNIVERSITAT ROVIRA I VIRGILI
CONTRIBUTIONS ON SPECTRAL CONTROL FOR THE ASYMMETRICAL FULL BRIDGE MULTILEVEL INVERTER
Oscar Mauricio Muñoz Ramírez
ISBN:978-84-693-7665-2/DL:T.1747-2010

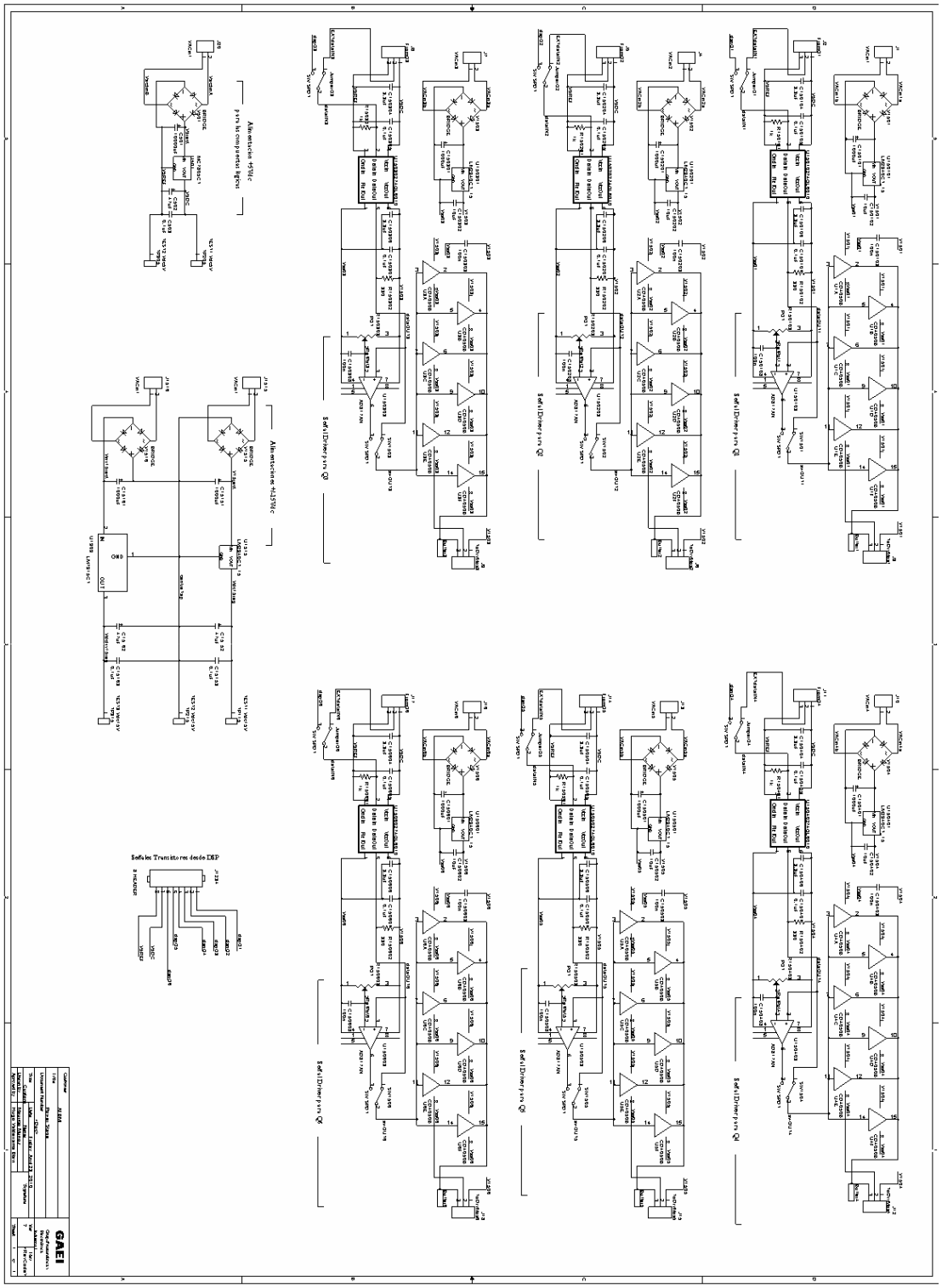

Figure C.2 Schematic of switching pulses drivers.

UNIVERSITAT ROVIRA I VIRGILI
CONTRIBUTIONS ON SPECTRAL CONTROL FOR THE ASYMMETRICAL FULL BRIDGE MULTILEVEL INVERTER
Oscar Mauricio Muñoz Ramírez
ISBN:978-84-693-7665-2/DL:T.1747-2010

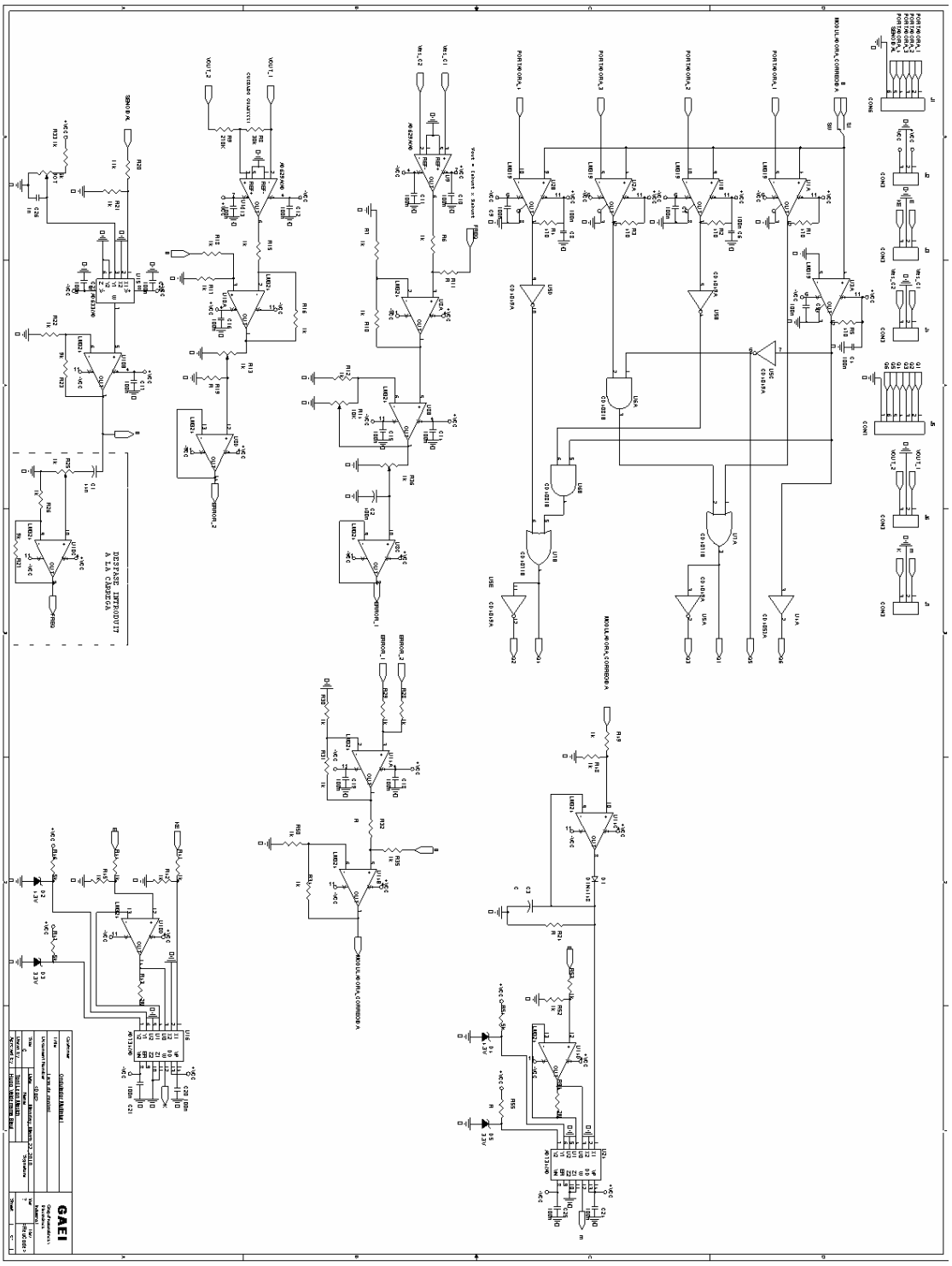

Figure C.3 Schematic of Analogic 5-level PD-PWM modulator and State Variables control loop.

UNIVERSITAT ROVIRA I VIRGILI
CONTRIBUTIONS ON SPECTRAL CONTROL FOR THE ASYMMETRICAL FULL BRIDGE MULTILEVEL INVERTER
Oscar Mauricio Muñoz Ramírez
ISBN:978-84-693-7665-2/DL:T.1747-2010

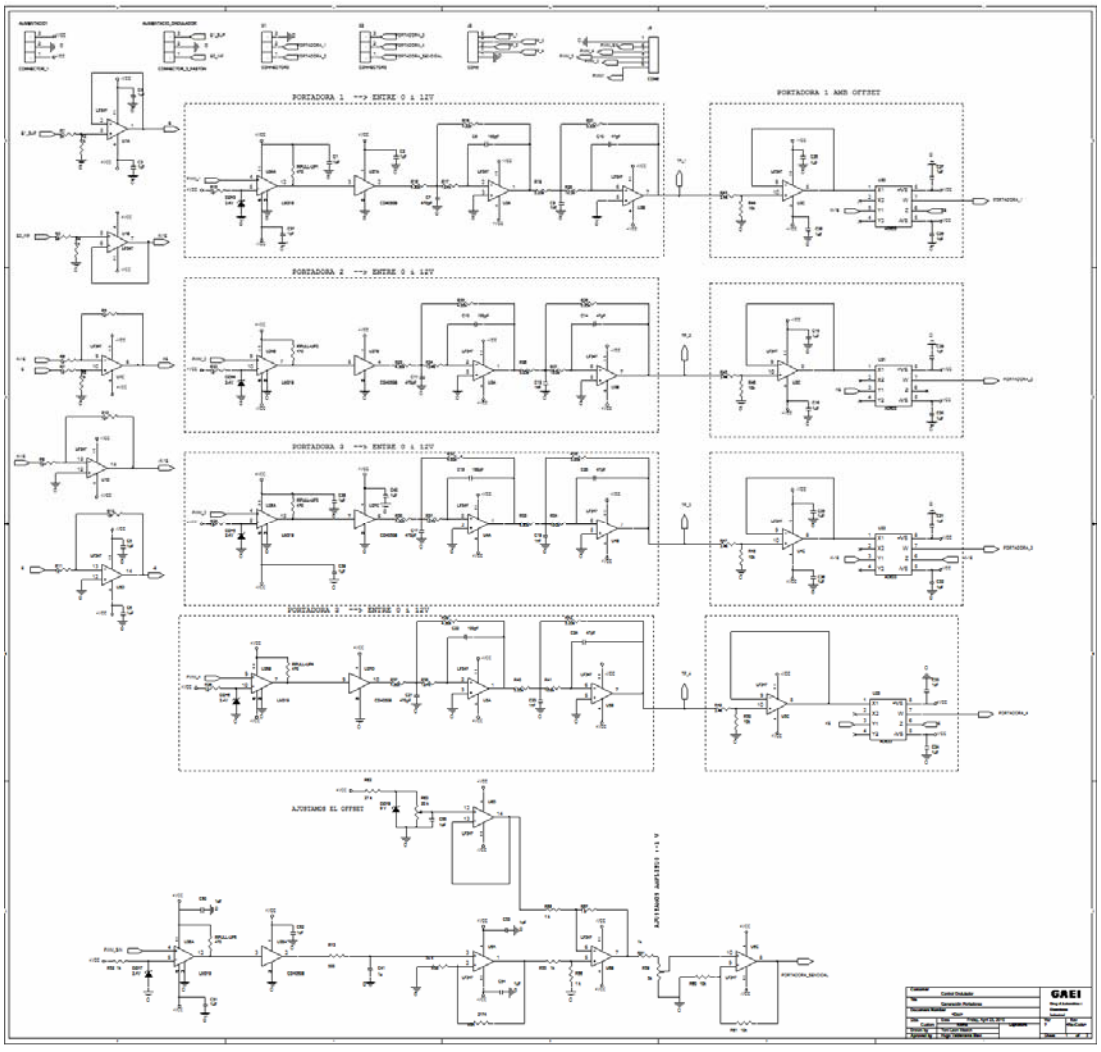

Figure C.4 Schematic of demodulation and filtering of carriers and modulator signal and Feedforward control loop.

UNIVERSITAT ROVIRA I VIRGILI
CONTRIBUTIONS ON SPECTRAL CONTROL FOR THE ASYMMETRICAL FULL BRIDGE MULTILEVEL INVERTER
Oscar Mauricio Muñoz Ramírez
ISBN:978-84-693-7665-2/DL:T.1747-2010

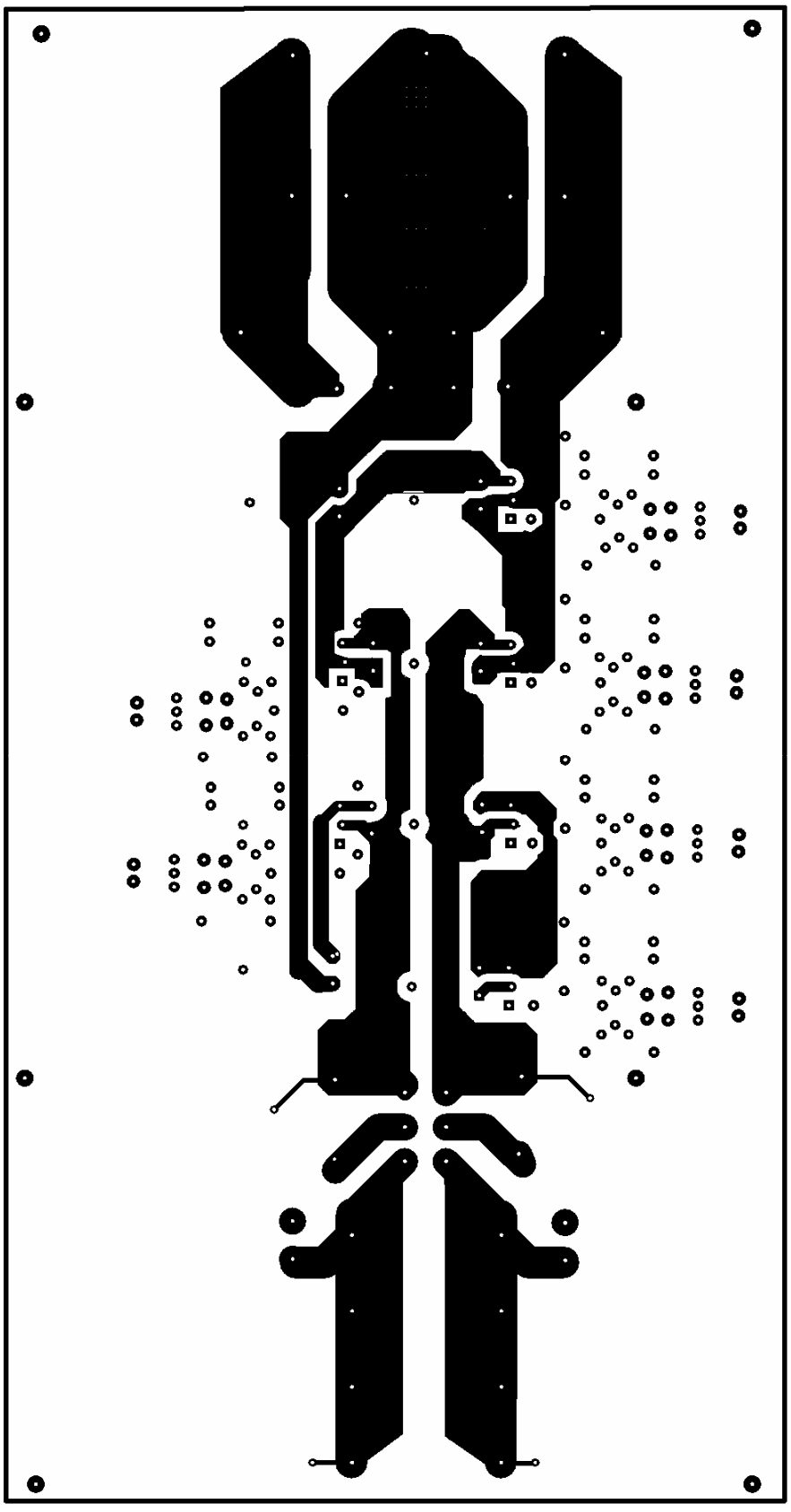

Figure C.5 PCB-Layout at 10:8 scale of AFBMI Power Stage, top face.

UNIVERSITAT ROVIRA I VIRGILI
CONTRIBUTIONS ON SPECTRAL CONTROL FOR THE ASYMMETRICAL FULL BRIDGE MULTILEVEL INVERTER
Oscar Mauricio Muñoz Ramírez
ISBN:978-84-693-7665-2/DL:T.1747-2010

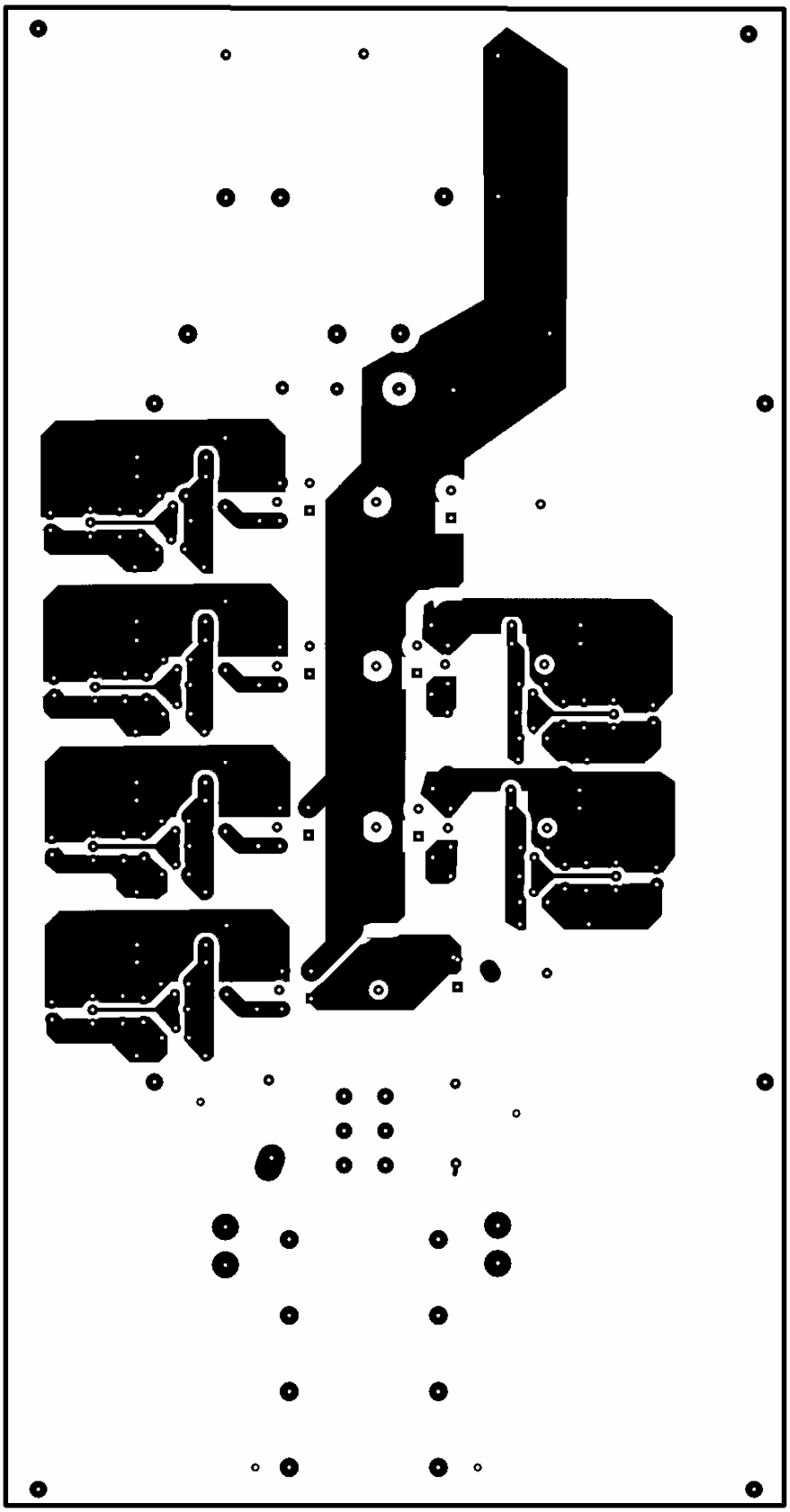

Figure C.6 PCB-Layout at 10:8 scale of AFBMI Power Stage, bottom face.

ISBN:978-84-693-7665-2/DL:T.1747-2010

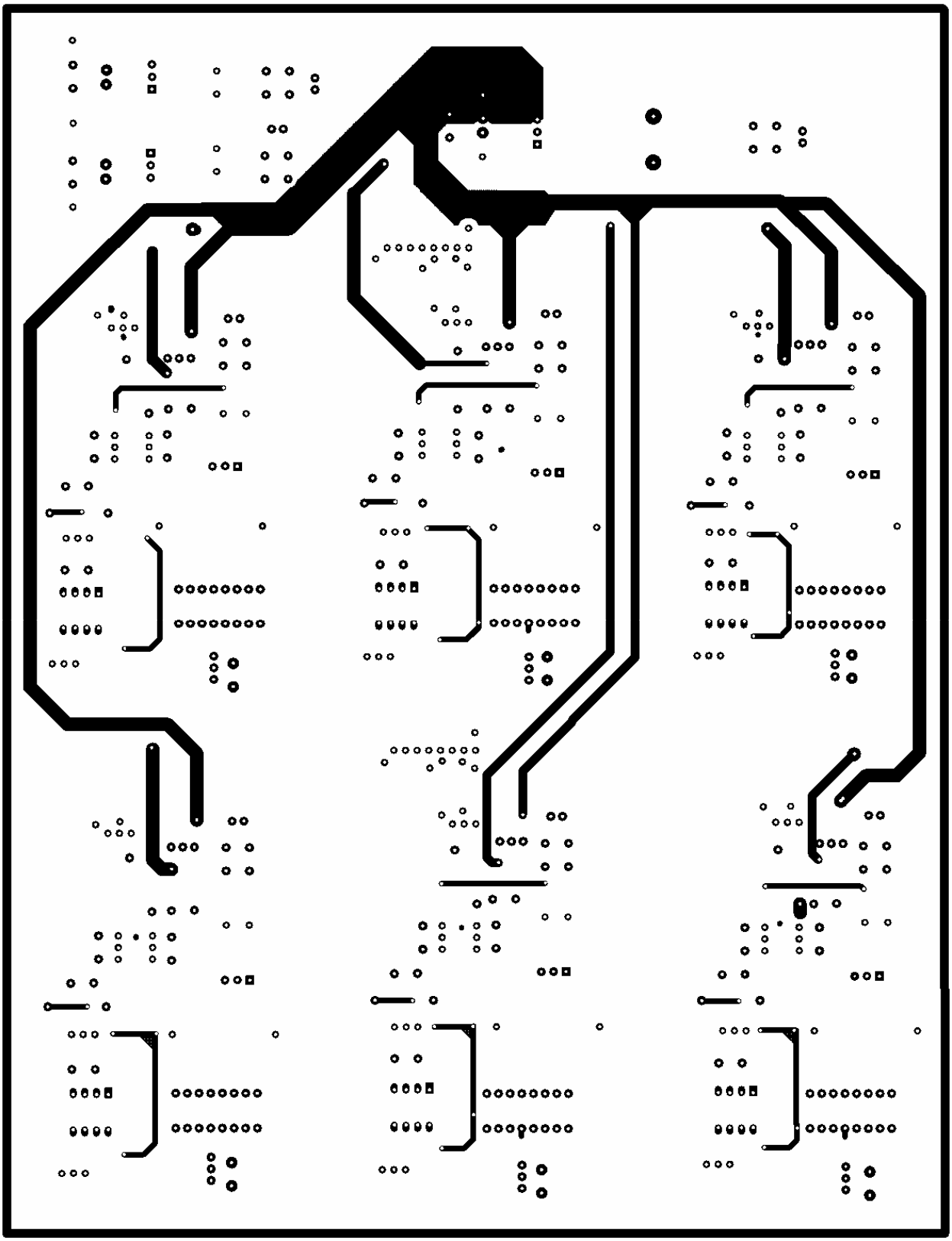

Figure C.7 PCB-Layout at 10:8 scale of Drivers Circuits, top face.

ISBN:978-84-693-7665-2/DL:T.1747-2010

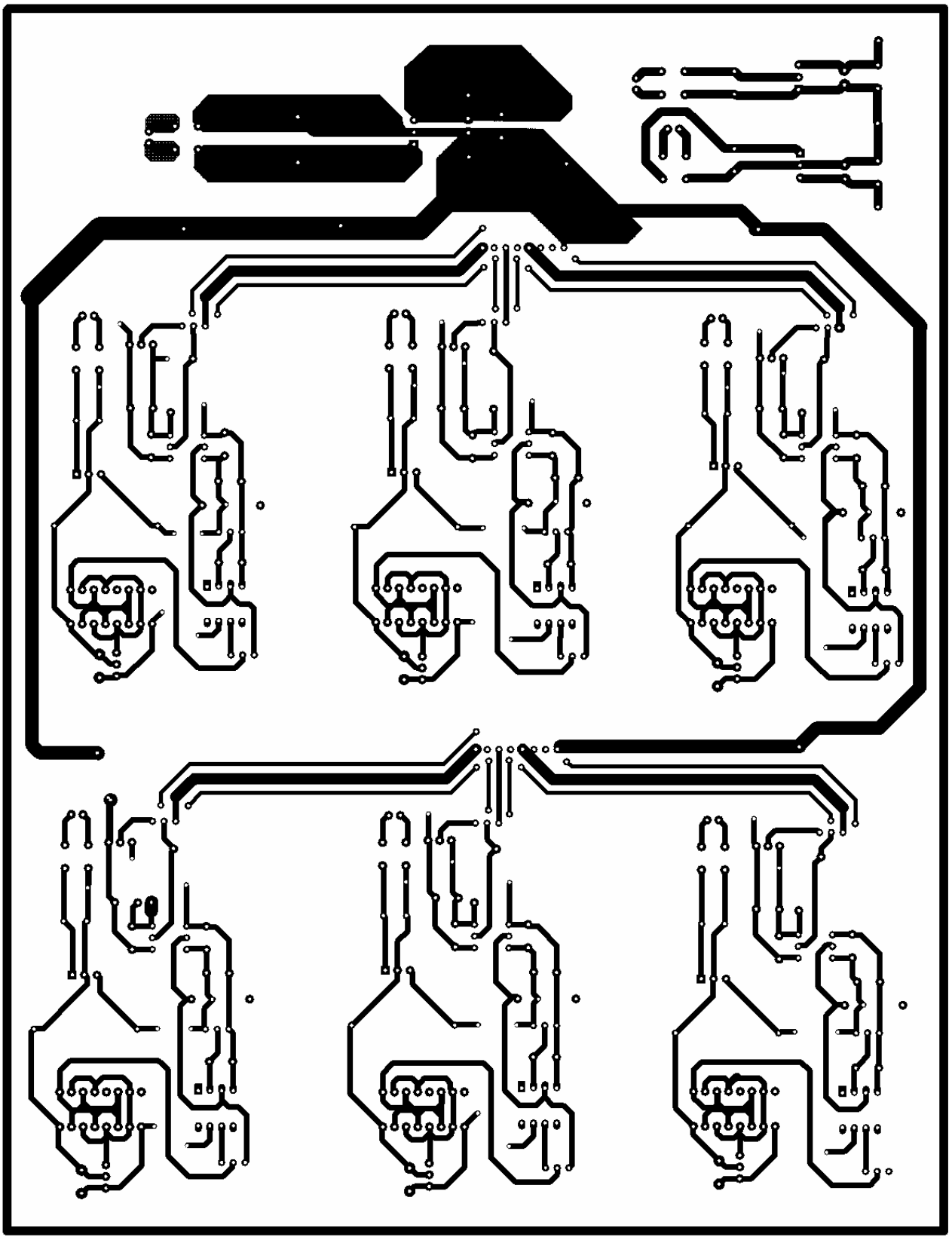

Figure C.8 PCB-Layout at 10:8 scale of Drivers Circuits, bottom face.

UNIVERSITAT ROVIRA I VIRGILI
CONTRIBUTIONS ON SPECTRAL CONTROL FOR THE ASYMMETRICAL FULL BRIDGE MULTILEVEL INVERTER
Oscar Mauricio Muñoz Ramírez
ISBN:978-84-693-7665-2/DL:T.1747-2010

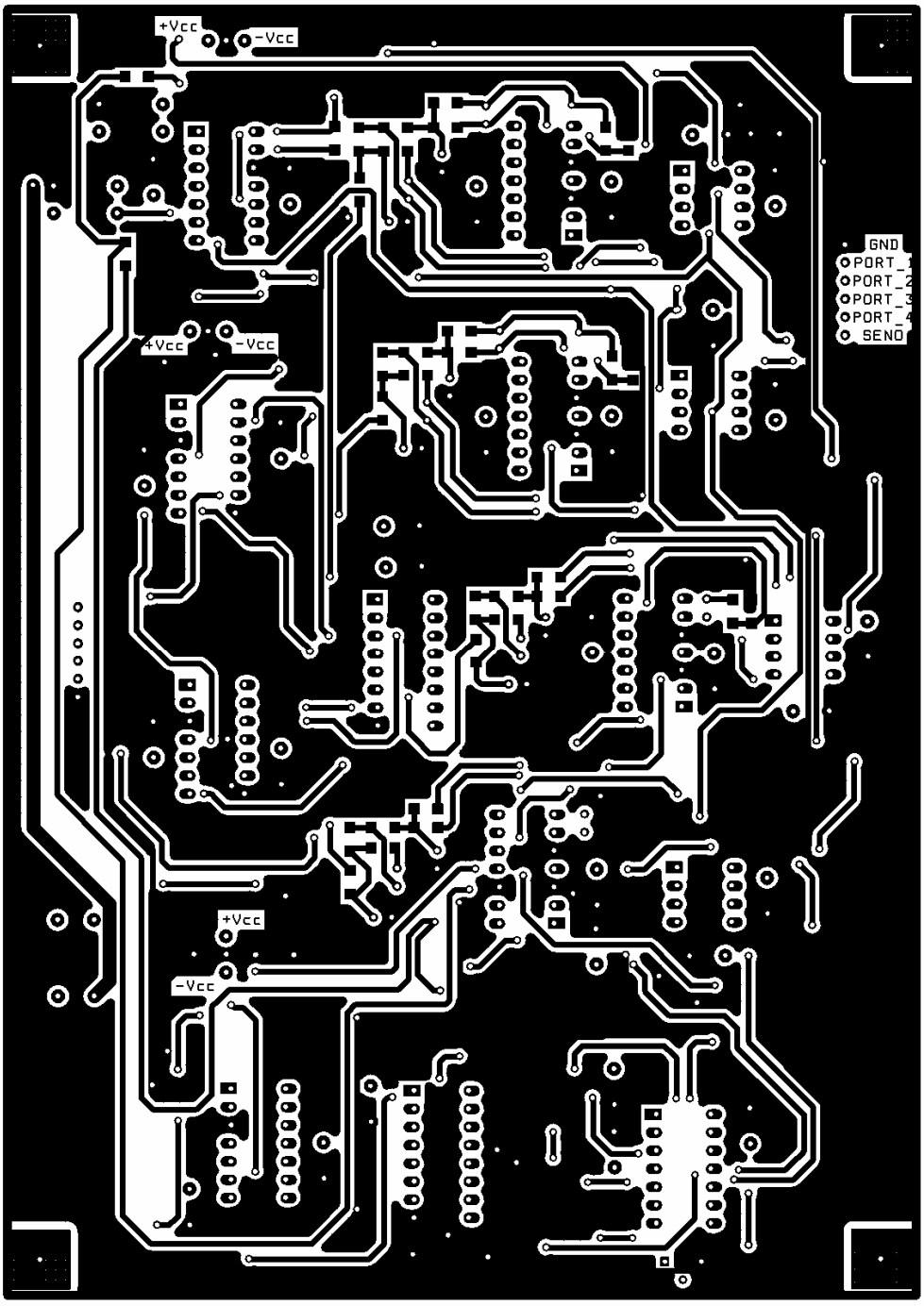

Figure C.9 PCB-Layout at 10:8 scale of Analogic 5-level PD-PWM modulator and State Variables control loop , top face.

UNIVERSITAT ROVIRA I VIRGILI
CONTRIBUTIONS ON SPECTRAL CONTROL FOR THE ASYMMETRICAL FULL BRIDGE MULTILEVEL INVERTER
Oscar Mauricio Muñoz Ramírez
ISBN:978-84-693-7665-2/DL:T.1747-2010

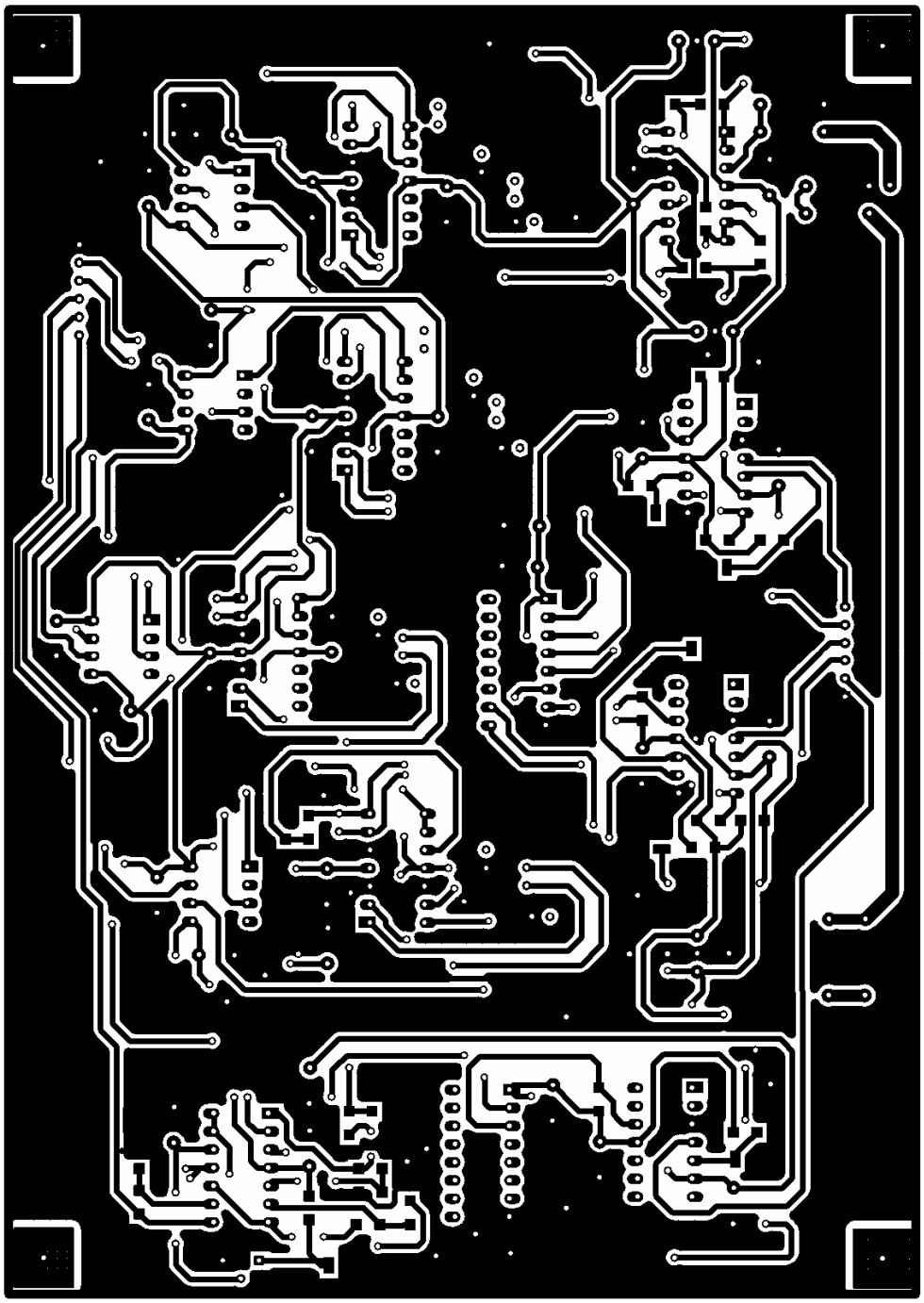

Figure C.10 PCB-Layout at 10:8 scale of of Analogic 5-level PD-PWM modulator and State Variables control loop , bottom face.

UNIVERSITAT ROVIRA I VIRGILI
CONTRIBUTIONS ON SPECTRAL CONTROL FOR THE ASYMMETRICAL FULL BRIDGE MULTILEVEL INVERTER
Oscar Mauricio Muñoz Ramírez
ISBN:978-84-693-7665-2/DL:T.1747-2010

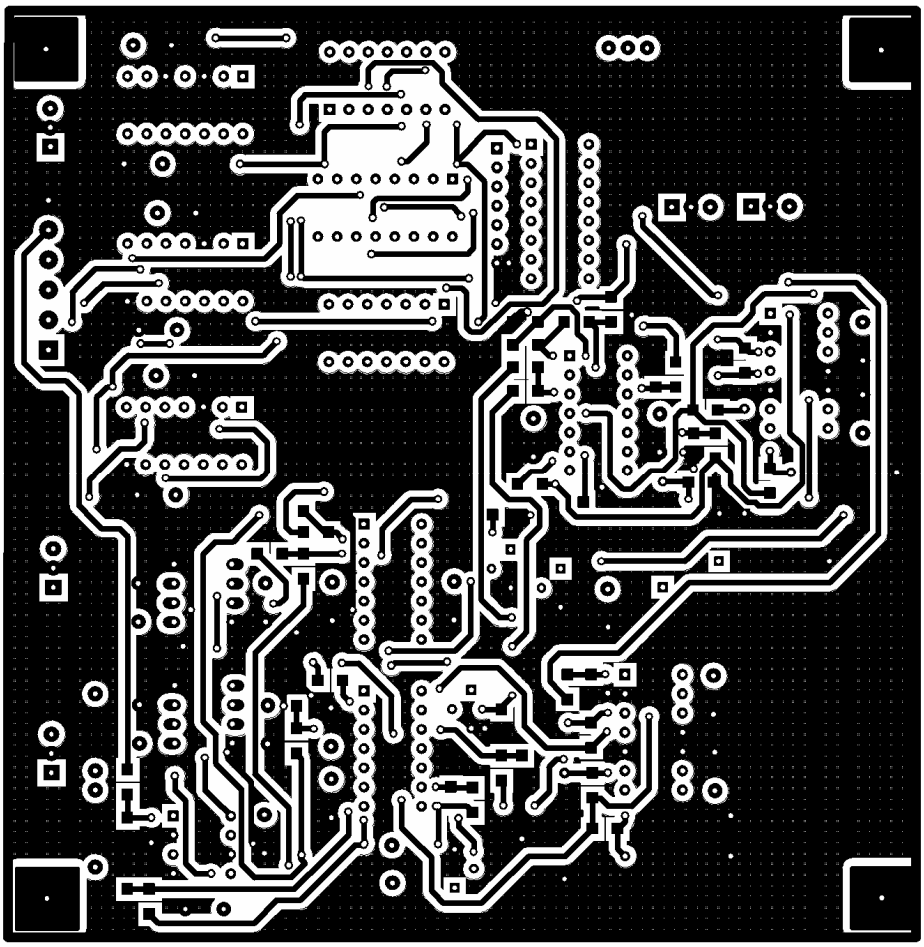

Figure C.11 PCB-Layout at 10:8 scale of demodulation and filtering of carriers and modulator signal and Feedforward control loop, top face.

UNIVERSITAT ROVIRA I VIRGILI
CONTRIBUTIONS ON SPECTRAL CONTROL FOR THE ASYMMETRICAL FULL BRIDGE MULTILEVEL INVERTER
Oscar Mauricio Muñoz Ramírez
ISBN:978-84-693-7665-2/DL:T.1747-2010

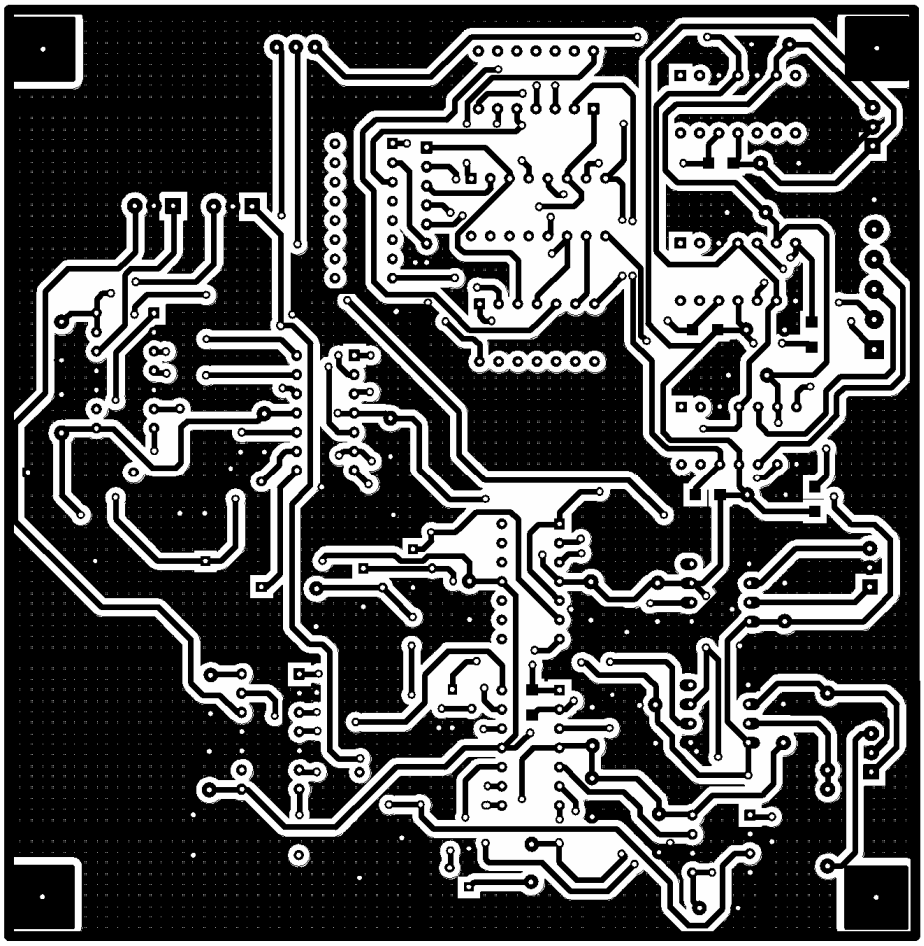

Figure C.12 PCB-Layout at 10:8 scale of demodulation and filtering of carriers and modulator signal and Feedforward control loop, bottom face.

UNIVERSITAT ROVIRA I VIRGILI
CONTRIBUTIONS ON SPECTRAL CONTROL FOR THE ASYMMETRICAL FULL BRIDGE MULTILEVEL INVERTER
Oscar Mauricio Muñoz Ramírez
ISBN:978-84-693-7665-2/DL:T.1747-2010

APPENDIX D. MATLAB Source Code

D.1 C_{mn}-Algorithm

% This is Matlab script of the program that calculates DFS C_{mn} coefficients in order to
%compose harmonics that satisfy condition $h = m \cdot M_f + n$
% harmonics as well as continuos time domain signal are plotted.

```
%Master Program Script that calls functions FcnC01, FcnC0n, FcnCm0 and FcnCmn
%File Name:    OneModulator5Level.m
%folder allocation: CmnByDFSAlgorithm
%functions File Names: FcnC01.m, FcnC0n.m, FcnCm0.m, FcnCmn.m

% Modulation of One Phase AFBMI 5 Level Operation Mode
% PLOTTING OF HARMONICS ARE NORMALIZED
close all; clc; clear all;
%        INPUT PARAMETERS
Vdc=100;        % sum of DC voltages
Mf=11;          % Frequency modulation Index
A=0.90;         % Amplitude modulation Index
K=0.30;         % Level Distribution
Alias=10;       % Carrier harmonic multiple
% r1 is the highest carrier and r4 lowest carrier
%r1=0.50; r2=0.50; r3=0.50; r4=0.50; % CASE 1
r1=1.00; r2=1.00; r3=1.00; r4=1.00; % CASE 2

Phi_l=acos( (K-1)/A ); Phi_u=acos( K/A );
solapamiento=3; % the effect oo flappping caused by base-band harmonics
N=solapamiento*Mf+ceil(Mf/2);
Qbessel=2*N; % Limit for Bessel Calculations
if (Qbessel>25)
   Qbessel=25;% Qbessel>25 is not necessary
end
M=Alias+solapamiento; % 2M+1 filas, Wc
Cmn=zeros(M+1,2*N+1);% vector of coefficients Cmn
%        To plot continuos time domain output signals:
Fmuestreo=20; ciclos=2;  Fo=1;
Rayas=Mf*Alias + floor(Mf/2);
format long
Rayas_A=zeros(1,Rayas);  % harmonics coseno
Rayas_B=zeros(1,Rayas);  % harmonics seno
Rayas_C=zeros(1,Rayas);  % harmonics phasor coseno
Rayas_Norm=zeros(1,Rayas);  % NORMALIZED harmonics
Phase_C=zeros(1,Rayas);  %
Phase_Degree=zeros(1,Rayas);
%    Cmn's for k-esims harmonics
   for m=0:M
      for n=-N:N
         if(m==0 && n==1)
           Cmn(m+1,n+N+1)=Vdc*FcnC01(K,A,r1,r2,r3,r4);
         end %if(m==0 && n==1)
         if(m==0 && n>1)
           Cmn(m+1,n+N+1)=Vdc*FcnC0n(K,A,r1,r2,r3,r4,n);
```

```
        end
        if(m>0 && n==0) %m~=0
          Cmn(m+1,n+N+1)=Vdc*FcnCm0(K,A,r1,r2,r3,r4,m,Qbessel);
        end
        if(m>0 && n~=0) %m~=0
          Cmn(m+1,n+N+1)=Vdc*FcnCmn(K,A,r1,r2,r3,r4,m,n,Qbessel);
        end
      end % for n=0:N
    end % for m=0:M
%%%  Harmonics generation by condition h = m · M_f + n
for k=1:Rayas
    for m=0:M
      for n=-N:N
        arm=Mf*m+n;
        if(arm==k)
        Rayas_C(k)=Rayas_C(k) +Cmn(m+1,n+N+1);
        end %if((Mf*m+n)==k)
      end %for n=-N:N
    end %for m=0:M
end % for k=1:Rayas
Rayas_Norm=abs(Rayas_C); Rayas_Norm=Rayas_Norm/Vdc;
%%%  Normalized Harmonics
figure(1);
stem(Rayas_Norm(1:Rayas),'xr');
title(['Normalized Harmonics: AFBMI Output Signal for 5-Level Mode Operation. Ma=',num2str(A),'
Mf=',num2str(Mf),' K=',num2str(K),' r1=',num2str(r1),' r2=',num2str(r2),' r3=',num2str(r3),'
r4=',num2str(r4)],'Color','b');
grid;
Rayas_A=real(Rayas_C); Rayas_B=imag(Rayas_C);
figure(2);
stem(Rayas_A(1:Rayas),'xk');
grid;
title('Cosines Terms','Color','b');
figure(3);
stem(Rayas_B(1:Rayas),'xm');
grid;
title('Sines Terms','Color','b');
%%%  Reproduction of 5-level waveform Vo
Fc=Rayas;  Fmuestreo=Fmuestreo*Fc;
To=1/Fo;  ciclos=ciclos*To;
t=0:1/Fmuestreo:ciclos;
Vo=zeros(1,Fmuestreo*ciclos+1);
VoSin=zeros(1,Fmuestreo*ciclos+1);
VoCos=zeros(1,Fmuestreo*ciclos+1);
aux_cos=0;  aux_sin=0;  aux_angle=0;
for z=1:Fmuestreo*ciclos+1  % instante t(z-1) % for z=1:Fmuestreo*ciclos+1
    for Arm=1:Rayas
      aux_angle=2*pi*Fo*Arm*t(z);
      aux_cos=Rayas_A(Arm)*cos(aux_angle);
      VoCos(z)=VoCos(z)+aux_cos;
      aux_sin=Rayas_B(Arm)*sin(aux_angle);
      VoSin(z)=VoSin(z)+aux_sin;
    end
    Vo(z)=VoCos(z)+VoSin(z);
    end
clear aux_cos;  clear aux_sin;  clear aux_angle;
```

```
figure(4);
plot(t,Vo);  grid;
title(['Full Bridge 5-Level VSI output Signal with Ma=',num2str(A),' Mf=',num2str(Mf),'
K=',num2str(K),' r1=',num2str(r1),' r2=',num2str(r2),' r3=',num2str(r3),' r4=',num2str(r4)],'Color','b');
%%%              END of Master Program OneModulator5Level.m   %%%


%%%              function FcnC01   %%%
function R = FcnC01(K,A,r1,r2,r3,r4)

format long;
Sum=0;
Phi_l=acos( (K-1)/A ); Phi_u=acos( K/A );
alpha1=pi + 2*pi*r1*(1-K)/K;      delta1= 2*pi*r1/K*A;
beta1=-pi -2*pi*(1-r1)*(1-K)/K;   lambda1=2*pi*(1-r1)/K*A;
alpha2=pi;                        delta2= 2*pi*r2/(1-K)*A;
beta2=-pi;                        lambda2=2*pi*(1-r2)/(1-K)*A;
alpha3=pi - 2*pi*r3;              delta3= 2*pi*r3/K*A;
beta3= pi - 2*pi*r3;              lambda3=2*pi*(1-r3)/K*A;
alpha4=pi - 2*pi*r4/(1-K);        delta4= 2*pi*r4/(1-K)*A;
beta4=-pi + 2*pi*(1-r4)/(1-K);    lambda4=2*pi*(1-r4)/(1-K)*A;
% NIVEL +Vdc:
%--------   Inicio de I9
factor1=(alpha4 - beta4)/2/pi/pi*-j;
factor2=(delta4 + lambda4)/2/pi/pi;
aux1=   exp(Phi_u*j)        -exp(-Phi_u*j);
aux2=-j*exp(2*Phi_u*j)/4 + j*exp(-2*Phi_u*j)/4  + (Phi_u + Phi_u)/2;
Sum=Sum + factor1*aux1 + factor2*aux2;
%--------   Fin de I9
% NIVEL +K*Vdc:
%--------   Inicio de I8 + I7
factor1=K*(2*pi + beta4 - alpha4)/2/pi/pi*-j;
factor2=-K*(delta4 + lambda4)/2/pi/pi;
aux1=   exp(Phi_u*j)        -exp(-Phi_u*j);
aux2=-j*exp(2*Phi_u*j)/4 + j*exp(-2*Phi_u*j)/4  + (Phi_u + Phi_u)/2;
Sum=Sum + factor1*aux1 + factor2*aux2;
%--------   Fin de I8 + I7
%--------   Inicio de I6
factor1=K*(alpha3 - beta3)/2/pi/pi*-j;
factor2=K*(delta3 + lambda3)/2/pi/pi;
aux1=   exp(-1*Phi_u*j)      -exp(-1*pi/2*j);
aux2=-j*exp(-2*Phi_u*j)/4  +j*exp(-2*pi/2*j)/4  + (-1*Phi_u + pi/2)/2;
Sum=Sum + factor1*aux1 + factor2*aux2;
%--------   Fin de I6
%--------   Inicio de I10
factor1=K*(alpha3 - beta3)/2/pi/pi*-j;
factor2=K*(delta3 + lambda3)/2/pi/pi;
aux1=   exp(pi/2*j)      -exp(Phi_u*j);
aux2=-j*exp(2*pi/2*j)/4  +j*exp(2*Phi_u*j)/4  + (pi/2 - Phi_u)/2;
Sum=Sum + factor1*aux1 + factor2*aux2;
%--------   Fin de I10
% NIVEL -(1-K)*Vdc:
%--------   Inicio de I2
factor1=(1-K)*(alpha1 - beta1)/2/pi/pi*j;
factor2=-1*(1-K)*(delta1 + lambda1)/2/pi/pi;
aux1=   exp(-Phi_l*j)      -exp(-pi*j);
```

UNIVERSITAT ROVIRA I VIRGILI
CONTRIBUTIONS ON SPECTRAL CONTROL FOR THE ASYMMETRICAL FULL BRIDGE MULTILEVEL INVERTER
Oscar Mauricio Muñoz Ramírez
ISBN:978-84-693-7665-2/DL:T.1747-2010


```
aux2=-j*exp(-2*Phi_l*j)/4  +j*exp(-2*pi*j)/4  + (-Phi_l +pi)/2;
Sum=Sum + factor1*aux1 + factor2*aux2;
%--------   Fin de I2
%--------   Inicio de I13
factor1=(1-K)*(alpha1 - beta1)/2/pi/pi*j;
factor2=-1*(1-K)*(delta1 + lambda1)/2/pi/pi;
aux1=   exp(pi*j)      -exp(Phi_l*j);
aux2=-j*exp(2*pi*j)/4  +j*exp(2*Phi_l*j)/4  + (pi -Phi_l)/2;
Sum=Sum + factor1*aux1 + factor2*aux2;
%--------   Fin de I13
%--------   Inicio de I5 + I4
factor1=(1-K)*(2*pi + beta2 - alpha2)/2/pi/pi*j;
factor2=(1-K)*(delta2 + lambda2)/2/pi/pi;
aux1=   exp(-1*pi/2*j)      -exp(-1*Phi_l*j);
aux2=-j*exp(-2*pi/2*j)/4  +j*exp(-2*Phi_l*j)/4  + (-1*pi/2 + Phi_l)/2;
Sum=Sum + factor1*aux1 + factor2*aux2;
%--------   Fin de I5 + I4
%--------   Inicio de I12 + I11
factor1=(1-K)*(2*pi + beta2 - alpha2)/2/pi/pi*j;
factor2=(1-K)*(delta2 + lambda2)/2/pi/pi;
aux1=   exp(Phi_l*j)      -exp(pi/2*j);
aux2=-j*exp(2*Phi_l*j)/4  +j*exp(2*pi/2*j)/4  + (Phi_l - pi/2)/2;
Sum=Sum + factor1*aux1 + factor2*aux2;
%--------   Fin de I12 + I11
% NIVEL -Vdc:
%--------   Inicio de I1 + I3
factor1=(2*pi +beta1 -alpha1)/2/pi/pi*j;
factor2=(delta1 + lambda1)/2/pi/pi;
aux1=   exp(-Phi_l*j)      -exp(-pi*j);
aux2=-j*exp(-2*Phi_l*j)/4  +j*exp(-2*pi*j)/4  + (-Phi_l +pi)/2;
Sum=Sum + factor1*aux1 + factor2*aux2;
%--------   Fin de I1 + I3
%--------   Inicio de I15 + I14
factor1=(2*pi +beta1 -alpha1)/2/pi/pi*j;
factor2=(delta1 + lambda1)/2/pi/pi;
aux1=   exp(pi*j)      -exp(Phi_l*j);
aux2=-j*exp(2*pi*j)/4  +j*exp(2*Phi_l*j)/4  + (pi -Phi_l)/2;
Sum=Sum + factor1*aux1 + factor2*aux2;
%--------   Fin de I15 + I14
R = Sum;
%%%             END of function FcnC01   %%%

%%%             function FcnC0n   %%%
function R = FcnC0n(K,A,r1,r2,r3,r4,n)
format long;
Sum=0;
Phi_l=acos( (K-1)/A ); Phi_u=acos( K/A );
alpha1=pi + 2*pi*r1*(1-K)/K;      delta1= 2*pi*r1/K*A;
beta1=-pi -2*pi*(1-r1)*(1-K)/K;   lambda1=2*pi*(1-r1)/K*A;
alpha2=pi;                        delta2= 2*pi*r2/(1-K)*A;
beta2=-pi;                        lambda2=2*pi*(1-r2)/(1-K)*A;
alpha3=pi - 2*pi*r3;              delta3= 2*pi*r3/K*A;
beta3= pi - 2*pi*r3;              lambda3=2*pi*(1-r3)/K*A;
alpha4=pi - 2*pi*r4/(1-K);        delta4= 2*pi*r4/(1-K)*A;
beta4=-pi + 2*pi*(1-r4)/(1-K);    lambda4=2*pi*(1-r4)/(1-K)*A;
% NIVEL +Vdc:
```

```
%--------   Inicio de I9
factor1=(alpha4 - beta4)/2/pi/pi*-j;
factor2=(delta4 + lambda4)/2/pi/pi*-j;
aux1=   exp(n*Phi_u*j)       -exp(-n*Phi_u*j);
aux1=aux1/n;
aux2=exp((n+1)*Phi_u*j) -exp((n+1)*-Phi_u*j);
aux2=aux2/2/(n+1);
aux3=exp((n-1)*Phi_u*j) -exp((n-1)*-Phi_u*j);
aux3=aux3/2/(n-1);
Sum=Sum + factor1*aux1 + factor2*(aux2 + aux3);
%--------   Fin de I9
% NIVEL +K*Vdc:
%--------   Inicio de I8 + I7
factor1=K*(2*pi + beta4 - alpha4)/2/pi/pi*-j;
factor2=K*(delta4 + lambda4)/2/pi/pi*j;
aux1=   exp(n*Phi_u*j)       -exp(-n*Phi_u*j);
aux1=aux1/n;
aux2=exp((n+1)*Phi_u*j) -exp((n+1)*-Phi_u*j);
aux2=aux2/2/(n+1);
aux3=exp((n-1)*Phi_u*j) -exp((n-1)*-Phi_u*j);
aux3=aux3/2/(n-1);
Sum=Sum + factor1*aux1 + factor2*(aux2 + aux3);
%--------   Fin de I8 + I7
%--------   Inicio de I6
factor1=K*(alpha3 - beta3)/2/pi/pi*-j;
factor2=K*(delta3 + lambda3)/2/pi/pi*-j;
aux1=   exp(-n*Phi_u*j)       -exp(-n*pi/2*j);
aux1=aux1/n;
aux2=exp(-(n+1)*Phi_u*j) -exp(-(n+1)*pi/2*j);
aux2=aux2/2/(n+1);
aux3=exp(-(n-1)*Phi_u*j) -exp(-(n-1)*pi/2*j);
aux3=aux3/2/(n-1);
Sum=Sum + factor1*aux1 + factor2*(aux2 + aux3);
%--------   Fin de I6
%--------   Inicio de I10
factor1=K*(alpha3 - beta3)/2/pi/pi*-j;
factor2=K*(delta3 + lambda3)/2/pi/pi*-j;
aux1=   exp(n*pi/2*j)       -exp(n*Phi_u*j);
aux1=aux1/n;
aux2=exp((n+1)*pi/2*j) -exp((n+1)*Phi_u*j);
aux2=aux2/2/(n+1);
aux3=exp((n-1)*pi/2*j) -exp((n-1)*Phi_u*j);
aux3=aux3/2/(n-1);
Sum=Sum + factor1*aux1 + factor2*(aux2 + aux3);
%--------   Fin de I10
% NIVEL -(1-K)*Vdc:
%--------   Inicio de I2
factor1=(1-K)*(alpha1 - beta1)/2/pi/pi*j;
factor2=(1-K)*(delta1 + lambda1)/2/pi/pi*j;
aux1=   exp(-n*Phi_l*j)       -exp(-n*pi*j);
aux1=aux1/n;
aux2=exp(-(n+1)*Phi_l*j) -exp(-(n+1)*pi*j);
aux2=aux2/2/(n+1);
aux3=exp(-(n-1)*Phi_l*j) -exp(-(n-1)*pi*j);
aux3=aux3/2/(n-1);
Sum=Sum + factor1*aux1 + factor2*(aux2 + aux3);
```

```
%--------   Fin de I2
%--------   Inicio de I13
factor1=(1-K)*(alpha1 - beta1)/2/pi/pi*j;
factor2=(1-K)*(delta1 + lambda1)/2/pi/pi*j;
aux1=   exp(n*pi*j)        -exp(n*Phi_l*j);
aux1=aux1/n;
aux2=exp((n+1)*pi*j) -exp((n+1)*Phi_l*j);
aux2=aux2/2/(n+1);
aux3=exp((n-1)*pi*j) -exp((n-1)*Phi_l*j);
aux3=aux3/2/(n-1);
Sum=Sum + factor1*aux1 + factor2*(aux2 + aux3);
%--------   Fin de I13
%--------   Inicio de I5 + I4
factor1=(1-K)*(2*pi + beta2 - alpha2)/2/pi/pi*j;
factor2=(1-K)*(delta2 + lambda2)/2/pi/pi*-j;
aux1=   exp(-n*pi/2*j)        -exp(-n*Phi_l*j);
aux1=aux1/n;
aux2=exp(-(n+1)*pi/2*j) -exp(-(n+1)*Phi_l*j);
aux2=aux2/2/(n+1);
aux3=exp(-(n-1)*pi/2*j) -exp(-(n-1)*Phi_l*j);
aux3=aux3/2/(n-1);
Sum=Sum + factor1*aux1 + factor2*(aux2 + aux3);
%--------   Fin de I5 + I4
%--------   Inicio de I12 + I11
factor1=(1-K)*(2*pi + beta2 - alpha2)/2/pi/pi*j;
factor2=(1-K)*(delta2 + lambda2)/2/pi/pi*-j;
aux1=   exp(n*Phi_l*j)        -exp(n*pi/2*j);
aux1=aux1/n;
aux2=exp((n+1)*Phi_l*j) -exp((n+1)*pi/2*j);
aux2=aux2/2/(n+1);
aux3=exp((n-1)*Phi_l*j) -exp((n-1)*pi/2*j);
aux3=aux3/2/(n-1);
Sum=Sum + factor1*aux1 + factor2*(aux2 + aux3);
%--------   Fin de I12 + I11
% NIVEL -Vdc:
%--------   Inicio de I1 + I3
factor1=(2*pi +beta1 -alpha1)/2/pi/pi*j;
factor2=(delta1 + lambda1)/2/pi/pi*-j;
aux1=   exp(-n*Phi_l*j)        -exp(-n*pi*j);
aux1=aux1/n;
aux2=exp(-(n+1)*Phi_l*j) -exp(-(n+1)*pi*j);
aux2=aux2/2/(n+1);
aux3=exp(-(n-1)*Phi_l*j) -exp(-(n-1)*pi*j);
aux3=aux3/2/(n-1);
Sum=Sum + factor1*aux1 + factor2*(aux2 + aux3);
%--------   Fin de I1 + I3
%--------   Inicio de I15 + I14
factor1=(2*pi +beta1 -alpha1)/2/pi/pi*j;
factor2=(delta1 + lambda1)/2/pi/pi*-j;
aux1=   exp(n*pi*j)        -exp(n*Phi_l*j);
aux1=aux1/n;
aux2=exp((n+1)*pi*j) -exp((n+1)*Phi_l*j);
aux2=aux2/2/(n+1);
aux3=exp((n-1)*pi*j) -exp((n-1)*Phi_l*j);
aux3=aux3/2/(n-1);
Sum=Sum + factor1*aux1 + factor2*(aux2 + aux3);
```

```
%--------   Fin de I15 + I14
R = Sum;
%%%             END of function FcnC0n   %%%


%%%             function FcnCm0   %%%
%%%             END of function FcnCm0   %%%
function R = FcnCm0(K,A,r1,r2,r3,r4,m,Qbessel)
format long;
Sum=0;
Phi_l=acos( (K-1)/A ); Phi_u=acos( K/A );
alpha1=pi + 2*pi*r1*(1-K)/K;      delta1= 2*pi*r1/K*A;
beta1=-pi -2*pi*(1-r1)*(1-K)/K;   lambda1=2*pi*(1-r1)/K*A;
alpha2=pi;                        delta2= 2*pi*r2/(1-K)*A;
beta2=-pi;                        lambda2=2*pi*(1-r2)/(1-K)*A;
alpha3=pi - 2*pi*r3;              delta3= 2*pi*r3/K*A;
beta3= pi - 2*pi*r3;              lambda3=2*pi*(1-r3)/K*A;
alpha4=pi - 2*pi*r4/(1-K);        delta4= 2*pi*r4/(1-K)*A;
beta4=-pi + 2*pi*(1-r4)/(1-K);    lambda4=2*pi*(1-r4)/(1-K)*A;
% NIVEL +Vdc:
%--------   Inicio de I9
factor=1/2/pi/pi/m; HighLim=Phi_u; LowLim=-Phi_u;
aux1= HighLim -LowLim;   aux1=aux1*real(besselj(0,m*delta4));
aux1=aux1*-j*exp(m*alpha4*j);
aux3= HighLim -LowLim;   aux3=aux3*real(besselj(0,m*lambda4));
aux3=aux3*j*exp(m*beta4*j);
aux2=0; aux4=0; sum_aux2=0; sum_aux4=0; aux_sin=0;
for q=1:Qbessel
   aux_sin=sin(HighLim*q) - sin(LowLim*q); aux_sin=aux_sin/q;
   sum_aux2=(j^(q+1))*real(besselj(q,m*delta4))*aux_sin;
   sum_aux4=(j^(-q+1))*real(besselj(q,m*lambda4))*aux_sin;
   aux2=aux2 +sum_aux2; aux4=aux4 +sum_aux4;
end
aux2=-2*aux2*exp(m*alpha4*j); aux4=2*aux4*exp(m*beta4*j);
Sum=Sum + factor*(aux1 +aux2 +aux3 +aux4);
%--------   Fin de I9
% NIVEL +K*Vdc:
%--------   Inicio de I8 + I7
factor=K/2/pi/pi/m;  HighLim=Phi_u; LowLim=-Phi_u; %K
aux1= HighLim -LowLim;   aux1=aux1*real(besselj(0,m*lambda4));
aux1=aux1*-j*exp(m*beta4*j);
aux3= HighLim -LowLim;   aux3=aux3*real(besselj(0,m*delta4));
aux3=aux3*j*exp(m*alpha4*j);
aux2=0; aux4=0; sum_aux2=0; sum_aux4=0; aux_sin=0;
for q=1:Qbessel
   aux_sin=sin(HighLim*q) - sin(LowLim*q); aux_sin=aux_sin/q;
   sum_aux2=(j^(-q+1))*real(besselj(q,m*lambda4))*aux_sin;
   sum_aux4=(j^(q+1))*real(besselj(q,m*delta4))*aux_sin;
   aux2=aux2 +sum_aux2; aux4=aux4 +sum_aux4;
end
aux2=-2*aux2*exp(m*beta4*j); aux4=2*aux4*exp(m*alpha4*j);
Sum=Sum + factor*(aux1 +aux2 +aux3 +aux4);
%--------   Fin de I8 + I7
%--------   Inicio de I6
factor=K/2/pi/pi/m;  HighLim=-Phi_u; LowLim=-pi/2; %K
aux1= HighLim -LowLim;   aux1=aux1*real(besselj(0,m*delta3));
```

```
aux1=aux1*-j*exp(m*alpha3*j);
aux3= HighLim -LowLim;   aux3=aux3*real(besselj(0,m*lambda3));
aux3=aux3*j*exp(m*beta3*j);
aux2=0; aux4=0; sum_aux2=0; sum_aux4=0; aux_sin=0;
for q=1:Qbessel
   aux_sin=sin(HighLim*q) - sin(LowLim*q); aux_sin=aux_sin/q;
   sum_aux2=(j^(q+1))*real(besselj(q,m*delta3))*aux_sin;
   sum_aux4=(j^(-q+1))*real(besselj(q,m*lambda3))*aux_sin;
   aux2=aux2 +sum_aux2; aux4=aux4 +sum_aux4;
end
aux2=-2*aux2*exp(m*alpha3*j); aux4=2*aux4*exp(m*beta3*j);
Sum=Sum + factor*(aux1 +aux2 +aux3 +aux4);
%--------   Fin de I6
%--------   Inicio de I10
factor=K/2/pi/pi/m;  HighLim=pi/2; LowLim=Phi_u;%K
aux1= HighLim -LowLim;   aux1=aux1*real(besselj(0,m*delta3));
aux1=aux1*-j*exp(m*alpha3*j);
aux3= HighLim -LowLim;   aux3=aux3*real(besselj(0,m*lambda3));
aux3=aux3*j*exp(m*beta3*j);
aux2=0; aux4=0; sum_aux2=0; sum_aux4=0; aux_sin=0;
for q=1:Qbessel
   aux_sin=sin(HighLim*q) - sin(LowLim*q); aux_sin=aux_sin/q;
   sum_aux2=(j^(q+1))*real(besselj(q,m*delta3))*aux_sin;
   sum_aux4=(j^(-q+1))*real(besselj(q,m*lambda3))*aux_sin;
   aux2=aux2 +sum_aux2; aux4=aux4 +sum_aux4;
end
aux2=-2*aux2*exp(m*alpha3*j); aux4=2*aux4*exp(m*beta3*j);
Sum=Sum + factor*(aux1 +aux2 +aux3 +aux4);
%--------   Fin de I10
% NIVEL -(1-K)*Vdc:
%--------   Inicio de I2
factor=(1-K)/2/pi/pi/m;  HighLim=-Phi_l; LowLim=-pi;%(1-K)
aux1= HighLim -LowLim;   aux1=aux1*real(besselj(0,m*delta1));
aux1=aux1*j*exp(m*alpha1*j);
aux3= HighLim -LowLim;   aux3=aux3*real(besselj(0,m*lambda1));
aux3=aux3*-j*exp(m*beta1*j);
aux2=0; aux4=0; sum_aux2=0; sum_aux4=0; aux_sin=0;
for q=1:Qbessel
   aux_sin=sin(HighLim*q) - sin(LowLim*q); aux_sin=aux_sin/q;
   sum_aux2=(j^(q+1))*real(besselj(q,m*delta1))*aux_sin;
   sum_aux4=(j^(-q+1))*real(besselj(q,m*lambda1))*aux_sin;
   aux2=aux2 +sum_aux2; aux4=aux4 +sum_aux4;
end
aux2=2*aux2*exp(m*alpha1*j); aux4=-2*aux4*exp(m*beta1*j);
Sum=Sum + factor*(aux1 +aux2 +aux3 +aux4);
%--------   Fin de I2
%--------   Inicio de I13
factor=(1-K)/2/pi/pi/m;  HighLim=pi; LowLim=Phi_l;%(1-K)
aux1= HighLim -LowLim;   aux1=aux1*real(besselj(0,m*delta1));
aux1=aux1*j*exp(m*alpha1*j);
aux3= HighLim -LowLim;   aux3=aux3*real(besselj(0,m*lambda1));
aux3=aux3*-j*exp(m*beta1*j);
aux2=0; aux4=0; sum_aux2=0; sum_aux4=0; aux_sin=0;
for q=1:Qbessel
   aux_sin=sin(HighLim*q) - sin(LowLim*q); aux_sin=aux_sin/q;
   sum_aux2=(j^(q+1))*real(besselj(q,m*delta1))*aux_sin;
```

```
   sum_aux4=(j^(-q+1))*real(besselj(q,m*lambda1))*aux_sin;
   aux2=aux2 +sum_aux2; aux4=aux4 +sum_aux4;
end
aux2=2*aux2*exp(m*alpha1*j); aux4=-2*aux4*exp(m*beta1*j);
Sum=Sum + factor*(aux1 +aux2 +aux3 +aux4);
%--------   Fin de I13
%--------   Inicio de I5 + I4
factor=(1-K)/2/pi/pi/m;  HighLim=-pi/2; LowLim=-Phi_l; %(1-K)
aux1= HighLim -LowLim;   aux1=aux1*real(besselj(0,m*lambda2));
aux1=aux1*j*exp(m*beta2*j);
aux3= HighLim -LowLim;   aux3=aux3*real(besselj(0,m*delta2));
aux3=aux3*-j*exp(m*alpha2*j);
aux2=0; aux4=0; sum_aux2=0; sum_aux4=0; aux_sin=0;
for q=1:Qbessel
   aux_sin=sin(HighLim*q) - sin(LowLim*q); aux_sin=aux_sin/q;
   sum_aux2=(j^(-q+1))*real(besselj(q,m*lambda2))*aux_sin;
   sum_aux4=(j^(q+1))*real(besselj(q,m*delta2))*aux_sin;
   aux2=aux2 +sum_aux2; aux4=aux4 +sum_aux4;
end
aux2=2*aux2*exp(m*beta2*j); aux4=-2*aux4*exp(m*alpha2*j);
Sum=Sum + factor*(aux1 +aux2 +aux3 +aux4);
%--------   Fin de I5 + I4
%--------   Inicio de I12 + I11
factor=(1-K)/2/pi/pi/m;  HighLim=Phi_l; LowLim=pi/2; %(1-K)
aux1= HighLim -LowLim;   aux1=aux1*real(besselj(0,m*lambda2));
aux1=aux1*j*exp(m*beta2*j);
aux3= HighLim -LowLim;   aux3=aux3*real(besselj(0,m*delta2));
aux3=aux3*-j*exp(m*alpha2*j);
aux2=0; aux4=0; sum_aux2=0; sum_aux4=0; aux_sin=0;
for q=1:Qbessel
   aux_sin=sin(HighLim*q) - sin(LowLim*q); aux_sin=aux_sin/q;
   sum_aux2=(j^(-q+1))*real(besselj(q,m*lambda2))*aux_sin;
   sum_aux4=(j^(q+1))*real(besselj(q,m*delta2))*aux_sin;
   aux2=aux2 +sum_aux2; aux4=aux4 +sum_aux4;
end
aux2=2*aux2*exp(m*beta2*j); aux4=-2*aux4*exp(m*alpha2*j);
Sum=Sum + factor*(aux1 +aux2 +aux3 +aux4);
%--------   Fin de I12 + I11
% NIVEL -Vdc:
%--------   Inicio de I1 + I3
factor=1/2/pi/pi/m;  HighLim=-Phi_l; LowLim=-pi;
aux1= HighLim -LowLim;   aux1=aux1*real(besselj(0,m*lambda1));
aux1=aux1*j*exp(m*beta1*j);
aux3= HighLim -LowLim;   aux3=aux3*real(besselj(0,m*delta1));
aux3=aux3*-j*exp(m*alpha1*j);
aux2=0; aux4=0; sum_aux2=0; sum_aux4=0; aux_sin=0;
for q=1:Qbessel
   aux_sin=sin(HighLim*q) - sin(LowLim*q); aux_sin=aux_sin/q;
   sum_aux2=(j^(-q+1))*real(besselj(q,m*lambda1))*aux_sin;
   sum_aux4=(j^(q+1))*real(besselj(q,m*delta1))*aux_sin;
   aux2=aux2 +sum_aux2; aux4=aux4 +sum_aux4;
end
aux2=2*aux2*exp(m*beta1*j); aux4=-2*aux4*exp(m*alpha1*j);
Sum=Sum + factor*(aux1 +aux2 +aux3 +aux4);
%--------   Fin de I1 + I3
%--------   Inicio de I15 + I14
```

```
factor=1/2/pi/pi/m; HighLim=pi; LowLim=Phi_l;
aux1= HighLim -LowLim;   aux1=aux1*real(besselj(0,m*lambda1));
aux1=aux1*j*exp(m*beta1*j);
aux3= HighLim -LowLim;   aux3=aux3*real(besselj(0,m*delta1));
aux3=aux3*-j*exp(m*alpha1*j);
aux2=0; aux4=0; sum_aux2=0; sum_aux4=0; aux_sin=0;
for q=1:Qbessel
   aux_sin=sin(HighLim*q) - sin(LowLim*q); aux_sin=aux_sin/q;
   sum_aux2=(j^(-q+1))*real(besselj(q,m*lambda1))*aux_sin;
   sum_aux4=(j^(q+1))*real(besselj(q,m*delta1))*aux_sin;
   aux2=aux2 +sum_aux2; aux4=aux4 +sum_aux4;
end
aux2=2*aux2*exp(m*beta1*j); aux4=-2*aux4*exp(m*alpha1*j);
Sum=Sum + factor*(aux1 +aux2 +aux3 +aux4);
%--------   Fin de I15 + I14
R = Sum;

%%%              function FcnCmn   %%%
function R = FcnCmn(K,A,r1,r2,r3,r4,m,n,Qbessel)

format long;
Sum=0;
Phi_l=acos( (K-1)/A ); Phi_u=acos( K/A );
alpha1=pi + 2*pi*r1*(1-K)/K;      delta1= 2*pi*r1/K*A;
beta1=-pi -2*pi*(1-r1)*(1-K)/K;   lambda1=2*pi*(1-r1)/K*A;
alpha2=pi;                        delta2= 2*pi*r2/(1-K)*A;
beta2=-pi;                        lambda2=2*pi*(1-r2)/(1-K)*A;
alpha3=pi - 2*pi*r3;              delta3= 2*pi*r3/K*A;
beta3= pi - 2*pi*r3;              lambda3=2*pi*(1-r3)/K*A;
alpha4=pi - 2*pi*r4/(1-K);        delta4= 2*pi*r4/(1-K)*A;
beta4=-pi + 2*pi*(1-r4)/(1-K);    lambda4=2*pi*(1-r4)/(1-K)*A;
% NIVEL +Vdc:
%--------   Inicio de I9
factor=1/2/pi/pi/m; HighLim=Phi_u; LowLim=-Phi_u;
aux1= exp(HighLim*n*j) -exp(LowLim*n*j); aux1=aux1*real(besselj(0,m*delta4));
aux1=-aux1*exp(m*alpha4*j)/n;
aux3= exp(HighLim*n*j) -exp(LowLim*n*j);   aux3=aux3*real(besselj(0,m*lambda4));
aux3=aux3*exp(m*beta4*j)/n;
aux2=0; aux4=0;
for q=1:Qbessel
   sum_aux2=0; sum_aux4=0; aux_exp1=0; aux_exp2=0;
   if(q~=abs(n))
   aux_exp1=exp((n+q)*HighLim*j) -exp((n+q)*LowLim*j); aux_exp1=aux_exp1/(n+q);
   aux_exp2=exp((n-q)*HighLim*j) -exp((n-q)*LowLim*j); aux_exp2=aux_exp2/(n-q);
   sum_aux2=(j^q)*real(besselj(q,m*delta4))*(aux_exp1 +aux_exp2);
   sum_aux4=(j^-q)*real(besselj(q,m*lambda4))*(aux_exp1 +aux_exp2);
   end
   if(q==-n)
   aux_exp1= (HighLim -LowLim)*j;%aux_exp1 se resuelve por integral sencilla de 1*dy
   aux_exp2= exp((n-q)*HighLim*j) -exp((n-q)*LowLim*j); aux_exp2=aux_exp2/(n-q);
   sum_aux2=(j^q)*real(besselj(q,m*delta4))*(aux_exp1 +aux_exp2);
   sum_aux4=(j^-q)*real(besselj(q,m*lambda4))*(aux_exp1 +aux_exp2);
   end
   if(q==n)
   aux_exp1= exp((n+q)*HighLim*j) -exp((n+q)*LowLim*j); aux_exp1=aux_exp1/(n+q);
   aux_exp2= (HighLim -LowLim)*j;%aux_exp2 se resuelve por integral sencilla de 1*dy
```

```
    sum_aux2=(j^q)*real(besselj(q,m*delta4))*(aux_exp1 +aux_exp2);
    sum_aux4=(j^-q)*real(besselj(q,m*lambda4))*(aux_exp1 +aux_exp2);
    end
    aux2=aux2 +sum_aux2; aux4=aux4 +sum_aux4;
end
aux2=-aux2*exp(m*alpha4*j); aux4=aux4*exp(m*beta4*j);
Sum=Sum + factor*(aux1 +aux2 +aux3 +aux4);
%--------   Fin de I9
% NIVEL +K*Vdc:
%--------   Inicio de I8 + I7
factor=K/2/pi/pi/m; HighLim=Phi_u; LowLim=-Phi_u; %K
aux1= exp(HighLim*n*j) -exp(LowLim*n*j); aux1=aux1*real(besselj(0,m*lambda4));
aux1=-aux1*exp(m*beta4*j)/n;
aux3= exp(HighLim*n*j) -exp(LowLim*n*j); aux3=aux3*real(besselj(0,m*delta4));
aux3=aux3*exp(m*alpha4*j)/n;
aux2=0; aux4=0;
for q=1:Qbessel
    sum_aux2=0; sum_aux4=0; aux_exp1=0; aux_exp2=0;
    if(q~=abs(n))
    aux_exp1=exp((n+q)*HighLim*j) -exp((n+q)*LowLim*j); aux_exp1=aux_exp1/(n+q);
    aux_exp2=exp((n-q)*HighLim*j) -exp((n-q)*LowLim*j); aux_exp2=aux_exp2/(n-q);
    sum_aux2=(j^-q)*real(besselj(q,m*lambda4))*(aux_exp1 +aux_exp2);
    sum_aux4=(j^q)*real(besselj(q,m*delta4))*(aux_exp1 +aux_exp2);
    end
    if(q==-n)
    aux_exp1= (HighLim -LowLim)*j;%aux_exp1 se resuelve por integral sencilla de 1*dy
    aux_exp2= exp((n-q)*HighLim*j) -exp((n-q)*LowLim*j); aux_exp2=aux_exp2/(n-q);
    sum_aux2=(j^-q)*real(besselj(q,m*lambda4))*(aux_exp1 +aux_exp2);
    sum_aux4=(j^q)*real(besselj(q,m*delta4))*(aux_exp1 +aux_exp2);
    end
    if(q==n)
    aux_exp1= exp((n+q)*HighLim*j) -exp((n+q)*LowLim*j); aux_exp1=aux_exp1/(n+q);
    aux_exp2= (HighLim -LowLim)*j;%aux_exp2 se resuelve por integral sencilla de 1*dy
    sum_aux2=(j^-q)*real(besselj(q,m*lambda4))*(aux_exp1 +aux_exp2);
    sum_aux4=(j^q)*real(besselj(q,m*delta4))*(aux_exp1 +aux_exp2);
    end
    aux2=aux2 +sum_aux2; aux4=aux4 +sum_aux4;
end
aux2=-aux2*exp(m*beta4*j); aux4=aux4*exp(m*alpha4*j);
Sum=Sum + factor*(aux1 +aux2 +aux3 +aux4);
%--------   Fin de I8 + I7
%--------   Inicio de I6
factor=K/2/pi/pi/m; HighLim=-Phi_u; LowLim=-pi/2; %K
aux1= exp(HighLim*n*j) -exp(LowLim*n*j); aux1=aux1*real(besselj(0,m*delta3));
aux1=-aux1*exp(m*alpha3*j)/n;
aux3= exp(HighLim*n*j) -exp(LowLim*n*j); aux3=aux3*real(besselj(0,m*lambda3));
aux3=aux3*exp(m*beta3*j)/n;
aux2=0; aux4=0;
for q=1:Qbessel
    sum_aux2=0; sum_aux4=0; aux_exp1=0; aux_exp2=0;
    if(q~=abs(n))
    aux_exp1=exp((n+q)*HighLim*j) -exp((n+q)*LowLim*j); aux_exp1=aux_exp1/(n+q);
    aux_exp2=exp((n-q)*HighLim*j) -exp((n-q)*LowLim*j); aux_exp2=aux_exp2/(n-q);
    sum_aux2=(j^q)*real(besselj(q,m*delta3))*(aux_exp1 +aux_exp2);
    sum_aux4=(j^-q)*real(besselj(q,m*lambda3))*(aux_exp1 +aux_exp2);
    end
```

```
    if(q==-n)
    aux_exp1= (HighLim -LowLim)*j;%aux_exp1 se resuelve por integral sencilla de 1*dy
    aux_exp2= exp((n-q)*HighLim*j) -exp((n-q)*LowLim*j); aux_exp2=aux_exp2/(n-q);
    sum_aux2=(j^q)*real(besselj(q,m*delta3))*(aux_exp1 +aux_exp2);
    sum_aux4=(j^-q)*real(besselj(q,m*lambda3))*(aux_exp1 +aux_exp2);
    end
    if(q==n)
    aux_exp1= exp((n+q)*HighLim*j) -exp((n+q)*LowLim*j); aux_exp1=aux_exp1/(n+q);
    aux_exp2= (HighLim -LowLim)*j;%aux_exp2 se resuelve por integral sencilla de 1*dy
    sum_aux2=(j^q)*real(besselj(q,m*delta3))*(aux_exp1 +aux_exp2);
    sum_aux4=(j^-q)*real(besselj(q,m*lambda3))*(aux_exp1 +aux_exp2);
    end
    aux2=aux2 +sum_aux2; aux4=aux4 +sum_aux4;
end
aux2=-aux2*exp(m*alpha3*j); aux4=aux4*exp(m*beta3*j);
Sum=Sum + factor*(aux1 +aux2 +aux3 +aux4);
%--------   Fin de I6
%--------   Inicio de I10
factor=K/2/pi/pi/m; HighLim=pi/2; LowLim=Phi_u; %K
aux1= exp(HighLim*n*j) -exp(LowLim*n*j); aux1=aux1*real(besselj(0,m*delta3));
aux1=-aux1*exp(m*alpha3*j)/n;
aux3= exp(HighLim*n*j) -exp(LowLim*n*j); aux3=aux3*real(besselj(0,m*lambda3));
aux3=aux3*exp(m*beta3*j)/n;
aux2=0; aux4=0;
for q=1:Qbessel
    sum_aux2=0; sum_aux4=0; aux_exp1=0; aux_exp2=0;
    if(q~=abs(n))
    aux_exp1=exp((n+q)*HighLim*j) -exp((n+q)*LowLim*j); aux_exp1=aux_exp1/(n+q);
    aux_exp2=exp((n-q)*HighLim*j) -exp((n-q)*LowLim*j); aux_exp2=aux_exp2/(n-q);
    sum_aux2=(j^q)*real(besselj(q,m*delta3))*(aux_exp1 +aux_exp2);
    sum_aux4=(j^-q)*real(besselj(q,m*lambda3))*(aux_exp1 +aux_exp2);
    end
    if(q==-n)
    aux_exp1= (HighLim -LowLim)*j;%aux_exp1 se resuelve por integral sencilla de 1*dy
    aux_exp2= exp((n-q)*HighLim*j) -exp((n-q)*LowLim*j); aux_exp2=aux_exp2/(n-q);
    sum_aux2=(j^q)*real(besselj(q,m*delta3))*(aux_exp1 +aux_exp2);
    sum_aux4=(j^-q)*real(besselj(q,m*lambda3))*(aux_exp1 +aux_exp2);
    end
    if(q==n)
    aux_exp1= exp((n+q)*HighLim*j) -exp((n+q)*LowLim*j); aux_exp1=aux_exp1/(n+q);
    aux_exp2= (HighLim -LowLim)*j;%aux_exp2 se resuelve por integral sencilla de 1*dy
    sum_aux2=(j^q)*real(besselj(q,m*delta3))*(aux_exp1 +aux_exp2);
    sum_aux4=(j^-q)*real(besselj(q,m*lambda3))*(aux_exp1 +aux_exp2);
    end
    aux2=aux2 +sum_aux2; aux4=aux4 +sum_aux4;
end
aux2=-aux2*exp(m*alpha3*j); aux4=aux4*exp(m*beta3*j);
Sum=Sum + factor*(aux1 +aux2 +aux3 +aux4);
%--------   Fin de I10
% NIVEL -(1-K)*Vdc:
%--------   Inicio de I2
factor=(1-K)/2/pi/pi/m; HighLim=-Phi_l; LowLim=-pi; %(1-K)
aux1= exp(HighLim*n*j) -exp(LowLim*n*j); aux1=aux1*real(besselj(0,m*delta1));
aux1=aux1*exp(m*alpha1*j)/n;
aux3= exp(HighLim*n*j) -exp(LowLim*n*j); aux3=aux3*real(besselj(0,m*lambda1));
aux3=-aux3*exp(m*beta1*j)/n;
```

```
aux2=0; aux4=0; sum_aux2=0; sum_aux4=0; aux_exp1=0; aux_exp2=0;
for q=1:Qbessel
   sum_aux2=0; sum_aux4=0; aux_exp1=0; aux_exp2=0;
   if(q~=abs(n))
   aux_exp1=exp((n+q)*HighLim*j) -exp((n+q)*LowLim*j); aux_exp1=aux_exp1/(n+q);
   aux_exp2=exp((n-q)*HighLim*j) -exp((n-q)*LowLim*j); aux_exp2=aux_exp2/(n-q);
   sum_aux2=(j^q)*real(besselj(q,m*delta1))*(aux_exp1 +aux_exp2);
   sum_aux4=(j^-q)*real(besselj(q,m*lambda1))*(aux_exp1 +aux_exp2);
   end
   if(q==-n)
   aux_exp1= (HighLim -LowLim)*j;%aux_exp1 se resuelve por integral sencilla de 1*dy
   aux_exp2= exp((n-q)*HighLim*j) -exp((n-q)*LowLim*j); aux_exp2=aux_exp2/(n-q);
   sum_aux2=(j^q)*real(besselj(q,m*delta1))*(aux_exp1 +aux_exp2);
   sum_aux4=(j^-q)*real(besselj(q,m*lambda1))*(aux_exp1 +aux_exp2);
   end
   if(q==n)
   aux_exp1= exp((n+q)*HighLim*j) -exp((n+q)*LowLim*j); aux_exp1=aux_exp1/(n+q);
   aux_exp2= (HighLim -LowLim)*j;%aux_exp2 se resuelve por integral sencilla de 1*dy
   sum_aux2=(j^q)*real(besselj(q,m*delta1))*(aux_exp1 +aux_exp2);
   sum_aux4=(j^-q)*real(besselj(q,m*lambda1))*(aux_exp1 +aux_exp2);
   end
   aux2=aux2 +sum_aux2; aux4=aux4 +sum_aux4;
end
aux2=aux2*exp(m*alpha1*j); aux4=-aux4*exp(m*beta1*j);
Sum=Sum + factor*(aux1 +aux2 +aux3 +aux4);
%--------   Fin de I2
%--------   Inicio de I13
factor=(1-K)/2/pi/pi/m; HighLim=pi; LowLim=Phi_l; %(1-K)
aux1= exp(HighLim*n*j) -exp(LowLim*n*j); aux1=aux1*real(besselj(0,m*delta1));
aux1=aux1*exp(m*alpha1*j)/n;
aux3= exp(HighLim*n*j) -exp(LowLim*n*j);   aux3=aux3*real(besselj(0,m*lambda1));
aux3=-aux3*exp(m*beta1*j)/n;
aux2=0; aux4=0;
for q=1:Qbessel
   sum_aux2=0; sum_aux4=0; aux_exp1=0; aux_exp2=0;
   if(q~=abs(n))
   aux_exp1=exp((n+q)*HighLim*j) -exp((n+q)*LowLim*j); aux_exp1=aux_exp1/(n+q);
   aux_exp2=exp((n-q)*HighLim*j) -exp((n-q)*LowLim*j); aux_exp2=aux_exp2/(n-q);
   sum_aux2=(j^q)*real(besselj(q,m*delta1))*(aux_exp1 +aux_exp2);
   sum_aux4=(j^-q)*real(besselj(q,m*lambda1))*(aux_exp1 +aux_exp2);
   end
   if(q==-n)
   aux_exp1= (HighLim -LowLim)*j;%aux_exp1 se resuelve por integral sencilla de 1*dy
   aux_exp2= exp((n-q)*HighLim*j) -exp((n-q)*LowLim*j); aux_exp2=aux_exp2/(n-q);
   sum_aux2=(j^q)*real(besselj(q,m*delta1))*(aux_exp1 +aux_exp2);
   sum_aux4=(j^-q)*real(besselj(q,m*lambda1))*(aux_exp1 +aux_exp2);
   end
   if(q==n)
   aux_exp1= exp((n+q)*HighLim*j) -exp((n+q)*LowLim*j); aux_exp1=aux_exp1/(n+q);
   aux_exp2= (HighLim -LowLim)*j;%aux_exp2 se resuelve por integral sencilla de 1*dy
   sum_aux2=(j^q)*real(besselj(q,m*delta1))*(aux_exp1 +aux_exp2);
   sum_aux4=(j^-q)*real(besselj(q,m*lambda1))*(aux_exp1 +aux_exp2);
   end
   aux2=aux2 +sum_aux2; aux4=aux4 +sum_aux4;
end
aux2=aux2*exp(m*alpha1*j); aux4=-aux4*exp(m*beta1*j);
```

```
Sum=Sum + factor*(aux1 +aux2 +aux3 +aux4);
%--------   Fin de I13
%--------   Inicio de I5 + I4
factor=(1-K)/2/pi/pi/m; HighLim=-pi/2; LowLim=-Phi_l; %(1-K)
aux1= exp(HighLim*n*j) -exp(LowLim*n*j); aux1=aux1*real(besselj(0,m*lambda2));
aux1=aux1*exp(m*beta2*j)/n;
aux3= exp(HighLim*n*j) -exp(LowLim*n*j);   aux3=aux3*real(besselj(0,m*delta2));
aux3=-aux3*exp(m*alpha2*j)/n;
aux2=0; aux4=0;
for q=1:Qbessel
   sum_aux2=0; sum_aux4=0; aux_exp1=0; aux_exp2=0;
   if(q~=abs(n))
   aux_exp1=exp((n+q)*HighLim*j) -exp((n+q)*LowLim*j); aux_exp1=aux_exp1/(n+q);
   aux_exp2=exp((n-q)*HighLim*j) -exp((n-q)*LowLim*j); aux_exp2=aux_exp2/(n-q);
   sum_aux2=(j^-q)*real(besselj(q,m*lambda2))*(aux_exp1 +aux_exp2);
   sum_aux4=(j^q)*real(besselj(q,m*delta2))*(aux_exp1 +aux_exp2);
   end
   if(q==-n)
   aux_exp1= (HighLim -LowLim)*j;%aux_exp1 se resuelve por integral sencilla de 1*dy
   aux_exp2= exp((n-q)*HighLim*j) -exp((n-q)*LowLim*j); aux_exp2=aux_exp2/(n-q);
   sum_aux2=(j^-q)*real(besselj(q,m*lambda2))*(aux_exp1 +aux_exp2);
   sum_aux4=(j^q)*real(besselj(q,m*delta2))*(aux_exp1 +aux_exp2);
   end
   if(q==n)
   aux_exp1= exp((n+q)*HighLim*j) -exp((n+q)*LowLim*j); aux_exp1=aux_exp1/(n+q);
   aux_exp2= (HighLim -LowLim)*j;%aux_exp2 se resuelve por integral sencilla de 1*dy
   sum_aux2=(j^-q)*real(besselj(q,m*lambda2))*(aux_exp1 +aux_exp2);
   sum_aux4=(j^q)*real(besselj(q,m*delta2))*(aux_exp1 +aux_exp2);
   end
   aux2=aux2 +sum_aux2; aux4=aux4 +sum_aux4;
end
aux2=aux2*exp(m*beta2*j); aux4=-aux4*exp(m*alpha2*j);
Sum=Sum + factor*(aux1 +aux2 +aux3 +aux4);
%--------   Fin de I5 + I4
%--------   Inicio de I12 + I11
factor=(1-K)/2/pi/pi/m; HighLim=Phi_l; LowLim=pi/2; %(1-K)
aux1= exp(HighLim*n*j) -exp(LowLim*n*j); aux1=aux1*real(besselj(0,m*lambda2));
aux1=aux1*exp(m*beta2*j)/n;
aux3= exp(HighLim*n*j) -exp(LowLim*n*j);   aux3=aux3*real(besselj(0,m*delta2));
aux3=-aux3*exp(m*alpha2*j)/n;
aux2=0; aux4=0;
for q=1:Qbessel
   sum_aux2=0; sum_aux4=0; aux_exp1=0; aux_exp2=0;
   if(q~=abs(n))
   aux_exp1=exp((n+q)*HighLim*j) -exp((n+q)*LowLim*j); aux_exp1=aux_exp1/(n+q);
   aux_exp2=exp((n-q)*HighLim*j) -exp((n-q)*LowLim*j); aux_exp2=aux_exp2/(n-q);
   sum_aux2=(j^-q)*real(besselj(q,m*lambda2))*(aux_exp1 +aux_exp2);
   sum_aux4=(j^q)*real(besselj(q,m*delta2))*(aux_exp1 +aux_exp2);
   end
   if(q==-n)
   aux_exp1= (HighLim -LowLim)*j;%aux_exp1 se resuelve por integral sencilla de 1*dy
   aux_exp2= exp((n-q)*HighLim*j) -exp((n-q)*LowLim*j); aux_exp2=aux_exp2/(n-q);
   sum_aux2=(j^-q)*real(besselj(q,m*lambda2))*(aux_exp1 +aux_exp2);
   sum_aux4=(j^q)*real(besselj(q,m*delta2))*(aux_exp1 +aux_exp2);
   end
   if(q==n)
```

```
    aux_exp1= exp((n+q)*HighLim*j) -exp((n+q)*LowLim*j); aux_exp1=aux_exp1/(n+q);
    aux_exp2= (HighLim -LowLim)*j;%aux_exp2 se resuelve por integral sencilla de 1*dy
    sum_aux2=(j^-q)*real(besselj(q,m*lambda2))*(aux_exp1 +aux_exp2);
    sum_aux4=(j^q)*real(besselj(q,m*delta2))*(aux_exp1 +aux_exp2);
    end
    aux2=aux2 +sum_aux2; aux4=aux4 +sum_aux4;
end
aux2=aux2*exp(m*beta2*j); aux4=-aux4*exp(m*alpha2*j);
Sum=Sum + factor*(aux1 +aux2 +aux3 +aux4);
%--------   Fin de I12 + I11
% NIVEL -Vdc:
%--------   Inicio de I1 + I3
factor=1/2/pi/pi/m; HighLim=-Phi_l; LowLim=-pi;
aux1= exp(HighLim*n*j) -exp(LowLim*n*j); aux1=aux1*real(besselj(0,m*lambda1));
aux1=aux1*exp(m*beta1*j)/n;
aux3= exp(HighLim*n*j) -exp(LowLim*n*j); aux3=aux3*real(besselj(0,m*delta1));
aux3=-aux3*exp(m*alpha1*j)/n;
aux2=0; aux4=0; sum_aux2=0; sum_aux4=0; aux_exp1=0; aux_exp2=0;
for q=1:Qbessel
    sum_aux2=0; sum_aux4=0; aux_exp1=0; aux_exp2=0;
    if(q~=abs(n))
    aux_exp1=exp((n+q)*HighLim*j) -exp((n+q)*LowLim*j); aux_exp1=aux_exp1/(n+q);
    aux_exp2=exp((n-q)*HighLim*j) -exp((n-q)*LowLim*j); aux_exp2=aux_exp2/(n-q);
    sum_aux2=(j^-q)*real(besselj(q,m*lambda1))*(aux_exp1 +aux_exp2);
    sum_aux4=(j^q)*real(besselj(q,m*delta1))*(aux_exp1 +aux_exp2);
    end
    if(q==-n)
    aux_exp1= (HighLim -LowLim)*j;%aux_exp1 se resuelve por integral sencilla de 1*dy
    aux_exp2= exp((n-q)*HighLim*j) -exp((n-q)*LowLim*j); aux_exp2=aux_exp2/(n-q);
    sum_aux2=(j^-q)*real(besselj(q,m*lambda1))*(aux_exp1 +aux_exp2);
    sum_aux4=(j^q)*real(besselj(q,m*delta1))*(aux_exp1 +aux_exp2);
    end
    if(q==n)
    aux_exp1= exp((n+q)*HighLim*j) -exp((n+q)*LowLim*j); aux_exp1=aux_exp1/(n+q);
    aux_exp2= (HighLim -LowLim)*j;%aux_exp2 se resuelve por integral sencilla de 1*dy
    sum_aux2=(j^-q)*real(besselj(q,m*lambda1))*(aux_exp1 +aux_exp2);
    sum_aux4=(j^q)*real(besselj(q,m*delta1))*(aux_exp1 +aux_exp2);
    end
    aux2=aux2 +sum_aux2; aux4=aux4 +sum_aux4;
end
aux2=aux2*exp(m*beta1*j); aux4=-aux4*exp(m*alpha1*j);
Sum=Sum + factor*(aux1 +aux2 +aux3 +aux4);
%--------   Fin de I1 + I3
%--------   Inicio de I15 + I14
factor=1/2/pi/pi/m; HighLim=pi; LowLim=Phi_l;
aux1= exp(HighLim*n*j) -exp(LowLim*n*j); aux1=aux1*real(besselj(0,m*lambda1));
aux1=aux1*exp(m*beta1*j)/n;
aux3= exp(HighLim*n*j) -exp(LowLim*n*j); aux3=aux3*real(besselj(0,m*delta1));
aux3=-aux3*exp(m*alpha1*j)/n;
aux2=0; aux4=0;
for q=1:Qbessel
    sum_aux2=0; sum_aux4=0; aux_exp1=0; aux_exp2=0;
    if(q~=abs(n))
    aux_exp1=exp((n+q)*HighLim*j) -exp((n+q)*LowLim*j); aux_exp1=aux_exp1/(n+q);
    aux_exp2=exp((n-q)*HighLim*j) -exp((n-q)*LowLim*j); aux_exp2=aux_exp2/(n-q);
    sum_aux2=(j^-q)*real(besselj(q,m*lambda1))*(aux_exp1 +aux_exp2);
```

```
   sum_aux4=(j^q)*real(besselj(q,m*delta1))*(aux_exp1 +aux_exp2);
   end
   if(q==-n)
   aux_exp1= (HighLim -LowLim)*j;%aux_exp1 se resuelve por integral sencilla de 1*dy
   aux_exp2= exp((n-q)*HighLim*j) -exp((n-q)*LowLim*j); aux_exp2=aux_exp2/(n-q);
   sum_aux2=(j^-q)*real(besselj(q,m*lambda1))*(aux_exp1 +aux_exp2);
   sum_aux4=(j^q)*real(besselj(q,m*delta1))*(aux_exp1 +aux_exp2);
   end
   if(q==n)
   aux_exp1= exp((n+q)*HighLim*j) -exp((n+q)*LowLim*j); aux_exp1=aux_exp1/(n+q);
   aux_exp2= (HighLim -LowLim)*j;%aux_exp2 se resuelve por integral sencilla de 1*dy
   sum_aux2=(j^-q)*real(besselj(q,m*lambda1))*(aux_exp1 +aux_exp2);
   sum_aux4=(j^q)*real(besselj(q,m*delta1))*(aux_exp1 +aux_exp2);
   end
   aux2=aux2 +sum_aux2; aux4=aux4 +sum_aux4;
end
aux2=aux2*exp(m*beta1*j); aux4=-aux4*exp(m*alpha1*j);
Sum=Sum + factor*(aux1 +aux2 +aux3 +aux4);
%--------   Fin de I15 + I14
R = Sum;

%%%            END of function FcnCmn   %%%
```

D.2 C_n-Algorithm

```
% This is Matlab script of the program that calculates SFS Cn coefficients in order to
%compose harmonics as well as continuous time domain signal are plotted.
%File Name:    CnBySFSAlgorithm.m
%folder allocation: CnBySFSAlgorithm
close all; clc; clear all;
format long;
Niveles=5;% Maximum number of levels: 5; 4,3 and 2 are permitted.
Alias=50;
Rayas=Alias;   Fmuestreo=50; ciclos=1;

Vdc=50;        K=0.5;          Ma=0.9*Vdc;          Mf=50;

Rayas_ML=zeros(1,Rayas);  % Harmonics for a Multilevel Signal
An=zeros(1,Rayas); % cosine terms
jBn=zeros(1,Rayas); % sinus terms
r1=0.5; r2=0.5; r3=0.5; r4=0.5;%caso 1
% r1=1.0; r2=1.0; r3=1.0; r4=1.0;%caso 2...or any case you wish to test
Fo=50;To=1/Fo;wo=2*pi*Fo;
Fc=Fo*Mf;Tc=To/Mf;wc=wo*Mf;
Fmuestreo=Fmuestreo*Fc;ciclos=ciclos*To;
switch(Niveles)
   case 5
      L1=Vdc;L2=K*Vdc;L3=0;L4=-1*(1-K)*Vdc;L5=-1*Vdc;
   case 4
      L1=Vdc;L2=K*Vdc;L3=-(1-K)*Vdc;L4=-Vdc;L5=0;
   case 3
      L1=Vdc;L2=0;L3=-Vdc;L4=0;L5=0;
   case 2
      L1=Vdc;L2=-Vdc;L3=0;L4=0;L5=0;
```

```
    otherwise
end
paso=To/Mf;
t=0:paso:To;
tTest=zeros(1,Mf+1);
TsampleA=zeros(1,Mf+1);TsampleB=zeros(1,Mf+1);TsampleMidi=zeros(1,Mf+1);
Xdown=zeros(1,Mf+1);Xup=zeros(1,Mf+1);Zonas=zeros(1,Mf+1);
FullSin=zeros(1,Mf+1);
for i=0:Mf
   FullSin(1,i+1)=sin(wo*i*paso)*Ma; % que es lo mismo que
   TsampleMidi(1,i+1)=i*Tc+0.5*Tc;
   SampleMidi(1,i+1)=sin(wo*TsampleMidi(1,i+1))*Ma;
end % for i=0:Mf
% Active TiBuck or Working Zone: Vj and Vj-1
for i=0:Mf
    Aux=SampleMidi(1,i+1);
  if(Aux<=L1&&Aux>L2)
      Lmax=L1;Lmin=L2;r=r1;Zonas(1,i+1)=1;
   elseif(Aux<=L2&&Aux>L3&&Niveles>=3)
      Lmax=L2;Lmin=L3;r=r2;Zonas(1,i+1)=2;
  elseif(Aux<=L3&&Aux>L4&&Niveles>=4)
      Lmax=L3;Lmin=L4;r=r3;Zonas(1,i+1)=3;
   elseif(Aux<=L4&&Aux>L5&&Niveles>=5)
      Lmax=L4;Lmin=L5;r=r4;Zonas(1,i+1)=4;
  end %if
    TsampleA(1,i+1)=i*Tc+0.25*Tc;
  TsampleB(1,i+1)=i*Tc+0.75*Tc;
  SampleA(1,i+1)=Ma*sin(wo*TsampleA(1,i+1));SampleB(1,i+1)=Ma*sin(wo*TsampleB(1,i+1));
   % Secant and Line Intersections
   y1=SampleMidi(1,i+1);   y2=SampleA(1,i+1);   yA=Lmax;   yB=Lmin;
     VoutXdown(1,i+1)=Lmax;
 if(r~=1.0)          %   2*a-M-Lh        Ll-Lh          M-a
   Xdown(1,i+1)=i*Tc +((((2*y2-y1-yA)*(1-r))/(yB-yA-(4*(1-r)*(y1-y2))))*Tc);
    if(Xdown(1,i+1)<i*Tc)
       Xdown(1,i+1)=i*Tc;
    end
    if(Xdown(1,i+1)>=((1-r)*Tc+(i*Tc)))
       Xdown(1,i+1)=i*Tc;        VoutXdown(1,i+1)=Lmin;
    end
 else
    Xdown(1,i+1)=i*Tc;
    if(y2<yB)
       VoutXdown(1,i+1)=Lmin;
    end
 end
   y1=SampleMidi(1,i+1);        y2=SampleB(1,i+1);     yA=Lmax;       yB=Lmin;
   VoutXup(1,i+1)=Lmin;
 if(r~=0.0)         %Lh-Ll     3*M-2*b  -Lh     Lh-Ll       b-M
    Xup(1,i+1)=i*Tc+((yA-yB+(r*(3*y1-2*y2-yA)))/(yA-yB-(4*r*(y2-y1)))*Tc);
   if(Xup(1,i+1)>(i+1)*Tc)
    Xup(1,i+1)=(i+1)*Tc;          VoutXup(1,i+1)=Lmax;
   end
   if(Xup(1,i+1)<=((1-r)*Tc+(i*Tc)))
    Xup(1,i+1)=(i+1)*Tc;
   end
 else
```

```
    Xup(1,i+1)=(i+1)*Tc;
    if(y2>yB)
        VoutXdown(1,i+1)=Lmax;
     end
 end
end % for i=1:Mf+1
%%% Continuos Time Domain Output Signal %%%
Hi=0.0;Lo=0.0;
a=0;b=0;aux1=0;aux2=0;aux3=0;aux4=0;
for n=1:Rayas % n-esim harmonic calculation
    a=0;b=0; A00=0;
    for m=1:Mf % ti  Mf-1
       A00=A00+( VoutXdown(1,m)   *(Xup(1,m)   -Xdown(1,m)   )...
            +VoutXup(1,m)  *(Xdown(1,m) -((m-1)*Tc)  )...
            +VoutXup(1,m) *((m*Tc)    -Xup(1,m)   ) );
      a=a+(VoutXdown(1,m)*(sin(n*wo*Xup(1,m))-sin(n*wo*Xdown(1,m)))...
        +VoutXup(1,m)*(sin(n*wo*Xdown(1,m))-sin(n*wo*(m-1)*Tc)+sin(n*wo*m*Tc)-
sin(n*wo*Xup(1,m))))/n;
     b=b+(VoutXdown(1,m)*(cos(n*wo*Xdown(1,m))-cos(n*wo*Xup(1,m)))...
        +VoutXup(1,m)*(cos(n*wo*(m-1)*Tc)-cos(n*wo*Xdown(1,m))+cos(n*wo*Xup(1,m))-
cos(n*wo*m*Tc)))/n;
    end % for t=1:Mf
    a=a/To/wo;b=b/To/wo;
    An(1,n)=a;jBn(1,n)=b;
end % fn=1:Rayas
Cn=abs(An+j*jBn);
% % Harmonics visualization
figure(5);
 stem(An(1:Rayas),'xr'); %colores por m,k,b,r
 title('Componentes Reales');
 grid;
 %          %%% Time Domain OutPut Signals %%%
to=0:1/Fmuestreo:ciclos;
Vo=zeros(1,Fmuestreo*ciclos+1);
VoCos=zeros(1,Fmuestreo*ciclos+1);
VoSin=zeros(1,Fmuestreo*ciclos+1);
aux_cos=0;aux_sin=0;aux_angle=0;
for z=1:Fmuestreo*ciclos+1  % instante t(z-1)
    for Arm=1:Rayas
        aux_angle=2*pi*Fo*Arm*to(z);
        aux_cos=An(Arm)*cos(aux_angle);
        VoCos(z)=VoCos(z)+aux_cos;
        aux_sin=jBn(Arm)*sin(aux_angle);
        VoSin(z)=VoSin(z)+aux_sin;
    end
end
Vo=VoCos+VoSin;
Vo=2*Vo; % Cn=1/2(An +jBn) and C-n=1/2(An -jBn)
clear aux_cos;  clear aux_sin;  clear aux_angle;
figure(7);plot(to,Vo);grid;
figure(8);
stem(1.41421356*Cn(1:Rayas),'.r'); %1.41421356 para osciloscopio
title(['Cn for Ma=',num2str(Ma/Vdc),' K=',num2str(K),' r1=',num2str(r1),' r2=',num2str(r2),'
r3=',num2str(r3),' r4=',num2str(r4)],'Color','b'); grid;
axis([-2 150 0 16]);%Ma/10
Thd=zeros(1,100); Wthd0=zeros(1,100);
```

```
THD10=sqrt(sum(abs(Cn(2:10)).^2))/(Cn(1,1))*100;
THD100=sqrt(sum(abs(Cn(2:40)).^2))/(Cn(1,1))*100;
figure (8);
text(50,2.7+10 ,['h=10: THD%=',num2str(THD10)],'FontSize',14);
text(50,1.7+9 ,['h=40: THD%=',num2str(THD100)],'FontSize',14);
figure(9);
semilogy(1.41421356*Cn(1:Rayas),'*k');hold;
semilogy(1.41421356*Cn(1:Rayas),'r-');
grid;
axis([0 150 0.01 100]);
text(74,30 ,['h=10: THD%=',num2str(THD10)],'FontSize', 14,'BackgroundColor',[1 1
1],'EdgeColor','black');
text(67,10 ,['h=100: THD%=',num2str(THD100)],'FontSize',14,'BackgroundColor',[1 1
1],'EdgeColor','black');
title(['Cn-Algorithm Ma=',num2str(Ma/Vdc),' K=',num2str(K),' r1=',num2str(r1),' r2=',num2str(r2),'
r3=',num2str(r3),' r4=',num2str(r4)],'Color','b','FontSize',12);
%%%             END of CnBySFSAlgorithm.m %%%
```

D.3 Genetic Algorithm For Matrix (M_a,K)

```
% This is Matlab script of the program that executes the GA in order to build up the matrix with two-
%dimensional range 0.7≤Ma≤1.0 and 0.3≤K≤0.7.
% 63 points can be calculated if resolution=0.05, 221 points can be calculated if resolution=0.025

% "CiclosEvolutivo.m" builds up the matrix by calling Master Program "evolutivo.m"
% then Master Program calls the funtions: " modulador5nivelesSSThdPasos.m"
%                                          and : " modulador5nivelesSSThdRstandard.m"
%harmonics are calculated using the same strategy of Cn-Algorithm

%folder allocation: GeneticAlgorithmForMatrixMaK

%%%             CiclosEvolutivo.m    %%%
clear;    clc;      tic;
for Cm=0.8:0.025:0.9
   for Ck=0.4:0.025:0.5
      ck=Ck; cm=Cm;
      evolutivo(ck,cm)
   end%for k=0.3:0.1:0.7
end%for m=0.8:0.1:1.0
tiempo=toc% tic and toc functions calculate the total execution time
load handel
sound(y,Fs)
%%%             END of CiclosEvolutivo.m    %%%

%%%             evolutivo.m    %%%
function [] = evolutivo(ck,cm)

format long
%condiciones electricas de operacion
pK=ck;%0.5; %distribucion niveles
pMa=cm;%modulacion amplitud
%IMPORTANTE,
pn=10; %armonicos sumatoria de THD, por escalones, cumpliendo requisito minimo
pVdc=50;     pMf=50;   pNiveles=5;
```

ISBN:978-84-693-7665-2/DL:T.1747-2010


```
pAlias=pn+2;%armonicos a considerar en espectro, Ejemplo: si THD considera n armonicos,
pAlias>=n+10;
pVdc=50;    pMf=50;   pNiveles=5;
[Thd10min,Thd11a20min,Thd21a30min,Thd31a40min]=modulador5nivelesSSThdRstandard(pVdc,p
K,pMa,pMf,pAlias,pNiveles,pn);
% ingreso de datos del algoritmo %
%poblacion forzada: hacer pf=1, lo contrario:pf=0;
pf=0;
%poblacion inicial
N=80;
%poblacion maxima a la que crece la poblacion
N_max=200;
%número de generaciones
G=500;
%variables a optimizar
vopt=4;
TasaMutacion=0.05;
%la variancia de la mutacion
variancia=0.2;
%%%%%%%%%%%%%%%%%%%%%%%%%%%%%%%%
% creacion de las poblaciones %
%%%%%%%%%%%%%%%%%%%%%%%%%%%%%%%%
%matriz de poblacion de soluciones
C=zeros(N,vopt);
% selecciono el el rango de cada una de las variables %
% k1 k2 k3 k4 A K
v_min=[0 0 0 0];
v_max=[1 1 1 1];
% creacion de la poblacion inicial aleatoria % POBLACION FORZADA
cnt=0;
for t3=0:0.5:1
    for t2=0:0.5:1
        for t1=0:0.5:1
            for t0=0:0.5:1
             cnt=cnt+1;
             RsTest(cnt,:)=[t3 t2 t1 t0];
            end
        end
    end
end
% MPF=[0.5 0.5 0.5 0.5; 1 1 1 1; 0 0 0 0; 0.75 0.75 0.75 0.75; 0.25 0.25 0.25 0.25;...
%          0.5 0 0 0.5; 0 0.5 0.5 0; 0 1 1 0; 1 0 0 1; 1 0.5 0.5 1; 0.5 1 1 0.5; 0 0 0.5 0.5;...
%           0 0 1 1; 0.5 0.5 0 0; 0.5 0.5 1 1; 1 1 0 0; 1 1 0.5 0.5; 0 0.5 1 0; 0 1 0.5 1];
MPF=RsTest;
if pf==1
    [a,b]=size(MPF);
    C(1:a,:)=MPF;
    for i=a+1:N
        C(i,:)=(((v_max-v_min)'.*rand(vopt,1))+v_min')';
    end
    for i=1:N
L(i,1)=modulador5nivelesSSThdPasos(C(i,:),pVdc,pK,pMa,pMf,pAlias,pNiveles,pn,Thd10min,Thd11
a20min,Thd21a30min,Thd31a40min);
    end
else
    for i=1:N
```

```
      C(i,:)=(((v_max-v_min)'.*rand(vopt,1))+v_min')';
L(i,1)=modulador5nivelesSSThdPasos(C(i,:),pVdc,pK,pMa,pMf,pAlias,pNiveles,pn,Thd10min,Thd11
a20min,Thd21a30min,Thd31a40min);
   end
end
%     while C(i,5)<C(i,6) | C(i,5)<abs(1-C(i,6))
%       C(i,:)=(((v_max-v_min)'.*rand(6,1))+v_min')';
%     end
 % Evalua la función objetivo para cada individuo  %
L(i,1)=modulador5nivelesSSThdPasos(C(i,:),pVdc,pK,pMa,pMf,pAlias,pNiveles,pn,Thd10min,Thd11
a20min,Thd21a30min,Thd31a40min);
   %end
% encumbente inicial %
 [a1,a2]=min(L);
En(1,1)=a1;             %almacena el valor minimo
En(1,2:(vopt+1))=C(a2,:); %almacena el valor de los parametros
En(1,(vopt+2))=1;              %almacena la generación en la que ocurrio
En(1,(vopt+3))=TasaMutacion;              %almacena la Tasa Mutacion
Solucion.valor_minimo=En(1,1);
Solucion.r1=En(1,2);
Solucion.r2=En(1,3);
Solucion.r3=En(1,4);
Solucion.r4=En(1,5);
% Solucion.A=En(1,6);
% Solucion.K=En(1,7);
Solucion.generacion=En(1,6);
Solucion;%descomentar para pantallazo
% generaciones %
for gen=1:G
   if gen~=1
%       if (gen>10) % REDUCIR POBLACION
%          N=20; N_max=50;
%       end
      % encumbente %
      [b1,b2]=size(En);
      if min(L(1,1)) < En(b1,1)
         [a1,a2]=min(L);
         En(b1+1,1)=a1;            %almacena el valor minimo
         En(b1+1,2:(vopt+1))=C(a2,:);      %almacena el valor de los parametros
         En(b1+1,(vopt+2))=gen;           %almacena la generación en la que ocurrio
         En(b1+1,(vopt+3))=TasaMutacion; %almacena la Tasa de Mutacion nueva
         clc;%quitar ;coma para pantallazo
         Solucion.valor_minimo=En(b1+1,1);
         Solucion.r1=En(b1+1,2);
         Solucion.r2=En(b1+1,3);
         Solucion.r3=En(b1+1,4);
         Solucion.r4=En(b1+1,5);
          if ((gen>300) & (b1-10)>10)
          distanciaGen=En(b1,6)-En(b1-10,6);
            if distanciaGen>5
               distanciaThd=abs(En(b1,1)-En(b1-10,1));
%                 cambio=distanciaThd/En(b1-10,1)*100;% en porcentaje %
               cambio=distanciaThd/En(b1-10,1)/(En(b1,6)-En(b1-10,6))*100;
               if cambio<20/100%por cada cien genraciones
               TasaMutacion=TasaMutacion + 0.05;
               variancia=variancia + 0.05;
```

UNIVERSITAT ROVIRA I VIRGILI
CONTRIBUTIONS ON SPECTRAL CONTROL FOR THE ASYMMETRICAL FULL BRIDGE MULTILEVEL INVERTER
Oscar Mauricio Muñoz Ramírez
ISBN:978-84-693-7665-2/DL:T.1747-2010


```
                if TasaMutacion>0.5
                    TasaMutacion=0.05;variancia=0.3;
                end
              %TasaMutacion=TasaMutacion + 0.1*rand;
              %TasaMutacion=0.2*rand;
              end
            end
        end
%           Solucion.A=En(b1+1,6);
%           Solucion.K=En(b1+1,7);
          Solucion.generacion=En(b1+1,6);
          Solucion.Mutacion=En(b1+1,7);
          Solucion.iteracion=gen;
          Solucion;%quitar ;coma para pantallazo
       else
          clc;%quitar ;coma para pantallazo
          Solucion.iteracion=gen;
          Solucion;%quitar ;coma para pantallazo
       end
    end
    % recombinacion %
    Cn=C;
    for i=N+1:2:N_max
       v=3;
       a=round(rand*(length(C)-1)+1); %selecciono un individuo en forma aleatoria
       b=round(rand*(length(C)-1)+1); %selecciono otro individuo en forma aleatoria
       for w=1:size(C,2)
          mu=rand;
          if mu<=0.5
             beta=(2*mu)^(1/(v+1));
          else
             beta=(1/(2*(1-mu)))^(1/(v+1));
          end
          Cn(i,w)=0.5*((1+beta)*C(a,w)+(1-beta)*C(b,w));
          Cn(i+1,w)=0.5*((1-beta)*C(a,w)+(1+beta)*C(b,w));
          if Cn(i,w)> v_max(w)
             Cn(i,w)= v_max(w);
          end
          if Cn(i,w)< v_min(w)
             Cn(i,w)= v_min(w);
          end
          if Cn(i+1,w)> v_max(w)
             Cn(i+1,w)= v_max(w);
          end
          if Cn(i+1,w)< v_min(w)
             Cn(i+1,w)= v_min(w);
          end
       end
    end
    Ln=L;
    %for i=N+1:N_max
    for i=1:N_max
   % Evalua la función objetivo para cada individuo %
Ln(i,1)=modulador5nivelesSSThdPasos(Cn(i,:),pVdc,pK,pMa,pMf,pAlias,pNiveles,pn,Thd10min,Thd
11a20min,Thd21a30min,Thd31a40min);
    end
```

UNIVERSITAT ROVIRA I VIRGILI
CONTRIBUTIONS ON SPECTRAL CONTROL FOR THE ASYMMETRICAL FULL BRIDGE MULTILEVEL INVERTER
Oscar Mauricio Muñoz Ramírez
ISBN:978-84-693-7665-2/DL:T.1747-2010


```
      % Función de selección
       %%%%%%%%%%%%%%%%%%%%%%%%%%%
  for i=1:N
    [a,b]=min(Ln); %determino el minimo y la posición
    L(i,1)=a;
    C(i,:)=Cn(b,:);
    Ln(b,1)=inf;
  end
  % mutacion %
   for i=1:N % mutacion para la poblacion elite
%     for i=N+1:N_max % mutacion para la poblacion descendiente
      if rand < TasaMutacion%0.15%tasa de mutacion 5antes en 0.05
         a=round(rand*(vopt-1))+1;
         C(i,a)= Cn(i,a)+sqrt(variancia)*randn; %realizo una mutación de una componente del
individuo
         if C(i,a)> v_max(a)
            C(i,a)= v_max(a);
         end
         if C(i,a)< v_min(a)
            C(i,a)= v_min(a);
         end
         Mutantes(gen,:)=C(i,:);
        % Evalua la función objetivo para cada individuo %
L(i,1)=modulador5nivelesSSThdPasos(C(i,:),pVdc,pK,pMa,pMf,pAlias,pNiveles,pn,Thd10min,Thd11
a20min,Thd21a30min,Thd31a40min);
      end
   end
  save seguridad
end%termina el ciclo de genes
IndexMa=num2str(floor(pMa*10000));  IndexK=num2str(floor(pK*10000));
cadena=[ 'puntoMa0',IndexMa,'K0',IndexK ];
save (cadena);
%%%            END of evolutivo.m    %%%

%%%   modulador5nivelesSSThdPasos.m    %%%
function [THDn] =
modulador5nivelesSSThdPasos(C,pVdc,pK,pMa,pMf,pAlias,pNiveles,pn,Thd10min,Thd11a20min,Th
d21a30min,Thd31a40min)
%SFS: Cn, donde n es un multiplo de la fundamental, Fo
r1=C(1);          r2=C(2);          r3=C(3);          r4=C(4);
%constantes
Vdc=pVdc;      K=pK;  Ma=pMa*Vdc;          Mf=pMf;
n=pn;             Niveles=pNiveles;                Alias=pAlias;%20;
Rayas=Alias;
Rayas_ML=zeros(1,Rayas);  % Harmonics for a Multilevel Signal
An=zeros(1,Rayas); % terminos coseno o Reales
jBn=zeros(1,Rayas); % terminos senos o Imaginarios
Arm=zeros(1,Rayas);
Fo=50;To=1/Fo;Tc=To/Mf;
wo=2*pi*Fo;
switch(Niveles)
   case 5
      L1=Vdc;L2=K*Vdc;L3=0;L4=-1*(1-K)*Vdc;L5=-1*Vdc;
   case 4
      L1=Vdc;L2=K*Vdc;L3=-(1-K)*Vdc;L4=-Vdc;L5=0;
   case 3
```

```
        L1=Vdc;L2=0;L3=-Vdc;L4=0;L5=0;
    case 2
        L1=Vdc;L2=-Vdc;L3=0;L4=0;L5=0;
     otherwise
end
paso=To/Mf;t=0:paso:To;
TsampleA=zeros(1,Mf+1);TsampleB=zeros(1,Mf+1);TsampleMidi=zeros(1,Mf+1);
Xdown=zeros(1,Mf+1);Xup=zeros(1,Mf+1);Zonas=zeros(1,Mf+1);
FullSin=zeros(1,Mf+1);
for i=0:Mf
   FullSin(1,i+1)=sin(wo*i*paso)*Ma;    TsampleMidi(1,i+1)=i*Tc+0.5*Tc;
   SampleMidi(1,i+1)=sin(wo*TsampleMidi(1,i+1))*Ma;
end % for i=0:Mf
% Determinar Zonas
for i=0:Mf
     Aux=SampleMidi(1,i+1);
  if(Aux<=L1&&Aux>L2)
       Lmax=L1;Lmin=L2;r=r1;Zonas(1,i+1)=1;
   elseif(Aux<=L2&&Aux>L3&&Niveles>=3)
       Lmax=L2;Lmin=L3;r=r2;Zonas(1,i+1)=2;
  elseif(Aux<=L3&&Aux>L4&&Niveles>=4)
       Lmax=L3;Lmin=L4;r=r3;Zonas(1,i+1)=3;
   elseif(Aux<=L4&&Aux>L5&&Niveles>=5)
       Lmax=L4;Lmin=L5;r=r4;Zonas(1,i+1)=4;
  end %if
  TsampleA(1,i+1)=i*Tc+0.25*Tc;   TsampleB(1,i+1)=i*Tc+0.75*Tc;
  SampleA(1,i+1)=Ma*sin(wo*TsampleA(1,i+1));SampleB(1,i+1)=Ma*sin(wo*TsampleB(1,i+1));
   y1=SampleMidi(1,i+1);    y2=SampleA(1,i+1);    yA=Lmax;    yB=Lmin;
   VoutXdown(1,i+1)=Lmax;
 if(r~=1.0)
   Xdown(1,i+1)=i*Tc +((((2*y2-y1-yA)*(1-r))/(yB-yA-(4*(1-r)*(y1-y2))))*Tc);
    if(Xdown(1,i+1)<i*Tc)
       Xdown(1,i+1)=i*Tc;
    end
    if(Xdown(1,i+1)>=((1-r)*Tc+(i*Tc)))
       Xdown(1,i+1)=i*Tc;         VoutXdown(1,i+1)=Lmin;
    end
else
    Xdown(1,i+1)=i*Tc;
    if(y2<yB)
       VoutXdown(1,i+1)=Lmin;
    end
 end
  y1=SampleMidi(1,i+1); y2=SampleB(1,i+1);  yA=Lmax;        yB=Lmin;
  VoutXup(1,i+1)=Lmin;
 if(r~=0.0)
   Xup(1,i+1)=i*Tc+((yA-yB+(r*(3*y1-2*y2-yA)))/(yA-yB-(4*r*(y2-y1)))*Tc);
   if(Xup(1,i+1)>(i+1)*Tc)
     Xup(1,i+1)=(i+1)*Tc;          VoutXup(1,i+1)=Lmax;
   end
  if(Xup(1,i+1)<=((1-r)*Tc+(i*Tc)))
     Xup(1,i+1)=(i+1)*Tc;
   end
 else
   Xup(1,i+1)=(i+1)*Tc;
   if(y2<yB)% activada en Nov22de2009
```

```
        VoutXup(1,i+1)=Lmin
        VoutXdown(1,i+1)=Lmin;
        %VoutXdown(1,i+1)=Lmax;
    end
 end
end % for i=1:Mf+1
Hi=0.0;Lo=0.0;
a=0;b=0;aux1=0;aux2=0;aux3=0;aux4=0;
for n=1:Rayas % n-esim harmonic calculation
   a=0;b=0;
   for m=1:Mf
     a=a+(VoutXdown(1,m)*(sin(n*wo*Xup(1,m))-sin(n*wo*Xdown(1,m)))...
        +VoutXup(1,m)*(sin(n*wo*Xdown(1,m))-sin(n*wo*(m-1)*Tc)+sin(n*wo*m*Tc)-
sin(n*wo*Xup(1,m))))/n;
     b=b+(VoutXdown(1,m)*(cos(n*wo*Xdown(1,m))-cos(n*wo*Xup(1,m)))...
        +VoutXup(1,m)*(cos(n*wo*(m-1)*Tc)-cos(n*wo*Xdown(1,m))+cos(n*wo*Xup(1,m))-
cos(n*wo*m*Tc)))/n;
   end % for t=1:Mf
   a=a/To/wo;b=b/To/wo;
   An(1,n)=a;jBn(1,n)=b;
end % fn=1:Rayas
Arm=abs(An+j*jBn);
n=pn;
%%%%%%%%%%%%%%%%    ArmR05=abs(An+j*jBn);
THDn=sqrt(sum(abs(Arm(2:10)).^2))/(Arm(1,1))*100;
auxTest=sqrt(sum(abs(Arm(3:10)).^2))/(Arm(1,1))*100;
 if ( auxTest >= Thd10min)
 THDn=THDn+THDn/100;
 end
 auxTest=sqrt(sum(abs(Arm(11:20)).^2))/(Arm(1,1))*100;
 if ( auxTest >= Thd11a20min)
 THDn=THDn+THDn/100;
 end
 auxTest=sqrt(sum(abs(Arm(21:30)).^2))/(Arm(1,1))*100;
 if ( auxTest >= Thd21a30min)
 THDn=THDn+THDn/100;
 end
 auxTest=sqrt(sum(abs(Arm(31:40)).^2))/(Arm(1,1))*100;
 if ( auxTest >= Thd31a40min)
 THDn=THDn+THDn/100;
 end

%%%   END of   modulador5nivelesSSThdPasos.m    %%%

%%%   modulador5nivelesSSThdRstandard.m      %%%
function [Thd10,Thd11a20,Thd21a30,Thd31a40] =
modulador5nivelesSSThdRstandard(pVdc,pK,pMa,pMf,pAlias,pNiveles,pn)

%SFS:Cn, donde n es un multiplo de la fundamental, Fo
%constantes
Vdc=pVdc;      K=pK;          Ma=pMa*Vdc;          Mf=pMf;
n=pn;          Niveles=pNiveles;                   Alias=pAlias;%20;
Rayas=Alias;
Rayas_ML=zeros(1,Rayas);  % Harmonics for a Multilevel Signal
An=zeros(1,Rayas); % terminos coseno o Reales
jBn=zeros(1,Rayas); % terminos senos o Imaginarios
```

```
Arm=zeros(1,Rayas);
Fo=50;To=1/Fo;Tc=To/Mf;
wo=2*pi*Fo;
r1=0.5; r2=0.5; r3=0.5; r4=0.5;
ArmR05=zeros(1,Rayas);
switch(Niveles)
   case 5
      L1=Vdc;L2=K*Vdc;L3=0;L4=-1*(1-K)*Vdc;L5=-1*Vdc;
   case 4
      L1=Vdc;L2=K*Vdc;L3=-(1-K)*Vdc;L4=-Vdc;L5=0;
   case 3
      L1=Vdc;L2=0;L3=-Vdc;L4=0;L5=0;
   case 2
      L1=Vdc;L2=-Vdc;L3=0;L4=0;L5=0;
    otherwise
end
paso=To/Mf;t=0:paso:To;
TsampleA=zeros(1,Mf+1);TsampleB=zeros(1,Mf+1);TsampleMidi=zeros(1,Mf+1);
Xdown=zeros(1,Mf+1);Xup=zeros(1,Mf+1);Zonas=zeros(1,Mf+1);
FullSin=zeros(1,Mf+1);
for i=0:Mf
   FullSin(1,i+1)=sin(wo*i*paso)*Ma; % que es lo mismo que
   TsampleMidi(1,i+1)=i*Tc+0.5*Tc;
   SampleMidi(1,i+1)=sin(wo*TsampleMidi(1,i+1))*Ma;
end % for i=0:Mf
for i=0:Mf
     Aux=SampleMidi(1,i+1);
  if(Aux<=L1&&Aux>L2)
      Lmax=L1;Lmin=L2;r=r1;Zonas(1,i+1)=1;
   elseif(Aux<=L2&&Aux>L3&&Niveles>=3)
      Lmax=L2;Lmin=L3;r=r2;Zonas(1,i+1)=2;
  elseif(Aux<=L3&&Aux>L4&&Niveles>=4)
      Lmax=L3;Lmin=L4;r=r3;Zonas(1,i+1)=3;
   elseif(Aux<=L4&&Aux>L5&&Niveles>=5)
      Lmax=L4;Lmin=L5;r=r4;Zonas(1,i+1)=4;
  end %if
  TsampleA(1,i+1)=i*Tc+0.25*Tc;
  TsampleB(1,i+1)=i*Tc+0.75*Tc;
  SampleA(1,i+1)=Ma*sin(wo*TsampleA(1,i+1));SampleB(1,i+1)=Ma*sin(wo*TsampleB(1,i+1));
   y1=SampleMidi(1,i+1); y2=SampleA(1,i+1); yA=Lmax; yB=Lmin;
   VoutXdown(1,i+1)=Lmax;
 if(r~=1.0)
   Xdown(1,i+1)=i*Tc +((((2*y2-y1-yA)*(1-r))/(yB-yA-(4*(1-r)*(y1-y2))))*Tc);
    if(Xdown(1,i+1)<i*Tc)
       Xdown(1,i+1)=i*Tc;
    end
    if(Xdown(1,i+1)>=((1-r)*Tc+(i*Tc)))
       Xdown(1,i+1)=i*Tc;        VoutXdown(1,i+1)=Lmin;
    end
 else
    Xdown(1,i+1)=i*Tc;
    if(y2<yB)
       VoutXdown(1,i+1)=Lmin;
    end
 end
   y1=SampleMidi(1,i+1);        y2=SampleB(1,i+1);     yA=Lmax;        yB=Lmin;
```

UNIVERSITAT ROVIRA I VIRGILI
CONTRIBUTIONS ON SPECTRAL CONTROL FOR THE ASYMMETRICAL FULL BRIDGE MULTILEVEL INVERTER
Oscar Mauricio Muñoz Ramírez
ISBN:978-84-693-7665-2/DL:T.1747-2010


```
  VoutXup(1,i+1)=Lmin;
 if(r~=0.0)
   Xup(1,i+1)=i*Tc+((yA-yB+(r*(3*y1-2*y2-yA)))/(yA-yB-(4*r*(y2-y1)))*Tc);
   if(Xup(1,i+1)>(i+1)*Tc)
     Xup(1,i+1)=(i+1)*Tc;
     VoutXup(1,i+1)=Lmax;
   end
  if(Xup(1,i+1)<=((1-r)*Tc+(i*Tc)))
     Xup(1,i+1)=(i+1)*Tc;
 end
 else
   Xup(1,i+1)=(i+1)*Tc;
   if(y2<yB)
       VoutXup(1,i+1)=Lmin;
       VoutXdown(1,i+1)=Lmin;
       %VoutXdown(1,i+1)=Lmax;
    end
 end
end % for i=1:Mf+1
Hi=0.0;Lo=0.0;
a=0;b=0;aux1=0;aux2=0;aux3=0;aux4=0;
for n=1:Rayas % n-esim harmonic calculation
   a=0;b=0;
   for m=1:Mf % ti  Mf-1???
     a=a+(VoutXdown(1,m)*(sin(n*wo*Xup(1,m))-sin(n*wo*Xdown(1,m)))...
        +VoutXup(1,m)*(sin(n*wo*Xdown(1,m))-sin(n*wo*(m-1)*Tc)+sin(n*wo*m*Tc)-
sin(n*wo*Xup(1,m))))/n;
     b=b+(VoutXdown(1,m)*(cos(n*wo*Xdown(1,m))-cos(n*wo*Xup(1,m)))...
        +VoutXup(1,m)*(cos(n*wo*(m-1)*Tc)-cos(n*wo*Xdown(1,m))+cos(n*wo*Xup(1,m))-
cos(n*wo*m*Tc)))/n;
   end % for t=1:Mf
   a=a/To/wo;b=b/To/wo;
   An(1,n)=a;jBn(1,n)=b;
end % fn=1:Rayas
ArmR05=abs(An+j*jBn);
Thd10=sqrt(sum(abs(ArmR05(2:10)).^2))/(ArmR05(1,1))*100;
Thd11a20=0;%sqrt(sum(abs(ArmR05(11:20)).^2))/(ArmR05(1,1))*100;
Thd21a30=0;%sqrt(sum(abs(ArmR05(21:30)).^2))/(ArmR05(1,1))*100;
Thd31a40=0;%sqrt(sum(abs(ArmR05(31:40)).^2))/(ArmR05(1,1))*100;
%%%   END of   modulador5nivelesSSThdRstandard.m %%%
```

UNIVERSITAT ROVIRA I VIRGILI
CONTRIBUTIONS ON SPECTRAL CONTROL FOR THE ASYMMETRICAL FULL BRIDGE MULTILEVEL INVERTER
Oscar Mauricio Muñoz Ramírez
ISBN:978-84-693-7665-2/DL:T.1747-2010

UNIVERSITAT ROVIRA I VIRGILI
CONTRIBUTIONS ON SPECTRAL CONTROL FOR THE ASYMMETRICAL FULL BRIDGE MULTILEVEL INVERTER
Oscar Mauricio Muñoz Ramírez
ISBN:978-84-693-7665-2/DL:T.1747-2010

APPENDIX E. TMS32F2812 Source Code (DSP)

Pseudo-Natural Modulator in TMS320F2812

```
#include "stdio.h"
#include "DSP281x_Device.h"     // DSP281x Headerfile Include File
#include "DSP281x_Examples.h"   // DSP281x Examples Include File
#include "qmath.h"
#include "math.h"
#define MaxCuentas    30000 // scale for 400us
#define Retardo       15
#define FactorCuentas 22.8 //29993cuentas/1310 (1 periodo de portadora, To/Mf)
#define UnidadesTc    1310.68  // 65536cuentas/Mf
#define PI 3.1415926535  // from Wikipedia: 3.14159 26535...

char tecla=0;
float Ma=0.9,K=0.7;
//float r=0.5,r1=0.5,r2=0.5,r3=0.5,r4=0.5; //Caso 1
//      set of carriers can be modified like this:
//float r=0.5,r1=1.0,r2=0.0,r3=0.47177,r4=0.0;          //CaseOpt1:Ma08 K05 Thd,n=40

unsigned Zona=0,MaUp=0,MaDown=0,CheckZonaActual=0,CheckZonaBefore=0;
unsigned NivelBajo=0,NivelAlto=0;
unsigned
contaT0=0,contaT1PER=0,contaT1CNT=0,i=0,reversa=0,Cocientes1Zero=0,Cocientes2Zero=0;
int portadora,auxI;
unsigned
contadorZ1=0,contadorZ2=0,contadorZ3=0,contadorZ4=0,contadorZonasOff=0,MilesCiclos=0;
Uint16 ciclos=0,ciclos1=0,ciclos2=0,ciclos3=0,ciclos4=0,ciclos5=0;
Uint16 Xd[50],Xu[50],pulse[50],testigo1[50],testigo2[50],testigopulse[50];
Uint16 PeriodoContador[50],CompararContador[50],UnomenosrTc=0;
Uint16 Mf=50,temp,PasoDeZonas[50],TestContador[50];
int contador=0,contador1=0,contador2=0,contador3=0,contador4=0,contador5=0;
float TablaSeno[50],MaSeno[50],TablaSeno_a[50],TablaSeno_b[50];
float step=0,stepMedio=0,angulo[50],angulo_a[50],angulo_b[50]; // formato flotante
float Lh,Ll,M,a,b,c,d,LimiteKE=0,Limite1menosKE=0;
float
temp1,temp2,temp3,cociente1[50],cociente2[50],cociente1num[50],cociente1den[50],cociente2num[5
0],cociente2den[50];
float auxr,aux1,aux2,aux4,Aux5,c1,c2,pos1,pos2;
// Prototype statements for functions found within this file.
interrupt void cpu_timer0_isr(void);
interrupt void IntTimer1_ISR(void);
void CalcularLhLl(void);   void DeterminarZona(void);
void ModularZonas(void);   void ModularZonasOFF(void);
void init_eva(void);
void main(void)
{
// Step 1. Initialize System Control:
  InitSysCtrl();
// Step 2. Initalize GPIO:
  EALLOW;
  GpioMuxRegs.GPAMUX.all = 0x00FF;        GpioMuxRegs.GPBMUX.all = 0x0000;
  GpioMuxRegs.GPDMUX.all = 0x0000;        GpioMuxRegs.GPEMUX.all = 0x0000;
```

```
   GpioMuxRegs.GPFMUX.all = 0x0000;        GpioMuxRegs.GPGMUX.all = 0x0000;
   GpioMuxRegs.GPADIR.all=0x18FF;          GpioMuxRegs.GPBDIR.all=0x00FF;
   GpioMuxRegs.GPDDIR.all=0x0000;          GpioMuxRegs.GPEDIR.all=0x0001;
   GpioMuxRegs.GPFDIR.all=0x03FF;          GpioMuxRegs.GPGDIR.all=0x0000;
   EDIS;
// Step 3. Clear all interrupts and initialize PIE vector table:
// Disable CPU interrupts
   DINT;
// Initialize the PIE control registers to their default state.
   InitPieCtrl();
// Disable CPU interrupts and clear all CPU interrupt flags:
   IER = 0x0000;   IFR = 0x0000;
// Initialize the PIE vector table with pointers to the shell
// Interrupt Service Routines (ISR).
   InitPieVectTable();
// Interrupts that are used in this example are re-mapped to
// ISR functions found within this file.
   EALLOW;  // This is needed to write to EALLOW protected registers
   PieVectTable.TINT0 = &cpu_timer0_isr;
   PieVectTable.T1PINT = &IntTimer1_ISR;
   EDIS;    // This is needed to disable write to EALLOW protected registers
// Step 4. Initialize all the Device Peripherals:
// InitPeripherals(); // Not required for this example
   InitCpuTimers(); // This function is found in DSP281x_InitPeripherals.c
// Configure CPU-Timer 0 to interrupt every second:
// 100MHz CPU Freq, Period (in uSeconds)
   ConfigCpuTimer(&CpuTimer0,150,400);
//   StartCpuTimer0();
// Step 5. User specific code, enable interrupts:
// Enable CPU INT1 which is connected to CPU-Timer 0:
//IER |= M_INT1;
IER |= (M_INT1 | M_INT2);
PieCtrlRegs.PIEIER1.all = M_INT7;
PieCtrlRegs.PIEIER2.all = M_INT4;
PieCtrlRegs.PIEIER3.all=0x0000;  PieCtrlRegs.PIEIER4.all=0x0000;
PieCtrlRegs.PIEIER5.all=0x0000;  PieCtrlRegs.PIEIER6.all=0x0000;
// Enable global Interrupts and higher priority real-time debug events:
EINT;   // Enable Global interrupt INTM
ERTM;   // Enable Global realtime interrupt DBGM
GpioDataRegs.GPADAT.all = 0x0000;
GpioDataRegs.GPBDAT.all = 0x0000;
GpioDataRegs.GPFDAT.all = 0x0000;
GpioDataRegs.GPADAT.bit.GPIOA11 = 0;
GpioDataRegs.GPADAT.bit.GPIOA12 = 0;
GpioDataRegs.GPEDAT.bit.GPIOE0 = 0; //pin 5, P8
LimiteKE=K; Limite1menosKE=K-1;
// pos1,pos2: Introduzco posicion media para muestra MaSeno_a y MaSeno_b
step=2*PI/50; stepMedio=step/2;
for(i=0;i<50;i++)
{angulo[i]=i*step + stepMedio;          TablaSeno[i]=sin(angulo[i]);
  MaSeno[i]=Ma*TablaSeno[i];            contaT0=i;
  DeterminarZona();
  pos1=stepMedio/2; pos2=pos1+stepMedio;
  angulo_a[i]=i*step+pos1;  angulo_b[i]=angulo_a[i]+stepMedio;
  TablaSeno_a[i]=sin(angulo_a[i]);  TablaSeno_b[i]=sin(angulo_b[i]);
  TablaSeno_a[i]=Ma*TablaSeno_a[i];  TablaSeno_b[i]=Ma*TablaSeno_b[i];
```

ISBN:978-84-693-7665-2/DL:T.1747-2010


```
   if(i<50)
   { Xd[i]=0;  Xu[i]=0;  pulse[i]=0;
    testigo1[i]=0;  testigo2[i]=0; testigopulse[i]=0;
    CompararContador[i]=0;  PeriodoContador[i]=0;
    cociente1num[i]=0;cociente1den[i]=0;
    cociente2num[i]=0;cociente2den[i]=0;
    PasoDeZonas[i]=777; TestContador[i]=777;
   }
};  //for(i=0;i<50;i++)
   aux1=0,aux2=0,c1=0,c2=0,aux4=0,Aux5=0;
for(i=0;i<50;i++) // para Mf=50 hay entonces 1310cuentas por paso(2^16/Mf)
{     contaT0=i; // lo necesita codigo de CalcularLhLl()
      DeterminarZona();//Toma la r-apropiada segun MaSeno,K,1menosK
      CalcularLhLl();// Define Lh y Ll según ZonaDeterminada
      UnomenosrTc=(int)((1-r)*MaxCuentas);
      a=TablaSeno_a[i];  M=MaSeno[i];  b=TablaSeno_b[i];
     if(r!=1.0)
           {      temp1=2*a; temp2=-1*M-Lh;  temp3=1-r;
                  aux2=temp1+temp2;  aux1=aux2*temp3;
                  c2=1-r; Aux5=M-a; Aux5=Aux5*4;  c1=c2*Aux5;
                  aux2=Ll-Lh;  aux4=aux2-c1;
                  cociente1num[i]=aux1;  cociente1den[i]=aux4;
                  cociente1[i]=aux1/aux4;
                  Xd[i]=(int)(cociente1[i]*MaxCuentas);
                  if((cociente1[i]<0.0001)||(cociente1[i]>(1-r)))
                  { TestContador[i]=i;
                    if(a>=Lh)
                      {Xd[i]=0;}
                    if(a<=Ll)
                      {Xd[i]=MaxCuentas+Retardo;}
                    }//if((cociente1[i]<0.0)||(cociente1[i]>(1-r)))
     }//if(r!=1.0)
                  else //if(r!=1.0)
                  {Xd[i]=0;}
c1=0; c2=0; auxr=0; aux1=0; aux2=0; aux4=0; temp1=0; temp2=0; temp3=0; Aux5=0;
   if(r!=0.0)
    {             c1=3*M;  c2=-2*b;  Aux5=c1+c2;  aux2=Aux5-Lh;  auxr=aux2*r;
                  temp1=Lh-Ll;  aux1=auxr+temp1;
                  c2=b-M;   temp2=-4*r; temp3=c2*temp2;
                  aux4=temp1+temp3;
                  cociente2num[i]=aux1;  cociente2den[i]=aux4;
                  cociente2[i]=aux1/aux4;
                  Xu[i]=(int)(cociente2[i]*MaxCuentas);
           if((cociente2[i]>0.9999)||(cociente2[i]<(1-r)))
           //if((Xu[i]>MaxCuentas)||(Xu[i]<UnomenosrTc))
                    {TestContador[i]=i;
                     if(b>=Lh)
                     {Xu[i]=MaxCuentas;}
                     if(b<=Ll)
                     {Xu[i]=0;}
                    }
    }//if(r!=0.0)
      else {Xu[i]=MaxCuentas;}
c1=0; c2=0; auxr=0; aux1=0; aux2=0; aux4=0; temp1=0; temp2=0; temp3=0; Aux5=0;
PeriodoContador[i]=Xu[i];  CompararContador[i]=Xd[i];
// Lineas para limitar Ma>1.0 OVERMODULATION //
```

```
    //Corte por límite superior
    //para no sobrepasar 400uS - Time.Atención.Rutina)
        if(CompararContador[i]<Retardo)//Retardo
          CompararContador[i]=Retardo;
        pulse[i]=PeriodoContador[i]-CompararContador[i];
};
init_eva();
StartCpuTimer0();
contaT0=0; i=0;
contador=0;  contador1=0;  contador3=0;
ciclos=0;    ciclos1=0;    ciclos3=0;
ModularZonasOFF();  DeterminarZona();
GpioDataRegs.GPBDAT.all=0x0000;
EvaRegs.COMCONA.bit.FCOMPOE=1; // 0: Hi-Z
// Step 6. IDLE loop. Just sit and loop forever (optional):
  for(;;)
  {
  } //end for(;;)
}
interrupt void cpu_timer0_isr(void)
{// Para medir tiempo de retardo
  GpioDataRegs.GPEDAT.bit.GPIOE0=1; //pin 5, P8
  contaT0=contador;
  DeterminarZona();
  //configurar timer y tenerlo ahi,aún sin arrancar 0x00C0:StopTimer
  EvaRegs.T1CON.all=0x00C0; EvaRegs.T2CON.all=0x00C0;
   //IMPORTANTE: the period register is reloaded if TxCNT=ZERO=underflow-condition
  EvaRegs.T1CNT=0x0000; EvaRegs.T2CNT=0x0000;
  EvaRegs.T1PR=PeriodoContador[contador];//shadow PER load after CNT==0
  EvaRegs.COMCONA.bit.CENABLE=0;//they became transparent
  EvaRegs.T1CMPR=CompararContador[contador];
  ModularZonas();
  //configurar timer y ahora si arrancar
  EvaRegs.T1CON.all=0x10C2; EvaRegs.T2CON.all=0x10C2;
  EvaRegs.COMCONA.bit.CENABLE=1;//enables all CMP'rs operations
                //poner preparado los flags:
        // habilita                    // resetea flag
  EvaRegs.EVAIMRA.bit.T1PINT=1;  EvaRegs.EVAIFRA.bit.T1PINT=1;
   // EvaRegs.EVAIMRB.bit.T2PINT=1;  EvaRegs.EVAIFRB.bit.T2PINT=1;
   PieCtrlRegs.PIEACK.all=0x0003;//0x000B;
   //  PieCtrlRegs.PIEACK.all = PIEACK_GROUP1;
   //testigo1[contador]=EvaRegs.T1PR;  testigo2[contador]=EvaRegs.CMPR1;
   testigopulse[contador]=EvaRegs.T1PR-EvaRegs.CMPR1;
   testigo1[contador]=EvaRegs.CMPR1;  testigo2[contador]=EvaRegs.ACTRA.all;
   contador++;
   if(contador>Mf-1)// 44)
   { contador=0;//31; //ciclos++;   contadorZ1=0; contadorZ2=0; contadorZ3=0; contadorZ4=0;
    }
    MilesCiclos++;
   if(MilesCiclos>25)// 44)
   { MilesCiclos=0;}
   GpioDataRegs.GPEDAT.bit.GPIOE0=0; //pin 5, P8
   GpioDataRegs.GPATOGGLE.bit.GPIOA11=1;//pin 17, P8
   }

interrupt void IntTimer1_ISR(void)    // EV-A GP Timer1 Period Interrupt
```

ISBN:978-84-693-7665-2/DL:T.1747-2010


```
{ //necesario detener el temporizador
 EvaRegs.T1CON.all=0x00C0; EvaRegs.T2CON.all=0x00C0; //0x1000Marzo4-2009, antes 0x10C0
 PieCtrlRegs.PIEACK.all=0x0003;//0x000B;
}
void init_eva()
{EvaRegs.T1PR=0x6000; EvaRegs.T1CMPR=0x8000; EvaRegs.T1CNT=0x0000;
 EvaRegs.EVAIMRA.bit.T1PINT=0; // habilita
 EvaRegs.EVAIFRA.bit.T1PINT=0; // resetea flag
 EvaRegs.T1CON.all=0x0048;//Marzo3-2009:0x5048; FEb25del2009 0x1048;//10C2;
 // Initalize EVA Timer2
 EvaRegs.T2PR=0x6000; EvaRegs.T2CMPR=0x8000; EvaRegs.T2CNT=0x0000;
 EvaRegs.EVAIMRB.bit.T2PINT=0;// habilita
 EvaRegs.EVAIFRB.bit.T2PINT=0; // resetea flag
 EvaRegs.T2CON.all=0x0048;//FEb25del2009 0x1048;//10C2;
 //activación del pin
 EvaRegs.GPTCONA.bit.TCMPOE=1;//1;//0: Hi-Z
 // Polarity of GP Timer 1 Compare = Active low
 EvaRegs.GPTCONA.bit.T1PIN=0;//2;
 EvaRegs.GPTCONA.bit.T2PIN=0;//2;
 EvaRegs.ACTRA.all=0x0000; //0AAA:todos ActivoAlto
 EvaRegs.DBTCONA.all=0x0AE8;//1uS //0x02FC;//1.6uS
  //Enable all FullCompare PWM1,2,3,4,5,6
 EvaRegs.EXTCONA.bit.INDCOE=0;
 EvaRegs.COMCONA.bit.FCOMPOE=1;
 EvaRegs.COMCONA.bit.FCMP1OE=1;
 EvaRegs.COMCONA.bit.FCMP2OE=1;
 EvaRegs.COMCONA.bit.FCMP3OE=1;
 // ACTRA ReLoad Condition:0:T1CNT=0; 1:T1CNT=0+T1CNT=T1PR; 2: Immediately
 EvaRegs.COMCONA.bit.ACTRLD=0;//Mar2:=0 saltosNiveles? =1no cambia
 EvaRegs.COMCONA.bit.CENABLE=1;
 //EvaRegs.COMCONA.all = 0x1000; // ya esta hecho en lineas anteriores
 // Enable compare for PWM1-PWM6
 EvaRegs.CMPR1=0x0000; EvaRegs.CMPR2=0x0000; EvaRegs.CMPR3=0x0000;
}
// Fcns:  //
void CalcularLhLl(void)
{
if(MaSeno[contaT0]>=LimiteKE)
 {Lh=1.0;    Ll=LimiteKE;}
if(MaSeno[contaT0]<LimiteKE && MaSeno[contaT0]>=0.0)
 {Lh=LimiteKE; Ll=0.0;}
if(MaSeno[contaT0]<0.0 && MaSeno[contaT0]>=Limite1menosKE)
 {Lh=0.0;       Ll=Limite1menosKE;}
if(MaSeno[contaT0]<Limite1menosKE)
 { Lh=Limite1menosKE; Ll=-1.0;}
}
void  DeterminarZona(void)
{  if(MaSeno[contaT0]>=LimiteKE)
   {  Zona=1;r=r1;PasoDeZonas[contador]=Zona;}
   if((MaSeno[contaT0]<LimiteKE) && (MaSeno[contaT0]>=0.0))
  {  Zona=2;r=r2;PasoDeZonas[contador]=Zona;}
    if((MaSeno[contaT0]<0.0) && (MaSeno[contaT0]>=Limite1menosKE))
 {  Zona=3;r=r3;PasoDeZonas[contador]=Zona;}
   if(MaSeno[contaT0]<Limite1menosKE)
 {  Zona=4;r=r4;PasoDeZonas[contaT0]=Zona;}
   if((MaSeno[contaT0]>1.001)||(MaSeno[contaT0]<-1.001))
```

```
   { ModularZonasOFF();
     Zona=0; r=0.777;  } }
void ModularZonas(void)
{  switch(Zona)
   { case 1:
     {EvaRegs.ACTRA.all=0x0C36;
      EvaRegs.CMPR1=EvaRegs.T1CMPR;
      EvaRegs.CMPR2=EvaRegs.T1CMPR;
      EvaRegs.CMPR3=MaxCuentas;
      } break;
     case 2:
      {EvaRegs.ACTRA.all=0x0C6C;
       EvaRegs.CMPR1=EvaRegs.T1CMPR;
      EvaRegs.CMPR2=EvaRegs.T1CMPR;
      EvaRegs.CMPR3=MaxCuentas;
      } break;
     case 3:
      {EvaRegs.ACTRA.all=0x0336;
      EvaRegs.CMPR1=EvaRegs.T1CMPR;
      EvaRegs.CMPR2=EvaRegs.T1CMPR;
      EvaRegs.CMPR3=0x0000;
      } break;
     case 4:
      {EvaRegs.ACTRA.all=0x036C;
      EvaRegs.CMPR1=EvaRegs.T1CMPR;//CompararContador[contador];
      EvaRegs.CMPR2=EvaRegs.T1CMPR;//CompararContador[contador];
      EvaRegs.CMPR3=0x0000;
      } break;
           case 0:
            {contadorZonasOff++;
             EvaRegs.ACTRA.all=0x0000;
             EvaRegs.CMPR1=0x0000;//0x0000;
             EvaRegs.CMPR2=0x0000;
             EvaRegs.CMPR3=0x0000;
             } break;
   }
} //void ModularZonas
void ModularZonasOFF(void)
{ contadorZonasOff++;
 EvaRegs.ACTRA.all = 0x0000;
 EvaRegs.CMPR1=0x0000;
 EvaRegs.CMPR2=0x0000;
 EvaRegs.CMPR3=0x0000;
 }
// No more.
```

UNIVERSITAT ROVIRA I VIRGILI
CONTRIBUTIONS ON SPECTRAL CONTROL FOR THE ASYMMETRICAL FULL BRIDGE MULTILEVEL INVERTER
Oscar Mauricio Muñoz Ramírez
ISBN:978-84-693-7665-2/DL:T.1747-2010

APPENDIX F. dsPIC30F6010A Source Code

Closed loop systmem assisted by optimized carriers generator dsPIC 30F6010A

```
//REALITZACIO DE ONES PORTADORES PER CONTROLAR  L'ONDULADOR
//************************************
# include <p30f6010.h>
# include <math.h>
//***   VARIABLES GLOBALS   ***
long int e1;                // Variable de prova per fer canvis de pendent
int ma;          char x;          char j;          char p;
int ka;          int muestra_actual;      int muestra_anterior;
int m;   int k;    long int v3;      long int v4;
// Cicles de traball dels BUFFER'S principals
float DutyC1;   float DutyC2;   float DutyC3;   float DutyC4;
// Variables de calculs de AY en les pendents positives de les portadores
float x1;          float x2;          float x3;          float x4;
// Variables de càlculs de AY en les pendents negatives de les portadores
float y1;          float y2;          float y3;          float y4;
// Cicles de treball dels BUFFER'S auxiliars
float DutyC1_aux;       float DutyC2_aux;       float DutyC3_aux;       float DutyC4_aux;
float x1_aux;    float x2_aux;    float x3_aux;    float x4_aux;
float y1_aux;    float y2_aux;    float y3_aux;    float y4_aux;
float DutyC5;   // Cicle de treball del PWM de la senoidal
unsigned int periode;           unsigned int flag;
unsigned int principal;         unsigned int auxiliar;
unsigned int pendiente_port;// Valor de la pendent de una portadora
unsigned int pendiente;         int pend;
unsigned int high;        unsigned int low;
// Si el valor no es float, al realitzar una operació amb un int, // el resultat pasa a ésser int
float pendiente1;          float pendiente2;          float pendiente3;          float pendiente4;
float pendiente1_aux;   float pendiente2_aux;   float pendiente3_aux;   float pendiente4_aux;
unsigned int numero_port;       // Número de la portadora a canviar
int passos_5;
int BUFFER_4[111];              // Buffer de memòria amb valors de la portadora 4
int BUFFER_3[111];              // Buffer de memòria amb valors de la portadora 3
int BUFFER_2[111];              // Buffer de memòria amb valors de la portadora 2
int BUFFER_1[111];              // Buffer de memòria amb valors de la portadora 1
int BUFFER_SENOIDE[201];  // Buffer de memòria amb valors de l'ona senoidal.
// Buffers de memòria de les portadores auxiliars
int BUFFER_4_AUX[111];      int BUFFER_3_AUX[111];
int BUFFER_2_AUX[111];      int BUFFER_1_AUX[111];
int BUFFER_GRADOS[201];
int b;
int passos_1;    int passos_2;    int passos_3;    int passos_4;
int passos_1aux;          int passos_2aux;          int passos_3aux;          int passos_4aux;
int CONJUNTOS [13][17][4]=
// MATRIU TRES DIMENSIONS AMB PUNTS CALCULATS MITJANÇANT (GA)
// Las 4 R's para m=0, k=0,// Las 4 R's para m=0, k=1  y así hasta k =17
        {
        {       {110,51,55,42},{110,68,27,110},{0,43,76,109},{110,53,73,0},
                {110,72,68,0},{0,45,39,98},{109,85,73,108},{109,99,80,110},
                {110,102,77,100},{106,110,81,93},{10,0,30,94},{90,110,70,74},
                {21,0,42,78},{88,110,56,81},{0,110,55,83},{105,0,53,56},
```

```
        {24,0,62,46},   },
{       {110,57,35,107},{0,72,27,107},{109,53,72,0},{110,56,65,0},
        {110,58,68,0},{109,80,66,110},{0,33,47,12},{109,93,69,100},
        {109,105,75,87},{0,2,40,57},{105,110,66,76},{97,110,63,51},
        {22,0,40,99},{91,110,55,81},{0,110,55,79},{105,0,53,58},
        {9,110,52,75},  },
{       {110,63,26,110},{110,50,71,0},{110,63,62,0},{0,55,42,110},
        {110,60,59,99},{110,73,61,95},{0,40,51,42},{110,88,61,84},
        {109,99,29,95},{0,7,69,0},{110,109,59,79},{5,0,51,59},
        {97,110,55,77},{89,110,56,77},{14,0,54,55},{0,110,55,50},
        {19,110,53,74},},
{       {0,59,39,109},{110,52,63,0},{110,58,52,109},{109,55,56,97},
        {109,58,59,84},{110,62,57,66},{109,84,60,83},{1,93,37,77},
        {0,100,21,92},{109,102,43,87},{109,104,41,77},{110,110,53,54},
        {105,110,52,75},{100,109,54,74},{13,0,54,57},{98,110,51,68},
        {0,110,52,72},  },
{       {0,59,51,102},{110,53,52,109},{110,52,63,34},{110,63,58,86},
        {0,53,51,44},{110,56,59,64},{0,95,49,79},{0,95,24,77},
        {1,99,32,87},{1,102,28,91},{0,8,75,30},{110,106,45,74},
        {110,109,50,72},{2,0,57,56},{99,109,54,51},{101,110,52,67},
        {104,22,83,67},  },
{       {41,87,29,110},{0,56,58,19},{110,53,57,79},{109,58,56,64},
        {109,54,60,65},{110,53,59,62},{0,101,40,68},{0,101,38,76},
        {0,100,30,85},{109,11,81,38},{110,97,25,74},{0,9,71,60},
        {0,6,65,69},{110,106,48,51},{1,6,64,65},{102,106,48,68},
        {0,64,0,75},    },
{       {41,89,32,110},{0,58,54,63},{0,58,53,48},{109,53,55,58},
        {110,63,56,62},{0,61,52,52},{109,10,76,42},{0,105,39,77},
        {0,101,30,68},{110,11,84,36},{0,104,36,68},{109,99,36,70},
        {0,11,69,57},{102,94,32,66},{109,100,42,65},{2,17,72,66},
        {105,52,106,33},  },
{       {33,86,59,89},{2,61,55,65},{104,44,55,53},{110,48,57,57},
        {109,61,54,67},{0,52,59,52},{110,11,76,50},{0,108,39,77},
        {109,87,11,65},{0,24,94,44},{110,11,79,56},{109,0,68,68},
        {109,91,34,54},{110,88,28,65},{109,87,33,75},{108,42,102,62},
        {110,46,101,22},  },
{       {37,91,59,82},{35,88,56,68},{43,110,57,69},{28,88,56,67},
        {40,107,43,62},{109,76,13,61},{0,33,102,66},{110,77,1,52},
        {110,80,8,60},{110,85,16,68},{0,27,93,59},{110,83,21,54},
        {109,82,21,60},{0,23,78,65},{0,26,75,73},{104,75,27,67},
        {0,59,5,84},  },
{       {48,104,31,70},{47,95,32,67},{46,110,51,67},{47,110,25,63},
        {45,108,19,66},{64,0,88,47},{0,37,105,62},{110,74,0,54},
        {110,76,5,58},{110,78,12,69},{0,32,97,64},{110,74,12,59},
        {109,75,15,63},{109,74,22,81},{0,32,82,64},{101,65,7,73},
        {97,66,15,78},  },
{       {48,103,27,65},{45,95,45,66},{46,94,21,59},{47,110,17,65},
        {67,3,90,50},{63,0,91,50},{43,92,3,60},{0,39,109,52},
        {0,38,109,55},{109,73,9,75},{109,73,6,52},{0,39,100,48},
        {0,39,102,51},{110,66,17,88},{102,63,0,64},{104,63,8,74},
        {89,60,0,80},   },
{       {65,3,83,51},{45,97,31,70},{45,97,15,61},{47,109,17,69},
        {63,1,93,47},{69,22,101,68},{43,92,5,65},{109,70,0,57},
        {0,41,110,58},{110,67,6,80},{109,70,3,54},{0,42,103,46},
        {0,41,103,61},{104,61,11,96},{102,59,0,68},{11,49,106,31},
        {90,61,6,109},  },
```

```
        {       {66,3,84,54},{48,107,23,54},{45,97,14,54},{62,0,90,42},
                {63,0,93,53},{37,88,0,54},{42,92,3,54},{73,33,110,43},
                {0,42,106,54},{110,64,0,52},{110,66,4,54},{0,47,110,53},
                {0,46,110,54},{0,48,109,54},{94,58,0,54},{99,57,0,54},
                {30,48,110,0},  }
        };      // FI DE MATRIU TRES DIMENSIONS

// ** PROTOTIPUS DE FUNCIONS **********
void _ISR _T1Interrupt (void);          // Rutina atenció interrupció del Timer 1
void _ISR _T3Interrupt (void);          // Rutina atenció interrupció del Timer 3
void _ISR _T2Interrupt (void);          // Rutina atenció interrupció del Timer 2
void _ISR _INT0Interrupt (void);        // Rutina d'atenció a la interrupció entrada externa 1
void _ISR_ADCInterrupt (void);
void configura (void);                  // Rutina de configuració dels registres utilitzats
void configura_AD (void);               // Configuración del conversor AD
void configura_PWM (void);              // Configuració del PWM
void main (void);                       // Funció principal
void DC4(void);                         // Cálculo de los valores del DC4
void DC3(void);                         // Cálculo de los valores del DC3
void DC2(void);                         // Cálculo de los valores del DC2
void DC1(void);                         // Cálculo de los valores del DC1
void senoidal(void);
void DC4_aux (void);   void DC3_aux (void);
void DC2_aux (void);   void DC1_aux (void);
void implementa_buffer4 (int, float);   // Funció que plena un buffer on guardem els punts dels dc de
cadascuna de les ones portadores
void implementa_buffer3 (int, float);
void implementa_buffer2 (int, float);
void implementa_buffer1 (int, float);
void implementa_buffer (int, float); // plena un buffer amb els punts de la senyal senoidal de 50 Hz
void implementa_buffer4_aux (int, float);
void implementa_buffer3_aux (int, float);// Funcions on plenem els buffers auxiliars
void implementa_buffer2_aux (int, float);
void implementa_buffer1_aux (int, float);
void configura_timer_buffer (void);// Configuració per actualitzar els valors de les R's
//** RUTINA D'ATENCIO A LA INTERRUPCIO DEL TIMER 1**
void _ISR _T1Interrupt (void)
{       switch (flag)
        {       case 0:
                {       PDC1 = BUFFER_1[passos_1++];
                        // Enviem al registre del PWM1 el valor calculat prèviament
                        PDC2 = BUFFER_2[passos_2++];
                        // Enviem al registre del PWM2 el valor calculat prèviament
                        PDC3 = BUFFER_3[passos_3++];
                        // Enviem al registre del PWM3 el valor calculat prèviament
                        PDC4 = BUFFER_4[passos_4++];
                        // Enviem al registre del PWM4 el valor calculat prèviament
                        if (passos_4>=110)
                                {       passos_4=0;
                                        passos_3=0;
                                        // Reiniciem els passos al arribar al final del BUFFER
                                        passos_2=0;
                                        passos_1=0;
                                }
                        if (passos_5>=200)
                                {passos_5=0;
```

```
                                }
                        break;
                }
                case 1:
                {       PDC1 = BUFFER_1_AUX[passos_1aux++];
                // Enviem al registre del PWM1 el valor calculat prèviament
                        PDC2 = BUFFER_2_AUX[passos_2aux++];
                // Enviem al registre del PWM2 el valor calculat prèviament
                        PDC3 = BUFFER_3_AUX[passos_3aux++];
                // Enviem al registre del PWM3 el valor calculat prèviament
                        PDC4 = BUFFER_4_AUX[passos_4aux++];
                // Enviem al registre del PWM4 el valor calculat prèviament
                        if (passos_4aux>=110)
                                {       passos_4aux=0;
                                        passos_3aux=0;
                                        passos_2aux=0;
                // Reiniciem els passos al arribar al final del BUFFER
                                        passos_1aux=0;
                                        e1++;
                                }
                        if (passos_5>=200)
                                {passos_5=0;
                                }
                        break;
                }
        }
        IFS0bits.T1IF = 0;
// Esborra el Flag de atenció a la irq
}
//** RUTINA D'ATENCIO A LA INTERRUPCIO DEL TIMER 3**
void _ISR _T3Interrupt (void)
{       OC1RS = BUFFER_SENOIDE[passos_5++];
        // Carreguem el valor del buffer calculat prèviament
        IFS0bits.T3IF = 0;
        // Esborra el Flag de atenció a la irq
}
//** RUTINA D'ATENCIO A LA INTERRUPCIO DEL AD**
void _ISR _ADCInterrupt (void)
{       x++;
        j++;
        if (x<210)
        {       muestra_actual=ADCBUF0;
                ka=ADCBUF3;
        //      muestra_anterior+=muestra_actual;
        //      v3=ADCBUF2;
        //      v4=ADCBUF3;
                        if (muestra_actual>muestra_anterior)
                                {muestra_anterior=muestra_actual;
                                }
                                else
                                {ma=muestra_anterior;
                                }

        }
        if(j>251)
        {       //ma=muestra_anterior>>5;
```

```
                x=0;    j=0;
        }
        IFS0bits.ADIF=0;
}
//**RUTINA D'ATENCIO A LA INTERRUPCIÓ EXTERNA INT0
// ( ADQUIRIM QUINES SON LES PENDENTS DE LES PORTADORES **
void _ISR _T2Interrupt (void)
{/*     if (ka<153) ka=153;
// Assegurem quins son els valors frontera, per tal de no sortir del cuadre de R's
        if (ka>358) ka=358;
        if (ma<358) ma=358;
        if (ma>512) ma=512;
*/
        k=(ka-153)/13;
// Calculem quin es l'index de posició a la taula de m i k en funció del seu valor de la lectura del A/D
        m=(ma-358)/13;
        switch (flag)
        {       case 0:
                {if (ka<153||ka>358||ma<358||ma>512)
                        {pendiente1_aux=55;   pendiente2_aux=55;
                         pendiente3_aux=55;   pendiente4_aux=55;
                        }
                        else
                        {pendiente1_aux=CONJUNTOS [m][k][0];
                         pendiente2_aux=CONJUNTOS [m][k][1];
                         pendiente3_aux=CONJUNTOS [m][k][2];
                         pendiente4_aux=CONJUNTOS [m][k][3];
                        }
                        DC1_aux();    DC3_aux();    DC2_aux();    DC4_aux();
//SI NO SE LLENAN BIEN AQUI, CAMBIAR AL MAIN COMO EN EL PRINCIPIO
                        break;
                }
                case 1:
                {if (ka<153||ka>358||ma<358||ma>512)
                        {pendiente1=55;         pendiente2=55;
                         pendiente3=55;         pendiente4=55;
                        }
                        else
                        {pendiente1=CONJUNTOS [m][k][0];
                         pendiente2=CONJUNTOS [m][k][1];
                         pendiente3=CONJUNTOS [m][k][2];
                         pendiente4=CONJUNTOS [m][k][3];
                        }
                  DC1();        DC2();          DC3();          DC4();
                        break;
                }
        }
        if (flag==0)
                                {       flag=1;         principal=1;
                                        muestra_anterior=0;
                                }
                                else
                                {       flag=0;         auxiliar=1;
                                        muestra_anterior=0;
                                }
IFS0bits.T2IF = 0;
```

```
}
//***************MENU PRINCIPAL*****************
void main (void)
  {       configura_PWM();//Configuració dels PWM's ( Portadores i senoidals )
          configura_AD();
          configura_timer_buffer();// Configurem el Timer 2 per tal de cambiar les R's
          configura();//Configuració de les interrupcions
//        TRISA = 0x00;
          TRISE = 0x00; //Port de sortida dels PWM's Portadores
          TRISG = 0xFF;
          TRISD = 0x7E;//<0> Sortida PWM ona senoidal, <1:7> Entrades pendent de portadores
          TRISF = 0xF3; //<6> Irq0 que ens indica que s'ha de llegir pendents,
                        //<0:1> Número de portadora a llegir.
          TRISB = 0xFFFF;// TODO PORTB
          e1=0;           flag=0;
          muestra_anterior=0;// Valor inicial de la mostra anterior, per al detector de pic
          x=0;            j=0;
          PORTGbits.RG0 = 0;//Flag comprovació de temps de durada de irq
          passos_5=0;
          principal=0;
          auxiliar=1;
          b=1;
          while (1)       //Bucle infinit
     {       while ((principal==1)&(flag==1))//Carreguem els BUFFERS principals
             {//                     pendiente1++;
                        //Indiquem el  pendent de les portadores
//                      pendiente2++;
//                      pendiente3++;
//                      pendiente4++;
                        if (pendiente1 == 110)
                        {       pendiente1 = 0;
                                pendiente2 = 0;
                                pendiente3 = 0;
                                pendiente4 = 0;
                        }

//                      DC1();  DC2();  DC3();          DC4();
                        if (numero_port>2) principal=0;
// Una vez hemos almacenado todas las portadoras, cambiamos el flag del buffer a seleccionar
//                      principal=0;
                  }
                  while ((auxiliar==1)&(flag==0))//Carreguem els BUFFERS auxiliars
                  {
//                      pendiente1_aux=101;
//                      pendiente2_aux=101;
//                      pendiente3_aux=101;
//                      pendiente4_aux=101;

//                       DC1_aux();  DC3_aux();  DC2_aux();  DC4_aux();
                         if (numero_port>2) auxiliar=0;
//                       auxiliar=0;
                  }
          }
  }// fi programa principal
//**CONFIGURACIO TIMER 1 I INTERRUPCIONS**
void configura (void)
```

```
{T1CON=0x0000;        //Parem el timer 1 i resetejem els seus registres
TMR1=0x0000;
PR1=0x006B;   //Una irq a 277kHz per tal de realitzar una senyal amb 110 passos
IPC0=0x4000;  //Interrupció del T1 prioritat (1)
IPC1=0x3100;  //Interrupció del T3 prioritat (5)
IPC2=0x1000;  //Interrupción de fi de conversió AD (6), Interrupció del T2 prioritat (4)
IEC0=0x08C8; //Habilitem les interrupcions del Timer 1 PR1=TMR1 ,
                  //Timer 3 PR3=TMR3 , ADIE = Fi conversió
IEC1=0x0000;
IEC2=0x0000;
INTCON1bits.NSTDIS = 0;      //Anidem les irq's
INTCON2bits.ALTIVT = 0;      //NO utilitzem la taula de prioritats auxiliar
T1CON=0x8000;          //T1 ON, Prescaler 1:1, temp 16 bits, Fosc
T3CONbits.TON = 1;   //Activem el Timer 3
T2CONbits.TON = 1;   //Activem el Timer 2
}
//**CONFIGURACIO DELS PWM**
void configura_PWM(void)
{
        //**CONFIGURACIÓ DELS PWM DE LES PORTADORES**
        PTCON = 0x8000;//Base temps desactivada, Postscaler=0, Prescaler =0, Mode NORMAL
        PWMCON1 = 0x0F96; //PWM's Independents, Activem les sortides High
        PWMCON2bits.UDIS=0;//Postscaler=0,
                                // La sortida 'sactualitza en el següent TCY, Actualitzem el PWM
        OVDCON=0xFF00;      //Les sortides estan controlades per els PWM
        PTPER = 57;    //Introduim el període de la senyal    100-->292,5 kHz
        //*****CONFIGURACIÓ DEL PWM DE LA SENOIDAL A 50Hz******
        senoidal();
        PR3 = 0x0B80;            //Introduim la freqüència del PWM --> 10kHz
        OC1RS = 0x0000;          //Introduim el Duty Cicle
        OC1CON = 0x000E;     //Configurem el simple PWM Mode
        T3CON = 0x0000;          //Configurem el Timer 3
        pendiente4=1;   //VALOR DE PRUEBA PARA COMPROBAR EL ALGORITMO
        pendiente3=30;
        pendiente2=75;
        pendiente1=109;
        DC1(); DC2(); DC3(); DC4();
}
//**CONFIGURACIO DEL TIMER 2**
void configura_timer_buffer(void)
{       PR2 = 0x44A9; //Introduim el valor a contar
        T2CON = 0x0030;//Configurem el Timer 2
}
//**CONFIGURACIO DEL CONVERSOR AD**
void configura_AD(void)
{       //**CONFIGURACIÓ DELS REGISTRES DE CONTROL**
        TRISB=0xFFFF;          //Todo el puerto B son salidas
        ADPCFG=0x87FF;
        ADCON1=0x00E0;       //
        ADCHS=0x0000;        //
        ADCSSL=0x7800;       //
        ADCON2=0x240C;       //
        ADCON3=0x1E06;       //
        ADCON1bits.ADON = 1;
        ADCON1bits.ASAM = 1;
}
```

```
//*FCN'S DE CALCUL DELS VALORS DELS CICLES DE TREBALL AMB FLAG 0*
void DC4(void)
{int p4; // Pasos a realizar como variables locales para asegurarnos
        // que solamente las cambiamos en esta función
        if (pendiente4==0)
        {               x4=110;         pendiente4=1;
// Ens assegurem de que en un cas extrem NO DIVIDIM PER 0 !!!
        }
        else x4=(110/pendiente4);
        if (pendiente4==110)
        {               y4=110;         pendiente4=109;
        }
        else y4=(110/(110-pendiente4));
    for (p4=0; p4<=110;p4+=1)
        {               if(p4<pendiente4) DutyC4+=x4;
                        else DutyC4-=y4;
                        implementa_buffer4(p4,DutyC4);
        }
p4=0;   DutyC4=0;
}
void DC3(void)
{int p3;
        if (pendiente3==0)
        {       x3=110;         pendiente3=1;
        }
        else x3=(110/pendiente3);
        if (pendiente3==110)
        {       y3=110;         pendiente3=109;
        }
        else y3=(110/(110-pendiente3));
                for (p3=0; p3<=110;p3+=1)
                {       if(p3<pendiente3) DutyC3+=x3;
        // Algoritme per plenar el BUFFER amb les pendents corresponents
                        else DutyC3-=y3;
                        implementa_buffer3(p3,DutyC3);
        }
p3=0;   DutyC3=0;
}
void DC2(void)
{int p2;
        if (pendiente2==0)
        {       x2=110;         pendiente2=1;
        }
        else x2=(110/pendiente2);
        if (pendiente2==110)
        {       y2=110;         pendiente2=109;
        }
        else y2=(110/(110-pendiente2));
                        for (p2=0; p2<=110;p2+=1)
        {
                        if(p2<pendiente2) DutyC2+=x2;
                        else DutyC2-=y2;
                        implementa_buffer2(p2,DutyC2);
        }
p2=0;   DutyC2=0;
}
```

```
void DC1(void)
{int p1;
        if (pendiente1==0)
        {       x1=110;         pendiente1=1;
        }
        else x1=(110/pendiente1);
        if (pendiente1==110)
        {       y1=110;         pendiente1=109;
        }
        else y1=(110/(110-pendiente1));
                for (p1=0; p1<=110;p1+=1)
        {       if(p1<pendiente1) DutyC1+=x1;
                else DutyC1-=y1;
                implementa_buffer1(p1,DutyC1);
        }
p1=0;   DutyC1=0;
}
void senoidal (void)
{       float n;        float inc_grados;       float PI;       PI=3.1416;
        n=0;
        inc_grados=((1.8*2*PI)/360);
                for (passos_5=0;passos_5<=200;passos_5+=1)
        {       DutyC5=1450+(1450*sin(n));
                n+=inc_grados;
                implementa_buffer(passos_5,DutyC5);
        }
passos_5=0;
}
//*FCN'S DE CALCUL DELS VALORS DELS CICLES DE TREBALL AMB FLAG 1*
void DC4_aux(void)
{int p4aux;
                if (pendiente4_aux==0)
        {               x4=110;         pendiente4_aux=1;
        }
        else x4=(110/pendiente4_aux);
        if (pendiente4_aux==110)
        {               y4=110;         pendiente4_aux=109;
        }
        else y4=(110/(110-pendiente4_aux));
        for (p4aux=0; p4aux<=110;p4aux+=1)
        {               if(p4aux<pendiente4_aux) DutyC4_aux+=x4;
                        // Plenem el buffer amb els valors del Duty Cicle desitjats
                        else DutyC4_aux-=y4;
                        implementa_buffer4_aux(p4aux,DutyC4_aux);
        }
p4aux=0;
// MUY IMPORTANTE - REINICIAMOS LOS PASOS
DutyC4_aux=0;
// MUCHO MÁS IMPORTANTE - REINICIAMOS EL VALOR DEL CICLO DE TRABAJO
}
void DC3_aux(void)
{int p3aux;
        if (pendiente3_aux==0)
        {       x3=110;         pendiente3_aux=1;
        }
        else x3=(110/pendiente3_aux);
```

```
        if (pendiente3_aux==110)
        {       y3=110;         pendiente3_aux=109;
        }
        else y3=(110/(110-pendiente3_aux));
        for (p3aux=0; p3aux<=110;p3aux+=1)
        {       if(p3aux<pendiente3_aux) DutyC3_aux+=x3;
                        else DutyC3_aux-=y3;
                        implementa_buffer3_aux(p3aux,DutyC3_aux);
        }
p3aux=0;        DutyC3_aux=0;
}
void DC2_aux(void)
{int p2aux;
        if (pendiente2_aux==0)
        {       x2=110;         pendiente2_aux=1;
        }
        else x2=(110/pendiente2_aux);
        if (pendiente2_aux==110)
        {       y2=110;         pendiente2_aux=109;
        }
        else y2=(110/(110-pendiente2_aux));
        for (p2aux=0; p2aux<=110;p2aux+=1)
        {       if(p2aux<pendiente2_aux) DutyC2_aux+=x2;
                else DutyC2_aux-=y2;
                implementa_buffer2_aux(p2aux,DutyC2_aux);
        }
p2aux=0;        DutyC2_aux=0;
}
void DC1_aux(void)
{int p1aux;
        if (pendiente1_aux==0)
        {       x1=110;         pendiente1_aux=1;
        }
        else x1=(110/pendiente1_aux);
        if (pendiente1_aux==110)
        {       y1=110;         pendiente1_aux=109;
        }
        else y1=(110/(110-pendiente1_aux));
                for (p1aux=0; p1aux<=110;p1aux+=1)
        {               if(p1aux<pendiente1_aux) DutyC1_aux+=x1;
                        else DutyC1_aux-=y1;
                        implementa_buffer1_aux(p1aux,DutyC1_aux);
        }
p1aux=0;        DutyC1_aux=0;
}
//*IMPLEMENTACIO DELS BUFFERS DE MEMORIA
//PER EMMAGATZEMAR ELS VALORS DELS DC FLAG 1****
void implementa_buffer4(int p4, float DutyC4)
{       BUFFER_4[p4++]=DutyC4;
}
void implementa_buffer3(int p3, float DutyC3)
{       BUFFER_3[p3++]=DutyC3;
}
void implementa_buffer2(int p2, float DutyC2)
{       BUFFER_2[p2++]=DutyC2;
}
```

UNIVERSITAT ROVIRA I VIRGILI
CONTRIBUTIONS ON SPECTRAL CONTROL FOR THE ASYMMETRICAL FULL BRIDGE MULTILEVEL INVERTER
Oscar Mauricio Muñoz Ramírez
ISBN:978-84-693-7665-2/DL:T.1747-2010


```
void implementa_buffer1(int p1, float DutyC1)
{       BUFFER_1[p1++]=DutyC1;
}
void implementa_buffer( int passos_5, float DutyC5)
{       BUFFER_SENOIDE[passos_5++]=DutyC5;
}
//**IMPLEMENTACIO DELS BUFFERS DE MEMORIA PER
//EMMAGATZEMAR ELS VALORS DELS DC AUXILIARS FLAG =0**
void implementa_buffer4_aux(int p4aux, float DutyC4_aux)
{       BUFFER_4_AUX[p4aux++]=DutyC4_aux;
}
void implementa_buffer3_aux(int p3aux, float DutyC3_aux)
{       BUFFER_3_AUX[p3aux++]=DutyC3_aux;
}
void implementa_buffer2_aux(int p2aux, float DutyC2_aux)
{       BUFFER_2_AUX[p2aux++]=DutyC2_aux;
}
void implementa_buffer1_aux(int p1aux, float DutyC1_aux)
{       BUFFER_1_AUX[p1aux++]=DutyC1_aux;
}
```